frontiers
RESEARCH TOPICS

CORTICAL NO INTERNEURONS: FROM EMBRYOGENESIS TO FUNCTIONS

Topic Editors
Bruno Cauli, Yoshiyuki Kubota and Ludovic Tricoire

frontiers in
NEURAL CIRCUITS

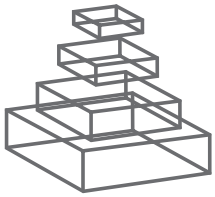

frontiers

ISSN 1664-8714
ISBN 978-2-88919-175-8
DOI 10.3389/978-2-88919-175-8

ABOUT FRONTIERS

Frontiers is more than just an open-access publisher of scholarly articles: it is a pioneering approach to the world of academia, radically improving the way scholarly research is managed. The grand vision of Frontiers is a world where all people have an equal opportunity to seek, share and generate knowledge. Frontiers provides immediate and permanent online open access to all its publications, but this alone is not enough to realize our grand goals.

FRONTIERS JOURNAL SERIES

The Frontiers Journal Series is a multi-tier and interdisciplinary set of open-access, online journals, promising a paradigm shift from the current review, selection and dissemination processes in academic publishing.
All Frontiers journals are driven by researchers for researchers; therefore, they constitute a service to the scholarly community. At the same time, the Frontiers Journal Series operates on a revolutionary invention, the tiered publishing system, initially addressing specific communities of scholars, and gradually climbing up to broader public understanding, thus serving the interests of the lay society, too.

DEDICATION TO QUALITY

Each Frontiers article is a landmark of the highest quality, thanks to genuinely collaborative interactions between authors and review editors, who include some of the world's best academicians. Research must be certified by peers before entering a stream of knowledge that may eventually reach the public - and shape society; therefore, Frontiers only applies the most rigorous and unbiased reviews.
Frontiers revolutionizes research publishing by freely delivering the most outstanding research, evaluated with no bias from both the academic and social point of view.
By applying the most advanced information technologies, Frontiers is catapulting scholarly publishing into a new generation.

WHAT ARE FRONTIERS RESEARCH TOPICS?

Frontiers Research Topics are very popular trademarks of the Frontiers Journals Series: they are collections of at least ten articles, all centered on a particular subject. With their unique mix of varied contributions from Original Research to Review Articles, Frontiers Research Topics unify the most influential researchers, the latest key findings and historical advances in a hot research area!
Find out more on how to host your own Frontiers Research Topic or contribute to one as an author by contacting the Frontiers Editorial Office: researchtopics@frontiersin.org

CORTICAL NO INTERNEURONS: FROM EMBRYOGENESIS TO FUNCTIONS

Topic Editors:
Bruno Cauli, Centre National de la Recherche Scientifique (CNRS), France
Yoshiyuki Kubota, National Institute for Physiological Sciences, Japan
Ludovic Tricoire, Université Pierre et Marie Curie, France

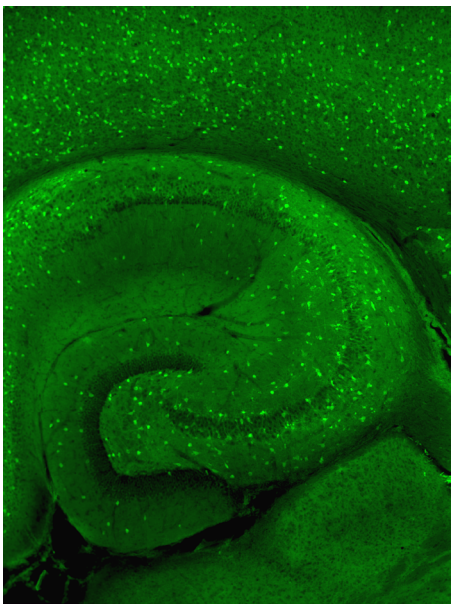

Fluorescence image of hippocampal and necortical interneurons originating from the medial ganglionic eminence . They were labeled with GFP (green) using the Nkx2-1Cre:RCE double transgenic mouse line.

Neuronal processing and physiology rely on a delicate interplay between glutamatergic excitatory neurons and GABAergic inhibitory interneurons in a spatially, temporally and cell-type specific manner. Understanding these processes is complicated further by the large diversity characterizing the cerebral cortex. Although recent advances have significantly improved our knowledge of its neuronal types, the identity and the roles of several subpopulations of GABAergic interneurons remain elusive. Presumably, because of their apparent paucity, their diversity, the highly labile nature of nitric oxide (NO) as well as its pleiotropic actions, the functional importance of NO-producing GABAergic interneurons is particularly enigmatic. This Research Topic will cover the different aspects of cortical NO interneurons, from their diversity, embryonic origins to their functions in the cortical circuit and physiology.

Table of Contents

frontiers in
NEURAL CIRCUITS

EDITORIAL
published: 03 June 2013
doi: 10.3389/fncir.2013.00105

Cortical NO interneurons: from embryogenesis to functions

Ludovic Tricoire[1], Yoshiyuki Kubota[2] and Bruno Cauli[1]*

[1] *CNRS UMR7102, Neurobiologie des Processus Adaptatifs, Université Pierre et Marie Curie, Paris, France*
[2] *Division of Cerebral Circuitry, National Institute for Physiological Sciences, Okazaki, Japan*
**Correspondence: bruno.cauli@snv.jussieu.fr*

Edited by:
Rafael Yuste, Columbia University, USA

Reviewed by:
Rafael Yuste, Columbia University, USA

Neuronal processing and physiology of cortical circuits rely on a delicate interplay between glutamatergic excitatory neurons and GABAergic inhibitory interneurons in a spatially, temporally, and cell-type specific manner. Understanding these processes is further complicated by the large diversity characterizing the cerebral cortex (Ascoli et al., 2008; DeFelipe et al., 2013). Although recent advances have significantly improved our knowledge of its neuronal types, the identity and the roles of several subpopulations of GABAergic interneurons remain elusive (Gentet, 2012). Presumably, because of their apparent paucity, their diversity, the highly labile nature of nitric oxide (NO) as well as its pleiotropic actions, the functional importance of NO-producing GABAergic interneurons is particularly enigmatic. In this e-book we present a collection of articles published in *Frontiers in Neural Circuits* in response to the "Special topic" entitled "Cortical NO interneurons: from embryogenesis to functions." Although it is practically impossible to address all aspects of NO interneurons, this special issue organized in four sections covers different facets of neocortical and hippocampal NO interneurons: from their diversity and embryonic origins to their functions in the cortical circuits and in neurovascular coupling.

Studying the functional roles of NO-producing cortical interneurons has been challenging. NO being a highly diffusible gas (Wood and Garthwaite, 1994) the identification and characterization of neurons producing it essentially rely on the direct or indirect detection of its synthesizing enzyme; the neuronal nitric oxide synthase isoform (nNOS). NO cortical interneurons have been historically classified as type I and type II on the basis of the size of their soma and by the intensity of their nNOS staining (Estrada and DeFelipe, 1998). Type I neurons, corresponding to heavily stained neurons with a large soma, have been studied at the molecular level but since they correspond to the rarest population of cortical interneurons (Kubota et al., 1994) their electrophysiological and pharmacological properties are poorly documented (Karagiannis et al., 2009; Kubota et al., 2011). In contrast type II neurons are much more numerous, but mainly for technical reasons inherent to the dimness of their staining, their properties and even their existence in the rodents has been questioned (Yan and Garey, 1997).

This issue was revaluated in the whisker-to-barrel cortex by using NADPH-diaphorase histochemistry (Nogueira-Campos et al., 2012) revealing that type I neurons were enriched in deep layers whereas type II NO interneurons were particularly dense in superficial layers. Consistently, using a combination of patch-clamp recordings, single cell RT-PCR and immunocytochemistry (Perrenoud et al., 2012a) disclosed that type I neurons were predominantly located in deeper layers and largely co-expressed somatostatin while type II neurons were concentrated in layers II/III and VI and heterogeneous at the molecular level. In contrast with the neocortex, the type I / type II subdivision does not hold in the hippocampus (Tricoire and Vitalis, 2012). By using an elegant spectral analysis to improve recognition of immunofluorescently labeled nNOS and neuropeptide-Y (NPY) expressing neurons (Somogyi et al., 2012), found that most NO interneurons with soma in the *stratum radiatum* of the CA1 area exhibit characteristic properties of ivy cells and express NPY. In contrast to their counterparts in the *stratum pyramidale* (Fuentealba et al., 2008), *stratum radiatum* ivy cells display a different pattern of axonal and dendritic arborizations suggesting that these two subpopulations of hippocampal NO interneurons are involved in different microcircuits.

Concomitantly with improvements in nNOS detection and the advent of genetic tools allowing lineage analysis of interneuron precursors, the developmental temporal and spatial origins of hippocampal and cortical nNOS neurons have been clarified with three studies showing that hippocampal and cortical type I NO interneurons originate from the medial ganglionic eminence (Jaglin et al., 2012; Magno et al., 2012; Perrenoud et al., 2012a), confirming and extending original findings (Tricoire et al., 2010). In contrast type II interneurons exhibited multiple embryonic origins (Magno et al., 2012; Perrenoud et al., 2012a). These works show that nNOS interneurons in addition of existing as different flavor also exhibit several and underestimated embryonic origins (Tricoire and Vitalis, 2012). These findings stress the still ongoing debate about the relative influences between the genetic programs and the molecular cues during embryogenesis.

Another important question addressed in this special topic, is how NO interneurons are modulated by afferent signals and what their main neuronal targets are. Type I NO interneurons were found to express selectively the NK1 receptor whose activation by its natural agonist substance P induced their depolarization (Dittrich et al., 2012). Using the phototoxicity of a NO indicator, selective damaging of cortical NO interneurons uncovered their role in lateral inhibition on neighboring columns and in the spatiotemporal dynamics of cortical activity (Shlosberg et al., 2012). A comprehensive review of the peculiar place of NO interneurons in cortical microcircuits is concluding this section (Armstrong et al., 2012).

Although NO is a well-established vasodilator, the relevance of NO interneurons in neurovascular coupling, the tight

relationship between neuronal activity and local blood perfusion, has been questioned for decades (Cauli and Hamel, 2010; Kilduff et al., 2011). Besides, NO is also interacting with numerous signaling pathways involved in this process. The particularly complex roles of NO interneurons in the control of blood perfusion is extensively reviewed by (Duchemin et al., 2012) as an introduction to this section. As a first step in the understanding of their neurovascular functions, the anatomical relationships of type I interneurons with blood vessels is described in the rat cortical gray matter (Nogueira-Campos et al., 2012) and monkey white matter (Rockland and Nayyar, 2012) confirming and extending previous findings (Cauli et al., 2004). Stimulation of 5HT3A receptors expressed by type II NO interneurons and other discrete subpopulations of interneurons (Perrenoud et al., 2012b) leads to both NO-mediated vasodilations and NPY-mediated vasoconstrictions. These observations indicate that the role of NO interneurons in neurovascular coupling is even more complex when considering their diversity. In summary this special issue provides new important findings and up-to-date reviews on NO interneurons diversity and physiology that will be useful for both established scientists in this field and new comers.

ACKNOWLEDGMENTS

We acknowledge financial support by the Agence Nationale pour la Recherche (ANR 2011 MALZ 003 01).

REFERENCES

Armstrong, C., Krook-Magnuson, E., and Soltesz, I. (2012). Neurogliaform and Ivy cells: a major family of nNOS expressing GABAergic neurons. *Front. Neural Circuits* 6:23. doi: 10.3389/fncir.2012.00023

Ascoli, G. A., Alonso-Nanclares, L., Anderson, S. A., Barrionuevo, G., Benavides-Piccione, R., Burkhalter, A., et al. (2008). Petilla terminology: nomenclature of features of GABAergic interneurons of the cerebral cortex. *Nat. Rev. Neurosci.* 9, 557–568. doi: 10.1038/nrn2402

Cauli, B., and Hamel, E. (2010). Revisiting the role of neurons in neurovascular coupling. *Front. Neuroenergetics* 2:9. doi: 10.3389/fnene.2010.00009

Cauli, B., Tong, X. K., Rancillac, A., Serluca, N., Lambolez, B., Rossier, J., et al. (2004). Cortical GABA interneurons in neurovascular coupling: relays for subcortical vasoactive pathways. *J. Neurosci.* 24, 8940–8949. doi: 10.1523/JNEUROSCI.3065-04.2004

DeFelipe, J., López-Cruz, P. L., Benavides-Piccione, R., Bielza, C., Larrañaga, P., Anderson, S., et al. (2013). New insights into the classification and nomenclature of cortical GABAergic interneurons. *Nat. Rev. Neurosci.* 14, 202–216. doi: 10.1038/nrn3444

Dittrich, L., Heiss, J. E., Warrier, D. R., Perez, X. A., Quik, M., and Kilduff, T. S. (2012). Cortical nNOS neurons co-express the NK1 receptor and are depolarized by Substance P in multiple mammalian species. *Front. Neural Circuits* 6:31. doi: 10.3389/fncir.2012.00031

Duchemin, S., Boily, M., Sadekova, N., and Girouard, H. (2012). The complex contribution of NOS interneurons in the physiology of cerebrovascular regulation. *Front. Neural Circuits* 6:51. doi: 10.3389/fncir.2012.00051

Estrada, C., and DeFelipe, J. (1998). Nitric oxide-producing neurons in the neocortex: morphological and functional relationship with intraparenchymal microvasculature. *Cereb. Cortex* 8, 193–203. doi: 10.1093/cercor/8.3.193

Fuentealba, P., Begum, R., Capogna, M., Jinno, S., Marton, L. F., Csicsvari, J., et al. (2008). Ivy cells: a population of nitric-oxide-producing, slow-spiking GABAergic neurons and their involvement in hippocampal network activity. *Neuron* 57, 917–929. doi: 10.1016/j.neuron.2008.01.034

Gentet, L. J. (2012). Functional diversity of supragranular GABAergic neurons in the barrel cortex. *Front. Neural Circuits* 6:52. doi: 10.3389/fncir.2012.00052

Jaglin, X. H., Hjerling-Leffler, J., Fishell, G., and Batista-Brito, R. (2012). The origin of neocortical nitric oxide synthase-expressing inhibitory neurons. *Front. Neural Circuits* 6:44. doi: 10.3389/fncir.2012.00044

Karagiannis, A., Gallopin, T., David, C., Battaglia, D., Geoffroy, H., Rossier, J., et al. (2009). Classification of NPY-expressing neocortical interneurons. *J. Neurosci.* 29, 3642–3659. doi: 10.1523/JNEUROSCI.0058-09.2009

Kilduff, T. S., Cauli, B., and Gerashchenko, D. (2011). Activation of cortical interneurons during sleep: an anatomical link to homeostatic sleep regulation? *Trends Neurosci.* 34, 10–19. doi: 10.1016/j.tins.2010.09.005

Kubota, Y., Hattori, R., and Yui, Y. (1994). Three distinct subpopulations of GABAergic neurons in rat frontal agranular cortex. *Brain Res.* 649, 159–173.

Kubota, Y., Shigematsu, N., Karube, F., Sekigawa, A., Kato, S., Yamaguchi, N., et al. (2011). Selective coexpression of multiple chemical markers defines discrete populations of neocortical GABAergic neurons. *Cereb. Cortex* 21, 1803–1817. doi: 10.1093/cercor/bhq252

Magno, L., Oliveira, M. G., Mucha, M., Rubin, A. N., and Kessaris, N. (2012). Multiple embryonic origins of nitric oxide synthase-expressing GABAergic neurons of the neocortex. *Front. Neural Circuits* 6:65. doi: 10.3389/fncir.2012.00065

Nogueira-Campos, A. A., Finamore, D. M., Imbiriba, L. A., Houzel, J. C., and Franca, J. G. (2012). Distribution and morphology of nitrergic neurons across functional domains of the rat primary somatosensory cortex. *Front. Neural Circuits* 6:57. doi: 10.3389/fncir.2012.00057

Perrenoud, Q., Geoffroy, H., Gauthier, B., Rancillac, A., Alfonsi, F., Kessaris, N., et al. (2012a). Characterization of Type I and Type II nNOS-expressing interneurons in the barrel cortex of mouse. *Front. Neural Circuits* 6:36. doi: 10.3389/fncir.2012.00036

Perrenoud, Q., Rossier, J., Ferezou, I., Geoffroy, H., Gallopin, T., Vitalis, T., et al. (2012b). Activation of cortical 5-HT(3) receptor-expressing interneurons induces NO mediated vasodilatations and NPY mediated vasoconstrictions. *Front. Neural Circuits* 6:50. doi: 10.3389/fncir.2012.00050

Rockland, K. S., and Nayyar, N. (2012). Association of type I neurons positive for NADPH-diaphorase with blood vessels in the adult monkey corpus callosum. *Front. Neural Circuits* 6:4. doi: 10.3389/fncir.2012.00004

Shlosberg, D., Buskila, Y., Abu-Ghanem, Y., and Amitai, Y. (2012). Spatiotemporal alterations of cortical network activity by selective loss of NOS-expressing interneurons. *Front. Neural Circuits* 6:3. doi: 10.3389/fncir.2012.00003

Somogyi, J., Szabo, A., Somogyi, P., and Lamsa, K. (2012). Molecular analysis of ivy cells of the hippocampal CA1 stratum radiatum using spectral identification of immunofluorophores. *Front. Neural Circuits* 6:35. doi: 10.3389/fncir.2012.00035

Tricoire, L., Pelkey, K. A., Daw, M. I., Sousa, V. H., Miyoshi, G., Jeffries, B., et al. (2010). Common origins of hippocampal ivy and nitric oxide synthase expressing neurogliaform cells. *J. Neurosci.* 30, 2165–2176. doi: 10.1523/JNEUROSCI.5123-09.2010

Tricoire, L., and Vitalis, T. (2012). Neuronal nitric oxide synthase expressing neurons: a journey from birth to neuronal circuits. *Front. Neural Circuits* 6:82. doi: 10.3389/fncir.2012.00082

Wood, J., and Garthwaite, J. (1994). Models of the diffusional spread of nitric oxide: implications for neural nitric oxide signalling and its pharmacological properties. *Neuropharmacology* 33, 1235–1244. doi: 10.1016/0028-3908(94)90022-1

Yan, X. X., and Garey, L. J. (1997). Morphological diversity of nitric oxide synthesising neurons in mammalian cerebral cortex. *J. Hirnforsch.* 38, 165–172.

Received: 15 April 2013; accepted: 15 May 2013; published online: 03 June 2013.

Citation: Tricoire L, Kubota Y and Cauli B (2013) Cortical NO interneurons: from embryogenesis to functions. Front. Neural Circuits 7:105. doi: 10.3389/fncir.2013.00105

frontiers in
NEURAL CIRCUITS

ORIGINAL RESEARCH ARTICLE
published: 06 November 2012
doi: 10.3389/fncir.2012.00057

Distribution and morphology of nitrergic neurons across functional domains of the rat primary somatosensory cortex

Anaelli A. Nogueira-Campos[1,2], Deborah M. Finamore[1], Luis A. Imbiriba[3], Jean C. Houzel[4] and João G. Franca[1]*

[1] Laboratório de Neurobiologia II, Programa de Neurobiologia, Instituto de Biofísica Carlos Chagas Filho, Universidade Federal do Rio de Janeiro, Rio de Janeiro, Brazil
[2] Departamento de Fisiologia, Instituto de Ciências Biológicas, Universidade Federal de Juiz de Fora, Juiz de Fora, Brazil
[3] Escola de Educação Física e Desportos, Universidade Federal do Rio de Janeiro, Rio de Janeiro, Brazil
[4] Laboratório de Fronteiras em Neurociências, Programa de Ciências Morfológicas, Instituto de Ciências Biomédicas, Universidade Federal do Rio de Janeiro, Rio de Janeiro, Brazil

Edited by:
Bruno Cauli, Centre National de la Recherche Scientifique, France

Reviewed by:
Kathleen S. Rockland, Massachussetts Institute of Technology, USA
Yoshiyuki Kubota, National Institute for Physiological Sciences, Japan

***Correspondence:**
João G. Franca, Centro de Ciências da Saúde, Instituto de Biofísica Carlos Chagas Filho, Universidade Federal do Rio de Janeiro, Avenida Carlos Chagas Filho, 373, Bloco G - 1° andar - Sala G1-019, Cidade Universitária - Ilha do Fundão, 21941-902 Rio de Janeiro, Brazil.
e-mail: jgfranca@biof.ufrj.br

The rat primary somatosensory cortex (S1) is remarkable for its conspicuous vertical compartmentalization in barrels and septal columns, which are additionally stratified in horizontal layers. Whereas excitatory neurons from each of these compartments perform different types of processing, the role of interneurons is much less clear. Among the numerous types of GABAergic interneurons, those producing nitric oxide (NO) are especially puzzling, since this gaseous messenger can modulate neural activity, synaptic plasticity, and neurovascular coupling. We used a quantitative morphological approach to investigate whether nitrergic interneurons, which might therefore be considered both as NO volume diffusers and as elements of local circuitry, display features that could relate to barrel cortex architecture. In fixed brain sections, nitrergic interneurons can be revealed by histochemical processing for NADPH-diaphorase (NADPHd). Here, the dendritic arbors of nitrergic neurons from different compartments of area S1 were 3D reconstructed from serial 200 μm thick sections, using 100x objective and the Neurolucida system. Standard morphological parameters were extracted for all individual arbors and compared across columns and layers. Wedge analysis was used to compute dendritic orientation indices. Supragranular (SG) layers displayed the highest density of nitrergic neurons, whereas layer IV contained nitrergic neurons with largest soma area. The highest nitrergic neuronal density was found in septa, where dendrites were previously characterized as more extense and ramified than in barrels. Dendritic arbors were not confined to the boundaries of the column nor layer of their respective soma, being mostly double-tufted and vertically oriented, except in SG layers. These data strongly suggest that nitrergic interneurons adapt their morphology to the dynamics of processing performed by cortical compartments.

Keywords: NADPH-diaphorase, dendritic morphometry, nitric oxide, inhibitory neurons, rat cortical area S1, barrel cortex

INTRODUCTION

The cortical nitrergic system is composed of inhibitory GABAergic neurons that express nitric oxide synthase (NOS) (Bredt et al., 1991; Dawson et al., 1991; Hope et al., 1991; Yan and Garey, 1997; Kubota et al., 2011), the enzyme responsible for synthesis of nitric oxide (NO). NO is a highly diffusible gas with a short half-life (0.5–5 s), whose range of action covers about 100–200 μm, rising within 10–15 s to a steady-state concentration (Malinski et al., 1993; Meulemans, 1994; Wood and Garthwaite, 1994). Thus, NO could spread out from its site of production to influence many different tissue elements (neuronal, glial, and vascular components) that are not necessarily in close anatomical juxtaposition (review in Garthwaite and Boulton, 1995). NO is an unusual neurotransmitter (Bredt et al., 1991; Dawson and Snyder, 1994), involved in a wide range of physiological and pathological events in the central nervous system, such as modulation of synaptic transmission and neurotoxicity (Wallace et al., 1996; Estevez et al., 1998; see Calabrese et al., 2007; Garthwaite, 2008 for review). NO has been associated with learning and memory in addition to neurovascular coupling (Bohme et al., 1991; Izumi et al., 1992; Iadecola, 1993). Activation of NOS is one of the factors that leads to vasodilation following neuronal activation, leading to an increase in local cerebral blood flow (Drake and Iadecola, 2007; Cauli and Hamel, 2010). Nitrergic neurons are part of the intrinsic neuronal circuitry. They release neuropeptide Y (NPY)—a potent vasoconstrictor—on blood vessels located distal to the cell body. Distal release of NPY may restrict the NO-induced vasodilation to the micro region around the

nitrergic neuronal cell body and dendrites (Estrada and DeFelipe, 1998; Cauli et al., 2004).

NADPH-diaphorase (NADPHd) is a generic term attributed to any enzyme that chemically reduces the co-factor NADP. Action of fixatives, especially paraformaldehyde, deactivates most endogenous diaphorases, except for NOS, rendering this enzyme detectable by histochemistry in fixed tissue (Matsumoto et al., 1993). Thus, histochemistry for NADPHd became a reliable tool for the study of the distribution of NOS in the nervous system. In the mammalian cerebral cortex, the population of NADPHd-stained neurons has been subdivided into two broad categories according to the intensity of histochemical staining and soma size. Type 1 neurons present intense Golgi-like staining of the cell body and dendrites, and large somas. Compared to type 1, type 2 neurons are smaller with lighter labeling of the cell body and, occasionally, some labeling in primary neurites (Sandell, 1986; Bredt et al., 1990; Dawson et al., 1991; Vincent and Kimura, 1992; Lüth et al., 1994; Yan and Garey, 1997; Iwase et al., 1998; Franca et al., 2000; Freire et al., 2004). Type 1 neurons comprise about 0.5–2% of all cortical neurons (Gabbott and Bacon, 1995) and are much less frequent in neocortex than type 2, which display a different laminar distribution (Cruz-Rizzolo et al., 2006). Finally, in addition to individual neurons, histochemistry for NADPHd also labels very thin neuronal processes that can be detected as a diffuse neuropil stain, especially along the thalamo-recipient layer IV. NADPHd-reactive neuropil depicts boundaries of cortical primary sensory areas in different species (Franca et al., 2000; Freire et al., 2012); and can additionally allow delineation of cortical modules in somatosensory cortex of rodents (Franca et al., 2000; Pereira et al., 2000; Freire et al., 2005, 2012) and in visual cortex of primates (Sandell, 1986; Franca et al., 1997).

Primary somatosensory area (S1) in the rat provides a useful model system for exploring details of cortical organization in mammalian brains (Petersen, 2007) because it presents generalized features, such as (1) a distinct laminar arrangement in six different parallel layers from the pia mater to the white matter; (2) a representation of sensory surfaces that form a topologically organized map (Santiago et al., 2007); and (3) a vertical organization with sharply defined anatomical units, the so-called "barrels" (Woolsey and Van der Loos, 1970, reviewed in Catania, 2002) that can be depicted by NAPDHd histochemistry (Franca and Volchan, 1995).

In rodent S1, recent studies on the distribution and morphology of nitrergic neurons (type 1 NAPDHd neurons) were mainly performed on tangential sections along layer IV of the posterior medial barrel subfield (PMBSF)—the region where mystacial vibrissae are represented and the barrels are large and very sharply-defined. Such studies revealed that nitrergic neurons concentrate in septal domains of the PMBSF (Valtschanoff et al., 1993; Franca and Volchan, 1995; Pereira et al., 2000; Freire et al., 2004, 2005), where they display larger and more complex dendritic trees than neurons located inside barrels (Freire et al., 2005). Nonetheless, the PMBSF does not represent the entire rodent S1 since additional barrel fields, representing the anterior snout, the forepaw, the hindpaw, and the trunk, plus an intervening "dysgranular" cortex in-between the barrel fields, are also part of this cortical area (Wallace, 1987). Additionally, S1 is composed of different cortical compartments representing different cortical layers in different processing columns (*i.e.*, barrel and septal columns) comprising different components of S1 cortical circuit (Lubke and Feldmeyer, 2007; Wester and Contreras, 2012). So far there is no description of the distribution and fine morphological arrangement displayed by the dendritic arbors of these cells along the entire S1, nor about how these neurons might relate to the barrel cortex architecture. While being both volume diffusers for NO and inhibitory (GABAergic) elements of cortical circuits, type 1 NAPDHd neurons might display different dendritic arrangements according to their position in the cortical circuitry.

Thus, after subdividing rat S1 into six basic compartments—supragranular (SG), granular (GR), and infragranular (IG) layers located in barrel or septal columns—we first quantified the distribution of nitrergic neuronal cell bodies in these compartments, and then studied the morphology and spatial arrangements of their dendritic trees. We observed that dendrites from single nitrergic neurons can cross cortical compartments, not being restricted by compartment borders. Septal columns tended to present higher concentration of nitrergic neurons than barrel columns. Additionally, in SG layers nitrergic neuronal density is the highest among laminar compartments. Dendritic fields in SG assumed various spatial organizations, being multipolar, horizontal or vertical. In contrast, most nitrergic neurons displayed vertically-oriented dendritic arbors in GR and IG layers. We propose that these subtle differences in the morphological organization of local nitrergic neurons reflect different spatial characteristics of the neurovascular coupling between local hyperemia and neuronal excitability that allow distinct processing dynamics in each cortical compartment.

MATERIALS AND METHODS

ANIMALS

The left hemispheres of three adult male Wistar rats were used in the present study. All efforts were made to minimize animal suffering and to reduce the number of animals used. Protocols for these experiments were approved by the Ethic Committee for Animal Use in Scientific Research of the Centro de Ciências da Saúde (CCS, Universidade Federal do Rio de Janeiro) and were in accordance with the NIH guidelines (assurance number "IBCCF 029").

PERFUSION AND HISTOLOGICAL PROCEDURES

Animals were deeply anesthetized by inhalation of ether vapor and perfused through the left ventricle, using a peristaltic pump, with 300 ml of 0.9% sodium chloride (NaCl), followed by 300–400 ml of 4% paraformaldehyde in pH 7.4, 0.1 M sodium phosphate buffer (PB). After removing the brain from the skull, a block containing the entire parietal lobe was prepared and cut coronally with a vibratome (Pelco International, Series 1000) into serial, 200 μm-thick sections. The sections were collected in PB and subsequently washed three times in this same solution. Next, the sections were incubated free-floating at 37°C in a solution for NADPHd histochemistry, consisting of 0.6% malic acid, 0.03% nitroblue tetrazolium, 1% dimethylsulfoxide, 0.03% manganese chloride, and 0.5% β-NADP in 0.1 M Tris buffer, pH 8.0 (modified from Scherer-Singler et al., 1983). To increase

penetration of reagents into the section thickness, the detergent Triton X-100 was added to the histochemical solution in a concentration of 1.5–3%. This concentration has been used for adequate penetration of NADPHd reagents through thick histological sections (Franca et al., 1997).

The reaction was monitored under light microscope, and usually interrupted after 2–4 h by rinsing the sections in PB. All procedures, from perfusion to NADPHd histochemistry were performed at the same day. Sections were then mounted onto gelatin-coated glass slides and left to air-dry overnight. Slides were dehydrated in alcohol, washed twice in xylene for 5 min and coverslipped with Entellan (Merck).

DEFINITION OF S1 COMPARTMENTS AND TRIDIMENSIONAL RECONSTRUCTIONS

In the rat, neuropil staining by NADPHd histochemistry allows the definition of boundaries of barrels and cortical layers in sections through S1 (Franca and Volchan, 1995). This cortical area can thus be subdivided in six cortical compartments corresponding to two vertical domains (barrel or septal column) and three horizontal compartments corresponding to SG layers, including layers I, II, and III; GR, corresponding to layer IV, where barrels and septa were most evident; and IG layers, including layers V and VI (for an example, see **Figure 4**).

All coronal sections through S1 were analyzed and reconstructed using a Zeiss Axioplan-2 microscope equipped with a color digital camera (1600 × 1200, 3/4" chip, 36bit, MBF), a motorized stage (Mac5000 LUDL), and an extra *z* encoder controlled by Neurolucida software (MBFBiosciences, Inc) running on a Dell workstation. Cortical boundaries and barrel contours defined by neuropil reactivity, and the relative position of S1 strongly reactive (type 1) NADPHd cell bodies (Yan and Garey, 1997) were digitized using 5x and 10x objectives, respectively. Individual neuronal profiles were three-dimensionally (3D) reconstructed using a 100x oil objective, and included both the contours of the cell body and the entire dendritic tree as apparent in the cortical section in which the cell body was contained.

Type 1 neurons in area S1 were selected for morphometric analysis based on apparent completeness of their dendritic trees. Only neurons displaying dendritic trees characterized by a tapering profile of all dendrites, with none of them ending abruptly in a stump, were selected for reconstruction. In each of the three hemispheres, 180 neurons were reconstructed, corresponding to 30 neurons for each of the six cortical compartments defined above. In hemisphere R06-10, all S1 type 1 neurons were reconstructed in all sections for qualitative appraisal of dendritic tree distribution, but only 180 of these neurons were chosen for morphometric analysis, based on the criteria described above.

DATA EXTRACTION AND STATISTICAL ANALYSIS

Definition and measurement of cortical compartment areas

Each barrel column was defined by a radial projection from the lateral borders of each layer IV barrel to the pial surface and the layerVI/white matter border (**Figure 4**). The area of the barrel column was then measured using ImaqVision 6.0 image processing software (ACD Systems). The total area of septal columns was obtained by subtracting the area occupied by barrel columns from the total area of S1. Similarly, the area occupied by SG, GR, and IG layers were also measured.

Stereological evaluation of cell density

In order to estimate the density of type 1 NAPDHd neurons in each compartment volume (N_v), we initially counted the number of cell body profiles (N) and divided it by the flat area (A) of the cortical compartment. Density per volume was then estimated for each cortical compartment adopting Abercrombie's stereological correction formula (Abercrombie, 1946):

$$N_v = (N/A) / (t + d)$$

where t was the section thickness, and d was the average cell body diameter in each compartment estimated by the procedures described by Schuz and Palm (1989). We assumed that t was constant, corresponding to the thickness set at the vibratome (200 μm). To calculate d, we first estimated d from the cell body area (a), using the formula of the circle:

$$d = 2\,(a/\pi)^{0,5}$$

The average cell body diameter (d) was calculated for each cortical compartment using all reconstructed neurons located in that given compartment. Then, the value of d was corrected using the stereological estimations defined by formulae (2) and (3) of Schuz and Palm (1989); yielding to values d_2 and d_3, respectively. Since d_2 and d_3 respectively overestimates and underestimates the actual value of d (Schuz and Palm, 1989), the final value of d applied in Abercrombie's formula was the mean obtained from d_2 and d_3. Values obtained for each compartment in each hemisphere are listed in **Table 1**.

Morphological parameters analyzed

A number of quantitative morphological parameters were extracted by NeuroExplorer software (MBFBiosciences, Inc) from the reconstructed type 1 NADPHd neurons. These parameters could be either related to the cell body or to the dendritic tree.

Cell body parameters included the cell body area (corresponding to the flat 2D surface occupied by the neuronal soma) and form factor. Form factor describes how spherical the cell body is. As the contour shape of cell body approaches that of a perfect circle it tends to a maximum value of 1. In contrast, as the contour shape flattens out, this value approaches a minimum of 0.

Morphological parameters related to the dendritic tree included: (1) number of first order dendrites; (2) dendritic length (DL), corresponding to the sum of the length of all segments of the dendritic tree; (3) number of nodes (each node corresponding to a point of dendritic branching originating two or more dendritic segments); (4) number of dendritic segments (each segment corresponding to a dendritic branch between two nodes, or between a node and the cell body, or to a terminal branch); (5) fractal dimension; and (6) area of the dendritic field (Wässle and Boycott, 1991). The fractal dimension gives a quantitative estimation of the complexity of the dendritic tree, describing the way the dendritic tree fills the area that comprised the dendritic field. The area of the dendritic field was accessed by convex hull analysis, which measures the size of the dendritic field by interpreting a branched structure as a solid object in a given volume or area.

Table 1 | Distribution of nitrergic neuronal cell bodies in the different cortical compartments.

Cortical compartments*	No. of cells (%)	Compartment area in mm^2 (%)	Cell body diameter (variance) in μm	Neuronal density in cells/mm^3**
R06-10 (*n* = 27 SECTIONS)				
SG	559 (26.3)	26.31 (19.6)	12.35 (3.43)	100
GR	268 (12.6)	26.67 (19.9)	13.07 (2.97)	47
IG	1298 (61.1)	81.00 (60.5)	12.32 (3.03)	75
BARRELS	1390 (65.4)	93.28 (69.6)	12.42 (3.05)	70
SEPTA	735 (34.6)	40.71 (30.4)	12.43 (3.43)	85
Total	**2125 (100)**	**133.98 (100)**	**12.42 (3.18)**	**75**
SG - barrels	357 (16.8)	19.23 (14.3)	12.30 (3.16)	86
SG - septa	202 (9.5)	7.09 (5.3)	12.44 (3.91)	128
GR - barrels	184 (8.6)	16.54 (12.4)	13.15 (3.07)	50
SR - septa	84 (3.9)	10.13 (7.6)	12.88 (2.75)	38
IG - barrels	849 (39.9)	57.51 (42.9)	12.31 (2.88)	66
IG - septa	449 (21.1)	23.49 (17.5)	12.33 (3.31)	86
R07-03 (*n* = 22 SECTIONS)				
SG	421 (27.0)	20.65 (19.3)	14.74 (4.40)	95
GR	284 (18.2)	23.02 (21.5)	16.0 (3.71)	57
IG	853 (54.8)	63.28 (59.2)	14.31 (2.59)	63
BARRELS	951 (61.0)	70.98 (66.4)	15.08 (4.28)	62
SEPTA	607 (39.0)	35.97 (33.6)	15.0 (3.83)	78
Total	**1558 (100)**	**106.95 (100)**	**15.0 (4.04)**	**68**
SG - barrels	258 (16.5)	14.14 (13.2)	15.0 (5.69)	86
SG - septa	163 (10.5)	6.51 (6.1)	14.57 (3.21)	128
GR - barrels	154 (9.9)	11.49 (10.7)	15.72 (3.69)	50
SR - septa	130 (8.3)	11.52 (10.8)	16.28 (3.68)	38
IG - barrels	539 (34.6)	45.34 (42.4)	14.64 (3.12)	66
IG - septa	314 (20.2)	17.95 (16.8)	14.0 (1.93)	86
R07-04 (*n* = 25 SECTIONS)				
SG	498 (32.6)	24.23 (20.5)	14.04 (2.23)	96
GR	305 (19.9)	23.73 (20.1)	14.90 (3.01)	60
IG	726 (47.5)	70.06 (59.4)	14.26 (2.16)	48
BARRELS	1018 (66.6)	70.52 (59.7)	14.41 (2.62)	67
SEPTA	511 (33.4)	47.50 (40.3)	14.39 (2.57)	50
Total	**1529 (100)**	**118.01 (100)**	**14.40 (2.58)**	**60**
SG - barrels	316 (20.7)	14.28 (12.1)	14.29 (1.92)	103
SG - septa	182 (11.9)	9.95 (8.4)	13.78 (2.47)	85
GR - barrels	206 (13.5)	12.38 (10.5)	14.72 (3.17)	77
SR - septa	99 (6.5)	11.35 (9.6)	15.09 (2.89)	41
IG - barrels	496 (32.4)	43.86 (37.2)	14.21 (2.78)	53
IG - septa	230 (15.0)	26.19 (22.2)	14.30 (1.62)	41

**Cortical compartments: SG, supragranular layers; GR, granular layer (layer IV); IG, infragranular layers.*

***Corresponding values were calculated after stereological corrections described in section "Stereological Evaluation of Cell Density".*

Additionally, dendritic field orientation of each neuron was defined using wedge analysis of DL. A Cartesian coordinate reference frame was centered at the cell body, with its principal axis oriented toward the pia mater, and dividing eight equiangular wedges. The summed length of dendritic segments contained in each wedge (DL_n) was measured to calculate a verticality index (*vi*) in which the sum of DLs in the four wedges close to the vertical axis was divided by the sum of DL measured in all eight wedges (total DL). The *vi* allowed the classification of type 1 neurons as horizontal- ($vi = 0 - 0.32$), multipolar- ($vi = 0.33 - 0.65$) or vertical-oriented ($vi = 0.66 - 1$). For vertically-oriented neurons, a dendritic directionality index (*di*) was calculated by subtracting DLs from the two wedges close to the white matter from DLs obtained in the opposite two wedges opening toward the pia, and dividing the result by the sum of DLs for those four wedges. This *di* further characterized whether vertically-oriented neurons were double-tufted ($di = -0.50$ *to* $+0.50$), or if their dendritic trees were oriented toward the pia ($di = +0.51$ *to* $+1.0$) or the white matter ($di = -1.0$ *to* -0.49).

Statistical analysis

Descriptive statistical analysis was used to characterize the cases, based on the mean value, standard deviation (SD) and coefficient of variation (CV) [(SD/mean)] for each parameter. Moreover, reconstructed neurons were grouped according to the compartment occupied by their respective cell body. All morphological parameters were compared employing Two-way analysis of variance (ANOVA) for repeated measures to access differences among each laminar (SG, GR, and IG) and columnar (septal *versus* barrels) compartments. Fisher *post-hoc* analysis was employed when significance was attained. Tests of normality were performed to determine the probability that the sample came from a normally distributed population (Shapiro–Wilk's W test) and, if the sphericity assumption was violated, Geisser-Greenhouse correction was applied. For the all analysis, the level of significance was set to 0.05, unless stated otherwise.

RESULTS

NEUROPIL STAINING AND MORPHOLOGICAL ASPECTS OF NITRERGIC NEURONS IN RAT PRIMARY SOMATOSENSORY CORTEX

In coronal sections of rat cortex, area S1 was easily identified due to the strong NADPHd-reactive neuropil characteristic of layer IV barrels, intercalated with less reactive septa (**Figure 1**). This pattern was found in the expected position for the barrel fields (Zilles and Wree, 1985), as previously described with this technique in tangential sections (Franca and Volchan, 1995). Differences in staining intensity of the diffuse NADPHd neuropil label additionally revealed cortical layer borders. Typically, layer I corresponded to a thin densely stained layer close to the cortical surface followed by the less reactive layers II and III. The border between layers II and III could not be reliably identified by means of NADPHd histochemistry. Below the strongly reactive layer IV was the less reactive layer V. Layer VI, although clearly more intensely stained than layer V, was not as dark as layer IV barrels (**Figures 1A,B**).

In addition to the conspicuous neuropil staining, NADPHd histochemistry labeled individual neurons with a Golgi-like pattern (**Figures 1C,D, 2**, and **3B,C**). These neurons presented non-pyramidal cell bodies and well-labeled dendritic trees. Because of these features they were identified as type 1 NADPHd neurons (Yan and Garey, 1997). Since all type 1 NADPHd neurons express constitutive NO synthase (Bredt et al., 1991; Dawson et al., 1991; Hope et al., 1991; Matsumoto et al., 1993), these cells will henceforth be referred here as nitrergic neurons, or simply as "neurons."

Nitrergic neurons presented round or oval cell bodies that gave rise to primary dendrites through an abrupt thinning of the soma profile detected in the same or along different focal planes (**Figure 2**). Their long dendrites usually ramified two or three times along their path (**Figure 2**), commonly crossing the limits of different S1 compartments (**Figures 3A** and **4**). Although we used a 100× oil-immersion objective to reconstruct individual neurons, the extent to which a given dendrite could be followed

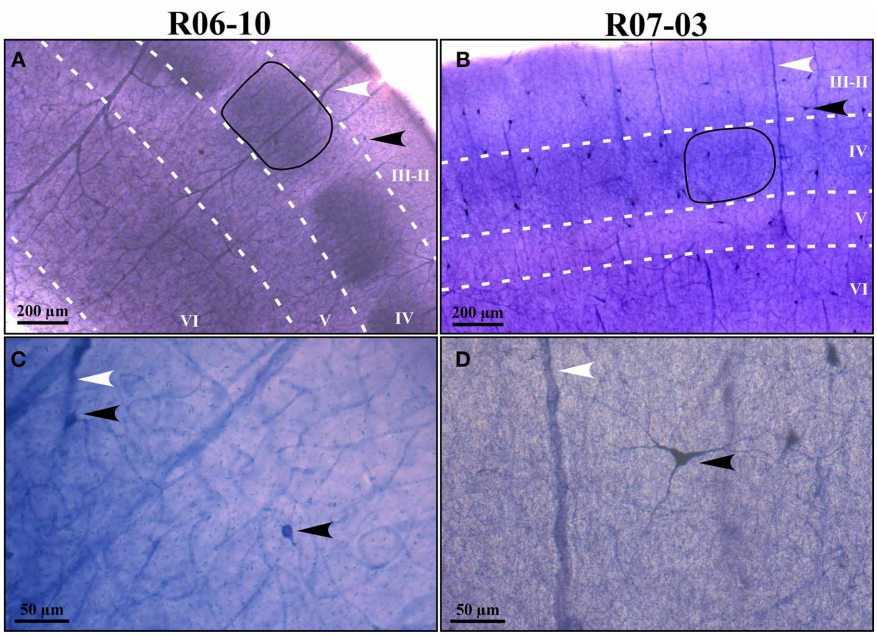

FIGURE 1 | NADPHd reactive neuropil and nitrergic (NADPHd type 1) neurons. (A,B) Low-magnification micrographs of cases R06-10 and R07-03, respectively, showing cortical layers (white dashed lines) and barrels in layer IV (the black continuous line depicts one example from each case). Layers IV and VI are more intensely labeled than layers II-III and V. It is not feasible by means of NAPDHd reactivity alone to identify the border between layers II and III. Intensely stained (type 1) NADPHd-reactive neurons can be identified (black arrowheads), and correspond to nitrergic interneurons. Blood vessels are also well-stained (white arrowheads). **(C,D)** Type 1 neurons and blood vessels framed in **(A)** and **(B)** observed in higher magnification (check arrowheads for correspondence). Higher neuropil reactivity in case R06-10 **(A)** provides a better contrast for delimitation of different compartments such as barrels and septa. On the other hand, more intense neuropil reactivity increases background noise making identification of thinner neuritic processes more difficult [such as in **(C)** as compared to **(D)**].

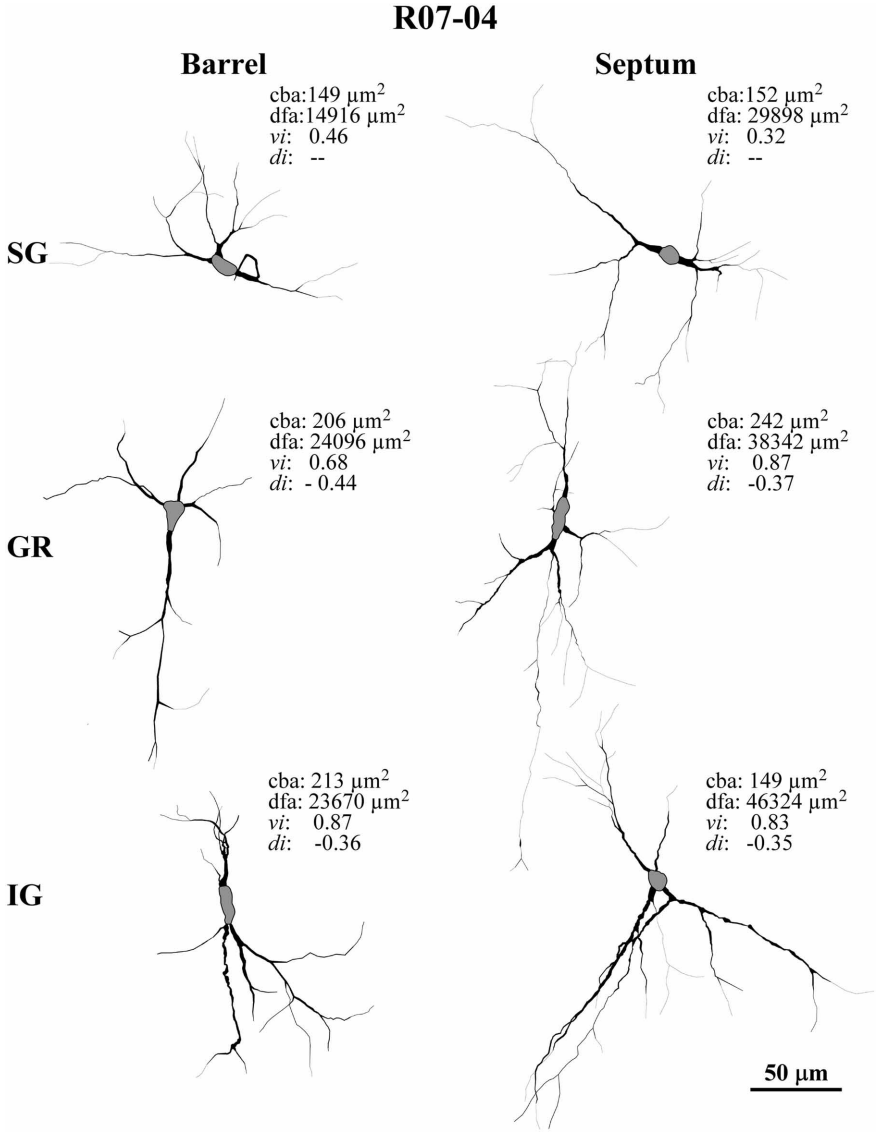

FIGURE 2 | Examples of typical nitrergic neurons from different cortical compartments in case R07-04 that were 3D-reconstructed in Neurolucida. All neurons are oriented as if the pia mater were parallel to the top of the figure. Barrel and septal neurons are represented respectively in the left and right columns of the figure. Accordingly, neurons in top, middle, and inferior rows of the figure were respectively located in supragranular (SG), granular (GR), and infragranular (IG) compartments. Neurons in GR and IG layers display more vertically-oriented dendritic trees, while in SG neurons tend to be horizontally-oriented or multipolar. Neurons found in septal columns have a tendency to display more complex dendritic morphology than those located in barrels. Values of four relevant morphological parameters are depicted for each neuron illustrated: cba, cell body area; dfa, dendritic field area; vi, verticality index; di, directionality index. In order to distinguish the limit with primary dendrites, each cell body is represented in gray.

seemed to be inversely proportional to the background activity (**Figure 1**). Horizontal, vertical, and multipolar nitrergic neurons were present along S1, but vertically-oriented neurons predominated, except in SG layers (**Figures 3A** and **4**, see "Quantitative analysis of morphological parameters of S1 nitrergic neurons."). In SG layers some nitrergic neurons displayed heavily ramified dendrites, giving them a bushy appearance (**Figure 3A**). Such SG "arachnoid" neurons were detected in some sections but not in others. They were found in two of the studied hemispheres (**Figures 3A** and **4**).

SPATIAL DISTRIBUTION OF NITRERGIC NEURONS ACROSS FUNCTIONAL DOMAINS OF PRIMARY SOMATOSENSORY CORTEX

Nitrergic neurons were detected in all cortical compartments of area S1. They were distributed in an apparently random fashion. In some instances, several neighboring nitrergic neurons were clustered, displaying dendrites seeming in close apposition to each other. However, regions devoid of these cells could also be observed in the same section (**Figures 3A** and **4**). It was apparent by qualitative observation that layers IV and V presented lower nitrergic cell densities than layers VI and SG (**Figure 5**).

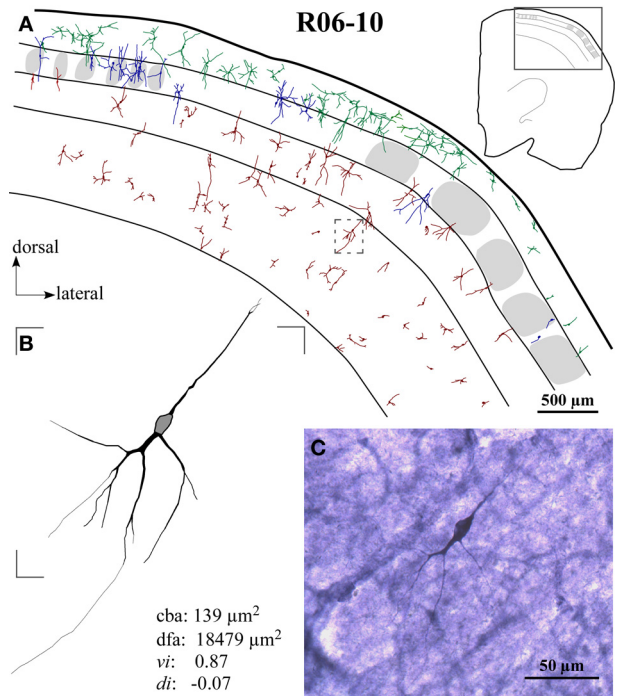

FIGURE 3 | Case R06-10. (A) All S1 nitrergic neurons in this 200 µm-coronal section were reconstructed. Neurons with cell bodies located in different cortical layers are represented with different colors. Their spatial distribution does not follow any apparent pattern or regularity. Parts of the section lack the presence of nitrergic neurons while in other parts these neurons are clustered. The absence of barrels in the middle part of this section suggests a cut through two different barrel fields (probably the hindpaw and the postero-medial barrel subfields) separated by the barrel-free dysgranular cortex. Bushy supragranular (SG) neurons observed in this section are not consistently found in other sections of this hemisphere. Nevertheless, they are observed in the other hemispheres analyzed (see **Figure 4** for another example). Note that in many instances, dendrites cross over laminar and/or columnar borders. Additionally, some layer IV barrels are devoid of nitrergic neurons, while in others nitrergic cell bodies are localized close to the external border of the barrel. The insert at the upper right corner illustrates the whole section in which a frame depicts the region enlarged in the main part of the figure. A small dashed box frames the neuron illustrated in **(B)**. **(B)** Neurolucida reconstruction of a typical vertically-oriented nitrergic neuron in layer VI. Morphometric parameters depicted for this neuron: cba, cell body area; dfa, dendritic field area; vi, vertically indices; di, directionally indices. Contour of cell body is delimited in gray. **(C)** High-magnification photomicrograph of the same neuron illustrated in **(B)**.

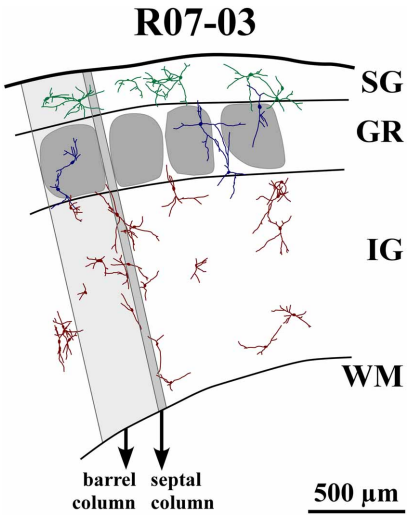

FIGURE 4 | Reconstruction of part of S1 from case R07-03. All nitrergic neurons in this part of the tissue are reconstructed and represented. Barrel and septal columns are delimited by lines that are roughly tangential to barrel borders and orthogonal to cortical surface and white matter (WM) boundaries. One barrel column (shaded light gray) and one septal column (shaded dark gray) are depicted for illustration. Neurons from different cortical layers are represented with different colors. Neurons seem randomly distributed with dendrites crossing the limits of barrels and cortical layers. Most neurons in layer IV (GR) and infragranular layers (IG) tend to display vertically-oriented dendritic trees, while in supragranular layers (SG) neurons are either multipolar or horizontally-oriented. Neurons inside layer IV barrels usually have cell bodies located far from the center of the barrel. Their dendritic trees may cross barrel and laminar borders. The same can be observed in the single GR septal neuron represented in this figure. Neurons seem to cluster in pairs or triplets; but, at the same time, leave blank spaces uncovered by their cell bodies and dendritic trees.

Nevertheless, regions in S1 presenting clusters of nitrergic neurons and regions lacking such cells did not alternate with any apparent regularity, nor could be correlated with different cortical compartments in any clear way (**Figures 3A**, **4**, and **5**). For instance, although nitrergic neurons were absent from many barrels in layer IV (**Figures 3A** and **5**), they could be found in some other barrels along S1, usually located close to barrel borders (**Figures 3A**, **4** and **5**). Additionally, nitrergic neurons located inside barrels tended to display vertically-oriented dendritic arbors that were usually not constrained by the barrel borders (**Figures 3A** and **4**).

In order to quantify the spatial distribution of nitrergic neurons along different cortical compartments of area S1, neuronal density was calculated for S1 in each hemisphere after summing up the number of cell bodies and the area size of individual compartments in all sections throughout S1. Since simple cell counting may result in biased estimations of the number of cellular profiles (Gundersen et al., 1988), adequate stereological corrections were adopted (see "Data extraction and statistical analysis"). **Table 1** and **Figure 6** present the results of this analysis. In each hemisphere studied, when compartment areas were summed up in all 200 µm-thick sections containing S1 (as if they were positioned side by side), total area of S1 ranged from 107 to 134 mm^2 (in R07-03 and R06-10, respectively). IG layers constituted 60% of S1 and, correspondingly, contained from 50 to 60% of all S1 nitrergic neurons. Nevertheless, the highest nitrergic neuronal density values were found in SG layers, corresponding to about 97 neurons/mm^3 (**Table 1**, **Figure 6**). These values were 35–100% higher than density measured in IG. The granular layer (GR or layer IV) had the lowest density values, except in case R07-04.

Comparisons between barrel and septal columns (**Table 1**) revealed that 60–70% of S1 consisted of barrel columns in which approximately 65% of nitrergic neuronal cell bodies were located. However, density in septal columns was approximately 25%

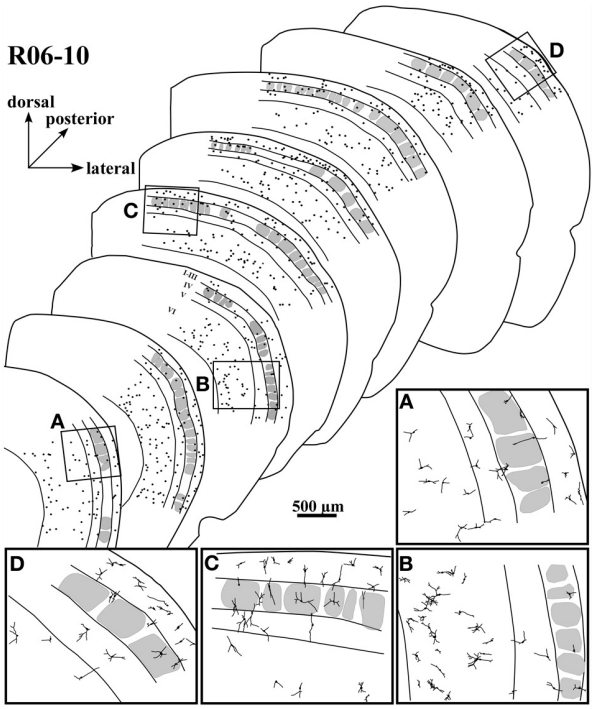

FIGURE 5 | Spatial distribution of nitrergic neuronal cell bodies in selected sections of hemisphere R06-10, disposed from anterior (lower left) to posterior (upper right). The four inserts below (from **A** to **D**) correspond to drawings in higher magnification from the respective regions framed in four of the sections. Most of the cells seem to concentrate in supragranular layers and in layer VI.

higher than in barrel columns, except in case R07-04 in which density measured in barrel columns was similar to that found in the other two hemispheres but 34% higher than that measured in septal columns (**Table 1**).

QUANTITATIVE ANALYSIS OF MORPHOLOGICAL PARAMETERS OF S1 NITRERGIC NEURONS

In hemisphere R06-10 we were able to collect all histological sections along S1 without significant tears or tissue loss. This hemisphere was thus used to perform a complete reconstruction of rat S1, including 3D reconstructions of all nitrergic neurons located in area S1 ($N = 2125$ neurons) as illustrated in **Figures 3A** and **5**. Nevertheless, because many dendrites were cut during tissue sectioning, quantitative parameters were extracted from 180 neurons (30 neurons per cortical compartment) located at mid-section depth and selected based on apparent completeness of all their dendrites. Hemispheres R07-03 ($N = 180$ neurons) and R07-04 ($N = 180$ neurons) also presented a clear neuropil staining pattern, revealing barrels and cortical layers plus well-stained nitrergic neurons that were selected for 3D-reconstruction using the same criteria mentioned above.

Morphological parameters could be either related to the cell body or to the dendritic tree (**Table 2**). Cell body parameters (cell body area and form factor) displayed mean values that were consistent between hemispheres, with low variation coefficients (up to 26%). However, most of the parameters related to the dendritic tree (*e.g.*, dendritic field area, number of segments, etc) displayed large variations in mean values across different hemispheres.

Morphometry of the reconstructed neurons (**Table 2**) revealed that the "generic" nitrergic neuron in rat S1 was a non-pyramidal cell (*i.e.*, a neuron displaying a rounded cell body with a form factor of 0.8); with a cell body size of 160 μm^2 from which 2 or 3 primary dendrites emerged. These dendrites tended to ramify once or twice, giving rise to secondary and tertiary dendrites. As depicted above, total DL and dendritic field area measured in the different hemispheres were extremely variable resulting in means ranging, respectively, from 504 to 1053 μm, and from 15×10^3 to 41×10^3 μm^2.

In hemispheres R07-03 and R07-04, quantitative analysis of cell body area revealed that nitrergic neurons located at layer IV (GR) were 10% larger than those located either in SG or in IG (**Figure 7**). This difference, although statistically significant ($p < 0.01$), was not noticeable under qualitative inspection. In hemisphere R06-10, no difference in cell body size was detected when neurons from different laminar compartments were compared (**Figure 7**).

There was no morphological difference when nitrergic neurons from barrel columns were compared with those of septal columns, except for hemisphere R07-04. In this case, DL, number of nodes and segments, dendritic field area, and fractal dimension (a measure of dendritic field complexity) were significantly higher for neurons located in septal columns as compared with those in barrel columns ($p < 0.01$).

SPATIAL ORGANIZATION OF NITRERGIC DENDRITIC TREES

An important and consistent finding of our study was related to orientation of the dendritic tree, as measured in coronal sections by wedge analysis (see "Morphological parameters analyzed"). In all three hemispheres, 50% or more of the nitrergic neurons presented dendritic trees that were vertically oriented (**Figure 8A**, **Table 3**). The other half of this neuronal population was composed of multipolar (ranging from 24 to 29% in R07-03 and R07-04, respectively) or horizontal neurons (from 7 to 26% of the nitrergic neurons in R06-10 and R07-03, respectively, **Figure 8A**).

Multipolar and horizontally-oriented nitrergic neurons were most common in SG. Verticality indices (*vi*) were significantly lower for this laminar compartment than for GR and IG (**Figure 8B**, $p < 0.01$ for all three hemispheres). Mean *vi* in SG ranged from 0.24 (R07-03) to 0.58 (R06-10), thus lower than the 0.66 threshold used to classify a dendritic tree as vertically-oriented. In GR and IG, mean *vi* ranged from 0.70 (GR in R07-04) to 0.81 (GR in R06-10). This confirmed our qualitative observation of predominance of horizontal and multipolar neurons in SG, whilst vertically-oriented neurons tended to predominate in GR and IG. Vertically-oriented nitrergic neurons were equally distributed in GR and IG, both in barrel and septal columns (**Table 3**). No significant difference in the orientation of the dendritic tree was detected when neurons from barrel and septal columns were compared against each other in all cases ($p > 0.05$).

Since a vertically-oriented neuron could present its dendritic arbors pointing to different directions, we further calculated the

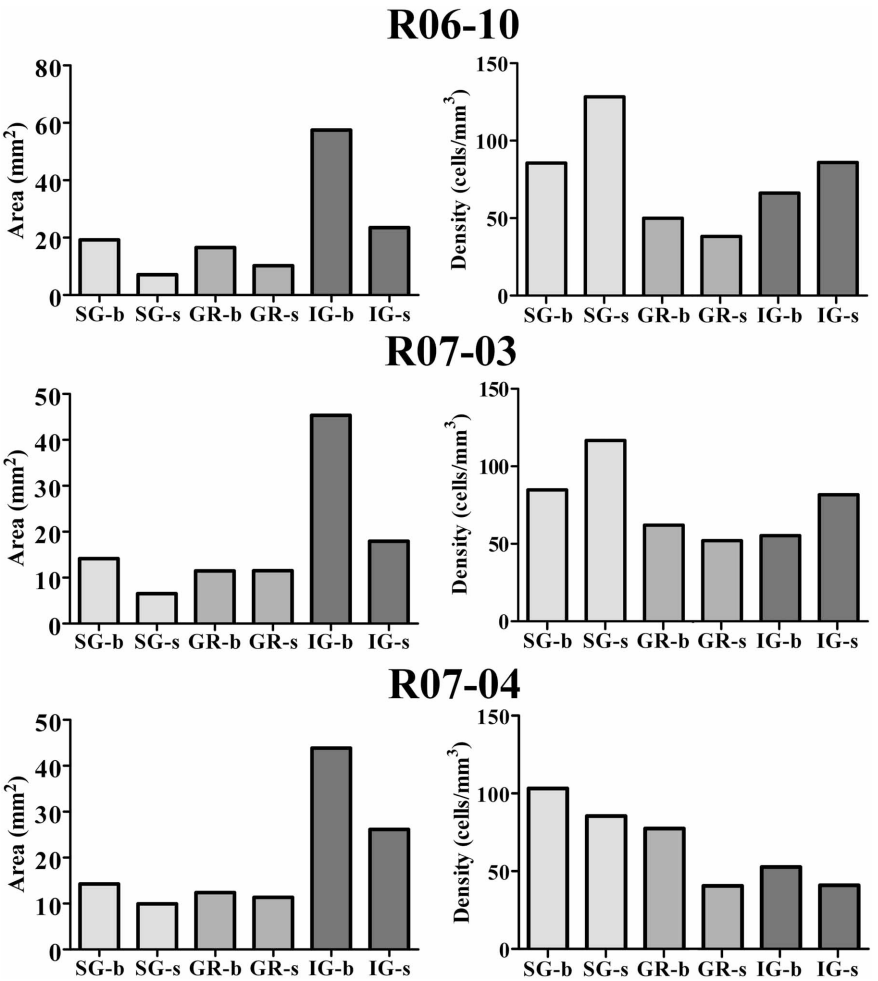

FIGURE 6 | Cortical compartment area (*left column*) and corresponding nitrergic neuronal density (*right column*) in the three hemispheres studied. Area measurements were estimated after summing up values obtained in all histological sections obtained in a given hemisphere. Likewise, density was calculated after counting the total number of cell bodies in the same sections. The infragranular layers (IG) correspond to 60% of S1. Barrel columns also correspond to 60% or more of S1. Although IG lodge more than 47% of nitrergic neurons, supragranular layers (SG) present the highest density of nitrergic neurons (about 97 cells/mm^3 against *circa* 62 cells/mm^3 in IG, see **Table 1**). SG-b, supragranular layer at barrel columns; SG-s, supragranular layer at septal columns; GR-b, granular layer at barrel columns; GR-s, granular layer at septal columns; IG-b, infragranular layer at barrel columns; IG-s, infragranular layers at septal column.

directionality index for nitrergic neurons with *vi* equal or higher than 0.66. In all three hemispheres, 55% or more of the vertically-oriented neurons were double tufted (**Figure 8C** and **Table 3**), *i.e.*, with dendritic branches extending both toward the white matter and the cortical surface. Moreover, 32% and 42% of the vertically-oriented neurons in hemispheres R06-10 and R07-03, respectively, displayed dendritic trees oriented toward the white matter only (**Figure 8C**, **Table 3**).

DISCUSSION

We described and quantified morphological parameters and the spatial distribution of strongly-reactive (type 1) NADPHd neurons in area S1 of the adult rat. These neurons are known to release NO, an unusual gaseous messenger in the central nervous system (Bredt and Snyder, 1992; Dawson and Snyder, 1994). Based on the pattern of NADPHd neuropil reactivity, we subdivided rat S1 into different vertical and horizontal anatomical compartments typically related to the organizational flow of functional processing in somatosensory cortex.

From qualitative inspection, except for the fact that cortical layers IV and V seemed to present fewer cells, spatial distribution of nitrergic neurons across compartments looked random. Their dendrites were also not necessarily confined inside the cortical compartment in which the parent cell body was located. Nevertheless, density of nitrergic neurons in SG was systematically higher than in other laminar compartments.

We compared morphological parameters from nitrergic neurons reconstructed from different hemispheres and from different compartments in a same hemisphere. Large coefficients of variation were obtained for most parameters, indicating that the

Table 2 | Morphometric parameters of nitrergic neurons per hemisphere.

Cases	R06-10		R07-03		R07-04	
Morphometric parameters	**Mean**	**CV***	**Mean**	**CV***	**Mean**	**CV***
Cell body area (μm^2)	145	0.24	180	0.26	165	0.22
Form factor	0.78	0.14	0.81	0.13	0.77	0.15
Number of 1st order dendrites (μm)	3.3	0.29	3.02	0.33	2.96	0.31
Total dendritic length (μm)	504	0.42	1052	0.48	581	0.58
Number of nodes	4.5	0.62	8.77	0.52	7.15	0.58
Number of segments	12.2	0.47	20.52	0.45	17.07	0.50
Fractal dimension	1.00	0.02	1.03	0.02	1.02	0.02
Dendritic field area (μm^2)	15×10^3	0.69	41×10^3	0.43	20×10^3	2.98
Verticality index	0.71	0.34	0.58	0.54	0.62	0.47

**CV, coefficient of variation.*

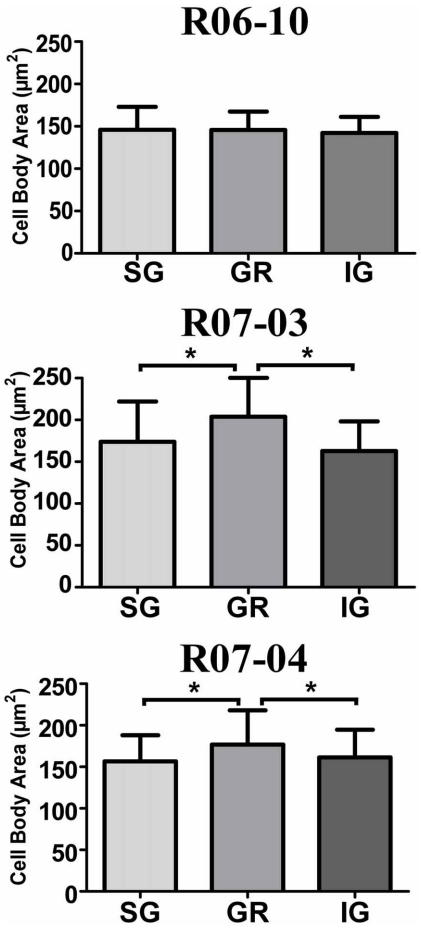

FIGURE 7 | Mean cell body area of nitrergic neurons. Layer IV (GR) neurons presented the largest cell body area in cases R07-03 and R07-04. Asterisk (*) represents $p < 0.01$.

morphology of these cells is variable across different animals (**Table 2**). Additionally, in the three hemispheres analyzed, nitrergic neurons in GR and IG tended to be vertically-oriented, while in SG multipolar, horizontally-, and vertically-oriented neurons were found in equal proportions. Cell body size was larger in layer IV (GR) than in SG and IG in two of these hemispheres. The significance of these results and some considerations about technical factors that might have influenced our results will be discussed below.

TECHNICAL CONSIDERATIONS AND THE VARIABILITY OF MORPHOLOGICAL PARAMETERS

Mean values for morphological parameters of nitrergic neurons were different across analyzed hemispheres (**Table 2**). For instance, in hemisphere R07-03 mean values for total DL and dendritic field area were about two times larger than those obtained for hemispheres R06-10 and R07-04 (**Table 2**). A similar trend occurred when cell body area was compared in the three hemispheres. This variability was not due to differences in data collection procedures, since all nitrergic neurons were reconstructed by the same investigator, following the same procedures. Completeness of each reconstructed dendritic tree was further confirmed by a second investigator.

Because aldehyde fixation causes tissue shrinkage, different fixation intensities in the three hemispheres could explain this result. Although we were careful in adopting the same perfusion and fixation procedures in all three animals, variations in fixation intensity are generally very difficult to avoid and might have occurred in our material. This interpretation is supported by the fact that morphological parameters not influenced by tissue shrinkage, such as number of first order dendrites, form factor, verticality index, and fractal dimension, did not vary much.

Although in principle resistant to fixatives such as paraformaldehyde, NAPDH-diaphorase activity of neuronal NOS can be compromised by the intensity of the fixation (Matsumoto et al., 1993; Franca et al., 2000). Thus, it is possible that a stronger fixation may reduce the staining of the dendritic arbor by inactivating histochemical activity of small pockets of NOS contained in thinner processes such as terminal dendrites, which might be more sensible or more exposed to the chemical action of the fixative. In an attempt to circumvent that, longer incubation times are usually performed in order to minimize the risk of not staining the entire dendritic tree. However, longer incubation times result in a darker background that might

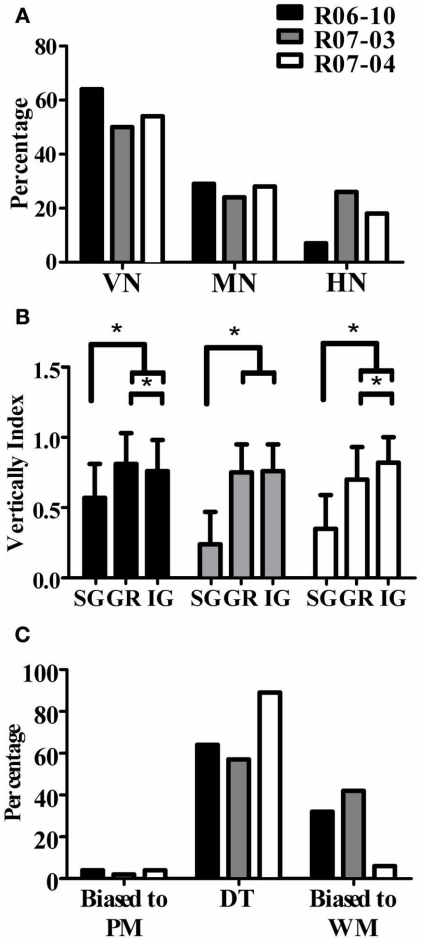

FIGURE 8 | Quantification of dendritic orientation. (A) Morphological types of S1 nitrergic neurons classified according to dendritic orientation. Half of these neurons display a vertically-oriented dendritic arbor (VN). The other half of the population is equally represented by multipolar (MN) and horizontally-oriented (HN) neurons. **(B)** Verticality index (*vi*) measured with wedge analysis of 3D-reconstructed S1 nitrergic neurons. Values obtained in supragranular layers (SG) are significantly lower than both granular (GR) and infragranular (IG) layers. This quantitative finding confirms the observation that vertically-oriented nitrergic neurons predominate in GR and IG, while in SG they tend to be horizontal or multipolar. Asterisk (*) represents $p < 0.01$. **(C)** Most vertically-oriented neurons in S1 (*i.e.*, presenting a verticality index equal or higher than 0.66) display their dendritic trees facing both the pia mater and the white matter, thus corresponding to double-tufted cells (DT). The second most common type of vertically-oriented neurons present a dendritic arbor facing the white matter only. PM: pia mater; WM: white matter.

render thinner processes hard to follow under conventional optical microscopy, thus compromising their reconstruction. We believe that we minimized the possibility of not representing the entire dendritic tree by carefully and systematically reconstructing all neuritic processes using an immersion 100x-objective. Nevertheless, since in hemisphere R07-03 we obtained the largest neurons and the weakest background activity (**Figure 1**, **Table 2**), we believe that in some cases very thin terminal dendrites might have been missed due to a darker (noisier) background, or simply because they fell below optical resolution limit (*ca.* 0.25 μm).

Ideally, fixation should be intense enough to render the tissue resistant to damage in histological processing, but light enough to allow histochemical detection of NOS in the most delicate neuronal processes. Assuming a perfect trade-off in fixation intensity, duration of the histochemical reaction is critical. During incubation in NAPDHd histochemical solution, neuronal cell bodies are the first profiles to stain. Primary, secondary, and tertiary dendrites follow suit in this order. Neuropil reactivity with enough contrast to allow identification of the different cortical compartments may be too dark for detection and reconstruction of thinner neuritic processes. Thus, setting the adequate intensity of the NADPHd reaction, either by manipulating intensity of fixation and/or timing of histochemical reaction is difficult to achieve. Probably the best way to optimize NADPHd histochemistry for labeling individual nitrergic neurons is to associate light tissue fixation with short periods of histochemical incubation, thus compromising neuropil reactivity and the identification of cortical compartments.

OTHER POSSIBLE SOURCES OF MORPHOLOGICAL VARIABILITY OF NITRERGIC NEURONS

It has been demonstrated that central nervous system expression of "constitutive" NOS corresponds to a plastic phenomenon. In the visual cortex, for instance, NOS expression in neuropil presents a 24 h (circadian) rhythmicity (Hilbig and Punkt, 1997) and can be regulated by visual experience (Aoki et al., 1993).

Experience-dependent regulation of the intracellular distribution of NOS, resulting in variability in the apparent DL and dendritic field size of nitrergic neurons, can occur in the superficial layers of rat superior colliculus (SC) (Tenorio et al., 1998). In the visually-deprived SC, nitrergic activity in distal dendrites diminishes as compared to the contralateral, visually-stimulated, SC. Thus, in the deprived SC, dendritic arbors of nitrergic neurons, as revealed by NAPDHd histochemistry, appear to shrink. This phenomenon corresponds to a subcellular redistribution of NOS, since intracellular injection of fluorescent tracers reveals that these cells have actually the same dendritic field size as those in the visually-stimulated contralateral SC (Tenorio et al., 1998).

Thus, intracellular distribution of NOS can depend on sensory experience, which might vary from animal to animal, possibly resulting in phenotypic variability of nitrergic neuronal morphology such as the one observed in **Table 2**. In line with this evidence, Romanelli et al. (2007) described a reversible up-regulation of nitrergic expression in rat S1 and other brain regions right after exposure to spatial novelty. In addition, the number and morphological complexity of nitrergic neurons in varying brain regions can also be regulated by numerous factors such as physical exercise (Torres et al., 2006), exposure to light (Chen et al., 2006), and emotional stress (Beijamini and Guimaraes, 2006), which might explain the phenotypic variation of nitrergic neurons obtained in different animals.

NITRERGIC NEURONS IN BARRELS AND SEPTA

When the postero medial barrel field (PMBSF) is analyzed in tangential sections through layer IV, it is clear that nitrergic neurons predominate inside septal as compared to barrel compartments (Valtschanoff et al., 1993; Franca and Volchan,

Table 3 | Distribution of different types of vertically-oriented nitrergic neurons across cortical compartments.

	SG-b[a]	SG-s	GR-b	GR-s	IG-b	IG-s	Total[b]	% of total population[c]
R06-10								
Vertical cells	11 (9.6%)	12 (10.4%)	23 (20.0%)	25 (21.7%)	25 (21.7%)	19 (16.5%)	115 (100.0%)	63.8
Biased Pia	0 (0.0%)	0 (0.0%)	0 (0.0%)	2 (1.7%)	2 (1.7%)	1 (0.9%)	5 (4.3%)	2.8
DT	5 (4.3%)	9 (7.8%)	15 (13.0%)	14 (12.2%)	14 (12.2%)	16 (13.9%)	73 (63.5%)	40.6
Biased WM	6 (5.2%)	3 (2.6%)	8 (7.0%)	9 (7.8%)	9 (7.8%)	2 (1.7%)	37 (32.2%)	20.6
R07-03								
Vertical cells	2 (2.2%)	3 (3.3%)	19 (21.1%)	23 (25.6%)	23 (25.6%)	20 (22.2%)	90 (100.0%)	50.0
Biased Pia	0 (0%)	0 (0%)	0 (0.0%)	0 (0%)	2 (2.2%)	0 (0%)	2 (2.2%)	1.1
DT	0 (0%)	0 (0%)	11 (12.2%)	9 (10.0%)	16 (17.8%)	14 (15.6%)	5 (55.6%)	27.8
Biased WM	2 (2.2%)	3 (3.3%)	8 (8.9%)	14 (15.6%)	5 (5.6%)	6 (6.7%)	38 (42.2%)	21.1
R07-04								
Vertical cells	4 (4.3%)	3 (3.2%)	21 (22.3%)	26 (27.7%)	21 (22.3%)	19 (20.2%)	94 (100.0%)	52.2
Biased Pia	0 (0%)	0 (0%)	0 (0.0%)	1 (1.1%)	2 (2.1%)	1 (1.1%)	4 (4.3%)	2.2
DT	4 (4.3%)	3 (3.2%)	20 (21.3%)	21 (22.3%)	18 (19.1%)	18 (19.1%)	84 (89.4%)	46.7
Biased WM	0 (0%)	0 (0%)	1 (1.1%)	4 (4.3%)	1 (1.1%)	0 (0%)	6 (6.4%)	3.3

[a] *Cortical compartments: SG-b, supragranular layer at barrel columns; SG-s, supragranular layer at septal columns; GR-b, granular layer at barrel columns; GR-s granular layer at septal columns; IG-b, infragranular layer at barrel columns; IG-s, infragranular layers at septal columns.*

[b] *Number of "vertically-oriented" neurons (i.e., presenting a verticality index higher than 0.65) in a given category. Percentage in parenthesis relates to the number of all vertically-oriented neurons found in the sample.*

[c] *Percentage considering the total number of reconstructed neurons in the sample (N = 180 cells per hemisphere).*

1995; Freire et al., 2004). According to our previous work in PMBSF (Franca and Volchan, 1995; Freire et al., 2004), the total area occupied by all barrels is equivalent to that of the interbarrel (septal) space, but the number of nitrergic cell bodies located in septal cortex is significantly higher than inside barrels. In our current analysis, when nitrergic neuronal density was calculated for the entire cortical column (summing up neurons and areal sizes of all laminar compartments), we verified in two of the hemispheres examined that density was higher in septal columns than in barrel columns (**Table 1**).

Curiously, in our material, when we compared the distribution of nitrergic neurons in layer IV only, cellular density is actually higher in barrel compartments in all three hemispheres (**Table 1**, **Figure 6**). We believe that a number of factors explain this apparent contradiction with previous findings (Valtschanoff et al., 1993; Franca and Volchan, 1995; Freire et al., 2004, 2005). First, our current analysis was not restricted to the PMBSF (where only the mystacial vibrissae are represented), but encompassed the entire S1, including barrel fields representing other body parts and the dysgranular cortex that separate different barrel fields (for a review see Rice, 1995). This would indicate that rules for distribution of nitrergic neurons vary in different parts of S1, possibly reflecting different cortical circuitries. In line with this hypothesis, recent data suggest that morphology of SG nitrergic neurons actually vary in different parts of primary visual cortex (V1) (Rocha et al., 2012). A second possibility is that we might have overestimated barrel borders, since, due to their oval shapes, they are not as sharply defined in thick coronal sections as in tangential sections through layer IV. Thus, a septal neuron located close to a barrel border might seem inside the barrel when, once observed through a transversal (non-tangential) plane of section, the neuron could be either in front or behind the barrel, but not actually inside it. Support to this notion comes with the fact that we found many cell bodies close to barrel borders. Additionally, different from our previous measurements in tangential sections (Franca and Volchan, 1995; Freire et al., 2004), barrel column total area was larger than that measured in the septal columns (**Table 1**), further supporting the idea of barrel borders overestimation.

One earlier morphometric analysis of nitrergic neurons in the mouse PMBSF indicated that septal neurons have larger and more complex dendritic fields than nitrergic neurons inside barrels (Freire et al., 2005). Again, this previous study did not encompass the whole S1, and was restricted to neurons located in layer IV. In the present analysis, we used a different species (the rat), and grouped neurons from all cortical layers located either in barrel or septal columns. Using this approach, we did not find morphological differences between neurons located in barrel columns and those of septal columns, except in hemisphere R07-04. In this case, a number of parameters related to dendritic field size and complexity was larger in septal than in barrel nitrergic neurons ($p < 0.01$).

NITRERGIC NEURONAL MORPHOLOGY AND THE CORTICAL CIRCUIT

We demonstrated that in GR and IG, dendritic trees of nitrergic neurons in rat S1 were predominantly vertically-oriented. Most of these vertically-oriented neurons were either double-tufted or bipolar. In SG, dendritic arbors of nitrergic neurons were equally distributed in horizontal, multipolar, and vertical orientations. Thus, mean verticality index measured in SG was significantly lower than that obtained in GR and IG (**Figure 8B**, **Table 3**). Assuming that nitrergic neurons are involved in neurovascular coupling (Drake and Iadecola, 2007; Cauli and Hamel, 2010), non-vertical nitrergic processes in SG could act in concert to

maintain the metabolic demands necessary for horizontal integration, while in GR and IG nitrergic neurons would simultaneously keep activity vertically restricted to the cortical column. However, important lateral transcolumnar projections occur in GR and IG of rat S1 (Schubert et al., 2007). In addition, nitrergic neurons are not necessarily confined to the anatomically-defined cortical compartments. Similar dendritic patterns have been described for pyramidal neurons located close to the borders of cytochrome oxidase blobs in V1 (Hubener and Bolz, 1992; Malach, 1992). These findings give support to the idea that cortical processing is not as strictly compartmentalized in vertical columns (Swindale, 1990; Horton and Adams, 2005; Rockland, 2010) as previously suggested (Mountcastle, 1997; Douglas and Martin, 2004).

We additionally observed that in two of our hemispheres (R07-03 and R07-04) cell body size was larger in nitrergic neurons located inside layer IV than in the other laminar compartments (*i.e.,* SG and IG). Functional significance of this finding is uncertain. Nitrergic cell bodies can be viewed as nodes for NO release. In principle, these larger cell bodies may release larger amounts of NO per neuron, in the same cortical layer (*i.e.,* GR) that presented the lowest numbers of nitrergic neurons (**Table 1**). On the flip side, it is already well-documented that, in primary sensory areas such as S1, GR has a high metabolic activity, as identified by intense histochemical reactivity for enzymes such as succinate deshydrogenase and cytochrome oxidase (Wong-Riley and Welt, 1980; Wallace, 1987; Riddle et al., 1993). This high concentration of metabolic enzymes in layer IV correlates with an intense reactivity to NAPDHd and NOS (Wong-Riley and Welt, 1980; Aoki et al., 1993; Wong-Riley et al., 1998), suggesting that NO synthase expression is coupled to neural activity, perhaps through a positive feedback loop in which NO acts as a retrograde messenger (Garthwaite and Boulton, 1995). NO can thus be released either through "large" cellular profiles such as neuronal cell bodies and dendrites, or through the fine processes (represented by axons, axon terminals, and terminal dendrites) that comprise the reactive neuropil. The precise role played by these two sources of NO should be relevant for cortical physiology, and needs to be further investigated.

ACKNOWLEDGMENTS

We would like to thank Dr. Carlomagno Pacheco Bahia and Mr. José Magalhães de Oliveira for help in our experiments. This work was supported by Fundação Carlos Chagas Filho de Amparo à Pesquisa do Estado do Rio de Janeiro (FAPERJ) and Conselho Nacional de Desenvolvimento Científico e Tecnológico (CNPq)—Programa de Núcleos de Excelência (PRONEX) e Rede Instituto Brasileiro de Neurociência (IBN Net/FINEP). This research is part of the Masters in Science thesis of Anaelli A. Nogueira-Campos, supported by the Coordenação de Aperfeiçoamento de Pessoal de Nível Superior (CAPES) and FAPERJ (Bolsa Nota 10) developed as part of the Curso de Pós-Graduação em Ciências Biológicas (Fisiologia) of the Instituto de Biofísica Carlos Chagas Filho of the Universidade Federal do Rio de Janeiro. The authors would also like to thank the reviewers for significant suggestions that were incorporated in this manuscript.

REFERENCES

Abercrombie, M. (1946). Estimation of nuclear population from microtome sections. *Anat. Rec.* 94, 239–247.

Aoki, C., Fenstemaker, S., Lubin, M., and Go, C.-G. (1993). Nitric oxide synthase in the visual cortex of monocular monkeys as revealed by light and electron microscopic immunocytochemistry. *Brain Res.* 620, 97–113.

Beijamini, V., and Guimaraes, F. S. (2006). Activation of neurons containing the enzyme nitric oxide synthase following exposure to an elevated plus maze. *Brain Res. Bull.* 69, 347–355.

Bohme, G. A., Bon, C., Stutzmann, J. M., Doble, A., and Blanchard, J. C. (1991). Possible involvement of nitric oxide in long-term potentiation. *Eur. J. Pharmacol.* 199, 379–381.

Bredt, D. S., Glatt, C. E., Hwang, P. M., Fotuhi, M., Dawson, T. M., and Snyder, S. H. (1991). Nitric oxide synthase protein and mRNA are discretely localized in neuronal populations of the mammalian CNS together with NADPH diaphorase. *Neuron* 7, 615–624.

Bredt, D. S., Huang, P. M., and Snyder, S. H. (1990). Localization of nitric oxide sythase indicating a neural role for nitric oxide. *Nature* 347, 768–770.

Bredt, D. S., and Snyder, S. H. (1992). Nitric oxide, a novel neuronal messenger. *Neuron* 8, 3–11.

Calabrese, V., Mancuso, C., Calvani, M., Rizzarelli, E., Butterfield, D. A., and Stella, A. M. (2007). Nitric oxide in the central nervous system: neuroprotection versus neurotoxicity. *Nat. Rev. Neurosci.* 8, 766–775.

Catania, K. C. (2002). Barrels, stripes, and fingerprints in the brain - implications for theories of cortical organization. *J. Neurocytol.* 31, 347–358.

Cauli, B., and Hamel, E. (2010). Revisiting the role of neurons in neurovascular coupling. *Front. Neuroenerg.* 2:9. doi: 10.3389/fnene.2010.00009

Cauli, B., Tong, X. K., Rancillac, A., Serluca, N., Lambolez, B., Rossier, J., et al. (2004). Cortical GABA interneurons in neurovascular coupling: relays for subcortical vasoactive pathways. *J. Neurosci.* 24, 8940–8949.

Chen, B., So, K. F., Yu, E., and Tay, D. K. (2006). Expression of nicotinamide adenine dinucleotide phosphate-diaphorase in the retina of postnatal golden hamsters deprived of light stimulation. *Neurosci. Lett.* 405, 74–78.

Cruz-Rizzolo, R. J., Horta-Junior, J. A., Bittencourt, J. C., Ervolino, E., de Oliveira, J. A., and Casatti, C. A. (2006). Distribution of NADPH-diaphorase-positive neurons in the prefrontal cortex of the Cebus monkey. *Brain Res.* 1083, 118–133.

Dawson, T. M., Bredt, D. S., Fotuhi, M., Hwang, P. M., and Snyder, S. H. (1991). Nitric oxide synthase and neuronal NADPH diaphorase are identical in brain and peripheral tissues. *Proc. Natl. Acad. Sci. U.S.A.* 88, 7797–7801.

Dawson, T. M., and Snyder, S. H. (1994). Gases as biological messengers: nitric oxide and carbon monoxide in the brain. *J. Neurosci.* 14, 5147–5159.

Douglas, R. J., and Martin, K. A. (2004). Neuronal circuits of the neocortex. *Annu. Rev. Neurosci.* 27, 419–451.

Drake, C. T., and Iadecola, C. (2007). The role of neuronal signaling in controlling cerebral blood flow. *Brain Lang.* 102, 141–152.

Estevez, A. G., Spear, N., Manuel, S. M., Radi, R., Henderson, C. E., Barbeito, L., et al. (1998). Nitric oxide and superoxide contribute to motor neuron apoptosis induced by trophic factor deprivation. *J. Neurosci.* 18, 923–931.

Estrada, C., and DeFelipe, J. (1998). Nitric oxide-neurons in the neocortex: morphological and functional relationship with intraparechymal microvasculature. *Cereb. Cortex* 8, 193–203.

Franca, J. G., do-Nascimento, J. L. M., Picanço-Diniz, C. W., Quaresma, J. A. S., and Silva, A. L. C. (1997). NADPH-diaphorase activity in area 17 of the squirrel monkey visual cortex: neuropil pattern, cell morphology and laminar distribution. *Braz. J. Med. Biol. Res.* 30, 1093–1105.

Franca, J. G., and Volchan, E. (1995). NADPH diaphorase histochemistry as a marker for barrels in rat somatosensory cortex. *Braz. J. Med. Biol. Res.* 28, 787–790.

Franca, J. G., Volchan, E., Jain, N., Catania, K. C., Oliveira, R. L. S., Hess, F. F., et al. (2000). Distribution of NADPH-diaphorase cells in visual and somatosensory cortex in

four mammalian species. *Brain Res.* 864, 163–175.

Freire, M. A., Faber, J., Picanco-Diniz, C. W., Franca, J. G., and Pereira, A. (2012). Morphometric variability of nicotinamide adenine dinucleotide phosphate diaphorase neurons in the primary sensory areas of the rat. *Neuroscience* 205, 140–153.

Freire, M. A., Franca, J. G., Picanco-Diniz, C. W., and Pereira, A. Jr. (2005). Neuropil reactivity, distribution and morphology of NADPH diaphorase type I neurons in the barrel cortex of the adult mouse. *J. Chem. Neuroanat.* 30, 71–81.

Freire, M. A., Gomes-Leal, W., Carvalho, W. A., Guimaraes, J. S., Franca, J. G., Picanco-Diniz, C. W., et al. (2004). A morphometric study of the progressive changes on NADPH diaphorase activity in the developing rat's barrel field. *Neurosci. Res.* 50, 55–66.

Gabbott, P. L. A., and Bacon, S. J. (1995). Co-localisation of NADPH diaphorase activity and GABA immunoreactivity in local circuit neurones in the medial prefrontal cortex (mPFC) of the rat. *Brain Res.* 699, 321–328.

Garthwaite, J. (2008). Concepts of neural nitric oxide-mediated transmission. *Eur. J. Neurosci.* 27, 2783–2802.

Garthwaite, J., and Boulton, C. L. (1995). Nitric oxide signaling in the central nervous system. *Ann. Rev. Neurosci.* 57, 683–706.

Gundersen, H. J., Bendtsen, T. F., Korbo, L., Marcussen, N., Moller, A., Nielsen, K., et al. (1988). Some new, simple and efficient stereological methods and their use in pathological research and diagnosis. *APMIS* 96, 379–394.

Hilbig, H., and Punkt, K. (1997). 24-hour rhythmicity of NADPH-diaphorase activity in the neuropil of rat visual cortex. *Brain Res. Bull.* 43, 337–340.

Hope, B. T., Michael, G. J., Knigge, K. M., and Vincent, S. R. (1991). Neuronal NADPH diaphorase is a nitric oxide synthase. *Proc. Natl. Acad. Sci. U.S.A.* 88, 2811–2814.

Horton, J. C., and Adams, D. L. (2005). The cortical column: a structure without a function. *Philos. Trans. R. Soc. Lond B Biol. Sci.* 360, 837–862.

Hubener, M., and Bolz, J. (1992). Relationships between dendritic morphology and cytochrome oxidase compartments in monkey striate cortex. *J. Comp. Neurol.* 324, 67–80.

Iadecola, C. (1993). Regulation of the cerebral microcirculation during neural activity: is nitric oxide the missing link? *Trends Neurosci.* 16, 206–214.

Iwase, K., Takemura, M., Shimada, T., Wakisawa, S., Nobuki, T., and Shigenaga, Y. (1998). Ontogeny of NADPH-diaphorase in rat forebrain and midbrain. *Anat. Embryol.* 197, 229–247.

Izumi, Y., Clifford, D. B., and Zorumski, C. F. (1992). Inhibition of long-term potentiation by NMDA-mediated nitric oxide release. *Science* 257, 1273–1276.

Kubota, Y., Shigematsu, N., Karube, F., Sekigawa, A., Kato, S., Yamaguchi, N., et al. (2011). Selective coexpression of multiple chemical markers defines discrete populations of neocortical GABAergic neurons. *Cereb. Cortex* 21, 1803–1817.

Lubke, J., and Feldmeyer, D. (2007). Excitatory signal flow and connectivity in a cortical column: focus on barrel cortex. *Brain Struct. Funct.* 212, 3–17.

Lüth, H.-J., Hedlich, A., Heidegard, H., Winkelmann, E., and Mayer, B. (1994). Morphological analyses of NADPH-diaphorase/nitric oxide synthase positive structures in human visual cortex. *J. Neurocytol.* 23, 770–782.

Malach, R. (1992). Dendritic sampling across processing streams in monkey striate cortex. *J. Comp. Neurol.* 315, 303–312.

Malinski, T., Taha, Z., Grunfeld, S., Patton, S., Kapturczak, M., and Tomboulian, P. (1993). Diffusion of nitric oxide in the aorta wall monitored *in situ* by porphyrinic microsensors. *Biochem. Biophys. Res. Commun.* 193, 1076–1082.

Matsumoto, T., Nakane, M., Pollock, J. S., Kuk, J. E., and Förstermann, U. (1993). A correlation between soluble brain nitric oxide synthase and NADPH-diaphorase activity is only seen after exposure of the tissue to fixative. *Neurosci. Lett.* 155, 61–64.

Meulemans, A. (1994). Diffusion coefficients and half-lives of nitric oxide and N-nitroso-L-arginine in rat cortex. *Neurosci. Lett.* 171, 89–93.

Mountcastle, V. B. (1997). The columnar organization of the neocortex. *Brain* 120, 701–722.

Pereira, A. Jr., Freire, M. A., Bahia, C. P., Franca, J. G., and Picanco-Diniz, C. W. (2000). The barrel field of the adult mouse SmI cortex as revealed by NADPH-diaphorase histochemistry. *Neuroreport* 11, 1889–1892.

Petersen, C. C. (2007). The functional organization of the barrel cortex. *Neuron* 56, 339–355.

Rice, F. L. (1995). "Comparative aspects of barrel structure and development," in *The Barrel Cortex of Rodents,* eds E. G. Jones and I. T. Diamond (New York, NY: Plenum Publishing Corporation), 1–75.

Riddle, D. R., Gutierrez, G., Zheng, D., White, L. E., Richards, A., and Purves, D. (1993). Differential metabolic and electrical activity in the somatic sensory cortex of juvenile and adult rats. *J. Neurosci.* 13, 4193–4213.

Rocha, E. G., Freire, M. A. M., Bahia, C. P., Pereira, A., Sossthenes, M. C. K., Silveira, L. C. L., et al. (2012). Dendritic structure varies as a function of eccentricity in V1, a quantitative study of NAPDH diaphorase neurons in the diurnal south american roden Agouti, *Dasyprocta prymnolopha*. *Neuroscience* 216, 94–102.

Rockland, K. S. (2010). Five points on columns. *Front. Neuroanat.* 4:22. doi: 10.3389/fnana.2010.00022

Romanelli, P., Di Matteo, L., Cobellis, G., Varriale, B., Menegazzi, M., Gironi Carnevale, U. A., et al. (2007). Transcription factor expression, RNA synthesis and NADPH-diaphorase across the rat brain and exposure to spatial novelty. *Behav. Brain Res.* 184, 91–100.

Sandell, J. H. (1986). NADPH diaphorase histochemistry in the macaque striate cortex. *J. Comp. Neurol.* 251, 388–397.

Santiago, L. F., Rocha, E. G., Freire, M. A., Dias, I. A., Lent, R., Houzel, J. C., et al. (2007). The organizational variability of the rodent somatosensory cortex. *Rev. Neurosci.* 18, 283–294.

Scherer-Singler, U., Vincent, S. R., Kimura, H., and McGeer, E. G. (1983). Demonstration of a unique population of neurons with NADPH-diaphorase histochemistry. *J. Neurosci. Meth.* 9, 229–234.

Schubert, D., Kotter, R., and Staiger, J. F. (2007). Mapping functional connectivity in barrel-related columns reveals layer- and cell type-specific microcircuits. *Brain Struct. Funct.* 212, 107–119.

Schuz, A., and Palm, G. (1989). Density of neurons and synapses in the cerebral cortex of the mouse. *J. Comp. Neurol.* 286, 442–455.

Swindale, N. V. (1990). Is the cerebral cortex modular? *Trends Neurosci.* 13, 487–492.

Tenorio, F., Giraldi-Guimaraes, A., Santos, H. R., Cintra, W. M., and Mendez-Otero, R. (1998). Eye enucleation alters intracellular distribution of NO synthase in the superior colliculus. *Neuroreport* 9, 145–148.

Torres, J. B., Assuncao, J., Farias, J. A., Kahwage, R., Lins, N., Passos, A., et al. (2006). NADPH-diaphorase histochemical changes in the hippocampus, cerebellum and striatum are correlated with different modalities of exercise and water-maze performances. *Exp. Brain Res.* 175, 292–304.

Valtschanoff, J. G., Weinberg, R. J., Kharazia, V. N., Schmidt, H. H., Nakane, M., and Rustioni, A. (1993). Neurons in rat cerebral cortex that synthesize nitric oxide: NADPH diaphorase histochemistry, NOS immunocytochemistry, and colocalization with GABA. *Neurosci. Lett.* 157, 157–161.

Vincent, S. R., and Kimura, H. (1992). Histochemical mapping of nitric oxide synthase in the rat brain. *Neuroscience* 46, 755–784.

Wallace, M. N. (1987). Histochemical demonstration of sensory maps in the rat and mouse cerebral cortex. *Brain Res.* 418, 178–182.

Wallace, M. N., Tayebjee, M. H., Rana, F. S., Farquhar, D. A., and Nyong'o, A. O. (1996). Pyramidal neurones in pathological human motor cortex express nitric oxide synthase. *Neurosci. Lett.* 212, 187–190.

Wässle, H., and Boycott, B. B. (1991). Functional architecture of the mammalian retina. *Physiol. Rev.* 71, 447–480.

Wester, J. C., and Contreras, D. (2012). Columnar interactions determine horizontal propagation of recurrent network activity in neocortex. *J. Neurosci.* 32, 5454–5471.

Wong-Riley, M. T. T., Anderson, B., Liebl, W., and Huang, Z. (1998). Neurochemical organization of the macaque striate cortex: correlation of cytochrome oxidase with Na^+K^+ ATPase, NADPH-diaphorase, nitric oxide synthase, and *N*-methyl-D-aspartate receptor subunit 1. *Neuroscience* 83, 1025–1045.

Wong-Riley, M. T. T., and Welt, C. (1980). Histochemical changes in cytochrome oxidase of cortical barrels after vibrissal removal in neonatal and adult mice. *Proc. Natl. Acad. Sci. U.S.A.* 77, 2333–2337.

Wood, J., and Garthwaite, J. (1994). Models of the diffusional spread of nitric oxide: implications for

neural nitric oxide signalling and its pharmacological properties. *Neuropharmacology* 33, 1235–1244.

Woolsey, T. A., and Van der Loos, H. (1970). The structural organization of layer IV in the somatosensory region (S1) of mouse cerebral cortex. The description of a cortical field composed of discrete cytoarchitectonic units. *Brain Res.* 17, 205–242.

Yan, X. X., and Garey, L. J. (1997). Morphological diversity of nitric oxide synthesising neurons in mammalian cerebral cortex. *J. Hirnforsch.* 38, 165–172.

Zilles, K., and Wree, A. (1985). "Cortex: areal and laminar structure," in *Forebrain and Midbrain,* ed G. Paxinos (Sydney, Orlando, San Diego, New York: Academic Press, Harcourt Brace Janovich), 375–415.

Conflict of Interest Statement: The authors declare that the research was conducted in the absence of any commercial or financial relationships that could be construed as a potential conflict of interest.

Received: 08 May 2012; accepted: 06 August 2012; published online: 06 November 2012.

Citation: Nogueira-Campos AA, Finamore DM, Imbiriba LA, Houzel JC and Franca JG (2012) Distribution and morphology of nitrergic neurons across functional domains of the rat primary somatosensory cortex. Front. Neural Circuits ***6****:57. doi: 10.3389/fncir.2012.00057*

frontiers in
NEURAL CIRCUITS

GENERAL COMMENTARY
published: 26 April 2013
doi: 10.3389/fncir.2013.00083

Distinct morphological features of NADPH diaphorase neurons across rodent's primary cortices

***Marco A. M. Freire*[1]* and *José R. Santos*[2]**

[1] *Laboratory of Cellular Neurobiology, Edmond and Lily Safra International Institute for Neuroscience of Natal, Natal, Brazil*
[2] *Department of Biology, Federal University of Sergipe, Aracaju, Brazil*
**Correspondence: freire.m@gmail.com*

Edited by:
Bruno Cauli, Centre National de la Recherché Scientifique and Université Pierre et Marie Curie, France

Reviewed by:
Kathleen S. Rockland, Massachusetts Institute of Technology, USA

A commentary on

Distribution and morphology of nitrergic neurons across functional domains of the rat primary somatosensory cortex
by Nogueira-Campos, A. A., Finamore, D. M., Imbiriba, L. A., Houzel, J. C., and Franca, J. G. (2012). Front. Neural Circuits 6:57. doi: 10.3389/fncir.2012.00057

Nitric oxide (NO) is a versatile gaseous molecule involved in several pathological and physiological functions in nervous system (Calabrese et al., 2007; Steinert et al., 2010; Freire, 2012). Its biosynthesis occurs after the stoichiometric conversion of L-arginine to L-citrulline in a process requiring the presence of NADPH and O_2 as co-substrates (Bredt and Snyder, 1994). A group of enzymes known as nitric oxide synthases (NOS) is responsible to synthesize NO (Stuehr et al., 2004). In the brain, neuronal NOS is strictly co-localized with NADPH diaphorase (NADPH-d), an oxidative enzyme present in a discrete population of interneurons (Dawson et al., 1991). NADPH-d histochemistry has been used to reveal the presence of NO dispersed in neuropil and to evaluate the presence and distribution of NO-synthesizing neurons across several species (Vincent et al., 1983; Sandell, 1986; Mizukawa et al., 1989; Yan et al., 1996; Franca et al., 2000; Freire et al., 2010, 2011).

Previous studies concerning NADPH-d/NOS reactive neurons focused mainly in its distribution around brain. Differences in morphology were described qualitatively. More recently, a growing amount of information regarding differences in morphometric parameters of this cell group, based in neuronal reconstructions, has emerged (Freire et al., 2007, 2012; Rocha et al., 2012). In light of this, an interesting question arises: could morphological differences of nitrergic neurons among distinct cortical areas or throughout subdivisions of a given area in rodents be associated to their distinct physiologies, as observed to pyramidal neurons (Elston et al., 2006)?

In rodents, primary somatosensory cortex (S1) is a suitable area to be explored since the complete body's representation delineates a topologically correlated cortical map (Rocha et al., 2007; Santiago et al., 2007) commonly revealed by NADPH-d histochemistry (Freire et al., 2012). The general pattern of NADPH-d-reactive neuropil is markedly similar to observed with cytochrome oxidase histochemistry, since both are oxidative enzymes involved in the energetic metabolism (Wong-Riley et al., 1998). The main representation of S1 in rats and mice corresponds to the posterior medial barrel subfield (PMBSF), the region where mystacial vibrissae are represented and the largest and more defined barrels are found. Previous studies have shown that, in a tangential view, NADPH-d neurons concentrate along the regions of PMBSF that separate barrels from each other, known as septa (Franca and Volchan, 1995; Freire et al., 2004). Nevertheless, other S1 regions were not explored in these studies.

In this context, a comprehensive work published by Nogueira-Campos et al. (2012) in Frontiers in Neural Circuits contributes to cover this gap. In that study the authors evaluated the entire population of NADPH-d neurons found across rat's S1 in order to quantify the distribution of these cells throughout all body's representation and also evaluate the morphological aspects and relationship of these neurons with barrels and septal regions. Similar to previously described to PMBSF (Franca and Volchan, 1995; Freire et al., 2004), NADPH-d neurons were not limited by compartment borders across S1. Besides, cell density in septal regions was higher than inside barrels. Regarding morphometric measurements, only in one case evaluated by the authors there was an evident difference between neurons found in septa and barrels, as previously reported (Franca and Volchan, 1995; Freire et al., 2004), what can be explained by the plan of section adopted (coronal *vs.* tangential). But what might these morphological differences represent, in terms of physiology, along distinct regions across rodent's S1? Septal and barrel regions are physiologically/functionally distinct (Alloway, 2008) since septal neurons display significant differences in response latencies related to variations in the frequency of whisker stimulation when compared to barrel neurons (Chakrabarti and Alloway, 2009). In addition both regions receive projections from separated thalamic nuclei (Killackey and Sherman, 2003). Accordingly, barrels and septa would require a segregated circuitry in these different zones, what may be correlated to morphometric differences observed in NADPH-d neurons in both regions. These structural differences could reflect specializations in the processing of sensory information across distinct cortical areas, meaning a difference in their capacity for synaptic integration because dendritic coverage is directly related to the amount of synaptic contacts a cell may receive. Accordingly, neurons possessing a smaller dendritic arbor cover a small cortical area and potentially establish fewer synaptic contacts

than more ramified cells. Because septal region is thought to be a segregated cortex from barrels (Killackey and Sherman, 2003), both regions represent two different processing streams that analyze distinct information (Alloway, 2008). So, more complex interneurons in septa could integrate a broader range of synaptic inputs than those found inside barrels.

In conclusion, data provided by Nogueira-Campos et al. (2012) offer new insights about the organization of interneuron circuitry across rat's S1. A further quantification of NADPH-d neuronal morphology in non-primary/association areas may contribute to a more complete notion of cortical differences in the inhibitory circuitry.

ACKNOWLEDGMENTS

The authors would like to thank Associação Alberto Santos Dumont para Apoio à Pesquisa (AASDAP)—Brazil for the logistical support.

REFERENCES

Alloway, K. D. (2008). Information processing streams in rodent barrel cortex: the differential functions of barrel and septal circuits. *Cereb. Cortex* 18, 979–989.

Bredt, D. S., and Snyder, S. H. (1994). Nitric oxide: a physiologic messenger molecule. *Annu. Rev. Biochem.* 63, 175–195.

Calabrese, V., Mancuso, C., Calvani, M., Rizzarelli, E., Butterfield, D. A., and Stella, A. M. (2007). Nitric oxide in the central nervous system: neuroprotection versus neurotoxicity. *Nat. Rev. Neurosci.* 8, 766–775.

Chakrabarti, S., and Alloway, K. D. (2009). Differential response patterns in the si barrel and septal compartments during mechanical whisker stimulation. *J. Neurophysiol.* 102, 1632–1646.

Dawson, T. M., Bredt, D. S., Fotuhi, M., Hwang, P. M., and Snyder, S. H. (1991). Nitric oxide synthase and neuronal NADPH diaphorase are identical in brain and peripheral tissues. *Proc. Natl. Acad. Sci. U.S.A.* 88, 7797–7801.

Elston, G. N., Elston, A., Freire, M. A. M., Gomes-Leal, W., Pereira, A. Jr., Silveira, L. C. L., et al. (2006). Specialization of pyramidal cell structure in the visual areas V1, V2 and V3 of the South American rodent, *Dasyprocta primnolopha*. *Brain Res.* 1106, 99–110.

Franca, J. G., and Volchan, E. (1995). NADPH diaphorase histochemistry as a marker for barrels in rat somatosensory cortex. *Braz. J. Med. Biol. Res.* 28, 787–790.

Franca, J. G., Volchan, E., Jain, N., Catania, K. C., Oliveira, R. L., Hess, F. F., et al. (2000). Distribution of NADPH-diaphorase cells in visual and somatosensory cortex in four mammalian species. *Brain Res.* 864, 163–175.

Freire, M. A. M. (2012). Pathophysiology of neurodegeneration following traumatic brain injury. *West Indian Med. J.* 61, 751–755.

Freire, M. A. M., Faber, J., Picanço-Diniz, C. W., Franca, J. G., and Pereira, A. (2012). Morphometric variability of nicotinamide adenine dinucleotide phosphate diaphorase neurons in the primary sensory areas of the rat. *Neuroscience* 205, 140–153.

Freire, M. A. M., Gomes-Leal, W., Carvalho, W. A., Guimaraes, J. S., Franca, J. G., Picanço-Diniz, C. W., et al. (2004). A morphometric study of the progressive changes on NADPH diaphorase activity in the developing rat's barrel field. *Neurosci. Res.* 50, 55–66.

Freire, M. A. M., Morya, E., Faber, J., Santos, J. R., Guimaraes, J. S., Lemos, N. A. M., et al. (2011). Comprehensive analysis of tissue preservation and recording quality from chronic multielectrode implants. *PLoS ONE* 6:e27554. doi: 10.1371/journal.pone.0027554

Freire, M. A. M., Oliveira, R. B., Picanço-Diniz, C. W., and Pereira, A. Jr. (2007). Differential effects of methylmercury intoxication in the rat's barrel field as evidenced by NADPH diaphorase histochemistry. *Neurotoxicology* 28, 175–181.

Freire, M. A. M., Rocha, E. G., Oliveira, J. L. F., Guimaraes, J. S., Silveira, L. C. L., Elston, G. N., et al. (2010). Morphological variability of NADPH diaphorase neurons across areas V1, V2, and V3 of the common agouti. *Brain Res.* 1318C, 52–63.

Killackey, H. P., and Sherman, S. M. (2003). Corticothalamic projections from the rat primary somatosensory cortex. *J. Neurosci.* 23, 7381–7384.

Mizukawa, K., Vincent, S. R., McGeer, P. L., and McGeer, E. G. (1989). Distribution of reduced-nicotinamide-adenine-dinucleotide-phosphate diaphorase-positive cells and fibers in the cat central nervous system. *J. Comp. Neurol.* 279, 281–311.

Nogueira-Campos, A. A., Finamore, D. M., Imbiriba, L. A., Houzel, J. C., and Franca, J. G. (2012). Distribution and morphology of nitrergic neurons across functional domains of the rat primary somatosensory cortex. *Front. Neural Circuits* 6:57. doi: 10.3389/fncir.2012.00057

Rocha, E. G., Freire, M. A. M., Bahia, C. P., Pereira, A., Sosthenes, M. C., Silveira, L. C., et al. (2012). Dendritic structure varies as a function of eccentricity in V1: A quantitative study of NADPH diaphorase neurons in the diurnal South American rodent agouti, *Dasyprocta prymnolopha*. *Neuroscience* 216, 94–102.

Rocha, E. G., Santiago, L. F., Freire, M. A. M., Gomes-Leal, W., Lent, R., Houzel, J. C., et al. (2007). Callosal axon arbors in the limb representations of the somatosensory cortex (SI) in the agouti (*Dasyprocta primnolopha*). *J. Comp. Neurol.* 500, 255–266.

Sandell, J. H. (1986). NADPH diaphorase histochemistry in the macaque striate cortex. *J. Comp. Neurol.* 251, 388–397.

Santiago, L. F., Rocha, E. G., Freire, M. A. M., Lent, R., Houzel, J. C., Picanço-Diniz, C. W., et al. (2007). The organizational variability of the rodent somatosensory cortex. *Rev. Neurosci.* 18, 283–294.

Steinert, J. R., Chernova, T., and Forsythe, I. D. (2010). Nitric oxide signaling in brain function, dysfunction, and dementia. *Neuroscientist* 16, 435–452.

Stuehr, D. J., Santolini, J., Wang, Z. Q., Wei, C. C., and Adak, S. (2004). Update on mechanism and catalytic regulation in the NO synthases. *J. Biol. Chem.* 279, 36167–36170.

Vincent, S. R., Johansson, O., Hokfelt, T., Skirboll, L., Elde, R. P., Terenius, L., et al. (1983). NADPH-diaphorase: a selective histochemical marker for striatal neurons containing both somatostatin- and avian pancreatic polypeptide (APP)-like immunoreactivities. *J. Comp. Neurol.* 217, 252–263.

Wong-Riley, M., Anderson, B., Liebl, W., and Huang, Z. (1998). Neurochemical organization of the macaque striate cortex: correlation of cytochrome oxidase with Na+K+ATPase, NADPH-diaphorase, nitric oxide synthase, and N-methyl-D-aspartate receptor subunit 1. *Neuroscience* 83, 1025–1045.

Yan, X. X., Jen, L. S., and Garey, L. J. (1996). NADPH-diaphorase-positive neurons in primate cerebral cortex colocalize with GABA and calcium-binding proteins. *Cereb. Cortex* 6, 524–529.

Received: 01 April 2013; accepted: 12 April 2013; published online: 26 April 2013.

Citation: Freire MAM and Santos JR (2013) Distinct morphological features of NADPH diaphorase neurons across rodent's primary cortices. Front. Neural Circuits 7:83. doi: 10.3389/fncir.2013.00083

frontiers in
NEURAL CIRCUITS

ORIGINAL RESEARCH ARTICLE
published: 29 June 2012
doi: 10.3389/fncir.2012.00036

Characterization of type I and type II nNOS-expressing interneurons in the barrel cortex of mouse

Quentin Perrenoud[1], Hélène Geoffroy[1], Benjamin Gauthier[1], Armelle Rancillac[1], Fabienne Alfonsi[2,3], Nicoletta Kessaris[2,3], Jean Rossier[1], Tania Vitalis[1†] and Thierry Gallopin[1*†]

[1] *Laboratoire de Neurobiologie, CNRS UMR 7637, ESPCI ParisTech, Paris, France*
[2] *Wolfson Institute for Biomedical Research, University College London, London, UK*
[3] *Department of Cell and Developmental Biology, University College London, London, UK*

Edited by:
Bruno Cauli, University Pierre et Marie Curie, France

Reviewed by:
Kathleen S. Rockland, Massachusetts Institute of Technology, USA
Thomas Kilduff, Stanford Research Institute International, USA

****Correspondence:***
Thierry Gallopin, Laboratoire de Neurobiologie, CNRS UMR 7637, ESPCI ParisTech, University Pierre et Marie Curie, 10 rue Vauquelin, 75005 Paris, France.
e-mail: thierry.gallopin@espci.fr

†Tania Vitalis and Thierry Gallopin have contributed equally to this work.

In the neocortex, neuronal nitric oxide (NO) synthase (nNOS) is essentially expressed in two classes of GABAergic neurons: type I neurons displaying high levels of expression and type II neurons displaying weaker expression. Using immunocytochemistry in mice expressing GFP under the control of the glutamic acid decarboxylase 67k (GAD67) promoter, we studied the distribution of type I and type II neurons in the barrel cortex and their expression of parvalbumin (PV), somatostatin (SOM), and vasoactive intestinal peptide (VIP). We found that type I neurons were predominantly located in deeper layers and expressed SOM (91.5%) while type II neurons were concentrated in layer II/III and VI and expressed PV (17.7%), SOM (18.7%), and VIP (10.2%). We then characterized neurons expressing nNOS mRNA ($n = 42$ cells) *ex vivo*, using whole-cell recordings coupled to single-cell reverse transcription-PCR and biocytin labeling. Unsupervised cluster analysis of this sample disclosed four classes. One cluster ($n = 7$) corresponded to large, deep layer neurons, displaying a high expression of SOM (85.7%) and was thus very likely to correspond to type I neurons. The three other clusters were identified as putative type II cells and corresponded to neurogliaform-like interneurons ($n = 19$), deep layer neurons expressing PV or SOM ($n = 9$), and neurons expressing VIP ($n = 7$). Finally, we performed nNOS immunohistochemistry on mouse lines in which GFP labeling revealed the expression of two specific developmental genes (Lhx6 and 5-HT_{3A}). We found that type I neurons expressed Lhx6 but never 5-HT_{3A}, indicating that they originate in the medial ganglionic eminence (MGE). Type II neurons expressed Lhx6 (63%) and 5-HT_{3A} (34.4%) supporting their derivation either from the MGE or from the caudal ganglionic eminence (CGE) and the entopeduncular and dorsal preoptic areas. Together, our results in the barrel cortex of mouse support the view that type I neurons form a specific class of SOM-expressing neurons while type II neurons comprise at least three classes.

Keywords: Immunohistochemistry, patch-clamp, development, nitric oxide, parvalbumin, somatostatin, vasointestinal peptide, neuropeptide Y

INTRODUCTION

The neuronal nitric oxide (NO) synthase (nNOS) isoform is expressed by distinct populations of neocortical neurons (Karagiannis et al., 2009; Kubota et al., 2011). NO is well known to play crucial roles in the induction or regulation of neuronal plasticity (Garthwaite and Boulton, 1995) and is involved in various neuronal functions such as learning and memory (Rancillac and Crepel, 2004; Garthwaite, 2008), neuronal death (Dawson and Dawson, 1998; Kiss, 2000), and cerebral blood flow control (Iadecola et al., 1993; Moro et al., 1995; Rancillac et al., 2006). Despite these pleiotropic effects of prime importance, cortical nNOS-expressing neurons are still poorly understood. Characterizing these neurons is thus an important step toward understanding their physiological functions.

In the neocortex nitrergic neurons are mainly GABAergic (Valtschanoff et al., 1993) and are generally divided in type I and type II neurons according to the intensity of NADPH diaphorase activity and/or nNOS immunoreactivity (Yan et al., 1996; Yan and Garey, 1997; Judas et al., 1999; Smiley et al., 2000; Lee and Jeon, 2005). Type I cells usually exhibit large somata, are intensely stained and represent about 2% of total GABAergic interneurons in the rat primary sensorimotor cortex (Kubota et al., 1994). In rodents, they are found in all cortical layers (Oermann et al., 1999), although they are more frequently observed in infragranular layers (Vercelli et al., 2000; Wiencken and Casagrande, 2000; Garbossa et al., 2001; Lee and Jeon, 2005). Immunohistochemical studies indicate that type I cells frequently co-express neuropeptide Y (NPY) and somatostatin (SOM; Dawson et al., 1991; Kubota et al., 1994; Gonchar and Burkhalter, 1997; Estrada and Defelipe, 1998; Smiley et al., 2000).

Type II cells, for their part, are much smaller and weakly stained (Yan et al., 1996). First described in the primate and human cortex (Aoki et al., 1993; Hashikawa et al., 1994; Gabbott and Bacon, 1995; Yan et al., 1996), they were recently reported in rodents (Lee

and Jeon, 2005). Because of the technical limitations in identifying type II neurons, they have largely been neglected and their neurochemical characteristics are not well studied. In addition, little information is available regarding the morphological and electrophysiological characteristics of type I and type II nNOS-expressing neurons (Kilduff et al., 2011).

In the present study, we characterized cortical nitrergic interneurons with immunohistochemical labeling of distinct chemical markers in GAD67:GFP knock-in mice (Tamamaki et al., 2003). Furthermore, a multiparametric analysis of neurons expressing nNOS mRNA was performed using whole-cell current-clamp recordings coupled to single-cell reverse transcription (scRT)-PCR in acute slices of mouse somatosensory barrel cortex. Unsupervised clustering revealed the presence of four major classes of nitrergic neurons whose properties correlated to type I and type II nNOS immunoreactivity. Finally, we assessed the embryonic origins of type I and type II interneurons by using immunohistochemistry on mouse lines co-expressing GFP/YFP and two specific precursors expressed in distinct embryonic territories; medial ganglionic eminence (MGE; Lhx6) and caudal ganglionic eminence (CGE)-entopeduncular and dorsal preoptic areas (AEP/PO; 5-HT_{3A}).

MATERIALS AND METHODS

All experimental procedures were performed as described previously (Perrenoud et al., 2012) and were in accordance with the guidelines of the European Community Council Directive of November 24, 1986 (86/609/EEC).

IMMUNOHISTOCHEMISTRY

Seven P17 GAD67:GFP knock-in (Δneo) transgenic mice (Tamamaki et al., 2003), three offspring of Lhx6-CRE and Rosa26R-YFP mice (Fogarty et al., 2007), and three 5-HT_{3A}:GFP mice (GENSAT, Vucurovic et al., 2010) were used. Mice were deeply anesthetized with an intraperitoneal (IP) injection of pentobarbital (150 mg/kg body weight) and perfused transcardially with 4% paraformaldehyde in 0.1 M phosphate buffered saline (PBS), pH 7.4 (PFA). Brains were dissected, embedded in 3% agarose diluted in PBS, and cut coronally on a vibratome (Leica; VT1000S). Free-floating 45 μm thick coronal sections were collected serially. Alternate sections were incubated for 48–72 h at 4°C with one of the following antibodies diluted in PBS containing triton (0.2%; PBST): rabbit anti-nNOS antibody (1:500; Santa-Cruz sc-648), rabbit anti-PV (1:800; Swant PV28), rat anti-SOM (1:500; Millipore MAB354), or rabbit anti-vasoactive intestinal peptide (VIP; 1:500, ImmunoStar 20077). After washing in PBST, sections were incubated with AlexaFluor 568 goat anti-rabbit antibody or AlexaFluor 568 goat anti-rat antibody (1:300; Invitrogen). Sections were rinsed in PBST, mounted in Vectashield (Vector) containing DAPI. Confocal images were acquired with an SP5 confocal microscope (Nikon).

COUNTING OF GABAergic IMMUNOSTAINED NEURONS

Counting was performed using the method described in Perrenoud et al. (2012). Briefly, immunostained slices of GAD67:GFP knock-in (Δneo) transgenic mice were observed with a fluorescent microscope (Zeiss, Axio Imager M1) equipped with an AxioCam MRm CCD camera (Zeiss). Mosaics were constructed from images spanning the region of the posteromedial barrel subfield (PMBSF; approximately between −0.94 and −2.06 mm from Bregma (Paxinos and Franklin, 2001), acquired using a 10× objective, with the AxioVision 4.7 software (Zeiss) and stored as gray scale bitmaps. Counts were performed using a procedure written in IGOR PRO 6 (WaveMetrics) with a custom made algorithm dividing the radial extent of the neocortex into 30 bins while following its curvature and adapting to variations in its thickness. Layer boundaries matched closely with edges of particular bins: layer I corresponded to bin 1 and 2; layer II/III to bin 3–9; layer IV to bin 10–13; layer V to bin 14–21; and layer VI to bin 22–30. Counts were repeated at least on three slices per animal. For each animal, final values of densities were computed, normalizing the sum of counted cells by the corresponding counted area.

SLICE PREPARATION FOR ELECTROPHYSIOLOGICAL RECORDINGS

Juvenile C57BL/6 mice (Janvier) aged P14–P17 were deeply anesthetized with halothane and decapitated. Brains were quickly removed and cut into 300 μm thick slices with a 30–40° inclination from the sagittal plane into an ice cold (approximately 4°C) slicing solution continuously aerated with carbogen (95% O_2/5% CO_2; Air Liquide), containing (in mM): 110 choline chloride, 11.6 sodium ascorbate, 7 $MgCl_2$, 2.5 KCl, 1.25 NaH_2PO_4, 25 glucose, 25 $NaHCO_3$, and 3.1 sodium pyruvate (Bureau et al., 2006). Prior to recording, slices were maintained at room temperature in a holding chamber containing artificial cerebrospinal fluid (aCSF) aerated with carbogen, containing (in mM): 126 NaCl, 2.5 KCl, 2 $CaCl_2$, 1 $MgCl_2$, 1.25 NaH_2PO_4, 20 glucose, and 26 $NaHCO_3$. In order to avoid excitotoxicity 1 mM of kynurenic acid (Sigma) was added to the solution.

WHOLE-CELL PATCH-CLAMP RECORDINGS

Slices were submerged in thermostat controlled recording chamber (Luigs and Neuman), placed on the stage of an Axioskop 2FS microscope (Carl Zeiss), equipped with Dodt gradient contrast optics (Luigs and Neuman), and a CoolSnap FX CCD camera (Roper scientific) and visualized under infrared (IR) illumination. The preparation was continuously superfused (1–2 ml/min) with oxygenated aCSF. Barrels were visualized in the absence of the light condenser and recordings were performed within the barrel cortex. Pipettes (4–6 MΩ) were pulled from borosilicate capillaries and filled with 8 μl of autoclaved internal solution containing 144 mM K-gluconate, 3 mM $MgCl_2$, 0.5 mM EGTA, 10 mM HEPES, pH 7.2 (285/295 mOsm), and 3 mg/ml biocytin (Sigma). Whole-cell recordings were performed at 30 ± 1°C in the current-clamp mode of a MultiClamp 700B amplifier (Molecular Devices). Signals were filtered at 4 kHz and digitized at 50 kHz with an analog signal converter (Digidata 1322A; Molecular Devices), and analyzed using pClamp 9.2 software (Molecular Devices). The sole criterion for selection of recorded cells was the absence of an apical dendrite. Junction potentials were not corrected.

SINGLE-CELL RT-PCR PROTOCOL

At the end of recordings, cytoplasms were aspirated into the patch pipette, expelled into a test tube in which reverse transcription was performed as described previously (Lambolez et al., 1992) and

stored at −80°C. The scRT-PCR protocol was designed to detect the presence of messenger mRNAs coding for the vesicular glutamate transporter 1 (VGluT1), the two isoforms of glutamic acid decarboxylase (GAD65 and GAD67), nNOS, the calcium binding proteins calbindin (CB) 28k, calretinin (CR), and parvalbumin (PV), and the neuropeptides SOM, NPY, VIP, and cholecystokinin (CCK; **Table 1**). Two successive rounds of amplification were performed using nested primer pairs (Cauli et al., 1997). All primer pairs (**Table 1**) were designed to target two different exons so as to differentiate transcripts from genomic DNA. Amplification products were detected on 2% agarose gels in presence of a standard molecular weight marker (100 bp Ladder; Promega).

HISTOCHEMICAL LABELING AND MORPHOLOGICAL RECONSTRUCTION OF RECORDED NEURONS

Recorded slices were fixed overnight at 4°C with 4% paraformaldehyde in 0.1 M phosphate buffer (PB) pH 7.4 and kept in PB at 4°C until further processed. Slices were then sequentially incubated in PB containing 1% H_2O_2 in order to quench endogenous peroxidases, and in PB containing Avidin Biotin Complex (Vector; 1:200) and Triton X-100 (0.5%). Neuronal morphology was visualized using diaminobenzidine nickel (DAB elite kit, Vector). Between each step slices were thoroughly rinsed in PB. Tissue sections were mounted in Mowiol (Calbiochem). For recorded cells with clearly visible dendritic arborizations, morphology was analyzed using a DMR microscope (Leica), equipped with a 100× objective together with a standard Neurolucida system (MBF Bioscience).

ELECTROPHYSIOLOGICAL ANALYSIS

Voltage responses of neurons induced by 800 ms hyperpolarizing and depolarizing current pulses were measured as described previously (Vucurovic et al., 2010; Perrenoud et al., 2012). In order to characterize the behavior of recorded neurons, 22 electrophysiological parameters were measured: (1) resting potential (RMP), (2) input resistance (R_m), (3) membrane time constant (τ_m), (4) membrane capacitance (C_m), (5) Sag index, (6) rheobase, (7) first spike latency, (8) adaptation ($m_{threshold}$), (9) minimal steady-state frequency (F_{min}; slope and y-intercept of a linear fit to the firing frequency at threshold, respectively), (10) amplitude accommodation (H_{ump}), (11) amplitude of early adaptation (A_{sat}), (12) time constant of early adaptation (τ_{sat}), (13) maximal steady-state frequency (m_{sat}), and (14) late adaptation (F_{max}; defined such that the function $F = A_{sat} \times \exp(-t/\tau_{sat}) + m_{sat} \times t + F_{max}$), was fitted to the firing frequency in the trace just prior to saturation (15) amplitude (A1), (16) duration (D1), (18) AHP maximum (AHP1m), (17) ADP, (19) AHP latencies (tAHP2m), and (20) ADP latencies of the first action potential, (21) amplitude reduction (Amp.Red), and (22) duration increase (Dur.Inc) of the second action potential relative to the first.

MORPHOLOGICAL ANALYSIS

Eighteen parameters related to features of the soma and dendrites of reconstructed neurons were extracted as described previously (Perrenoud et al., 2012). In order to describe somata of reconstructed neurons, (1) the area, (2) perimeter, (3) maximal, and (4) minimal diameters of the soma were computed from IR pictures acquired prior to whole-cell recording. (5) Elongation was defined as the ratio between the maximal and minimal diameters (Karagiannis et al., 2009). The dendritic properties of vectorized neurons were extracted using Neurolucida explorer (MBF Bioscience) and analyzed using Excel (Microsoft). The following parameters were quantified: (6) number of primary dendrites, (7) total dendritic

Table 1 | PCR primer.

Genes	Size	First PCR primers	Size	Second PCR primers
VGlut1	593	Sense, 124 CCCTTAGAACGGAGTCGGCT	367	Sense, 148 ACGACAGCCTTTTGCGGTTC
NM_182993.1		Antisense, 697 TATCCGACCACCAGCAGCAG		Antisense, 495 CAAAGTAGGCGGGCTGAGAG
GAD65	375	Sense, 99 CCAAAAGTTCACGGGCGG	248	Sense, 219 CACCTGCGACCAAAAACCCT
NM_008078.1		Antisense, 454 TCCTCCAGATTTTGCGGTTG		Antisense, 447 GATTTTGCGGTTGGTCTGCC
GAD67	253	Sense, 83 ATGATACTTGGTGTGGCGTAGC	177	Sense, 159 CAATAGCCTGGAAGAGAAGAGTCG
NM_008077.3		Antisense, 314 GTTTGCTCCTCCCCGTTCTTAG		Antisense, 314 GTTTGCTCCTCCCCGTTCTTAG
CA	426	Sense, 139 CGAAAGAAGGCTGGATTGGAG	295	Sense, 194 ATGGACAGAGAGATGATGGAAAAA
NM_009788.2		Antisense, 544 CCCACACATTTTGATTCCCTG		Antisense, 467 TCCAGCTTTCCGTCATTATTTG
CR	265	Sense, 83 TTGATGCTGACGGAAATGGGTA	151	Sense, 141 GCTGGAGAAGGCAAGGAAGG
NM_007586.1		Antisense, 327 CAAGCCTCCATAAACTCAGCG		Antisense, 271 ATTCTCTTCGGTCGGCAGGAT
PV	275	Sense, 104 GCCTGAAGAAAAAGAACCCG	163	Sense, 122 CGGATGAGGTGAAGAAGGTGT
NM_013645.2		Antisense, 275 AATCTTGCCGTCCCCATCCT		Antisense, 265 TCCCCATCCTTGTCTCCAGC
nNOS	373	Sense, 1668 CCTGGGGCTCAAATGGTATG	236	Sense, 1742 CCTGTCCCTTTAGTGGCTGGTA
NM_008712.2		Antisense, 2021 CACAATCCACACCCAGTCGG		Antisense, 1957 GATGAAGGACTCGGTGGCAGA
NPY	294	Sense, 16 CGAATGGGGCTGTGTGGA	220	Sense 38 CCCTCGCTCTATCTCTGCTCGT
NM_023456.2		Antisense, 286 AAGTTTCATTTCCCATCACCACAT		Antisense, 236 GCGTTTTCTGTGCTTTCCTTCA
SOM	250	Sense, 1 ATGCTGTCCTGCCGTCTCCA	170	Sense, 41 GCATCGTCCTGGCTTTGGG
NM_009215.1		Antisense, 231 GCCTCATCTCGTCCTGCTCA		Antisense, 191 GGGCTCCAGGGCATCATTCT
VIP	419	Sense, 3 GGAAGCCAGAAGCAAGCCTC	276	Sense, 113 TGGATGACAGGATGCCGTTT
NM_011702.1		Antisense, 402 GCTTTCTGAGGCGGGTGTAG		Antisense, 369 CGGCATCAGAGTGTCGTTTG
CCK	202	Sense, 259 ATACATCCAGCAGGTCCGCA	156	Sense, 305 CTTAAGAACCTGCAGAGCCTGG
NM_031161.2		Antisense, 440 TTTCCTCATTCCACCTCCTCC		Antisense, 440 TTTCCTCATTCCACCTCCTCC

length, (8) average length of segments, (9) ratio of the total dendritic length to the total dendritic surface, (10) average tortuosity of dendritic segments, (11) number of dendritic nodes, and (12) fractal index (calculated using the box counting method; Douketis et al., 1995). According to the Sholl procedure (Sholl, 1953): (13) The length of the dendritic arborization enclosed within a radius of 100 μm around the cell body, (14) between 100 and 200 μm radii, (15) between 200 and 300 μm radii, (16) and outside a 300-μm radius were extracted and expressed as a fraction of the total dendritic length. Finally, a wedge analysis was performed where the volume around each reconstructed neuron was divided into 12 wedges centered on the soma (Dumitriu et al., 2007; Vucurovic et al., 2010). (17) Vertical extent and (18) horizontal extent were defined as the fraction of the dendritic arborization, respectively, enclosed in the four wedges closest to the radial cortical axis or to the tangential cortical axis.

UNSUPERVISED CLUSTERING

Using Ward's (1963) method, cells are grouped in clusters so as to minimize the Euclidean distances between cells and cluster-centroids in multiparametric space. An advantage of this unsupervised clustering algorithm is that definition of the number of classes to be characterized is not required prior to analysis. However, a drawback of Ward's method is that miss-assigned cells are not corrected during the iterative process. Clusters generated with Ward's method were thus corrected using the K-means algorithm. This method initiates with k arbitrarily assigned cluster centers and assigns each observation to one of k corresponding clusters by minimizing the distance of the observation to the centers. The actual cluster-centroids are subsequently computed and the process is repeated until an optimum solution is reached whereby observations are allocated into k non-overlapping groups. Here, initial cluster centers were chosen so as to correspond to the centroids of the clusters generated with Ward's methods. This combination allowed the generation of non-overlapping clusters without making prior assumptions about the number of groups into which neurons should be separated. The threshold defining the number of clusters on Ward's dendrogram was set to the value maximizing the mean silhouette value of classified neurons after K-means correction. In silhouette analysis (Karagiannis et al., 2009), the value $S(i)$ is computed for each data point as: $S(i) = [b(i) - a(i)]/\max[a(i), b(i)]$ where, for a data point i, $a(i)$ corresponds to the average distance between i and the points belonging to the same cluster and $b(i)$ corresponds to the average distance between i and the points of the closest cluster. In our case, a positive silhouette value indicates that on average, the neuron is closer to the neurons of its own cluster than from the neurons belonging to other clusters in the parameter space. By contrast, a negative value indicates a potential misclassification. Thus, a decrease of the mean silhouette value of the cells following randomization was interpreted as a lower quality of clustering. In order to maximize the consistency of the clustering results, parameters were not used for clustering (i) if they were dependent upon other parameters, (ii) if they were subjected to excessive variability from trial to trial, or (iii) if they were invariant in all observed cells. Based on these criteria, electrophysiological parameters used for clustering analysis were RMP, R_m, τ_m, C_m, Sag index, H_{ump}, A_{sat}, t_{sat}, C_{sat}, m_{sat}, A1, D1, AHP1max, tADP1, tAHP1max, Amp.Red, and Dur.Inc. Molecular parameters included in the clustering analysis were computed, as binary variables set to 1 if the marker was present and 0 if absent and corresponded to CB, PV, CR, NPY, VIP, and SOM. For all parameters, distributions were centered and reduced prior to clustering in order to eliminate any weighting effects induced by differences of scaling. This appeared sufficient to ensure that binary and continuous parameters had a similar effect on clustering analysis (Perrenoud et al., 2012).

STATISTICAL ANALYSIS

For electrophysiological and morphological variables, differences were tested using Kruskal–Wallis non-parametric ANOVAs followed by Mann–Whitney U-tests for pair comparisons. In order to test differences in the occurrence of molecular markers, we computed the statistic $|\varepsilon| = |p_a - p_b|/\sqrt{[(p_q/n_a) + (p_q/n_b)]}$ where p_a and p_b represent the percentages of occurrence of the marker, and n_a and n_b the number of individuals in cluster a and b. The percentages of occurrence and of absence of the marker in the overall population were represented by p and $q = 1 - p$, respectively. p-Values of the difference of expression were computed by plotting this statistic against a standard normal distribution (Karagiannis et al., 2009). Variations in the density of labeled GABAergic cells between neocortical layers were tested using a one-way ANOVA on repeated measures test, followed by Student Newman–Keuls tests for pair comparisons. Kruskal–Wallis ANOVA, one-way ANOVA on repeated measures, and Student Newman–Keuls test were performed using Sigma Stat (LogiLabo). Mann–Whitney U-tests were performed within the Matlab environment (MathWorks) and statistical tests for molecular expression were performed in Excel (Microsoft).

RESULTS

LAMINAR DISTRIBUTION OF TYPE I AND TYPE II nNOS IMMUNOLABELED NEURONS

The aim of this study was to characterize the populations of neocortical interneurons defined by nNOS immunoreactivity. In order to fulfill this goal we examined the density and the laminar distribution of these cells using immunohistochemistry. Cells defined by nNOS immunolabeling were counted in each layer of the barrel cortex from juvenile mice (P17; PMBSF; approximately between −0.94 and −2.06 mm from Bregma; Paxinos and Franklin, 2001). In order to ensure that all counted neurons were GABAergic, counts were performed on a strain of GAD67:GFP mice where GFP is thought to be restricted to and expressed in all GABAergic cells. Counts were normalized by the area of the counted region so as to provide a measure of density and were repeated on three animals. Counts were averaged between barrels and septa.

In agreement with previous reports (Yan et al., 1996; Yan and Garey, 1997; Smiley et al., 2000; Lee and Jeon, 2005) we found that two types of cells are defined on the basis of nNOS immunoreactivity. Type I cells corresponded to strongly labeled cells displaying large somata (**Figure 1A2**). By contrast, type II cells corresponded to smaller interneurons displaying weaker labeling, typically restricted to the perikaryon. The densities of these types of cell were assessed separately and each appeared to adopt a specific distribution and to concentrate in particular neocortical

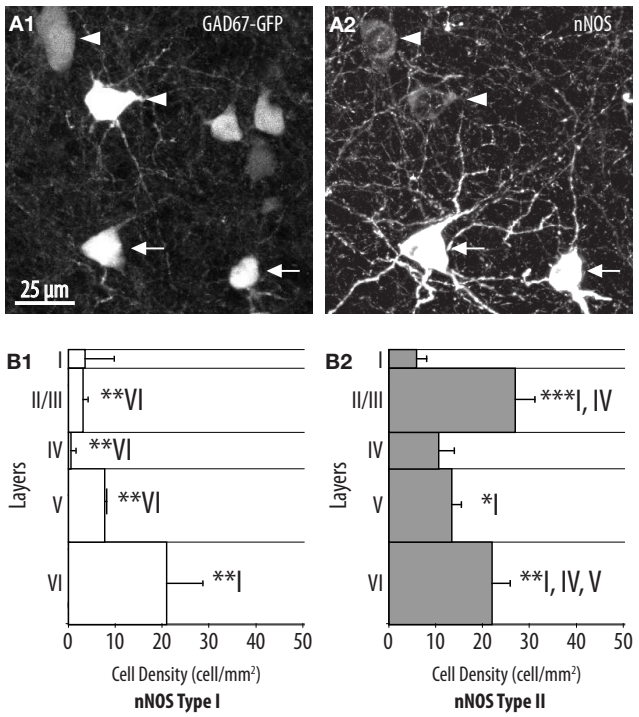

FIGURE 1 | Distribution of type I and type II nNOS-expressing GABAergic interneurons in the mouse barrel cortex. (A) Colocalization of GFP **(1)** with nNOS immunolabeling **(2)** in GAD67:GFP mice. Arrows point to examples of type I (heavily labeled) nNOS-expressing GABAergic neurons and arrowheads point to examples of type II (weakly labeled) nNOS-expressing GABAergic cells. **(B)** Histogram of the density of type I **(1)** and type II **(2)** nNOS immunolabeled GFP-expressing cells in cortical layers I–VI ($n = 3$ mice; error bars: standard deviation; *, **, and *** indicate statistically significant differences with $p \leq 0.05$, $p \leq 0.01$, and $p \leq 0.001$, respectively; roman numerals refer to neocortical layers).

layers. Type I neurons were sparse (9.4 ± 2.7 cells/mm^2 overall) and accumulated preferentially in layer VI where they had a density of 21.1 ± 7 cells/mm^2. Type I neurons could be found at more moderate densities in layer V and layer II/III but were almost absent from layer I to IV (**Figure 1B1**). The overall density of type II neurons was higher than the density of type I neurons (18.3 ± 2.5 cells/mm^2 overall). Type II neurons populated all neocortical layers but accumulated preferentially in layer II/III and layer VI (**Figure 1B2**).

IMMUNODETECTION OF PV, SOM, AND VIP IN TYPE I AND TYPE II nNOS INTERNEURONS

PV, SOM, and VIP immunoreactivity profiles define three well-characterized non-overlapping populations of interneurons in the cerebral cortex (Kubota et al., 1994; Gonchar and Burkhalter, 1997; Gonchar et al., 2007; Xu et al., 2010). In order to further characterize type I and type II nNOS-expressing interneurons, we investigated the expression of SOM, PV, and VIP using triple immunofluorescent labeling performed on GAD67:GFP knock-in mice. As apparent in **Figures 2A,D1**, 91.5 ± 4.0% of type I neurons expressed SOM. These results are consistent with previous reports indicating that SOM is a distinctive marker of type I neurons (Smiley et al., 2000). In agreement, only 11.0 ± 6.9% of type I neurons expressed PV and none expressed VIP (**Figures 2E1,F1**). By contrast, type II cells did not display a distinct immunoreactivity profile since PV, SOM, and VIP were expressed by 17.8 ± 5.0, 18.7 ± 6.9, and 10.2 ± 5.5% of type II interneurons, respectively. Interestingly, PV and SOM immunoreactive type II neurons were preferentially concentrated in deep neocortical layers while VIP immunoreactive type II neurons were located at the highest density in layers II/III (**Figures 2D2,E2,F2**). Thus, our results suggest that type II interneurons represent a heterogeneous population of interneurons.

CHARACTERIZATION OF INTERNEURONS EXPRESSING nNOS mRNA

To further characterize nNOS-expressing interneurons, a sample of 42 cells expressing nNOS mRNA were selected from a large database of neocortical interneurons characterized *ex vivo* using whole-cell patch-clamp recordings coupled to scRT-PCR and biocytin labeling on juvenile mice (P17-P14). The properties of these neurons were quantified using a set of 49 defined parameters. Twenty-two electrophysiological parameters (**Tables 2–5**) were measured from neuronal responses to hyperpolarizing and depolarizing current pulses. In accordance with the Petilla terminology (Ascoli et al., 2008), these parameters took into account passive membrane properties (five parameters, **Table 2**), the properties of the discharges at threshold (four parameters, **Table 3**), and saturation (five parameters, **Table 4**), in addition to properties of action potentials (eight parameters, **Table 5**). Nine molecular markers were detected by scRT-PCR alongside with nNOS: VGluT1, GAD [i.e., expression of either glutamic acid decarboxylase 65K or glutamic acid decarboxylase 67K (GAD65 and GAD67)], the calcium binding proteins CB, PV, and CR, and the neuropeptides NPY, VIP, SOM, and CCK (**Figure 3**). Finally, for a subset of 29 GABAergic neurons, morphological variables were measured from IR images of somata and from Neurolucida reconstructions of the dendritic trees. Eighteen morphometric parameters describing the soma (five parameters; **Table 6**), the local features of the dendrites (seven parameters; **Table 7**), and the spatial organization of the dendritic arborization (six parameters; **Table 8**) were extracted for each cell. Due to the fact that high scRT-PCR efficiency requires that up to one third of the cytoplasmic content is harvested (Tsuzuki et al., 2001); a procedure which has a negative effect on biocytin labeling (Karagiannis et al., 2009; Vucurovic et al., 2010), characterization of the axon was not possible for every neuron analyzed for gene expression and electrophysiological behavior. Nevertheless, representative examples of axons were obtained cells in each identified population.

UNSUPERVISED CLASSIFICATION OF INTERNEURONS EXPRESSING nNOS mRNA

In order to determine whether interneurons expressing nNOS mRNA can be divided into subgroups based on functional and molecular parameters, we applied Ward's method; an algorithm which has been widely used in the categorization of interneurons (Tamas et al., 1997; Cauli et al., 2000; Gallopin et al., 2006). Ward's clustering was applied on the basis of 17 electrophysiological variables and 6 molecular parameters representing the properties of sampled neurons (see Materials and Methods). As illustrated in

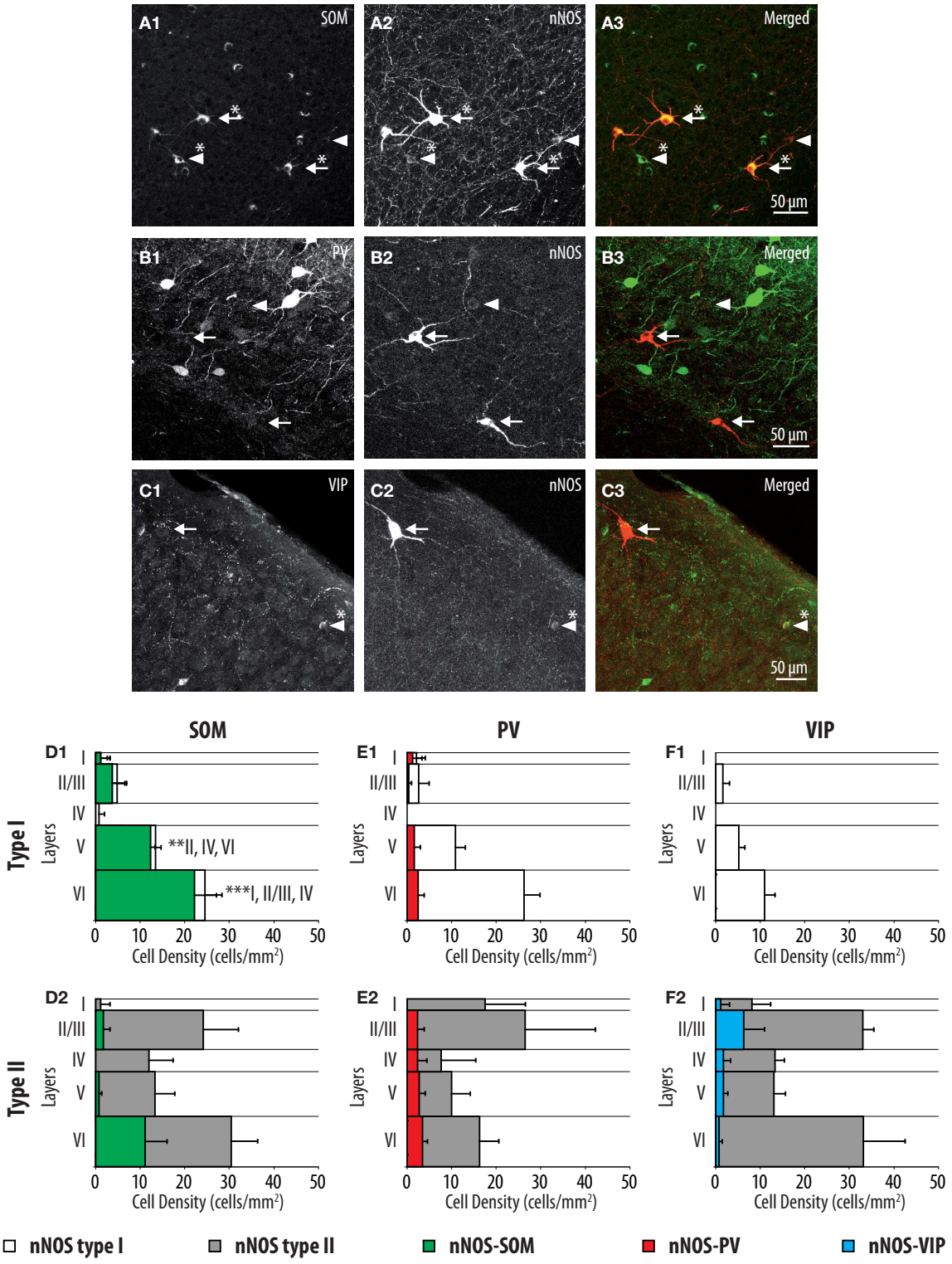

FIGURE 2 | Distributions of SOM, PV, and VIP expressing cells within type I and type II nNOS immunolabeled GABAergic interneurons. (A–C) Colocalization of SOM, PV, and VIP **(1)** with nNOS immunolabeling **(2)** in GAD67:GFP knock-in mice. Arrows point to examples of type I (heavily labeled) nNOS-expressing neurons, arrowheads point to examples of type II nNOS (weakly labeled) expressing neurons. Double-labeled cells are marked by an asterisk. **(D–F)** Histograms reflecting the densities of SOM (green), PV (red), and VIP (blue) expressing neurons within type I **(1)** and type II **(2)** nNOS-GFP-expressing interneuron classes in cortical layers I–VI. The densities of doubled labeled cells are superimposed on the overall densities of nNOS type I (white) and nNOS type II (gray) interneurons ($n = 3$ mice; error bars: standard deviation; *, **, and *** indicate significant differences with $p \leq 0.05$, $p \leq 0.01$, and $p \leq 0.001$, respectively; roman numerals refer to neocortical layers).

Table 2 | Passive membrane properties.

	Cluster 1 put-T2: Ad-NPY *n* = 19	**Cluster 2 put-T1: Ad-SOM *n* = 7**	**Cluster 3 put-T2: non-Ad-PV/SOM *n* = 9**	**Cluster 4 put-T2: Ad-VIP/CR *n* = 7**
(1) Resting potential (mV)	−68.9 ± 4.1	−65.4 ± 3.9	−68.8 ± 4.7	−64.1 ± 6.8
ANOVA: N.S.				
(2) Input resistance (MΩ)	359.7 ± 142.8	519.7 ± 89.4	303.1 ± 185.5	546.5 ± 242.6
ANOVA: 0.016	<C2	>C1, C3	<C2	
(3) Membrane time constant (ms)	25.8 ± 14.2	56.2 ± 24.3	27.7 ± 14.6	40.6 ± 12.4
ANOVA: 0.004	<<C2, <C4	>>C1, >C3	<C2	>C1
(4) Membrane capacitance (pF)	71.8 ± 24.2	113.8 ± 62.6	99.5 ± 32.5	106.2 ± 98.3
ANOVA: N.S.				
(5) Sag index (%)	89.0 ± 4.0	80.6 ± 11.4	89.4 ± 4.7	91.8 ± 5.2
ANOVA: N.S.				

n, number of cells; N.S., non-significant; <, <<, and <<<, inferior with $p \leq 0.05$, $p \leq 0.01$, and $p \leq 0.001$, respectively; >, >>, and >>>, superior with $p \leq 0.05$, $p \leq 0.01$, and $p \leq 0.001$, respectively; C1, cluster 1; C2, cluster 2; C3, cluster 3; C4, cluster 4.

Table 3 | Just above threshold properties.

	Cluster 1 put-T2: Ad-NPY *n* = 19	**Cluster 2 put-T1: Ad-SOM *n* = 7**	**Cluster 3 put-T2: non-Ad-PV/SOM *n* = 9**	**Cluster 4 put-T2: Ad-VIP/CR *n* = 7**
(6) Rheobase (pA)	71.1 ± 33.1	45.7 ± 35.1	83.3 ± 63.6	24.3 ± 9.8
ANOVA: 0.001	>>>C4, >C2			<<<C1, C3
(7) First spike latency (ms)	340.0 ± 242.2	358.4 ± 225.0	276.8 ± 183.1	180.0 ± 89.4
ANOVA: N.S.				
(8) Adaptation (Hz/s)	3.5 ± 15.3	−5.7 ± 22.8	11.9 ± 110.0	−4.2 ± 13.1
ANOVA: N.S.				
(9) Minimal steady-state frequency (Hz)	6.8 ± 2.5	14.5 ± 10.2	16.9 ± 14.6	8.3 ± 2.7
ANOVA: N.S.				

n, number of cells; N.S., non-significant; <, <<, and <<<, inferior with $p \leq 0.05$, $p \leq 0.01$, and $p \leq 0.001$, respectively; >, >>, and >>>, superior with $p \leq 0.05$, $p \leq 0.01$, and $p \leq 0.001$, respectively; C1, cluster 1; C2, cluster 2; C3, cluster 3; C4, cluster 4.

Table 4 | Firing properties.

	Cluster 1 put-T2: Ad-NPY *n* = 19	**Cluster 2 put-T1: Ad-SOM *n* = 7**	**Cluster 3 put-T2: non-Ad-PV/SOM *n* = 9**	**Cluster 4 put-T2: Ad-VIP/CR *n* = 7**
(10) Amplitude accommodation (mV)	6.8 ± 5.2	0.7 ± 1.2	0.8 ± 1.2	1.7 ± 3.2
ANOVA: <0.001	<<<C2, C3, <<C4	>>>C1	>>>C1	>>C1
(11) Amplitude of late adaptation (Hz)	112.5 ± 32.3	54.4 ± 10.7	37.8 ± 11.7	42.7 ± 30.2
ANOVA: <0.001	>>>C2, C3, C4	<<<C1, <C3	<<<C1, >C2	<<<C1
(12) Time constant of late adaptation (ms)	20.2 ± 5.3	27.7 ± 9.9	16.9 ± 13.6	33.6 ± 28.7
ANOVA: N.S.	<C2, >C3	>C1, C3	<C1, C2	
(13) Maximal steady-state frequency (Hz)	84.6 ± 17.0	93.5 ± 35.8	164.9 ± 25.2	61.8 ± 12.9
ANOVA: <0.001	<<<C3, >>C4	<<C3	>>>C1, C4, >>C2	<<<C3, <<C1
(14) Late adaptation (Hz/s)	−27.4 ± 12.8	−22.1 ± 14.1	−31.4 ± 16.2	−13.5 ± 12.3
ANOVA: N.S.				

n, number of cells; N.S., non-significant; <, <<, and <<<, inferior with $p \leq 0.05$, $p \leq 0.01$, and $p \leq 0.001$, respectively; >, >>, and >>>, superior with $p \leq 0.05$, $p \leq 0.01$, and $p \leq 0.001$, respectively; C1, cluster 1; C2, cluster 2; C3, cluster 3; C4, cluster 4.

Table 5 | Action potential properties.

	Cluster 1 put-T2: Ad-NPY $n = 19$	Cluster 2 put-T1: Ad-SOM $n = 7$	Cluster 3 put-T2: non-Ad-PV/SOM $n = 9$	Cluster 4 put-T2: Ad-VIP/CR $n = 7$
(15) First spike amplitude (mV)	72.1 ± 7.2	69.3 ± 8.8	70.3 ± 5.8	78.0 ± 8.2
ANOVA: N.S.				
(16) First spike duration (ms)	1.0 ± 0.2	0.9 ± 0.2	0.6 ± 0.1	0.8 ± 0.1
ANOVA: <0.001	>>>C3	>>>C3	<<<C1, C2, C4	>>>C3
(17) First spike ADP (mV)	0.1 ± 0.4	0.0 ± 0.0	0.0 ± 0.0	1.8 ± 1.9
ANOVA: <0.001	<<C4	<<C4	<C4	>>C1, C3, >C2
(18) First spike AHP maximum (mV)	−21.3 ± 4.2	−22.9 ± 4.0	−25.5 ± 3.6	−16.2 ± 6.1
ANOVA: 0.007	>>C3	<C4	<<C1, C4	>>C3, >C2
(19) First spike ADP latency (ms)	0.8 ± 2.3	0.0 ± 0.0	0.0 ± 0.0	7.1 ± 5.2
ANOVA: <0.001	<<C4	<<C4	<C4	>>C1, C3, >C2
(20) First spike AHP max latency (ms)	12.9 ± 6.2	4.4 ± 4.0	2.1 ± 0.3	7.4 ± 11.2
ANOVA: <0.001	>>>C3, >>C2, >C4	>>>C3, <<C1	<<<C1, C2, C4	>>>C3, <C1
(21) Amplitude reduction (%)	0.9 ± 2.6	3.0 ± 9.8	−1.8 ± 5.5	4.0 ± 2.7
ANOVA: N.S.				
(22) Duration increase (%)	4.7 ± 2.8	4.4 ± 8.2	0.1 ± 3.0	6.6 ± 1.9
ANOVA: 0.004	>>C3		<<<C4, <<C1	>>>C3

n, number of cells; N.S., non-significant; <, <<, and <<<, inferior with $p \leq 0.05$, $p \leq 0.01$, and $p \leq 0.001$, respectively; >, >>, and >>>, superior with $p \leq 0.05$, $p \leq 0.01$, and $p \leq 0.001$, respectively; C1, cluster 1; C2, cluster 2; C3, cluster 3; C4, cluster 4.

the resulting aggregation dendrogram (**Figure 3A**), four groups of cells could be identified in our sample of nNOS transcribing neurons. These groups were designated as clusters 1, 2, 3, and 4 and represented 20, 5, 9, and 8 neurons, respectively. As outlined previously (see Materials and Methods), due to its iterative nature, Ward's method has the advantage that no assumptions are required regarding the number of groups into which observations should be classified. However, a drawback of this method is that miss-assigned cells are not corrected through the iterative process. So as to eliminate potential mistakes occurring, Ward's clusters were corrected using the K-means algorithm (see Materials and Methods, Karagiannis et al., 2009; McGarry et al., 2010; Perrenoud et al., 2012). Following correction, two cells of cluster 1 were reassigned to cluster 2, and one neuron of cluster 4 was reassigned to cluster 1 (**Figure 3B**). In order to determine whether the allocation of neurons into four groups based on these parameters was the optimal outcome of the clustering process, our results were compared with clustering trials whereby thresholds were set to define fewer or higher numbers of groups. After K-means correction, the mean silhouette value for cluster analysis yielding four groups was 0.3014 (see Materials and Methods; Karagiannis et al., 2009; McGarry et al., 2010; Perrenoud et al., 2012). By comparison, clusterings obtained after correction for three or five groups resulted in smaller mean silhouette values (0.2879 and 0.2023, respectively), indicating a loss of clustering quality. Thus, the subdivision of neurons into four groups was retained for further analysis. The neurons of clusters 1, 2, and 3 displayed adapting action potential discharges and were characterized by a high expression of NPY, SOM, and VIP/CR, respectively. These clusters were thus named adapting NPY (Adapt-NPY), adapting SOM (Adapt-SOM), and adapting VIP/CR (Adapt-VIP/CR). By contrast, cluster 4 neurons showed little adaptation of firing frequencies and expressed PV or SOM. Cluster 4 was thus termed non-adapting PV/SOM (non-Ad-PV/SOM).

IDENTIFICATION OF PUTATIVE TYPE I AND TYPE II CELLS WITHIN INTERNEURONS EXPRESSING nNOS mRNA

To determine whether identified clusters of cells expressing nNOS mRNA could correspond to type I or type II nNOS immunoreactivity, we examined the laminar distribution of nNOS neurons (**Figures 3C,D**) and their expression of the molecular markers PV, SOM, and VIP (**Figure 3E**). Particular attention was paid to the level of transcription of SOM as the expression of this marker was a distinctive feature of type I neurons at the protein level (**Figure 2C2**). As apparent in **Figure 3E**, SOM was present in 85.7% of the neurons in cluster 2 (Adapt-SOM), a proportion highly consistent with the level of expression of SOM in type I interneurons. The laminar distribution of neurons within cluster 2 (**Figure 3C**) also appeared to replicate the distribution of type I neurons as assessed by immunohistochemistry (**Figure 1B1**). The cumulated laminar distribution (**Figure 3D**) and levels of PV, SOM, and VIP expression for neurons in clusters 1, 3, and 4 (**Figure 3F**) also appeared to be in strong agreement with results obtained at the protein level for type II neurons (**Figures 1** and **2**). Consistent with the expression of PV and SOM in deep layer type II neurons (**Figures 2C2,D2**), these mRNAs were highly expressed in neurons within cluster 3 (non-Ad-PV/SOM) which were preferentially found in layer VI (**Figures 3D,E**). In addition, the expression of VIP in superficial type II neurons (**Figure 2E2**) corresponded reasonably well with the high levels of VIP expression (**Figure 3E**) and the preferential localization in layers II/III of cluster 4 neurons (Adapt-VIP/CR; **Figure 3D**). Thus, based on the striking agreement of our multiparametric results with the distribution and marker expression of type I and

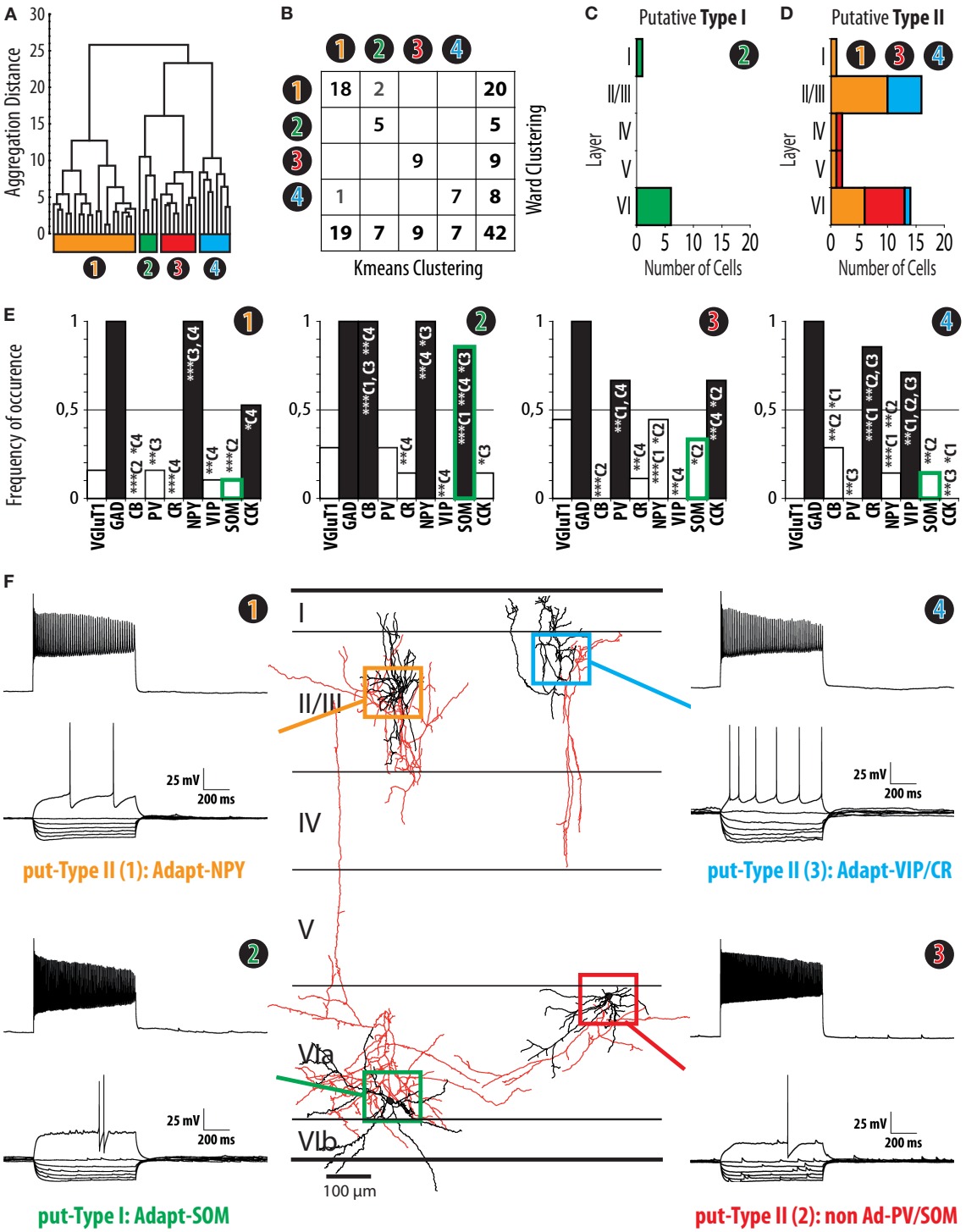

FIGURE 3 | Clustering of interneurons expressing nNOS mRNA. (A) Ward's clustering of 42 nNOS interneurons sampled from slices of the barrel cortex of juvenile (P14–P17) mice. Individual cells are represented along the *x*-axis. The *y*-axis represents the distance of aggregation in a space of 17 electrophysiological variables and 6 molecular markers. Four clusters, termed Adapt-NPY (cluster 1, yellow), Adapt-SOM (cluster 2, green), non-Ad-PV/SOM (cluster 3, red), and Adapt-VIP/CR (cluster 4, blue) were identified. **(B)** Table corresponding to Ward's clustering in **(A)** and a clustering output generated by the K-means algorithm with the same sample and parameters with non-overlapping components in gray font. Note that the clusters are mostly overlapping. **(C)** Laminar distribution of cluster 2. Note that the distribution is consistent with the distribution of type I nNOS immunolabeled neurons (**Figure 1**). **(D)** Cumulated laminar distribution of clusters 1 (yellow), 3 (red), and 4 (blue). Note that the distribution is consistent with the distribution of type II nNOS immunolabeled neurons (**Figure 1**). **(E)** Histograms of the

(Continued)

FIGURE 3 | Continued
expression of Vglut1, GAD, CB, PV, CR, NPY, VIP, SOM, and CCK in clusters 1, 2, 3, and 4. Note that the expression of SOM mRNA in cluster 2 closely resembles the profile of SOM expression in type I nNOS immunolabeled neurons (**Figure 2**) while this is not the case for other clusters (green contour on histogram bars; C1: cluster 1; C2 cluster 2; C3: cluster 3; C4: cluster 4; *, **, and *** indicate significant differences with $p \leq 0.05$, $p \leq 0.01$, and $p \leq 0.001$, respectively). **(F)** Representative examples of electrophysiological properties (left and right panels) and morphology (central panel) from neurons from clusters 1 (yellow, upper left), 2 (green, lower left), 3 (red, lower right), and 4 (blue, upper right). Electrophysiological traces correspond to voltage responses induced by current injections (bottom traces: −100 to 0 pA by increments of 10 pA and rheobase; top trace: last step of current before saturation). For the morphological reconstructions of corresponding neurons, somatodendritic trees are illustrated in black, axons in red. Neurons are represented at their respective laminar positions.

Table 6 | Soma under infrared microscopy.

	Cluster 1 put-T2: Ad-NPY $n = 18$	**Cluster 2 put-T1: Ad-SOM $n = 6$**	**Cluster 3 put-T2: non-Ad-PV/SOM $n = 9$**	**Cluster 4 put-T2: Ad-VIP/CR $n = 7$**
(1) Area (μm^2)	125.6 ± 31.8	151.4 ± 27.8	170.2 ± 52.8	131.5 ± 28.5
ANOVA: N.S.				
(2) Perimeter (μm)	42.0 ± 5.6	45.6 ± 5.1	49.5 ± 9.4	47.9 ± 9.6
ANOVA: N.S.				
(3) Maximal diameter (μm)	15.3 ± 2.4	16.3 ± 1.9	17.8 ± 4.1	19.6 ± 5.0
ANOVA: N.S.				
(4) Minimal diameter (μm)	10.3 ± 1.5	11.7 ± 1.3	12.0 ± 1.6	9.1 ± 0.9
ANOVA: 0.002	<C2, C3	>>C4, >C1	>>C4, >C1	<<C2, C3
(5) Elongation	1.5 ± 0.3	1.4 ± 0.2	1.5 ± 0.3	2.2 ± 0.6
ANOVA: 0.038	<C4	<C4	<C4	>C1, C2, C3

n, number of cells; N.S., non-significant; <, <<, and <<<, inferior with $p \leq 0.05$, $p \leq 0.01$, and $p \leq 0.001$, respectively; >, >>, and >>>, superior with $p \leq 0.05$, $p \leq 0.01$, and $p \leq 0.001$, respectively; C1, cluster 1; C2, cluster 2; C3, cluster 3; C4, cluster 4.

Table 7 | Local metric of dendrites.

	Cluster 1 put-T2: Ad-NPY $n = 11$	**Cluster 2 put-T1: Ad-SOM $n = 6$**	**Cluster 3 put-T2: non-Ad-PV/SOM $n = 8$**	**Cluster 4 put-T2: Ad-VIP/CR $n = 4$**
(6) Number of primary dendrites	8.0 ± 1.9	5.0 ± 1.9	6.4 ± 1.4	3.3 ± 1.5
ANOVA: 0.003	>>C4, >C2	<C1	>C4	<<C1, <C3
(7) Total dentritic length (μm)	2073.0 ± 1063.2	2127.8 ± 1066.0	2101.9 ± 825.6	2298.8 ± 1016.2
ANOVA: N.S.				
(8) Length of segments (average; μm)	28.2 ± 9.7	51.0 ± 16.4	47.9 ± 12.9	44.9 ± 16.0
ANOVA: 0.005	<<C2, C3, <C4	>>C1	>>C1	>C1
(9) Length/surface	0.97 ± 0.18	0.82 ± 0.38	0.80 ± 0.23	0.96 ± 0.26
ANOVA: N.S.				
(10) Dendritic segments tortuosity (average)	1.18 ± 0.03	1.19 ± 0.06	1.18 ± 0.05	1.22 ± 0.07
ANOVA: N.S.				
(11) Number of nodes	31.6 ± 11.5	18.5 ± 10.6	18.8 ± 6.0	27.5 ± 17.9
ANOVA: N.S.				
(12) Fractal index	1.11 ± 0.04	1.08 ± 0.03	1.08 ± 0.03	1.11 ± 0.05
ANOVA: N.S.				

n, number of cells; N.S., non-significant; <, <<, and <<<, inferior with $p \leq 0.05$, $p \leq 0.01$, and $p \leq 0.001$, respectively; >, >>, and >>>, superior with $p \leq 0.05$, $p \leq 0.01$, and $p \leq 0.001$, respectively; C1, cluster 1; C2, cluster 2; C3, cluster 3; C4, cluster 4.

type II nNOS-expressing neurons, cluster 2 cells were identified as putative type I interneurons, while neurons within clusters 1, 3, and 4 were identified as putative type II cells. To further investigate this hypothesis, we next undertook a multiparametric characterization of putative type I and type II nNOS-expressing neurons.

MULTIPARAMETRIC CHARACTERISTICS OF PUTATIVE TYPE I INTERNEURONS

Putative type I neurons belonging to the Adapt-SOM cluster ($n = 7$) displayed distinctive properties. Electrophysiological data showed that putative type I neurons were characterized by medium to high input resistances and significantly higher membrane time

Table 8 | Spatial distribution of the dendritic arbor.

	Cluster 1 put-T2: Ad-NPY $n = 11$	Cluster 2 put-T1: Ad-SOM $n = 6$	Cluster 3 put-T2: non-Ad-PV/SOM $n = 8$	Cluster 4 put-T2: Ad-VIP/CR $n = 4$
(13) Dendritic Sholl (0–100 μm; %)	85.1 ± 19.6	56.1 ± 17.2	59.3 ± 12.1	54.4 ± 23.9
ANOVA: 0,01	>>C3, >C2, C4	>C1	>>C1	>C1
(14) Dendritic Sholl (100–200 μm; %)	12.4 ± 13.2	32.9 ± 10.0	32.5 ± 9.1	32.6 ± 12.2
ANOVA: 0.008	<<C2, C3, <C4	>>C1	>>C1	>C1
(15) Dendritic Sholl (200–300 μm; %)	2.2 ± 7.3	10.4 ± 10.3	7.9 ± 7.3	11.2 ± 13.8
ANOVA: 0.025	<<C3, <C2	>C1		
(16) Dendritic Sholl (>300 μm; %)	0.2 ± 0.7	0.6 ± 1.4	0.3 ± 0.7	1.7 ± 3.5
ANOVA: N.S.				
(17) Vertical extent (%)	40.8 ± 13.6	42.9 ± 22.6	43.9 ± 20.2	60.3 ± 28.0
ANOVA: N.S.				
(18) Horizontal extent (%)	30.6 ± 13.2	31.6 ± 15.5	29.2 ± 14.5	19.6 ± 19.6
ANOVA: N.S.				

n, number of cells; N.S., non-significant; <, <<, and <<<, inferior with $p \leq 0.05$, $p \leq 0.01$, and $p \leq 0.001$, respectively; >, >>, and >>>, superior with $p \leq 0.05$, $p \leq 0.01$, and $p \leq 0.001$, respectively; C1, cluster 1; C2, cluster 2; C3, cluster 3; C4, cluster 4.

constants than the neurons of other clusters (**Table 2**). They displayed a marked adaptation of frequency at threshold (**Table 3**) and saturation (**Table 4**) and fired long duration spikes followed by fast AHPs (**Table 5**; **Figure 3F**). Alongside their previously mentioned high expression of SOM, putative type I neurons displayed significantly higher levels of CB (100%) and NPY (100%) than neurons in other clusters (**Figure 3E**). Putative type I neurons typically displayed large somata (**Table 6**), exhibiting an average of five primary dendrites (**Table 7**), which ramified to form a wide dendritic arbor extending up to 300 μm away from the cell body (**Table 8**). The axon of two putative type I cells could be reconstructed to a length in excess of 1 mm and appeared to ramify extensively within the layer of origin (illustrated in **Figure 3F**). Finally, concurring with immunohistochemical results, putative type I neurons were principally sampled in layer VI (six of seven neurons) but also occurred in layer II/III (one of seven neurons; **Figure 3D**).

MULTIPARAMETRIC CHARACTERISTICS OF PUTATIVE TYPE II INTERNEURONS

Our results suggest that type II neurons comprise three populations of neurons, each with distinct characteristics: Adapt-NPY (cluster 1), non-Ad-PV/SOM (cluster 3), and Adapt-VIP/CR (cluster 4). Adapt-NPY neurons ($n = 19$) populated all neocortical layers but were most abundant in layers II/III and VI (**Figure 3D**). Electrophysiological data showed that Adapt-NPY were characterized by medium range input resistances (**Table 2**). Their action potential discharges were accelerating at threshold (**Table 3**), adapting at saturation and displayed a significantly larger accommodation of spike amplitude than for neurons in other clusters (**Table 4**). Adapt-NPY neurons displayed long duration action potential spikes and were characterized by significantly slower AHP duration than other neurons (**Table 5**). Interestingly, Adapt-NPY neurons did not show a notable expression of calcium binding proteins such as PV, CB, or CR (**Figure 3E**). Alongside NPY (100%), they mostly expressed CCK (52.6%). Finally, Adapt-NPY neurons showed a highly distinctive morphological profile. They had small somata (**Table 6**) and exhibited a significantly higher number of primary dendrites than other neurons (**Table 7**). Their dendrites ramified extensively (**Table 7**) and tended to stay confined within a radius of 200 μm around the soma (**Table 8**). The axons of three cells could be reconstructed extending in excess of 1 mm and also appeared to ramify extensively around the cell body. These characteristics suggest that Adapt-NPY very likely correspond to neurogliaform cells (Kawaguchi, 1995).

Non-Ad-PV/SOM neurons ($n = 9$) were principally sampled in layer VI (seven of nine neurons) and displayed the most distinctive electrophysiological characteristic of our sample. They had depolarized membrane potentials and short time constants (**Table 2**). They showed little or no adaptation at threshold (**Table 3**), fired at a significantly higher maximal rate (**Table 4**), with significantly faster spike durations and AHP dynamics than other neurons (**Table 5**). Non-Ad-PV/SOM expressed either PV (66.7%) or SOM (33.3%) but never co-expressed both markers. They were also characterized by a high occurrence of CCK expression (66.7%). Finally, on a morphological basis, non-Ad-PV/SOM neurons appeared as multipolar cells with large somata. The axon of one non-Ad-PV/SOM was reconstructed extending in excess of 1 mm from the soma and appeared to ramify within its layer of origin (**Figure 3F**).

Adapt-VIP/CR neurons ($n = 7$) appeared to concentrate preferentially in superficial layers (**Figure 3D**). They were characterized by high input resistances (**Table 2**), low rheobases, adapting discharges at threshold (**Table 3**) and saturation, and fired at significantly lower maximal frequencies than other neurons (**Table 4**). Some of them displayed double AHPs (**Table 5**). They mostly expressed CR (85.7%) and VIP (71.4%; **Figure 3E**). On a morphological basis, they appeared as fusiform neurons, having significantly higher soma aspect ratio than other neurons (**Table 6**). Most of them were of bipolar morphology resulting in a significantly lower number of dendrites than other cells (**Table 7**). The axon of one Adapt-VIP/CR was reconstructed in excess of 1 mm and appeared to be descending (**Figure 3F**).

EMBRYONIC ORIGIN OF TYPE I AND TYPE II nNOS-EXPRESSING INTERNEURONS

Most neocortical interneurons originate in the embryonic subpallium (Wonders and Anderson, 2006). This region is subdivided into several progenitor domains each giving rise to specific populations of interneurons (Gelman and Marin, 2010). In order to complement the characterization of nNOS-expressing interneurons, we attempted to obtain insight about their embryonic origins. To achieve this goal, we performed nNOS immunostaining in two transgenic mouse lines where specific and non-overlapping regions of the subpallium are labeled with fluorescent proteins (Flames et al., 2007; Fogarty et al., 2007; Lee et al., 2010; Vucurovic et al., 2010; Vitalis and Rossier, 2011): Lhx6-Cre/R26R-YFP mice (**Figure 4A**) where fluorescence is found in neurons originating from the MGE and 5-HT_{3A}:GFP mice (**Figure 4B**) where labeled neurons originate in the CGE, and in the AEP/PO. Nearly all type I neurons ($98.6 \pm 2.5\%$) expressed GFP in Lhx6-Cre/R26R-YFP (**Figure 4C1**) indicating that all originate in the MGE. Accordingly type I neurons never expressed GFP in 5-HT_{3A}:GFP mice (**Figure 4D1**). By contrast $63.0 \pm 6.8\%$ of type II neurons expressed GFP in Lhx6-Cre/R26R-YFP mice while $34.4 \pm 0.9\%$ were labeled in 5-HT_{3A}:GFP mice (**Figures 4C2,D2**). This indicated that type II neurons comprise neurons originating both in the CGE-AEP/PO and the MGE, reinforcing the idea that they form a heterogeneous population. Interestingly, GFP-expressing type II neurons appeared to accumulate in deeper layers in Lhx6-Cre/R26R-YFP mice while they accumulated in upper neocortical layers in 5-HT_{3A}:GFP.

DISCUSSION

In this study, we characterized neocortical nitrergic neurons using a multi-disciplinary approach combining immunohistochemical labeling of nNOS-expressing neurons and multiparametric analysis of nNOS transcribing neurons in acute slices of mouse somatosensory barrel cortex. We found that type I cells constitute a relatively homogeneous population of interneurons originating from MGE as a specific embryonic territory. In contrast, type II cells are divided into three interneuron subtypes originating from the MGE as well as the CGE-AEP/PO.

CHARACTERIZATION OF NEOCORTICAL NITRERGIC INTERNEURONS

In the neocortex, as is apparent using immunohistochemistry or NADPH diaphorase immunoreactivity, nNOS concentrates in a sparse population of GABAergic neurons which subdivide in two subtypes: heavily labeled type I cells and lightly labeled type II cells (Yan et al., 1996; Yan and Garey, 1997; Smiley et al., 2000; Lee and Jeon, 2005). However, these nitrergic neurons remain poorly characterized (Kilduff et al., 2011). Although the molecular identity of types I nitrergic neurons has been well investigated in primate and rodents (Estrada and Defelipe, 1998), very few studies have characterized the expression of markers of interneurons in type II cells (Kubota et al., 2011). In addition, due to their paucity, electrophysiological recordings of nitrergic interneurons have rarely been achieved in brain slices (Cauli et al., 2004; Karagiannis et al., 2009). Therefore, our understanding of the neocortical mechanisms underlying NO release as a response to neuronal activity remains elusive.

In this study, the properties of type I and type II neocortical nitrergic interneurons were extensively characterized in the barrel cortex of juvenile (P14–17) mouse. Firstly, using nNOS immunohistochemistry in GAD67:GFP knock-in mice (Tamamaki et al., 2003), we described the laminar distribution of type I and type II nitrergic interneurons. Using double labeling immunohistochemistry, the molecular properties of the two classes of neurons was investigated by assessing their expression of PV, SOM, and VIP which constitute non-overlapping markers whose expression is restricted to specific interneuron populations (Kubota et al., 1994, 2011; Gonchar and Burkhalter, 1997; Gonchar et al., 2007; Xu et al., 2010). Secondly, we analyzed the properties of 42 interneurons expressing nNOS mRNA and characterized with patch-clamp recordings combined with biocytin labeling and scRT-PCR. This sample of cells was extracted from a dataset of more than 300 interneurons harvested in all layers of the barrel cortex (20 of the cells used in this study were also used in a previous report; Perrenoud et al., 2012). Unsupervised cluster analysis (see Materials and Methods and Perrenoud et al., 2012), disclosed four groups of nitrergic neurons exhibiting distinct electrophysiological, molecular, and morphological properties. Interestingly, by analyzing the laminar distribution and the molecular markers transcribed in these groups, each could be putatively related to type I or type II immunoreactivity. Finally, we provided insights into the embryonic origin of type I and type II nitrergic interneurons by using immunohistochemistry on two mouse strains (Lhx6-Cre/R26R-YFP and 5-HT_{3A}:GFP) in which interneurons originating from specific regions of the embryonic subpallium are identified by GFP fluorescence (Du et al., 2008; Lee et al., 2010; Vucurovic et al., 2010).

Together these data provide a comprehensive characterization of neocortical nitrergic neurons. As detailed in the following section, the results generated using different approaches in this study were strikingly coherent and resulted in a consistent picture of the properties of type I and type II nNOS-expressing cells. Thus, we are confident that our results constitute an accurate description of the properties of nitrergic neurons in the barrel cortex of juvenile mouse.

TYPE I INTERNEURONS ARE SOM-EXPRESSING CELLS ORIGINATING FROM THE MGE

Type I nitrergic neurons are the object of considerable attention because of their unique properties. Firstly, though they are GABAergic (Valtschanoff et al., 1993), they differ from other neocortical inhibitory neurons in that they send long distance horizontal projections to remote neocortical areas (Tomioka et al., 2005; Higo et al., 2007, 2009; Tomioka and Rockland, 2007). Thus, although they constitute a subset of the so-called "neocortical interneurons," type I nitrergic cells are not interneurons *per se*. Interestingly, it has also been recently demonstrated that type I neurons are specifically activated during a long period of slow wave sleep obtained after sleep deprivation (Gerashchenko et al., 2008; Kilduff et al., 2011).

Our study confirms and significantly improves current descriptions of type I nitrergic neocortical neurons. As reported in other studies, type I interneurons displayed intense nNOS immunoreactivities (Yan et al., 1996; Yan and Garey, 1997; Smiley et al., 2000;

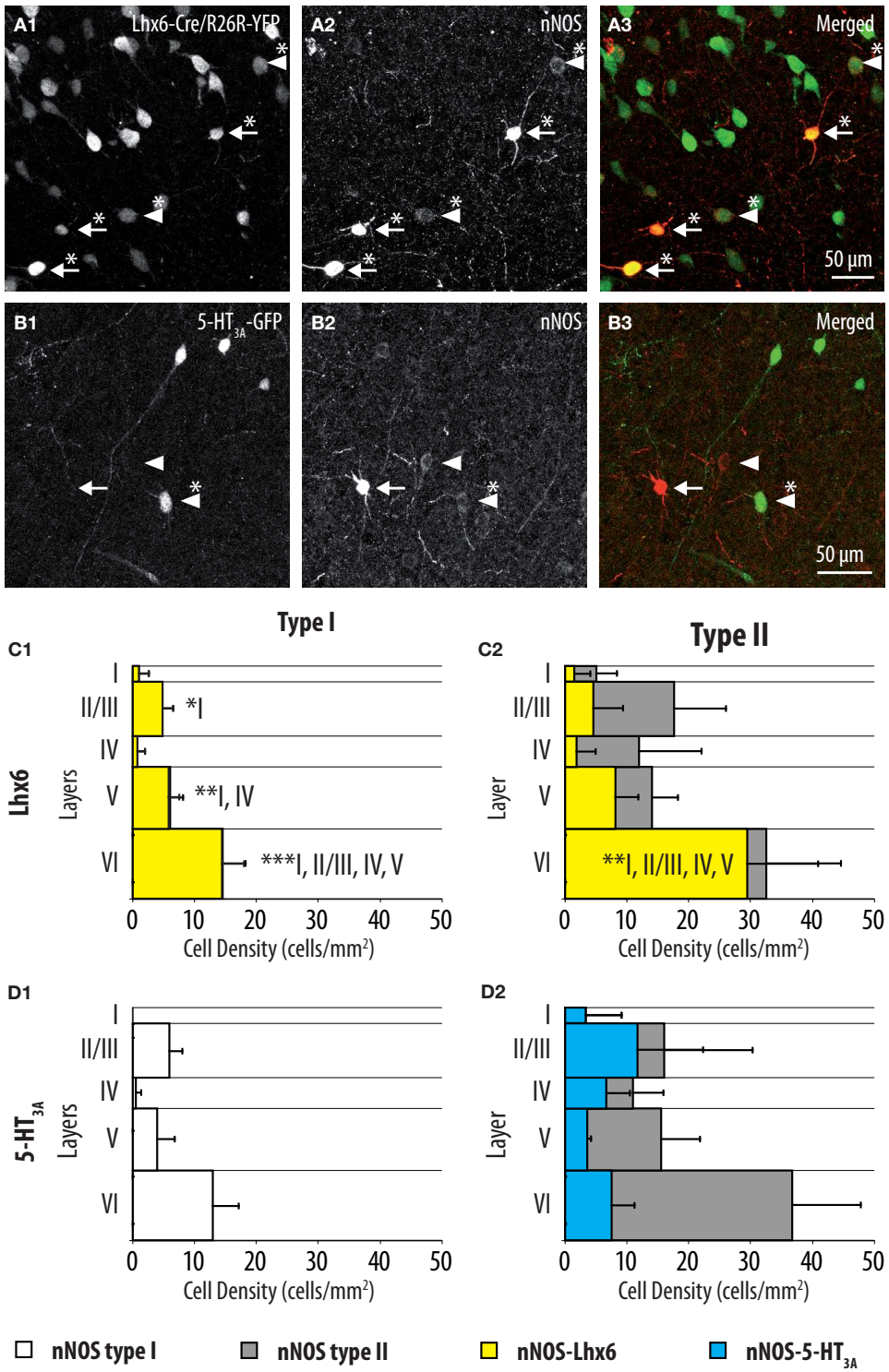

FIGURE 4 | Distributions of GFP-expressing cells among type I and type II nNOS immunolabeled neurons in Lhx6-Cre/R26R-YFP and 5-HT$_{3A}$:GFP mice. (A) Colocalization of GFP **(1)** with nNOS immunolabeling **(2)** in Lhx6-Cre/R26R-YFP. **(B)** Colocalization of GFP **(1)** with nNOS immunolabeling **(2)** in 5-HT$_{3A}$:GFP mice. Arrows point to examples of type I (heavily labeled) nNOS-expressing neurons, arrowheads point to examples of type II nNOS (weakly labeled) expressing neurons. Double-labeled cells are marked by an asterisk. **(C)** Histograms reflecting the density of GFP-expressing type I **(1)** and type II **(2)** nNOS immunolabeled cells in cortical layer I–VI of Lhx6-Cre/R26R-YFP mice (yellow). **(D)** Histograms reflecting the density of GFP-expressing type I **(1)** and type II **(2)** nNOS immunolabeled cells in cortical layer I–VI of 5-HT$_{3A}$:GFP mice (blue). In **(C)** and **(D)** the densities of nNOS type I (white) and nNOS type II (gray) neurons are superimposed ($n = 3$ mice; error bars: standard deviation; *, **, and *** indicate significant differences with $p \leq 0.05$, $p \leq 0.01$, and $p \leq 0.001$, respectively; roman numerals refer to neocortical layers).

Lee and Jeon, 2005) and preferentially populated layer VI and V (Vercelli et al., 2000; Wiencken and Casagrande, 2000; Garbossa et al., 2001; Lee and Jeon, 2005). By comparison, they were less frequent in layer II/III and relatively infrequent in layers I and IV. Combined immunofluorescent labeling revealed that type I interneurons predominantly expressed SOM, confirming that they constitute a subset of SOM-expressing interneurons (Kubota et al., 1994, 2011; Smiley et al., 2000; Karagiannis et al., 2009). However, although rarely, PV immunoreactivity was detected in some type I cells, as reported in the mouse visual cortex (Lee and Jeon, 2005).

The electrophysiological properties of type I cells have been largely neglected due to the scarcity of these cells in the cortex (Kilduff et al., 2011). Here we performed unsupervised cluster analysis on a sample of interneurons expressing nNOS mRNA, disclosing a cluster of cells (Adapt-SOM) that likely correspond to type I interneurons. Indeed, these neurons were mainly recorded in deep layers and co-expressed SOM and NPY mRNAs well-matching with the features of type I cells (Kubota et al., 1994, 2011; Karagiannis et al., 2009). Putative type I cells displayed adapting discharges, fired long duration action potential spikes followed by fast AHPs and had significantly slower membrane time constant than other interneurons (**Table 2**). Type I cells had large somas (**Table 6**) and displayed an average of five primary dendrites (**Table 7**) which ramified into a wide arbor (**Table 8**). The axon of one putative type I cell could be satisfactorily reconstructed and appeared to ramify extensively within its layer of origin (**Figure 3**).

Finally, our study is, to our knowledge, the first attempt to provide indications about the embryonic origin of type I neurons. We found that all type I neurons were GFP labeled in Lhx6-Cre/R26R-YFP mice. As Lhx6 is a distinctive marker of the neurons originating from the MGE (Fogarty et al., 2007; Du et al., 2008), our results strongly suggest that type I neurons originate in this embryonic region. In agreement, we found that no type I nitrergic neurons expressed GFP in a 5-HT_{3A}:GFP strain where fluorescence is found in neurons originating from the adjacent CGE and AEP/PO (Lee et al., 2010; Vucurovic et al., 2010). This finding is also in strong agreement with the notion that type I neurons constitute a subset of SOM-expressing GABAergic interneurons, since most originate in the MGE (Butt et al., 2005; Xu et al., 2005; Miyoshi et al., 2007; Wonders et al., 2008).

The features of type I interneurons appear well conserved across mammalian species (Yan and Garey, 1997; Franca et al., 2000). The morphology and the laminar distribution of type I neurons is consistent in rat (Gabbott and Bacon, 1995; Gabbott et al., 1997; Kubota et al., 2011), mouse (Lee and Jeon, 2005; present study), rabbit (Lee and Jeon, 2005), cat (Higo et al., 2007), monkey (Sandell, 1986; Smiley et al., 2000), and human (Judas et al., 1999). Similarly, SOM expression is a signature of type I nitrergic cells in rat (Vruwink et al., 2001; Kubota et al., 2011), monkey (Smiley et al., 2000), and human (Judas et al., 1999). Interestingly, type I nitrergic neurons also occur in substantial numbers in the subcortical white matter (Franca et al., 2000; Clancy et al., 2001). Thus, type I nitrergic neurons seem to be a ubiquitous and conserved feature of the mammalian cerebral cortex.

The consistent and comprehensive description of the properties of type I nitrergic cells provided in this study might prove useful to study the function of these neurons in the future. However, one should keep in mind that the features of type I neurons reported here might vary according to experimental conditions. Firstly, in rodents and primates, variations in neuronal density (Franca et al., 2000) and morphology (Freire et al., 2012) of type I neurons can occur between neocortical areas. Secondly, the features of type I neurons seem to be subjected to inter-species variations. For instance, type I cells do not express CB in rat (Gabbott et al., 1997) and human (Judas et al., 1999), while they express this marker in rabbit and mouse (Lee and Jeon, 2005; present study). More importantly, the modest expression of PV in type I cells which occurs in mouse (Lee and Jeon, 2005; present study) contrasts with data obtained in rat (Gabbott et al., 1997; Vruwink et al., 2001; Kubota et al., 2011), monkey (Smiley et al., 2000), and human (Judas et al., 1999) where type I cells only express SOM. This can give the impression that type I interneurons form two distinct classes in mouse. However, in our multiparametric analysis, the properties of PV expressing putative type I neurons were consistent with those of the other neurons of this cluster. Thus, we suggest that PV expression in mouse type I neurons is more likely to reflect intra-class variability. Further studies will be needed to explore whether variations in the properties of type I neurons translate functionally.

TYPE II INTERNEURONS REPRESENT A HETEROGENEOUS GROUP OF CELLS

Type II cells have initially been described in the neocortex of many mammalian species especially in primate and human neocortex (Aoki et al., 1993; Hashikawa et al., 1994; Yan et al., 1996). Although early studies failed to detect type II neurons in rodents (Gabbott and Bacon, 1995; Yan and Garey, 1997; Oermann et al., 1999) recent reports have evidenced that they were also present in these species (Freire et al., 2005; Lee and Jeon, 2005). Studies have illustrated the functional importance of this class in the modulation of the vascular tone (Cauli et al., 2004). However, because of the difficulties of visualizing type II interneurons, the characterization of these cells has been neglected.

In this study, we characterized type II cells in the somatosensory cortex of mouse. With double immunolabeling, we found that a significant proportion of these cells were immunoreactive either for PV, SOM, or VIP. PV has previously been observed in some faintly stained nNOS-expressing cells in rat (Kubota et al., 2011). However, to our knowledge this is the first report of expression of SOM and VIP in type II nitrergic interneurons. Interestingly, PV and SOM immunoreactive type II cells were preferentially aggregated in deep neocortical layers while VIP immunoreactive type II neurons accumulated in layer II/III. Since PV, SOM, and VIP reportedly never co-express in the cortex of mouse (Xu et al., 2010), and their expression did not sum to the total density of type II nitrergic cells, our data also indicated that a substantial part of type II neurons do not express either of these markers. Therefore, our immunological data strongly suggested that in the barrel cortex of mouse, type II interneurons corresponded to a heterogeneous population comprised of distinct subgroups exhibiting particular laminar preferences.

Agreeing with this hypothesis, our multiparametric analysis disclosed three groups of cells that putatively corresponded to type II cells. The laminar distributions and the expression of

PV, SOM, and VIP mRNAs of these three clusters appeared in strong agreement with results obtained at the protein level for type II neurons. The most prominent group; Adapt-NPY ($n = 19$) populated all layers and corresponded to small, neurogliaform-like interneurons which did not express PV, SOM, or VIP. Our data are thus consistent with previous findings indicating that neurogliaform cells constitute the main subset of type II cells (Karagiannis et al., 2009; Kubota et al., 2011). Consistent with immunohistochemical data, the two other groups corresponded to non-adapting neurons accumulating in deep layers and expressing PV or SOM (non-Ad-PV/SOM; $n = 9$), and to adapting bipolar neurons expressing VIP and CR, which were preferentially found in layer II/III (Adapt-VIP/CR; $n = 7$).

The relevance of these three groups of type II neurons was further strengthened by our developmental study. Consistent with the known origin of VIP/CR neurons in the CGE (Butt et al., 2005; Lee et al., 2010; Vucurovic et al., 2010), our data indicate that type II cells preferentially express the CGE-AEP/PO specific marker 5-HT_{3A} in superficial layers. Conversely, in deep layers, type II neurons preferentially expressed Lhx6, consistent with the notion that PV and SOM-expressing neurons originate in the MGE (Butt et al., 2005; Xu et al., 2005; Miyoshi et al., 2007; Wonders et al., 2008). Finally, our data are consistent with the finding that neurogliaform cells can arise both in the MGE (Butt et al., 2005) and in the CGE (Lee et al., 2010; Vucurovic et al., 2010).

Thus, our study strongly suggests that type II neurons constitute a heterogeneous population of interneurons comprised of three classes: neurogliaforms expressing NPY, deep layers non-adapting cells expressing PV, or SOM and superficial bipolar cells expressing VIP/CR. Because of the consistency of our results, we are confident that the strategies employed here successfully disclosed the diversity of type II nitrergic interneurons in the neocortex of juvenile mouse. However, our data regarding type II interneurons display inconsistencies with data obtained in other cortical areas and animal models. Firstly, while we report that the densities of type I and type II cells are approximately equal in layer VI, another study performed in the visual cortex of mouse and rabbit found that type II cells were half as concentrated as type I cells in this layer (Lee and Jeon, 2005). Secondly, two previous studies performed in rat did not identify type II nitrergic interneurons expressing VIP or SOM at the histochemical level (Kubota et al., 2011) or in a similar multiparametric sample of interneurons (Karagiannis et al., 2009). Our finding regarding type II cells highlights further discrepancies with data obtained in primates. Indeed, we found that type II were about twofold more numerous than type I cells and populated all neocortical layers. By contrast, type II cells appeared about 20-fold more abundant than type I cells and exclusively located in supragranular layers in monkey (Yan et al., 1996; Yan and Garey, 1997; Smiley et al., 2000) and human (Judas et al., 1999). The molecular signature of type II cells also varies markedly in primates where they are characterized by the expression of CB but never express SOM or NPY (Smiley et al., 2000). Thus, this raises the intriguing possibility that type II cells might correspond to distinct cell types in different species.

CONCLUSION

In the CNS, NO modulates a wealth of functions ranging from synaptic plasticity and neuronal excitability to blood perfusion (Garthwaite, 2008). Among the three isoforms of NO synthase, nNOS is specifically expressed in neurons and thus provides a specific substrate enabling NO signaling to integrate changes of neuronal activity (Zhou and Zhu, 2009). The present study provides a comprehensive characterization of the properties of nNOS-expressing neurons in the barrel cortex of juvenile mouse. Our results indicate that nNOS is expressed in several classes of interneurons. These groups are likely to be differentially recruited by oncoming signals underlying specific epochs of neocortical processing (Burkhalter, 2008). Thus, our study indicates that NO signaling is coupled, in a complex manner, to a wide array of processes performed in the neocortical network.

ACKNOWLEDGMENTS

This work was supported by ESPCI ParisTech, CNRS, and INSERM. Research in Nicoletta Kessaris's laboratory is supported by the European Research Council (Grant 207807). We warmly thank Dr. Elisa L. Hill for her help with the writing of the manuscript, as well as Bastien Fournié for his precious help in the project.

REFERENCES

Aoki, C., Fenstemaker, S., Lubin, M., and Go, C. G. (1993). Nitric oxide synthase in the visual cortex of monocular monkeys as revealed by light and electron microscopic immunocytochemistry. *Brain Res.* 620, 97–113.

Ascoli, G. A., Alonso-Nanclares, L., Anderson, S. A., Barrionuevo, G., Benavides-Piccione, R., Burkhalter, A., Buzsáki, G., Cauli, B., Defelipe, J., Fairén, A., Feldmeyer, D., Fishell, G., Fregnac, Y., Freund, T. F., Gardner, D., Gardner, E. P., Goldberg, J. H., Helmstaedter, M., Hestrin, S., Karube, F., Kisvárday, Z. F., Lambolez, B., Lewis, D. A., Marin, O., Markram, H., Muñoz, A., Packer, A., Petersen, C. C., Rockland, K. S., Rossier, J., Rudy, B., Somogyi, P., Staiger, J. F., Tamas, G., Thomson, A. M., Toledo-Rodriguez, M., Wang, Y., West, D. C., and Yuste, R. (2008). Petilla terminology: nomenclature of features of GABAergic interneurons of the cerebral cortex. *Nat. Rev. Neurosci.* 9, 557–568.

Bureau, I., von Saint, P. F., and Svoboda, K. (2006). Interdigitated paralemniscal and lemniscal pathways in the mouse barrel cortex. *PLoS Biol.* 4, e382. doi:10.1371/journal.pbio.0040382

Burkhalter, A. (2008). Many specialists for suppressing cortical excitation. *Front. Neurosci.* 2:2. doi:10.3389/neuro.01.026.2008

Butt, S. J., Fuccillo, M., Nery, S., Noctor, S., Kriegstein, A., Corbin, J. G., and Fishell, G. (2005). The temporal and spatial origins of cortical interneurons predict their physiological subtype. *Neuron* 48, 591–604.

Cauli, B., Audinat, E., Lambolez, B., Angulo, M. C., Ropert, N., Tsuzuki, K., Hestrin, S., and Rossier, J. (1997). Molecular and physiological diversity of cortical nonpyramidal cells. *J. Neurosci.* 17, 3894–3906.

Cauli, B., Porter, J. T., Tsuzuki, K., Lambolez, B., Rossier, J., Quenet, B., and Audinat, E. (2000). Classification of fusiform neocortical interneurons based on unsupervised clustering. *Proc. Natl. Acad. Sci. U.S.A.* 97, 6144–6149.

Cauli, B., Tong, X. K., Rancillac, A., Serluca, N., Lambolez, B., Rossier, J., and Hamel, E. (2004). Cortical GABA interneurons in neurovascular coupling: relays for subcortical vasoactive pathways. *J. Neurosci.* 24, 8940–8949.

Clancy, B., Silva-Filho, M., and Friedlander, M. J. (2001). Structure and projections of white matter neurons in the postnatal rat visual cortex. *J. Comp. Neurol.* 434, 233–252.

Dawson, T. M., Bredt, D. S., Fotuhi, M., Hwang, P. M., and Snyder, S. H. (1991). Nitric oxide synthase and neuronal NADPH diaphorase are identical in brain and peripheral tissues. *Proc. Natl. Acad. Sci. U.S.A.* 88, 7797–7801.

Dawson, V. L., and Dawson, T. M. (1998). Nitric oxide in neurodegeneration. *Prog. Brain Res.* 118, 215–229.

Douketis, C., Wang, Z., Haslett, T. L., and Moskovits, M. (1995). Fractal character of cold-deposited silver films determined by low-temperature scanning tunneling microscopy. *Phys. Rev. B Condens. Matter* 51, 11022–11031.

Du, T., Xu, Q., Ocbina, P. J., and Anderson, S. A. (2008). NKX2.1 specifies cortical interneuron fate by activating Lhx6. *Development* 135, 1559–1567.

Dumitriu, D., Cossart, R., Huang, J., and Yuste, R. (2007). Correlation between axonal morphologies and synaptic input kinetics of interneurons from mouse visual cortex. *Cereb. Cortex* 17, 81–91.

Estrada, C., and Defelipe, J. (1998). Nitric oxide-producing neurons in the neocortex: morphological and functional relationship with intraparenchymal microvasculature. *Cereb. Cortex* 8, 193–203.

Flames, N., Pla, R., Gelman, D. M., Rubenstein, J. L., Puelles, L., and Marin, O. (2007). Delineation of multiple subpallial progenitor domains by the combinatorial expression of transcriptional codes. *J. Neurosci.* 27, 9682–9695.

Fogarty, M., Grist, M., Gelman, D., Marin, O., Pachnis, V., and Kessaris, N. (2007). Spatial genetic patterning of the embryonic neuroepithelium generates GABAergic interneuron diversity in the adult cortex. *J. Neurosci.* 27, 10935–10946.

Franca, J. G., Volchan, E., Jain, N., Catania, K. C., Oliveira, R. L., Hess, F. F., Jablonka, M., Rocha-Miranda, C. E., and Kaas, J. H. (2000). Distribution of NADPH-diaphorase cells in visual and somatosensory cortex in four mammalian species. *Brain Res.* 864, 163–175.

Freire, M. A., Faber, J., Picanco-Diniz, C. W., Franca, J. G., and Pereira, A. (2012). Morphometric variability of nicotinamide adenine dinucleotide phosphate diaphorase neurons in the primary sensory areas of the rat. *Neuroscience* 205, 140–153.

Freire, M. A., Franca, J. G., Picanco-Diniz, C. W., and Pereira, A. Jr. (2005). Neuropil reactivity, distribution and morphology of NADPH diaphorase type I neurons in the barrel cortex of the adult mouse. *J. Chem. Neuroanat.* 30, 71–81.

Gabbott, P. L., and Bacon, S. J. (1995). Co-localisation of NADPH diaphorase activity and GABA immunoreactivity in local circuit neurones in the medial prefrontal cortex (mPFC) of the rat. *Brain Res.* 699, 321–328.

Gabbott, P. L., Dickie, B. G., Vaid, R. R., Headlam, A. J., and Bacon, S. J. (1997). Local-circuit neurones in the medial prefrontal cortex (areas 25, 32 and 24b) in the rat: morphology and quantitative distribution. *J. Comp. Neurol.* 377, 465–499.

Gallopin, T., Geoffroy, H., Rossier, J., and Lambolez, B. (2006). Cortical sources of CRF, NKB, and CCK and their effects on pyramidal cells in the neocortex. *Cereb. Cortex* 16, 1440–1452.

Garbossa, D., Fontanella, M., Pagni, C. A., and Vercelli, A. (2001). Nitric oxide synthase and cytochrome c oxidase changes in the tumoural and peritumoural cerebral cortex. *Acta Neurochir. (Wien)* 143, 897–908.

Garthwaite, J. (2008). Concepts of neural nitric oxide-mediated transmission. *Eur. J. Neurosci.* 27, 2783–2802.

Garthwaite, J., and Boulton, C. L. (1995). Nitric oxide signaling in the central nervous system. *Annu. Rev. Physiol.* 57, 683–706.

Gelman, D. M., and Marin, O. (2010). Generation of interneuron diversity in the mouse cerebral cortex. *Eur. J. Neurosci.* 31, 2136–2141.

Gerashchenko, D., Wisor, J. P., Burns, D., Reh, R. K., Shiromani, P. J., Sakurai, T., de la Iglesia, H. O., and Kilduff, T. S. (2008). Identification of a population of sleep-active cerebral cortex neurons. *Proc. Natl. Acad. Sci. U.S.A.* 105, 10227–10232.

Gonchar, Y., and Burkhalter, A. (1997). Three distinct families of GABAergic neurons in rat visual cortex. *Cereb. Cortex* 7, 347–358.

Gonchar, Y., Wang, Q., and Burkhalter, A. (2007). Multiple distinct subtypes of GABAergic neurons in mouse visual cortex identified by triple immunostaining. *Front. Neuroanat.* 1:3. doi:10.3389/neuro.05.003.2007

Hashikawa, T., Leggio, M. G., Hattori, R., and Yui, Y. (1994). Nitric oxide synthase immunoreactivity colocalized with NADPH-diaphorase histochemistry in monkey cerebral cortex. *Brain Res.* 641, 341–349.

Higo, S., Akashi, K., Sakimura, K., and Tamamaki, N. (2009). Subtypes of GABAergic neurons project axons in the neocortex. *Front. Neuroanat.* 3:25. doi:10.3389/neuro.05.025.2009

Higo, S., Udaka, N., and Tamamaki, N. (2007). Long-range GABAergic projection neurons in the cat neocortex. *J. Comp. Neurol.* 503, 421–431.

Iadecola, C., Beitz, A. J., Renno, W., Xu, X., Mayer, B., and Zhang, F. (1993). Nitric oxide synthase-containing neural processes on large cerebral arteries and cerebral microvessels. *Brain Res.* 606, 148–155.

Judas, M., Sestan, N., and Kostovic, I. (1999). Nitrinergic neurons in the developing and adult human telencephalon: transient and permanent patterns of expression in comparison to other mammals. *Microsc. Res. Tech.* 45, 401–419.

Karagiannis, A., Gallopin, T., David, C., Battaglia, D., Geoffroy, H., Rossier, J., Hillman, E. M. C., Staiger, J. F., and Cauli, B. (2009). Classification of NPY-expressing neocortical interneurons. *J. Neurosci.* 29, 3642–3659.

Kilduff, T. S., Cauli, B., and Gerashchenko, D. (2011). Activation of cortical interneurons during sleep: an anatomical link to homeostatic sleep regulation? *Trends Neurosci.* 34, 10–19.

Kiss, J. P. (2000). Role of nitric oxide in the regulation of monoaminergic neurotransmission. *Brain Res. Bull.* 52, 459–466.

Kawaguchi, Y. (1995). Physiological subgroups of nonpyramidal cells with specific morphological-characteristics in layer II/III of rat frontal cortex. *J. Neurosci.* 15, 2638–2655.

Kubota, Y., Hattori, R., and Yui, Y. (1994). Three distinct subpopulations of GABAergic neurons in rat frontal agranular cortex. *Brain Res.* 649, 159–173.

Kubota, Y., Shigematsu, N., Karube, F., Sekigawa, A., Kato, S., Yamaguchi, N., Hirai, Y., Morishima, M., and Kawaguchi, Y. (2011). Selective coexpression of multiple chemical markers defines discrete populations of neocortical GABAergic neurons. *Cereb. Cortex* 21, 1803–1817.

Lambolez, B., Audinat, E., Bochet, P., Crepel, F., and Rossier, J. (1992). AMPA receptor subunits expressed by single Purkinje cells. *Neuron* 9, 247–258.

Lee, J. E., and Jeon, C. J. (2005). Immunocytochemical localization of nitric oxide synthase-containing neurons in mouse and rabbit visual cortex and co-localization with calcium-binding proteins. *Mol. Cells* 19, 408–417.

Lee, S., Hjerling-Leffler, J., Zagha, E., Fishell, G., and Rudy, B. (2010). The largest group of superficial neocortical GABAergic interneurons expresses ionotropic serotonin receptors. *J. Neurosci.* 30, 16796–16808.

McGarry, L. M., Packer, A. M., Fino, E., Nikolenko, V., Sippy, T., and Yuste, R. (2010). Quantitative classification of somatostatin-positive neocortical interneurons identifies three interneuron subtypes. *Front. Neural Circuits* 4:12. doi:10.3389/fncir.2010.00012

Miyoshi, G., Butt, S. J., Takebayashi, H., and Fishell, G. (2007). Physiologically distinct temporal cohorts of cortical interneurons arise from telencephalic Olig2-expressing precursors. *J. Neurosci.* 27, 7786–7798.

Moro, V., Badaut, J., Springhetti, V., Edvinsson, L., Seylaz, J., and Lasbennes, F. (1995). Regional study of the co-localization of neuronal nitric oxide synthase with muscarinic receptors in the rat cerebral cortex. *Neuroscience* 69, 797–805.

Oermann, E., Bidmon, H. J., Mayer, B., and Zilles, K. (1999). Differential maturational patterns of nitric oxide synthase-I and NADPH diaphorase in functionally distinct cortical areas of the mouse cerebral cortex. *Anat. Embryol.* 200, 27–41.

Paxinos, G., and Franklin, K. B. J. (2001). *The Mouse Brain in Stereotaxic Coordinates.* San Diego: Elsevier.

Perrenoud, Q., Rossier, J., Geoffroy, H., Vitalis, T., and Gallopin, T. (2012). Diversity of GABAergic interneurons in layer VIa and VIb of mouse barrel cortex. *Cereb. Cortex.* PMID: 22357664, [Epub ahead of print].

Rancillac, A., and Crepel, F. (2004). Synapses between parallel fibres and stellate cells express long-term changes in synaptic efficacy in rat cerebellum. *J. Physiol. (Lond.)* 554, 707–720.

Rancillac, A., Rossier, J., Guille, M., Tong, X. K., Geoffroy, H., Amatore, C., Arbault, S., Hamel, E., and Cauli, B. (2006). Glutamatergic control of microvascular tone by distinct GABA neurons in the cerebellum. *J. Neurosci.* 26, 6997–7006.

Sandell, J. H. (1986). NADPH diaphorase histochemistry in the macaque striate cortex. *J. Comp. Neurol.* 251, 388–397.

Sholl, D. A. (1953). Dendritic organization in the neurons of the visual and motor cortices of the cat. *J. Anat.* 87, 387–406.

Smiley, J. F., McGinnis, J. P., and Javitt, D. C. (2000). Nitric oxide synthase interneurons in the monkey cerebral cortex are subsets of the somatostatin, neuropeptide Y, and calbindin cells. *Brain Res.* 863, 205–212.

Tamamaki, N., Yanagawa, Y., Tomioka, R., Miyazaki, J., Obata, K., and Kaneko, T. (2003). Green fluorescent protein expression and colocalization with calretinin, parvalbumin, and somatostatin in the

GAD67-GFP knock-in mouse. *J. Comp. Neurol.* 467, 60–79.

Tamas, G., Buhl, E. H., and Somogyi, P. (1997). Fast IPSPs elicited via multiple synaptic release sites by different types of GABAergic neurone in the cat visual cortex. *J. Physiol. (Lond.)* 500(Pt 3), 715–738.

Tomioka, R., Okamoto, K., Furuta, T., Fujiyama, F., Iwasato, T., Yanagawa, Y., Obata, K., Kaneko, T., and Tamamaki, N. (2005). Demonstration of long-range GABAergic connections distributed throughout the mouse neocortex. *Eur. J. Neurosci.* 21, 1587–1600.

Tomioka, R., and Rockland, K. S. (2007). Long-distance corticocortical GABAergic neurons in the adult monkey white and gray matter. *J. Comp. Neurol.* 505, 526–538.

Tsuzuki, K., Lambolez, B., Rossier, J., and Ozawa, S. (2001). Absolute quantification of AMPA receptor subunit mRNAs in single hippocampal neurons. *J. Neurochem.* 77, 1650–1659.

Valtschanoff, J. G., Weinberg, R. J., Kharazia, V. N., Schmidt, H. H., Nakane, M., and Rustioni, A. (1993). Neurons in rat cerebral cortex that synthesize nitric oxide: NADPH diaphorase histochemistry, NOS immunocytochemistry, and colocalization with GABA. *Neurosci. Lett.* 157, 157–161.

Vercelli, A., Garbossa, D., Biasiol, S., Repici, M., and Jhaveri, S. (2000). NOS inhibition during postnatal development leads to increased ipsilateral retinocollicular and retinogeniculate projections in rats. *Eur. J. Neurosci.* 12, 473–490.

Vitalis, T., and Rossier, J. (2011). New insights into cortical interneurons development and classification: contribution of developmental studies. *Dev. Neurobiol.* 71, 34–44.

Vruwink, M., Schmidt, H. H., Weinberg, R. J., and Burette, A. (2001). Substance P and nitric oxide signaling in cerebral cortex: anatomical evidence for reciprocal signaling between two classes of interneurons. *J. Comp. Neurol.* 441, 288–301.

Vucurovic, K., Gallopin, T., Ferezou, I., Rancillac, A., Chameau, P., van Hooft, J. A., Geoffroy, H., Monyer, H., Rossier, J., and Vitalis, T. (2010). Serotonin 3A receptor subtype as an early and protracted marker of cortical interneuron subpopulations. *Cereb. Cortex* 20, 2333–2347.

Ward, J. H. (1963). Hierarchical grouping to optimize an objective function. *J. Am. Stat. Assoc.* 58, 236–244.

Wiencken, A. E., and Casagrande, V. A. (2000). The distribution of NADPH diaphorase and nitric oxide synthetase (NOS) in relation to the functional compartments of areas V1 and V2 of primate visual cortex. *Cereb. Cortex* 10, 499–511.

Wonders, C. P., and Anderson, S. A. (2006). The origin and specification of cortical interneurons. *Nat. Rev. Neurosci.* 7, 687–696.

Wonders, C. P., Taylor, L., Welagen, J., Mbata, I. C., Xiang, J. Z., and Anderson, S. A. (2008). A spatial bias for the origins of interneuron subgroups within the medial ganglionic eminence. *Dev. Biol.* 314, 127–136.

Xu, Q., Wonders, C. P., and Anderson, S. A. (2005). Sonic hedgehog maintains the identity of cortical interneuron progenitors in the ventral telencephalon. *Development* 132, 4987–4998.

Xu, X., Roby, K. D., and Callaway, E. M. (2010). Immunochemical characterization of inhibitory mouse cortical neurons: three chemically distinct classes of inhibitory cells. *J. Comp. Neurol.* 518, 389–404.

Yan, X. X., and Garey, L. J. (1997). Morphological diversity of nitric oxide synthesising neurons in mammalian cerebral cortex. *J. Hirnforsch.* 38, 165–172.

Yan, X. X., Jen, L. S., and Garey, L. J. (1996). NADPH-diaphorase-positive neurons in primate cerebral cortex colocalize with GABA and calcium-binding proteins. *Cereb. Cortex* 6, 524–529.

Zhou, L., and Zhu, D. Y. (2009). Neuronal nitric oxide synthase: structure, subcellular localization, regulation, and clinical implications. *Nitric Oxide* 20, 223–230.

Conflict of Interest Statement: The authors declare that the research was conducted in the absence of any commercial or financial relationships that could be construed as a potential conflict of interest.

Received: 28 March 2012; paper pending published: 16 April 2012; accepted: 31 May 2012; published online: 29 June 2012.

Citation: Perrenoud Q, Geoffroy H, Gauthier B, Rancillac A, Alfonsi F, Kessaris N, Rossier J, Vitalis T and Gallopin T (2012) Characterization of type I and type II nNOS-expressing interneurons in the barrel cortex of mouse. Front. Neural Circuits ***6****:36. doi: 10.3389/fncir.2012.00036*

frontiers in
NEURAL CIRCUITS

ORIGINAL RESEARCH ARTICLE
published: 31 May 2012
doi: 10.3389/fncir.2012.00035

Molecular analysis of ivy cells of the hippocampal CA1 stratum radiatum using spectral identification of immunofluorophores

Jozsef Somogyi[1], Andras Szabo[2], Peter Somogyi[1] and Karri Lamsa[2]*

[1] *Medical Research Council Anatomical Neuropharmacology Unit, Department of Pharmacology, Oxford University, Oxford, UK*
[2] *Department of Pharmacology, Oxford University, Oxford, UK*

Edited by:
Bruno Cauli, CNRS/Université Pierre et Marie Curie, France

Reviewed by:
Gianmaria Maccaferri, Northwestern University, USA
Ludovic Tricoire, Université Pierre et Marie Curie, France

***Correspondence:**
Karri Lamsa, Department of Pharmacology, Oxford University, Mansfield Road, Oxford OX1 3QT, UK.
e-mail: karri.lamsa@pharm.ox.ac.uk

Neuronal nitric oxide synthase-expressing (nNOS+) GABAergic interneurons are common in hippocampal stratum (str.) radiatum. However, these cells are less well characterized than nNOS+ ivy cells in str. pyramidale or neurogliaform cells (NGC) in str. lacunosum-moleculare. Here we have studied the laminar distribution of the axons and dendrites, and the immunoreactivity of these neurons recorded in rat hippocampal slices. We have used spectral analysis of antibody- or streptavidin-conjugated fluorophores to improve recognition of genuine signals in reactions for molecules such as nNOS and neuropeptide-Y (NPY). We found that most nNOS+ cells with soma in the CA1 area str. radiatum exhibit characteristic properties of ivy cells, and were positive for NPY and negative for reelin. However, laminar distributions of their neurites differ from original characterization of ivy cells with the soma in or close to str. pyramidale. Both their dendrites and axon are mainly in str. radiatum and to a lesser extent in str. oriens, and in addition often extend to str. lacunosum-moleculare. We conclude that ivy cells in str. radiatum may predominantly be feedforward inhibitory interneurons in the CA1 area, and their axonal output delivering GABA, NPY, and NO can influence both the entorhinal cortex innervated and the CA3 innervated zones pre- and post-synaptically. Spectral analysis of fluorophores provides an objective algorithm to analyze signals in immunoreactions for neurochemical markers.

Keywords: feedforward inhibition, feedback inhibition, slow GABA action, dendritic modulation, spectral imaging

INTRODUCTION

In the CA1 area of the hippocampus, three major types of neuronal nitric oxide synthase (nNOS)-expressing GABAergic interneurons have been identified with different laminar distribution. Large intensely nNOS+ projection neurons are rare and have mostly horizontal dendrites in stratum (str.) oriens. These cells are most frequently located at the border with the subiculum (Freund and Buzsáki, 1996; Somogyi, 2010). Of the other two related neuron types, neurogliaform cells (NGC) are located predominantly in str. lacunosum-moleculare where their dendrites receive excitatory synapses from the perforant pathway and the efferent axons form connections to other interneurons and pyramidal cell apical dendrites (Somogyi, 2010; Capogna, 2011; Maccaferri, 2011). The cell bodies of the closely related nNOS+ ivy cells were reported to be most numerous in str. pyramidale and their axons and dendrites extend from str. oriens through str. radiatum, rarely entering str. lacunosum-moleculare (Fuentealba et al., 2008; Szabadics and Soltesz, 2009; Tricoire et al., 2010, 2011). Although interneuron somata expressing nNOS are also common in str. radiatum (Catania et al., 1995; Fuentealba et al., 2008; Tricoire et al., 2010; Krook-Magnuson et al., 2011), the distributions of their processes have rarely been reported.

Here we have studied the laminar distribution of axons and dendrites of ivy cells with soma in str. radiatum of the CA1 area. Cells were filled with neurobiotin in rat acute hippocampal slices using whole-cell patch technique and reconstructed. Most studied nNOS-expressing cells showed co-labeling for neuropeptide-Y (NPY) (Fuentealba et al., 2008; Karagiannis et al., 2009; Tricoire et al., 2010; Krook-Magnuson et al., 2011). Because whole-cell recording and *in vitro* slice conditions reduce immunoreactivity for certain molecules, we spectrally analyzed fluorophore emissions and measured the intensity of antibody-conjugated fluorophore signals to conclude visual observations of laser confocal microscope images.

We report here that nNOS-expressing neurons, which have soma in the CA1 str. radiatum, show many characteristics of ivy cells reported in the pyramidal layer, but some may differ from those characterized previously in their laminar distribution of axons and dendrites (Fuentealba et al., 2008). Spectral analysis improves the evaluation of immunoreactions, which are often compromised in slice preparations and in neurons studied with whole-cell clamp technique.

MATERIALS AND METHODS

HIPPOCAMPAL SLICES AND CELL LABELING

Three- to four-week-old-male Sprague–Dawley rats were killed according to the Animals (Scientific Procedures) Act 1986 and transverse hippocampal slices were prepared as described

previously (Oren et al., 2009). Slices (350 μm) were cut with a vibrating microtome (Microm HM650V, Carl Zeiss Ltd., Germany) and kept submerged at 32°C in sucrose solution for 20–25 min before transferred to an interface chamber. The sucrose solution contained the following (in mM): sucrose (75), NaCl (87), KCl (2.5), $CaCl_2$ (0.5), $MgCl_2$ (7), NaH_2PO_4 (1), $NaHCO_3$ (25), glucose (25), pH 7.4, bubbled with 95% O_2/5% CO_2. Slices were maintained in Earle's balanced salt solution (EBSS, Gibco-Invitrogen, with 3 mM Mg^{2+} and 1 mM Ca^{2+}) at room temperature (20–25°C) for at least 60 min in an interface chamber (gassed with 95% O_2/5% CO_2) before starting experiments. Then, slices were placed in a recording chamber (Luigs & Neumann, Germany) mounted on the stage of an upright microscope (Olympus BX51WI, Japan), where they were held under a nylon mesh grid and superfused at a rate of 3–5 mL min^{-1} with artificial cerebrospinal fluid (ACSF) at 31–33°C. The recording solution contained (in mM): NaCl (119), KCl (2.5), $CaCl_2$ (2.5), $MgSO_4$ (1.3), NaH_2PO_4 (1.25), $NaHCO_3$ (25), glucose (11); osmolarity 295 mOsm/L and final pH 7.4 (equilibrated with 95% O_2/5% CO_2). Slices were visualized using a 20× water immersion objective with 2–4× zoom and infra-red differential interference contrast (DIC) optics and camera.

Neurons were filled with neurobiotin (0.2–0.3%) using whole-cell clamp with a solution containing (mM): CsCl (145), HEPES (20), Cs-EGTA (0.2), NaCl (8), Mg-ATP (2), GTP (0.3), QX-314 Br (1), pH 7.2, 290 mOsm/L. Following at least 20 min of filling, the pipette was retracted and the slice was transferred to a perfused (3–5 mL min^{-1}) and heated (30–32°C) submerged chamber for recovery (1 h). Electrophysiological data recorded from some of the ivy cells reported here have been published elsewhere (Szabo et al., 2012).

TISSUE PROCESSING AND ANALYSIS

The slices were fixed overnight at 4°C in a solution containing 4% paraformaldehyde, 0.05% glutaraldehyde, and ∼0.2% picric acid in 0.1 M sodium phosphate buffer (PB) (pH 7.3–7.4) (Oren et al., 2009). The next day, slices were washed thoroughly in 0.1 M phosphate-buffer and stored in PB containing 0.05% sodium azide at 4°C. For re-sectioning, slices were embedded and fixed in 20% gelatin and re-sectioned at 70 μm thickness using a vibrating microtome (Leica VT1000S, Leica Microsystems, Germany). The sections were washed once in 0.1 M PB, and several times in 50 mM Tris-buffered saline (TBS, Sigma, UK) with 0.3% Triton X-100, and then incubated for at least 5 h with Alexa Fluor 488-labeled streptavidin (Invitrogen, UK, diluted 1:2000) in TBS with 0.3% Triton X-100. Sections were mounted in Vectashield (Vector Laboratories, Burlingame, CA, USA) under coverslips. Cells were digitally imaged from two to four 70 μm thick sections using Axio Imager.Z1 epifluorescence microscope (Carl Zeiss Microimaging Gmbh, Germany) with filter set 38HE, 20× (0.8 NA) or 40× (1.3 NA) immersion objectives and AxioVision 4.7.1 software with modules for Multichannel Fluorescent, Mosaic, and *Z*-stack imaging. Using maximum intensity projection, *Z*-stacks (step size 1.3 μm) were collapsed and inverted to show cells on white background in ImageJ 1.42 (NIH, USA). To ensure match the eight-bit images were joined with GIMP (GNU Image Manipulation Program) as linked layers. For quantification NeuronJ plugin for ImageJ was used for neurite tracing at a preset pixel width (3 pixels). We observed dye coupling (multiple-cell staining) only in one (k031192) of the 23 studied cells.

Somata were removed from reconstructed images before analysis. The Plot Profile function of ImageJ was used to detect and summate pixels covering the traced axons and dendrites. For binning the images were divided into 10 μm wide horizontal laminae starting from str.oriens/alveus to the distal end of str. lacunosum-moleculare. Horizontal histograms in **Figure 1** show pixels over axons and dendrites in each 10 μm bin as proportion of the total number of pixels in all laminae. Since line thickness was uniform in the reconstructed image, the pixel count is an approximate representation of the proportion of the axon or dendrites in the analyzed layers.

As layers have different curvatures in different slices, curvatures were digitally flattened to horizontal lines using the curve bend filtering options of the GIMP. This has a small effect on the relative number of pixels. Due to projection onto the X-Y plane, the Z component of fiber lengths was omitted. Because of the square form of pixels, the length of diagonally oriented lines may have been underestimated. Laminar distribution data of ivy cells in **Figure 1** were pooled and reported with additional cells in a summary histogram in Szabo et al. (2012).

IMMUNOHISTOCHEMISTRY

Non-specific binding of antibodies was blocked by 20% normal horse serum (NHS, Vector Laboratories, Burlingame, CA, USA) in TBS for 1 h and the sections were incubated in mixtures of appropriate primary antibodies for 48 h at 4°C as described previously (Oren et al., 2009). All antibodies were diluted in TBS containing 0.3% Triton-X and 1% NHS. After washing in TBS, sections were incubated in a mixture of appropriate secondary antibodies conjugated with indocarbocyanine 3 (Cy3) or indodicarbocyanine 5 (Cy5) overnight at 4°C. Sections were then washed in TBS, mounted in Vectashield (Vector Laboratories, Burlingame, CA, USA). Method specificity was tested by omitting the primary antibodies and using the full range of secondary antibodies and imaging parameters as with the full reaction. Under these conditions, no cell specific signal resembling those produced by the primary antibodies was detected. Some autofluorescence was detected (**Figure 2**), but easily differentiated from the antibody signal. Secondary antibody cross-reactivity was not detected in the tests of applying only one primary antibody with the full range of secondary antibodies and the same imaging conditions for recording as with the full reaction. Selected sections were examined under a confocal laser-scanning microscope using sequential multitrack, single channel operation mode. Hence, only one laser was applied at any one time. Control incubations using two primary antibodies and only one secondary antibody resulted in the detection of only the appropriate primary antibody. When fluorescence was not detectable in the relevant area of the section where similar parts of other non-recorded cells were immunopositive, cells were considered immunonegative. Details of primary antibodies are reported in **Table 1**. Secondary antibodies were purchased from Jackson ImmunoResearch Lab (Cy3-conjugated products 706165148, 711165152, and 715165151, dilution 1:400;

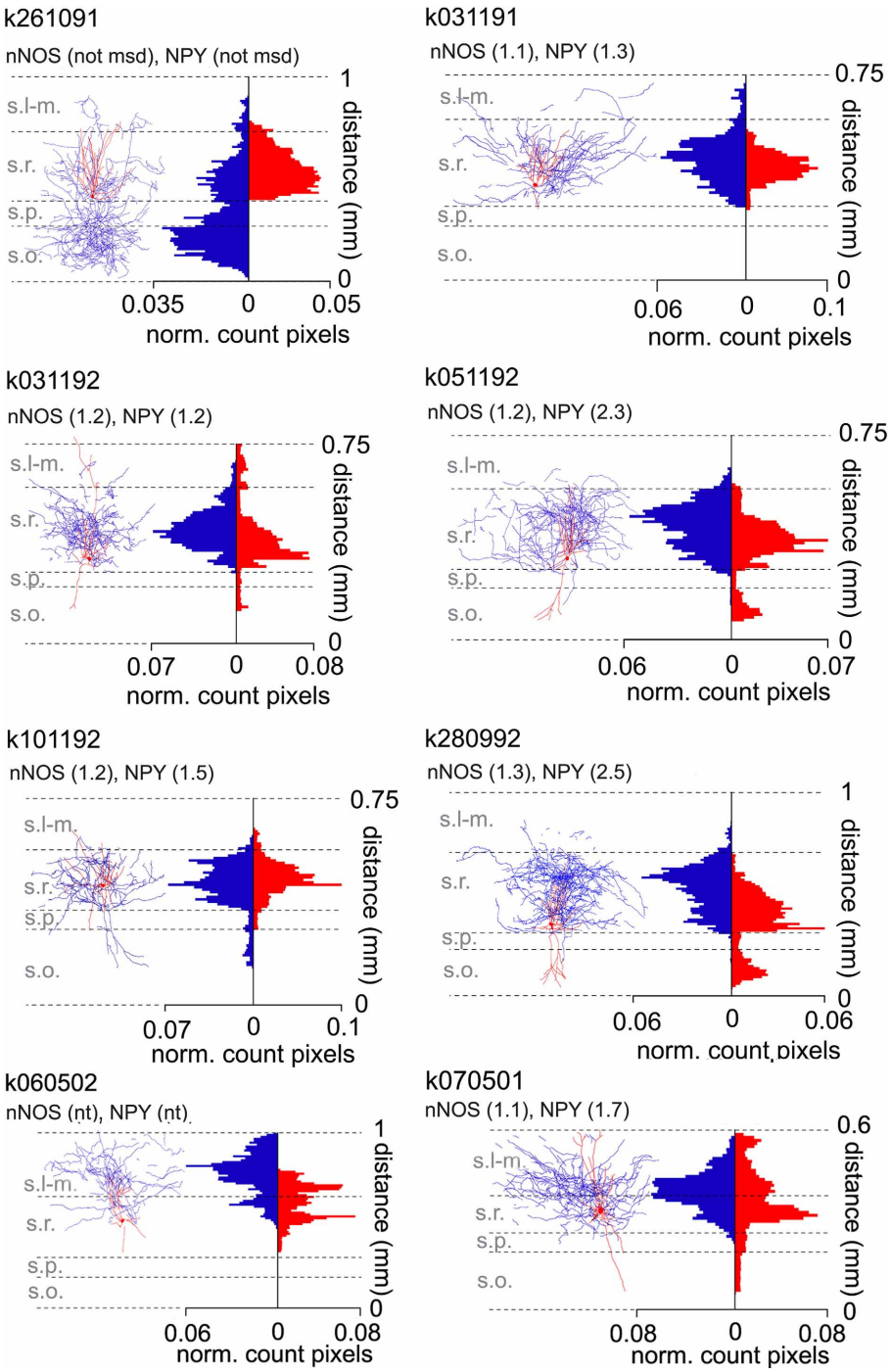

FIGURE 1 | Laminar distribution of axons and dendrites of ivy cells with soma in the CA1 stratum radiatum. Eight reconstructed ivy cells with soma in str. radiatum. Individual images show digital, two-dimensional reconstructions of soma and dendrite (red) and axon (blue) from fluorescence image stacks of 2–4 merged sections, each 70 μm thick. Cell K261091 has most of its axonal arbor in str. oriens, whereas five cells have axon predominantly in str. radiatum and two (k060502, k070501) in strata radiatum and lacunosum-moleculare (s.l-m.). The axons and dendrites of most cells penetrate into s.l-m to a varying extent. The distributions of axons and dendrites in different laminae are illustrated as histograms on the right which show normalized pixel count detected for the axon and dendrites in the two-dimensional representations. Each bar shows proportion of pixels per bin (10 μm); the sum of all bins being 1. Ordinate: radial distance from the alveus towards the hippocampal fissure in mm. The cells were tested for nNOS and NPY immunoreactivity by epifluorescence and/or confocal spectral imaging. Semiquantitative fluorescence analysis values by confocal microscopy are shown above the cells as a ratio of cytoplasmic to neuropil pixel brightness. An arbitrary threshold of 1.5 was set as lower limit to consider a cell immunopositve. Cells showing ratios below 1.5 could either have a reduced immunoreactivity due to dialysis of the cytoplasm during whole-cell recording, or might not express the molecule. Laminae are indicated by abbreviations. not msd, not measured; nt, not tested because of damaged soma.

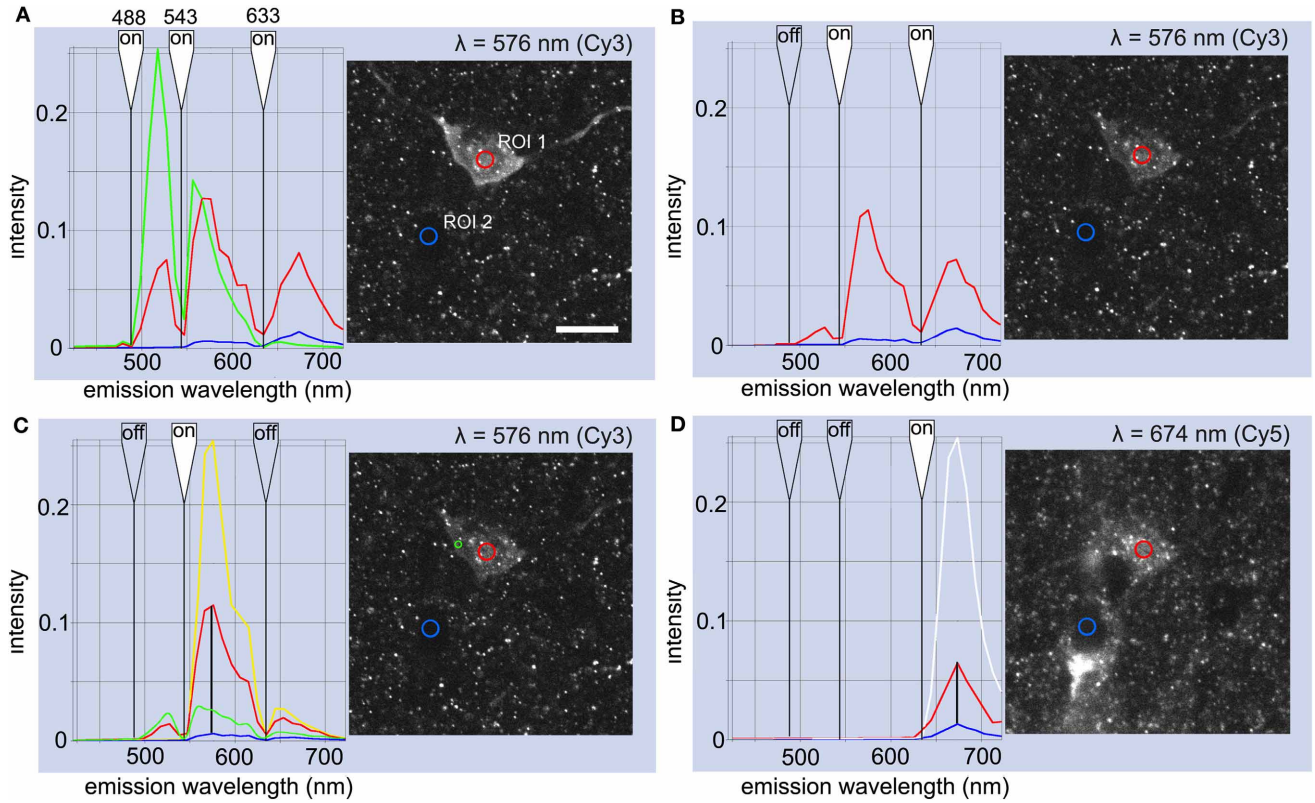

FIGURE 2 | Evaluation of immunoreactions for cytoplasmic nNOS and NPY using semi-quantitative spectral analysis of fluorophore emission in one ivy cell (k111291). Fluorophore-specific spectral peak amplitudes were used to evaluate the specificity of emissions. **(A)** The red line illustrates emission spectrum from a region of interest (ROI 1) in the cytosol when three lasers are simultaneously activated in a cell reacted with streptavidin-Alexa Fluor 488, Cy3-conjugated secondary antibody testing for nNOS, and Cy5-conjugated secondary antibody testing for NPY. Blue line shows corresponding emission signal from a reference area (ROI 2) in the nucleus of a non-recorded cell nearby. Green line in plot A represents Alexa Fluor 488 emission reference spectrum recorded separately from another section which was labeled only with a secondary antibody-conjugated to Alexa Fluor 488. The sharp drop of signal strength at each laser wavelength (flagged as white indicates "on") is caused by the triple band primary beam splitter. Ordinate values stand for emission intensity normalized to the maximum (255) in eight-bit images. Micrograph illustrates emission detected in one bin at the maximum wavelength ($\lambda = 576$ nm). Scale bar 10 μm. **(B)** The same cell when the 488 nm laser was switched off showing emission spectra measured in the two ROIs (line colors as in **A**). **(C)** Emission spectra from the cytoplasm (red) and reference area (blue) when only the 543 nm laser was activated (yellow line shows the reference emission spectrum of Cy3 fluorophore). Vertical black line at 576 nm points to amplitudes measured in the two ROIs at Cy3 emission peak wavelength. Green line shows emission from another somatic area with non-granular fluorescence pattern. In this area, the 543 nm laser elicits proportionally larger amplitude response in the Alexa-488 emission band, indicating the excitation of the Alexa488 fluorophore. In addition, a significant emission signal may emerge from autofluorescence over a wide range of wavelengths. Note that the amplitude ratios are higher here than in the cells reported in **Table 2**, because of the very low level of background in the reference area over the nucleus of an unlabeled cell, rather than from neuropil or from the nucleus of the recorded cell. **(D)** Emission spectrum when the 633 nm laser was activated alone. White line shows the reference emission spectrum from Cy5 measured separately. Vertical black line at 674 nm points to the amplitudes in the two ROIs at the peak emission wavelength of Cy5. Micrograph illustrates emission detected in one bin at the maximum wavelength ($\lambda = 674$ nm). The presence or absence of fluorophore-specific emission in the cell can be established, because the emission spectrum of each fluorophore has its characteristic peak at specific wavelength, as seen on both sides of the beam splitter (see green spectral line for Alexa Fluor 488 in **A** and yellow line for Cy3 in **C**). Because in spectrum **B** (red line) the emission amplitude is low at the wavelength of the peak of the emission from Alexa Fluor 488, while it is several times higher at the Cy3-specific emission peak, we can conclude that Cy3 emission provides the bulk of the signal. No significant cross-talk or shine-through from the Alexa Fluor 488 emission contributes to the signal measured from a ROI in the cytoplasm.

Cy5-conjugated products 706175148 and 711175152, dilution 1:250), and Thermo Scientific (Cy5-conjugated product 33515, dilution 1:250).

SEMIQUANTITATIVE FLUOROPHORE SPECTRAL ANALYSIS (SFSA) OF IMMUNOREACTION

Spectral analysis and quantification of fluorophore-specific emissions were used to evaluate specificity of immunoreactions in ivy cells. First, using the QUASAR spectral detector of Zeiss Axio Imager.Z1-LSM 710 confocal microscope, cells were imaged in lambda mode to record emission spectra from 400 to 730 nm (collected in 32 bins, 10.3 nm wide each) using all three lasers individually. Because the emission spectrum of each fluorophore has specific wavelengths, the presence or absence of fluorophore emission can be established in the area. Analysis of the fluorophore-specific wavelengths in the recorded cell cytoplasm

Table 1 | Primary antibody list.

Immunoreactivity	Dilution	Species	Source	Source code	Antibody, antigene, and specificity
CB1R	1:1000	gp	Frontier Institute Co., Hokkaido, Japan	CB1-GP-Af530-1	Polyclonal, mouse CB1R C terminal sequence 31 aa., Fukudome et al., 2004.
nNOS	1:500	m	Sigma-Aldrich	N2280	Monoclonal, raised against recombinant protein residues 1–181. Labeling pattern as published previously with other antibodies.
NPY	1:5000	rb	Diasorin (Immunostar)	22940	Polyclonal, NPY-coupled to bovine thyroglubulin with glutaraldehyde. Absorption tested by manufacturer to six similar peptides. Labeling pattern as published with other antibodies.
parvalbumin (PV)	1:1000	rb	Swant, Bellinzona, Switzerland	PV-28	Polyclonal, rat muscle parvalbumin, Kägi et al., 1987; Schwaller et al., 1999.
somatostatin (SM)	1:200	m	GeneTex, Irvine, CA, USA	GTX71935	Monoclonal, human somatostatin conjugated to protein carrier. Labeling pattern similar to that published with other antibodies.
reelin	1:1000	m	Millipore	MAB5364	Monoclonal (G10), recombinant reelin aa. residues 164–496; Western blot analysis; de Bergeyck et al., 1998.

Species (s): gp, guinea pig; m, mouse; rb, rabbit.

and in neuropil were used to test presence of the fluorophore. The ratio values are reported in **Table 2** with details on immunoreactions. In some cells the nucleus was damaged by retrieval of the pipette and therefore nuclear analysis was omitted and only cytoplasmic and neuropil values were compared to judge labeling specificity.

RESULTS

We labeled interneurons in the str. radiatum of rat acute hippocampal slices with neurobiotin using the whole-cell recording method. Under visual guidance using infrared-DIC video microscopy, we targetted neurons with small soma characteristic of nNOS- and NPY-expressing neurons (Fuentealba et al., 2008; Karayannis et al., 2010; Tricoire et al., 2010; Krook-Magnuson et al., 2011). Following over-night fixation, slices were re-sectioned to allow full penetration of reagents and cells were visualized with streptavidin-fluorophore conjugate (Oren et al., 2009). Data on some ivy cells presented here have been published recently in Szabo et al. (2012) (see Materials and Methods).

Putative nNOS-expressing neurons were selected by their characteristic dense axon with small boutons (Tamas et al., 2003; Price et al., 2005; Szabadics et al., 2007; Fuentealba et al., 2008; Szabadics and Soltesz, 2009; Karayannis et al., 2010; Somogyi, 2010; Armstrong et al., 2011; Krook-Magnuson et al., 2011). Eight cells were reconstructed for analysis of the laminar distribution of their axons and dendrites (**Figure 1**).

AXONAL AND DENDRITIC LAMINAR DISTRIBUTION OF IVY CELLS WITH SOMA IN STRATUM RADIATUM

To express the laminar distribution of neurites, we counted pixels in digital images of the reconstructed cells. First, streptavidin-Alexa488-visualized neurites were imaged from sections and stacks of pictures were collapsed to two-dimensional digital images. Dendrites and axons identified by visual inspection of the sections were marked with a preset line thickness and the extent of lines was expressed as the number of pixels covering them. Finally, pixel counts in laminae from different sections of a cell were merged.

The distribution of pixels over neurites showed that ivy cells, which had soma in str. radiatum, also had their axons mostly in this layer and to a lesser extent in str. oriens. In addition, the axon of these cells regularly projected to str. lacunosum-moleculare to a small extent (**Figure 1**). Their dendrites were mostly in str. radiatum, although some penetrated into strata oriens, pyramidale, and lacunosum-moleculare.

Although laminar properties of many cells moderately differ from the ivy cells characterized in or in the vicinity of str. pyramidale, their translaminar axon, and dendrites indicate that they are ivy cells (Fuentealba et al., 2008). The axonal and dendritic distributions of these cells are different from NGC, which are focused on str. lacunosum-moleculare (Price et al., 2005; Capogna, 2011; Maccaferri, 2011).

The two ivy cells in **Figure 1** with their somata closest to the border of str. radiatum with str. lacunosum-moleculare had

Table 2 | Semiquantitive fluorophore spectral analysis results of nNOS and NPY immunoreactions in ivy cells.

Cell code	Cy3	Visual score	SFSA		Cy5	Visual score	SFSA		Other tested immunoreactions (visual evaluation)
			Ratios s/nu, s/ne	Score			Ratios s/nu, s/ne	Score	
k030682	NPY	+	na, 3.7	+	nNOS	+	nt	+	
k131081	NPY	+	3.9, 3.5	+	nNOS	nt	nt	na	CB1R-
k150192	NPY	+	2.4, 3.6	+	nNOS	nt	nt	na	SM-
k090793	NPY	+	2.5, 1.7	+	nNOS	−	1.1, 1.4	−	CB1R-, PV-
k090794	NPY	+	na, 3.9	+	nNOS	+	na, 2.0	+	CB1R-, PV-
k220792	NPY	+	na, 2.8	+	nNOS	nc	na, 1.7	+	
k070891	NPY	+	na, 2.1	+	nNOS	nc	na, 1.8	+	CB1R-, PV-
k090891	NPY	+	2.9, 1.8	+	nNOS	−	na, 1.3	−	CB1R-, PV-
k111291	NPY	+	3.5, 7.2	+	nNOS	+	2.4, 5.3	+	CB1R-, PV-
k060101	NPY	nt	nt	na	nNOS	+	2.4, 2.0	+	CB1R-, PV-
k060105	NPY	+	2.5, 6.6	+	nNOS	+	1.7, 2.3	+	CB1R-, PV-
k250502	nNOS	+	2.7, 1.0	+	NPY	+	3.2, 1.8	+	reelin-
k260502	nNOS	+	1.9, 0.9	+	NPY	nc	1.4, 0.9	−	reelin-
k130701	nNOS	nc	na, 1.3	−	NPY	+	1.2, 2.0	+	reelin-
k130702	nNOS	−	1.4, 1.1	−	NPY	nc	1.6, 1.7	+	reelin-
K261091	NPY	+	nt	na	nNOS	nt	nt	na	CB1R-,
K031191	NPY	−	1.3, 1.3	−	nNOS	−	1.2, 1.1	−	CB1R-,
K031192	NPY	nc	1.3, 1.2	−	nNOS	nc	1.3, 1.2	−	PV-, CB1R-
K051192	NPY	+	2.2, 2.3	+	nNOS	nc	1.4, 1.2	−	CB1R-
K101192	NPY	nc	1.5, 1.5	+	nNOS	nc	1.4, 1.2	−	CB1R-
K280992	NPY	+	1.6, 2.5	+	nNOS	+	1.2, 1.3	−	PV-, CB1R-
K060502	nNOS	nt	nt	na	NPY	nt	nt	na	CB1R-, reelin-
K070501	Nnos	−	1.3, 1.1	−	NPY	nc	1.8, 1.7	+	CB1R-, reelin-

Reactions for nNOS and NPY in ivy cells were analyzed with laser confocal microscope using visual observation as well as SFSA. Immunoreactions were visualized by secondary antibodies conjugated with fluorophores (Cy3 and Cy5). Visual scoring was based on estimation of staining intensity in the cytoplasm relative to the ambient neuropil and/or nucleus, and characteristic patterns of the protein expression. In SFSA the emission amplitudes at fluorophore-specific wavelengths were tested in the soma, nucleus, and ambient neuropil. Amplitude ratios soma vs. nucleus (s/nu) and soma vs. neuropil (s/ne) were used in scoring immunoreactivity in the cytoplasm. A threshold was set for immunopositivity at ≥ 1.5× higher emission from the cytoplasm than from control areas (nucleus or neuropil). Immunopositivity is indicated by plus sign (+), cells below this threshold are considered negative (−). The tested ivy cells in str. radiatum did not show immunoreactivity for reelin (n = 6), none of the ivy cells showed immunopositivity either for parvalbumin (PV) (tested in dendrites) or cannabinoid receptor type 1 (CB1R) (tested in axons). In three cells (k111291, k060101, and k060105) cytoplasmic content was harvested from the soma into whole-cell pipette. If the nucleus was damaged by the electrode, a ratio was taken between cytoplasm and the neuropil. Absence of nuclear ratio is indicated as na, not applicable; nc, non conclusive; nt, not tested.

a large proportion of both the axons and dendrites in str. lacunosum-moleculare. Both cells appeared to be negative for reelin, although the negative results can be due to the whole-cell recording conditions. We conclude that laminar distribution of ivy cell somata in the CA1 area extends to distal str. radiatum.

SEMI-QUANTITATIVE SPECTRAL ANALYSIS OF IMMUNOREACTIONS FOR nNOS AND NPY IN IVY CELLS

In addition to the cells analyzed above, we labeled 15 ivy cells which had soma and dense axon in str. radiatum. The intracellular recording techniques of the whole-cell method often compromise cytoplasmic protein detection by immunohistochemistry due to the dilution of proteins. In addition, cytoplasm was harvested from the soma of three of the cells into pipette for single-cell RT-PCR analysis reported in Szabo et al. (2012) compromising the detection of the proteins by immunohistochemistry (see **Table 2**) (Lambolez et al., 1992).

In conventional channel imaging, two fluorophores may be excited simultaneously, one sub-optimally by the laser used in neighboring channels resulting in an excitation crosstalk, which is impossible to separate even by sequential scanning. This poses a problem when the amount of the two fluorophores in a cell are grossly different, like intense AlexaFluor-488 reporting the injected neurobiotin and weak Cy3 signal from immunoreactivity of a diluted cytoplasmic molecule. Similarly, crosstalk may apply if fluorescence is strong in Cy3 channel and weak in Cy5. In order to establish a reproducible lower threshold for immunopositivity, we applied Semi-quantitative Fluorophore Spectral Analysis (SFSA) to quantify immunofluorophore emissions in subcellular domains and to judge immunoreaction quality and specificity.

Peak amplitudes of Alexa Fluor488, Cy3 and Cy5 fluorophore emissions at their specific spectral wavelengths were used to assess specificity for NPY and nNOS immunofluorescence. Firstly, by

exciting a fluorophore with its specific laser, the emission spectral profile was recorded from 400 to 730 nm. This was obtained in lambda mode for each fluorophore by stimulating control cells in reference sections containing one of these fluorophores only (e.g., cells filled with neurobiotin and visualized with AlexaFluo 488, but not exposed to any secondary antibodies. Similarly, reference spectra were obtained from Cy3 and Cy5 emissions from sections tested either for nNOS or NPY antibody and their secondary antibody only).

Secondly, the amplitude at each fluorophore's maximum emission wavelength (referred here as a specific lambda wavelength) was obtained in the recorded cell cytoplasm. As an example, when the emission amplitude is low at the wavelength specific to Alexa Fluor 488 when stimulating with 543 nm laser while it is several times higher at the Cy3-specific emission wavelength, we can conclude that the cytosol contains Cy3 emission and no significant cross-talk or shine through from the Alexa Fluor 488 emission contributes to the signal measured.

Thirdly, when the presence of Cy3 or Cy5 fluorophore in the cell was confirmed, we evaluated specificity of the fluorophore-conjugated antibody binding. We compared emission peaks from selected areas in the recorded cell; cytoplasm, nucleus, and ambient neuropil (**Figure 2**). A signal was considered positive if the fluorophore emission peak amplitude from the cytoplasm was at least 1.5 times larger than from reference areas.

We found that 17 of the 23 ivy cells identified on the basis of their axons were positive for NPY by SFSA and 15 of 23 when scored by visual evaluation only. Correspondingly, nNOS+ was verified in eight cells with SFSA and in seven cells when evaluated visually only (of the 18 cells evaluated with both). All analyzed cells with ratio values and fluorophores are shown in **Table 2**. In conclusion, SFSA can be used to detect and deal with excitation cross-talk in weak cytoplasmic immunoreactions. This facilitates the recognition of genuine weak signals in a reproducible and quantitative manner.

DISCUSSION

We report here that nNOS-immunopositive and/or NPY GABAergic ivy cell somata are widely distributed in str. radiatum of the rat hippocampal CA1 area. The laminar distribution of ivy cell axons and dendrites varies and this may be related to soma location. Cells characterized in this study had somata, efferent axon, and dendrites predominantly in str. radiatum and the processes regularly penetrated into str. lacunosum-moleculare.

The laminar distribution of axon and dendrites is somewhat different from earlier illustrations of ivy cells with their soma close to str. pyramidale and axon densely innervating both strata oriens and radiatum, but hardly ever penetrating str. lacunosum-moleculare (Fuentealba et al., 2008). This indicates that ivy cells in strata pyramidale and radiatum may be differently connected in the hippocampus. The major proportion of dendritic length in str. radiatum indicates predominant glutamatergic input form the CA3 area pyramidal cells, whereas dendrites in str. oriens receive synapses both form CA3 and CA1 pyramidal cells. Therefore, we suggest that ivy cells in str. radiatum are predominantly involved in feedforward inhibition, whereas ivy cells close to str. pyramidale probably are in addition under feedback influence from CA1 pyramidal cells (Fuentealba et al., 2008; Somogyi, 2010). Moreover, it is likely that many ivy cells in str. radiatum also receive input from the perforant pathway and innervate post-synaptic domains in str. lacunosum-moleculare (Price et al., 2008; Szabo et al., 2012).

Although ivy and NGC share many features, the nNOS and/or NPY-expressing neurons reported here in str. radiatum resemble ivy cells because of their afferent and efferent connections (Armstrong et al., 2011; Capogna, 2011; Maccaferri, 2011). Their dendrites and axon extended from str. oriens and pyramidale to radiatum and lacunosum-moleculare (Szabo et al., 2012). In addition, these cells were different from NGCs immunohistochemically, because they failed to show reelin expression, which is a characteristic of NGC in str. lacunosum-moleculare (Fuentealba et al., 2008; Somogyi, 2010).

Fluorophores with selective binding specificity provide a powerful tool for analysis of localization of biomolecules, but identification of individual fluorophores can be challenging when they have similar localization and strongly overlapping emission spectra (Valm et al., 2011) or when their emission is observed against high fluorescent background (Leavesley et al., 2012). We employed spectral analysis of antibody-conjugated fluorophore emission for neuron type identification. This method allowed us to verify the presence of fluorophores (Cy3 or Cy5) in recorded and labeled cells and to make judgments on emission specificity by comparing emission values in relevant subcellular sites and in control areas. Both nNOS and NPY immunoreactivity is cytoplasmic, probably associated with the Golgi apparatus and secretory granules for NPY and various protein complexes for nNOS. Therefore, nuclear and ambient neuropil areas provide good test for unspecific antibody binding. In this study a ratio of 1.5 was used as a threshold of immunopositivity and specificity of the immunoreactions. However, this value is arbitrary and it is highly possible that future studies with analysis of larger sample pools will show that lower ratios could be used. The major benefit of SFSA is that emission intensities can be measured at selected lambda values for linear unmixing and thus quantifying cross-talk in imaging channels. Furthermore, unmixed values render comparison of staining intensities. We conclude that this SFSA method provides an objective and quantitative way to judge immunohistochemical reactions in subcellular regions where multiple fluorophores need to be tested simultaneously. Based on an algorithm, the analysis improves reproducibility and recognition of genuine positive signals in weak reactions. This approach may be critically important when intracellular recording techniques such as the whole-cell method is used for cell labeling, because these can compromise intracellular protein immunoreaction by dialyzing the cytoplasm.

ACKNOWLEDGMENTS

Supported by the Wellcome Trust and The John Fell Fund (Andras Szabo, Karri Lamsa), Medical Research Council (Jozsef Somogyi, Peter Somogyi). We thank Dr. Rachel Ingram and Ms. Linda Katona for helpful discussions and comments on the manuscript and Dr. Damien Lapray for microscopic screening of putative ivy cells for axon distribution.

REFERENCES

Armstrong, C., Szabadics, J., Tamas, G., and Soltesz, I. (2011). Neurogliaform cells in the molecular layer of the dentate gyrus as feed-forward gamma-aminobutyric acidergic modulators of entorhinal-hippocampal interplay. *J. Comp. Neurol.* 519, 1476–1491.

Capogna, M. (2011). Neurogliaform cells and other interneurons of stratum lacunosum-moleculare gate entorhinal-hippocampal dialogue. *J. Physiol.* 589, 1875–1883.

Catania, M. V., Tolle, T. R., and Monyer, H. (1995). Differential expression of AMPA receptor subunits in NOS-positive neurons of cortex, striatum, and hippocampus. *J. Neurosci.* 15, 7046–7061.

de Bergeyck, V., Naerhuyzen, B., Goffinet, A. M., and Lambert de Rouvroit, C. (1998). A panel of monoclonal antibodies against reelin, the extracellular matrix protein defective in reeler mutant mice. *J. Neurosci. Methods* 82, 17–24.

Freund, T. F., and Buzsáki, G. (1996). Interneurons of the hippocampus. *Hippocampus* 6, 347–470.

Fuentealba, P., Begum, R., Capogna, M., Jinno, S., Marton, L. F., Csicsvari, J., Thomson, A., Somogyi, P., and Klausberger, T. (2008). Ivy cells: a population of nitric-oxide-producing, slow-spiking GABAergic neurons and their involvement in hippocampal network activity. *Neuron* 57, 917–929.

Fukudome, Y., Ohno-Shosaku, T., Matsui, M., Omori, Y., Fukaya, M., Tsubokawa, H., Taketo, M. M., Watanabe, M., Manabe, T., and Kano, M. (2004). Two distinct classes of muscarinic action on hippocampal inhibitory synapses: M2-mediated direct suppression and M1/M3-mediated indirect suppression through endocannabinoid signalling. *Eur. J. Neurosci.* 19, 2682–2692.

Kägi, U., Berchtold, M. W., and Heizmann, C. W. (1987). Ca^{2+}-binding parvalbumin in rat testis. Characterization, localization, and expression during development. *J. Biol. Chem.* 262, 7314–7320.

Karagiannis, A., Gallopin, T., David, C., Battaglia, D., Geoffroy, H., Rossier, J., Hillman, E. M., Staiger, J. F., and Cauli, B. (2009). Classification of NPY-expressing neocortical interneurons. *J. Neurosci.* 29, 3642–3659.

Karayannis, T., Elfant, D., Huerta-Ocampo, I., Teki, S., Scott, R. S., Rusakov, D. A., Jones, M. V., and Capogna, M. (2010). Slow GABA transient and receptor desensitization shape synaptic responses evoked by hippocampal neurogliaform cells. *J. Neurosci.* 30, 9898–9909.

Krook-Magnuson, E., Luu, L., Lee, S. H., Varga, C., and Soltesz, I. (2011). Ivy and neurogliaform interneurons are a major target of mu-opioid receptor modulation. *J. Neurosci.* 31, 14861–14870.

Lambolez, B., Audinat, E., Bochet, P., Crépel, F., and Rossier, J. (1992). AMPA receptor subunits expressed by single Purkinje cells. *Neuron* 9, 247–258.

Leavesley, S. J., Annamdevula, N., Boni, J., Stocker, S., Grant, K., Troyanovsky, B., Rich, T. C., and Alvarez, D. F. (2012). Hyperspectral imaging microscopy for identification and quantitative analysis of fluorescently-labeled cells in highly autofluorescent tissue. *J. Biophotonics* 5, 67–84.

Maccaferri, G. (2011). Modulation of hippocampal stratum lacunosum-moleculare microcircuits. *J. Physiol.* 589, 1885–1891.

Oren, I., Nissen, W., Kullmann, D. M., Somogyi, P., and Lamsa, K. P. (2009). Role of ionotropic glutamate receptors in long-term potentiation in rat hippocampal CA1 oriens-lacunosum moleculare interneurons. *J. Neurosci.* 29, 939–950.

Price, C. J., Cauli, B., Kovacs, E. R., Kulik, A., Lambolez, B., Shigemoto, R., and Capogna, M. (2005). Neurogliaform neurons form a novel inhibitory network in the hippocampal CA1 area. *J. Neurosci.* 25, 6775–6786.

Price, C. J., Scott, R., Rusakov, D. A., and Capogna, M. (2008). GABA(B) receptor modulation of feedforward inhibition through hippocampal neurogliaform cells. *J. Neurosci.* 27, 6974–6982.

Schwaller, B., Dick, J., Dhoot, G., Carroll, S., Vrbova, G., Nicotera, P., Pette, D., Wyss, A., Bluethmann, H., Hunziker, W., and Celio, M. R. (1999). Prolonged contraction-relaxation cycle of fast-twitch muscles in parvalbumin knockout mice. *Am. J. Physiol.* 276, C395–C403.

Somogyi, P. (2010). "Hippocampus: intrinsic organization," in *Handbook of Brain Microcircuits*, eds G. M. Shepherd and S. Grillner (New York, NY: Oxford University Press), 148–164.

Szabadics, J., and Soltesz, I. (2009). Functional specificity of mossy fiber innervation of GABAergic cells in the hippocampus. *J. Neurosci.* 29, 4239–4251.

Szabadics, J., Tamas, G., and Soltesz, I. (2007). Different transmitter transients underlie presynaptic cell type specificity of GABAA, slow and GABAA, fast. *Proc. Natl. Acad. Sci. U.S.A.* 104, 14831–14836.

Szabo, A., Somogyi, J., Cauli, B., Lambolez, B., Somogyi, P., and Lamsa, K. (2012). Calcium-permeable AMPA receptors provide a common mechanism for LTP in glutamatergic synapses of distinct hippocampal interneuron types. *J. Neurosci.* 32, 6511–6516.

Tamas, G., Lorincz, A., Simon, A., and Szabadics, J. (2003). Identified sources and targets of slow inhibition in the neocortex. *Science* 299, 1902–1905.

Tricoire, L., Pelkey, K. A., Daw, M. I., Sousa, V. H., Miyoshi, G., Jeffries, B., Cauli, B., Fishell, G., and McBain, C. J. (2010). Common origins of hippocampal Ivy and nitric oxide synthase expressing neurogliaform cells. *J. Neurosci.* 30, 2165–2176.

Tricoire, L., Pelkey, K. A., Erkkila, B. E., Jeffries, B. W., Yuan, X., and McBain, C. J. (2011). A blueprint for the spatiotemporal origins of mouse hippocampal interneuron diversity. *J. Neurosci.* 31, 10948–10970.

Valm, A. M., Mark Welch, J. L., Rieken, C. W., Hasegawa, Y., Sogin, M. L., Oldenbourg, R., Dewhirst, F. E., and Borisy, G. G. (2011). Systems-level analysis of microbial community organization through combinatorial labeling and spectral imaging. *Proc. Natl. Acad. Sci. U.S.A.* 108, 4152–4157.

Conflict of Interest Statement: The authors declare that the research was conducted in the absence of any commercial or financial relationships that could be construed as a potential conflict of interest.

Received: 02 April 2012; paper pending published: 12 April 2012; accepted: 18 May 2012; published online: 31 May 2012.

Citation: Somogyi J, Szabo A, Somogyi P and Lamsa K (2012) Molecular analysis of ivy cells of the hippocampal CA1 stratum radiatum using spectral identification of immunofluorophores. Front. Neural Circuits ***6****:35. doi: 10.3389/fncir.2012.00035*

frontiers in
NEURAL CIRCUITS

ORIGINAL RESEARCH ARTICLE
published: 09 July 2012
doi: 10.3389/fncir.2012.00044

The origin of neocortical nitric oxide synthase-expressing inhibitory neurons

Xavier H. Jaglin[1], Jens Hjerling-Leffler[2], Gord Fishell[1,3] and Renata Batista-Brito[1]*†

[1] *NYU Neuroscience Institute, New York University Langone Medical Center, New York, NY, USA*
[2] *Division of Molecular Neurobiology, Department of Medical Biochemistry and Biophysics, Karolinska Institute, Stockholm, Sweden*
[3] *Departments of Cell Biology and Neural Science, New York University Langone Medical Center, New York, NY, USA*

Edited by:
Ludovic Tricoire, Université Pierre et Marie Curie, France

Reviewed by:
Kenneth A. Pelkey, National Institutes of Health, USA
Armelle Rancillac, Centre National de la Recherche Scientifique, France
Alessandra Pierani, Université Paris Diderot, France

****Correspondence:***
Renata Batista-Brito, Department of Neurobiology, NYU Neuroscience Institute, Yale University, 333 Cedar St., PO Box 208001, New Haven, CT 06520-8001, USA.
e-mail: renata.brito@yale.edu

†Present address:
Renata Batista-Brito, Department of Neurobiology, Yale University, 333 Cedar St., PO Box 208001, New Haven, CT 06520-8001, USA.

Inhibitory neurons are critical for regulating effective transfer of sensory information and network stability. The precision of inhibitory function likely derives from the existence of a variety of interneuron subtypes. Their specification is largely dependent on the locale of origin of interneuron progenitors. Neocortical and hippocampal inhibitory neurons originate the subpallium, namely in the medial and caudal ganglionic eminences (MGE and CGE), and in the preoptic area (POA). In the hippocampus, neuronal nitric oxide synthase (nNOS)-expressing cells constitute a numerically large GABAergic interneuron population. On the contrary, nNOS-expressing inhibitory neurons constitute the smallest of the known neocortical GABAergic neuronal subtypes. The origins of most neocortical GABAergic neuron subtypes have been thoroughly investigated, however, very little is known about the origin of, or the genetic programs underlying the development of nNOS neurons. Here, we show that the vast majority of neocortical nNOS-expressing neurons arise from the MGE rather than the CGE. Regarding their molecular signature, virtually all neocortical nNOS neurons co-express the neuropeptides somatostatin (SST) and neuropeptide Y (NPY), and about half of them express the calcium-binding protein calretinin (CR). nNOS neurons thus constitute a small cohort of the MGE-derived SST-expressing population of cortical inhibitory neurons. Finally, we show that conditional removal of the transcription factor *Sox6* in MGE-derived GABAergic cortical neurons results in an absence of SST and CR expression, as well as reduced expression of nNOS in neocortical nNOS neurons. Based on their respective abundance, origin and molecular signature, our results suggest that neocortical and hippocampal nNOS GABAergic neurons likely subserve different functions and have very different physiological relevance in these two cortical structures.

Keywords: inhibition, interneuron, cortex, hippocampus, nNOS, GABAergic, fate mapping, MGE

INTRODUCTION

Brain activity is regulated by the interaction of two major types of neural cells: excitatory neurons that use the neurotransmitter glutamate and inhibitory neurons that use the neurotransmitter γ-aminobutyric acid (GABA). Inhibitory neurons are critical for maintaining the excitatory-inhibitory balance necessary for the effective transfer of information while preventing runaway excitation, and consequently play important roles in regulating network activity (Pouille and Scanziani, 2001; Markram et al., 2004; Haider and McCormick, 2009). Severe disruption of GABAergic inhibition profoundly alters neocortical activity patterns and leads to seizures, while milder changes in inhibitory neuron number and function are strongly linked to psychiatric disorders, such as schizophrenia and autism (Volk et al., 2002; Yau et al., 2003; Belmonte et al., 2004; Levitt et al., 2004; Cossart et al., 2005; Dani et al., 2005; Caceda et al., 2007; Gonzalez-Burgos and Lewis, 2008; Morris et al., 2008). Inhibition is thus hypothesized to be a critical regulator of normal brain function and a key cause of dysfunction in disease. Inhibitory function relies on the existence of a variety of GABAergic inhibitory neuronal subtypes. Most inhibitory neurons display locally projecting axons and have been consequently named interneurons. Besides this morphological variety, different classes of inhibitory neurons exhibit distinct intrinsic membrane properties, molecular markers, connectivity, and synaptic specializations, and therefore likely mediate specific roles within cortical circuits (Fishell and Rudy, 2011). In the murine system, although many characteristics are not acquired until several weeks postnatally, the specification of GABAergic neurons in the mature animal is largely established during embryonic development, through the function of specific transcription factors exclusive to different spatial regions (Flames et al., 2004; Butt et al., 2005, 2008; Wonders and Anderson, 2006; Fogarty et al., 2007; Wonders et al., 2008; Batista-Brito and Fishell, 2009; Gelman et al., 2009).

While the majority of neocortical GABAergic neurons project a highly ramified axon locally, these interneurons are not the sole source of inhibition within the neocortex. A small portion of GABAergic neurons projects axons to distant neocortical areas, including regions in the ipsilateral hemisphere and contralateral hemispheres (McDonald and Burkhalter, 1993; Gonchar et al.,

1995; Aroniadou-Anderjaska and Keller, 1996; Chowdhury et al., 1996; Salin and Prince, 1996; Kimura and Baughman, 1997). A study combining labeling of GABAergic projection neurons, retrograde labeling and axon tracing methods revealed that the vast majority of neocortical long-range projecting GABAergic neurons belong to a group of cells expressing the neuronal isoform of nitric oxide synthase (nNOS) (Tomioka et al., 2005). This result suggests that even though low in number (Gonchar et al., 2007), neocortical nNOS GABAergic neurons have the potential to strongly influence neocortical networks. Most of the studies on the origin and function of nNOS cells have focused on the hippocampus where nNOS is expressed in a numerically large population of GABAergic neurons (Fuentealba et al., 2008; Tricoire et al., 2010, 2011). However, the function and origin of nNOS-expressing inhibitory neurons in the neocortex remain largely unexplored.

Neocortical and hippocampal GABAergic inhibitory neurons are produced in the neurogenic ganglionic eminences of the ventral telencephalon (or subpallium) and migrate tangentially toward the neocortex and hippocampus (Anderson et al., 1997a; Lavdas et al., 1999; Sussel et al., 1999; Pleasure et al., 2000; Marin and Rubenstein, 2001; Wichterle et al., 2001). The ventral ganglionic eminences express numerous genes known to be essential for the generation of GABAergic cells. These include genes with widespread expression throughout the subpallium, such as the *Distaless homeobox* (*Dlx*) family of genes (*Dlx1*, *2*, *5*, and *6*) (Anderson et al., 1997a,b; Cobos et al., 2005; Ghanem et al., 2007; Potter et al., 2009), which have been shown to be critical for interneuron migration and specification (Anderson et al., 1997b; Pleasure et al., 2000; Petryniak et al., 2007). Most neocortical and hippocampal GABAergic neurons are produced in the embryonic proliferative regions named the medial and caudal ganglionic eminences (MGE and CGE, respectively) (Wichterle et al., 2001; Nery et al., 2002; Xu et al., 2004, 2008; Butt et al., 2005; Flames et al., 2007; Fogarty et al., 2007; Miyoshi et al., 2010; Tricoire et al., 2011), and a smaller percentage are produced in the embryonic preoptic area (POA) (Gelman et al., 2009, 2011).

In the neocortex, near all parvalbumin (PV) and somatostatin (SST) expressing inhibitory neuron subtypes are produced in the MGE (Wichterle et al., 1999; Butt et al., 2005; Fogarty et al., 2007; Wonders et al., 2008; Xu et al., 2008). The genetic cascade necessary for proper specification, differentiation, and development of MGE-derived interneurons is starting to be elucidated. *Nkx2.1* has been shown to direct the MGE-subtype specification and *Lhx6* is necessary for the proper migration and maturation of both PV- and SST-expressing interneurons (Sussel et al., 1999; Liodis et al., 2007). The transcription factor *Sox6*, which is also expressed in MGE-derived interneuron lineages (Azim et al., 2009; Batista-Brito et al., 2009), acts downstream of *Lhx6* and is required for the positioning and maturation of PV cells, and to a lesser extent, SST cells (Batista-Brito et al., 2009).

In addition to the MGE, the CGE is the second largest source of neocortical inhibitory neurons, contributing approximately 30% of all GABAergic neurons (Lee et al., 2010). Recently, it has been shown that all CGE-derived neocortical interneurons specifically express the serotonin receptor 3a (5-Ht3a) (Lee et al., 2010; Vucurovic et al., 2010), while the transcription factors CoupTF1/2 are widely but not selectively expressed within the CGE (Sousa et al., 2009). The 5-Ht3a-expressing CGE-derived GABAergic neocortical interneurons, includes the entire vasoactive intestinal peptide (VIP) and cholecystokinin (CCK)-expressing population as well as the entire SST-negative populations of calretinin (CR) and Reelin (RLN)-expressing interneurons (Nery et al., 2002; Lee et al., 2010; Miyoshi et al., 2010).

It has been recently shown that different parts of the POA selectively express *Nkx5.1* and *Dbx1*, respectively, and produce a small and highly diverse fraction of neocortical GABAergic interneurons (Gelman et al., 2009, 2011). The interneurons types produced in the *Dbx1* population are largely overlapping with the MGE-derived subtypes while it is possible that the *Nkx5.1* expressing population is included in the population expressing *5-Ht3a* (Gelman et al., 2009, 2011; Lee et al., 2010).

Similarly to neocortical interneurons, PV- and SST-expressing hippocampal interneurons originate in the MGE, whereas hippocampal interneurons expressing CCK, CR, and VIP are produced in the CGE (Tricoire et al., 2011; Keimpema et al., 2012). Neuropeptide Y (NPY) expressing hippocampal interneurons encompass a mixed repertoire of subtypes originating from the MGE, CGE and the POA (Gelman et al., 2009). Despite largely originating in the MGE, the majority of nNOS-expressing hippocampal GABAergic neuron subpopulations do not overlap with PV- or SST-expressing interneurons (Fuentealba et al., 2008; Tricoire et al., 2010, 2011), and few nNOS-positive cells co-express CR (Jinno and Kosaka, 2002a). In the hippocampus, nNOS is expressed in the majority of neurogliaform cells (NGC) and Ivy cells (IvCs) interneuron subtypes (Fuentealba et al., 2008; Tricoire et al., 2010). Within the hippocampus, nNOS colocalizes with a variety of markers (Fuentealba et al., 2008; Szabadics and Soltesz, 2009; Tricoire et al., 2010) and has been reported to be the numerically largest interneuron population (Fuentealba et al., 2008). It remains unknown if there are any homologs of the nNOS-expressing neurogliaform and Ivy interneurons within the neocortex.

Here we show that contrary to the hippocampus, nNOS-expressing cells constitute a small minority of the total neocortical GABAergic neurons. In order to investigate the developmental origin of nNOS-expressing cells, we did genetic fate mapping using cre-drivers specific for different domains of the MGE (*Nkx2.1*^{Cre} and *Lhx6*^{Cre}) as well as the *5-Ht3a*^{EGFP}-reporter line that labels the CGE-derived lineage. Our findings suggest that nNOS-expressing neocortical GABAergic neurons originate from the MGE, mainly from the most dorsal domain of the MGE (dMGE). In the hippocampus, similarly to what has been previously shown, we observed that a majority of the nNOS interneurons are derived from the MGE, but a significant portion originate within the CGE and/or POA (Tricoire et al., 2010). Both neocortical and hippocampal nNOS-expressing cells also express NPY, but in contrast to the hippocampus virtually all neocortical nNOS neurons express SST, and about half express CR. Finally, we show that the transcription factor *Sox6* has a role in the differentiation of neocortical nNOS cells, since loss of *Sox6* leads to a total absence of SST expression in neocortical nNOS cells, and possibly stunts the development of neurites.

Our results show that nNOS-expressing neocortical and hippocampal inhibitory neurons have different origins, suggesting that neocortical and hippocampal nNOS-expressing cells constitute an example of unrelated subtypes, both having acquired/retained the expression of nNOS. Understanding the functional role of this sparse population of neocortical long-range projection inhibitory neurons and the relevance of the nitrinergic signaling in cortical circuits are questions of considerable interest.

MATERIALS AND METHODS

MOUSE LINES

All animal handling and maintenance were performed according to the regulations of the Institutional Animal Care and Use Committee of the NYU School of Medicine. The *Dlx6*^{Cre} (GENSAT project at Rockefeller University), *Lhx6*^{Cre} (Fogarty et al., 2007), *Nkx2.1*^{Cre} (Xu et al., 2008), *SST*^{Cre} (Taniguchi et al., 2011), *5-Ht3a*^{EGFP} (GENSAT project at Rockefeller University), *Sox6*$^{F/+}$ (Dumitriu et al., 2006), and *RCE*^{EGFP} (Sousa et al., 2009) mouse lines were maintained in a mixed background (Swiss Webster and C57Bl/6), and genotyped as previously described (Stenman et al., 2003; Dumitriu et al., 2006; Fogarty et al., 2007; Butt et al., 2008; Xu et al., 2008; Taniguchi et al., 2011).

In vivo GENETIC FATE MAPPING

To perform genetic fate mapping of neocortical and hippocampal GABAergic neurons transgenic males heterozygous for the driver line *Dlx6*^{Cre} (GENSAT project at Rockefeller University) were crossed to female homozygous for the *RCE*^{EGFP} allele reporter allele (Sousa et al., 2009). To fate map MGE-derived lineages, males heterozygous for the transgenic driver lines *Lhx6*^{Cre} (Fogarty et al., 2007) and *Nkx2.1*^{Cre} (Xu et al., 2008) were crossed to female mice homozygous for the *RCE*^{EGFP} reporter allele (Sousa et al., 2009). Fate mapping of the CGE-derived lineage was accomplished by using the BAC-transgenic line *5-Ht3a*^{EGFP} (GENSAT project at Rockefeller University).

In vivo Sox6 CONDITIONAL LOSS OF FUNCTION

Male *Sox6*$^{F/+}$; *Lhx6*^{Cre} or *Sox6*$^{F/+}$; *SST*^{Cre} mice were crossed to *Sox6*$^{F/F}$; *RCE*$^{EGFP/EGFP}$ females to generate productive *Sox6*$^{F/+}$; *Lhx6*^{Cre}; *RCE*^{EGFP} (control) and *Sox6*$^{F/F}$; *Lhx6*^{Cre}; *RCE*^{EGFP} (mutant); or *Sox6*$^{F/+}$; *SST*^{Cre}; *RCE*^{EGFP} (control) and *Sox6*$^{F/F}$; *SST*^{Cre}; *RCE*^{EGFP} (mutant) offspring.

TISSUE PREPARATION FOR IMMUNOCYTOCHEMISTRY

The brains of juvenile mice (P21) were fixed by transcardiac perfusion of 4% paraformaldehyde (PFA)/phosphate buffered saline (PBS) solution followed by a one hour post-fixation on ice with 4% PFA/PBS solution. Brains were rinsed with PBS and cryoprotected by using 30% sucrose/PBS solution overnight at 4°C. Tissues were embedded in Tissue Tek, frozen on dry ice, and cryosectioned at 20 μm thickness.

IMMUNOHISTOCHEMISTRY

Sections for immunohistochemistry analysis were processed using 2% normal goat serum/0.1% Triton X-100 in all procedures except washing steps, where only PBS was used. Sections were blocked for 1 h, followed by incubation with the primary antibodies overnight at 4°C. Cryostat tissue sections were stained with the following primary antibodies: rabbit anti-GFP (1:1000; Molecular Probes), rat anti-GFP (1:1000, Nacalai Tesque), chicken anti-GFP (1:1000, AbCam), mouse anti-Parvalbumin (1:1000; Sigma), rat anti-SST (1:500; Chemicon), rabbit anti-NPY (1:500; Incstar), sheep anti-NPY (1:500; Chemicon), mouse anti-Reelin (1:500; MBL international), rabbit anti-nNOS (1:1000, Chemicon), mouse anti-calretinin (1:750; Chemicon). Secondary antibodies conjugated with Alexa fluoro-dyes 488, 594, or 649 (Molecular Probes) raised from the same host were then used as blocking serum and were applied for 30 min at room temperature for visualizing the signals. Nuclear counterstaining was performed with 100 ng/ml 4,6-diamidino-2-phenylindole (DAPI) solution in PBS for 1 min. Fluorescent images were captured using a cooled-CCD camera (Princeton Scientific Instruments, NJ) using Metamorph software (Universal imaging, Dwoningtown, PA). For all embryonic and postnatal stages, counting was performed on a minimum of four coronal sections from at least two animals using the image processing and analysis software ImageJ (Wayne Rasband, NIH). Neocortical analyses were performed in the somatosensory barrel cortex (S1BF). Hippocampal analyses were carried out in CA3, CA1, and dentate gyrus. To minimize counting bias we compared sections of equivalent bregma positions (from −1.5 mm to −2.0 mm relative to bregma), defined according to the Mouse Brain atlas (Franklin and Paxinos, 2001). All data were represented as mean ± SEM.

RESULTS

NEOCORTICAL nNOS-EXPRESSING CELLS CONSTITUTE A SMALL MINORITY OF NEOCORTICAL GABAergic NEURONS

Previous work has shown that nNOS cells in the hippocampus and neocortex express markers characteristic of inhibitory neurons (Jinno et al., 2002; Gonchar et al., 2007; Fuentealba et al., 2008). In order to determine the percentage of nNOS neurons that are GABAergic, as well as the percentage of GABAergic neurons that express nNOS we performed immunostaining for nNOS in brain slices where the entire GABAergic cortical neuronal population was labeled with EGFP, using genetic fate mapping of cells expressing the pan-GABAergic gene *Dlx6* (Batista-Brito et al., 2008). Genetic fate mapping experiments using Cre/loxP technology are based on the combined use of a *driver allele* (whereby the promoter of a gene of interest drives the expression of a Cre recombinase) and a *floxed-reporter allele* (whereby the expression of the reporter gene is triggered by a recombination event mediated by the Cre recombinase). Upon recombination, the expression of the reporter gene allows for selective and cumulative labeling of cells sharing the common expression of the gene of interest at any point in their history. Here we used the *Dlx6*^{Cre} driver mouse line combined with the *RCE*^{EGFP} reporter line, whereby Cre activity removes the floxed-STOP cassette at the *Rosa* locus, resulting in permanent EGFP expression in cells that have once expressed *Dlx6*. We show that all the neocortical and hippocampal interneurons (100 ± 0.9% and 99.5 ± 1.1%, respectively) expressing nNOS also express EGFP. Therefore, we conclude that nNOS labeling in the neocortex and hippocampus is restricted to GABAergic neurons (**Figures 1A–C**). The number

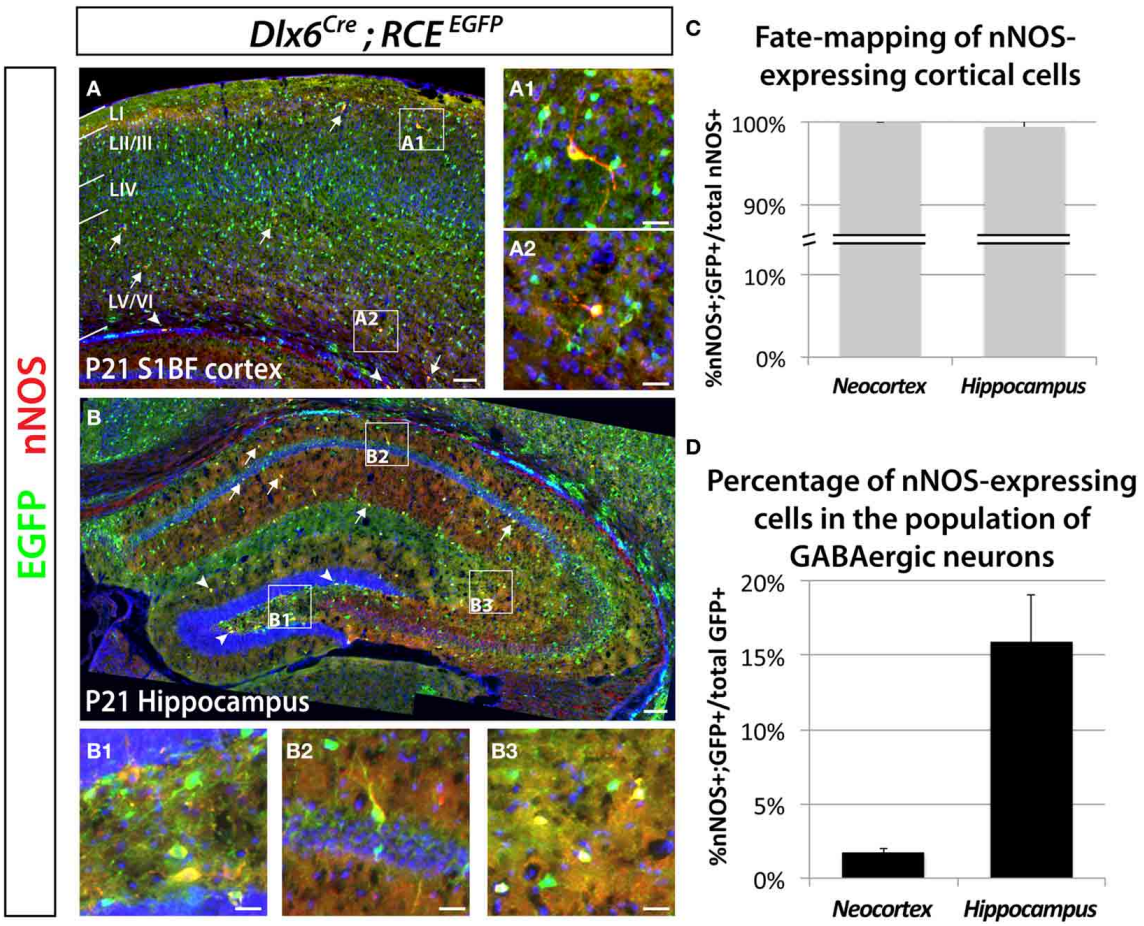

FIGURE 1 | Genetic fate mapping reveals that neocortical and hippocampal nNOS-expressing cells are GABAergic inhibitory neurons. The inhibitory fate was verified using the pan-interneuronal driver *Dlx6*^{Cre} allowing the expression of the EGFP from the RCE reporter in the neocortex (somatosensory cortex) **(A)** and hippocampus **(B)**. Using this fate mapping strategy we determined the percentage of neocortical and hippocampal GABAergic neurons expressing the neuronal Nitric Oxide Synthase (nNOS) on telencephalic coronal sections. **(A)** Representative section showing sparse cells that express nNOS in the mouse barrel cortex at P21 (arrows), mainly in superficial (layer II/III) (A1) and deep (layer VI) (A2) layers as shown by the DAPI counterstaining. Note the presence of EGFP in every nNOS-expressing cell. A few nNOS-expressing neurons are also located in the white matter (arrowheads). **(B)** Scattered nNOS staining is found throughout the mouse hippocampus at P21, in all layers of the Ammon's horns CA1–3 (arrows) as well as in all layers of the dentate gyrus (arrowheads). Similar to the neocortex and irrespective of the cell's location within the hippocampus (B1, hilar region and subgranular layer of the dentate gyrus; B2, CA1 stratum pyramidale and stratum oriens; B3, CA3 stratum radiatum and stratum lacunosum-moleculare), nNOS-expressing cells are GABAergic neurons as revealed by the expression of EGFP. **(C)** Histogram showing the percentage of nNOS-expressing neurons that are fate mapped by the *Dlx6*^{Cre}*; RCE*^{EGFP} line in mouse cortex and hippocampus ($100 \pm 0.0\%$ and $99.5 \pm 1.1\%$) ($n = 3$ independent brains for each genotype). **(D)** Histogram showing the percentage of *Dlx6*^{Cre}*; RCE*^{EGFP} fate mapped interneurons that express nNOS in mouse cortex and hippocampus ($1.7 \pm 0.3\%$ and $15.9 \pm 3.2\%$) ($n = 3$ independent brains for each genotype). Data represent mean ± SEM. Scale bars correspond to 100 μm **(A,B)** and 25 μm (A1,A2,B1–3).

of neocortical GABAergic neurons expressing nNOS is much lower relative to the number of nNOS-expressing cells in the hippocampus (**Figures 1A–C**). Within the neocortex only $1.7 \pm 0.3\%$ of the total number of *Dlx6* fate mapped cells express nNOS, compared to $15.9 \pm 3.2\%$ in the hippocampus (**Figure 1D**). All our analyses were confined to cells that express high levels of nNOS, also known as nNOS type I neurons (Yan et al., 1996; Judas et al., 1999; Lee and Jeon, 2005). For simplicity, and because the used antibody does not allow the identification of cells expressing low levels of nNOS (type II nNOS neurons), we will refer to the cells that unambiguously express high levels of nNOS as nNOS-expressing cells throughout the manuscript. Neocortical nNOS neocortical neurons are preferentially distributed in deeper layers (V–VI), although some are located in the superficial layers (II/III) (**Figure 1A**). Furthermore, a few nNOS-expressing neurons are also located in the white matter. Neocortical nNOS neurons display highly elaborated processes as described elsewhere (Tomioka et al., 2005). By contrast, nNOS staining is present throughout the mouse hippocampus at P21, including all layers of the Ammon's horns CA1-3 as well as in the dentate gyrus' layers (except the granular layer) (**Figure 1B**).

THE MAJORITY OF NEOCORTICAL nNOS GABAergic NEURONS ORIGINATE WITHIN THE dMGE

In order to determine the origin of nNOS-expressing neocortical inhibitory neurons, we fate mapped neurons produced in the ventral telencephalon and located in the somatosensory cortex of P21 mice. Fate mapping of the MGE was accomplished by using the *Nkx2.1*^{Cre} (Xu et al., 2008) and *Lhx6*^{Cre} (Fogarty et al., 2007) driver lines in combination with the *RCE*^{EGFP} reporter allele. In *Nkx2.1*^{Cre}; *RCE*^{EGFP} mice, EGFP labeled cells originate in most of the MGE (except for its most dorsal part; dMGE), and the POA (Xu et al., 2008; Sousa et al., 2009). In *Lhx6*^{Cre}; *RCE*^{EGFP} mice cells originating within the entire MGE, and POA are permanently labeled with EGFP (Fogarty et al., 2007). *Lhx6* is also expressed in blood vessels, therefore, fate mapping using this line also labels blood vessels with EGFP (Fogarty et al., 2007). We labeled CGE-derived cells with the transgenic line *5-Ht3a*^{EGFP} (Lee et al., 2010).

Our results show that nNOS neurons colocalize with EGFP in the *Nkx2.1*^{Cre}; *RCE*^{EGFP} and *Lhx6*^{Cre}; *RCE*^{EGFP} mice (**Figures 2A,B**), but not in the *5-Ht3a*^{EGFP} animals (**Figure 2C**).

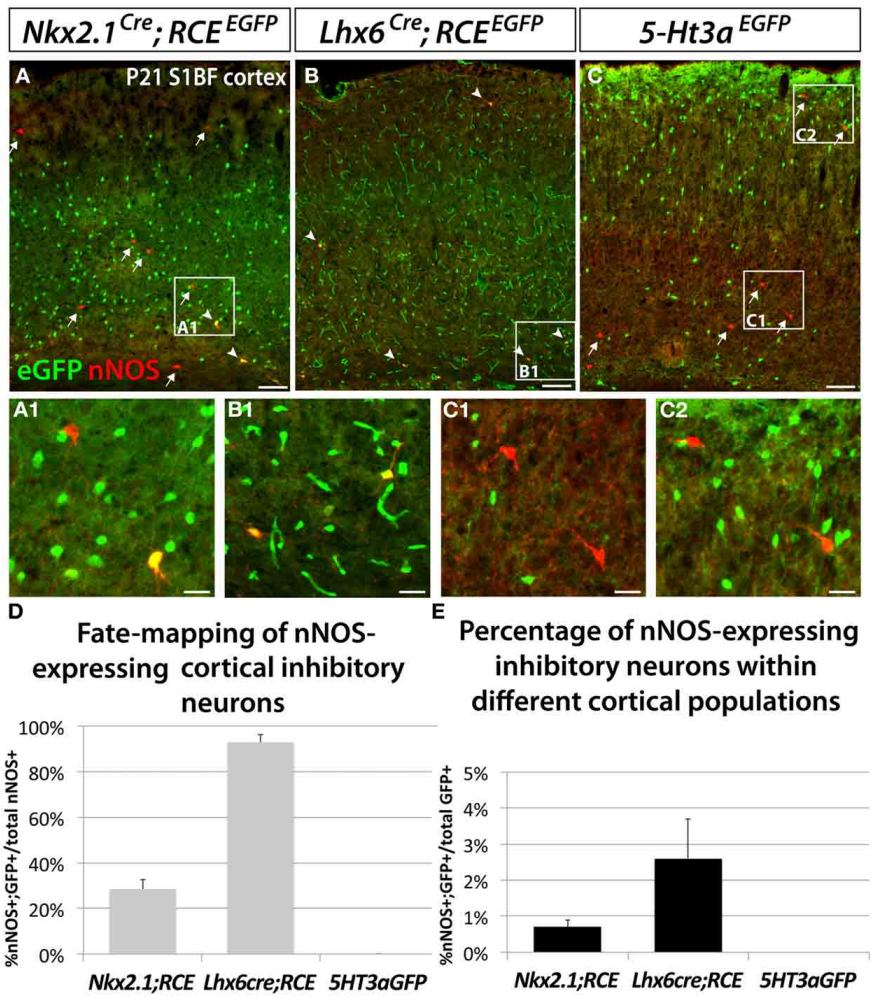

FIGURE 2 | Neocortical nNOS-expressing inhibitory neurons are derived from the medial ganglionic eminence. To ascertain and quantify the spatial origin of cortical nNOS inhibitory neurons, we employed different fate mapping strategies based on the use of *Nkx2.1*^{Cre}; *RCE*^{EGFP} **(A)**, *Lhx6*^{Cre}; *RCE*^{EGFP} **(B)**, or *5-Ht3a*^{EGFP} mice **(C)**. **(A–C)** Representative pictures of coronal sections of P21 mouse somatosensory neocortex immunolabeled with EGFP and nNOS. Fate mapped cells expressing EGFP and nNOS are indicated by arrowheads. Arrows indicated cells expressing nNOS only. **(D,E)** Histograms showing the fate mapping of cortical nNOS GABAergic neurons and the contribution of nNOS-expressing cells to MGE and CGE populations, expressed as the percentage of nNOS+/GFP+ cells in the entire nNOS positive population **(D)**, or in the entire EGFP positive population **(E)**. The *Nkx2.1*^{Cre}; *RCE*^{EGFP} fate mapping indicates that 28.5 ± 4.3% of nNOS GABAergic neurons originate from the MGE domain covered by the *Nkx2.1*^{Cre} driver line **(A,D)** and that nNOS cells account for 0.7 ± 0.2% of this *Nkx2.1*^{Cre}-derived population **(A,E)** ($n = 3$ independent brains). The *Lhx6*^{Cre}; *RCE*^{EGFP} and *5-Ht3a*^{EGFP} fate mapping strategies revealed that virtually all nNOS-cINs originate from the MGE (93.0 ± 3.3%) **(B,D)** and not from the CGE (no cells co-express nNOS and GFP) **(C,D)**, respectively ($n = 3$ independent brains for each genotype). On the other hand, nNOS cells account for 2.6 ± 1.1% of MGE-derived inhibitory neurons fate mapped by the *Lhx6*^{Cre}; *RCE*^{EGFP} **(B,E)**. Data represent mean ± SEM. Scale bars correspond to 100 μm **(A–C)** and 25 μm (A1,B1,C1,C2).

Since *5-Ht3a*^{EGFP} labels cells migrating out from the CGE, our results suggest that the CGE do not produce nNOS inhibitory neurons of the neocortex.

In contrast, 93 ± 3.3% of nNOS cells in the somatosensory cortex of *Lhx6*^{Cre}*; RCE*^{EGFP} mice express EGFP (**Figures 2B,D**), leading us to conclude that the vast majority of the neocortical nNOS cells originate within the MGE. Surprisingly, only 28.5 ± 4.3% of nNOS cells also express EGFP when we used the *Nkx2.1*^{Cre}; *RCE*^{EGFP} transgenic line. Comparison of the results from the *Nkx2.1*^{Cre}; *RCE*^{EGFP} and *Lxh6*^{Cre}; *RCE*^{EGFP} lines indicate that 70–75% of the total of nNOS cells in the somatosensory cortex originates within the dMGE, while the remaining 20–25% originates from the *Nkx2.1*^{Cre} domain. Moreover, this fate mapping strategy also confirmed that nNOS inhibitory neurons only account for a small portion of the MGE- and dMGE-derived cortical interneurons (respectively, 0.7 ± 0.19% of fate mapped interneurons in *Nkx2.1*^{Cre}; *RCE*^{EGFP} mice and 2.6 ± 1.1% of fate mapped interneurons in *Lhx6*^{Cre}; *RCE*^{EGFP} mice) (**Figure 2E**).

HIPPOCAMPAL nNOS GABAergic NEURONS DO NOT ORIGINATE WITHIN THE dMGE

We used the fate mapping approaches previously described to test if hippocampal nNOS neurons have the same origin as their neocortical counterparts. In accordance with previous studies (Tricoire et al., 2010), we observed that the majority of hippocampal nNOS neurons are derived from the MGE, as indicated by the observation that 76.5 ± 1.9% and 77.9 ± 5.7% of nNOS inhibitory neurons coexpress EGFP in the transgenic lines *Nkx2.1*^{Cre}; *RCE*^{EGFP} (**Figures 3A–C,J**) and *Lxh6*^{Cre}; *RCE*^{EGFP} (**Figures 3D–F,J**), respectively. Comparison of the results from the *Nkx2.1*^{Cre}; *RCE*^{EGFP} and *Lxh6*^{Cre}; *RCE*^{EGFP} lines indicate that, contrary to what is observed in the neocortex, only a small minority (less than 2%) of hippocampal nNOS cells originate from the dMGE. Furthermore, we observed in the hippocampus that 43.1 ± 0.4% of nNOS neurons were co-labeled with EGFP in the transgenic *5-Ht3a*^{EGFP} line (**Figures 3G–I,J**). While it has been previously recognized that the CGE produces some hippocampal nNOS neurons by using the transgenic lines *Gad65*^{GFP} (Tricoire et al., 2010) and *Mash1*^{CreER} (Tricoire et al., 2010), the contribution of the CGE towards nNOS hippocampal neurons perhaps have been underestimated. This could be due to the fact that the *Gad65*^{GFP} lineage does not recapitulate the totality of the CGE-derived lineage of interneurons, and due to the mosaic inducible nature of the *Mash1*^{CreER} line. However, the fact that 77.9 ± 5.7% (from the *Lhx6*^{Cre}) and 43.1 ± 0.4% (from *5-Ht3a*^{EGFP}) adds up to more than a 100% it is likely that *5-Ht3a*^{EGFP} is less a specific CGE-marker in the hippocampus compared to the cortex. Another possible explanation, which is not mutally exclusive of these observations, is that cell arising in the POA are both EGFP-positive in the *Lhx6*^{Cre}*; RCE*^{EGFP} and in the *5-Ht3a*^{EGFP} lines in the hippocampus. If the latter is the case, up to 21% of the nNOS population could be POA-derived, a much higher number than in the cortex.

Moreover, this fate mapping analysis in the hippocampus revealed that nNOS inhibitory neurons account for 39.4 ± 0.9% of *Nkx2.1*^{Cre}; *RCE*^{EGFP} fate mapped cells, 23.6 ± 5.4% of *Lhx6*^{Cre}; *RCE*^{EGFP} fate mapped cells and 15.1 ± 4.5% of of *5-Ht3a*^{EGFP} fate mapped cells (**Figure 3K**).

Interestingly, we observed that despite the striatum being typically thought of as a structure less related to the neocortex than the hippocampus, the origins of striatal and neocortical nNOS cells are more similar than the origins of hippocampal and neocortical nNOS cells. The vast majority of striatal nNOS cells originate from the MGE, as indicated by *Lhx6*^{Cre} fate mapping (Compare **Figure 4A** to **B**, **Figure 4C**) (Gittis et al., 2010). Similarly to the neocortex, the dMGE is a major source of striatal nNOS neurons, producing about 40% of this population (substract 45.9% of nNOS cells fate-mapped with the line *Nkx2.1*^{Cre}; *RCE*^{EGFP} to 86.7% of nNOS cells fate mapped with the line *Lhx6*^{Cre}; *RCE*^{EGFP}) (**Figure 4C**).

NEOCORTICAL nNOS NEURONS BELONG TO THE MGE-DERIVED SOMATOSTATIN-POSITIVE POPULATION OF GABAergic INHIBITORY NEURONS

In order to eludicate the neurochemical profile of the dMGE-derived nNOS-expressing inhibitory neurons, we performed immunostaining for nNOS and SST, PV, NPY, CR, and RLN, which are characteristic markers of inhibitory neuron subtypes. Double immunostaining performed with the antibodies nNOS and SST or PV in the juvenile somatosensory mouse cortex (P21) shows that virtually all nNOS cells co-express SST but not PV (data not shown). A further genetic fate mapping analysis carried out using the *SST*^{Cre}; *RCE*^{EGFP} line confirmed that all neocortical nNOS cells belong to the SST-expressing population, and none of them express PV (**Figures 5A,B**). In addition, we did triple labeling, to discern between the SST/CR and SST/RLN co-expressing populations versus the STT-negative/CR and /RLN expressing cells that are CGE-derived (Rudy et al., 2011). It is worth mentioning that NPY expression also seems to be shared by subpopulations of several different non-overlapping subtypes that have been shown to originate from the MGE, CGE, and POA (Fogarty et al., 2007; Xu et al., 2008; Gelman et al., 2009; Lee et al., 2010; Miyoshi et al., 2010). All the nNOS/SST double positive cells also co-express NPY (**Figures 5B,C**), 60 ± 15% express CR (**Figures 5B,D**), and none of the nNOS/SST double positive cells expressed RLN (**Figures 5B,E**). This is in contrast to the SST population in general, among which only around 25% co-express CR. This further supports a dorsal MGE origin for nNOS neocortical neurons since this population has been shown to also be enriched in SST/CR double positive interneurons (Sousa et al., 2009). In contrary, the majority of hippocampal nNOS cells do not express SST (**Figure 5F**), except for a small proportion of nNOS interneurons, mainly located in the dentate gyrus hilus (**Figure 5F1**). Interestingly, virtually all the striatal nNOS neurons also express SST (**Figure 5G**), once again suggesting that striatal, but not nNOS hippocampal neurons, are related to nNOS neocortical neurons in terms of origin and phenotype.

THE TRANSCRIPTION FACTOR *Sox6* IS REQUIRED FOR THE SPECIFICATION OF NEOCORTICAL nNOS GABAergic NEURONS

We have previously shown that the transcription factor *Sox6* is present in most if not all MGE-derived neocortical inhibitory neurons (Batista-Brito et al., 2009). *Sox6* expression is dependent

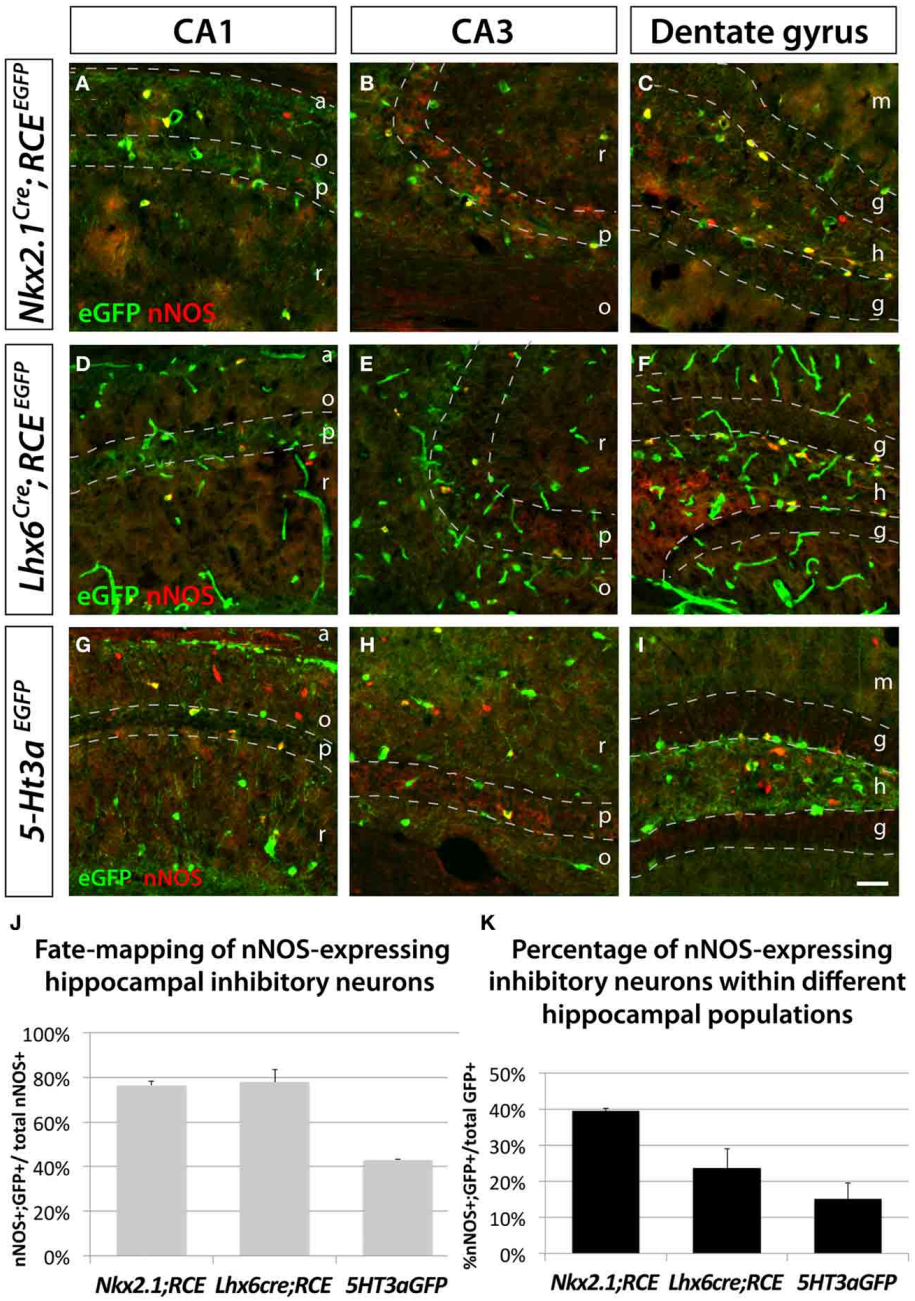

FIGURE 3 | Hippocampal nNOS-expressing inhibitory neurons are not generated from the dMGE. To ascertain and quantify the spatial origin of nNOS inhibitory neurons scattered through the entire hippocampus (CA1–3 and dentate gyrus), we employed different fate mapping strategies based on the use of *Nkx2.1^{Cre}; RCE^{EGFP}* **(A–C)**, *Lhx6^{Cre}; RCE^{EGFP}* **(D–E)**, or *5-Ht3a^{EGFP}* mice **(F–H)**. **(A,D,G; B,E,H; C,F,I)** Representative pictures of EGFP and nNOS immunolabeled P21 mouse hippocampus that illustrate the CA1, CA3 and dentate gyrus, respectively. Although MGE-derived nNOS GABAergic neurons are found in the different layers of the CA1 and CA3 regions, they are mostly found in the hilus and subgranular layer of the dentate gyrus **(A,B,D,E)** but are absent from the granular layer **(C,F)**. Similarly, CGE-derived nNOS cells are located in the different layers of CA1, CA3 **(G,H)** and dentate gyrus, with the exception of the dentate gyrus granular layer **(I)**. **(J,K)** Histograms showing the fate mapping of hippocampal nNOS GABAergic neurons and the contribution of nNOS-expressing cells to MGE- and CGE-derived populations of hippocampal inhibitory neurons. The *Nkx2.1^{cre}; RCE^{EGFP}* and *Lhx6^{Cre}; RCE^{EGFP}* fate mappings indicates that 76.5 ± 1.9% and 77.9 ± 5.7% of nNOS GABAergic neurons originate from the MGE domains covered by the *Nkx2.1^{Cre}* or *Lhx6^{Cre}* driver lines, respectively **(J)**. Note that comparable numbers of nNOS inhibitory neurons are fate mapped by both *Nkx2.1^{Cre}* or *Lhx6^{Cre}* driver lines suggesting that the dMGE is not an origin for hippocampal nNOS inhibitory neurons. By contrast, the nNOS cells account for 39.4 ± 0.9% and 23.6 ± 5.4% of the *Nkx2.1^{Cre}*- and *Lhx6^{Cre}*-derived population, respectively **(K)**. The *5-Ht3a^{EGFP}* fate mapping strategy revealed that 43.1 ± 0.4% of nNOS inhibitory neurons originate from the CGE. While conversely, nNOS GABAergic neurons account for 15.1 ± 4.5% of CGE-derived inhibitory neurons fate mapped by the *5-Ht3a^{EGFP}*. a, alveus; o, stratum oriens; p, stratum pyramidale; r, stratum radiatum; m, molecular layer; g, granular layer; h, hilus. Data represent mean ± SEM ($n = 3$ independent brains for each genotype). Scale bar corresponds to 100 μm.

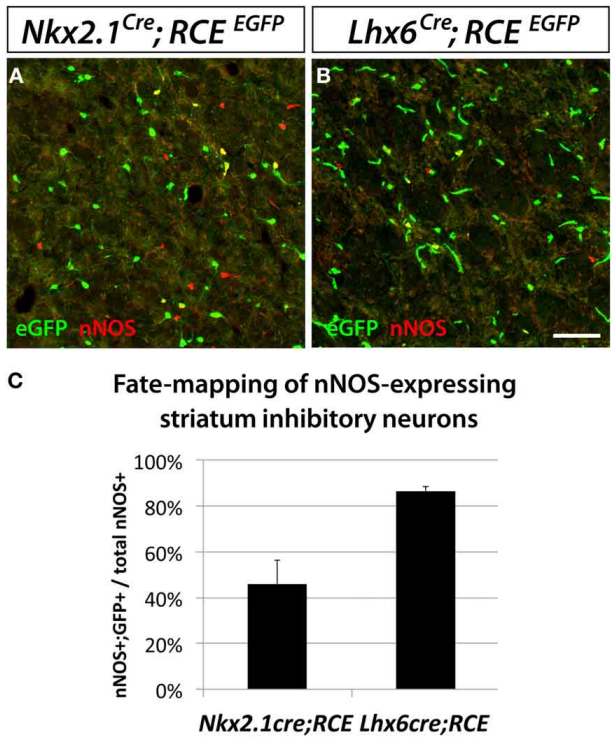

FIGURE 4 | Striatal nNOS GABAergic neurons are derived from the entire MGE. To determine and quantify the spatial origin of nNOS GABAergic neurons present in the striatum, we performed fate mapping experiments based on the use of *Nkx2.1*^{Cre}*; RCE*^{loxP} **(A)**, and *Lhx6*^{Cre}*; RCE*^{EGFP} **(B)**. This set of experiments revealed that 45.9 ± 10.5% and 86.7 ± 1.7% of nNOS GABAergic neurons originate from the MGE domains covered by the *Nkx2.1*^{Cre} or *Lhx6*^{Cre} driver lines, respectively **(C)**. Data represent mean ± SEM ($n = 3$ independent brains for each genotype). Scale bar corresponds to 50 μm.

on the activity of the transcription factor *Lhx6,* which is specifically expressed in all MGE-derived interneurons (Du et al., 2008). We reported that conditionally removing *Sox6* in MGE interneurons leads to a 30% reduction of the number of neocortical neurons expressing SST, and a complete loss of SST/CR-expression in mutant cells. In the present study, to address if in *Sox6* mutants the nNOS subtype was among the affected SST population, we removed *Sox6* from neocortical MGE-derived interneurons while simultaneously fate mapping the cells. To this end we used a conditional allele of *Sox6* (*Sox6*$^{F/F}$) (Dumitriu et al., 2006) crossed with the *Lhx6*^{Cre} driver line and the *RCE*^{EGFP} reporter line. The conditional mutant and control generated are *Sox6*$^{F/F}$; *Lhx6*^{Cre}; *RCE*^{EGFP} and *Sox6*$^{F/+}$; *Lhx6*^{Cre}; *RCE*^{EGFP}, respectively. In *Sox6*$^{F/F}$; *Lhx6*^{Cre}; *RCE*^{EGFP} mutants we could still identify nNOS neurons, however, nNOS somatic expression appeared to be diminished relatively to control animals (**Figures 6A,B**). While the total number of neocortical nNOS neurons tends to be slightly decreased in control vs mutant (4.8 ± 1.8 nNOS+ cells/mm^2 vs 3.4 ± 2.1 nNOS+ cells/mm^2, respectively), nNOS cells were rarely found in the superficial layers of *Sox6* conditional mutants. We next asked if the neurochemical markers NPY, SST, and CR were affected in neocortical mutant nNOS neurons. The somatic nNOS staining, in combination with the EGFP expression of fate mapped cells allowed for the identification of *Sox6* mutant MGE-derived inhibitory neurons. *Sox6* mutant nNOS neurons no longer express SST (**Figure 6C**) or CR (**Figure 6D**), but do retain the expression of NPY (**Figure 6E**). While cortical nNOS expressing neurons are affected by the conditional loss of *Sox6*, their hippocampal counterparts remain largely unaffected in the conditional *Sox6* mutants (data not shown). In agreement to what we reported previously (Batista-Brito et al., 2009), we observed a non-cell autonomous increase in the number of cells expressing NPY, as well as a diffuse and non-cell autonomous increase in the background of nNOS staining (data not shown). Furthermore, the cell morphology of mutant nNOS cells seemed to be severely affected, with these cells possessing considerably less dendritic and axonic arborization (compare **Figures 6A1** and **6B1**). However, it is not clear if this represents an alteration in the morphology of the cells, or if it is the result of weaker immunostaining. A more careful characterization, such as filling the mutant cells with a dye will be necessary to resolve this issue. However, since this cell population is so sparse, we did not succeed in identifying nNOS cells for detailed morphological analysis.

As previously described, *Sox6*$^{F/F}$; *Lhx6*^{Cre}; *RCE*^{EGFP} mutants develop generalized seizures by P16 followed by death of the animals between P17 and P19 from prolonged seizures, most likely due to a severe loss of inhibition from the affected PV-expressing basket cells (Batista-Brito et al., 2009). To test if the phenotype observed in nNOS cells was a non-cell autonomous consequence of seizure activity, we generated the mutant mice, *Sox6*$^{F/F}$; *SST*^{Cre}; *RCE*^{EGFP}, in which *Sox6* is only removed in SST-expressing MGE-derived inhibitory neurons, leaving the PV interneurons unaffected. *Sox6*$^{F/F}$; *SST*^{Cre}; *RCE*^{EGFP} mice appear to be phenotypically normal and do not show premature death nor develop obvious seizures. We confirmed that similarly to what we observed in *Sox6*$^{F/F}$; *Lhx6*^{Cre}; *RCE*^{EGFP} mutants, nNOS neocortical neurons in *Sox6*$^{F/F}$; *SST*^{Cre}; *RCE*^{EGFP} animals still fail to express SST and CR (data not shown) and have reduced nNOS expression at the soma level (**Figures 6F,G**), as well as seemingly less elaborated arborization of their processes (**Figures 6F1,G1**). Our results suggest that the transcription factor *Sox6* is necessary for the proper specification of nNOS neocortical neurons, and possibly necessary for the development of complex arborization of their processes (**Figure 7**).

DISCUSSION

In the present study, we characterized the contribution of nNOS-expressing cells in cortical GABAergic populations, as well as their place of origin and genes involved in their development. We show that contrary to the hippocampus, where nNOS interneurons are a numerous GABAergic class, nNOS (type I) neurons in the neocortex only constitute a very small portion of the GABAergic population. In accordance with previous studies, we observed that the majority of hippocampal nNOS GABAergic neurons originate within the MGE (Tricoire et al., 2010, 2011), however, a considerable percentage of this neuronal type also arises from the more ventral structures CGE and/ or POA. In contrast, the vast majority of neocortical nNOS GABAergic neurons

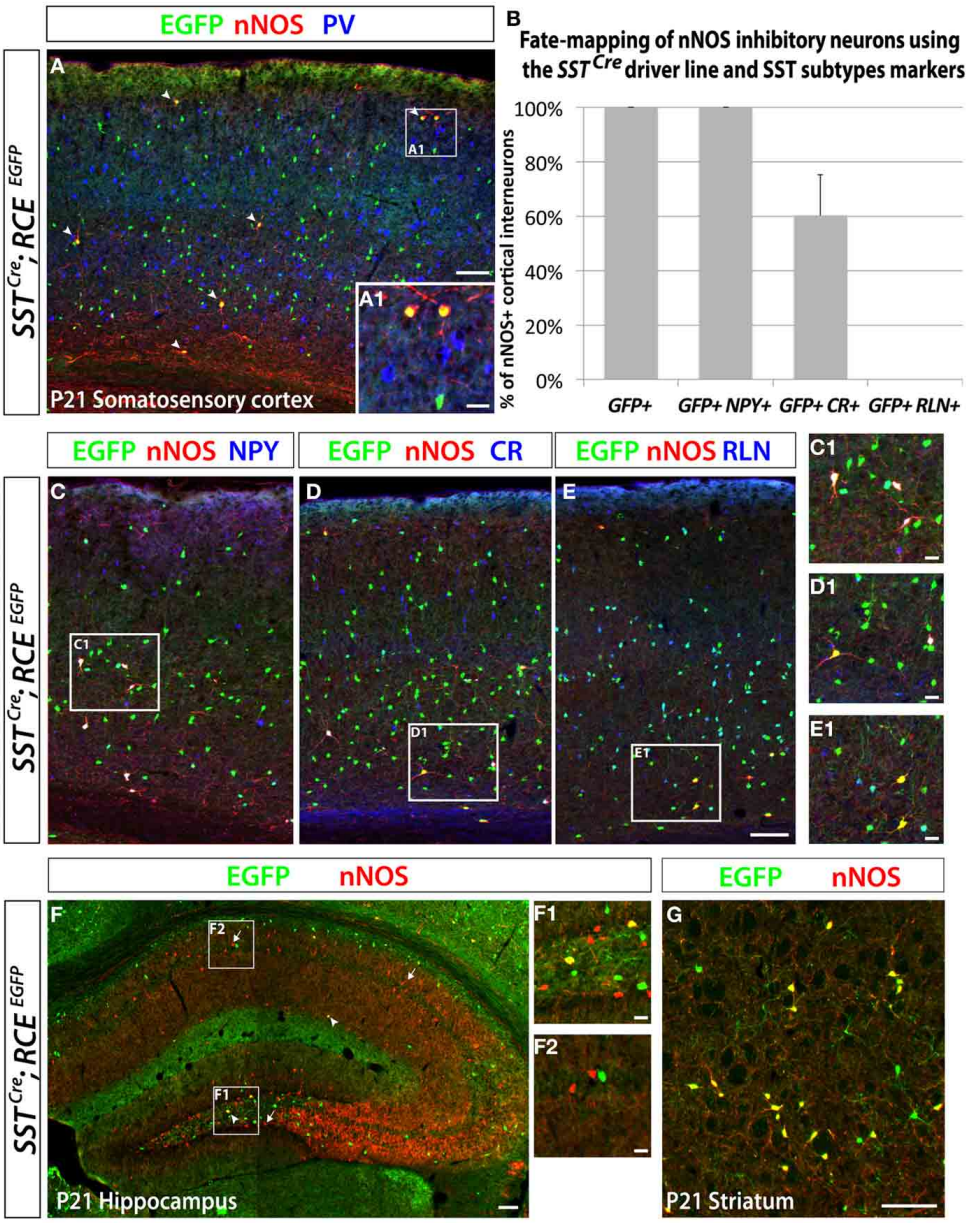

FIGURE 5 | Neocortical nNOS+ cells belong to the medial ganglionic eminence-derived somatostatin population of interneurons. Use of the *SST*^{Cre} driver in combination with the RCE reporter allows the identification of the SST-expressing population of inhibitory neurons both in the neocortex and the hippocampus. MGE-derived interneurons represent ~70% of the entire interneuron population and express either somatostatin (SST) (~30%) or parvalbumin (PV) (~40%). Immunostaining using those two markers permits visualization of the entire population of inhibitory neurons that come from the MGE. **(A)** The entire number of nNOS cells (red) in *SST*^{Cre}*; RCE*^{EGFP} P21 somatosensory cortex also expressed GFP (arrows) but not PV (blue only), either in deep or superficial (A1) layers. **(B–E)** Histograms and representative pictures of triple stainings performed on the *SST*^{Cre}*; RCE*^{EGFP} P21 somatosensory cortex to determine the proportion of nNOS cells co-expressing neurochemical markers found in the SST-expressing population of inhibitory neurons, such as Neuropeptide Y (NPY), Calretinin (CR), Reelin (RLN). The entire neocortical nNOS cells population belongs to the MGE-derived SST-expressing population of GABAergic neurons and account for 4.1 ± 0.8% of it (data not show). Moreover, 100% of SST+/nNOS+ neurons co-express NPY, 60 ± 15% co-express CR, and none of them co-express RLN. **(F)** To determine if hippocampal nNOS neurons belong to the MGE-derived SST-expressing population of inhibitory neurons, we performed immunolabeling of nNOS and EGFP on *SST*^{Cre}*; RCE*^{EGFP} P21 hippocampus. Only a small number of nNOS neurons express EGFP (arrowheads) in *SST*^{Cre}*; RCE*^{EGFP} P21 hippocampus, thus revealing their inclusion in the SST-expressing population of MGE-derived interneurons. This scarce population, as compared to the majority of nNOS neurons that do not express GFP (arrows), is most consistently found in the dentate gyrus hilus (F1) (F1, hilar region and subgranular layer of the dentate gyrus; F2, CA1 stratum oriens, pyramidale and radiatum). **(G)** To determine if striatal nNOS neurons belong to the MGE-derived SST-expressing population of interneurons, we performed immunolabeling of nNOS and EGFP on *SST*^{Cre}*; RCE*^{lEGFP} P21 striatum and revealed that about 93% of nNOS expressing striatal neurons belong the SST-expressing population. Data represent mean ± SEM ($n = 3$ independent brains). Scale bars correspond to 100 μm **(A,C–E,F,G)** and 25 μm (A1,C1–E1,F1,F2).

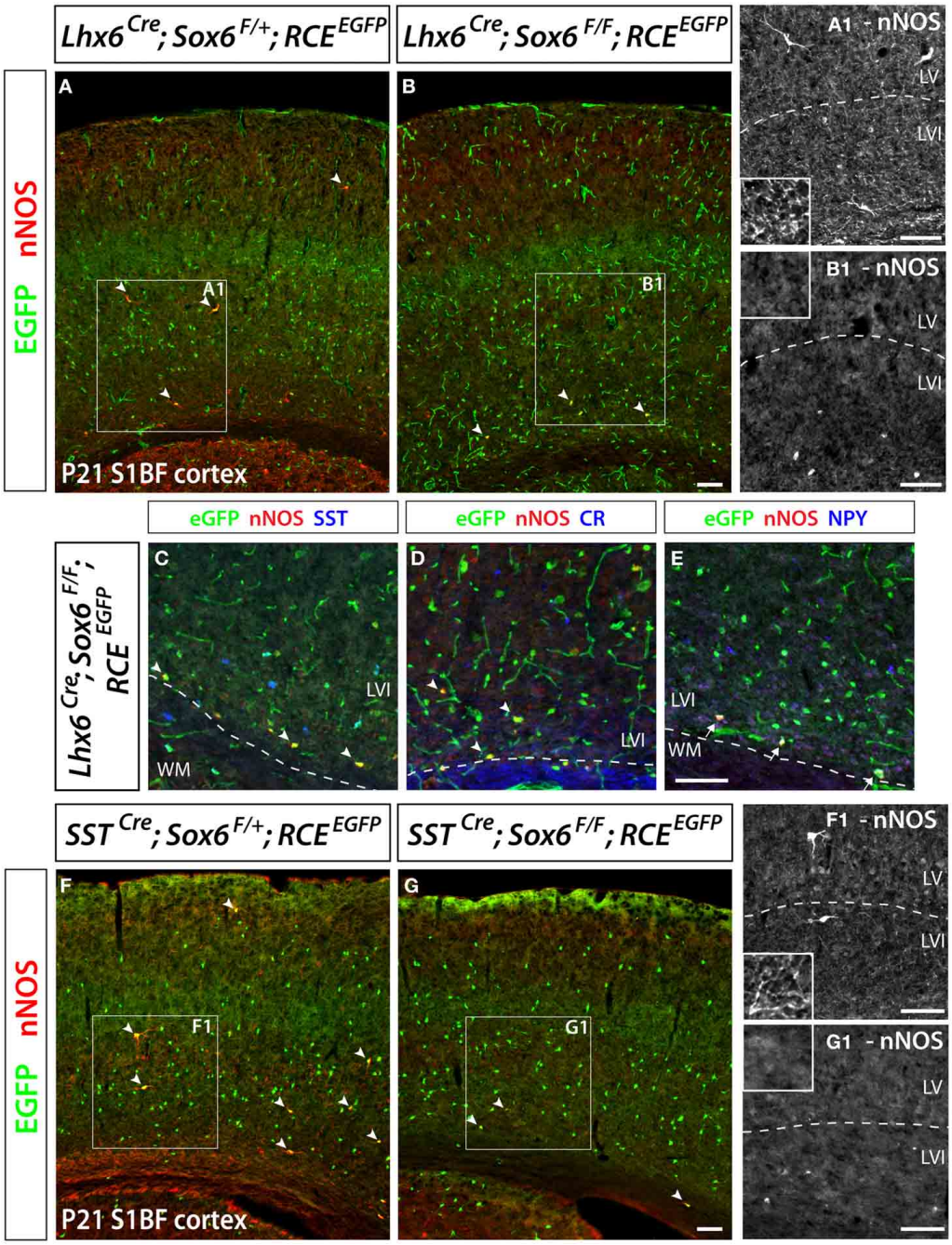

FIGURE 6 | Conditional removal of the transcription factor *Sox6* affects the nNOS-expressing population of neocortical GABAergic inhibitory neurons. The *Lhx6*^{Cre} driver line is used to conditionally inactivate *Sox6* in MGE-derived GABAergic neurons and simultaneously fate map the recombined population. **(A,B)** The expression of nNOS and their axonal and dendritic arborization are affected within the population of nNOS+/GFP+ cells (arrowheads) in the P21 somatosensory mouse cortex of *Sox6* mutants (*Lhx6*^{Cre}; *Sox6*$^{F/F}$; RCE^{EGFP}) (**B**–B1) vs. control (*Lhx6*^{Cre}; *Sox6*$^{F/+}$; RCE^{EGFP}) (**A**–A1). Note the absence of nNOS-expressing neurons in superficial layers (II/III), the weaker intensity of nNOS staining in deep layers (V/VI) of *Sox6* mutants vs. control (compare A1 and B1), as well as the absence of nNOS-containing neurites spanning the entire cortical thickness in *Sox6* mutants vs. control (compare close-up insets in A1 and B1). **(C–E)** To determine if the removal of *Sox6* in nNOS cells affects their specification, we performed triple staining of EGFP, nNOS (red) in combination with SST, CR, or NPY (blue). This revealed that nNOS-expressing inhibitory neurons no longer express SST and CR in *Sox6* mutants (arrowheads) **(C,D)**. However, NPY expression is unaffected in *Sox6* mutants (arrows) **(E)**. **(F,G)** To exclude any non-cell autonomous effect on the phenotype, we sought to determine if the *SST*^{cre} removal of *Sox6* recapitulates the phenotype observed upon *Lhx6*^{cre} removal of *Sox6*. EGFP/nNOS double staining of P21 somatosensory cortex revealed that MGE-derived SST/nNOS-expressing GABAergic neurons (arrowheads) are consistently affected by the loss of *Sox6*, as evidenced by the absence of nNOS cells in layer II/III, the decreased intensity of nNOS labeling in layer V/VI and the absence of nNOS+ neurites in the cortex. Data represent mean ± SEM ($n = 3$ independent brains for each genotype). Scale bars correspond to 100 μm.

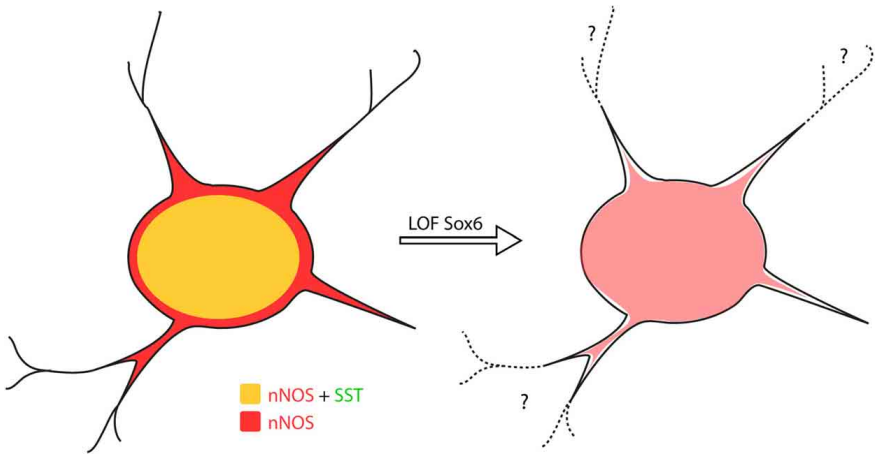

FIGURE 7 | *Sox6* loss-of-function phenotype in nNOS neocortical inhibitory neurons. Removal of *Sox6* in nNOS neocortical inhibitory neurons leads to the absence of SST expression, decreased levels of nNOS in the soma and absence of nNOS-expression in neurites, which are no longer visible. It remains to be determined whether the inability to detect neurites is caused by their truncation, or due to weak nNOS-expression.

are produced in the MGE, mainly in the dMGE. Hippocampal nNOS GABAergic neurons are also more diverse than their neocortical counterparts with regards to their molecular heterogenity. Neocortical nNOS cells appear to be a rather homogeneous population consisting perhaps of only two sub-populations. All nNOS-expressing neocortical inhibitory neurons express SST and NPY while 60% of them express CR. However, hippocampal nNOS GABAergic neurons express a variety of molecular markers such as NPY, SST, VIP, CR (Tricoire et al., 2010), and can further be subdivided on neurogliaform cells (NGC) and Ivy cells (IvC) accordingly to their morphology and the laminar location on their soma (Fuentealba et al., 2008). Finally we show that while neocortical nNOS cells require the transcription factor *Sox6* in order to develop their mature morphology and express characteristic molecular markers, the maturation of the hippocampal nNOS cells appears to be unaffected by *Sox6* loss of function. This again strengthens the evidence supporting that nNOS GABAergic neurons in these two distinct, but highly related cortical structures, are generated through independent developmental programs. Interestingly neocortical nNOS neurons appear to be more closely related to their striatal counterparts.

NEOCORTICAL nNOS GABAergic NEURONS MAINLY ORIGINATE IN THE DORSAL MGE

Neocortical GABAergic neurons arise from three telencephalic transient embryonic structures, the MGE, CGE, and POA (Batista-Brito and Fishell, 2009). In **Figure 8**, we show a schematic of genes expressed in those regions, which are important for the production and specification of neocortical and hippocampal GABAergic neurons. The MGE expresses *Nkx2.1* (Sussel et al., 1999) (red domain in **Figure 8**). In order to fate map the MGE we used the BAC line *Nkx2.1*^{Cre}, in which Cre expression is driven by the *Nkx2.1* promoter (Xu et al., 2008). While Nkx2.1 protein is expressed throughout the MGE and POA, Cre expression in the *Nkx2.1*^{Cre} driver spares the most dorsal part of the MGE (dMGE) (purple domain in **Figure 8**) (Xu et al., 2008). The absence of Cre expression in the dMGE of this BAC transgenic line might be due to positional effects or the absence of a critical part of the *Nkx2.1* promoter. However, because the expression of *Nkx2.1* mRNA is weaker in the dMGE than the rest of the MGE (Sussel et al., 1999), it has been suggested that the absence of Cre expression in the dMGE reflects a weaker *Nkx2.1* gene activation in this domain (Xu et al., 2008). The fact that the expression of another independently produced *Nkx2.1*^{Cre} BAC line is also absent from the dMGE (Kessaris et al., 2006; Fogarty et al., 2007) further supports this idea. Fate mapping of the totality of the MGE can be accomplished by using the BAC transgenic line *Lhx6*^{Cre} (Fogarty et al., 2007). *Lhx6* is expressed in postmitotic neurons derived from the MGE, as well as the POA (blue domain in **Figure 8**) (Fogarty et al., 2007; Du et al., 2008).

The most significant insight into the developmental origin of neocortical nNOS GABAergic was provided by the comparison between the fate mapping of *Nkx2.1*- and *Lhx6*-derived lineages. A minority of the neocortical nNOS cells (about 30%) could be accounted by *Nkx2.1* fate mapping, but virtually all of the neocortical nNOS cells could be accounted by *Lhx6* fate mapping (about 95%). Since the only progenitor region labeled by *Lhx6* but not *Nkx2.1*- fate mapping is the dMGE, our data strongly suggests that the dMGE is the source of the majority of neocortical nNOS neurons.

In our experience, no nNOS-positive neocortical neurons were labeled by the *5-Ht3a*^{EGFP} line, which labels the CGE and possibly part of the POA (Lee et al., 2010). Given that previous studies have shown that a small fraction of the cortical nNOS-expressing cortical neurons originate in the *Dbx1* domain of the POA (Gelman et al., 2009, 2011), we conclude that the *5-Ht3a*^{EGFP} BAC transgenic allele is unlikely expressed in the *Dbx1*-positive domain within the POA. This is further supported by the presence of markers typical for MGE (and thus not *5-Ht3a*^{EGFP}) such as PV and SST in the *Dbx1*-fate mapped population.

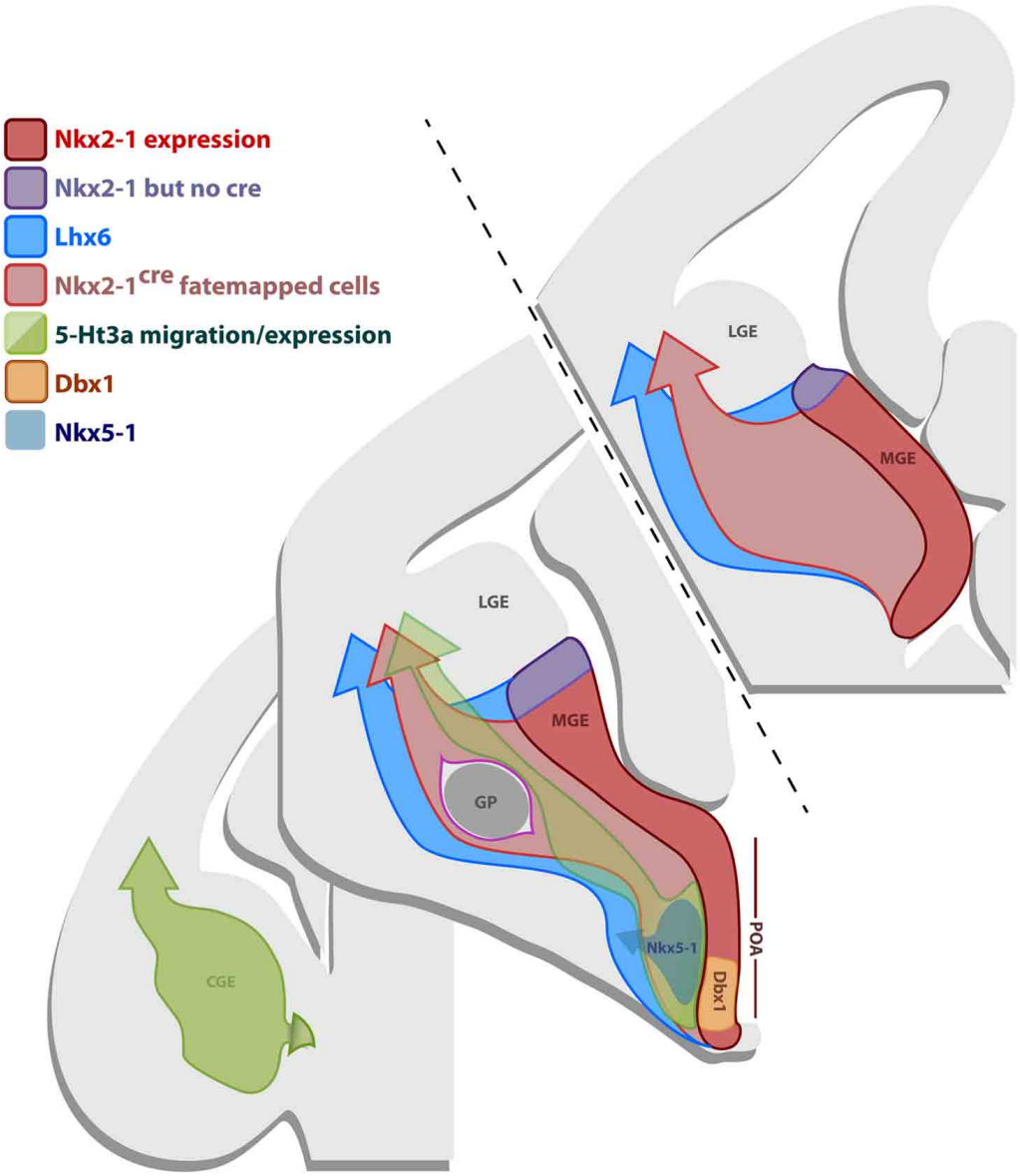

FIGURE 8 | Gene expression in the subpallial proliferative regions. Schematic representation of coronal sections of an E12.5 brain illustrating the gene expression profile of the progenitor regions MGE, CGE and POA. The most frontal section in the anterior/posterior axis (upper-left section) only comprises the MGE, the middle section contains the MGE, CGE and the POA, while the most caudal section (lower-right section) only shows the CGE. The MGE expresses Nkx2.1 (red domain), however, the BAC line *Nkx2.1*^{Cre} expresses the Cre recombinase in most of the MGE, except for its most dorsal part (dMGE) (purple domain). Nkx2.1 and Cre in the line *Nkx2.1*^{Cre} are also expressed in some of the POA. Consequently, fate mapping with the line *Nkx2.1*^{Cre} labels cells originating from the majority of the MGE, except for the dMGE (purple domain), and some of the POA, that migrate into the dorsal telencephalon (light-red arrow). *Lhx6* is downstream of *Nkx2.1* and is expressed in postmitotic neurons originating from the MGE and part of the POA. Fate mapping with the *Lhx6*^{Cre} line labels cells derived from the MGE (including dMGE-purple domain) and part of the POA that migrate into the dorsal telencephalon (blue arrow). The CGE and part of the POA express *5-Ht3a* (green domain). Fate mapping with the BAC line *5-Ht3a*^{EGFP} labels cells arising from the CGE and part of the POA that migrate into the dorsal thelencephalon (green arrow). Specific domains of the POA also express *Nkx5.1* (gray) and *Dbx1* (orange).

DIVERSE ORIGINS OF nNOS NEOCORTICAL AND HIPPOCAMPAL GABAergic NEURONS AND THE USE OF NEUROCHEMICAL MARKERS

Fate mapping studies have shown that the neocortical interneuron subtypes arising from the MGE and CGE are, for the most part, mutually exclusive (Rudy et al., 2011). For instance the hippocampal and neocortical PV-expressing fast spiking basket cells are solely produced in the MGE (Butt et al., 2005; Tricoire et al., 2011), while the CGE is the source of the VIP-expressing bipolar interneuron populations (Butt et al., 2005; Lee et al., 2010; Tricoire et al., 2011). This suggests that interneuron precursors

are subjected to distinct genetic programs initiated within the eminences that at least in part, determine their subtype identity. However, some molecular markers, such as the neurotransmitter NPY, are not specific for a particular interneuron subtype. Both neocortical and hippocampal NPY-expressing inhibitory neurons comprise a wide variety of subtypes (Karagiannis et al., 2009; Tricoire et al., 2011) and are derived from the MGE, CGE, and POA (Fogarty et al., 2007; Gelman et al., 2009; Lee et al., 2010; Tricoire et al., 2011). Furthermore, the level of expression of NPY is highly dependent on neuronal activity (Sperk et al., 1992; Schwarzer et al., 1995; Baraban et al., 1997). Taken together, these observations suggest that NPY should be used with caution as a marker of subtype identity.

Here we show that similar to PV neurons, neocortical nNOS cells are solely derived from the MGE and constitute a rather homogeneous subset of long range projections SST-expressing neurons (Tomioka et al., 2005), therefore, suggesting that in the neocortex nNOS might be a good indicator of neuronal subtype. By contrast, hippocampal nNOS cells are produced from a number of subpallial regions, have different morphologies and express a variety of neurochemical markers (Tricoire et al., 2010, 2011). This suggests that using nNOS as a subtype marker must be done carefully, especially when comparing structures. Moreover, the comparison between subtype diversity of hippocampal and neocortical cells expressing nNOS suggests that the location of birth of nNOS neurons is not the sole factor determining their marker expression, and that environmental cues present in the neocortex and hippocampus likely influence the expression of nNOS. It is likely that, except for nNOS expression, neocortical and hippocampal nNOS neurons are unrelated, and involved in different functions. Interestingly, neocortical nNOS neurons appear to have more in common with their counterparts in the striatum. Although being the largest striatal subtype, nNOS neurons are largely derived from the *Nkx2.1* domain and similar to the cortex express both SST and NPY.

THE TRANSCRIPTION FACTOR *Sox6* IS REQUIRED FOR THE SPECIFICATION OF NEOCORTICAL nNOS GABAergic NEURONS

Previous work has shown that loss of function of Nkx2.1 at the progenitor level results in a decreased number of nNOS-expressing neurons migrating tangentially into the cortex during development (Anderson et al., 2001), and a vast reduction of nNOS interneurons in the hippocampus at adult ages (Tricoire et al., 2010). We have previously shown that loss of the transcription factor Sox6, a gene downstream of Nkx2.1 and Lhx6 affects the radial migration and maturation of PV- and to a lesser extent SST-expressing neocortical inhibitory neurons. PV expression in fast-spiking basket cells is by and large lost in *Sox6* mutants while the effect on SST expression is much more modest. One SST-positive population that is affected by the loss of *Sox6* is the SST/CR double positive population where CR expression is lost completely (Batista-Brito et al., 2009). Given that in the neocortex nNOS neurons constitute a subpopulation of SST-neurons, we investigated whether the neurochemical characteristics, number, positioning or morphology of nNOS cells would be affected when *Sox6* is conditionally removed in Lhx6 expressing cells. Removal of *Sox6* had a marked effect on nNOS expressing neocortical inhibitory neurons. While nNOS persists (at low but detectable levels), *Sox6* mutant nNOS-expressing cells no longer express SST or CR, and are possibly less numerous, as indicated by the fact that in mutant animals nNOS neocortical neurons tend to be absent from the superficial layers. Furthermore, it appears based on nNOS staining, that mutant nNOS neurons display underdeveloped arborization of their processes. This contrasts with our previous results showing that even though *Sox6* mutant PV cells are immature, they still develop normal morphology (Batista-Brito et al., 2009). Taken together, our data show that removal of *Sox6* in nNOS neocortical neurons compromises their specification and also perhaps their morphology. Since the phenotype of nNOS mutant cells remained the same when *Sox6* was selectively removed in SST-expressing neurons, we argue that the effect is cell autonomous, or at least not caused by disrupted cortical network activity associated with PV-expressing fast spiking interneuron dysfunction. Similar to the neocortex, nNOS cells deprived of *Sox6* gene function in the striatum have reduced SST staining (data not shown). However, we did not detect any obvious defects in hippocampal nNOS interneurons in *Sox6* mutants (data not shown).

FUNCTIONAL ROLE OF nNOS GABAergic NEURONS

In the hippocampus (Jinno and Kosaka, 2002b), and likely in the neocortex, nNOS-expressing GABAergic neurons are the major source of nitric oxide (NO). NO regulates synaptic plasticity of glutamatergic and GABAergic synapses (Garthwaite and Boulton, 1995; Arancio et al., 1996; Burette et al., 2002; Szabadits et al., 2007; Garthwaite, 2008), and in the hippocampus potentiates GABA release (Li et al., 2002; Yu and Eldred, 2005). Even though neocortical nNOS neurons are distinct, and possibly differently regulated than their hippocampal counterparts, nNOS cells in the neocortex also function to control the level of GABA release and synaptic plasticity (Hardingham and Fox, 2006; Dachtler et al., 2011). While the number of nNOS neurons in the neocortex is small, their impact on the neocortical network through NO release might be significant as they are highly ramified, and project long distances rostro-caudally and medio-laterally, connecting neocortical areas up to 6–8 mm apart (Tomioka et al., 2005). In fact, it has been recently shown that specifically damaging nNOS neurons in the neocortex results in dysinhibition of the entire neocortical network and strong alterations of the spatio-temporal dynamics of the neocortex (Shlosberg et al., 2012). Cortical nNOS expressing neurons are also implicated in regulating local blood flow by transforming neuronal signals into vascular responses (Cauli et al., 2004), suggesting that neurogliaform-like neurons that express nNOS are likely to mediate cortical vasodilatations and/or vasoconstrictions that happen *in vivo* (Karagiannis et al., 2009). Moreover, it has also been shown that nNOS neurons are active during sleep (Gerashchenko et al., 2008). It has been reported that the functional activation of nNOS neurons during sleep is restricted to the cortex (Pasumarthi et al., 2010), suggesting that neocortical nNOS are major players in homeostatic sleep regulation (Gerashchenko et al., 2008; Pasumarthi et al., 2010). Importantly, while the regulation of the levels of NO is critical, an excessive production of NO can lead to neurotoxicity

(Dawson and Dawson, 1998), suggesting that the nNOS population in addition to normal brain function can result in disease states when perturbed.

In the future, in order to understand the contribution of nNOS expressing inhibitory neurons in the neocortical circuit, it would be interesting to investigate the intrinsic properties of nNOS neocortical neurons, as well as their synaptic inputs and outputs. However, in order to address these questions in such a sparse neuronal type, it will be necessary to specifically target nNOS cells, a goal that is achievable using recently developed genetic tools, such as the inducible Cre-diver line, *nNOS^{creER}* (Taniguchi et al., 2011). It would be particularly interesting to compare the electrophysiological properties of nNOS neocortical neurons to those of other SST expressing cells. Our hypothesis is that similar to nNOS cells in the striatum (Kawaguchi et al., 1995; Centonze et al., 2002) and SST neocortical interneurons (Kawaguchi and Kubota, 1996), nNOS cells in the neocortex will exhibit low threshold-spiking characteristics. However, due to the very different range of their output domains, we suspect that their functional roles in the network may be very different from those of SST$^+$/nNOS$^-$ neocortical interneurons. To address the functional role of neocortical nNOS neurons at both synaptic and circuit levels, it would be very interesting to selectively activate and suppress their activity using genetic methods such as opto- or pharmaco-genetics.

ACKNOWLEDGMENTS

Xavier H. Jaglin was supported by a Long-Term fellowship from the European Molecular Biology Organization (EMBO ALTF 303-2010), by the Bettencourt Schueller Foundation and by a fellowship from the Human Frontier Science Program (HFSP LT000078/2011-L).

REFERENCES

Anderson, S. A., Eisenstat, D. D., Shi, L., and Rubenstein, J. L. (1997a). Interneuron migration from basal forebrain to neocortex: dependence on Dlx genes. *Science* 278, 474–476.

Anderson, S. A., Qiu, M., Bulfone, A., Eisenstat, D. D., Meneses, J., Pedersen, R., and Rubenstein, J. L. (1997b). Mutations of the homeobox genes Dlx-1 and Dlx-2 disrupt the striatal subventricular zone and differentiation of late born striatal neurons. *Neuron* 19, 27–37.

Anderson, S. A., Marin, O., Horn, C., Jennings, K., and Rubenstein, J. L. (2001). Distinct cortical migrations from the medial and lateral ganglionic eminences. *Development* 128, 353–363.

Arancio, O., Kiebler, M., Lee, C. J., Lev-Ram, V., Tsien, R. Y., Kandel, E. R., and Hawkins, R. D. (1996). Nitric oxide acts directly in the presynaptic neuron to produce long-term potentiation in cultured hippocampal neurons. *Cell* 87, 1025–1035.

Aroniadou-Anderjaska, V., and Keller, A. (1996). Intrinsic inhibitory pathways in mouse barrel cortex. *Neuroreport* 7, 2363–2368.

Azim, E., Jabaudon, D., Fame, R. M., and Macklis, J. D. (2009). SOX6 controls dorsal progenitor identity and interneuron diversity during neocortical development. *Nat. Neurosci.* 12, 1238–1247.

Baraban, S. C., Hollopeter, G., Erickson, J. C., Schwartzkroin, P. A., and Palmiter, R. D. (1997). Knock-out mice reveal a critical antiepileptic role for neuropeptide Y. *J. Neurosci.* 17, 8927–8936.

Batista-Brito, R., and Fishell, G. (2009). The developmental integration of cortical interneurons into a functional network. *Curr. Top. Dev. Biol.* 87, 81–118.

Batista-Brito, R., Machold, R., Klein, C., and Fishell, G. (2008). Gene expression in cortical interneuron precursors is prescient of their mature function. *Cereb. Cortex* 18, 2306–2317.

Batista-Brito, R., Rossignol, E., Hjerling-Leffler, J., Denaxa, M., Wegner, M., Lefebvre, V., Pachnis, V., and Fishell, G. (2009). The cell-intrinsic requirement of Sox6 for cortical interneuron development. *Neuron* 63, 466–481.

Belmonte, M. K., Cook, E. H. Jr., Anderson, G. M., Rubenstein, J. L., Greenough, W. T., Beckel-Mitchener, A., Courchesne, E., Boulanger, L. M., Powell, S. B., Levitt, P. R., Perry, E. K., Jiang, Y. H., DeLorey, T. M., and Tierney, E. (2004). Autism as a disorder of neural information processing: directions for research and targets for therapy. *Mol. Psychiatry* 9, 646–663.

Burette, A., Zabel, U., Weinberg, R. J., Schmidt, H. H., and Valtschanoff, J. G. (2002). Synaptic localization of nitric oxide synthase and soluble guanylyl cyclase in the hippocampus. *J. Neurosci.* 22, 8961–8970.

Butt, S. J., Fuccillo, M., Nery, S., Noctor, S., Kriegstein, A., Corbin, J. G., and Fishell, G. (2005). The temporal and spatial origins of cortical interneurons predict their physiological subtype. *Neuron* 48, 591–604.

Butt, S. J., Sousa, V. H., Fuccillo, M. V., Hjerling-Leffler, J., Miyoshi, G., Kimura, S., and Fishell, G. (2008). The requirement of Nkx2-1 in the temporal specification of cortical interneuron subtypes. *Neuron* 59, 722–732.

Caceda, R., Kinkead, B., and Nemeroff, C. B. (2007). Involvement of neuropeptide systems in schizophrenia: human studies. *Int. Rev. Neurobiol.* 78, 327–376.

Cauli, B., Tong, X. K., Rancillac, A., Serluca, N., Lambolez, B., Rossier, J., and Hamel, E. (2004). Cortical GABA interneurons in neurovascular coupling: relays for subcortical vasoactive pathways. *J. Neurosci.* 24, 8940–8949.

Centonze, D., Bracci, E., Pisani, A., Gubellini, P., Bernardi, G., and Calabresi, P. (2002). Activation of dopamine D1-like receptors excites LTS interneurons of the striatum. *Eur. J. Neurosci.* 15, 2049–2052.

Chowdhury, S. A., Kawashima, T., Konishi, T., and Matsunami, K. (1996). GABAergic characteristics of transcallosal activity of cat motor cortical neurons. *Neurosci. Res.* 26, 323–333.

Cobos, I., Calcagnotto, M. E., Vilaythong, A. J., Thwin, M. T., Noebels, J. L., Baraban, S. C., and Rubenstein, J. L. (2005). Mice lacking Dlx1 show subtype-specific loss of interneurons, reduced inhibition and epilepsy. *Nat. Neurosci.* 8, 1059–1068.

Cossart, R., Bernard, C., and Ben-Ari, Y. (2005). Multiple facets of GABAergic neurons and synapses: multiple fates of GABA signalling in epilepsies. *Trends Neurosci.* 28, 108–115.

Dachtler, J., Hardingham, N. R., Glazewski, S., Wright, N. F., Blain, E. J., and Fox, K. (2011). Experience-dependent plasticity acts via GluR1 and a novel neuronal nitric oxide synthase-dependent synaptic mechanism in adult cortex. *J. Neurosci.* 31, 11220–11230.

Dani, V. S., Chang, Q., Maffei, A., Turrigiano, G. G., Jaenisch, R., and Nelson, S. B. (2005). Reduced cortical activity due to a shift in the balance between excitation and inhibition in a mouse model of Rett syndrome. *Proc. Natl. Acad. Sci. U.S.A.* 102, 12560–12565.

Dawson, V. L., and Dawson, T. M. (1998). Nitric oxide in neurodegeneration. *Prog. Brain Res.* 118, 215–229.

Du, T., Xu, Q., Ocbina, P. J., and Anderson, S. A. (2008). NKX2.1 specifies cortical interneuron fate by activating Lhx6. *Development* 135, 1559–1567.

Dumitriu, B., Dy, P., Smits, P., and Lefebvre, V. (2006). Generation of mice harboring a Sox6 conditional null allele. *Genesis* 44, 219–224.

Fishell, G., and Rudy, B. (2011). Mechanisms of inhibition within the telencephalon: "where the wild things are". *Annu. Rev. Neurosci.* 34, 535–567.

Flames, N., Long, J. E., Garratt, A. N., Fischer, T. M., Gassmann, M., Birchmeier, C., Lai, C., Rubenstein, J. L., and Marin, O. (2004). Short- and long-range attraction of cortical GABAergic interneurons by neuregulin-1. *Neuron* 44, 251–261.

Flames, N., Pla, R., Gelman, D. M., Rubenstein, J. L., Puelles, L., and Marin, O. (2007). Delineation of multiple subpallial progenitor domains by the combinatorial expression of transcriptional codes. *J. Neurosci.* 27, 9682–9695.

Fogarty, M., Grist, M., Gelman, D., Marin, O., Pachnis, V., and Kessaris, N. (2007). Spatial genetic patterning of the embryonic neuroepithelium generates GABAergic interneuron diversity in the adult cortex. *J. Neurosci.* 27, 10935–10946.

Franklin, K. B. J., and Paxinos, G. (2001). *The Mouse Brain in Stereotaxic coordinates*, 3rd Edn. San Diego, CA: Academic Press.

Fuentealba, P., Begum, R., Capogna, M., Jinno, S., Marton, L. F., Csicsvari, J., Thomson, A., Somogyi, P., and Klausberger, T. (2008). Ivy cells: a population of nitric-oxide-producing, slow-spiking GABAergic neurons and their involvement in hippocampal network activity. *Neuron* 57, 917–929.

Garthwaite, J. (2008). Concepts of neural nitric oxide-mediated transmission. *Eur. J. Neurosci.* 27, 2783–2802.

Garthwaite, J., and Boulton, C. L. (1995). Nitric oxide signaling in the central nervous system. *Annu. Rev. Physiol.* 57, 683–706.

Gelman, D., Griveau, A., Dehorter, N., Teissier, A., Varela, C., Pla, R., Pierani, A., and Marin, O. (2011). A wide diversity of cortical GABAergic interneurons derives from the embryonic preoptic area. *J. Neurosci.* 31, 16570–16580.

Gelman, D. M., Martini, F. J., Nobrega-Pereira, S., Pierani, A., Kessaris, N., and Marin, O. (2009). The embryonic preoptic area is a novel source of cortical GABAergic interneurons. *J. Neurosci.* 29, 9380–9389.

Gerashchenko, D., Wisor, J. P., Burns, D., Reh, R. K., Shiromani, P. J., Sakurai, T., de la Iglesia, H. O., and Kilduff, T. S. (2008). Identification of a population of sleep-active cerebral cortex neurons. *Proc. Natl. Acad. Sci. U.S.A.* 105, 10227–10232.

Ghanem, N., Yu, M., Long, J., Hatch, G., Rubenstein, J. L., and Ekker, M. (2007). Distinct cis-regulatory elements from the Dlx1/Dlx2 locus mark different progenitor cell populations in the ganglionic eminences and different subtypes of adult cortical interneurons. *J. Neurosci.* 27, 5012–5022.

Gittis, A. H., Nelson, A. B., Thwin, M. T., Palop, J. J., and Kreitzer, A. C. (2010). Distinct roles of GABAergic interneurons in the regulation of striatal output pathways. *J. Neurosci.* 30, 2223–2234.

Gonchar, Y. A., Johnson, P. B., and Weinberg, R. J. (1995). GABA-immunopositive neurons in rat neocortex with contralateral projections to S-I. *Brain Res.* 697, 27–34.

Gonchar, Y., Wang, Q., and Burkhalter, A. (2007). Multiple distinct subtypes of GABAergic neurons in mouse visual cortex identified by triple immunostaining. *Front. Neuroanat.* 1:3. doi: 10.3389/neuro.05.003.2007

Gonzalez-Burgos, G., and Lewis, D. A. (2008). GABA neurons and the mechanisms of network oscillations: implications for understanding cortical dysfunction in schizophrenia. *Schizophr. Bull.* 34, 944–961.

Haider, B., and McCormick, D. A. (2009). Rapid neocortical dynamics: cellular and network mechanisms. *Neuron* 62, 171–189.

Hardingham, N., and Fox, K. (2006). The role of nitric oxide and GluR1 in presynaptic and postsynaptic components of neocortical potentiation. *J. Neurosci.* 26, 7395–7404.

Jinno, S., Jeromin, A., Roder, J., and Kosaka, T. (2002). Immunocytochemical localization of neuronal calcium sensor-1 in the hippocampus and cerebellum of the mouse, with special reference to presynaptic terminals. *Neuroscience* 113, 449–461.

Jinno, S., and Kosaka, T. (2002a). Immunocytochemical characterization of hippocamposeptal projecting GABAergic nonprincipal neurons in the mouse brain: a retrograde labeling study. *Brain Res.* 945, 219–231.

Jinno, S., and Kosaka, T. (2002b). Patterns of expression of calcium binding proteins and neuronal nitric oxide synthase in different populations of hippocampal GABAergic neurons in mice. *J. Comp. Neurol.* 449, 1–25.

Judas, M., Sestan, N., and Kostovic, I. (1999). Nitrinergic neurons in the developing and adult human telencephalon: transient and permanent patterns of expression in comparison to other mammals. *Microsc. Res. Tech.* 45, 401–419.

Karagiannis, A., Gallopin, T., David, C., Battaglia, D., Geoffroy, H., Rossier, J., Hillman, E. M., Staiger, J. F., and Cauli, B. (2009). Classification of NPY-expressing neocortical interneurons. *J. Neurosci.* 29, 3642–3659.

Kawaguchi, Y., and Kubota, Y. (1996). Physiological and morphological identification of somatostatin- or vasoactive intestinal polypeptide-containing cells among GABAergic cell subtypes in rat frontal cortex. *J. Neurosci.* 16, 2701–2715.

Kawaguchi, Y., Wilson, C. J., Augood, S. J., and Emson, P. C. (1995). Striatal interneurones: chemical, physiological and morphological characterization. *Trends Neurosci.* 18, 527–535.

Keimpema, E., Straiker, A., Mackie, K., Harkany, T., and Hjerling-Leffler, J. (2012). Sticking out of the crowd: the molecular identity and development of cholecystokinin-containing basket cells. *J. Physiol.* 590, 703–714.

Kessaris, N., Fogarty, M., Iannarelli, P., Grist, M., Wegner, M., and Richardson, W. D. (2006). Competing waves of oligodendrocytes in the forebrain and postnatal elimination of an embryonic lineage. *Nat. Neurosci.* 9, 173–179.

Kimura, F., and Baughman, R. W. (1997). GABAergic transcallosal neurons in developing rat neocortex. *Eur. J. Neurosci.* 9, 1137–1143.

Lavdas, A. A., Grigoriou, M., Pachnis, V., and Parnavelas, J. G. (1999). The medial ganglionic eminence gives rise to a population of early neurons in the developing cerebral cortex. *J. Neurosci.* 19, 7881–7888.

Lee, J. E., and Jeon, C. J. (2005). Immunocytochemical localization of nitric oxide synthase-containing neurons in mouse and rabbit visual cortex and co-localization with calcium-binding proteins. *Mol. Cells* 19, 408–417.

Lee, S., Hjerling-Leffler, J., Zagha, E., Fishell, G., and Rudy, B. (2010). The largest group of superficial neocortical GABAergic interneurons expresses ionotropic serotonin receptors. *J. Neurosci.* 30, 16796–16808.

Levitt, P., Eagleson, K. L., and Powell, E. M. (2004). Regulation of neocortical interneuron development and the implications for neurodevelopmental disorders. *Trends Neurosci.* 27, 400–406.

Li, D. P., Chen, S. R., and Pan, H. L. (2002). Nitric oxide inhibits spinally projecting paraventricular neurons through potentiation of presynaptic GABA release. *J. Neurophysiol.* 88, 2664–2674.

Liodis, P., Denaxa, M., Grigoriou, M., Akufo-Addo, C., Yanagawa, Y., and Pachnis, V. (2007). Lhx6 activity is required for the normal migration and specification of cortical interneuron subtypes. *J. Neurosci.* 27, 3078–3089.

Marin, O., and Rubenstein, J. L. (2001). A long, remarkable journey: tangential migration in the telencephalon. *Nat. Rev. Neurosci.* 2, 780–790.

Markram, H., Toledo-Rodriguez, M., Wang, Y., Gupta, A., Silberberg, G., and Wu, C. (2004). Interneurons of the neocortical inhibitory system. *Nat. Rev. Neurosci.* 5, 793–807.

McDonald, C. T., and Burkhalter, A. (1993). Organization of long-range inhibitory connections with rat visual cortex. *J. Neurosci.* 13, 768–781.

Miyoshi, G., Hjerling-Leffler, J., Karayannis, T., Sousa, V. H., Butt, S. J., Battiste, J., Johnson, J. E., Machold, R. P., and Fishell, G. (2010). Genetic fate mapping reveals that the caudal ganglionic eminence produces a large and diverse population of superficial cortical interneurons. *J. Neurosci.* 30, 1582–1594.

Morris, H. M., Hashimoto, T., and Lewis, D. A. (2008). Alterations in somatostatin mRNA expression in the dorsolateral prefrontal cortex of subjects with schizophrenia or schizoaffective disorder. *Cereb. Cortex* 18, 1575–1587.

Nery, S., Fishell, G., and Corbin, J. G. (2002). The caudal ganglionic eminence is a source of distinct cortical and subcortical cell populations. *Nat. Neurosci.* 5, 1279–1287.

Pasumarthi, R. K., Gerashchenko, D., and Kilduff, T. S. (2010). Further characterization of sleep-active neuronal nitric oxide synthase neurons in the mouse brain. *Neuroscience* 169, 149–157.

Petryniak, M. A., Potter, G. B., Rowitch, D. H., and Rubenstein, J. L. (2007). Dlx1 and Dlx2 control neuronal versus oligodendroglial cell fate acquisition in the developing forebrain. *Neuron* 55, 417–433.

Pleasure, S. J., Anderson, S., Hevner, R., Bagri, A., Marin, O., Lowenstein, D. H., and Rubenstein, J. L. (2000). Cell migration from the ganglionic eminences is required for the development of hippocampal GABAergic interneurons. *Neuron* 28, 727–740.

Potter, G. B., Petryniak, M. A., Shevchenko, E., McKinsey, G. L., Ekker, M., and Rubenstein, J. L. (2009). Generation of Cre-transgenic mice using Dlx1/Dlx2 enhancers and their characterization in GABAergic interneurons. *Mol. Cell. Neurosci.* 40, 167–186.

Pouille, F., and Scanziani, M. (2001). Enforcement of temporal fidelity in pyramidal cells by somatic feed-forward inhibition. *Science* 293, 1159–1163.

Rudy, B., Fishell, G., Lee, S., and Hjerling-Leffler, J. (2011). Three groups of interneurons account for nearly 100% of neocortical GABAergic neurons. *Dev. Neurobiol.* 71, 45–61.

Salin, P. A., and Prince, D. A. (1996). Electrophysiological mapping of GABAA receptor-mediated inhibition in adult rat somatosensory cortex. *J. Neurophysiol.* 75, 1589–1600.

Schwarzer, C., Williamson, J. M., Lothman, E. W., Vezzani, A., and Sperk, G. (1995). Somatostatin, neuropeptide Y, neurokinin B and cholecystokinin immunoreactivity in two chronic models of temporal lobe epilepsy. *Neuroscience* 69, 831–845.

Shlosberg, D., Buskila, Y., Abu-Ghanem, Y., and Amitai, Y. (2012). Spatiotemporal alterations of cortical network activity by selective loss of NOS-expressing interneurons. *Front. Neural Circuits* 6:3. doi: 10.3389/fncir.2012.00003

Sousa, V. H., Miyoshi, G., Hjerling-Leffler, J., Karayannis, T., and Fishell, G. (2009). Characterization of Nkx6-2-derived neocortical interneuron lineages. *Cereb. Cortex* 19(Suppl. 1), i1–i10.

Sperk, G., Marksteiner, J., Gruber, B., Bellmann, R., Mahata, M., and Ortler, M. (1992). Functional changes in neuropeptide Y- and somatostatin-containing neurons induced by limbic seizures in the rat. *Neuroscience* 50, 831–846.

Stenman, J., Toresson, H., and Campbell, K. (2003). Identification of two distinct progenitor populations in the lateral ganglionic eminence: implications for striatal and olfactory bulb neurogenesis. *J. Neurosci.* 23, 167–174.

Sussel, L., Marin, O., Kimura, S., and Rubenstein, J. L. (1999). Loss of Nkx2.1 homeobox gene function results in a ventral to dorsal molecular respecification within the basal telencephalon: evidence for a transformation of the pallidum into the striatum. *Development* 126, 3359–3370.

Szabadics, J., and Soltesz, I. (2009). Functional specificity of mossy fiber innervation of GABAergic cells in the hippocampus. *J. Neurosci.* 29, 4239–4251.

Szabadits, E., Cserep, C., Ludanyi, A., Katona, I., Gracia-Llanes, J., Freund, T. F., and Nyiri, G. (2007). Hippocampal GABAergic synapses possess the molecular machinery for retrograde nitric oxide signaling. *J. Neurosci.* 27, 8101–8111.

Taniguchi, H., He, M., Wu, P., Kim, S., Paik, R., Sugino, K., Kvitsiani, D., Fu, Y., Lu, J., Lin, Y., Miyoshi, G., Shima, Y., Fishell, G., Nelson, S. B., and Huang, Z. J. (2011). A resource of Cre driver lines for genetic targeting of GABAergic neurons in cerebral cortex. *Neuron* 71, 995–1013.

Tomioka, R., Okamoto, K., Furuta, T., Fujiyama, F., Iwasato, T., Yanagawa, Y., Obata, K., Kaneko, T., and Tamamaki, N. (2005). Demonstration of long-range GABAergic connections distributed throughout the mouse neocortex. *Eur. J. Neurosci.* 21, 1587–1600.

Tricoire, L., Pelkey, K. A., Daw, M. I., Sousa, V. H., Miyoshi, G., Jeffries, B., Cauli, B., Fishell, G., and McBain, C. J. (2010). Common origins of hippocampal Ivy and nitric oxide synthase expressing neurogliaform cells. *J. Neurosci.* 30, 2165–2176.

Tricoire, L., Pelkey, K. A., Erkkila, B. E., Jeffries, B. W., Yuan, X., and McBain, C. J. (2011). A blueprint for the spatiotemporal origins of mouse hippocampal interneuron diversity. *J. Neurosci.* 31, 10948–10970.

Volk, D. W., Pierri, J. N., Fritschy, J. M., Auh, S., Sampson, A. R., and Lewis, D. A. (2002). Reciprocal alterations in pre- and postsynaptic inhibitory markers at chandelier cell inputs to pyramidal neurons in schizophrenia. *Cereb. Cortex* 12, 1063–1070.

Vucurovic, K., Gallopin, T., Ferezou, I., Rancillac, A., Chameau, P., van Hooft, J. A., Geoffroy, H., Monyer, H., Rossier, J., and Vitalis, T. (2010). Serotonin 3A receptor subtype as an early and protracted marker of cortical interneuron subpopulations. *Cereb. Cortex* 20, 2333–2347.

Wichterle, H., Garcia-Verdugo, J. M., Herrera, D. G., and Alvarez-Buylla, A. (1999). Young neurons from medial ganglionic eminence disperse in adult and embryonic brain. *Nat. Neurosci.* 2, 461–466.

Wichterle, H., Turnbull, D. H., Nery, S., Fishell, G., and Alvarez-Buylla, A. (2001). In utero fate mapping reveals distinct migratory pathways and fates of neurons born in the mammalian basal forebrain. *Development* 128, 3759–3771.

Wonders, C. P., and Anderson, S. A. (2006). The origin and specification of cortical interneurons. *Nat. Rev. Neurosci.* 7, 687–696.

Wonders, C. P., Taylor, L., Welagen, J., Mbata, I. C., Xiang, J. Z., and Anderson, S. A. (2008). A spatial bias for the origins of interneuron subgroups within the medial ganglionic eminence. *Dev. Biol.* 314, 127–136.

Xu, Q., Cobos, I., De La Cruz, E., Rubenstein, J. L., and Anderson, S. A. (2004). Origins of cortical interneuron subtypes. *J. Neurosci.* 24, 2612–2622.

Xu, Q., Tam, M., and Anderson, S. A. (2008). Fate mapping Nkx2.1-lineage cells in the mouse telencephalon. *J. Comp. Neurol.* 506, 16–29.

Yan, X. X., Jen, L. S., and Garey, L. J. (1996). NADPH-diaphorase-positive neurons in primate cerebral cortex colocalize with GABA and calcium-binding proteins. *Cereb. Cortex* 6, 524–529.

Yau, H. J., Wang, H. F., Lai, C., and Liu, F. C. (2003). Neural development of the neuregulin receptor ErbB4 in the cerebral cortex and the hippocampus: preferential expression by interneurons tangentially migrating from the ganglionic eminences. *Cereb. Cortex* 13, 252–264.

Yu, D., and Eldred, W. D. (2005). Nitric oxide stimulates gamma-aminobutyric acid release and inhibits glycine release in retina. *J. Comp. Neurol.* 483, 278–291.

Conflict of Interest Statement: The authors declare that the research was conducted in the absence of any commercial or financial relationships that could be construed as a potential conflict of interest.

Received: 29 March 2012; accepted: 20 June 2012; published online: 09 July 2012.

*Citation: Jaglin XH, Hjerling-Leffler J, Fishell G and Batista-Brito R (2012) The origin of neocortical nitric oxide synthase-expressing inhibitory neurons. Front. Neural Circuits **6**:44. doi: 10.3389/fncir.2012.00044*

frontiers in
NEURAL CIRCUITS

ORIGINAL RESEARCH ARTICLE
published: 24 September 2012
doi: 10.3389/fncir.2012.00065

Multiple embryonic origins of nitric oxide synthase-expressing GABAergic neurons of the neocortex

Lorenza Magno, Marcio G. Oliveira†, Mariusz Mucha†, Anna N. Rubin and Nicoletta Kessaris*

Wolfson Institute for Biomedical Research and Department of Cell and Developmental Biology, University College London, London, UK

Edited by:
Bruno Cauli, Université Pierre et Marie Curie, France

Reviewed by:
Bruno Cauli, Université Pierre et Marie Curie, France
Ludovic Tricoire, Université Pierre et Marie Curie, France

***Correspondence:**
Nicoletta Kessaris, Wolfson Institute for Biomedical Research and Department of Cell and Developmental Biology, University College London, Gower Street, London WC1E 6BT, UK.
e-mail: n.tekki-kessaris@ucl.ac.uk
† These authors contributed equally to this work.

Cortical GABAergic interneurons in rodents originate in three subcortical regions: the medial ganglionic eminence (MGE), the lateral/caudal ganglionic eminence (LGE/CGE), and the preoptic area (POA). Each of these neuroepithelial precursor domains contributes different interneuron subtypes to the cortex. Neuronal NOS (nNOS)-expressing neurons represent a heterogenous population of cortical interneurons. We examined the development of these cells in the mouse embryonic cortex and their abundance and distribution in adult animals. Using genetic lineage tracing in transgenic mice we find that nNOS type I cells originate only in the MGE whereas type II cells have a triple origin in the MGE, LGE/CGE, and POA. The two populations are born at different times during development, occupy different layers in the adult cortex and have distinct neurochemical profiles. nNOS neurons are more numerous in the adult cortex than previously reported and constitute a significant proportion of the cortical interneuron population. Our data suggest that the heterogeneity of nNOS neurons in the cortex can be attributed to their multiple embryonic origins which likely impose distinct genetic specification programs.

Keywords: nNOS, interneurons, development, mouse, birthdating

INTRODUCTION

The gaseous biological messenger nitric oxide (NO) was originally described as a vasodilator (Furchgott and Zawadzki, 1980; Palmer et al., 1987) and has since been implicated in a variety of physiological processes. In the nervous system NO is involved in the regulation of cerebral blood flow, neurotransmission, synaptic plasticity and memory formation, modulation of neuroendocrine functions, and behavioral activity (Szabo, 1996). A role for NO in neurogenesis has also been proposed (Gibbs, 2003). NO is synthesized by the enzyme NO synthase (NOS) from the amino acid L-arginine. Three NOS-encoding genes have been identified and named according to the tissue in which they were first found: endothelial NOS (eNOS), neuronal NOS (nNOS), and the inducible form of NOS found in a variety of tissues (iNOS) (Alderton et al., 2001).

Cortical nNOS neurons are mainly GABAergic. They have been identified by immunohistochemical detection of nNOS and/or nicotinamide adenine dinucleotide phosphate diaphorase (NADPHd) staining (Dawson et al., 1991; Hope et al., 1991; Vincent, 2010). nNOS cortical neurons have been subdivided into two types according to the intensity of NOS/NADPHd staining: heavily labeled type I neurons that have large somata, and weakly labeled type II cells that have smaller somata (Hashikawa et al., 1994; Yan et al., 1996; Smiley et al., 2000; Lee and Jeon, 2005). Type I cells comprise around 0.5–2% of the cortical interneuron population (Kubota et al., 1994; Gonchar and Burkhalter, 1997). Type II cells are more numerous than type I in all species examined although their numbers vary in different cortical areas and across species (Yan et al., 1996; Smiley et al., 2000; Lee and Jeon, 2005). The two types of nNOS neurons have distinct but overlapping distributions within the cortex (Hashikawa et al., 1994; Kubota et al., 1994; Yan et al., 1996; Gonchar and Burkhalter, 1997; Smiley et al., 2000; Gotti et al., 2005; Lee and Jeon, 2005).

Detecting weakly-stained NOS cells has been challenging and consequently many studies have focussed on type I cells. The aspiny/sparsely spiny type I cells have round or oval cell bodies with bitufted, multipolar, or stellate morphologies (Valtschanoff et al., 1993; Gonchar and Burkhalter, 1997; Smiley et al., 2000; Gotti et al., 2005; Lee and Jeon, 2005). Type II cells have round cell bodies and at least some may correspond to neurogliaform cells (Smiley et al., 2000; Price et al., 2005; Karagiannis et al., 2009). The two populations have distinct neurochemical content and physiological features and are therefore thought to represent two functionally different neuronal populations within the cortical network (Dawson et al., 1991; Kubota et al., 1994, 2011; Gonchar and Burkhalter, 1997; Smiley et al., 2000; Lee and Jeon, 2005; Karagiannis et al., 2009).

Some characteristics of cortical interneurons are specified at the time when these cells are born. A number of studies have examined where interneurons are generated in order to understand how heterogeneity is established (Wonders and Anderson, 2006; Gelman and Marin, 2010; Rubin et al., 2010; Gelman et al., 2011). Unlike cortical pyramidal neurons which are born sequentially from a common pool of local precursors, interneurons are born outside the cortex, and migrate into the cortex during embryogenesis (Wonders and Anderson, 2006). Genetic fate-mapping has confirmed that the two main sources of cortical interneurons are the medial ganglionic eminence (MGE) and the lateral/caudal ganglionic eminence (LGE/CGE) in the

subpallium (Fogarty et al., 2007; Miyoshi et al., 2007, 2010; Xu et al., 2008; Sousa et al., 2009; Rubin et al., 2010). The preoptic area (POA) has also been shown to generate small numbers of interneurons for the cortex (Gelman et al., 2009, 2011). Cortical interneurons originating from these three spatially segregated precursor pools are born at different times and have distinct neurochemical phenotypes and physiological properties. The origin of cortical nNOS cells has not been determined.

In this study we examined the timing of generation of nNOS-expressing cortical interneurons and emergence of the two subtypes. Using a series of transgenic mice that genetically label distinct neuroepithelial domains in the subpallium we identified the embryonic origin of the two populations and characterized their distribution patterns and neurochemical profiles within the adult somatosensory cortex.

MATERIALS AND METHODS

TRANSGENIC MICE

All transgenic mouse lines used in this study have been described previously: *Nkx2.1–Cre*^{Tg}, *Lhx6-Cre*^{Tg}, *Nkx6.2-Cre*^{Tg} (Kessaris et al., 2006; Fogarty et al., 2007), *Dlx1-lox-Venus-lox*^{Tg} (Rubin et al., 2010), *Nkx5.1-Cre*^{Tg} (Gelman et al., 2009), *Shh-GFPCre*^{KI} (Harfe et al., 2004). Herein we refer to them as *Nkx2.1-Cre*, *Lhx6-Cre*, *Nkx6.2-Cre*, *Dlx1-Venus*^{fl}, *Nkx5.1-Cre, and Shh-Cre*, respectively. Mice were maintained on a mixed C57BL/6/CBA background at the Wolfson Institute for Biomedical Research, University College London, and the National Institute for Medical Research, London, in accordance with United Kingdom legislation.

Three reporter mice for Cre recombinase have been used in this study: *Rosa26R–Green Fluorescent Protein (GFP) (R26R-GFP)* (Mao et al., 2001), *Rosa26R–yellow fluorescent protein (YFP) (R26R-YFP)* (Srinivas et al., 2001), and *Rosa26R–LacZ* (Soriano, 1999). Upon Cre-mediated recombination, the three mice express GFP, YFP, and β-galactosidase, respectively, under control of the Rosa26 promoter.

In situ HYBRIDIZATION

Tissue preparation and *in situ* hybridization were carried out as previously described (Rubin et al., 2010). To detect *nNos* transcripts we used several different RNA probes that recognize the full length *nNosα* transcript and one or more of its splice variants (*nNosβ*, *nNosγ*, *nNosμ*, and *nNos*-2). All probes gave comparable results (data not shown). We present images using a probe spanning exon 2 of the mouse *nNOS* gene which encodes the PDZ domain (PSD-95 discs large/ZO-1 homology domain), a unique feature of *nNos* that distinguishes it from *eNos* and *iNos*. This probe spans 660 bp from the mouse *nNos* gene and detects *nNosα*, *nNosμ*, and *nNos*-2 (Alderton et al., 2001). It was generated by PCR amplification from genomic DNA using the following primers: 5′-CCAACGTCATTTCTGTCCGTC-3′ and 5′-TTCCTGTGTCTTTCATCTCTGC-3′. The PCR product was cloned into pCRII-TOPO (Invitrogen). The plasmid was linearized with *SpeI* and an antisense digoxigenin (DIG)-labeled RNA probe was transcribed using T7 RNA polymerase (Promega).

IMMUNOHISTOCHEMISTRY

Unless otherwise stated, immunohistochemical detection of calbindin (CB), calretinin (CR), parvalbumin (PV), somatostatin (SST), neuropeptide Y (NPY), reelin (RLN), nNOS, GFP/YFP, and β-galactosidase (β-gal) was carried out as described previously (Rubin et al., 2010). To amplify the nNOS signal and detect the weak-expressing type II cells we used the Vectastain ABC kit (Vector Laboratories) followed by either Tyramide-Cy3 (Perkin Elmer) as a fluorescent enzyme substrate or DAB reagent (Vector Laboratories) as a chromogenic substrate, according to manufacturers' instructions. Briefly, endogenous peroxidase activity was quenched with 0.6% H_2O_2 for 20 min and anti-nNOS was applied overnight. A biotin-conjugated secondary antibody was used to detect the primary anti-nNOS antibody followed by the Avidin/Biotinylated enzyme Complex (ABC) (prepared according to manufacturer's instructions). Tyramide-Cy3 (Perkin Elmer) (1:300 in amplification buffer) or DAB substrate reagent (Vector Laboratories) were applied for 3 min or 1 min, respectively, before sections were mounted.

Primary antibodies used were the following: rat anti-GFP IgG2a (1:1000; Nacalai Tesque; Cat no. 0440484); rabbit anti-β-galactosidase (1:2000; MP Biomedicals; Cat no. 55976); mouse anti-CB (1:1000; Swant; Cat no. 300); rabbit anti-CR (1:1000; Swant; Cat no. 7699/3H); mouse anti-PV (1:1000; Chemicon/Millipore; Cat no. MAB1572); rabbit anti-SST (1:200 Peninsula Laboratories; Cat no. T410300); rabbit anti-NPY (1:1000, ImmunoStar; Cat no. 22940); mouse anti-RLN (1:200) (kindly provided by A. Goffinet). To detect nNOS we used several different antibodies that recognize different regions of the nNOS protein in an effort to identify the optimal conditions for detecting nNOS type II cells. These included the following: rabbit anti-nNOS that recognizes 195 amino acids from N-terminus of the rat nNOS (1:500; Invitrogen; Cat no. 61-7000), sheep anti-nNOS generated against recombinant rat nNOS [1:1000; (kindly provided by P. Emson) (Herbison et al., 1996)], mouse monoclonal anti-nNOS that recognizes amino acids 1095–1289 from the C terminus of human nNOS (1:200; BD Biosciences; Cat no. N31020-050), and rabbit anti-nNOS generated against amino acids 1419–1433 from the C terminus of human nNOS (1:1000; Immunostar; Cat no. 24287). All antibodies gave comparable results. Data presented in this study were generated using the rabbit anti-nNOS (Immunostar) and the sheep anti-nNOS (Herbison et al., 1996).

Secondary antibodies used were biotin-conjugated donkey anti-rabbit IgG (1:500; Millipore), biotin-conjugated donkey anti-sheep IgG (1:200; Thermo Scientific), AlexaFluor 488- and AlexaFluor 568-conjugated goat anti-rabbit IgG, or goat anti-rat IgG or goat anti-mouse IgG (all used at 1:750; Invitrogen).

EdU BIRTHDATING

5-ethynyl-2′-deoxyuridine (EdU, Molecular Probes) was dissolved in sterile PBS at 2 mg/ml. Pregnant females were administered five intraperitoneal injections of EdU (10 mg/Kg body weight) at 2 h intervals starting at 10:00 am. The pups were perfused at P30 with 4% PFA and tissue was further fixed for 45 min at room temperature by immersion in the same solution. EdU detection was carried out after nNOS

immunohistochemistry using the Click-iT EdU Alexa Fluor 647 Imaging Kit (Molecular Probes) according to manufacturer's instructions. Briefly, following detection of nNOS, the sections were incubated in Click-iT EdU reaction cocktail (prepared according to manufacturer's instructions) in the dark for 45 min before being washed and mounted.

QUANTIFICATION

The extent of co-localization between nNOS and other markers was determined as previously described (Fogarty et al., 2007). In all experiments quantification was carried out in the somatosensory cortex between Bregma position 0.74 and −1.22 mm. Cells were counted in a defined area spanning the pial–white matter extent of the cortex (450 μm width and 30 μm depth). In some cases this was subdivided into 10 equal bins along the dorsoventral axis and the number of cells in each bin was determined. For all quantification experiments a minimum of three mice were used. Counts were performed on at least three consecutive sections (six hemispheres) from each mouse. Results are expressed as mean ± standard error of the mean (SEM). Graphical representations of the data and statistical analysis were performed using GraphPadPrism for Microsoft Windows.

RESULTS

nNOS-EXPRESSING INTERNEURONS IN THE DEVELOPING CORTEX

We examined *nNos* mRNA and protein expression in the telencephalon at embryonic and postnatal stages. We detected nNOS transcripts in the cortex at E12.5 (**Figure 1A**). At this stage, expression was confined to the marginal zone and/or the cortical plate (black arrowhead in **Figure 1A**). This may correspond to Cajal-Retzius and cortical plate cells as previously described in the rat (Bredt and Snyder, 1994; Santacana et al., 1998). *nNos* was also expressed in scattered cells in the subventricular zone of the MGE (red arrowheads in **Figures 1A**,**B**) which is one of the sources of interneurons for the cortex. A clear but transient expression in the cortical plate was observed at E14.5, E18.5 (**Figures 1B**,**C**), and P5 (not shown). This was largely downregulated by P10 (**Figure 1D**). Presumptive cortical interneurons intensely labeled for *nNos* appeared scattered within the subventricular/intermediate zone of the lateral cortex at E18.5 (**Figures 1C**,**C'**). Later on these cells populated the entire medio-lateral extent of the cortex and the hippocampus and resided mainly within the deeper layers in postnatal animals (**Figures 1D**,**E**). Cells expressing high levels of *nNos* were also observed in the striatum (**Figures 1C–E**). A similar expression pattern was observed by nNOS immunohistochemistry (**Figures 1F–J**). Strong immunolabeling of nNOS protein was detected in a few scattered cells in the cortex at E18.5 and these increased in numbers thereafter (black arrows in **Figures 1I**,**J**). These are thought to represent nNOS type I cortical interneurons which express high levels of nNOS (Hashikawa et al., 1994; Yan et al., 1996; Smiley et al., 2000; Lee and Jeon, 2005). We could detect weakly-labeled putative nNOS type II cells from P10 onwards (red arrows in **Figures 1I**,**J**). We could not determine whether this represented the true onset of nNOS expression or the timing of appearance of type II cells because at earlier stages the strong nNOS signal in the cortical plate may have masked any weak expression in interneurons. A transient diffuse nNOS signal was observed in the deep cortical layers and in layer IV at P10 (**Figure 1I**). The barrel-like nNOS immunolabeling in layer IV (blue arrowheads in **Figure 1I**) may correspond to staining in the barrel centers, which are formed by afferents from the thalamus, or the barrel walls, which contain layer IV neurons. We

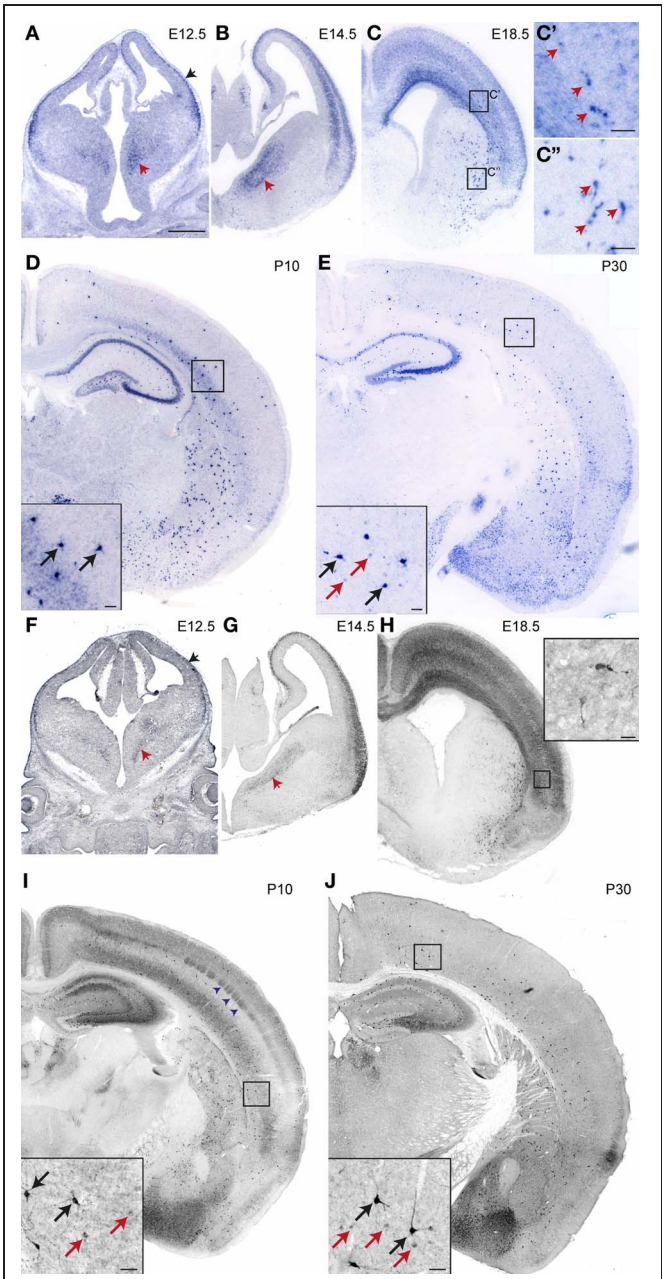

FIGURE 1 | Developmental expression of nNOS in the neocortex. **(A–E)** *nNos* mRNA expression at different embryonic and postnatal stages. Black and red arrowheads in **(A)** and **(B)** point to expression in the superficial cortex and the ventral MGE, respectively. Arrowheads in **(C')** and **(C")** point to cells expressing high levels of nNOS in the cortex and striatum, respectively. **(F–J)** nNOS protein expression at different embryonic and postnatal stages. Type I and type II cells are marked by black and red arrows, respectively in **(I)** and **(J)**. Scale bars: **A–J**, 500 μm. **C, C"** and inserts in **D**, **E**, **I**, **J**, 50 μm. Insert in **H**, 20 μm.

could not detect *nNOS* mRNA expression in layer IV at this stage (**Figure 1D**) suggesting that afferent inputs from the thalamus, where nNOS immunoreactivity has been observed (Terada et al., 2001), may account for the signal.

Our data show that interneurons expressing nNOS appear in the cortex just before birth. This suggests that either nNOS cortical interneurons are born late and enter the cortex late or that nNOS activation occurs in these cells only after they invade the cortex. To distinguish between the two possibilities we birthdated nNOS interneurons using EdU labeling at different embryonic stages and analysis at P30. nNOS type I and type II cells incorporating EdU could be detected at all stages examined (E10, E12, E14, E16, E18) (**Figure 2A**). Quantification of the extent of co-localization between EdU and nNOS showed that the majority of nNOS type I cells are born between E12 and E14 with E12 being the peak generation time (**Figure 2B**). Neurogenesis of type II cells spanned a longer period of time (**Figure 2D**). We also determined whether laminar fate is dependent on birthdate. We subdivided the cortex into two equal halves along the dorso-ventral axis and quantified the extent of EdU/nNOS colocalization. Although upper and lower layer nNOS neurons had overlapping neurogenesis periods, they had different peak generation times with most lower layer nNOS neurons being born earlier than the bulk of upper layer ones (**Figures 2C**,**E**). Collectively, our data indicate that nNOS cortical interneurons are born early during embryogenesis but express their definitive marker nNOS at later stages. Type II cells have a more protracted neurogenesis period compared to type I cells. In addition, settling of nNOS interneurons within the cortex occurs in an inside-out manner, as previously described for other cortical interneuron subtypes (Fairen et al., 1986; Rymar and Sadikot, 2007).

nNOS TYPE I AND TYPE II INTERNEURON DISTRIBUTION IN THE ADULT SOMATOSENSORY CORTEX

We examined in detail the distribution of nNOS-expressing interneurons in the adult cortex using immunohistochemistry for nNOS and Venus in *Dlx1-Venus^{fl}* transgenic mice. These mice express Venus in all GABAergic interneurons of the cortex (Rubin et al., 2010) and therefore allow us to definitively distinguish GABAergic nNOS interneurons from the few nNOS-expressing pyramidal cells which are found in upper cortical layers (**Figure 3A**). All nNOS-expressing neurons in the cortex, with the exception of a few cells in layer II, coexpressed Venus in the *Dlx1-Venus^{fl}* transgenic mice confirming their GABAergic phenotype (**Figure 3A**). In addition to the gray matter, nNOS/Venus coexpressing cells were also found in the white matter of the cortex (blue arrowheads in **Figure 3A**). nNOS type I cells showed distinctive immunoreactivity for nNOS: the cell body was intensely labeled and processes were clearly visible (**Figure 3B**). Type II cells had weaker immunoreactivity, processes were often indistinguishable and the cell body had uneven staining (**Figure 3B**). To quantify the density and distribution of nNOS interneurons in the cortex we counted double labeled Venus/nNOS type I and type II cells in different cortical layers: for this we subdivided the cortex into 10 equal bins along the white matter-pial axis and counted the double positive cells within each bin. Most type I cells were located within layer VI whereas type II cells had a maximum density in layers II/III and VI (**Figure 3C**). nNOS type I cells were rare and represented ∼2.5% of the total GABAergic interneuron population whereas type II cells represented ∼17% of cortical interneurons. Type II cells were ∼6.5 fold more abundant than type I cells in the somatosensory cortex although their relative abundance varied across different layers (**Figure 3D**). Our data indicate that there exists a clear heterogeneity of nNOS-expressing interneurons that is based not only on the level of expression of nNOS but also on the distribution and abundance of these cells within the cortex.

COEXPRESSION OF nNOS WITH OTHER INTERNEURON MARKERS IN TYPE I AND TYPE II CELLS

To determine whether nNOS type I cells can be subdivided further based on expression of other neurochemical markers, we examined the extent of co-localization between nNOS and CB, PV, SST, NPY, CR, and RLN. To avoid potential bleed-through artifacts arising from the strong fluorescence of type I cells detected by our amplification method, we quantified the extent of marker coexpression in nNOS in type I cells using regular immunohistochemistry whereby the primary anti-nNOS antibody was detected by an Alexa-conjugated secondary antibody. In the absence of signal amplification, only type I cells can be detected in the cortex. We found no co-localization between nNOS and CB, PV, or RLN in type I cells (**Figures 4A**,**B**). In contrast, all nNOS type I cells coexpressed NPY, nearly all coexpressed SST and ∼60% coexpressed CR (**Figures 4A**,**B**). Coexpression of nNOS with NPY and SST was also confirmed by *in situ* hybridization for NPY or SST followed by immunohistochemistry for nNOS (not shown). nNOS type I cells represented less than 10% of the total population of cortical NPY, SST, or CR interneurons ($8.7 \pm 1.6\%$ for NPY, $11.3 \pm 1\%$ for SST, and $8.2 \pm 1.1\%$ for CR) (**Figure 4C**). In contrast to nNOS type I cells, type II cells showed some co-localization with all markers examined (**Figures 4D–F**). A large number of nNOS type II cells coexpressed NPY (**Figure 4E**).

THE EMBRYONIC ORIGIN OF CORTICAL nNOS INTERNEURONS

The origin of cortical interneurons has been identified and it is clear that distinct interneuron cohorts originate from different neuroepithelial domains in the developing telencephalon. To a large extent, the apparent heterogeneity of interneurons observed in the adult cortex is laid down early on when these cells are born. We therefore examined whether the two types of nNOS interneurons originate from different neuroepithelial regions. For this we made use of a series of transgenic mice that express Cre recombinase in different domains of the developing telencephalon. When crossed to suitable reporters, these mice indelibly label the entire cell lineage originating in each domain. The mice used for lineage tracing in this study were the following: *Lhx6-Cre/R26R-YFP* which label all MGE-derived interneurons (Fogarty et al., 2007), *Nkx2.1-Cre/R26R-GFP* and *Nkx6.2-Cre/R26R-GFP* which label different populations of MGE-derived interneurons (as well as POA-derived neurons) (Fogarty et al., 2007), *Dlx1-Venus^{fl}/Nkx2.1-Cre* which label all LGE/CGE-derived cells (Rubin et al., 2010), and *Nkx5.1-Cre/R26R-YFP* and *Shh-Cre/R26R-LacZ* which label different

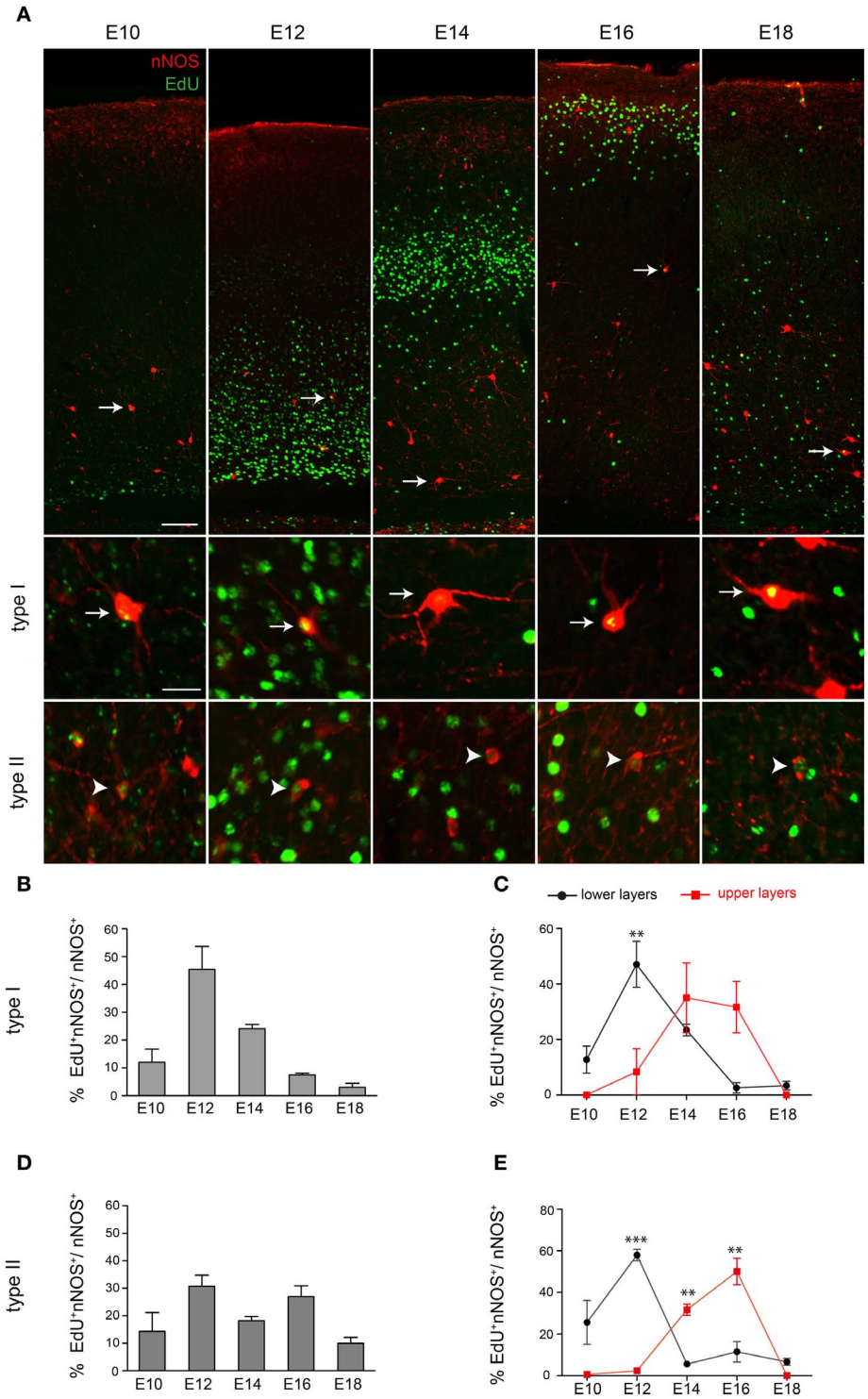

FIGURE 2 | Neurogenesis period of cortical nNOS cells. (A) nNOS-positive neurons and EdU-incorporating cells at P30 following EdU administration at different developmental stages. White arrows and arrowheads indicate nNOS-immunoreactive neurons colabeled with EdU. These are shown at higher magnification in the lower panel for type I (arrows) and type II cells (arrowheads). **(B)** Histogram showing the EdU labeling index for nNOS type I cells. **(C)** Neurogenesis periods of nNOS type I cells residing in lower and upper cortical layers. A significant difference is detected at E12. $^{**}P < 0.01$ (Two-way ANOVA with Bonferroni *post-hoc* test). **(D)** Histogram showing the EdU labeling index for nNOS type II cells. **(E)** Neurogenesis periods of nNOS type II cells residing in lower and upper cortical layers. A significant difference is detected at E12, E14, and E16. $^{**}P < 0.01$ $^{***}P < 0.001$ (Two-Way ANOVA with Bonferroni *post-hoc* test). Error bars indicate SEM. Scale bars: **A**, upper panel, 100 μm, lower panel, 20 μm.

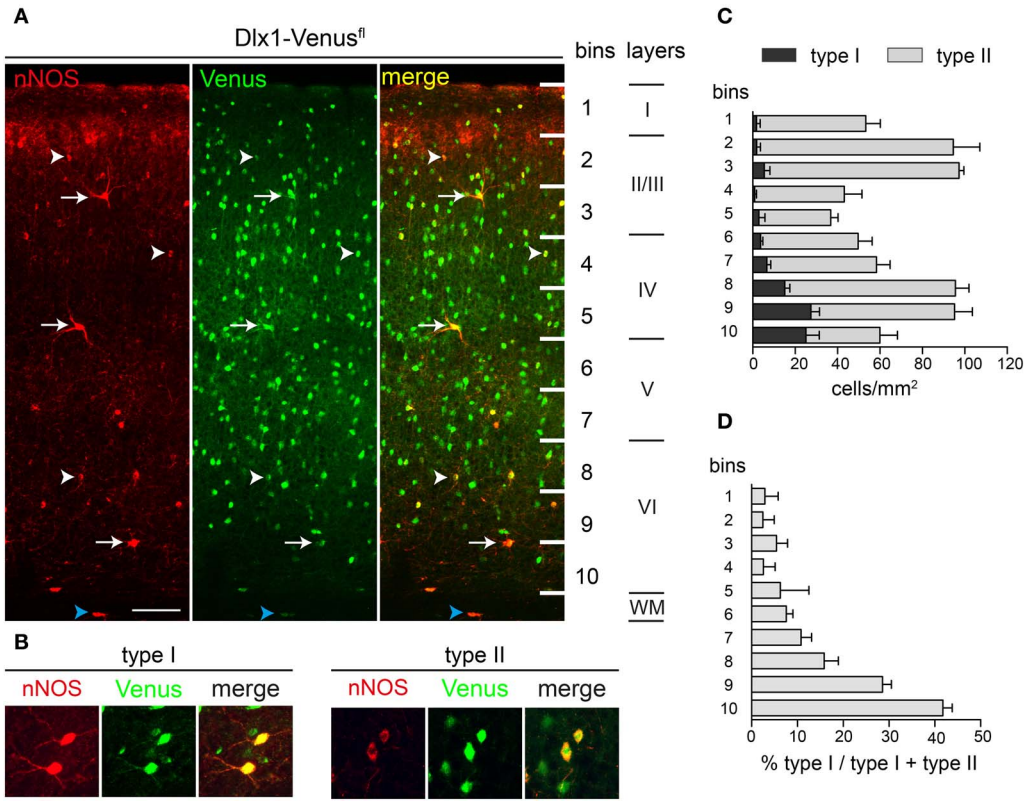

FIGURE 3 | nNOS-expressing type I and type II cells in the adult somatosensory cortex. (A) nNOS and Venus expression in the somatosensory cortex of *Dlx1-Venus*^{fl} mice. Arrows and arrowheads point to type I and type II cells respectively. Blue arrowheads mark nNOS-expressing cells in the white matter (WM). **(B)** High magnification images of type I and type II cells. Note the strong labeling for nNOS in the soma and the processes of type I cells and the pale nNOS staining in type II cells. **(C)** Quantification of type I and type II cell densities across cortical bins. **(D)** Abundance of type I cells across bins as a fraction of the total nNOS cells in each bin. Error bars indicate SEM. Scale bars: **A**, 50 μm; **B**, 20 μm.

subpopulations of POA-derived cortical interneurons (Gelman et al., 2009, 2011). Herein we refer to them as *Lhx6-Cre/YFP*, *Nkx2.1-Cre/GFP*, *Nkx6.2-Cre/GFP*, *Dlx1-V*^{fl}*/Nkx2.1-Cre*, *Nkx5.1-Cre/YFP,* and *Shh-Cre/LacZ*. We examined the co-localization of nNOS with GFP/YFP/Venus/β-gal (referred to as XFP/β-gal) and quantified this for type I and type II cells in the somatosensory cortex in adult mice. Where necessary, immunodetection of type I cells without signal amplification for nNOS was used to avoid any bleed-through artifacts arising from the strong fluorescence of type I cells. This was carried out in *Nkx2.1-Cre/GFP*, *Nkx6.2-Cre/GFP*, *Nkx5.1-Cre/YFP,* and *Shh-Cre/LacZ* transgenic mice. The strong Venus/YFP fluorescence in *Dlx1-V*^{fl}*/Nkx2.1-Cre* and *Lhx6-Cre/YFP* (two copies of the YFP reporter) transgenic mice circumvented all bleed-through problems.

All type I cells coexpressed YFP in *Lhx6-Cre/YFP* mice indicating that they are all derived from the MGE (**Figures 5A**,**B**). In previous studies we were able to distinguish between the contribution of the dorsal MGE (dMGE) and the rest of the MGE neuroepithelium using transgenic mice expressing *Nkx6.2-Cre* and *Nkx2.1-Cre* (Fogarty et al., 2007). *Nkx6.2-Cre* mice activate the *R26R-GFP* reporter mainly in the dMGE with only scattered activation in the rest of the MGE. In contrast, *Nkx2.1-Cre* transgenic mice label most of the MGE with the exception of a small dorsal domain that expresses high levels of *Nkx6.2*. Both mice express Cre in the POA. The two transgenic mice therefore have complementary albeit partly overlapping patterns of Cre expression. We found that, unlike *Lhx6-Cre/YFP* transgenic mice where all nNOS type I cells coexpressed YFP, in *Nkx2.1-Cre/GFP* or *Nkx6.2-Cre/YFP* transgenic mice less than 50% of the type I cells co-localized with GFP/YFP (**Figures 5A**,**B**). This suggests that there is contribution of nNOS type I cells from both the *Nkx6.2-Cre*-expressing dMGE neuroepithelium as well as the rest of the MGE. There was no Venus or YFP expression in nNOS type I cells in the LGE/CGE- or the POA-tracing mice confirming that these two regions do not generate cortical nNOS type I cells (**Figures 5A**,**B**). Consistent with nNOS type I cells being very few, they represented less than 5% of the cortical interneurons generated from the MGE which is the main source of interneurons for the cortex (**Figure 5C**).

In contrast to type I cells, type II cells appear to have a triple MGE, LGE/CGE, and POA origin (**Figures 5D–F**). Most of these cells are generated in the MGE and the LGE/CGE. The POA contributes only a small number (**Figures 5D–F**). Intriguingly, the contribution of *Nkx2.1-Cre*-expressing precursors to the total population of nNOS type II cells is similar to that of the entire MGE in *Lhx6-Cre/YFP* mice (**Figure 6E**). This suggests that

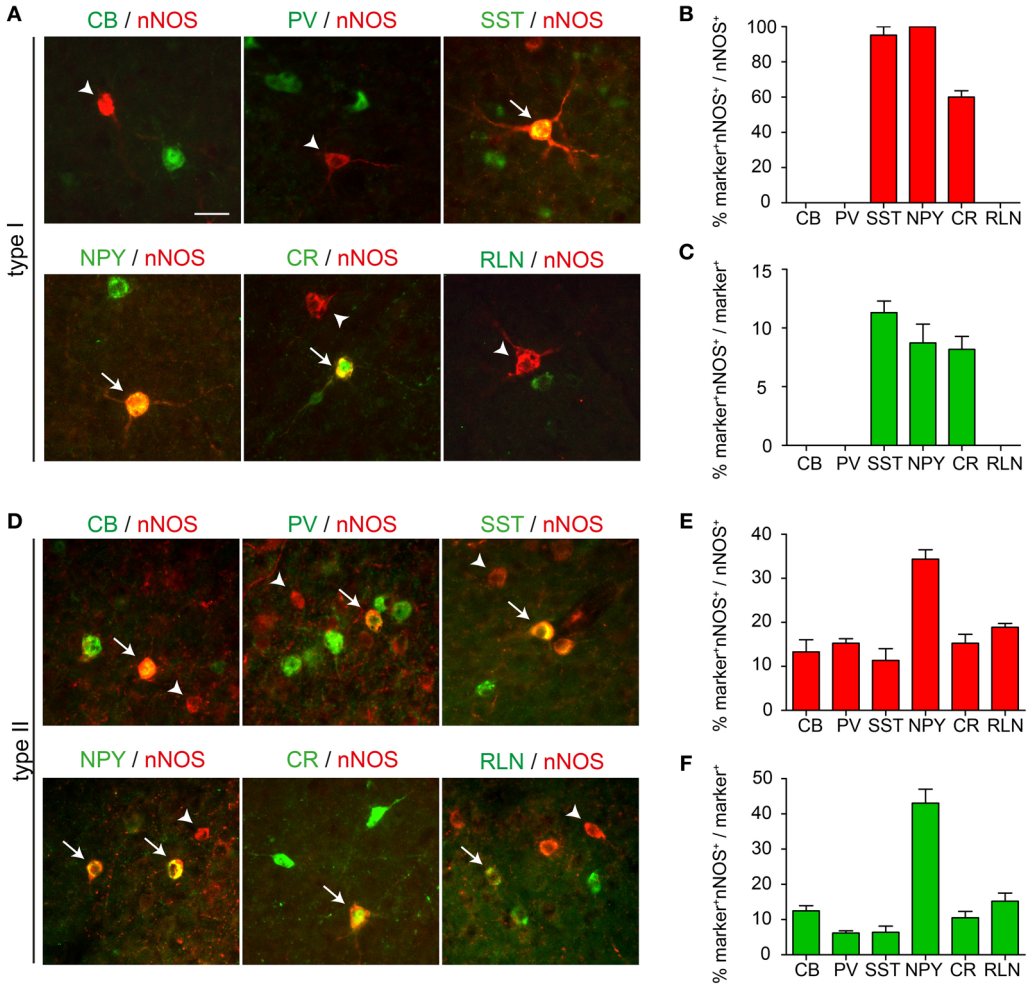

FIGURE 4 | Coexpression of nNOS with other interneuron markers. **(A)** Expression of CB, PV, SST, NPY, CR, or RLN in nNOS type I cells. **(B)** Quantification of the extent of coexpression between nNOS and the different interneuron markers in type I cells. **(C)** The number of marker$^+$ nNOS type I cells is presented as a percentage of the total number of marker$^+$ cells. **(D)** Expression of CB, PV, SST, NPY, CR, or RLN in nNOS type II cells. **(E)** Quantification of the extent of coexpression between nNOS and the different interneuron markers in type II cells. **(F)** The number of marker$^+$ nNOS type II cells is presented as a percentage of the total number of marker$^+$ cells. Error bars indicate SEM. Scale bar: 20 μm.

most MGE-derived type II cells are born outside the dMGE neuroepithelium.

LAMINAR DISTRIBUTION OF nNOS INTERNEURONS FROM DIFFERENT EMBRYONIC ORIGINS

Previous genetic fate-mapping work had shown that interneurons that have different embryonic origins settle in different layers within the adult cortex (Miyoshi et al., 2007, 2010; Gelman et al., 2009, 2011; Rubin et al., 2010). We examined the laminar distribution of nNOS/XFP/β-gal cells in the six transgenic mouse lines described above (**Figures 6A–L**). Type I cells originating from *Lhx6*-expressing precursors and representing the entire type I population settle within the lower layers of the cortex (**Figure 6A**). Whilst *Nkx2.1*-derived type I cells had a tendency to populate middle and lower layers, *Nkx6.2*-derived type I cells populated mainly middle layers (**Figures 6B**,**C**). MGE- and LGE/CGE-derived type II cells occupied respectively lower and upper layers of the cortex (**Figures 6G**,**J**), as previously described for other cortical interneuron subtypes originating from these two regions (Xu et al., 2004; Miyoshi et al., 2007, 2010; Rubin et al., 2010). A tendency for *Nkx2.1*-derived type II cells to populate lower layers than *Nkx6.2*-derived ones was also observed (**Figures 6H**,**I**). The few nNOS type II cells originating from *Nkx5.1*- and *Shh*-expressing domains occupied different cortical layers, suggesting that they represent distinct populations of type II neurons (**Figures 6K**,**L**).

DISCUSSION

We examined the development and origin of nNOS type I and type II interneurons in the neocortex. The two populations of nNOS neurons have different origins within the embryonic telencephalon: all type I cells are derived from the MGE whereas type II cells have a triple MGE, LGE/CGE, and POA origin (**Figure 7**). Neurogenesis of type I cells takes place during a narrower time-window compared to type II cells. Layer acquisition for both populations occurs in an inside-out manner

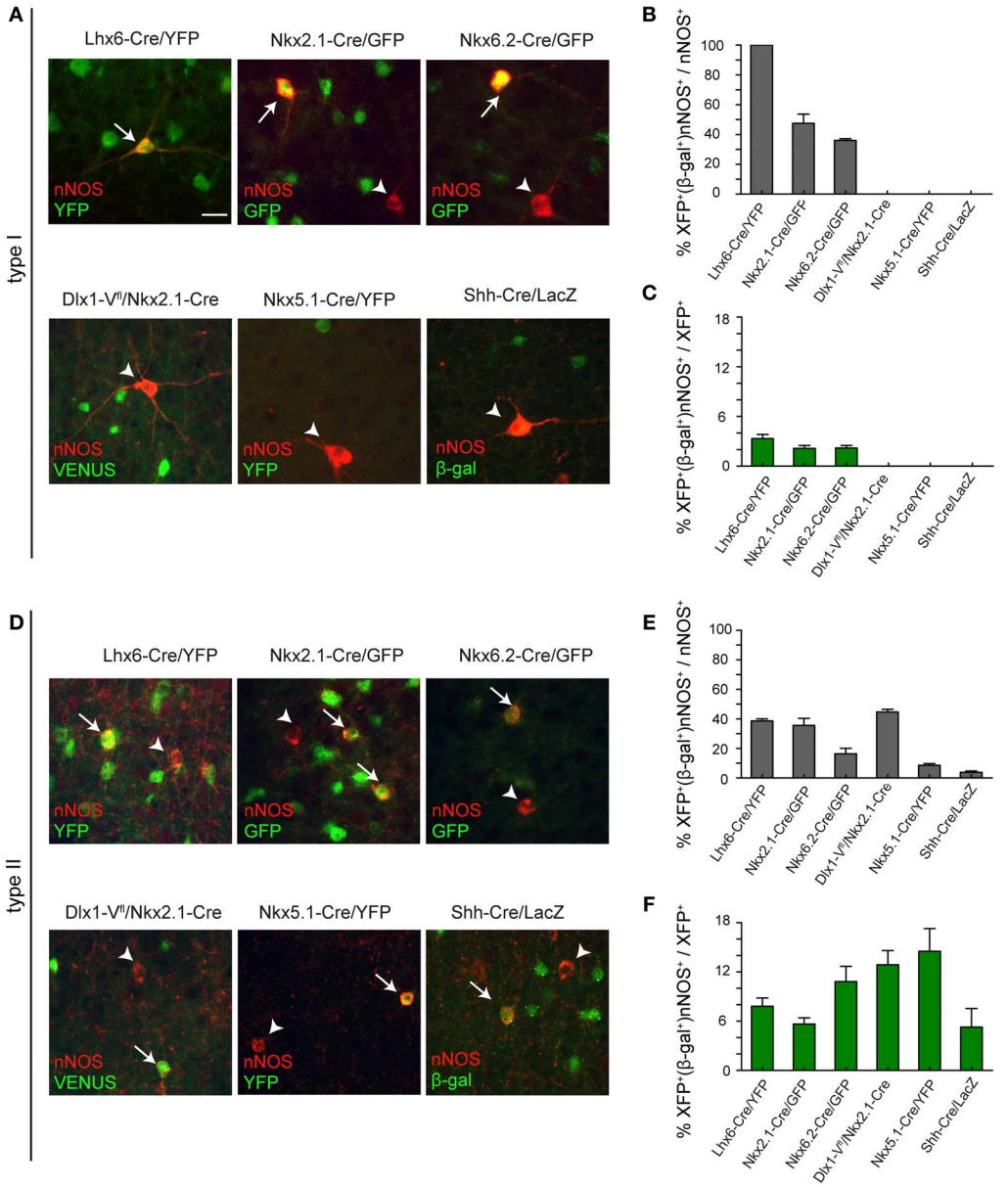

FIGURE 5 | Embryonic origin of type I and type II nNOS cortical interneurons. (A) Coexpression of nNOS and GFP/YFP/Venus/β-gal in type I cells in different transgenic mouse lines. Arrows and arrowheads point to double and single-labeled type I cells, respectively. **(B)** Contribution of different progenitor pools to type I cortical interneurons. The extent of co-localization between nNOS and GFP/YFP/Venus/β-gal in type I cells is shown as a percentage of the total nNOS type I cells **(B)** or as a percentage of the total GFP/YFP/Venus/ β-gal-expressing interneurons **(C)**. **(D)** Coexpression of nNOS and GFP/YFP/Venus/β-gal in type II cells in different transgenic mouse lines. Arrows and arrowheads point to double and single-labeled type II cells, respectively. **(E)** Contribution of different progenitor pools to type II cells. The extent of co-localization between nNOS and GFP/YFP/Venus/β-gal in type II cells is shown as a percentage of the total nNOS type II cells (**E**) or as a percentage of the total GFP/YFP/Venus/β-gal-expressing interneurons **(F)**. Error bars indicate SEM. Scale bar: 20 μm.

and is dependent on birthplace. nNOS neurons are more abundant in the adult cortex than previously thought and represent ∼20% of the entire cortical interneuron population. Type I and type II nNOS neurons have different distributions within the adult cortex. Most type I cells are located within lower cortical layers whereas type II cells are distributed in all layers. All type I cells in the mouse somatosensory cortex coexpress NPY and SST and about half express CR. Type I cells do not express CB, PV, or RLN (**Figure 7**). Type II cells show some coexpression with all markers examined (**Figure 7**). Our data confirm the previously described heterogeneity of the nNOS interneuron population based on the levels of nNOS expression, morphology, and coexpression of other interneuron markers. Our fate-mapping suggests that this heterogeneity is laid down during embryonic development when these cells are specified from neuroepithelial precursor cells.

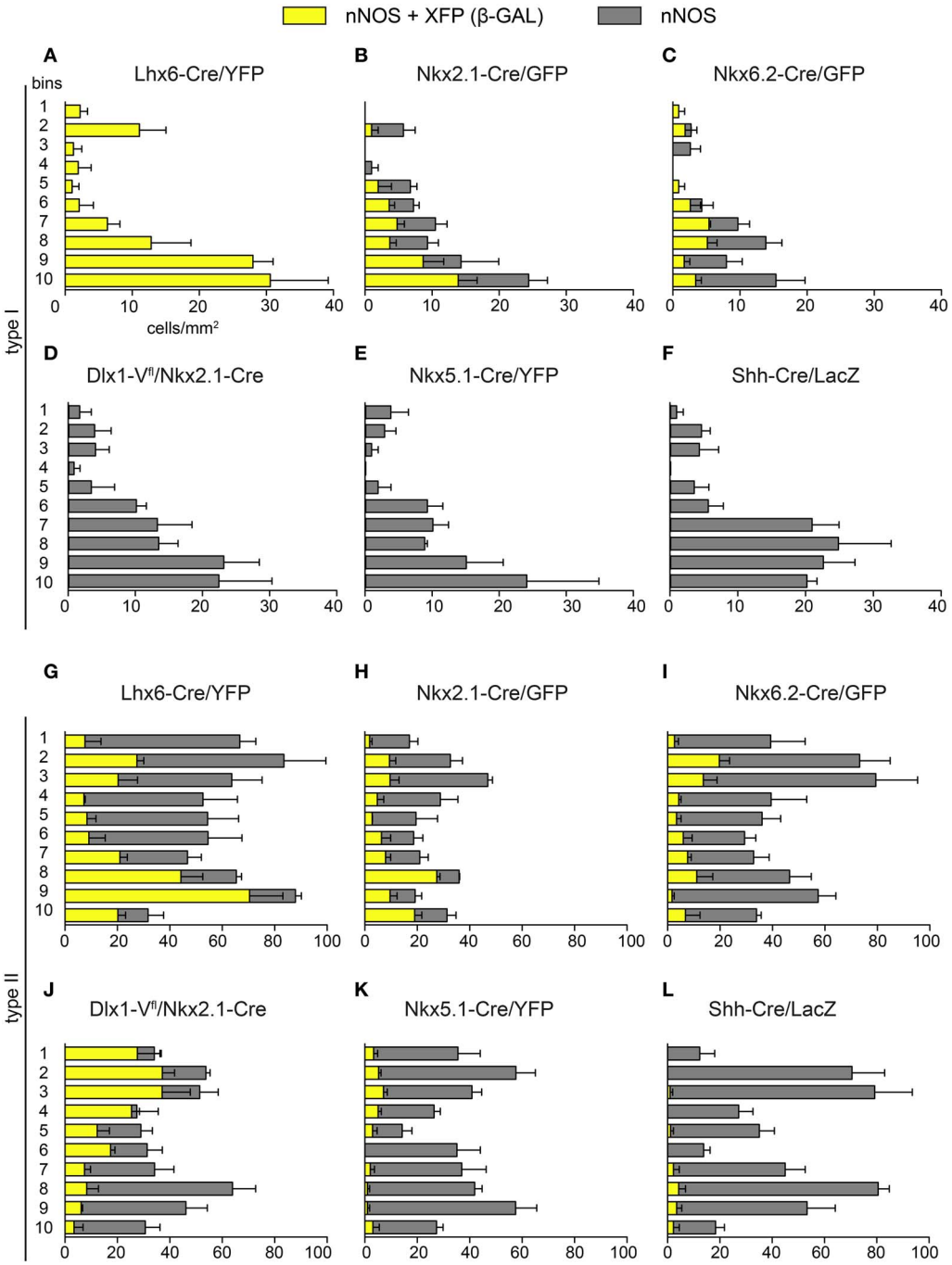

FIGURE 6 | Laminar distribution of nNOS immunoreactive cells originating in different embryonic neuroepithelial regions. The density of type I **(A–F)** and type II cells **(G–L)** coexpressing GFP/YFP/Venus/β-gal (yellow) as well as the total number of nNOS-expressing cells (gray) across cortical bins are shown for each transgenic mouse line. Error bars indicate SEM.

nNOS CORTICAL INTERNEURONS ARE BORN EARLY BUT UPREGULATE nNOS JUST BEFORE BIRTH

We detected putative nNOS cortical interneurons in the cortex only at E18.5 whereas most interneurons in the cortex are born earlier during embryogenesis (Fairen et al., 1986; Rymar and Sadikot, 2007). We demonstrate that both type I and type II cells are born early during gestation and suggest that they upregulate nNOS well after they enter the cortex. We cannot exclude the possibility of a subpallial delay in their migration and a late invasion of the cortex. However, an earlier marker that identifies these cells is required to address this question. Interestingly, we found that most type I cells were born at E12.5 whereas neurogenesis of

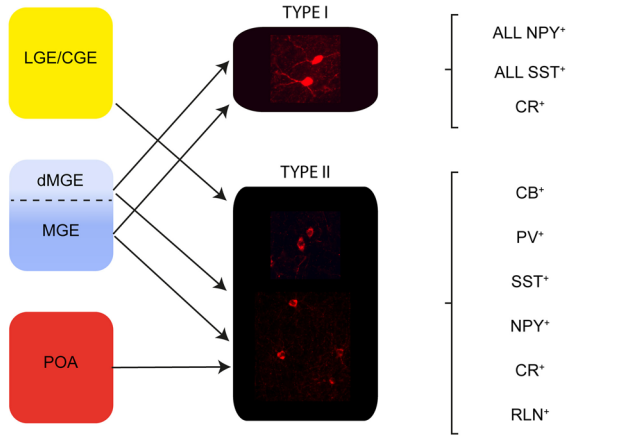

FIGURE 7 | The embryonic origin and neurochemical content of nNOS interneurons in the adult somatosensory mouse cortex. Type I cells originate in the MGE. Type II cells have a triple origin in the LGE/CGE, MGE and POA. All type I cells coexpress SST and NPY and some coexpress CR. Heterogeneity of neurochemical marker expression is observed in type II cells.

type II cells spanned a wider time-window. This is in line with their embryonic origin: type I cells are all MGE-derived whereas type II cells have a triple origin in the MGE, LGE/CGE, and POA. The three germinal zones generate cortical interneurons at different times during development (Miyoshi et al., 2007, 2010; Gelman et al., 2009, 2011).

DIFFERENTIAL DISTRIBUTION AND ABUNDANCE OF nNOS TYPE I AND TYPE II INTERNEURONS IN THE ADULT CORTEX

In mice and monkeys the two types of nNOS neurons are distributed differently within cortical layers, with type I cells found mainly in deeper layers and the white matter and type II cells found throughout the cortex, especially layers II/III (Hashikawa et al., 1994; Yan et al., 1996; Smiley et al., 2000; Gotti et al., 2005; Lee and Jeon, 2005; Rockland and Nayyar, 2012). In rats however, the distribution seems to vary according to the area examined with type I cells being abundant in deep layers in the frontal cortex (Kubota et al., 1994) and in superficial layers in the visual cortex (Gonchar and Burkhalter, 1997). Our analysis was focused on the mouse somatosensory cortex and we found a consistent abundance of type I cells in lower layers (highest in layer VI) and in the white matter and type II cells in upper (II/III) and lower layers (VI). As described in other species, type II cells were always more numerous than type I cells.

nNOS TYPE I CELLS COEXPRESS NPY, SST, AND CR BUT NOT CB, PV, OR RLN WHEREAS SUBPOPULATIONS OF TYPE II CELLS SHOW EXPRESSION OF ALL MARKERS EXAMINED

In rats, monkeys, and rabbits nearly all type I cells coexpress SST and NPY and a large number express substance P receptor, whereas hardly any express PV or CR (Dawson et al., 1991; Kubota et al., 1994, 2011; Gonchar and Burkhalter, 1997; Smiley et al., 2000; Lee and Jeon, 2005; Karagiannis et al., 2009). Expression of PV and CR in type I cells in the mouse is controversial (Lee and Jeon, 2005; Gonchar et al., 2007) and CB expression varies in different cortical areas and across species (Kubota et al., 1994; Gonchar and Burkhalter, 1997; Smiley et al., 2000; Lee and Jeon, 2005). We found that all nNOS type I cells in the mouse somatosensory cortex coexpress SST and NPY and ~60% coexpress CR. We did not find any type I cells co-localizing with CB, PV, or RLN. In contrast, small numbers of type II cells coexpressed CB, CR, PV, SST, RLN, and to a greater extent NPY. This heterogeneity of marker expression observed within the type II population is consistent with findings in rats where expression of NPY and PV has been observed albeit not SST (Karagiannis et al., 2009; Kubota et al., 2011). In monkeys some expression of SST and NPY in type II cells has been detected although not CB, CR, or PV (Smiley et al., 2000). These differences in co-localization studies for type I and type II cells may reflect differences amongst species, cortical areas, methodology used or technical differences in detecting and distinguishing type II from type I cells.

DISTINCT ORIGINS FOR nNOS TYPE I AND TYPE II INTERNEURONS IN THE EMBRYONIC TELENCEPHALON

The embryonic origin of cortical nNOS interneurons has not been established. Analysis of mice lacking the MGE transcription factor NKX2.1 showed a complete absence of nNOS-expressing cells at prenatal stages suggesting an MGE-origin (Anderson et al., 2001) and lineage tracing in the POA identified some nNOS cortical interneurons being derived from this region (Gelman et al., 2009, 2011). However, no distinction had been made between type I and type II cells in either of these two studies. We used a series of transgenic mouse lines that allowed us to fate map the three subpallial sources of interneurons and we demonstrate that type I and type II cells have different origins: type I nNOS interneurons are generated exclusively from the MGE whereas type II cells have multiple origins in the MGE, LGE/CGE, and the POA. This is in agreement with a recent fate-mapping study that showed an exclusive MGE origin of nNOS type I cells (Jaglin et al., 2012). Type II cells had not been examined (Jaglin et al., 2012).

Using our transgenic mice we were able to subdivide the MGE and directly fate-map the dMGE and more ventral MGE regions. We found that the dMGE which expresses high levels of *Nkx6.2*, generates a large number of nNOS type I cells. Our previous finding that all SST^+CR^+ interneurons for the cortex originate in the dMGE (Fogarty et al., 2007) suggests that type I cells generated within this region include the entire CR-expressing population. Type I cells that do not express CR may originate from more ventrally-located MGE precursors. We demonstrate that *Nkx2.1-Cre*-generated type I cells occupy lower layers whereas *Nkx6.2-Cre*-derived cells are more evenly distributed across the layers. Altogether, the data indicate that CR^+ and CR^- type I cells have different origins within the MGE and their layer distribution within the cortex is dependent on their birthplace.

Whilst most type I cells were found to be settled in lower layers in the adult cortex, type II cells were found in upper and lower layers. Layer selection for type II cells was dependent on the

origin because MGE-derived type II cells had a bias for the lower layers and LGE/CGE and POA-derived cells were more abundant in upper layers. This is in line with previous genetic fate-mapping studies that showed distinct distribution patterns of interneurons originating in the three subcortical germinal zones (Miyoshi et al., 2007, 2010; Gelman et al., 2009, 2011; Rubin et al., 2010).

FUNCTIONAL HETEROGENEITY OF TYPE I AND TYPE II CELLS IN THE NEOCORTEX

Very little is known about the function and participation of nNOS interneurons in cortical circuits. An axo-dendritic subcellular targeting has been described but no distinction has been made between type I and type II cells (Seress et al., 2005). The two populations in the rat somatosensory cortex have distinct physiological features (Karagiannis et al., 2009). Our findings that type I and type II cells have different embryonic origins and settle in different layers of the cortex are consistent with the notion that the two cohorts represent distinct interneuron subtypes.

Recent evidence has shown that nNOS type I neurons are projecting neurons (Tomioka et al., 2005; Higo et al., 2009; Tamamaki and Tomioka, 2010) and form a population of neurons that are activated during sleep (Gerashchenko et al., 2008; Kilduff et al., 2011). We find that type I cells share common features: they are all generated from MGE precursors during a narrow neurogenesis window and coexpress NPY and SST. However, even type I cells may represent functionally distinct cell types given that (a) they originate from the *Nkx6.2*-expressing region in the dMGE as well as more ventrally-located MGE neuroepithelial cells, (b) they occupy different layers according to their origin, and (c) they show heterogeneity in CR expression. Detailed analysis of CR^+ and CR^- SST-expressing Martinotti cells had found significant differences in their morphology and intrinsic physiology (Xu et al., 2006). This suggests that $nNOS^+SST^+CR^+$ and $nNOS^+$ SST^+CR^- type I cells may differ in their morphological and/or electrophysiological features. Their differential distribution across layers may also be suggestive of distinct roles in cortical networks.

Hippocampal Ivy cells and a subpopulation of nNOS-expressing neurogliaform cells are two examples of MGE-derived interneuron subpopulations that have similar molecular profiles and common intrinsic physiological and morphological characteristics. Yet, the two populations reside in different layers in the hippocampus and participate at different times during network function, suggesting that they may represent functionally distinct interneuron subtypes (Price et al., 2005; Fuentealba et al., 2008; Szabadics and Soltesz, 2009; Tricoire et al., 2010, 2011). Whether Ivy cells and neurogliaform cells of the hippocampus have different origins within the MGE or have diverged functionally because of their differential lamination is unknown.

Within the type II population there is diversity in terms of birthdate, embryonic origin, laminar distribution and neurochemical content indicating that type II cells represent a heterogenous pool of neurons. nNOS type II cells coexpressing RLN in the cortex may correspond to a subpopulation of late-spiking neurogliaform cells that originate in the CGE (Lee et al., 2010; Miyoshi et al., 2010). To date cortical and hippocampal interneurons that have similar properties have been found to originate within the same progenitor zone. Late-spiking neurogliaform cells are an exemption to this because cortical neurogliaform cells originate within the CGE whereas hippocampal neurogliaform cells have a dual MGE/CGE origin (Lee et al., 2010; Miyoshi et al., 2010; Tricoire et al., 2010, 2011). Alternatively, there might be an MGE-derived neurogliaform cell in the cortex that has yet to be identified.

Interneurons that originate from the three major subpallial sources clearly have distinct neurochemical, morphological, and electrophysiological profiles. These are likely to be genetically imposed at their birthplace. Dissection of genetic specification pathways that confer subtype identity will provide insight into the development and ultimately the function of these cells in cortical circuits.

ACKNOWLEDGMENTS

We thank our colleagues at the Wolfson Institute for Biomedical Research (University College London) for helpful comments and discussions. We also thank S.-L. Ang, S. Claxton, and N. Anthwal (National Institute for Medical Research, UK) for providing us with tissue from Shh-Cre mice. Marcio G. Oliveira and Anna N. Rubin are supported by PhD studentships from the Portuguese Fundação para a Ciência e Tecnologia (SFRH/BD/69008/2010) and the Wellcome Trust, respectively. Financial support for the work was provided to Nicoletta Kessaris by a European Research Council (ERC) Starting Grant under the European Community's Seventh Framework Programme (Grant agreement no. 207807).

REFERENCES

Alderton, W. K., Cooper, C. E., and Knowles, R. G. (2001). Nitric oxide synthases: structure, function and inhibition. *Biochem. J.* 357, 593–615.

Anderson, S. A., Marin, O., Horn, C., Jennings, K., and Rubenstein, J. L. (2001). Distinct cortical migrations from the medial and lateral ganglionic eminences. *Development* 128, 353–363.

Bredt, D. S., and Snyder, S. H. (1994). Transient nitric oxide synthase neurons in embryonic cerebral cortical plate, sensory ganglia, and olfactory epithelium. *Neuron* 13, 301–313.

Dawson, T. M., Bredt, D. S., Fotuhi, M., Hwang, P. M., and Snyder, S. H. (1991). Nitric oxide synthase and neuronal NADPH diaphorase are identical in brain and peripheral tissues. *Proc. Natl. Acad. Sci. U.S.A.* 88, 7797–7801.

Fairen, A., Cobas, A., and Fonseca, M. (1986). Times of generation of glutamic acid decarboxylase immunoreactive neurons in mouse somatosensory cortex. *J. Comp. Neurol.* 251, 67–83.

Fogarty, M., Grist, M., Gelman, D., Marin, O., Pachnis, V., and Kessaris, N. (2007). Spatial genetic patterning of the embryonic neuroepithelium generates GABAergic interneuron diversity in the adult cortex. *J. Neurosci.* 27, 10935–10946.

Fuentealba, P., Begum, R., Capogna, M., Jinno, S., Marton, L. F., Csicsvari, J., Thomson, A., Somogyi, P., and Klausberger, T. (2008). Ivy cells: a population of nitric-oxide-producing, slow-spiking GABAergic neurons and their involvement in hippocampal network activity. *Neuron* 57, 917–929.

Furchgott, R. F., and Zawadzki, J. V. (1980). The obligatory role of endothelial cells in the relaxation of arterial smooth muscle by acetylcholine. *Nature* 288, 373–376.

Gelman, D., Griveau, A., Dehorter, N., Teissier, A., Varela, C., Pla, R., Pierani, A., and Marin, O. (2011). A wide diversity of cortical GABAergic interneurons derives from the embryonic preoptic area. *J. Neurosci.* 31, 16570–16580.

Gelman, D. M., and Marin, O. (2010). Generation of interneuron diversity in the mouse cerebral cortex. *Eur. J. Neurosci.* 31, 2136–2141.

Gelman, D. M., Martini, F. J., Nobrega-Pereira, S., Pierani, A., Kessaris, N., and Marin, O. (2009). The embryonic preoptic area is a novel source of cortical GABAergic interneurons. *J. Neurosci.* 29, 9380–9389.

Gerashchenko, D., Wisor, J. P., Burns, D., Reh, R. K., Shiromani, P. J., Sakurai, T., de la Iglesia, H. O., and Kilduff, T. S. (2008). Identification of a population of sleep-active cerebral cortex neurons. *Proc. Natl. Acad. Sci. U.S.A.* 105, 10227–10232.

Gibbs, S. M. (2003). Regulation of neuronal proliferation and differentiation by nitric oxide. *Mol. Neurobiol.* 27, 107–120.

Gonchar, Y., and Burkhalter, A. (1997). Three distinct families of GABAergic neurons in rat visual cortex. *Cereb. Cortex* 7, 347–358.

Gonchar, Y., Wang, Q., and Burkhalter, A. (2007). Multiple distinct subtypes of GABAergic neurons in mouse visual cortex identified by triple immunostaining. *Front. Neuroanat.* 1:3. doi: 10.3389/neuro.05.003.2007

Gotti, S., Sica, M., Viglietti-Panzica, C., and Panzica, G. (2005). Distribution of nitric oxide synthase immunoreactivity in the mouse brain. *Microsc. Res. Tech.* 68, 13–35.

Harfe, B. D., Scherz, P. J., Nissim, S., Tian, H., McMahon, A. P., and Tabin, C. J. (2004). Evidence for an expansion-based temporal Shh gradient in specifying vertebrate digit identities. *Cell* 118, 517–528.

Hashikawa, T., Leggio, M. G., Hattori, R., and Yui, Y. (1994). Nitric oxide synthase immunoreactivity colocalized with NADPH-diaphorase histochemistry in monkey cerebral cortex. *Brain Res.* 641, 341–349.

Herbison, A. E., Simonian, S. X., Norris, P. J., and Emson, P. C. (1996). Relationship of neuronal nitric oxide synthase immunoreactivity to GnRH neurons in the ovariectomized and intact female rat. *J. Neuroendocrinol.* 8, 73–82.

Higo, S., Akashi, K., Sakimura, K., and Tamamaki, N. (2009). Subtypes of GABAergic neurons project axons in the neocortex. *Front. Neuroanat.* 3:25. doi: 10.3389/neuro.05.025.2009

Hope, B. T., Michael, G. J., Knigge, K. M., and Vincent, S. R. (1991). Neuronal NADPH diaphorase is a nitric oxide synthase. *Proc. Natl. Acad. Sci. U.S.A.* 88, 2811–2814.

Jaglin, X. H., Hjerling-Leffler, J., Fishell, G., and Batista-Brito, R. (2012). The origin of neocortical nitric oxide synthase-expressing inhibitory neurons. *Front. Neural Circuits* 6:44. doi: 10.3389/fncir.2012.00044

Karagiannis, A., Gallopin, T., David, C., Battaglia, D., Geoffroy, H., Rossier, J., Hillman, E. M., Staiger, J. F., and Cauli, B. (2009). Classification of NPY-expressing neocortical interneurons. *J. Neurosci.* 29, 3642–3659.

Kessaris, N., Fogarty, M., Iannarelli, P., Grist, M., Wegner, M., and Richardson, W. D. (2006). Competing waves of oligodendrocytes in the forebrain and postnatal elimination of an embryonic lineage. *Nat. Neurosci.* 9, 173–179.

Kilduff, T. S., Cauli, B., and Gerashchenko, D. (2011). Activation of cortical interneurons during sleep: an anatomical link to homeostatic sleep regulation? *Trends Neurosci.* 34, 10–19.

Kubota, Y., Hattori, R., and Yui, Y. (1994). Three distinct subpopulations of GABAergic neurons in rat frontal agranular cortex. *Brain Res.* 649, 159–173.

Kubota, Y., Shigematsu, N., Karube, F., Sekigawa, A., Kato, S., Yamaguchi, N., Hirai, Y., Morishima, M., and Kawaguchi, Y. (2011). Selective coexpression of multiple chemical markers defines discrete populations of neocortical GABAergic neurons. *Cereb. Cortex* 21, 1803–1817.

Lee, J. E., and Jeon, C. J. (2005). Immunocytochemical localization of nitric oxide synthase-containing neurons in mouse and rabbit visual cortex and co-localization with calcium-binding proteins. *Mol. Cells* 19, 408–417.

Lee, S., Hjerling-Leffler, J., Zagha, E., Fishell, G., and Rudy, B. (2010). The largest group of superficial neocortical GABAergic interneurons expresses ionotropic serotonin receptors. *J. Neurosci.* 30, 16796–16808.

Mao, X., Fujiwara, Y., Chapdelaine, A., Yang, H., and Orkin, S. H. (2001). Activation of EGFP expression by Cre-mediated excision in a new ROSA26 reporter mouse strain. *Blood* 97, 324–326.

Miyoshi, G., Butt, S. J., Takebayashi, H., and Fishell, G. (2007). Physiologically distinct temporal cohorts of cortical interneurons arise from telencephalic Olig2-expressing precursors. *J. Neurosci.* 27, 7786–7798.

Miyoshi, G., Hjerling-Leffler, J., Karayannis, T., Sousa, V. H., Butt, S. J., Battiste, J., Johnson, J. E., Machold, R. P., and Fishell, G. (2010). Genetic fate mapping reveals that the caudal ganglionic eminence produces a large and diverse population of superficial cortical interneurons. *J. Neurosci.* 30, 1582–1594.

Palmer, R. M., Ferrige, A. G., and Moncada, S. (1987). Nitric oxide release accounts for the biological activity of endothelium-derived relaxing factor. *Nature* 327, 524–526.

Price, C. J., Cauli, B., Kovacs, E. R., Kulik, A., Lambolez, B., Shigemoto, R., and Capogna, M. (2005). Neurogliaform neurons form a novel inhibitory network in the hippocampal CA1 area. *J. Neurosci.* 25, 6775–6786.

Rockland, K. S., and Nayyar, N. (2012). Association of type I neurons positive for NADPH-diaphorase with blood vessels in the adult monkey corpus callosum. *Front. Neural Circuits* 6:4. doi: 10.3389/fncir.2012.00004

Rubin, A. N., Alfonsi, F., Humphreys, M. P., Choi, C. K., Rocha, S. F., and Kessaris, N. (2010). The germinal zones of the basal ganglia but not the septum generate GABAergic interneurons for the cortex. *J. Neurosci.* 30, 12050–12062.

Rymar, V. V., and Sadikot, A. F. (2007). Laminar fate of cortical GABAergic interneurons is dependent on both birthdate and phenotype. *J. Comp. Neurol.* 501, 369–380.

Santacana, M., Uttenthal, L. O., Bentura, M. L., Fernandez, A. P., Serrano, J., Martinez de, V., Alonso, D., Martinez-Murillo, R., and Rodrigo, J. (1998). Expression of neuronal nitric oxide synthase during embryonic development of the rat cerebral cortex. *Brain Res. Dev. Brain Res.* 111, 205–222.

Seress, L., Abraham, H., Hajnal, A., Lin, H., and Totterdell, S. (2005). NOS-positive local circuit neurons are exclusively axo-dendritic cells both in the neo- and archi-cortex of the rat brain. *Brain Res.* 1056, 183–190.

Smiley, J. F., McGinnis, J. P., and Javitt, D. C. (2000). Nitric oxide synthase interneurons in the monkey cerebral cortex are subsets of the somatostatin, neuropeptide Y, and calbindin cells. *Brain Res.* 863, 205–212.

Soriano, P. (1999) Generalized lacZ expression with the ROSA26 Cre reporter strain. *Nat. Genet.* 21, 70–71.

Sousa, V. H., Miyoshi, G., Hjerling-Leffler, J., Karayannis, T., and Fishell, G. (2009). Characterization of Nkx6-2-derived neocortical interneuron lineages. *Cereb. Cortex* 19(Suppl. 1), i1–i10.

Srinivas, S., Watanabe, T., Lin, C. S., William, C. M., Tanabe, Y., Jessell, T. M., and Costantini, F. (2001). Cre reporter strains produced by targeted insertion of EYFP and ECFP into the ROSA26 locus. *BMC Dev. Biol.* 1, 4.

Szabadics, J., and Soltesz, I. (2009). Functional specificity of mossy fiber innervation of GABAergic cells in the hippocampus. *J. Neurosci.* 29, 4239–4251.

Szabo, C. (1996). Physiological and pathophysiological roles of nitric oxide in the central nervous system. *Brain Res. Bull.* 41, 131–141.

Tamamaki, N., and Tomioka, R. (2010). Long-range GABAergic connections distributed throughout the neocortex and their possible function. *Front. Neurosci.* 4:202. doi: 10.3389/fnins.2010.00202

Terada, H., Nagai, T., Okada, S., Kimura, H., and Kitahama, K. (2001). Ontogenesis of neurons immunoreactive for nitric oxide synthase in rat forebrain and midbrain. *Brain Res. Dev. Brain Res.* 128, 121–137.

Tomioka, R., Okamoto, K., Furuta, T., Fujiyama, F., Iwasato, T., Yanagawa, Y., Obata, K., Kaneko, T., and Tamamaki, N. (2005). Demonstration of long-range GABAergic connections distributed throughout the mouse neocortex. *Eur. J. Neurosci.* 21, 1587–1600.

Tricoire, L., Pelkey, K. A., Daw, M. I., Sousa, V. H., Miyoshi, G., Jeffries, B., Cauli, B., Fishell, G., and McBain, C. J. (2010). Common origins of hippocampal Ivy and nitric oxide synthase expressing neurogliaform cells. *J. Neurosci.* 30, 2165–2176.

Tricoire, L., Pelkey, K. A., Erkkila, B. E., Jeffries, B. W., Yuan, X., and McBain, C. J. (2011). A blueprint for the spatiotemporal origins of mouse hippocampal interneuron diversity. *J. Neurosci.* 31, 10948–10970.

Valtschanoff, J. G., Weinberg, R. J., Kharazia, V. N., Schmidt, H. H., Nakane, M., and Rustioni, A. (1993). Neurons in rat cerebral cortex that synthesize nitric oxide: NADPH diaphorase histochemistry, NOS immunocytochemistry, and colocalization with GABA. *Neurosci. Lett.* 157, 157–161.

Vincent, S. R. (2010). Nitric oxide neurons and neurotransmission. *Prog. Neurobiol.* 90, 246–255.

Wonders, C. P., and Anderson, S. A. (2006). The origin and specification of cortical interneurons. *Nat. Rev. Neurosci.* 7, 687–696.

Xu, Q., Cobos, I., de la Cruz, E., Rubenstein, J. L., and Anderson, S. A. (2004). Origins of cortical interneuron subtypes. *J. Neurosci.* 24, 2612–2622.

Xu, Q., Tam, M., and Anderson, S. A. (2008). Fate mapping Nkx2.1-lineage cells in the mouse telencephalon. *J. Comp. Neurol.* 506, 16–29.

Xu, X., Roby, K. D., and Callaway, E. M. (2006). Mouse cortical inhibitory neuron type that coexpresses somatostatin and calretinin. *J. Comp. Neurol.* 499, 144–160.

Yan, X. X., Jen, L. S., and Garey, L. J. (1996). NADPH-diaphorase-positive neurons in primate cerebral cortex colocalize with GABA and calcium-binding proteins. *Cereb. Cortex* 6, 524–529.

Conflict of Interest Statement: The authors declare that the research was conducted in the absence of any commercial or financial relationships that could be construed as a potential conflict of interest.

Received: 02 May 2012; paper pending published: 16 May 2012; accepted: 30 August 2012; published online: 24 September 2012.

Citation: Magno L, Oliveira MG, Mucha M, Rubin AN and Kessaris N (2012) Multiple embryonic origins of nitric oxide synthase-expressing GABAergic neurons of the neocortex. Front. Neural Circuits ***6****:65. doi: 10.3389/fncir.2012.00065*

frontiers in
NEURAL CIRCUITS

REVIEW ARTICLE
published: 05 December 2012
doi: 10.3389/fncir.2012.00082

Neuronal nitric oxide synthase expressing neurons: a journey from birth to neuronal circuits

Ludovic Tricoire*[1] *and* ***Tania Vitalis*[2]***

[1] *CNRS-UMR 7102, Laboratoire de Neurobiologie des Processus Adaptatifs, Université Pierre et Marie Curie, Paris, France*
[2] *CNRS-UMR 7637, Laboratoire de Neurobiologie, ESPCI ParisTech, Paris, France*

Edited by:
Bruno Cauli, CNRS and UPMC, France

Reviewed by:
Karri P. Lamsa, University of Oxford, UK
Bernardo Rudy, New York University School of Medicine, USA

****Correspondence:***
Tania Vitalis, CNRS-UMR 7637, Laboratoire de Neurobiologie, ESPCI ParisTech, 10 rue Vauquelin, 75005, Paris, France.
e-mail: tnvitalis@gmail.com; tania.vitalis@espci.fr

Ludovic Tricoire, CNRS-UMR 7102, Laboratoire de Neurobiologie des Processus Adaptatifs, Université Pierre et Marie Curie, 75005 Paris, France.
e-mail: ludovic.tricoire@snv.jussieu.fr

Nitric oxide (NO) is an important signaling molecule crucial for many physiological processes such as synaptic plasticity, vasomotricity, and inflammation. Neuronal nitric oxide synthase (nNOS) is the enzyme responsible for the synthesis of NO by neurons. In the juvenile and mature hippocampus and neocortex nNOS is primarily expressed by subpopulations of GABAergic interneurons. Over the past two decades, many advances have been achieved in the characterization of neocortical and hippocampal nNOS expressing neurons. In this review, we summarize past and present studies that have characterized the electrophysiological, morphological, molecular, and synaptic properties of these neurons. We also discuss recent studies that have shed light on the developmental origins and specification of GABAergic neurons with specific attention to neocortical and hippocampal nNOS expressing GABAergic neurons. Finally, we summarize the roles of NO and nNOS-expressing inhibitory neurons.

Keywords: interneurons, GABA, development, nNOS, specification, classification

INTRODUCTION

Information processing within neocortical and hippocampal circuits relies upon complex interactions between glutamatergic excitatory projection neurons and GABAergic inhibitory neurons. Coordinated cell–cell communication amongst and between these two neuronal populations is essential to maintain a delicate balance between excitatory and inhibitory signaling within the brain and is subject to dynamic regulation by many neuromodulatory substances such as various neuropeptides and nitric oxide (NO) (Krimer and Goldman-Rakic, 2001; Baraban and Tallent, 2004; Somogyi and Klausberger, 2005). Disruption of this excitatory-inhibitory balance often precipitates pathological disorders such as epilepsy, autism, and schizophrenia (McBain and Fisahn, 2001; Rubenstein and Merzenich, 2003; Levitt et al., 2004; Batista-Brito et al., 2009; Lewis et al., 2011; Marin, 2012). Understanding normal brain functions and the bases of these pathologies requires thorough characterization of telencephalic neurons and their development. For GABAergic neurons this has proven particularly difficult due to their remarkable diversity. Indeed a prerequisite in determining the circuit properties of this cell group is to first define each specific class of interneuron that populates the telencephalon. Helpful criteria for such classification were recently established by the Petilla inteneuron nomenclature group (PING). These include morphological, electrophysiological and molecular properties (Petilla Interneuron Nomenclature Group et al., 2008). Among the established subtypes of interneurons the subpopulation expressing neuronal nitric oxide synthase (nNOS) was recently shown to represent the most prevalent interneuron subpopulation in the hippocampus (Fuentealba et al., 2008). Though historically these cells had received relatively little attention a wave of recent studies have implicated interneurons expressing nNOS in important physiological processes such as the homeostatic regulation of sleep (Kilduff et al., 2011), neurovascular coupling to control neocortical blood flow (Cauli et al., 2004; Cauli and Hamel, 2010; Perrenoud et al., 2012b in this issue), and synaptic integration of adult born neurons (Overstreet and Westbrook, 2003). Moreover, these interneurons may contribute to pathological states related to dysfuntion of NO production/release as has been documented in neuronal death and epilepsy (Gholipour et al., 2010). Despite the common expression of nNOS there exists considerable heterogeneity within this cohort of interneurons yielding even further subdivision and overlap with other subpopulations defined by criteria unrelated to nNOS expression. During the past decade studies focusing on the developmental origins (place and date of birth) and genetic programs underlying fate specification have produced additional criteria that help make sense of interneuron diversity. In this review we will summarize recent advances in the characterization of neocortical and hippocampal nNOS expressing interneurons with particular emphasis on the genetic programs governing their genesis and specification. We will also briefly review the current understanding of circuit roles played by interneurons expressing nNOS in the development and plasticity of the hippocampus and neocortex.

GABAergic NEURONS EXPRESSING NEURONAL NITRIC OXIDE SYNTHASE IN THE JUVENILE OR MATURE HIPPOCAMPUS AND NEOCORTEX

Using a combination of intracellular recoding, dye filling, single cell RT-PCR, NADPH-diaphorase (NADPH-d) reactivity and immunostaining with various antibodies against calcium binding proteins, neuropeptides and nNOS, several groups have shown that nNOS GABAergic neurons can be subdivided into several hippocampal and neocortical sub-populations that are summarized in **Tables 1** and **2** and **Figure 3** (see below).

GABAergic NEURONS EXPRESSING NEURONAL NITRIC OXIDE SYNTHASE IN THE HIPPOCAMPUS

The hippocampus is subdivided in two main anatomical areas, the dentate gyrus (DG) and the cornu ammonis (CA). The CA region is classically further divided into CA1–4. In this section of the review, we will mainly focus on results obtained in CA1 where interneuron diversity has been best characterized but will detail other areas when data are available. As in the neocortex, nNOS expressing neurons comprise primarily inhibitory GABAergic neurons although nNOS immunoreactivity is also found in CA1 pyramidal cells. In these glutamatergic excitatory cells staining intensity in mature brain is much weaker than in interneurons and nNOS is observed preferentially in dendritic spines (Burette et al., 2002). Hippocampal nNOS expressing interneurons differ from their neocortical homologs in that they are much more abundant and the level of nNOS expression is more homogenous (Jinno and Kosaka, 2002). Indeed, while neocortical nNOS$^+$ interneurons may be subdivided based on intensity of nNOS immunoreactivity (see next section), no such distinction exists in the hippocampus. Furthermore, a recent study revealed that interneurons expressing nNOS comprise the most abundant interneuron subpopulation in the hippocampus, in contrast to neocortical observations where parvalbumin (PV) expressing interneurons are considered to be the most abundant interneuron subtypes (Fuentealba et al., 2008). Like in the neocortex, nNOS expressing interneurons are found in all hippocampal layers of CA and in the DG. One study in the mouse has shown that the density of nNOS interneurons is higher in the septal/dorsal part compared to the temporal/ventral part of the hippocampus (Jinno and Kosaka, 2002).

In rats and mice, at least five interneuron subpopulations have been described to express nNOS: (1) the neurogliaform cells (NGFC), (2) Ivy cells (IvC), (3) interneurons co-expressing the vasoactive intestinal peptide (VIP) and calretinin (CR), (4) interneurons expressing PV and (5) projection cells. This latter subtype of nNOS$^+$ cells has been shown to accumulate close to the subiculum (Freund and Buzsáki, 1996). The subpopulation coexpressing nNOS and PV principally resides in the DG (Dun et al., 1994; Jinno and Kosaka, 2002, 2004). However species differences between rat and mouse have been noted as co-expression of nNOS and PV in rat DG is much lower than in mouse (Dun et al., 1994 for rat; Jinno and Kosaka, 2002 for mouse). Additionally, a subset of somatostatin (SOM) expressing interneurons in CA1, CA3, and DG areas has been shown to express nNOS (Jinno and Kosaka, 2004). Similar to the case with PV, species differences have been encountered with nNOS/SOM coexpression being higher in rat than mouse (Dun et al., 1994 for rat; Jinno and Kosaka, 2004 for mouse). Examples of the morphology and firings of three of these cell groups are provided in **Figure 1**.

NEUROGLIAFORM AND IVY CELLS

Hippocampal NGFCs derive their name from their neocortical homologs with which they share common morphological features. NGFC bodies are typically found in stratum lacunosum moleculare (slm) and its border with s. radiatum (sr) of CA1-3, as well as within s. moleculare of the DG (Vida et al., 1998; Price et al., 2005, 2008; Elfant et al., 2008; Karayannis et al., 2010; Szabadics et al., 2010; Armstrong et al., 2011; Krook-Magnuson

Table 1 | Characteristics of rodent hippocampal GABAergic neurons expressing neuronal nitric oxide synthase.

Markers	Morphology location	Axonal targeting on pyramidal neurons	Firing pattern*	Transcription factors or lineage markers	Place of genesis[£]
nNOS$^+$/NPY$^+$ (IVCs)	Multipolar[1,2,3] s.r.; s.p.; s.o.	Dendrite[1,2,3]	Late spiking[3] Non-adapting	Nkx2.1/Lhx6[3,4]	MGE[3,4,5] AEP/POA?
nNOS$^+$/NPY$^+$ (NGFCs)	Multipolar[3,6,7] neurogliaform s.l.m./s.r. bd s.l.m./s.m. bd	Dentritic shaft[6,7] Blood vessels	Late spiking[3,5,6] Non-adapting	Nkx2.1/Lhx6[3,4] CoupTFII	MGE[3,4,5] AEP/POA ?
nNOS$^+$/VIP$^+$/CR$^+$	Bipolar[8] s.p.	SOM$^+$ neurons[8] of the s.o.	Non-LS[3]	CoupTFII[4] 5-HT$^4_{3A}$	CGE[3,4] LGE ? AEP/POA ?
nNOS$^+$/PV$^+$	Basket? DG specific	Granule cell layer?	Fast spiking?	Nkx2.1?	MGE?

**Firing pattern elicited from intracellular injections of depolarizing currents. [£]AEP, entopeduncular area; CGE, caudal ganglionic eminence; LGE, lateral ganglionic eminence; MGE, medial ganglionic eminence; POA, preoptic area; s.l.m.; stratum lacunosum molecular; s.m.; startum molecular; s.o.; stratum oriens; s.p.; stratum pyramidale; s.r.; stratum radiatum.*

[1]Fuentealba et al., 2008, [2]Somogyi et al., 2012, [3]Tricoire et al., 2010, [4]Tricoire et al., 2011, [5]Jaglin et al., 2012, [6]Price et al., 2005, [7]Zsiros and Maccaferri, 2005, [8]Freund and Buzsáki, 1996.

Table 2 | Characteristics of rodent neocortical GABAergic neurons expressing neuronal nitric oxide synthase.

Markers	% cells within nNOS-type II	Morphology	Axonal targeting	Firing pattern*	Transcription factors or lineage markers	Place of genesis
Highly nNOS$^+$SOM$^+$/NPY$^{+3,4,5,6,7,8}$ (nNOS-type I)		Long projection[1,2]	Blood vessels[1,2] Neurons[1,2]	Late spiking[3,8] Adapting[3,8]	Nkx2.1/Lhx6[3,4,5]	MGE[3,4,5]
Lightly nNOS$^+$ NPY$^{+3,5,6,8,9}$ (nNOS-type II)	55	Neurogliaform[3,6]	Blood vessels ? Dentritic shaft	Adapting[3,8]	Nkx2.1/Lhx6[3,4] 5-HT$_{3A}$[3,4,6]	MGE[3,4] CGE/AEP[3,4]
Lightly nNOS$^+$ PV$^+$ or SOM$^{+3,5,6,8,10}$ (nNOS-type II)	35	Multipolar[3]	Blood vessels ? Proximal dendrites Soma Axonal initial segment	Fast spiking[3]	Nkx2.1/Lhx6[3,4]	MGE[3,4]
Lightly nNOS VIP$^+$/CR$^{+3,5,6,8}$ (nNOS-type II)	10	Bipolar[3,6] Double-bouquet[3,6]	Blood vessels ? Soma	Adapting[3]	5-HT$_{3A}$[3,4,6]	AEP/PO? [3] CGE[3,4] SVZ/Ctx?

**Firing pattern elicited from intracellular injections of depolarizing currents: AEP, entopeduncular area; CGE, caudal ganglionic eminence; Ctx, cortex; LGE, lateral ganglionic eminence; MGE, medial ganglionic eminence; POA, preoptic area; SVZ, subventricular zone.*

[1] Tomioka et al., 2005, [2] Higo et al., 2009, [3] Perrenoud et al., 2012a, [4] Magno et al., 2012, [5] Jaglin et al., 2012, [6] Perrenoud et al., 2012b, [7] Kubota et al., 2011, [8] Karagiannis et al., 2009, [9] Oláh et al., 2009, [10] Vruwink et al., 2001.

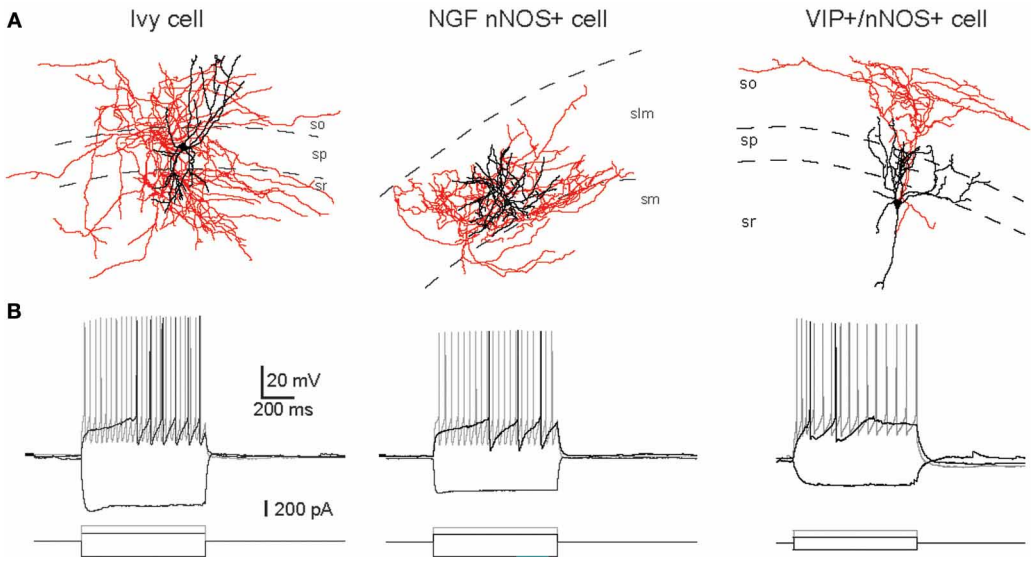

FIGURE 1 | Examples of IvC, NGFC, and VIP$^+$/nNOS$^+$ interneurons. **(A)** Neurolucida reconstructions of biocytin-filled cells (black, dendrite; red, axon). **(B)** Voltage responses of cells shown in **(A)** to three current step injections (-200 pA, just suprathreshold, and twice the current for just suprathreshold). Adapted from Tricoire et al. (2010).

et al., 2011; Markwardt et al., 2011). Their soma is relatively small in comparison with those of other interneuron subtypes such as somatostatin$^+$ (SOM$^+$) and PV$^+$ interneurons. NGFCs exhibit a multipolar dendritic network with a high degree of ramification close to the soma without any privileged orientation. The axonal arborization is extremely dense with extensive ramification within the local network and usually radiates beyond the spatial boundaries of the dendritic field (Price et al., 2005; Tricoire et al., 2010). In addition, both fields are restricted to slm and typically penetrate very little into the sr. However, several studies reported that the axons of CA1 NGFCs may penetrate s. moleculare of the DG (Price et al., 2005; Fuentealba et al., 2010;

Tricoire et al., 2010). Similarly axons of DG NGFCs can cross the hippocampal fissure and penetrate into slm of nearby CA1 and subiculum (Armstrong et al., 2011).

Closely related to NGFCs, are the recently described hippocampal IvCs (Fuentealba et al., 2008, 2010; Tricoire et al., 2010, 2011; Krook-Magnuson et al., 2011) and the existence of an equivalent interneuron subpopulation in the neocortex is a matter of debate. These cells were first reported by Peter Somogyi's group and named for the English Ivy-like appearance of their axons which profusely branch close to their origin providing dense thin branches with numerous small varicosities (Fuentealba et al., 2008; Somogyi et al., 2012 in this issue). In contrast to NGFCs, the cell bodies and processes of IvCs are found in s. oriens, s. pyramidale and sr without infiltrating slm (Fuentealba et al., 2008; Tricoire et al., 2010). However, recent results indicate that IvCs whose soma is located in sr regularly send axons and dendrites to some extent in slm. (Somogyi et al., 2012 in this special issue and Szabo et al., 2012).

From a molecular point of view, NGFCs and IvCs express several common markers/receptors resulting in convergent neurochemical profiles for these two nNOS$^+$ interneurons subtypes. The neuropeptide Y (NPY) has been found to colocalize with nNOS in both NGFCs and IvCs (Fuentealba et al., 2008; Tricoire et al., 2010; Somogyi et al., 2012 in this issue). However, NPY is not specific to nNOS$^+$ interneurons as it is also frequently coexpressed with SOM and PV in yet other distinct interneuron subpopulations (Klausberger and Somogyi, 2008). Whereas IvC and NGFC subpopulations of CA constitute a distinct population from PV and SOM expressing subpopulation, nNOS and PV often colocalize in the DG. The alpha1 GABAA receptor subunit is also frequently encountered in IvCs and nNOS$^+$ NGFCs (Fuentealba et al., 2008; Tricoire et al., 2010) but, like NPY, it cannot be considered as a specific marker of IvCs or NGFCs as it is also expressed in other interneuron subtypes (Baude et al., 2007). More recently, the delta GABAA receptor subunit that underlies tonic inhibition was demonstrated to preferentially localize to NGFC/IvC interneurons (Oláh et al., 2009). However this subunit is not specific of interneurons and is also found in excitatory granule cells in DG (Wei et al., 2003). IvCs and NGFCs are inhibited by mu opioid agonists, such as DAMGO, consistent with the expression of mu opioid receptors (MORs) on both interneuron subpopulations (Krook-Magnuson et al., 2011). Interestingly, MORs are also found in PV$^+$ interneurons in CA1. This expression pattern is distinct from that observed in neocortex where MORs are found on interneurons co-expressing VIP and cholecystokinin (CCK) (Férézou et al., 2007). The microtubule associated protein alpha actinin 2 has been shown to be selective for NGFCs and IvCs in rat hippocampus (Price et al., 2005; Fuentealba et al., 2008). It is not clear if it is also the case in mouse hippocampus. In rat, the chicken ovalbumin upstream promoter transcription factor II (CoupTFII) is frequently observed in both IvCs and NGFCs (Fuentealba et al., 2010), whereas in mouse it is rarely found in IvCs despite frequent expression in NGFCs (Tricoire et al., 2010). So far reelin appears to be the only marker that is differentially expressed between IvCs and NGFCs although this marker is also commonly found in SOM$^+$ interneurons (Alcántara et al., 1999). Indeed, reelin has been detected in NGFCs but not in IvCs (Fuentealba et al., 2010; Somogyi et al., 2012 in this issue).

In CA1, IvCs receive their main excitatory inputs from CA1 and CA3 pyramidal cells (Fuentealba et al., 2008; Somogyi et al., 2012 in this issue) while NGFCs receive excitatory inputs from the entorhinal cortex via the temporo-ammonic pathway and from CA3 via the Schaffer collateral pathway (Price et al., 2005). Both cell subpopulations inhibit down-stream targets via GABAA receptors. However, in addition, NGFCs generate long lasting postsynaptic inhibitory currents through the activation of GABAB receptors on their postsynaptic targets (Price et al., 2005, 2008). Interestingly, NGFCs are highly interconnected via both electrical and chemical synapses (Price et al., 2005; Zsiros and Maccaferri, 2005). In contrast, IvCs have thus far only been found to signal via chemical synapses on postsynaptic cells (Fuentealba et al., 2008). In terms of neuronal activity, IvCs and NGFCs exhibit very similar electrophysiological properties regarding their passive membrane and firing properties (Tricoire et al., 2010). For example, they all show a late spiking phenotype, i.e., a delay to generate action potentials when challenged by just suprathreshold current injection (Price et al., 2005; Zsiros and Maccaferri, 2005; Tricoire et al., 2010). None of these cell types exhibit adaptation of firing frequency at threshold stimulation. However, upon stronger stimulation, they all switch to an adaptive spiking profile (Tricoire et al., 2010). Nonetheless, *in vivo* recordings in anesthetized rats revealed that IvCs and NGFCs exhibit different firing characteristics during rhythmic hippocampal activities. NGFCs fire at the peak of theta oscillations detected extracellularly in s. pyramidale, whereas IvCs fire at the trough of these oscillations (Fuentealba et al., 2010; Lapray et al., 2012).

VIP$^+$/CR$^+$/nNOS$^+$ INTERNEURONS IN CA1-3

The third interneuron subpopulation expressing nNOS consists of a subset of VIP$^+$/CR$^+$ interneurons (Jinno and Kosaka, 2002; Tricoire et al., 2010). This population is specialized to innervate other GABAergic cells exclusively. To date, three types of interneuron-specific (IS) interneurons have been described on the basis of their anatomical and neurochemical features (Acsády et al., 1996a,b; Gulyás et al., 1996). Among them, nNOS has been found in the IS-3 subset (Tricoire et al., 2010). These cells have somas located in stratum pyramidale (s.p.) or in stratum radiatum (s.r.) close to the pyramidal layer, dendritic fields that are vertically oriented, and a primary axon descending to emit several horizontally oriented branches at the s.o.-alveus border. Consistent with their axonal morphology, they constitute a major local source of inhibition to SOM$^+$ O–LM cells (Acsády et al., 1996a,b; Gulyás et al., 1996; Chamberland et al., 2010). Electrophysiologically, they exhibit an irregular firing pattern when depolarized with current injection which differs from the late spiking and more regular firing profile of IvC/NGFC (Tricoire et al., 2010). The position of these neurons in the hippocampal network in terms of input is still to be determined.

PV$^+$/nNOS$^+$ INTERNEURONS IN DG

The expression pattern of nNOS in the DG differs from that observed in CA areas. Indeed, nNOS is found in about 20% of PV$^+$ interneurons (Jinno and Kosaka, 2002) whereas there was

no overlap between nNOS and PV expression in CA areas. While PV^+ interneurons in DG are well characterized in terms of morphology and neurophysiology (Bartos et al., 2007), so far no study has examined if $nNOS^+/PV^+$ cells represent a specific interneuron subpopulation compared to other DG PV^+ interneurons. Briefly, PV^+ interneurons exhibit a fast spiking firing profile, which means that they are able to generate a train of action potentials at high frequency and little to no accommodation when injected with depolarizing current. Action potentials in these neurons are much shorter in duration that those in IvC/NGF (Tricoire et al., 2011) and their axons preferentially target the perisomatic region of granule cells making them ideally suited to rapidly regulate DG output.

GABAergic NEURONS EXPRESSING NEURONAL NITRIC OXIDE SYNTHASE IN THE NEOCORTEX

In the cerebral cortex, nNOS GABAergic neurons comprise an average of 20% of the neocortical GABAergic population (Kubota et al., 1994; Gonchar and Burkhalter, 1997; Magno et al., 2012 and Perrenoud et al., 2012a in this issue). Classically, two types of GABAergic $nNOS^+$ neurons have been distinguished at the histochemical level (**Figure 2**). The first one corresponds to the subpopulation of GABAergic neurons expressing high levels of nNOS and NADPH-d activity, the so called "nNOS-type I" that display fast-spiking and adapting properties. They account for 0.5–2% of the neocortical GABAergic population (Kubota et al., 1994; Gonchar and Burkhalter, 1997; Magno et al., 2012 and Perrenoud et al., 2012a in this issue). In these neurons nNOS is associated with SOM and NPY expression and immunoreactivity as well as with the substance P receptor NK1 (Kubota et al., 2011). Further, it was recently shown that these neurons are depolarized by substance P application (Dittrich et al., 2012 in this issue). They mainly correspond to projection neurons that are sparsely distributed in all neocortical layers but preferentially located in lower layer VI (Perrenoud et al., 2012a in this issue; Magno et al., 2012 in this issue) and to a lesser extent in superficial layers. Using NADPH-d activity these GABAergic neurons were recently shown to send long (>1.5 mm in the mouse) thick axonal fascicles running between the gray and white matter in cat and mouse neocortex invading both the corpus callosum and the fimbria (Tomioka et al., 2005; Higo et al., 2009). Their projections innervate both GABAergic neurons and pyramidal neurons and they are suspected to interconnect the two controlateral hemispheres as well as the archi- and paleo-cortex. Interestingly, nNOS-type I cells were recently shown to be selectively activated during sleep as they showed c-Fos accumulation during sleep recovery following sleep deprivation (Gerashchenko et al., 2008). Kilduff et al. proposed that nNOS-type I GABAergic neurons could synchronize EEG activity across neocortical regions (detailed in the last chapter; Kilduff et al., 2011).

The second classically defined subpopulation of neocortical nNOS expressing GABAergic neurons exhibits weak nNOS soma staining and low NADPH-d activity. This group corresponds to "nNOS-type II" cells that were initially reported in the primate (Yan et al., 1996; Smiley et al., 2000) but have more recently been described in rodents (Cho et al., 2010; Kubota et al., 2011). In rodents nNOS-type II GABAergic neurons comprise an average of 17% of the neocortical GABAergic population (Kubota et al., 2011; Magno et al., 2012 and Perrenoud et al., 2012a in this issue) and have often been underestimated due to the difficulty of their visualization. These cells mainly concentrate into the superficial layers II–III and in deep layers V–VI. Although poorly described "nNOS-type II" cells appear to form a heterogeneous cell population regarding the neuronal markers they co-express and the few electrophysiological properties that have been reported. Indeed, a fraction of "nNOS-type II" cells was reported to express SOM and another PV (Kubota et al., 2011; Vruwink et al., 2001) with both of these distinct subsets emerging clearly in the cluster analysis (Karagiannis et al., 2009). Another subpopulation of nNOS-type II neurons comprises the group of adapting neurogliaform interneurons that mediates slow GABAergic inhibition of pyramidal cells and interneurons (Karagiannis et al., 2009; Oláh et al., 2009). Indeed, in their classification of NPY^+ interneurons Karragiannis and colleagues revealed that a fraction of interneurons expressing NPY^+, but not PV, SOM, or VIP, and displaying adapting firing properties with neurogliaform

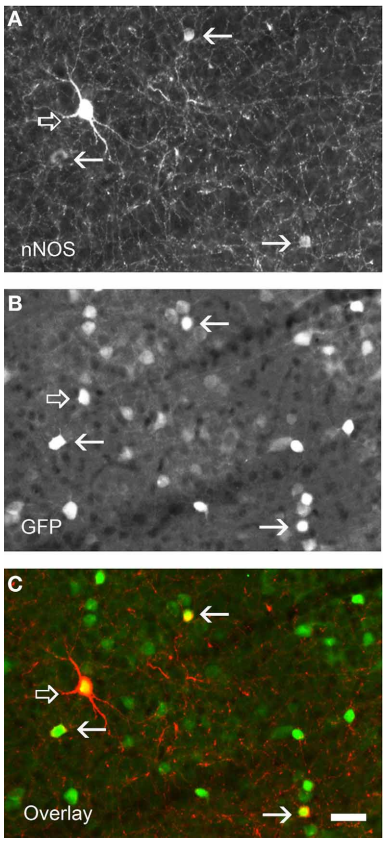

FIGURE 2 | Immunolabeling for nNOS in a neocortical sections of GAD67:GFP mouse strain showing the two nNOS populations. **(A)** Fluorescence picture showing immunohistochemical expression of nNOS. **(B)** Expression pattern of GFP. **(C)** Overlay of **(A)** and **(B)**. nNOS-type I neurons display strong immunolabeling (open arrows) and a large soma whereas nNOS-type II (arrows) are weakly stained and display smaller soma. Note that all nNOS-positive neurons are GABAergic. Scale bar: 30 μm. Unpublished caption obtained from preparations used for the study presented by Perrenoud et al. (2012a).

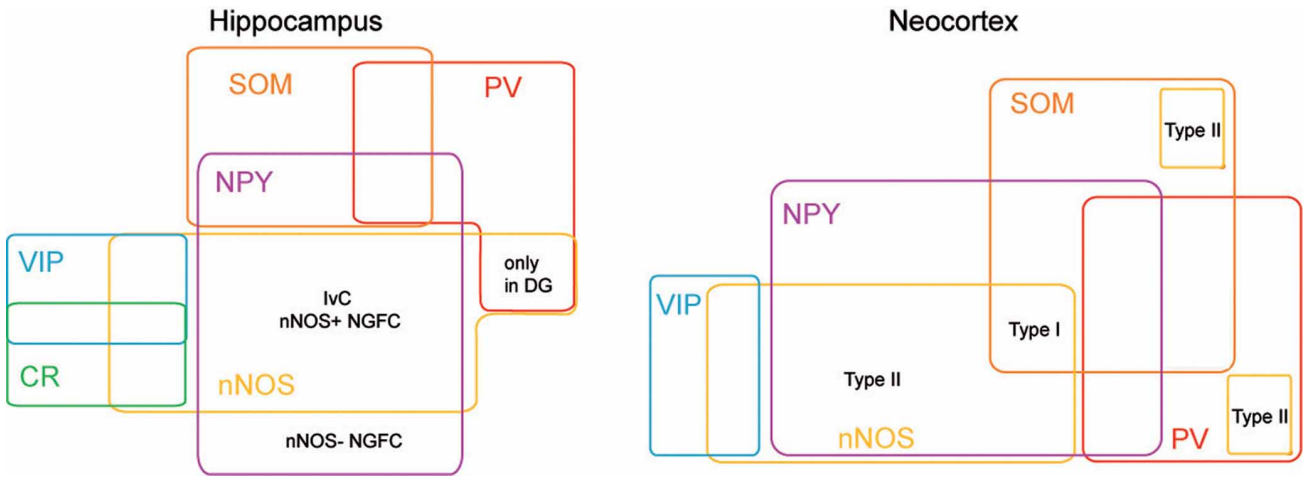

FIGURE 3 | nNOS expressing interneurons in cortex and hippocampus. Scheme summarizing the molecular profiles of neocortical and hippocampal nNOS$^+$ interneurons. This diagram is based on previous report (Tricoire et al., 2010, 2011) and on Perrenoud et al. (2012a in this issue).

morphologies could be further subdivided into two groups one expressing NPY "only" and another that accounts for 50% of the neurogliaform cluster in which NPY is co-expressed with nNOS (Karagiannis et al., 2009). In addition this cluster also included neurons expressing nNOS only but sharing electrophysiological and morphological similarities with adapting NPY interneurons.

More recently, Perrenoud et al performed a multiparametric analysis of "nNOS-type I" and "nNOS-type II" cells that intended to clarify nNOS expressing cell classification schemes and shed light on the physiological relevance of the different subgroups (Perrenoud et al., 2012a in this issue). This multiparametric analysis used an unsupervised classification of nNOS expressing GABAergic neurons and demonstrated clear segregation of nNOS cells into four clusters. One group contained GABAergic nNOS neurons co-expressing SOM and NPY that might correspond to the well-described population of nNOS-type I interneurons (Karagiannis et al., 2009; Kubota et al., 2011). Electrophysiologically these cells displayed adapting discharges fired long duration spikes followed by fast AHPs and had significantly slower membrane time constants than other interneurons. The three other clusters presumably corresponded to subpopulations of nNOS-type II interneurons. One cluster consisted of a population of interneurons co-expressing nNOS and CR and/or VIP that was to our knowledge not reported before. They were characterized by high input resistances, low firing threshold, adapting discharges to threshold and saturating current injections and they fired at significantly lower maximal frequencies than other neurons. A second cluster included a population of interneurons coexpressing nNOS and NPY with the exclusion of other classical markers (except CCK) that might correspond to neurogliaform interneurons. On an electrophysiological basis these NPY$^+$/nNOS$^+$ neurons were characterized by medium range input resistances. They displayed action potential discharges that were accelerating at threshold, adapting at saturation and a significantly larger accommodation of spike amplitude than in other clusters. In addition, these GABAergic neurons displayed long duration spikes followed by significantly slower AHPs than observed in other neurons. The third cluster included nNOS$^+$ interneurons expressing PV or SOM that are mainly located in the infragranular layers. These neurons displayed several unique electrophysiological characteristics. They had depolarized membrane potentials and short time constants. Moreover, these cells showed little or no adaptation at threshold, fired at significantly higher maximal rates, and displayed significantly faster spike and AHP dynamics than other neurons.

DEVELOPMENT OF TELENCEPHALIC INTERNEURONS

In rodents numerous studies have demonstrated that telencephalic interneurons mainly derive from subpallial territories (**Figure 4**). Pioneering *in vitro* studies and phenotypical descriptions of mutant mice lacking germinal zones that showed reduced interneuron numbers in the neocortex and hippocampus suggested that telencephalic interneurons expressing SOM and PV originate from the medial ganglionic eminence (MGE) and/or the preoptic area (POA) (Lavdas et al., 1999; Sussel et al., 1999; Wichterle et al., 1999; Pleasure et al., 2000; Wonders and Anderson, 2006; Batista-Brito and Fishell, 2009; Vitalis and Rossier, 2011). Indeed, in mice deficient for Nkx2.1, a transcription factor expressed in MGE and POA, the MGE appears to undergo a respecification into an LGE-like region and SOM and PV interneurons are dramatically reduced in the cortex and hippocampus. (Sussel et al., 1999; Pleasure et al., 2000; **Figure 5**). More recently, it was demonstrated that Nkx2.1 was necessary for the expression of Lhx6, a Lim homeobox transcription factor that is specifically expressed in the MGE and needed for the specification of MGE-derived interneurons (Liodis et al., 2007; Du et al., 2008). Grafting experiments and the use of transgenic mice often in association with "Cre-Lox strategy"

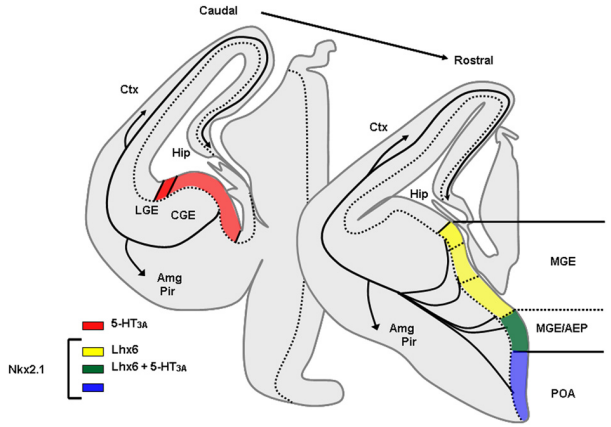

FIGURE 4 | Origins of GABAergic neurons populating the cerebral cortex and hippocampus at embryonic stages. Transversal schematic sections of E13–E14 embryonic mouse brain showing regions relevant to origin/birth of cortical interneurons. Territories expressing specific transcription factors or molecules classically used to determine the place of genesis of specific interneurons subpopulation are drawn. AEP, entopeduncular region, Amg, amygdala, CGE, caudal ganglionic eminence; Ctx, cortex; Hip, hippocampus; LGE, lateral ganglionic eminence; MGE, medial ganglionic eminence; Pir, piriform cortex; POA, preoptic area.

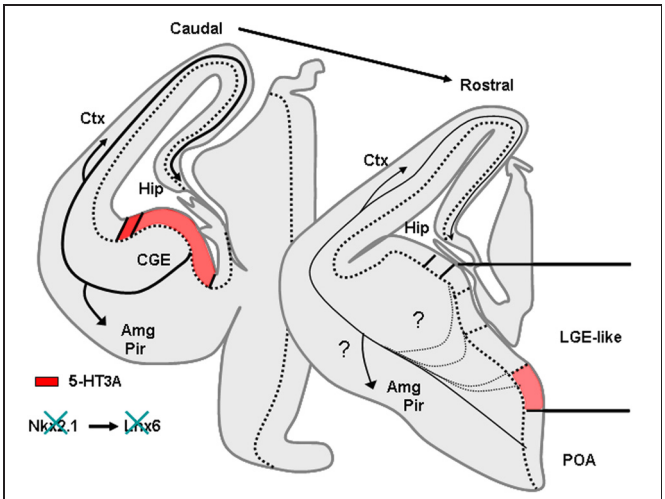

FIGURE 5 | Phenotype of mice lacking Nkx2.1. Nkx2.1 knockout mice show a MGE respecified into a "LGE-like" territory. Since Nkx2.1 is necessary for Lhx6 expression, Lhx6 is not observed in these animals that lack most PV and SOM expressing neurons in the cortex and hippocampus. AEP, entopeduncular region, Amg, amygdala, CGE, caudal ganglionic eminence; Ctx, cortex; Hip, hippocampus; LGE, lateral ganglionic eminence; MGE, medial ganglionic eminence; Pir, piriform cortex; POA, preoptic area.

have refined these analyses and confirmed that in the cerebral cortex fast spiking PV interneurons (Xu et al., 2004; Butt et al., 2005, 2007; Wonders et al., 2008) originate preferentially from the ventral part of the MGE (MGEv). By contrast, similar studies revealed that neocortical bursting and adapting SOM interneurons arise preferentially from the dorsal part of the MGE (MGEd) (Butt et al., 2005; Miyoshi et al., 2007). In the cerebral cortex, Martinotti cells co-expressing SOM and CR were further shown to be derived from the most dorsal MGE territory (LGE4 as named in Flames et al., 2007) that expresses the transcription factor Nkx6.2 (Fogarty et al., 2007). While initial *in vitro* experiments revealed that the CGE produces mainly CR expressing interneurons (Xu et al., 2004), more recent studies have demonstrated a much larger contribution of this region in generating telencephalic interneuron diversity (Butt et al., 2005; Fogarty et al., 2007; Miyoshi et al., 2007; Lee et al., 2010; Vucurovic et al., 2010). Indeed, together these studies showed that telencephalic (hippocampal and neocortical) interneurons expressing VIP, CR, and a subpopulation of neocortical neurogliaform interneurons expressing NPY (Lee et al., 2010; Tricoire et al., 2010, 2011; Vucurovic et al., 2010) are all CGE-derived. Interneurons arising from CGE pogenitors all appear to express the 5-HT receptor type 3A (5-HT_{3A}) (Lee et al., 2010; Vucurovic et al., 2010) and the transcription factor Gsh2 (Fogarty et al., 2007) while lacking Nkx2.1, Nkx6.2, and Lhx6 (Flames et al., 2007). However, it should be noted that the entopeduncular region (AEP), also defined as the more ventral extension of the MGE (Flames et al., 2007) co-expresses 5-HT_{3A}, NKx2.1, and Lhx6. Homochronic grafting of the AEP has revealed that this region does not appear to contribute importantly to the genesis of neocortical neurons expressing 5-HT_{3A}. By contrast, these experiments have shown that the AEP generates subpopulations of 5-HT^{+}_{3A} hippocampal interneurons (Vucurovic et al., 2010; Jaglin et al., 2012).

Besides contributions from the MGE, CGE, and AEP other regions have been implicated in the genesis of neocortical and hippocampal interneurons such as the preoptic regions and the neocortex. Recently, homochronic graftings of dorsal preoptic territories (POA1) have revealed that Nkx5.1^{+} progenitors generate neocortical interneurons expressing NPY^{+} with the exclusion of other markers classically used to discriminate interneurons populations (Gelman et al., 2009). The anatomical features and firing patterns of these neurons in the neocortex suggested they represent an additional subset of neurogliaform interneurons (Gelman et al., 2009). Further, Gelman et al have shown that the Dbx1-derived progenitors arising from the ventral POA (POA2) contribute to the genesis of various interneurons including fast spiking PV^{+}, SOM^{+}, multipolar late spiking NOS^{+}, neurogliaform, and bituftued/bipolar irregular spiking VIP/CR interneurons that mainly populate deep neocortical layers and hippocampal subfield (Gelman et al., 2011).

Together these studies have successfully correlated the place of genesis and the contribution of specific transcription factors or molecular markers with a preferential interneuron phenotype and location. Specific guidance molecules are preferentially expressed in different subterritories and participate to the targeting of specific interneuron subpopulations. Recent studies suggest that motility and guidance of interneurons depend on several molecular cues that are already differentially expressed in ganglionic eminences and neocortical compartments (Powell et al., 2001; Polleux et al., 2002; Pozas and Ibanez, 2005; Kanatani et al., 2008; López-Bendito et al., 2008). However, other mechanisms have been shown to participate in the correct positioning of specific classes of interneurons. Indeed, the selective cell death of specific

interneurons during early postnatal development may contribute to remove those that are abnormally positioned or not appropriately integrated in neocortical circuits (De Marco García et al., 2011). For instance it has recently been shown that reelin$^+$ and CR$^+$, but not VIP$^+$, interneurons depend on neocortical activity for their correct migration and positioning (De Marco García et al., 2011).

In addition to the embryonic genesis of neocortical interneurons recent studies have also shown that during the three first postnatal weeks the neocortex produces CR-positive interneurons (Cameron and Dayer, 2008; Inta et al., 2008; Riccio et al., 2012). Such postnatally generated populations may participate in distinct physiological processes including the appropriate targeting of callosal projections.

ORIGIN OF INTERNEURONS EXPRESSING nNOS

ORIGIN OF HIPPOCAMPAL INTERNEURONS EXPRESSING nNOS

As mentioned above, hippocampal nNOS$^+$ interneurons differ from their neocortical homologs in terms of neuronal diversity and distribution among hippocampal subfields and layers. Therefore specific studies have addressed their embryonic origin using lineage analysis, conditional fate-mapping, and loss of function (Fogarty et al., 2007; Tricoire et al., 2010, 2011; **Figure 6**). Using an Nkx2.1-Cre driver line in combination with different Cre-dependant GFP reporter lines, it has been shown that IvCs and nNOS$^+$/NGFCs derive essentially from the MGE. This was also supported by the expression of Lhx6 in these subpopulations (Tricoire et al., 2011; **Figure 6**). Accordingly, when a CGE preferred tamoxifen dependant driver line was used (Mash1-CreER, Miyoshi et al., 2010), very few fate-mapped neurons expressed nNOS (Tricoire et al., 2010). These few nNOS expressing CGE-derived neurons typically exhibited morphologies and distributions consistent with VIP$^+$/CR$^+$ interneurons rather than IvCs and NGFCs. Moreover, conditional loss of Nkx2.1 function (constitutive knock out die at birth) caused an almost complete loss of nNOS$^+$ GABAergic neurons in the hippocampus except for few bipolar interneurons in s.p. reminiscent of the VIP$^+$/CR$^+$ interneurons revealed in the CGE reporter (Tricoire et al., 2010; **Figures 6A,B**). In parallel, analysis of a GAD65-GFP transgenic line that labels a subset of CGE-derived interneurons (López-Bendito et al., 2004) further confirmed that some VIP$^+$ interneurons also express nNOS. Their electrophysiological and morphological properties were different from those of IvCs and NGFCs but were reminiscent of the IS-3 cell type that inhibits a subset of SOM$^+$ interneurons located in stratum oriens (s.o.) that project in turn to the stratum lacunosum molecular (Freund and Buzsáki, 1996; Chamberland et al., 2010).

Surprisingly, the lineage analysis also revealed that classically defined NGFCs can be subdivided into two groups with nNOS$^+$/NGFCs being derived from the MGE and nNOS-/NGFCs arising from CGE progenitors (Tricoire et al., 2010, 2011). This contrasts with findings in the neocortex where the CGE is the dominant source of NGFCs (Butt et al., 2005; Miyoshi et al., 2007, 2010) and of nNOS-type II interneurons (Perrenoud et al., 2012a in this issue). The surprising lack of nNOS in the CGE-derived subset of NGFCs may partially explain the reduced levels of nNOS in the neocortex compared to the hippocampus (Yan and Garey, 1997; Lee and Jeon, 2005). The striking difference between hippocampal and neocortical NGFCs suggests that interneuron precursors could be fated early during embryogenesis to reside in either the hippocampus or neocortex, perhaps reflecting differential sensitivities to specific sorting factors like chemokines (Li et al., 2008; López-Bendito et al., 2008) that promote migration of nNOS$^+$/NGFC and IvC precursors into the hippocampus. Alternatively, these cells may adopt a different fate depending on whether they integrate into the hippocampus or neocortex due to differential expression of morphogenic molecules within these local environments.

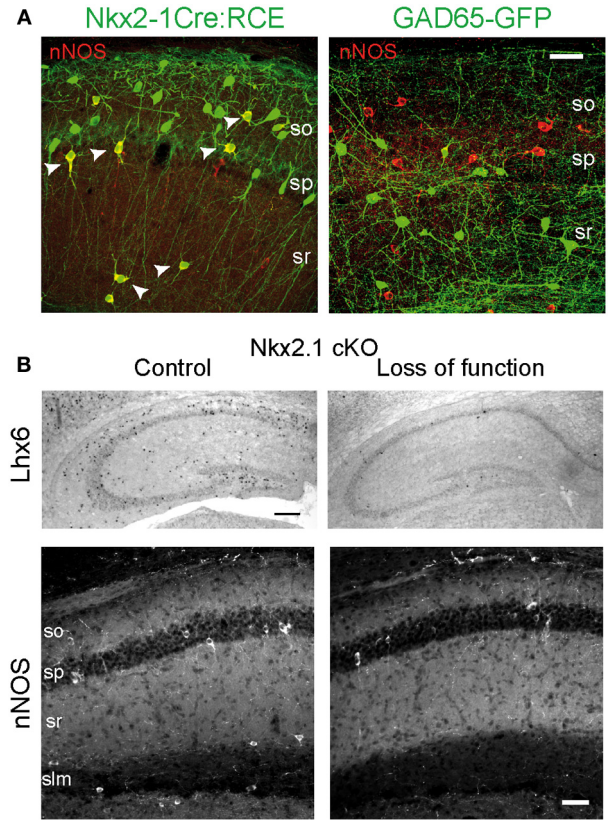

FIGURE 6 | Embryonic origin of nNOS$^+$ hippocampal interneurons. **(A)** Images illustrating the coexpression of GFP and nNOS in the Nkx2.1Cre:RCE (left) and GAD65-GFP (right) mouse lines. Scale bar: 25 μm. **(B)** Nkx2.1 is necessary for the specification of nNOS$^+$ interneurons. Top, *In situ* hybridization against Lhx6 transcripts on hippocampus of control (left) and mutant (right) P15 mice after conditional loss of Nkx2.1 function at E10.5. Scale bar: 200 μm. Bottom, Immunohistochemical expression patterns of nNOS in CA1 of control and mutant mice. Scale bar: 50 μm. Adapted from Tricoire et al. (2010, 2011).

ORIGIN OF NEOCORTICAL INTERNEURONS EXPRESSING nNOS

Investigations into the developmental origins of neocortical GABAergic neurons expressing nNOS are only in their infancy due to the fact that this population in the juvenile brain is largely heterogeneous and thus poorly defined. This is especially true for nNOS-type II interneurons that display low NADPH-d activity and nNOS-immunoreactivity making them difficult to identify

histologically. The study presented by Perrenoud et al. in this special issue is to our knowledge the first study to specifically characterize neocortical interneurons expressing nNOS using a multiparametric approach and to elucidate their developmental origins (see **Table 1**). The first group identified is homologous to previously described nNOS-type I cells being relatively homogeneous comprised of $nNOS^+$ GABAergic cells that coexpress SOM and display fast-spiking properties (Perrenoud et al., 2012a in this issue; see above). These properties clearly suggest that they belong to a subgroup of well-defined SOM^+ interneurons that were previously shown to derive from the MGE. Indeed, Perrenoud et al. demonstrate that all members of this subgroup express Lhx6 in agreement with two recent studies—presented in this issue—that have used various transgenic mouse lines to clarify the origin of nNOS expressing interneurons (Jaglin et al., 2012; Magno et al., 2012). Interestingly, it was recently shown that the specification of a large fraction of nNOS-type I neurons required the Lhx6-mediated activation of Sox6 for proper specification (Batista-Brito et al., 2009; Jaglin et al., 2012). Indeed, deletion of Sox6 in Lhx6 expressing cells suppressed SOM expression in nNOS-type-I neurons and altered their morphology by decreasing process complexity (Jaglin et al., 2012). In contrast to this first cluster, nNOS-type II cells displayed considerable heterogeneity segregating into three clusters with embryonic origins in both the MGE and the CGE/AEP territories. Indeed, not all nNOS-type II cells express Lhx6 (Jaglin et al., 2012 in this issue; Perrenoud et al., 2012a). A subpopulation of nNOS-type II cells express 5-HT_{3A}, a CGE/AEP marker, and colocalization between nNOS, 5-HT_{3A}, and VIP was observed (average 10% of the 5-HT_{3A} population; Perrenoud et al., 2012a,b in this issue). These cells are mainly localized in the superficial layers where they may participate in neuro-vascular coupling. Another group of cells expressing nNOS and NPY but not SOM may derived from MGE and CGE territories and could correspond to neurogliaform cells located in the most superficial layers where they may bidirectionally regulate blood flow. The recent genesis of a transgenic line expressing a tamoxifen inducible Cre recombinase under the control of the nNOS promoter (nNOS-CreER) will help to analyze the physiological roles that these populations may play (Taniguchi et al., 2011).

PRIMATES AND HUMAN TELENCEPHALON: SPECIFIC ASPECTS OF GABAergic DEVELOPMENT

Rodents, specifically mice, are of great interest due to the availability of transgenic models (Taniguchi et al., 2011) that allow for thorough dissection of the genetic programs needed for interneuron development and specification. However, it is difficult to relate neocortical development in mice to the much longer timescale and complexity of primate development (Uylings et al., 1990; Rakic, 2009). Indeed, comparative studies across species indicate that the first postnatal week in mice corresponds broadly to gestational days 85–130 in macaques and to 110–170 in humans (Clancy et al., 2001). The much longer timescale in these higher order species is certainly due to the important brain expansion in size and therefore to the increasing distance of subpalial and pallial territories and concerns the place of origins of telencephalic interneurons (see Molnar et al., 2006; Rakic, 2009). Indeed, while the vast majority of telencephalic GABAergic neurons originate from supallial territories in rodents (see above), in humans (from 5 to 15 gestational weeks) and primates this is only the case for the first generated ones that mainly arise from MGE (Letinic et al., 2002; Jakovcevski et al., 2011; Zecevic et al., 2011). Later, neurogenesis occurs in dorsal pallial territories and presumably in the CGE (Petanjek et al., 2009a,b; Jakovcevski et al., 2011). Indeed, it is known that late proliferations from pallial territories mainly generate CR^+ interneurons that are more numerous in humans and primates than in rodents and display distinct morphologies in each species (Jones, 2009; Rakic, 2009).

Recently, analysis of interneuron densities in postmortem brain tissue from humans suffering from holoprosencephaly associated with agenesis of GE showed a strong correlation between massive reductions in Nkx2.1 expression and depletion of nNOS/NPY/SST^+ and PV^+ interneurons (Fertuzinhos et al., 2009). These observations suggest that, like in mice, these populations of putative nNOS-type I cells are generated in the GE. Despite the fact that nNOS-type II largely outnumbered nNOS-type I neurons in primate and human brains their place of genesis has not been analyzed in these species.

DEVELOPMENT AND MATURATION OF NEOCORTICAL AND HIPPOCAMPAL INTERNEURONS EXPRESSING nNOS

The pattern of nNOS immunoreactivity in the rodent telencephalon undergoes sterotyped changes during development. From embryonic day 13 (E13) to the first postnatal day (P0), a period of intense neuronal migration, nNOS is strikingly expressed by distinct cells types. Indeed, cells migrating in the marginal zone displaying Cajal-Rezius like morphologies express nNOS (Santacana et al., 1998). In addition, by E15 in rats, nNOS labeling is clearly seen in the ganglionic eminence and the AEP/PO region (**Figure 2A** in Santacana et al., 1998) suggesting that nNOS could also label the early populations of GABAergic neurons that continue to express nNOS at mature stages. Later on, from E17 to E19, in rats, neurons displaying leading processes oriented along the intermediate zone or toward the pial surface, presumably migrating neurons were reported to express nNOS (Santacana et al., 1998). However, it is not clear whether they correspond solely to GABAergic neurons or to subpopulations of GABAergic and glutamatergic neurons.

In rat visual cortex, $nNOS^+$ neurons appear as early as postnatal day 1 in the intermediate (white matter) and subplate (layers V and VI) regions as small and undifferentiated neurons. Differences in intensity of nNOS immunoreactivity (later mentioned as type I and type II neurons) become evident as early as P7 (Chung et al., 2004; Kanold and Luhmann, 2010). nNOS GABAergic neurons reach their typical morphology in the second postnatal week and appear in all layers. Neurons in layers V and VI precede those in the superficial layers in acquiring their final morphology. By P30, NADPH-d active neurons are no longer detected in layer I suggesting they die off or migrate to deeper layers residing only transiently in layer I (Lüth et al., 1995).

In rat barrel cortex, an area that integrates sensory inputs coming from the whiskers, between P10 and P90, the neuropilic distributions of NADPH-d and cytochrome oxidase (CO) activities exhibit a remarkable similarity. NADPH-d activity is denser

in barrel hollows, regions that receive somatotopic sensory thalamic inputs, and is less active in barrel septa (Furuta et al., 2009). The number of NADPH-d active neurons increases significantly in the barrel fields between P10 and P23, with a peak at P23. The dendritic arborizations of NADPH-d active neurons become more elaborate during barrel development. At all ages evaluated, the number of NADPH-d^+/NOS^+ cells, mostly type I cells, was always higher in the septa than in the barrel hollows (Vercelli et al., 1999; Freire et al., 2004).

In the hippocampus, nNOS is transiently expressed in the pyramidal cell layer between P3 and P7 (Chung et al., 2004). While NADPH-d reactive soma and processes are present from the day of birth until adulthood in Ammon's horn, expression of NOS is delayed in the DG appearing only by the end of the first postnatal week (Moritz et al., 1999).

ROLE OF nNOS AND NO IN DEVELOPMENT, MATURATION, AND PLASTICITY

PRODUCTION OF NITRIC OXIDE BY NEURONAL NITRIC OXIDE SYNTHASE

NO is a free radical gas that can move rapidly across plasma membranes in anterograde and retrograde directions to act presynaptically, postsynaptically or within the cell that has produced it. NO is generated following the activation of NO synthases (Bredt and Synder, 1990; Daff, 2003). So far three NOS isoforms have been identified, two of which, endothelial (eNOS) and the neuronal (nNOS), are constitutively expressed while the third one is inducible and rarely present under basal conditions. Each NOS subtype has distinct functional and structural features. Depending on the neuronal cell type and the mode of neuronal excitation, nNOS, which is a $Ca2^+$/calmodulin-regulated enzyme, can be activated by Ca^{2+} influx through N-methyl-D-aspartate (NMDA) receptors or other calcium permeable channels (i.e., the ionotropic 5-HT_{3A} receptor; Rancillac et al., 2006; see also Perrenoud et al., 2012b in this issue). Alternatively, calcium liberated from intracellular stores such as the endoplasmic reticulum (i.e., through activation of metabotropic receptors coupled to activation of Gq protein) may promote nNOS activity. Arginine transported into the cell by the anion-cation tranporter is oxidised by nNOS into citrulline in a nicotinamide adenine dinucleothide phosphate (NADPH)-dependant manner (Snyder et al., 1998) generating NO that is considered to be stable in physiological conditions for approximately 1–2 s (1 s half-life; Garthwaite, 2008). Within cells, NO has the capacity to trigger several transduction pathways. The most well-known involves activation of guanylyl cyclase (Arnold et al., 1997) leading to the conversion of GTP into cGMP and subsequent activation of protein kinase G (PKG). PKG activity in turn promotes Erk activation and the induction of various immediate early genes such as c-fos, Arc, and BDNF. Indeed, in neuronal cultures NOS inhibition attenuates bicuculine-induced activation of Erk as well as the rise in c-Fos, Egr-1, and Arc that are all implicated in experience-dependant plasticity in the barrel cortex. Moreover, although NOS inhibition does not affect the phosphorylation of CREB it decreases accumulation of the CREB coactivator TORC1 (Gallo and Iadecola, 2011; **Figure 7**).

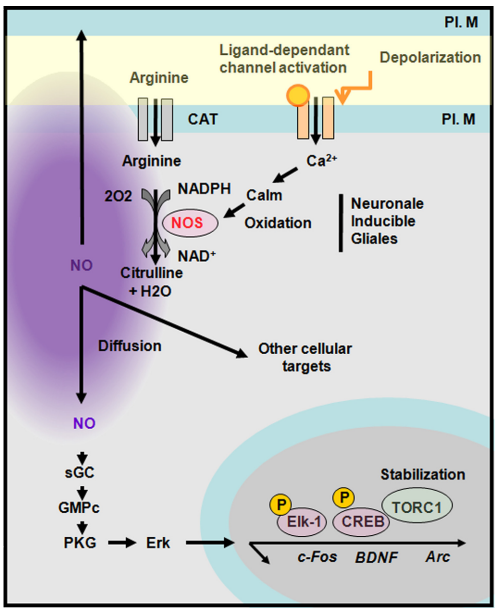

FIGURE 7 | Synthesis of nitric oxide and transduction cascades. Neuronal nitric oxide synthase (nNOS) is activated by a calcium-dependant calmodulin. NOS produces nitric oxide (NO) upon oxidation of arginine into citrulline. NO diffuses and act on presynaptic or postsynaptic targets. A well-known pathway of NO is through the activation of guanylyl cyclase (GC) that activates a protein kinase G (PKG) leading to Erk activation and the stabilization of TORC1 a CREB co-activator. CAT, cation and anion transporter; PL. M, plasma membrane. Adapted from Gallo and Iadecola (2011).

Activation of the NO/cGMP pathway is implicated in various neurophysiological processes including neuronal development, synaptic modulation, learning and memory. In addition several cGMP-independent effects of NO related to nervous system function have been reported. For instance, various presynaptic targets for NO have been identified such as SNAP25, synthaxin Ia, n-Sec 1, neurogranin as well as the postsynaptic targets ADP ribosyltransferase and NMDA receptors (Gallo and Iadecola, 2011). Finally, excessive NO production is potentially neurotoxic but this aspect is beyond the scope of this revue (Steinert et al., 2010).

ROLE OF nNOS AND NO DURING EARLY DEVELOPMENT

Numerous papers and reviews have described the role of nNOS and NO in various neuronal populations during development. Here, we will briefly focus on some of the best understood roles for NO/nNOS in neurons at early stages. nNOS or NADPH-d activity are transiently expressed in the embryonic hippocampal and neocortical anlagen during the peak of neurogenesis and the period of developmental synaptogenesis (Bredt and Snyder, 1994). It has been shown that NO acts as a paracrine messenger in newly generated neurons to control the proliferation and differentiation of mouse brain neural progenitor cells (NPC). Treatments with the NO synthase inhibitor L-NAME or the NO scavenger hemoglobin increase cell proliferation and decrease the differentiation of NPCs into neurons (Barnabé-Heider and Miller, 2003).

Interestingly, a similar role of NO was demonstrated in the subventricular zone of adult mice, a region that retains the capacity to generate neurons at mature stages (Xiong et al., 1999; Cheng et al., 2003; Matarredona et al., 2004). Both BDNF and epidermal growth factor (EGF) have been largely implicated in these events (Barnabé-Heider and Miller, 2003; Matarredona et al., 2004).

In addition to regulating neurogenesis, NO has also been implicated in the formation of cerebral maps. This role has been largely investigated and demonstrated in the visual system where NO induces synaptic refinement or elimination of immature synaptic connections at retino-collicular and retino-thalamic levels (Cramer et al., 1995, 1996; Wu et al., 1996, 2000; Cramer and Sur, 1999; Cuderio and Rivadulla, 1999; Vercelli et al., 2000). However, outside of retino-collicular and retino-thalamic organization, NO appears dispensible for the establishment of patterned neocortical maps since animals receiving daily injection of nitroarginine prior to and during the period of ocular dominance column formation, as well as nNOS knockout mice, display normal organization of the somatosensory cortex and barrel field plasticity (Van der Loos and Woolsey, 1973; Finney and Shatz, 1998). Nevertheless, though apparently not instructive, NO may still participate in establishing and refining neocortical connectivity. Indeed, when NADPH-d activity is altered in the barrel field, as observed in mice lacking NMDAR1 specifically in neocortical neurons, abnormal segregation of thalamocortical axons occurs (Iwasato et al., 2000; Lee et al., 2005). In these animals thalamocortical axons display fewer branch points in layer IV and abnormally expansive thalamocortical arbors, a feature that corresponds to a rudimentary whisker-specific pattern. These results suggest that NO could promote thalamocortical sprouting and participates in the consolidation of synaptic strength in layer IV of the primary somatosensory cortex.

Finally, it has been shown that between P6 and P10 in rodents, NO also affects neuronal gap-junction coupling. Indeed, Rörig and colleagues have shown that following preincubation with sodium nitroprusside (an NO donor), the number of gap-junction coupled neurons decreased (Rörig and Sutor, 1996a,b; Roerig and Feller, 2000). In the developing neocortex, gap-junctions represent a transient metabolic and electrical communication system occurring between glutamatergic or GABAergic neurons belonging to the same radial column. Thus, NO mediated regulation of gap junctions has the capacity to affect electrical coupling, synchronization of metabolic states and, coordination of transcriptional activity amongst connected neurons.

ROLE OF nNOS AND NO IN MICROCIRCUITS PLASTICITY

The idea that NO might modulate synaptic transmission, first proposed in 1988 by Garthwaite and colleagues (Garthwaite et al., 1988), has been confirmed in several brain regions including the hippocampus, striatum, hypothalamus, and locus coeruleus (Prast and Philippu, 2001). Indeed, studies using NO donors suggest that release of several transmitters, including acetylcholine, catecholamines, glutamate and GABA are regulated by endogenous NO. As a gaseous very weakly polar molecule without net electric charge and due to its small size, NO can diffuse readily across cell membranes. However, the high reactivity of NO as a free radical limits activity to within a micrometer of its site of synthesis allowing for synapse specificity in modulating presynaptic function (Garthwaite, 2008).

In acute hippocampal slices from neonatal rat, NO signaling was found to decrease GABAergic and glutamatergic postsynaptic currents, whereas network calcium imaging indicated that inhibition or stimulation of NO signaling enhanced or suppressed synchronous network events, respectively (Cserép et al., 2011). The regulation of GABAergic and glutamatergic synaptic transmission in early postnatal development, NO is considered particulalrly critical for fine-tuning synchronous network activity in the developing hippocampus (Cserép et al., 2011). In more mature hippocampus NO regulates LTP at the Schaffer collateral/CA1 synapses and acts as a retrograde messenger (for review see Malenka and Bear, 2004; Lisman and Raghavachari, 2006). This occurs via the activation of postsynaptic NMDA receptors, synthesis of NO by NOS expressed in pyramidal cells and then retrograde activation of guanylate cyclase located in axon terminals (See Feil and Kleppisch, 2008 for detailed intracellular mechanisms). In contrast, in the cerebellum NO serves as an anterograde messenger that is produced in parallel fiber terminals or cerebellar interneurons and then diffuses to the postsynaptic Purkinje cell to induce LTD through a cGMP-dependent mechanism (for review see Feil et al., 2005).

ROLE OF NO AND INTERNEURONS EXPRESSING nNOS IN HIPPOCAMPAL AND NEOCORTICAL NETWORK

Studies investigating synaptic modulation by NO have typically considered it to be derived from NOS localized in pyramidal cell postsynaptic densities. However, as described above, nNOS is largely expressed in GABAergic interneurons. Even if NO can modulate GABAergic transmission, it is still unclear if the NO released by interneurons principally regulates transmitter release or instead participates in other homeostatic processes such as regulation blood flow or neuronal excitability (Iadecola et al., 1993). Indeed bath application of an NO donor onto acute rat neocortical slices cause dilation of blood vessels (Cauli et al., 2004) and this hemodynamic change can similarly be elicited electrical stimulation of a single neocortical nNOS expressing interneuron (Cauli et al., 2004). Such tight coupling between neuronal activity of interneurons expressing nNOS and vasomotricity has also been reported in other brain structures such as cerebellum where pharmacological or electrical stimulation of stellate cells, which strongly express nNOS, induces vasodilation by release of NO that can be measured using NO-sensitive electrode (Rancillac et al., 2006). Given this interneuron mediated regulation of brain blood perfusion, it is interesting to note that most of $nNOS^+$ interneurons also coexpress NPY which is a potent vasoconstrictor (Dacey et al., 1988; Cauli et al., 2004). Consistently, we have shown that activation of serotonin type 3 receptors which are present on nNOS-type II interneurons co-expressing

NPY and/or VIP (Vucurovic et al., 2010; Perrenoud et al., 2012a in this issue), induces both vasodilation and vasoconstriction (Perrenoud et al., 2012b in this issue) via direct release of NO and NPY respectively. Therefore, it appears that both neocortical and hippocampal NGFCs, which coexpress NPY and nNOS, likely exert dual control over cerebral blood flow. To resolve these conflicting observations we propose that NPY, which is likely released at axon terminals, controls blood vessel tone distally from the cell body while NO released by the somato-dendritic compartment acts more proximally via volume transmission. These differential effects would permit fine-tuning of energy and oxygen supply by creating locally a microsphere with increased blood perfusion consequently to increased neural activity (Estrada and DeFelipe, 1998).

Regarding excitability, NO can regulate several conductances via the cGMP/PGK pathway in central neurons (Garthwaite, 2008). Indeed the hyperpolarization activated current that serves as a pacemaker to generate rhythmic activity amongst thalamic neurons (Pape and Mager, 1992) is regulated by NO (Biel et al., 2009). NO also acts on several potassium conductances such as the delayed rectifier Kv3 channels (Rudy and McBain, 2001). It has been shown that NO donors inhibit both Kv3.1 and Kv3.2 channels in CHO cells via activation of the cGMP/PKG pathway (Moreno et al., 2001). Such inhibition of Kv3 current has also been observed in the central nervous system via volume transmission in the auditory brain stem and the hippocampus (Steinert et al., 2008, 2011). It is interesting to note that Kv3 channels are responsible for the short duration of action potentials in auditory neurons as well as in hippocampal/neocortical PV^+ and SOM^+ interneurons (Atzori et al., 2000; Tansey et al., 2002; Lien and Jonas, 2003). NO-mediated modulation of Kv3 would therefore regulate the spike timing of these neurons (Lien and Jonas, 2003).

Recently, the role of NO in sleep regulation has been challenged. Indeed, the group of Kilduff has shown that long range projecting nNOS-type I GABAergic neurons are specifically activated during sleep by demonstrating that these cells specifically accumulate c-Fos during sleep rebound following sleep deprivation (Gerashchenko et al., 2008). The mechanism behind this activation is not completely understood. However, it is suspected that during the waking period $NPY^+/SOM^+/nNOS^+$ GABAergic neurons (putative nNOS-type I) are inhibited by neuromodulatory afferents driving arousal such as acetylcholine, noradrenaline, serotonin, and histamine and that they would be activated when arousal systems are depressed when sleep-promoting substances are released (i.e., adenosine, cytokines, growth hormone, releasing hormone, and cortistatin). Once activated nNOS neurons could synchronize EEG activity across neocortical regions through the release of NO, GABA or NPY. Interestingly it has been reported that nNOS knockout mice spend more time than controls in slow wave sleep as monitored by EEG. This suggests that nNOS-type I GABAergic neurons may regulate sleep homeostasis (Kilduff et al., 2011). However additional experiments remain to be performed to fully address this point.

CONCLUSION AND PERSPECTIVES

The development and plasticity of $nNOS^+$ interneurons needs to be confronted with more general questions that are central to understand interneurons development and specification. One important issue to address is to determine the extent to which interneurons are fully specified by their place and time of genesis. In other words are these cells hard wired from the progenitor stage or allowed a certain degree of "developmental plasticity" after the last division of the progenitors to adapt to their migratory and ultimately circuit environment? At mature stages interneuron subtypes are characterized by a combination of: (1) their laminar position within different circuits; (2) specific combinations of neurochemical markers; (3) their basic morphology; and (4) their electrophysiological features including passive membrane properties, spiking behavior and synaptic connectivity. Various studies including some highlighted above have shown that these criteria are largely dictated by an interneuron's site and time of genesis. However, some studies have also pointed to a role for the cellular environment an interneuron ultimately occupies in refining these properties such as their stratification (i.e., CR- and reelin-positive interneurons) and their expression of certain activity regulated markers like NPY. In this respect it should be mentioned that the expression of nNOS appears to be developmentally regulated in various neuronal populations and could be modulated by cellular targets in subpopulations of interneurons (i.e., in an activity-dependent manner). Thus, although challenging, it will be important to determine whether nNOS interneurons are guided to their final location early on, like most interneurons, or are eliminated if inaccurately positioned or if they stop expressing/fail to induce nNOS. An understanding of subtle differences in the genetic makeup/molecular characteristics of divergent nNOS interneuron cohorts may provide insight into these issues. The recent generation and use of Cre reporter animals in association with other techniques have been successfully used to determine the embryonic origin and birthdating of nNOS type I and type II interneurons revealing for the first time their heterogeneity and specificities (lineage and characteristics displayed at mature stage; in this issue). The increasing array of transgenic models and genetic tools available (i.e., optogenetic) will help advance the pace of this research.

Interestingly, the unique features that have been shown to depend on neuronal activity (Verhage et al., 2000) for wiring and plasticity are the density and strength of GABAergic innervations. It remains to be established if and how NO could participate in the maturation and refinement of axonal and/or dendritic arborization of specific classes of interneurons.

ACKNOWLEDGMENTS

We thank Thierry Gallopin, Hélène Geoffroy, Quentin Perrenoud and Armelle Rancillac of the "sleep neuronal networks" team for constant and fruitful interactions. We thank Gord Fishell and Renata Batista-Brito and, Nicoletta Kessaris for sharing the results of their studies before publication. We thank Kenneth Pelkey for suggestions to improve the manuscript. Financial support was provided by the CNRS, ESPCI ParisTech and INSERM.

REFERENCES

Acsády, L., Arabadzisz, D., and Freund, T. F. (1996a). Correlated morphological and neurochemical features identify different subsets of vasoactive intestinal polypeptide-immunoreactive interneurons in rat hippocampus. *Neuroscience* 73, 299–315.

Acsády, L., Görcs, T. J., and Freund, T. F. (1996b). Different populations of vasoactive intestinal polypeptide-immunoreactive interneurons are specialized to control pyramidal cells or interneurons in the hippocampus. *Neuroscience* 173, 317–334.

Alcántara, S., Ruiz, M., D'Arcangelo, G., Ezan, F., de Lecea, L., Curran, T., et al. (1999). Regional and cellular patterns of reelin mRNA expression in the forebrain of the developing and adult mouse. *J. Neurosci.* 18, 7779–7799.

Armstrong, C., Szabadics, J., Tamás, G., and Soltesz, I. (2011). Neurogliaform cells in the molecular layer of the dentate gyrus as feed-forward γ-aminobutyric acidergic modulators of entorhinal-hippocampal interplay. *J. Comp. Neurol.* 519, 1476–1491.

Arnold, W. P., Mittal, C. K., Katsuki, S., and Murad, F. (1997). Nitric oxide activates guanylate cyclase and increases guanosine 3′:5′-cyclic monophosphate levels in various tissue preparations. *Proc. Natl. Acad. Sci. U.S.A.* 74, 3203–3207.

Atzori, M., Lau, D., Tansey, E. P., Chow, A., Ozaita, A., Rudy, B., et al. (2000). H2 histamine receptor-phosphorylation of Kv3.2 modulates interneuron fast spiking. *Nat. Neurosci.* 3, 791–798.

Baraban, S. C., and Tallent, M. K. (2004). Interneuron diversity series: interneuronal neuropeptides–endogenous regulators of neuronal excitability. *Trends Neurosci.* 27, 135–142.

Barnabé-Heider, F., and Miller, F. D. (2003). Endogenously produced neurotrophins regulate survival and differentiation of cortical progenitors via distinct signaling pathways. *J. Neurosci.* 23, 5149–5160.

Bartos, M., Vida, I., and Jonas, P. (2007). Synaptic mechanisms of synchronized gamma oscillations in inhibitory interneuron networks. *Nat. Rev. Neurosci.* 8, 45–56.

Batista-Brito, R., and Fishell, G. (2009). The developmental integration of cortical interneurons into a functional network. *Curr. Top. Dev. Biol.* 87, 81–118.

Batista-Brito, R., Rossignol, E., Hjerling-Leffler, J., Denaxa, M., Wegner, M., Lefebvre, V., et al. (2009). The cell-intrinsic requirement of Sox6 for cortical interneuron development. *Neuron* 63, 466–481.

Baude, A., Bleasdale, C., Dalezios, Y., Somogyi, P., and Klausberger, T. (2007). Immunoreactivity for the GABAA receptor alpha1 subunit, somatostatin and Connexin36 distinguishes axoaxonic, basket, and bistratified interneurons of the rat hippocampus. *Cereb. Cortex* 17, 2094–2107.

Biel, M., Wahl-Schott, C., Michalakis, S., and Zong, X. (2009). Hyperpolarization-activated cation channels: from genes to function. *Physiol. Rev.* 89, 847–885.

Bredt, D. S., and Synder, S. H. (1990). Isolation of nitric oxide synthase, a calmodulin-requiring enzyme. *Proc. Natl. Acad. Sci. U.S.A.* 87, 682–685.

Bredt, D. S., and Snyder, S. H. (1994). Transient nitric oxide synthase neurons in embryonic cerebral cortical plate, sensory ganglia, and olfactory epithelium. *Neuron* 13, 301–313.

Burette, A., Zabel, U., Weinberg, R. J., Schmidt, H. H., and Valtschanoff, J. G. (2002). Synaptic localization of nitric oxide synthase and soluble guanylyl cyclase in the hippocampus. *J. Neurosci.* 22, 8961–8970.

Butt, S. J., Cobos, I., Golden, J., Kessaris, N., Pachnis, V., and Anderson, S. (2007). Transcriptional regulation of cortical interneuron development. *J. Neurosci.* 27, 11847–11850.

Butt, S. J., Fucillo, M., Nery, S., Noctor, S., Kriegstein, A., Corbin, J. G., et al. (2005). The temporal and spatial origins of cortical interneurons predict their physiological subtype. *Neuron* 48, 591–604.

Cameron, H. A., and Dayer, A. G. (2008). New interneurons in the adult neocortex: small, sparse, but significant. *Biol. Psychiatry* 63, 650–655.

Cauli, B., and Hamel, E. (2010). Revisiting the role of neurovascular coupling. *Front. Neuroenerg.* 2:9. doi: 10.3389/fnene.2010.00009

Cauli, B., Tong, X. K., Rancillac, A., Serluca, N., Lambolez, B., Rossier, J., et al. (2004). Cortical GABA interneurons in neurovascular coupling: relays for subcortical vasoactive pathways. *J. Neurosci.* 24, 8940–8949.

Chamberland, S., Salesse, C., Topolnik, D., and Topolnik, L. (2010). Synapse-specific inhibitory control of hippocampal feedback inhibitory circuit. *Front. Cell. Neurosci.* 4:130. doi: 10.3389/fncel.2010.00130

Cheng, A., Wang, S., Cai, J., Rao, M. S., and Mattson, M. P. (2003). Nitric oxide acts in a positive feedback loop with BDNF to regulate neural progenitor cell proliferation and differentiation in tha mammalian brain. *Dev. Biol.* 258, 319–333.

Cho, K. H., Jang, J. H., Jang, H. J., Kim, M. J., Yoon, S. H., Fukuda, T., et al. (2010). Subtype-specific dendritic Ca(2+) dynamics of inhibitory interneurons in the rat visual cortex. *J. Neurophysiol.* 104, 840–853.

Chung, Y. H., Kim, Y. S., and Lee, W. B. (2004). Distribution of nitric oxide synthase-immunoreactive neurons in the cerebral cortex and hippocampus during postnatal development. *J. Mol. Histol.* 35, 765–770.

Clancy, B., Darlington, R. B., and Finlay, B. L. (2001). Translating developmental time across mammalian species. *Neuroscience* 105, 7–17.

Cramer, K. S., Angelucci, A., Hahm, J. O., Bogdanov, M. B., and Sur, M. (1996). A role for nitric oxide in the development of the ferret retinogeniculate projection. *J. Neurosci.* 16, 7995–8004.

Cramer, K. S., Moore, C. I., and Sur, M. (1995). Transient expression of NADPH-diaphorase in the lateral geniculate nucleus of the ferret during early postnatal development. *J. Comp. Neurol.* 353, 306–316.

Cramer, K. S., and Sur, M. (1999). The neuronal form of nitric oxide synthase is requiered for pattern formation by retinal afferents in the ferret lateral geniculate nucleus. *Dev. Brain Res.* 116, 79–86.

Cserép, C., Szonyi, A., Veres, J. M., Németh, B., Szabadits, E., de Vente, J., et al. (2011). Nitric oxide signaling modulates synaptic transmission during early postnatal development. *Cereb. Cortex* 21, 2065–2074.

Cuderio, J., and Rivadulla, C. (1999). Sight and insight- on the physiological role of nitric oxide in the visual system. *Trends Neurosci.* 22, 109–116.

Dacey, R. G. Jr., Bassett, J. E., and Takayasu, M. (1988). Vasomotor responses of rat intracerebral arterioles to vasoactive intestinal peptide, substance P, neuropeptide Y, and bradykinin. *J. Cereb. Blood Flow Metab.* 8, 254–261.

Daff, S. (2003). Calmodulin-dependent regulation of mammalian nitric oxide synthase. *Biochem. Soc. Trans.* 31, 502–505.

Dayer, A. G., Jenny, B., Potter, G., Sauvain, M. O., Szabó, G., Vutskits, L., et al. (2008). Recruiting new neurons from the subventricular zone to the rat postnatal cortex: an organotypic slice culture model. *Eur. J. Neurosci.* 27, 1051–1060.

De Marco García, N. V., Karayannis, T., and Fishell, G. (2011). Neuronal activity is required for the development of specific cortical interneuron subtypes. *Nature* 472, 351–355.

Dittrich, L., Heiss, J. E., Warrier, D. R., Perez, X. A., Quik, M., and Kilduff, T. S. (2012). Cortical nNOS neurons co-express the NK1 receptor and are depolarized by Substance P in multiple mammalian species. *Front. Neural Circuits* 6:31. doi: 10.3389/fncir.2012.00031

Dun, N. J., Dun, S. L., Wong, R. K., and Förstermann, U. (1994). Colocalization of nitric oxide synthase and somatostatin immunoreactivity in rat dentate hilar neurons. *Proc. Natl. Acad. Sci. U.S.A.* 91, 2955–2959.

Du, T., Xu, Q., Ocbina, P. J., and Anderson, S. A. (2008). NKX2.1 specifies cortical interneuron fate by activating Lhx6. *Development* 135, 1559–1567.

Elfant, D., Pál, B. Z., Emptage, N., and Capogna, M. (2008). Specific inhibitory synapses shift the balance from feedforward to feedback inhibition of hippocampal CA1 pyramidal cells. *Eur. J. Neurosci.* 27, 104–113.

Estrada, C., and DeFelipe, J. (1998). Nitric oxide-producing neurons in the neocortex: morphological and functional relationship with intraparenchymal microvasculature. *Cereb. Cortex* 8, 193–203.

Feil, R., Hofmann, F., and Kleppisch, T. (2005). Function of cGMP-dependent protein kinases in the nervous system. *Rev. Neurosci.* 16, 23–41.

Feil, R., and Kleppisch, T. (2008). NO/cGMP-dependent modulation of synaptic transmission. *Handb. Exp. Pharmacol.* 184, 529–560.

Férézou, I., Hill, E. L., Cauli, B., Gibelin, N., Kaneko, T., Rossier, J., et al. (2007). Extensive overlap of mu-opioid and nicotinic sensitivity in cortical interneurons. *Cereb. Cortex* 17, 1948–1957.

Fertuzinhos, S., Krsnik, Z., Kawasawa, Y. I., Rasin, M. R., Kwan, K. Y., Chen, J. G., et al. (2009). Selective depletion of molecularly defined cortical interneurons in human holoprosencephaly with severe striatal hypoplasia. *Cereb. Cortex* 19, 2196–2207.

Finney, E. M., and Shatz, C. J. (1998). Establishment of patterned thalamocortical connections does

not require nitric oxide synthase. *J. Neurosci.* 18, 8826–8838.

Flames, N., Pla, R., Gelman, D. M., Rubenstein, J. L., Puelles, L., and Marín, O. (2007). Delineation of multiple subpallial progenitor domains by the combinatorial expression of transcriptional codes. *J. Neurosci.* 27, 9682–9695.

Fogarty, M., Grist, M., Gelman, D., Marín, O., Pachnis, V., and Kessaris, N. (2007). Spatial genetic patterning of the embryonic neuroepithelium generates GABAergic interneuron diversity in the adult cortex. *J. Neurosci.* 27, 10935–10946.

Freire, M. A., Gomes-Leal, W., Carvalho, W. A., Guimarães, J. S., Franca, J. G., Picanço-Diniz, C. W., et al. (2004). A morphometric study of the progressive changes on NADPH diaphorase activity in the developing rat's barrel field. *Neurosci. Res.* 50, 55–66.

Freund, T. F., and Buzsáki, G. (1996). Interneurons of the hippocampus. *Hippocampus* 6, 347–470.

Fuentealba, P., Begum, R., Capogna, M., Jinno, S., Márton, L. F., Csicsvari, J., et al. (2008). Ivy cells: a population of nitric-oxide-producing, slow-spiking GABAergic neurons and their involvement in hippocampal network activity. *Neuron* 57, 917–929.

Fuentealba, P., Klausberger, T., Karayannis, T., Suen, W. Y., Huck, J., Tomioka, R., et al. (2010). Expression of COUP-TFII nuclear receptor in restricted GABAergic neuronal populations in the adult rat hippocampus *J. Neurosci*. 30, 1595–1609.

Furuta, T., Kaneko, T., and Deschênes, M. (2009). Septal neurons in barrel cortex derive their receptive field input from the lemniscal pathway. *J. Neurosci.* 29, 4089–4095.

Gallo, E. F., and Iadecola, C. (2011). Neuronal nitric oxide contributes to neuroplasticity-associated protein expression through cGMP, protein kinase G, and extracellular signal-regulated kinase. *J. Neurosci.* 31, 6947–6955.

Garthwaite, J. (2008). Concepts of neural nitric oxide-mediated transmission. *Eur. J. Neurosci.* 27, 2783–2802.

Garthwaite, J., Charles, S. L., and Chess-Williams, R. (1988). Endothelium-derived relaxing factor release on activation of NMDA receptors suggests role as intercellular messenger in the brain. *Nature* 336, 385–388.

Gelman, D., Griveau, A., Dehorter, N., Teissier, A., Varela, C., Pla, R., et al. (2011). A wide diversity of cortical GABAergic interneurons derives from the embryonic preoptic area. *J. Neurosci.* 31, 16570–16580.

Gelman, D. M., Martini, F. J., Pereira, S. N., Pierani, A., Kessaris, N., and Marín, O. (2009). The embryonic preoptic area is a novel source of cortical GABAergic interneurons. *J. Neurosci.* 29, 9380–9389.

Gerashchenko, D., Wisor, J. P., Burns, D., Reh, R. K., Shiromani, P. J., Sakurai, T., et al. (2008). Identification of a population of sleep-active cerebral cortex neurons. *Proc. Natl. Acad. Sci. U.S.A.* 105, 10227–10232.

Gholipour, T., Ghasemi, M., Riazi, K., Ghaffarpour, M., Dehpour, A. R. (2010). Seizure susceptibility alteration through 5-HT(3) receptor: modulation by nitric oxide. *Seizure* 19, 17–22.

Gonchar, Y., and Burkhalter, A. (1997). Three distinct families of GABAergic neurons in rat visual cortex. *Cereb. Cortex* 7, 347–358.

Gulyás, A. I., Hájos, N., and Freund, T. F. (1996). Interneurons containing calretinin are specialized to control other interneurons in the rat hippocampus. *J. Neurosci.* 16, 3397–3411.

Higo, S., Akashi, K., Sakimura, K., and Tamamaki, N. (2009). Subtypes of GABAergic neurons project axons in the neocortex. *Front. Neuroanat.* 3:25. doi: 10.3389/neuro.05.025.2009

Iadecola, C., Beitz, A. J., Renno, W., Xu, X., Mayer, B., and Zhang, F. (1993). Nitric oxide synthase-containing neural processes on large cerebral arteries and cerebral microvessels. *Brain Res.* 606, 148–155.

Inta, D., Alfonso, J., von Engelhardt, J., Kreuzberg, M. M., Meyer, A. H., van Hooft, J. A., et al. (2008). Neurogenesis and widespread forebrain migration of distinct GABAergic neurons from the postnatal subventricular zone. *Proc. Natl. Acad. Sci. U.S.A.* 105, 20994–20999.

Iwasato, T., Datwani, A., Wolf, A. M., Nishiyama, H., Taguchi, Y., Tonegawa, S., et al. (2000). Cortex-restricted disruption of NMDAR1 impairs neuronal patterns in the barrel cortex. *Nature* 406, 726–731.

Jaglin, X. H., Hjerling-Leffer, J., Fishell, G., and Batista-Brito, R. (2012). The origin of neocortical nitric oxide synthase-expressing inhibitory neurons. *Front. Neural Circuits* 6:44. doi: 10.3389/fncir.2012.00044

Jakovcevski, I., Mayer, N., and Zecevic, N. (2011). Multiple origins of human neocortical interneurons are supported by distinct expression of transcription factors. *Cereb. Cortex* 21, 1771–1782.

Jinno, S., and Kosaka, T. (2002). Patterns of expression of calcium binding proteins and neuronal nitric oxide synthase in different populations of hippocampal GABAergic neurons in mice. *J. Comp. Neurol.* 449, 1–25.

Jinno, S., and Kosaka, T. (2004). Patterns of colocalization of neuronal nitric oxide synthase and somatostatin-like immunoreactivity in the mouse hippocampus: quantitative analysis with optical disector. *Neuroscience* 124, 797–808.

Jones, E. G. (2009). The origins of cortical interneurons: mouse versus monkey and human. *Cereb. Cortex* 19, 1953–1956.

Kanatani, S., Yozu, M., Tabata, H., and Nakajima, K. (2008). COUP-TFII is preferentially expressed in the caudal ganglionic eminence and is involved in the caudal migratory stream. *J. Neurosci.* 28, 13582–13591.

Kanold, P. O., and Luhmann, H. J. (2010). The subplate and early cortical circuits. *Annu. Rev. Neurosci.* 33, 23–48.

Karagiannis, A., Gallopin, T., Dávid, C., Battaglia, D., Geoffroy, H., Rossier, J., et al. (2009). Classification of NPY-expressing neocortical interneurons. *J. Neurosci.* 29, 3642–3659.

Karayannis, T., Elfant, D., Huerta-Ocampo, I., Teki, S., Scott, R. S., Rusakov, D. A., et al. (2010). Slow GABA transient and receptor desensitization shape synaptic responses evoked by hippocampal neurogliaform cells. *J. Neurosci.* 30, 9898–9909.

Kilduff, T. S., Cauli, B., and Gerashchenko, D. (2011). Activation of cortical interneurons during sleep: an anatomical link to homeostatic sleep regulation? *Trends Neurosci.* 34, 10–19.

Klausberger, T., and Somogyi, P. (2008). Neuronal diversity and temporal dynamics: the unity of hippocampal circuit operations. *Science* 321, 53–57.

Krimer, L. S., and Goldman-Rakic, P. S. (2001). Prefrontal microcircuits: membrane properties and excitatory input of local, medium, and wide arbor interneurons. *J. Neurosci.* 21, 3788–3796.

Krook-Magnuson, E., Luu, L., Lee, S. H., Varga, C., and Soltesz, I. (2011). Ivy and neurogliaform interneurons are a major target of μ-opioid receptor modulation. *J. Neurosci.* 31, 14861–14870.

Kubota, Y., Hattori, R., and Yui, Y. (1994). Three distinct subpopulations of GABAergic neurons in the rat frontal cortex. *Brain Res.* 649, 159–173.

Kubota, Y., Shigematsu, N., Karube, F., Sekigawa, A., Kato, S., Yamaguchi, N., et al. (2011). Selective coexpression of multiple chemical markers defines discrete populations of neocortical GABAergic neurons. *Cereb. Cortex* 21, 1803–1807.

Lapray, D., Lasztoczi, B., Lagler, M., Viney, T. J., Katona, L., Valenti, O., et al. (2012). Behavior-dependent specialization of identified hippocampal interneurons. *Nat. Neurosci.* 15, 1265–1271.

Lavdas, A. A., Grigoriou, M., Pachnis, V., and Parnavelas, J. G. (1999). The medial ganglionic eminence gives rise to a population of early neurons in the developing cerebral cortex. *J. Neurosci.* 19, 7881–7888.

Lee, L. J., Iwasato, T., Itohara, S., and Erzurumlu, R. S. (2005). Exuberant thalamocortical axon arborization in cortex-specific NMDAR1 knockout mice. *J. Comp. Neurol.* 485, 280–292.

Lee, J. E., and Jeon, C. J. (2005). Immunocytochemical localization of nitric oxide synthase-containing neurons in mouse and rabbit visual cortex and co-localization with calcium-binding proteins. *Mol. Cells* 19, 408–417.

Lee, S., Hjerling-Leffler, J., Zagha, E., Fishell, G., and Rudy, B. (2010). The largest group of superficial neocortical GABAergic interneurons expresses ionotropic serotonin receptors. *J. Neurosci.* 30, 16796–16808.

Letinic, K., Zoncu, R., and Rakic, P. (2002). Origin of GABAergic neurons in the human neocortex. *Nature* 417, 645–649.

Levitt, P., Eagleson, K. L., and Powell, E. M. (2004). Regulation of neocortical interneuron development and the implications for neurodevelopmental disorders. *Trends Neurosci.* 27, 400–406.

Lewis, D. A., Fish, K. N., Arion, D., and Gonzalez-Burgos, G. (2011). Perisomatic inhibition and cortical circuit dysfunction in schizophrenia. *Curr. Opin. Neurobiol.* 21, 866–872.

Lien, C. C., and Jonas, P. (2003). Kv3 potassium conductance is necessary and kinetically optimized for high-frequency action potential generation in hippocampal interneurons. *J. Neurosci.* 23, 2058–2068.

Li, G., Adesnik, H., Li, J., Long, J., Nicoll, R. A., Rubenstein, J. L., et al. (2008). Regional distribution

of cortical interneurons and development of inhibitory tone are regulated by Cxcl12/Cxcr4 signaling. *J. Neurosci.* 2, 1085–1098.

Liodis, P., Denaxa, M., Grigoriou, M., Akufo-Addo, C., Yanagawa, Y., and Pachnis, V. (2007). Lhx6 activity is required for the normal migration and specification of interneuron subtypes. *J. Neurosci.* 27, 3078–3089.

Lisman, J., and Raghavachari, S. (2006). A unified model of the presynaptic and postsynaptic changes during LTP at CA1 synapses. *Sci. STKE* 2006, re11.

López-Bendito, G., Sánchez-Alcañiz, J. A., Pla, R., Borrell, V., Picó, E., Valdeolmillos, M., et al. (2008). Chemokine signaling controls intracortical migration and final distribution of GABAergic interneurons. *J. Neurosci.* 28, 1613–1624.

López-Bendito, G., Sturgess, K., Erdélyi, F., Szabó, G., Molnár, Z., and Paulsen, O. (2004). Preferential origin and layer destination of GAD65-GFP cortical interneurons. *Cereb. Cortex* 14, 1122–1133.

Lüth, H. J., Hedlich, A., Hilbig, H., Winkelmann, E., and Mayer, B. (1995). Postnatal development of NADPH-diaphorase/nitric oxide synthase positive nerve cells in the visual cortex of the rat. *J. Hirnforsch.* 36, 313–328.

Magno, L., Oliveira, M. G., Mucha, M., Rubin, A. N., and Kessaris, N. (2012). Multiple embryonic origins of nitric oxide synthase-expressing GABAergic neurons of the neocortex. *Front. Neural Circuits* 6:65. doi: 10.3389/fncir.2012.00065

Malenka, R. C., and Bear, M. F. (2004). LTP and LTD:an embarrassment of riches. *Neuron* 44, 5–21.

Marin, O. (2012). Interneuron dysfunction in phsychiatric disorders. *Nat. Neurosci. Rev.* 13, 107–120.

Markwardt, S. J., Dieni, C. V., Wadiche, J. I., and Overstreet-Wadiche, L. (2011). Ivy/neurogliaform interneurons coordinate activity in the neurogenic niche. *Nat. Neurosci.* 14, 1407–1409.

Matarredona, E. R., Murillo-Carretero, M., Moreno-López, B., and Estrada, C. (2004). Nitric oxide synthesis inhibition increases proliferation of neural precursors isolated from the postnatal mouse subventricular zone. *Brain Res.* 995, 274–284.

McBain, C. J., and Fisahn, A. (2001). Interneurons unbound. *Nat. Rev. Neurosci.* 2, 11–23.

Miyoshi, G., Butt, S. J., Takebayashi, H., and Fishell, G. (2007). Physiologically distinct temporal cohorts of cortical interneurons arise from telencephalic Olig2-expressing precursors. *J. Neurosci.* 27, 7786–7798.

Miyoshi, G., Hjerling-Leffler, J., Karayannis, T., Sousa, V. H., Butt, S. J., Battiste, J., et al. (2010). Genetic fate mapping reveals that the caudal ganglionic eminence produces a large and diverse population of superficial cortical interneurons. *J. Neurosci.* 30, 1582–1594.

Molnar, Z., Metin, C., Stoykova, A., Tarabykin, V., Price, D. J., Francis, F., et al. (2006). Comparative aspects of cerebral cortical development. *Eur. J. Neurosci.* 23, 921–934.

Moreno, H., Vega-Saenz de Miera, E., Nadal, M. S., Amarillo, Y., and Rudy, B. (2001). Modulation of Kv3 potassium channels expressed in CHO cells by a nitric oxide-activated phosphatase. *J. Physiol.* 530, 345–358.

Moritz, G. C., Tenorio, F., Allodi, S., and Mendez-Otero, A. (1999). Expression of nitric oxide synthase in the developing rat hippocampus. *Neurosci. Lett.* 263, 89–92.

Oláh, S., Füle, M., Komlósi, G., Varga, C., Báldi, R., Barzó, P., et al. (2009). Regulation of cortical microcircuits by unitary GABA-mediated volume transmission. *Nature* 461, 1278–1281.

Overstreet, L. S., and Westbrook, G. L. (2003). Synapse density regulates independence at unitary inhibitory synapses. *J. Neurosci.* 23, 2618–2626.

Pape, H. C., and Mager, R. (1992). Nitric oxide controls oscillatory activity in thalamocortical neurons. *Neuron* 9, 441–448.

Perrenoud, Q., Geoffroy, H., Gautier, B., Rancillac, A., Alfonsi, F., Kessaris, N., et al. (2012a). Characterisation of type I and type II nNOS-expressing interneurons in the barrel cortex of mouse. *Front. Neural Circuits* 6:36. doi: 10.3389/fncir.2012.00036

Perrenoud, Q., Rossier, J., Férézou, I., Geoffroy, H., Gallopin, T., Vitalis, T., et al. (2012b). Activation of cortical 5-HT_3 receptor-expressing interneurons induces NO mediated vasodilatations and NPY mediated vasoconstrictions. *Front. Neural Circuits* 6:50. doi: 10.3389/fncir.2012.00050

Petanjek, Z., Berger, B., and Esclapez, M. (2009a). Origins of cortical GABAergic neurons in the cynomolgus monkey. *Cereb. Cortex* 19, 249–262.

Petanjek, Z., Kostovic, I., and Esclapez, M. (2009b). Primate-specific origins and migration of cortical GABAergic neurons. *Front. Neuroanat.* 3:26. doi: 10.3389/neuro.05.026.2009

Petilla Interneuron Nomenclature Group, Ascoli, G. A., Alonso-Nanclares, L., Anderson, S. A., Barrionuevo, G., Benavides-Piccione, R., Burkhalter, A., et al. (2008). Petilla terminology: nomenclature of features of GABAergic interneurons of the cerebral cortex. *Nat. Rev. Neurosci.* 9, 557–568.

Pleasure, S. J., Anderson, S., Hevner, R., Bagri, A., Marin, O., Lowenstein, D. H., et al. (2000). Cell migration from the ganglionic eminences is required for the development of hippocampal GABAergic interneurons. *Neuron* 28, 727–740.

Polleux, F., Whitford, K. L., Dijkhuizen, P. A., Vitalis, T., and Ghosh, A. (2002). Control of cortical interneuron migration by neurotrophins and PI3-kinase signaling. *Development* 129, 3147–3160.

Powell, E. M., Mars, W. M., and Levitt, P. (2001). Hepatocyte growth factor/scatter factor is a motogen for interneurons migrating from the ventral to dorsal telencephalon. *Neuron* 30, 79–89.

Pozas, E., and Ibanez, C. F. (2005). GDNF and GFRalpha1 promote differentiation and tangential migration of cortical GABAergic neurons. *Neuron* 45, 701–713.

Prast, H., and Philippu, A. (2001). Nitric oxide as modulator of neuronal function. *Prog. Neurobiol.* 64, 51–68.

Price, C. J., Cauli, B., Kovacs, E. R., Kulik, A., Lambolez, B., Shigemoto, R., et al. (2005). Neurogliaform neurons form a novel inhibitory network in the hippocampal CA1 area. *J. Neurosci.* 25, 6775–6786.

Price, C. J., Scott, R., Rusakov, D. A., and Capogna, M. (2008). GABA(B) receptor modulation of feedforward inhibition through hippocampal neurogliaform cells. *J. Neurosci.* 28, 6974–6982.

Rakic, P. (2009). Evolution of the neocortex: a perspective from developmental biology. *Nat. Rev. Neurosci.* 10, 724–735.

Rancillac, A., Rossier, J., Guille, M., Tong, X. K., Geoffroy, H., Amatore, C., et al. (2006). Glutamatergic control of microvascular tone by distinct GABA neurons in the cerebellun. *J. Neurosci.* 26, 6997–7006.

Riccio, O., Murthy, S., Szabo, G., Vutskits, L., Kiss, J. Z., Vitalis, T., et al. (2012). New pool of cortical interneuron precursors in the early postnatal dorsal white matter. *Cereb. Cortex* 22, 86–98.

Roerig, B., and Feller, M. B. (2000). Neurotransmitters and gap junctions in developing neural circuits. *Brain Res. Brain Res. Rev.* 32, 86–114.

Rörig, B., and Sutor, B. (1996a). Regulation of gap junction coupling in the developing neocortex. *Mol. Neurobiol.* 12, 225–249.

Rörig, B., and Sutor, B. (1996b). Nitric oxide-stimulated increase in intracellular cGMP modulates gap junction coupling in rat neocortex. *Neuroreport* 7, 569–572.

Rubenstein, J. L., and Merzenich, M. M. (2003). Model of autism: increased ratio of excitation/inhibition in key neural systems. *Genes Brain Behav.* 2, 255–267.

Rudy, B., and McBain, C. J. (2001). Kv3 channels: voltage-gated K^+ channels designed for high-frequency repetitive firing. *Trends Neurosci.* 24, 517–526.

Santacana, M., Uttenthal, L. O., Bentura, M. L., Fernandez, A. P., Serrano, J., Martinez de Velasco, J., et al. (1998). Expression of neuronal nitric oxide synthase during embryonic development of the rat cerebral cortex. *Dev. Brain Res.* 111, 205–222.

Smiley, J. F., McGinnis, J. P., and Javitt, D. C. (2000). Nitric oxide synthase interneurons in the monkey cerebral cortex are subsets of the somatostatin, neuropeptide Y, and calbindin cells. *Brain Res.* 863, 205–212.

Snyder, S. H., Jaffrey, S. R., and Zakhary, R. (1998). Nitric oxide and carbon monoxide: parallel roles as neural messengers. *Brain Res. Rev.* 26, 167–175.

Somogyi, J., Szabo, A., Somogyi, P., and Lamsa, K. (2012). Molecular analysis of ivy cells of the hippocampal CA1 stratum radiatum using spectral identification of immunofluorophores. *Front. Neural Circuits* 6:35. doi: 10.3389/fncir.2012.00035

Somogyi, P., and Klausberger, T. (2005). Defined types of cortical interneurone structure space and spike timing in the hippocampus. *J. Physiol.* 562, 9–26.

Steinert, J. R., Chenova, T., and Forsythe, I. D. (2010). Nitric oxide signaling in brain function, dysfunction, and dementia. *Neuroscientist* 16, 435–452.

Steinert, J. R., Kopp-Scheinpflug, C., Baker, C., Challiss, R. A., Mistry, R., Haustein, M. D., et al. (2008). Nitric oxide is a

volume transmitter regulating postsynaptic excitability at a glutamatergic synapse. *Neuron* 60, 642–656.

Steinert, J. R., Robinson, S. W., Tong, H., Haustein, M. D., Kopp-Scheinpflug, C., and Forsythe, I. D. (2011). Nitric oxide is an activity-dependent regulator of target neuron intrinsic excitability. *Neuron* 71, 291–305.

Sussel, L., Marin, O., Kimura, S., and Rubenstein, J. L. (1999). Loss of Nkx2.1 homeobox gene function results in a ventral to dorsal molecular respecification within the basal telencephalon: evidence for a transformation of the pallidum into the striatum. *Development* 126, 3359–3370.

Szabadics, J., Varga, C., Brunner, J., Chen, K., and Soltesz, I. (2010). Granule cells in the CA3 area. *J. Neurosci.* 30, 8296–8307.

Szabo, A., Somogyi, J., Cauli, B., Lambolez, B., Somogyi, P., and Lamsa, K. P. (2012). Calcium-permeable AMPA receptors provide a common mechanism for LTP in glutamatergic synapses of distinct hippocampal interneuron types. *J. Neurosci.* 32, 6511–6516.

Taniguchi, H., He, M., Wu, P., Kim, S., Paik, R., Sugino, K., et al. (2011). A resource of Cre driver lines for genetic targeting of GABAergic neurons in cerebral cortex. *Neuron* 71, 995–1013.

Tansey, E. P., Chow, A., Rudy, B., and McBain, C. J. (2002). Developmental expression of potassium-channel subunit Kv3.2 within subpopulations of mouse hippocampal inhibitory interneurons. *Hippocampus* 12, 137–148.

Tomioka, R., Okamoto, K., Furuta, T., Fujiyama, F., Iwasato, T., Yanagawa, Y., et al. (2005). Demonstration of long-range GABAergic connections distributed throughout the mouse neocortex. *Eur. J. Neurosci.* 21, 1587–1600.

Tricoire, L., Pelkey, K. A., Daw, M. I., Sousa, V. H., Miyoshi, G., Jeffries, B., et al. (2010). Common origins of hippocampal Ivy and nitric oxide synthase expressing neurogliaform cells. *J. Neurosci.* 30, 2165–2176.

Tricoire, L., Pelkey, K. A., Erkkila, B. E., Jeffries, B. W., Yuan, X., and McBain, C. J. (2011). A blueprint for the spatiotemporal origins of mouse hippocampal interneuron diversity. *J. Neurosci.* 31, 10948–10970.

Uylings, H. B. M., Van Eden, C. G., Parnavelas, J. G., Kalsbeek, A. (1990). "The prenatal and postnatal development of the rat cerebral cortex," in *The Cerebral Cortex of the Rat,* eds B. Kolb and R. C. Tees (Cambridge, MA: MIT Press), 35–76.

Van der Loos, H., and Woolsey, T. A. (1973). Somatosensory cortex: structural alterations following early injury to sense organs. *Science* 179, 395–398.

Vercelli, A., Garbossa, D., Biasiol, S., Repici, M., and Jhaveri, S. (2000). NOS inhibition during postnatal development leads to increased ipsilateral retinocollicular and retinogeniculate projections in rats. *Eur. J. Neurosci.* 1, 473–490.

Vercelli, A., Repici, M., Biasiol, S., and Jhaveri, S. (1999). Maturation of NADPH-d activity in the rat barrel-field cortex and its relationship to cytochrome oxidase activity. *Exp. Neurol.* 156, 294–315.

Verhage, M., Maia, A. S., Plomp, J. J., Brussaard, A. B., Heerona, J. H., Vermeer, H., et al. (2000). Synaptic assembly of the brain in absence of neurotransmitter secretion. *Science* 287, 864–869.

Vida, I., Halasy, K., Szinyei, C., Somogyi, P., and Buhl, E. H. (1998). Unitary IPSPs evoked by interneurons at the stratum radiatum-stratum lacunosum-moleculare border in the CA1 area of the rat hippocampus *in vitro*. *J. Physiol.* 506, 755–773.

Vitalis, T., and Rossier, J. (2011). New insights into cortical interneurons development and cl assification: contribution of developmental studies. *Dev. Neurobiol.* 71, 34–44.

Vruwink, M., Schmidt, H. H., Weinberg, R., and Burette, A. (2001). Substance P and nitric oxide signaling in cerebral cortex: anatomical evidence for reciprocal signaling between two classes of interneurons. *J. Comp. Neurol.* 441, 288–301.

Vucurovic, K., Gallopin, T., Ferezou, I., Rancillac, A., Chameau, P., van Hooft, J., et al. (2010). Serotonin 3A receptor subtype as an early and protracted marker of cortical interneuron subpopulations. *Cereb. Cortex* 20, 2333–2347.

Wei, W., Zhang, N., Peng, Z., Houser, C. R., and Mody, I. (2003). Perisynaptic localization of delta subunit-containing GABA(A) receptors and their activation by GABA spillover in the mouse dentate gyrus. *J. Neurosci.* 23, 10650–10661.

Wichterle, H., Garcia-Verdugo, J. M., Herrera, D. G., and Alvarez-Buylla, A. (1999). Young neurons from medial ganglionic eminence disperse in adult and embryonic brain. *Nat. Neurosci.* 2, 461–466.

Wonders, C. P., and Anderson, S. A. (2006). The origin and specification of cortical interneurons. *Nat. Rev. Neurosci.* 7, 687–696.

Wonders, C. P., Taylor, L., Welagen, J., Mbata, I. C., Xiang, J. Z., and Anderson, S. A. (2008). A spatial bias for the origins of interneuron subgroups within the medial ganglionic eminence. *Dev. Biol.* 314, 127–136.

Wu, H. H., Cork, R. J., Huang, P. L., Shuman, D. L., and Mize, R. R. (2000). Refinement of the ispilateral retinocollicular projection is disrupted in double endothelial and neuronal nitric oxide sythase gene knockout mice. *Dev. Brain Res.* 120, 105–111.

Wu, H. H., Waid, D. K., and McLoon, S. C. (1996). Nitric oxide and the developmental remodeling of retinal connections in the brain. *Prog. Brain Res.* 108, 273–286.

Xiong, H., Yamada, K., Han, D., Nabeshima, T., Enikolopov, G., Carnahan, J., et al. (1999). Mutual regulation between the intercellular messenger nitric oxide and brain-derived neurotrophic factor in rodent neocortical neurons. *Eur. J. Neurosci.* 11, 1567–1576.

Xu, Q., Cobos, I., De La Cruz, E., Rubenstein, J. L., and Anderson, S. A. (2004). Origins of cortical interneuron subtypes. *J. Neurosci.* 24, 2612–2622.

Yan, X. X., and Garey, L. J. (1997). Morphological diversity of nitric oxide synthesising neurons in mammalian cerebral cortex. *J. Hirnforsch.* 38, 165–172.

Yan, X. X., Jen, L. S., and Garey, L. J. (1996). NADPH-diaphorase-positive neurons in primate cerebral cortex colocalize with GABA and calcium-binding proteins. *Cereb. Cortex* 6, 524–529.

Zecevic, N., Hu, F., and Jakovcevski, I. (2011). Interneurons in the developing human neocortex. *Dev. Neurobiol.* 71, 18–33.

Zsiros, V., and Maccaferri, G. (2005). Electrical coupling between interneurons with different excitable properties in the stratum lacunosum-moleculare of the juvenile CA1 rat hippocampus. *J. Neurosci.* 25, 8686–8695.

Conflict of Interest Statement: The authors declare that the research was conducted in the absence of any commercial or financial relationships that could be construed as a potential conflict of interest.

Received: 25 May 2012; accepted: 25 October 2012; published online: 05 December 2012.

Citation: Tricoire L and Vitalis T (2012) Neuronal nitric oxide synthase expressing neurons: a journey from birth to neuronal circuits. Front. Neural Circuits ***6****:82. doi: 10.3389/fncir.2012.00082*

frontiers in
NEURAL CIRCUITS

ORIGINAL RESEARCH ARTICLE
published: 05 June 2012
doi: 10.3389/fncir.2012.00031

Cortical nNOS neurons co-express the NK1 receptor and are depolarized by Substance P in multiple mammalian species

Lars Dittrich[1]*†, Jaime E. Heiss[1†], Deepti R. Warrier[1], Xiomara A. Perez[2], Maryka Quik[2] and Thomas S. Kilduff[1]

[1] Biosciences Division, Center for Neuroscience, SRI International, Menlo Park, CA, USA
[2] Policy Division, Center for Health Sciences, SRI International, Menlo Park, CA, USA

Edited by:
Bruno Cauli, Université Pierre et Marie Curie, France

Reviewed by:
Yoshiyuki Kubota, National Institute for Physiological Sciences, Japan
Thierry Gallopin, Ecole Supérieur de Physique et de Chimie Industrielle, France

***Correspondence:**
Lars Dittrich, Biosciences Division, Center for Neuroscience, SRI International, 333 Ravenswood Avenue, LA 229, Menlo Park, CA 94025, USA.
e-mail: lars.dittrich@sri.com

† These authors contributed equally to this work.

We have previously demonstrated that Type I neuronal nitric oxide synthase (nNOS)-expressing neurons are sleep-active in the cortex of mice, rats, and hamsters. These neurons are known to be GABAergic, to express Neuropeptide Y (NPY) and, in rats, to co-express the Substance P (SP) receptor NK1, suggesting a possible role for SP in sleep/wake regulation. To evaluate the degree of co-expression of nNOS and NK1 in the cortex among mammals, we used double immunofluorescence for nNOS and NK1 and determined the anatomical distribution in mouse, rat, and squirrel monkey cortex. Type I nNOS neurons co-expressed NK1 in all three species although the anatomical distribution within the cortex was species-specific. We then performed *in vitro* patch clamp recordings in cortical neurons in mouse and rat slices using the SP conjugate tetramethylrhodamine-SP (TMR-SP) to identify NK1-expressing cells and evaluated the effects of SP on these neurons. Bath application of SP (0.03–1 μM) resulted in a sustained increase in firing rate of these neurons; depolarization persisted in the presence of tetrodotoxin. These results suggest a conserved role for SP in the regulation of cortical sleep-active neurons in mammals.

Keywords: nitric oxide, NOS-1, bNOS, sleep homeostasis, cerebral cortex, neurogliaform, *tac1, tac1r*

INTRODUCTION

Sleep is homeostatically regulated, such that increasing time awake causes elevation in sleep pressure. The neurobiological substrates of this homeostasis remain unclear (Kilduff et al., 2011). Using Fos immunoreactivity as a neural activity marker, we recently found that GABAergic cortical interneurons expressing neuronal nitric oxide synthase (nNOS) are selectively activated during sleep in three rodent species (Gerashchenko et al., 2008). Since the proportion of nNOS neurons expressing Fos was correlated with slow wave energy, an electroencephalographic (EEG) indicator of sleep pressure, we have proposed that these neurons are involved in the regulation or mediation of the homeostatic recovery process that occurs during sleep (Kilduff et al., 2011).

Two morphological types of cortical nNOS neurons have been identified in primates (Aoki et al., 1993; Lüth et al., 1994). Type I nNOS neurons have larger somata and show intense labeling with antisera to nNOS, as well as with histochemical staining of nicotinamide adenine dinucleotide phosphate diaphorase (NADPH-d), whereas type II neurons have smaller somata and show weaker labeling. More recently, both types of nNOS neurons were confirmed in rodents using NADPH-d staining (Pereira et al., 2000; Freire et al., 2004, 2005) and immunohistochemistry to nNOS (Yousef et al., 2004; Lee and Jeon, 2005; Cho et al., 2010). The sleep-active cortical nNOS neurons are intensely labeled for nNOS and thus correspond to type I cells (Gerashchenko et al., 2008).

In a detailed classification study of rat cortical interneurons (Kubota et al., 2011), type I nNOS neurons were found to be one of the smallest classes of interneurons and a subgroup of the cells immunoreactive for both neuropeptide Y (NPY) and somatostatin (SST). This study also confirmed an earlier finding (Vruwink et al., 2001) that type I nNOS neurons co-express the Substance P (SP) receptor NK1. These reports imply that cortical SP may act as a modulator of cortical sleep-active neurons. To date, no data are available about co-expression of nNOS and NK1 in the cortex of other mammals.

SP is one of the most abundant peptides in the central nervous system and has been implicated in a variety of physiological and pathophysiological processes. Most of the early research focused on its role in nociception, particularly in the spinal cord (reviewed by Hill, 2000). More recent research has established a role for SP in other nervous system functions, such as stress and addiction (reviews in Ebner and Singewald, 2006; Commons, 2010). However, evidence for a role of SP in sleep/wake regulation is sparse and inconclusive (see Nishino and Fujiki, 2007). While activation of the NK1 receptor on neurons usually causes depolarization (Dreifuss and Raggenbass, 1986; Maubach et al., 1998; Zaninetti and Raggenbass, 2000; Ito et al., 2002; Bailey et al., 2004; Blomeley and Bracci, 2008; Morozova et al., 2008;

Paul and Cox, 2010), NK1 activation can also have hyperpolarizing effects (Jafri and Weinreich, 1996). The effects of NK1 agonists in most cortical areas and on nNOS neurons in particular are unexplored to this point.

The aims of this study were to identify whether the presence of the NK1 receptor in type I nNOS neurons generalizes to other mammals and to determine the effects of SP on cortical NK1/nNOS neurons. To address these questions, we performed double immunofluorescence for nNOS and NK1 in mouse, rat, and squirrel monkey cortical tissue and conducted *in vitro* patch clamp recordings of NK1 neurons in cortical slices from mice and rats.

MATERIALS AND METHODS

ANIMALS

Five male C57BL/six mice (4–5 weeks of age), five male Sprague–Dawley rats (5–6 months of age), and three squirrel monkeys (*Saimiri sciureus* two female, 687 g and 740 g; one male, 908 g; approximately five-years old) were used for immunofluorescence. Nine male Sprague–Dawley rats (3–6 weeks of age) and 29 NPY-hrGFP mice [*B6.FVB-Tg(Npy-hrGFP)1Lowl/J*, JAX® Mice, Sacramento, CA; 3–6 weeks of age] of both sexes were used for *in vitro* recordings. NPY-hrGFP mice express humanized *Renilla* green fluorescent protein under control of the mouse NPY promoter (van den Pol et al., 2009). An additional NPY-hrGFP mouse was used for nNOS immunofluorescence. Mice and rats were housed with *ad libitum* access to food and water under a 12 h light/dark cycle for at least seven days before use in an experiment. Squirrel monkeys were purchased from Worldwide Primates (Miami, FL) and quarantined for one month according to California state regulations. All studies were performed according to guidelines approved by the SRI International Institutional Animal Care and Use Committee in conformance with the United States Public Health Service *Guidelines on Care and Use of Animals in Research*. Every effort was made to minimize the number of animals utilized in this study and to eliminate suffering.

IMMUNOFLUORESCENCE

Tissue preparation

Mice and rats were anesthetized with an overdose of euthanasia solution (0.1 ml and 1 ml, respectively, 390 mg/ml sodium pentobarbital and 50 mg/ml phenytoin sodium, Beuthanasia-D, Intervet, Summit, NJ) i.p. and intracardially perfused with heparinized phosphate buffered saline (PBS, 0.01 M, pH 7.2–7.4) followed by 4% paraformaldehyde in PBS. Brains were postfixed in the fixative overnight at 4°C. Monkeys were injected with 1.5 ml euthanasia solution (390 mg/ml sodium pentobarbital and 50 mg/ml phenytoin sodium, Euthasol, Henry Schein, Melville, NY) i.p., followed by 1.5 ml/kg of the same solution administered intravenously. The brains were rapidly removed, rinsed in cold PBS, placed in a squirrel monkey brain mold, and cut into 2 mm-thick blocks using stainless steel blades. For each animal, two blocks were immersion fixed in 4% paraformaldehyde in PBS overnight at 4°C. The remaining blocks were used for unrelated studies. All tissue was cryoprotected in 30% sucrose in PBS at 4°C. Coronal 40 μm sections were cut on a freezing microtome and stored at –20°C in 30% ethylene glycol and 20% glycerol in PBS until use.

Labeling and visualization

All incubations were performed on free-floating sections at room temperature (RT). From each brain, one anterior and one posterior section were selected. The anterior-posterior levels were +1.1 and −2.3 mm from bregma for mice (Paxinos and Franklin, 2001) and +2.04 and −4.44 for rats (Paxinos and Watson, 2007). For monkeys, the frontal section was anterior of the striatum (frontal of A15 according to Emmers and Akert (1963) and about section 180 of the squirrel monkey brain atlas at http://brainmuseum.org) and P0.5 (Emmers and Akert, 1963). For monkeys, only about half of the anterior section was available for this study. For two monkeys, this was mainly the superior frontal gyrus; for the other monkey, it was mainly the inferior frontal gyrus.

Endogenous peroxidase activity was quenched by 15 min incubation in 1% H_2O_2 in PBS. Sections were preincubated for 1 h in 5% normal donkey serum with 0.3% Triton and 0.1% sodium azide in PBS. Endogenous biotin was blocked by 15 min incubation in avidin solution followed by 15 min incubation in biotin solution (Vector Laboratories, Burlingame, CA). Incubation in primary antibody was performed overnight with a cocktail of mouse anti-nNOS antibody (N2280, Sigma-Aldrich, Milwaukee, WI) and rabbit anti-NK1 antibody (gift from Prof. R. Shigemoto, National Institute for Physiological Sciences, Okazaki, Japan). For immunofluorescence of one NPY-hrGFP mouse, the NK1 antibody was omitted. The concentrations utilized were determined by titration for optimal labeling for each species and were 0.25 μg/ml anti-NK1 and 180 μg/ml anti-nNOS for mouse, 0.1 μg/ml anti-NK1 and 180 μg/ml anti-nNOS for rat, and 0.5 μg/ml anti-NK1 and 450 μg/ml anti-nNOS for monkey tissue. As a negative control, the primary antibodies were omitted on additional sections of each species. nNOS was visualized with a donkey anti-mouse secondary antibody conjugated to Alexa Fluor 546 (Invitrogen, Chicago, IL, 1:500, 2 h). NK1 was visualized using a Tyramide Signal Amplification Fluorescein system (Perkin-Elmer, Los Angeles, CA), preceded by a 2 h incubation with biotinylated secondary antibody (Jackson ImmunoResearch, West Grove, PA, 2.6 μg/ml for rodents, 1.3 μg/ml for monkeys) and a 2 h incubation with an avidin-biotinylated peroxidase complex (Vector Laboratories, 1:200). Sections were mounted on glass slides, dehydrated in a graded series of alcohol, cleared with xylenes, and cover slipped in Depex (Electron Microscopy Sciences, Hatfield, PA) for permanent mounting (Espada et al., 2005). Labeled cell profiles in the neocortex and underlying white matter in one hemisphere of each section were counted at 400× magnification using Stereoinvestigator software (MBF Bioscience, Williston, VT).

In vitro ELECTROPHYSIOLOGY

Slice preparation

Rodents were deeply anesthetized with isofluorane and then decapitated. Brains were isolated in ice-cold oxygenated high sucrose solution containing (mM): sucrose 234, KCl 2.5, $CaCl_2$ 0.5, NaH_2PO_4 1.25, $MgSO_4$ 10, glucose 11, bubbled with 95% O_2–5% CO_2. Coronal brain slices (250 μm thickness) of the

region containing the rostral-most 2 mm of the striatum were cut with a microtome (VT-1000S, Leica, Germany). Slices were then transferred to an incubation chamber where they were superfused with physiological bicarbonate solution containing (mM): NaCl 123, KCl 3, $CaCl_2$ 2, $NaHCO_3$ 26, glucose 11, NaH_2PO_4 1.25, $MgCl_2$ 1, bubbled with 95% O_2–5% CO_2 at RT (22–24°C) for at least 1 h before recordings. The osmolarity of these external solutions was checked by a vapor pressure osmometer (Advanced Instruments, Norwood, MA) and ranged between 295 and 305 mOsmol l^{-1}.

Whole-cell patch clamp recordings

Patch pipettes were prepared from borosilicate capillary glass (G150F-4, Warner Instruments LLC, Hamden, CT) with a micropipette puller (P-97, Sutter Instruments, Novato, CA). The pipettes were routinely filled with a KGlu-internal solution containing (mM): KGluconate 125, KCl 10, $MgCl_2$ 1, EGTA 5, Hepes 10, MgATP 1, NaGTP 0.5, adjusted to pH 7.25 with KOH. For some experiments, 8 mM biocytin was added to the internal solution for *post-hoc* characterization of the recorded neurons. The osmolarity of these internal solutions was between 290 and 305 mOsmol l^{-1}. Pipette resistance measured in the external solution was 4–8 MΩ. The series resistance during recording was 12–48 MΩ and was compensated while recording in current-clamp mode. The reference electrode was an Ag–AgCl pellet immersed in the bath solution. The liquid junction potential was estimated to be 15 mV and was subtracted from the recorded membrane potential.

For electrophysiological recordings, a single slice was transferred to a recording chamber (RC-26G, Warner Instruments LLC, Hamden, CT) and superfused with the physiological bicarbonate solution at RT at a flow rate of 2 ml/min. For *in vitro* identification of live neurons expressing the NK1 receptor, 50–80 nM of tetramethylrhodamine conjugated to Substance P (TMR-SP) from Enzo Life Sciences, NY (Labrakakis and MacDermott, 2003; Pagliardini et al., 2005; Torsney and MacDermott, 2006) was added to the bath for 3 min (from a 56 μM stock solution in H_2O stored at −20°C) and slices were washed for at least 30 min before identification of labeled neurons. Cortical cells were visualized under an upright microscope (Leica DM LFSA, Leica Microsystems, Germany) using both infrared-differential interference contrast (IR-DIC) microscopy and fluorescence microscopy. Infrared images were acquired via a charge-coupled device (CCD) camera optimized for infrared wavelengths (DAGE-MITI, Michigan City, IN); fluorescence images were acquired using a digital microscope camera (ProgRes® MF, JENOPTIK Optical Systems GmbH, Germany). Recording pipettes were advanced toward individual NPY and/or TMR-SP fluorescent labeled cells in the slice under positive pressure and, on contact, tight seals between the pipette and the cell membrane on the order of 1–4 GΩ were made by negative pressure. The membrane patch was then ruptured by suction and membrane potential was monitored in current-clamp mode using a Multiclamp 700A amplifier (Molecular Devices, Sunnyvale, CA). Only cells in which the resting membrane potential (E_r) was below −50 mV were included in this study. The output voltage signal was low-pass filtered at 3 kHz and digitized at 10 kHz. Data were recorded on a computer through a Digidata 1320A A/D converter using pCLAMP software version 9.2 (Molecular Devices, Sunnyvale, CA). Recorded data were processed and plotted using Matlab R2010b (Mathworks, Natick, MA). For statistical comparisons, values were compared using analysis of variance (ANOVA) and the two samples, unpaired *t*-test with the program GNU Octave (http://www.gnu.org/software/octave/).

Characterization of recorded neurons at rest and after application of SP

At the initiation of whole-cell recordings, three different negative pulses of 1 s were delivered every 2 s in order to obtain three levels of hyperpolarization. The cell capacitance was determined by fitting the initial 300 ms of the hyperpolarizing pulse to a single exponential and averaging the three values obtained. The input resistance (R_{in}) at each hyperpolarization level was calculated as the maximal change in voltage obtained within these 300 ms divided by the injected current. R_{in} in absence of injected current was calculated by linear regression. E_r of the cells was calculated by averaging 100 ms of membrane potential at rest. 1 mM stock solutions of SP in H_2O (Sigma Aldrich, St. Louis, MO) were stored at −20°C in 0.2 ml aliquots. After verifying that the whole-cell recording was stable, SP was further diluted in bubbling artificial cerebrospinal fluid (ACSF) to obtain a final concentration of 0.03–1 μM and was applied in the bath for 30–120 s. In a similar fashion, tetrodotoxin (TTX; Abcam, Cambridge, MA) was also added to an additional container of oxygenated ACSF with or without SP at a final concentration of 1 μM prior to bath application. With SP in the bath, hyperpolarizing pulses (40–50 pA, 200 ms duration) were applied to cells at 10 s intervals to monitor R_{in} over time. SP-induced changes in firing rate were calculated by averaging the firing rate every 10 s. In order to detect spikes, traces were high-pass filtered over 100 Hz using a zero-phase forward and reverse digital Butterworth filter of sixth order. For every filtered trace, an amplitude threshold was manually determined and the onset of the spike was determined as the crossing of the threshold in the positive direction.

RESULTS

CORTICAL nNOS NEURONS CO-EXPRESS NK1

In all three species, almost all cortical nNOS neurons were found to co-express NK1: 90.8% (466 of 513) of nNOS neurons in mice, 98.7% (912 of 914) of nNOS neurons in rats, and 90.9% (1320 of 1452) of nNOS neurons in monkeys were co-labeled for NK1. In contrast, the proportion of single-labeled NK1 neurons differed greatly between species. While they were virtually absent in mice (3.5%, 17 of 483), single-labeled NK1 neurons constituted a significant population in rats (30.7%, 403 of 1315). In monkeys, single-labeled NK1 neurons outnumbered those co-labeled for nNOS (58.2%, 1834 of 3154).

The distribution of labeled neurons also differed between species. In mice, nNOS neurons were located mainly in the deep gray matter (**Figures 1A,A'**). In rats, nNOS neurons were scattered throughout all cortical layers (**Figures 1B,B'**). In monkeys, nNOS neurons were concentrated on both sides of the white matter-gray matter border (**Figures 1C,C'**). Single-labeled NK1 neurons were

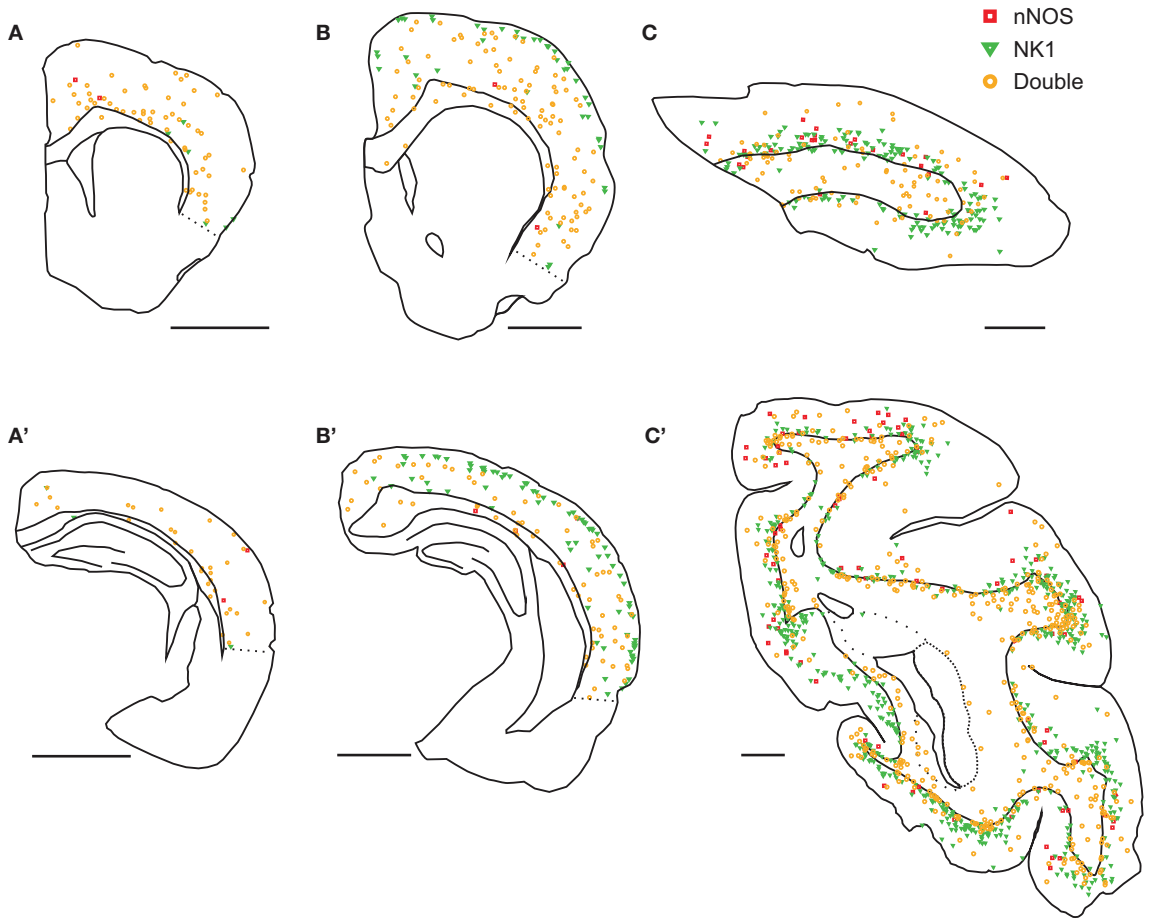

FIGURE 1 | Distribution of nNOS and NK1 cells in the neocortex of three mammalian species. In mice **(A,A')**, virtually all cells were double-labeled for nNOS and NK1 (orange) and were most abundant in deep gray matter. Neurons single-labeled for nNOS (red) or NK1 (green) were virtually absent. In rats **(B,B')**, double-labeled neurons were scattered throughout the cortex and underlying white matter; single-labeled nNOS neurons were virtually absent. Neurons single-labeled for NK1 were concentrated in superficial layers. In monkeys **(C,C')**, double-labeled neurons were most abundant in the deep gray matter and the underlying white matter and single-labeled nNOS neurons were rare. Neurons single-labeled for NK1 were concentrated in deep gray matter. Labeled neurons were more abundant in gyri than in sulci. **A, B,** and **C** are anterior sections, **A', B',** and **C'** are posterior sections. Scale bars denote 2 mm.

concentrated in the superficial gray matter in rats (**Figures 1B,B'**) and deep gray matter in monkeys (**Figures 1C,C'**). In monkeys, both cell types were more abundant in gyri than in sulci (**Figure 1C'**).

In all species, nNOS neurons showed a variable dendritic morphology with two or more primary dendrites (**Figure 2**). We observed some variability in cell size, with some neurons exhibiting exceptionally large somata. In rats and monkeys, single-labeled NK1 neurons were found to have a different morphology than those co-labeled for nNOS. In rats, single-labeled neurons were noticeably less intensely labeled and mostly smaller than double-labeled cells (**Figure 2B**). In monkeys, neurogliaform-like morphology with a round or oval soma and highly arborized short dendrites were the most distinctive characteristics of single-labeled NK1 neurons (**Figure 2D**). These cells were also often less intensely labeled and smaller than the double-labeled neurons (**Figure 2C**). In contrast, single-labeled nNOS neurons did not show apparent morphological differences from double-labeled neurons in any of the three species.

IDENTIFICATION OF SP-RESPONSIVE NEURONS *In vitro*

Since strongly immunoreactive cortical nNOS cells are a subgroup of NPY neurons in rats and mice (Tomioka et al., 2005; Gerashchenko et al., 2008; Kubota et al., 2011) and are concentrated in infragranular layers in mice, we initially targeted NPY neurons in infragranular layers of NPY-hrGFP mice in search of nNOS/NK1 neurons. However, only 16% (6 of 38) of neurons recorded in this manner were affected by application of 0.3–1 μM of SP in the bath. The low proportion of GFP-expressing neurons immunoreactive for nNOS in NPY-hrGFP mice is illustrated in **Figure 3**. Given the high degree of co-expression of nNOS and NK1 across species demonstrated above, we therefore used the NK1 ligand TMR-SP to increase the yield of nNOS neurons among NPY cells recorded *in vitro* in NPY-hrGFP mice

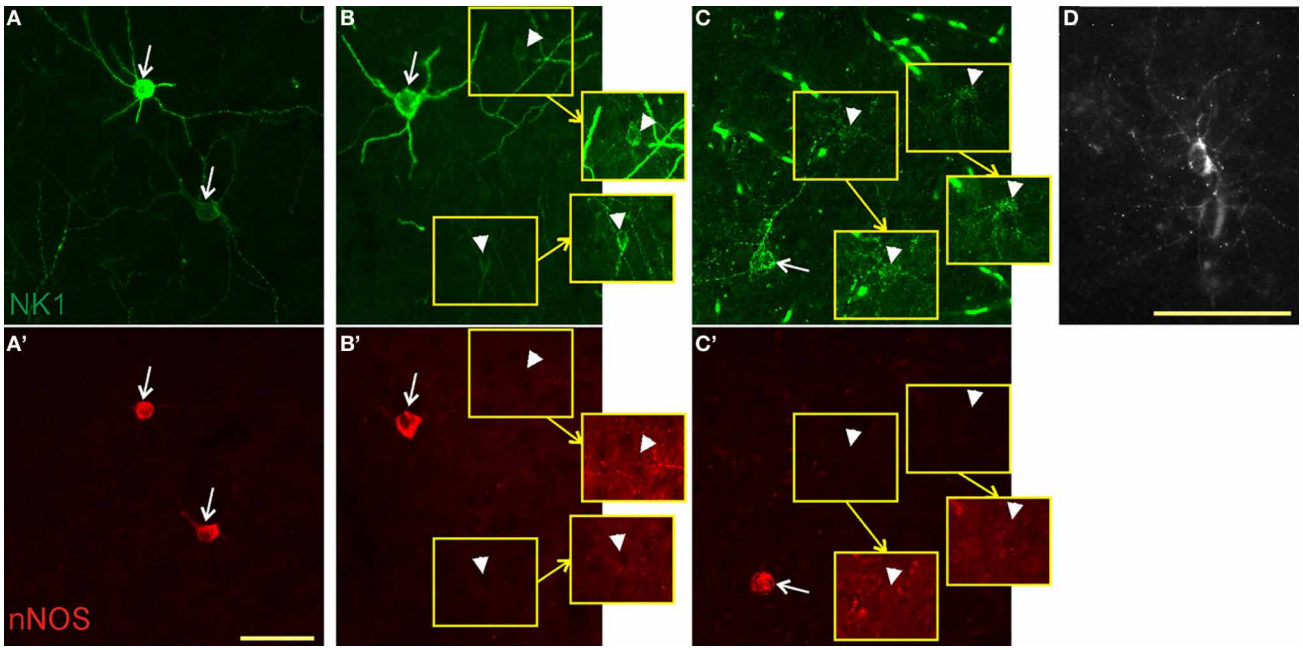

FIGURE 2 | Colocalization of NK1 and nNOS. In mice **(A,A')**, virtually all neurons were double-labeled (arrows) for NK1 (green, top panels) and nNOS (red, bottom panels). In rats **(B,B')**, we found both double-labeled neurons and neurons labeled for NK1 only (arrowheads). Neurons staining for NK1 alone had smaller somata and less intense labeling. Portions of the micrographs containing the weakly labeled NK1 neurons are displayed in the insets (yellow squares) with enhanced brightness to enable visibility. Note the absence of nNOS labeling in these neurons in **B'**. In monkeys **(C,C')**, double-labeled neurons had a dendritic arborization pattern similar to that of the other species, whereas neurons single-labeled for NK1 had round somata surrounded by short, thin, highly arborized dendrites. Fluorescent blood vessels are visible because monkeys were not perfused before fixation. The punctate pattern of NK1 labeling in **C** and the bottom cell in **A** is typical for NK1 endocytosis upon ligand binding. **(D)** A single-labeled NK1 neuron of monkey cortex at higher magnification for better visibility of the morphology. Note the highly arborized, short dendrites. Scale bars denote 50 μm. Micrographs were taken as monochrome pictures and pseudocolored for representation.

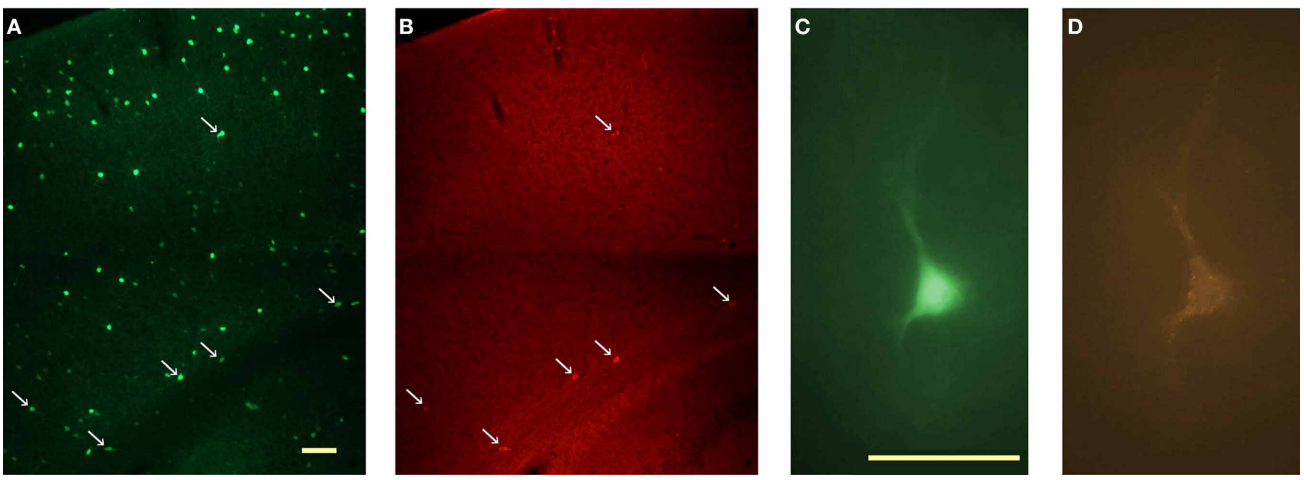

FIGURE 3 | *In vitro* identification of NK1$^+$ neurons in the cortex of NPY-hrGFP transgenic mice. (A) Visualization of NPY neurons in the cortex of NPY-hrGFP transgenic mice. This 40 μm section was processed for nNOS immunofluorescence. **(B)** nNOS-immunoreactive cells in the same section illustrated in **A**. nNOS neurons are located mainly in layer 6, adjacent to the white matter. Arrows in **A** and **B** denote neurons that show both green (GFP) and red (nNOS) fluorescence. Note the small proportion of NPY neurons co-expressing nNOS. **(C)** *In vitro* visualization of an NPY neuron for targeted patching. **(D)** Same cell as **C** illuminated with green light after a 3-min bath application of 56 nM TMR-SP followed by a 30 min wash. Micrographs in **C** and **D** are pseudocolored to resemble the original colors. Scale bar denotes 200 μm in **A**; 50 μm in **C**.

and to identify these neurons also in rats. A 3-min bath application of TMR-SP (56 nM) was sufficient to label neurons for more than 2 h. Since TMR-SP might produce effects in NK1 neurons comparable to SP itself, at least 30 min elapsed between TMR-SP application and initiation of a search for labeled cells for subsequent patching. **Figure 3C** shows a healthy NPY neuron visualized *in vitro*. After confirming the viability of the neuron by visualizing it under IR-DIC, the blue excitation was replaced by green illumination, thereby enabling visualization of TMR-SP-labeled neurons (**Figure 3D**). TMR-SP fluorescence was dim and could only be detected at 400× magnification. GFP fluorescence from NPY neurons could be detected at 50× magnification and was, therefore, used to aid identification of TMR-SP-labeled neurons in mice. No significant differences in E_r, R_{in}, capacitance, or time constant (τ) were observed when cells identified by TMR-SP ($N = 8$) were compared to SP-responsive NPY-hrGFP neurons that had not been exposed to TMR-SP ($N = 6$). Consequently, all SP-responsive neurons were considered as a single group for statistical analysis.

SP DIRECTLY DEPOLARIZES SP-RESPONSIVE NEURONS IN MICE AND RATS

To evaluate the effect of SP on neuronal firing rate, mouse cortical neurons were initially hyperpolarized with 0–10 pA to reduce spontaneous firing. Application of 0.03–1 μM SP induced on average (all values correspond to mean ± standard deviation) an increase in firing rate of 10.2 ± 4.9 spikes/s ($N = 11$). Blockade of voltage-dependent sodium channels by >5 min of bath application of 1 μM TTX was tested in seven cells. Addition of 0.03–0.3 μM SP induced a depolarization of 11.9 ± 4.6 mV ($N = 7$). SP-induced depolarization in the presence of TTX was found in all cells tested, indicating that the action of SP is most likely direct. **Figure 4A** shows an example of SP-induced depolarization of a neuron in mouse cortex. **Figure 4B** shows the membrane potential of a different neuron under TTX and its response to two successive applications of SP. The large variability observed in both the amplitude and the duration of the SP-induced depolarization for a given SP concentration precludes the elaboration of a dose response curve at the present time. Similar results were obtained for TMR-SP fluorescent neurons selected for recording in rat cortical slices, where bath application of 0.1–0.3 μM SP induced an increase of 5 ± 2 spikes/s ($N = 9$) in firing rate and, under 1 μM TTX, a depolarization of 8.1 ± 3.6 mV ($N = 5$ out of 5 neurons tested). **Figure 4C** shows an example of an SP-induced increase in firing rate of a TMR-SP-responsive cell in a rat cortical slice. **Figure 4D** shows a different neuron exhibiting a prolonged depolarization after 1 min application of SP.

SP-RESPONSIVE NEURONS HAVE DIFFERENT ELECTRICAL PROPERTIES THAN NON-SP-RESPONSIVE CELLS

By visual inspection of NPY neurons in mice, we did not observe a clear morphological difference that allowed distinction between SP-responsive ($NK1^+$) NPY cells and NPY neurons that did not respond to SP ($NK1^-$). However, during whole-cell recordings, striking differences were found in E_r, R_{in}, and τ of these cells. **Figure 5A** shows an example of the membrane potential of an $NK1^+$ neuron (orange trace) and an $NK1^-$ cell (black trace) during 1 s current pulses of −25, −50, and −75 pA. Although both cells were injected with the same three

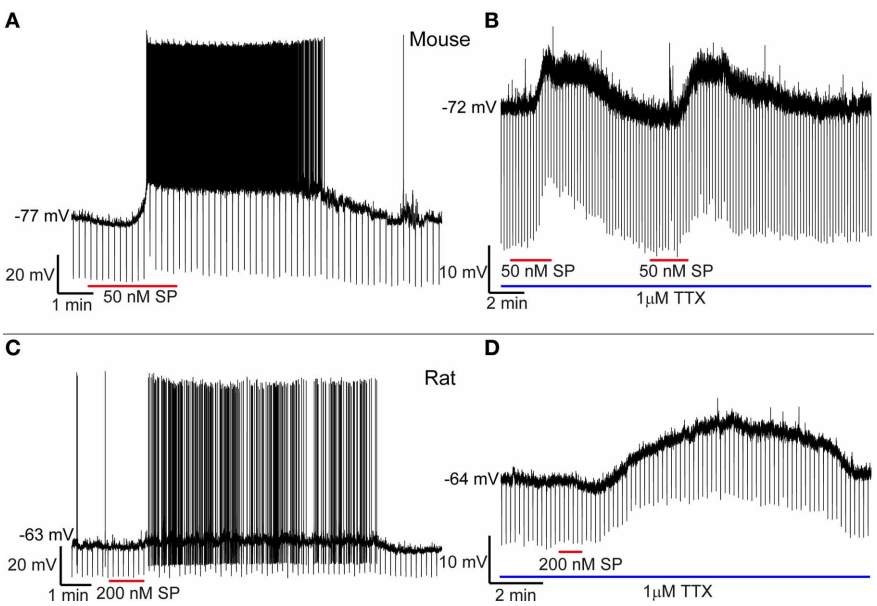

FIGURE 4 | SP depolarizes cortical $NK1^+$ neurons. (A) Application of 50 nM SP to the bath depolarizes an $NK1^+$ neuron in the mouse cortex and generates an increase in firing rate that persists for about 10 min. **(B)** Successive applications of 50 nM SP elicit similar responses during blockade of voltage-dependent Na^+ channels with TTX. **(C)** SP increases the firing rate of cortical $NK1^+$ neurons in the rat. **(D)** Under TTX blockade, rat $NK1^+$ cortical neurons can be depolarized for a prolonged period despite the short duration of SP bath application.

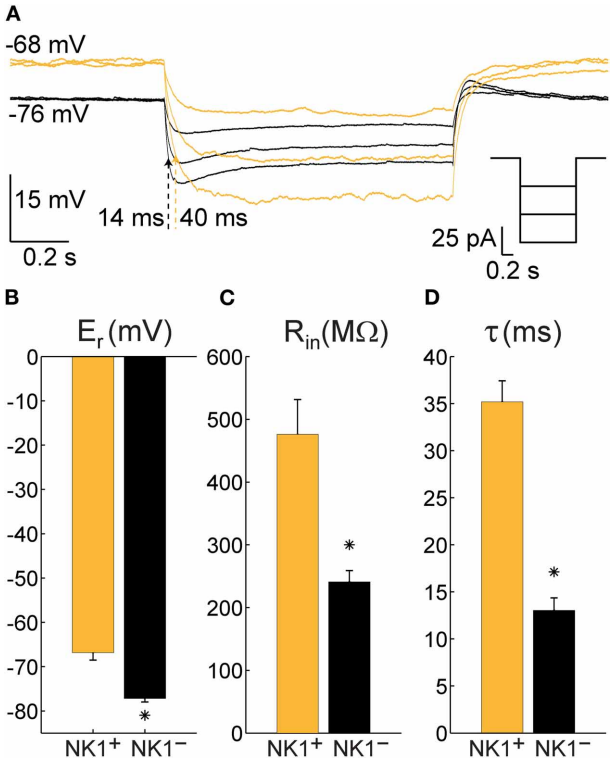

FIGURE 5 | Electrophysiological characteristics of NPY neurons recorded in cortical slices from NPY-hrGFP transgenic mice that are either NK1$^+$ ($N = 14$) or NK1$^-$ ($N = 31$). (A) Typical single trials of the membrane potential of an NK1$^+$ neuron (orange) and an NK1$^-$ neuron (black) in response to hyperpolarizing current injections showing a large difference in time constant (indicated by dotted arrows) and resting potential. Right inset depicts the injected currents for both neurons. **(B)** Mean and standard error of the membrane potential at rest (E_r) for all recorded NK1$^+$ and NK1$^-$ cells. **(C)** Mean and standard error of the input resistance at rest (R_{in}) for all recorded NK1$^+$ and NK1$^-$ neurons. **(D)** Mean and standard error of the time constant (τ, calculated as the product between input resistance and capacitance) for all cells where at least three steps of current were injected. The differences between NK1$^+$ and NK1$^-$ were highly significant in all three cases ($p < 3 \times 10^{-6}$).

levels of current, the larger R_{in} of the NK1$^+$ cell resulted in a greater change in membrane potential for a given amount of current injected and a longer τ (40 ms for the highest current injected, compared to $\tau = 14$ ms for the NK1$^-$ cell). One-way ANOVAs revealed that E_r, R_{in}, and τ were significantly different between mouse NK1$^+$, mouse NK1$^-$, and rat NK1$^+$ neurons [$F_{(2,\ 51)} = 35.98$, $p < 2 \times 10^{-10}$, $F_{(2,\ 51)} = 12.58$, $p < 4 \times 10^{-5}$; $F_{(2,\ 33)} = 31.21$, $p < 3 \times 10^{-8}$, respectively]. *Post-hoc* comparisons were performed using *t*-tests with Bonferroni-adjusted alpha levels of 0.017 (0.05/3). **Figure 5B** illustrates that mouse NK1$^+$ cells ($E_r = -66.9 \pm 5.9$ mV, $N = 14$) were more depolarized at rest than NK1$^-$ cells ($E_r = -77 \pm 4.4$ mV, $N = 31$), $t_{(43)} = 6.53$, $p < 6 \times 10^{-8}$. **Figure 5C** illustrates that R_{in} also differed between mouse NK1$^+$ cells (476 ± 192 MΩ, $N = 14$) and NK1$^-$ cells (241 ± 101 MΩ, $N = 31$), $t_{(43)} = 5.42$, $p < 3 \times 10^{-6}$; and **Figure 5D** illustrates that τ was longer for mouse NK1$^+$ cells (35.2 ± 7.4 ms, $N = 13$) than for NK1$^-$ cells (13 ± 4.9 ms, $N = 14$), $t_{(23)} = 9.24$, $p < 2 \times 10^{-9}$. The electrical parameters of rat NK1$^+$ neurons ($E_r = -63.1 \pm 6.3$ mV, $R_{in} = 332 \pm 195$ MΩ, and $\tau = 31 \pm 11$ ms) were not statistically different from mouse NK1$^+$ neurons [$t_{(21)} = 1.45$, $p = 0.16$; $t_{(21)} = 1.74$, $p = 0.10$; $t_{(20)} = 1.12$, $p = 0.28$, respectively]. However, E_r and τ of rat NK1$^+$ neurons differed from that of mouse mouse NK1$^-$ neurons [$t_{(38)} = 7.60$, $p < 4 \times 10^{-9}$; $t_{(21)} = 5.35$, $p < 3 \times 10^{-5}$, respectively].

DISCUSSION

In the three species investigated here, virtually all cortical nNOS neurons were co-labeled for NK1 while the proportion of single-labeled NK1 neurons varied among species. *In vitro* patch clamp recordings showed that 0.03–1 μM SP elicited persistent depolarization and a robust increase in firing rate of putative nNOS neurons in mice and rats. These results suggest that SP can activate cortical nNOS neurons across species. Combined with our previous findings that cortical nNOS neurons are sleep-active, these results suggest a possible role for SP in sleep regulation.

TYPE I AND TYPE II nNOS NEURONS

We assume that all nNOS neurons we detected were type I because their morphology and distribution matches that of previous reports for the species investigated here (e.g., Wiencken and Casagrande, 2000; Freire et al., 2004, 2005). Our nNOS antibody failed to detect the weakly labeled type II nNOS neurons that have previously been reported in mice (Freire et al., 2005; Lee and Jeon, 2005), rats (Freire et al., 2004; Yousef et al., 2004; Cho et al., 2010; Kubota et al., 2011), and squirrel monkeys (Franca et al., 1997; Wiencken and Casagrande, 2000). Our antibody is raised against an N-terminal fragment of rat nNOS and, therefore, likely detects only the most abundant alpha splice variant (Mardsen et al., 2011). Using a different N-terminal-directed antibody, Vruwink et al. (2001) also failed to report type II nNOS neurons in rats. Thus, it is possible that type II nNOS neurons mainly express an alternative splice variant, resulting in our inability to detect such cells in the present study. In support of that notion, Eliasson et al. (1997) report immunolabeling of nNOS in absence of nNOS-alpha in the cortex to be restricted to soma and proximal dendrites, which is typical for type II neurons.

SINGLE-LABELED NK1 NEURONS

The proportion of neurons immunoreactive for NK1 but not for nNOS that we found in rats (30.7%, 403 of 1315) was similar to that reported by Vruwink et al. (26.4%, 174 of 659). However, Kaneko et al. (1994) reported a much higher number of weakly labeled NK1 neurons (84.1%, 328 of 390), with the number of intensely labeled NK1 neurons per section being comparable to NK1/nNOS neurons in the present study. Since the immunofluorescence protocols in our study were optimized for detection of intense NK1 neurons, it is possible that some weakly labeled NK1 neurons in rats were below our detection limit. However, Kaneko et al. reported a very similar distribution of weakly labeled NK1 neurons in the cortex as we do, suggesting that they likely observed the same cell type.

Weakly labeled NK1 neurons share several characteristics with type II nNOS neurons. For example, both are concentrated in

superficial layers (Freire et al., 2004; Cho et al., 2010) and co-express parvalbumin but not SST in rats (Vruwink et al., 2001; Kubota et al., 2011). Like the single-labeled NK1 neurons in our study, type II nNOS neurons have a neurogliaform-like morphology in primates (Smiley et al., 2000). However, squirrel monkey type II nNOS neurons are distributed throughout all cortical laminae with highest abundance in layers II/III (Franca et al., 1997; Wiencken and Casagrande, 2000). In contrast, we found the single-labeled NK1 neurons to be concentrated in deep gray matter. Kubota et al. (2011) found a small number of supragranular NK1 neurons in rats that did not co-label for SST, and thus probably correspond to the same cell type. However, Kubota et al. did not report whether these cells were nNOS positive. Taken together, these results suggest that the weakly labeled NK1 neurons and type II nNOS neurons could be overlapping populations in rats and monkeys. More work will be needed to test this possibility.

Rats and primates used for histology in this study were young adults (sexual maturity develops around six weeks and three years, respectively), whereas mice were around onset of sexual maturity. Although maturation of type I nNOS neurons appears to precede sexual maturity in rodents (Chung et al., 2004; Eto et al., 2010), no such data are available for weakly labeled cortical NK1 neurons. Ontogenetic studies will be needed to evaluate if differences in cortical maturation contributed to the differences in distribution of weakly labeled NK1 neurons reported here.

In vitro RECORDINGS

In both species investigated, bath application of SP elicited TTX-insensitive depolarization of SP-responsive neurons. These observations are in agreement with the finding that NK1 agonists elicit action potentials in putative interneurons and increase the frequency of inhibitory postsynaptic currents in principal neurons in the rat entorhinal cortex (Stacey et al., 2002). The depolarization in response to SP that we observed lasted several minutes, similar to findings in other electrophysiological studies using NK1 agonists (Dreifuss and Raggenbass, 1986; Maubach et al., 1998; Zaninetti and Raggenbass, 2000; Ito et al., 2002; Bailey et al., 2004; Blomeley and Bracci, 2008; Morozova et al., 2008; Paul and Cox, 2010). Determination of the type of channels involved in the reported neuronal activation was beyond the scope of the present study.

Our findings that SP-responsive neurons have a higher resting membrane potential, a higher input resistance, and a longer time constant than other NPY neurons suggest the possibility of a specialized function of this population. This difference is underlined by the finding that electrical properties of mouse $NK1^+$ neurons were more similar to rat $NK1^+$ neurons than to mouse $NK1^-$ neurons. A detailed comparison of morphology and membrane protein composition might shed light on the source of this significant difference.

The virtually complete overlap of nNOS and NK1 expression in mice implies that the neurons recorded *in vitro* were type I nNOS neurons. Labeling with TMR-SP in live tissue was reliable but faint, requiring exposure times of several seconds in order to obtain a clear picture with our fluorescent camera; this probably caused a detection bias toward more intensely labeled cells. In the rat, the characteristic weak immunolabeling for NK1 in the single-labeled NK1 neurons suggests that these cells express less receptor and likely show even fainter labeling with TMR-SP, making them unlikely to be detected. For the same reasons we do not expect to have detected binding to the low-affinity SP receptors NK2 and NK3, which are also present in the cortex (Mileusnic et al., 1999; Saffroy et al., 2003; Duarte et al., 2006). Therefore, we assume that most, if not all, cells that we recorded in rats were of the type that showed intense NK1 immunolabeling and thus were likely type I nNOS neurons.

The large variation in the response to SP that hindered the elaboration of a dose response curve likely reflects variability within the population of intense NK1 neurons rather than between intense ones and weak ones. This conclusion is consistent with the previously described heterogeneity of expression of calcium binding proteins among type I nNOS neurons (Pasumarthi et al., 2010, and references therein). It is currently unclear whether this heterogeneity reflects a further functional subdivision of type I nNOS neurons or rather differences in neuronal states. A larger number of recordings are needed to address this question and will be the subject of a subsequent study.

SOURCE OF CORTICAL SP

Despite the direct effects of SP on NK1 neurons described here, there is a spatial mismatch between the NK1 receptor and SPergic axon terminals in the cortex (Liu et al., 1994; Vruwink et al., 2001; Wolansky et al., 2007). Cortical SPergic neurons are GABAergic and about 70% of this population co-express Parvalbumin in the rat (Kaneko et al., 1998; Vruwink et al., 2001). These neurons also co-express the NO receptor soluble guanylyl cyclase (Vruwink et al., 2001). Therefore, it was suggested that SPergic neurons release SP as a volume transmitter and are, in turn, modulated by NO released from the NK1/nNOS neurons, forming a non-synaptic cortical feedback loop (Vruwink et al., 2001). However, SPergic afferents to the cortex have also been found to originate from the laterodorsal tegmental nucleus (Vincent et al., 1983) and it cannot be excluded that other subcortical sources exist (see Wolansky et al., 2007). Furthermore, NK1 is the preferred receptor not only for SP, but also for the more recently discovered tachykinins hemokinin-1 and endokinin A and B (Page, 2004). The ligands neurokinin A and B can also activate the NK1 receptor, although with lower affinity (Ingi et al., 1991). Clearly, more work is needed to identify the source of NK1 activation of cortical nNOS neurons *in vivo*.

PHYSIOLOGICAL FUNCTION

Type I nNOS neurons are sleep-active in mice, rats, and hamsters (Gerashchenko et al., 2008; Pasumarthi et al., 2010). This unusual activation pattern has not yet been tested in primates. However, the similar dendritic and axonal morphology of these neurons in rodents (Tomioka et al., 2005), cats (Higo et al., 2007, 2009), and primates (Tomioka and Rockland, 2007) and the conserved co-expression of NPY and SST (Smiley et al., 2000; Kubota et al., 2011), as well as NK1 receptors (shown in this study), suggest that this neuronal population has a conserved function in mammals. The similar electrophysiological properties we found in mice and rats support this notion.

The potential involvement of SP in sleep regulation has been little studied to date. Local injection of SP into the ventrolateral preoptic area (VLPO) facilitated sleep in mice (Zhang et al., 2004). In contrast, intracerebroventricular SP injections disturbed sleep in mice (Andersen et al., 2006) and intravenous injection disturbed sleep in humans (Lieb et al., 2002). These results indicate that wake-promoting neurons in one or more subcortical areas expressing NK1 (Nakaya et al., 1994) such as the locus coeruleus, the dorsal raphe nucleus, or the cholinergic basal forebrain (Hahn and Bannon, 1999; Chen et al., 2001; Lacoste et al., 2006) override activation of sleep-promoting neurons in the VLPO (and possibly cortex) after systemic injection. SP depolarizes noradrenergic neurons of the locus coeruleus *in vitro* (Cheeseman et al., 1983) and increased SP levels in this nucleus have been linked to increased release of noradrenaline in the prefrontal cortex of rats (Ebner and Singewald, 2007). SP has been reported to excite (Liu et al., 2002) or inhibit (Valentino et al., 2003) dorsal raphe neurons, and to increase (Gradin et al., 1992) or decrease (Guiard et al., 2007) serotonin release. This was suggested to reflect region dependence of SP effects within the nucleus (Valentino et al., 2003; Guiard et al., 2007). A sleep-disturbing effect of systemic applications of SP is also in agreement with reports that such application induces stress and fear responses (reviewed in Ebner and Singewald, 2006).

NK1 desensitizes upon prolonged stimulation with SP and resensitization takes about 30 min in neurons (McConalogue et al., 1998). Given the long timescale of NK1 desensitization and our finding that the activating effects of a brief exposure to SP can persist for several minutes, the cortical SP/NK1 system would be suitable to regulate slow aspects of sleep/wake regulation, such as the buildup or decay of sleep need. This idea is supported by the finding that cortical mRNA levels of the gene encoding SP are upregulated by sleep deprivation in mice (Martinowich et al., 2011).

POTENTIAL RELEVANCE FOR PATHOLOGIES

Given the presumed ability of nNOS/NK1 neurons to elicit widespread cortical inhibition by long range axons and release of the volume transmitter NO (Kilduff et al., 2011; also see Shlosberg et al., 2012), it is conceivable that an imbalance in their regulation could lead to imbalance in overall cortical excitability. In agreement with that view, NK1 agonists exerted a powerful antiepileptic effect in a slice preparation of the entorhinal cortex (Maubach et al., 1998). Alterations in the gene coding for NK1 have been linked to attention deficit hyperactivity disorder in humans (Yan et al., 2010). Pharmacological or genetic disruption of NK1 also induces hyperactivity in mice (Herpfer et al., 2005; Yan et al., 2010); reduced activation of cortical nNOS neurons could contribute to that phenotype. Depressed patients, on the other hand, show increased levels of SP in the cerebrospinal fluid (Geracioti et al., 2006). NK1 levels in the orbitofrontal cortex of depressed patients are decreased (Stockmeier et al., 2002), which might be a compensatory response to increased levels of SP. Similarly, frontal cortical SP levels are increased in different animal models of depression (Husum et al., 2001; Roche et al., 2012). Abnormally high cortical SP levels might be linked to a depressive phenotype by excitation of inhibitory cortical nNOS neurons.

CONCLUSION

Cortical type I nNOS neurons in all three species investigated showed an almost complete co-expression of the NK1 receptor. SP application elicited a direct and persistent activation of putative nNOS neurons *in vitro*. Cortical release of SP may be involved in aspects of sleep/wake regulation mediated by sleep-active type I nNOS neurons. Type I nNOS neurons might also be involved in mediating psychopathologies of SP/NK1 imbalances, such as attention deficit hyperactivity disorder or depression.

ACKNOWLEDGMENTS

The project described was supported by Award Number R01HL059658 from the National Heart, Lung, and Blood Institute and R01NS59910 from the National Institute of Neurological Disorders and Stroke. The content is solely the responsibility of the authors and does not necessarily represent the official views of the National Heart, Lung, and Blood Institute, the National Institute of Neurological Disorders and Stroke, or the National Institutes of Health. This research was supported by funds provided by The Regents of the University of California, Tobacco-related Disease Research Program, Grant Number 17RT-0119A. The opinions, findings, and conclusion herein are those of the author and not necessarily represent The Regents of the University of California, or any of its programs. This research was also supported by Deutsche Forschungsgemeinschaft fellowship DI 1718/1-1 to Lars Dittrich. We thank Prof. R. Shigemoto for the generous gift of NK1 antibody and Dr. Michael Schwartz for helpful comments on the manuscript.

REFERENCES

Andersen, M. L., Nascimento, D. C., Machado, R. B., Roizenblatt, S., Moldofsky, H., and Tufik, S. (2006). Sleep disturbance induced by substance P in mice. *Behav. Brain Res.* 167, 212–218.

Aoki, C., Fenstemaker, S., Lubin, M., and Go, C. G. (1993). Nitric oxide synthase in the visual cortex of monocular monkeys as revealed by light and electron microscopic immunocytochemistry. *Brain Res.* 620, 97–113.

Bailey, C. P., Maubach, K. A., and Jones, R. S. (2004). Neurokinin-1 receptors in the rat nucleus tractus solitarius: pre- and postsynaptic modulation of glutamate and GABA release. *Neuroscience* 127, 467–479.

Blomeley, C., and Bracci, E. (2008). Substance P depolarizes striatal projection neurons and facilitates their glutamatergic inputs. *J. Physiol.* 586, 2143–2155.

Cheeseman, H. J., Pinnock, R. D., and Henderson, G. (1983). Substance P excitation of rat locus coeruleus neurones. *Eur. J. Pharmacol.* 94, 93–99.

Chen, L. W., Wei, L. C., Liu, H. L., Qiu, Y., and Chan, Y. S. (2001). Cholinergic neurons expressing substance P receptor (NK1) in the basal forebrain of the rat: a double immunocytochemical study. *Brain Res.* 904, 161–166.

Cho, K. H., Jang, J. H., Jang, H. J., Kim, M. J., Yoon, S. H., Fukuda, T., Tennigkeit, F., Singer, W., and Rhie, D. J. (2010). Subtype-specific dendritic Ca(2+) dynamics of inhibitory interneurons in the rat visual cortex. *J. Neurophysiol.* 104, 840–853.

Chung, Y. H., Joo, K. M., Lee, Y. J., Shin, D. H., and Cha, C. I.

(2004). Postnatal development and age-related changes in the distribution of nitric oxide synthase-immunoreactive neurons in the visual system of rats. *Neurosci. Lett.* 360, 1–4.

Commons, K. G. (2010). Neuronal pathways linking substance P to drug addiction and stress. *Brain Res.* 1314, 175–182.

Dreifuss, J. J., and Raggenbass, M. (1986). Tachykinins and bombesin excite non-pyramidal neurones in rat hippocampus. *J. Physiol.* 379, 417–428.

Duarte, C. R., Schutz, B., and Zimmer, A. (2006). Incongruent pattern of neurokinin B expression in rat and mouse brains. *Cell Tissue Res.* 323, 43–51.

Ebner, K., and Singewald, N. (2006). The role of substance P in stress and anxiety responses. *Amino Acids* 31, 251–272.

Ebner, K., and Singewald, N. (2007). Stress-induced release of substance P in the locus coeruleus modulates cortical noradrenaline release. *Naunyn Schmiedebergs Arch. Pharmacol.* 376, 73–82.

Eliasson, M. J., Blackshaw, S., Schell, M. J., and Snyder, S. H. (1997). Neuronal nitric oxide synthase alternatively spliced forms: prominent functional localizations in the brain. *Proc. Natl. Acad. Sci. U.S.A.* 94, 3396–3401.

Emmers, R., and Akert, K. (1963). *A Stereotaxic Atlas of the Brain of the Squirrel Monkey (Saimiri Sciureus)*. Madison, WI: University of Wisconsin Press.

Espada, J., Juarranz, A., Galaz, S., Canete, M., Villanueva, A., Pacheco, M., and Stockert, J. C. (2005). Non-aqueous permanent mounting for immunofluorescence microscopy. *Histochem. Cell Biol.* 123, 329–334.

Eto, R., Abe, M., Kimoto, H., Imaoka, E., Kato, H., Kasahara, J., and Araki, T. (2010). Alterations of interneurons in the striatum and frontal cortex of mice during postnatal development. *Int. J. Dev. Neurosci.* 28, 359–370.

Franca, J. G., Do-Nascimento, J. L., Picanco-Diniz, C. W., Quaresma, J. A., and Silva, A. L. (1997). NADPH-diaphorase activity in area 17 of the squirrel monkey visual cortex: neuropil pattern, cell morphology and laminar distribution. *Braz. J. Med. Biol. Res.* 30, 1093–1105.

Freire, M. A., Franca, J. G., Picanco-Diniz, C. W., and Pereira, A. Jr. (2005). Neuropil reactivity, distribution and morphology of NADPH diaphorase type I neurons in the barrel cortex of the adult mouse. *J. Chem. Neuroanat.* 30, 71–81.

Freire, M. A., Gomes-Leal, W., Carvalho, W. A., Guimaraes, J. S., Franca, J. G., Picanco-Diniz, C. W., and Pereira, A. Jr. (2004). A morphometric study of the progressive changes on NADPH diaphorase activity in the developing rat's barrel field. *Neurosci. Res.* 50, 55–66.

Geracioti, T. D. Jr., Carpenter, L. L., Owens, M. J., Baker, D. G., Ekhator, N. N., Horn, P. S., Strawn, J. R., Sanacora, G., Kinkead, B., Price, L. H., and Nemeroff, C. B. (2006). Elevated cerebrospinal fluid substance p concentrations in post-traumatic stress disorder and major depression. *Am. J. Psychiatry* 163, 637–643.

Gerashchenko, D., Wisor, J. P., Burns, D., Reh, R. K., Shiromani, P. J., Sakurai, T., de la Iglesia, H. O., and Kilduff, T. S. (2008). Identification of a population of sleep-active cerebral cortex neurons. *Proc. Natl. Acad. Sci. U.S.A.* 105, 10227–10232.

Gradin, K., Qadri, F., Nomikos, G. G., Hillegaart, V., and Svensson, T. H. (1992). Substance P injection into the dorsal raphe increases blood pressure and serotonin release in hippocampus of conscious rats. *Eur. J. Pharmacol.* 218, 363–367.

Guiard, B. P., Guilloux, J. P., Reperant, C., Hunt, S. P., Toth, M., and Gardier, A. M. (2007). Substance P neurokinin 1 receptor activation within the dorsal raphe nucleus controls serotonin release in the mouse frontal cortex. *Mol. Pharmacol.* 72, 1411–1418.

Hahn, M. K., and Bannon, M. J. (1999). Stress-induced C-fos expression in the rat locus coeruleus is dependent on neurokinin 1 receptor activation. *Neuroscience* 94, 1183–1188.

Herpfer, I., Hunt, S. P., and Stanford, S. C. (2005). A comparison of neurokinin 1 receptor knockout ($NK1^{-/-}$) and wildtype mice: exploratory behaviour and extracellular noradrenaline concentration in the cerebral cortex of anaesthetised subjects. *Neuropharmacology* 48, 706–719.

Higo, S., Akashi, K., Sakimura, K., and Tamamaki, N. (2009). Subtypes of GABAergic neurons project axons in the neocortex. *Front. Neuroanat.* 3:25. doi: 10.3389/neuro.05.025.2009

Higo, S., Udaka, N., and Tamamaki, N. (2007). Long-range GABAergic projection neurons in the cat neocortex. *J. Comp. Neurol.* 503, 421–431.

Hill, R. (2000). NK1 (substance P) receptor antagonists–why are they not analgesic in humans? *Trends Pharmacol. Sci.* 21, 244–246.

Husum, H., Vasquez, P. A., and Mathe, A. A. (2001). Changed concentrations of tachykinins and neuropeptide Y in brain of a rat model of depression: lithium treatment normalizes tachykinins. *Neuropsychopharmacology* 24, 183–191.

Ingi, T., Kitajima, Y., Minamitake, Y., and Nakanishi, S. (1991). Characterization of ligand-binding properties and selectivities of three rat tachykinin receptors by transfection and functional expression of their cloned cDNAs in mammalian cells. *J. Pharmacol. Exp. Ther.* 259, 968–975.

Ito, K., Rome, C., Bouleau, Y., and Dulon, D. (2002). Substance P mobilizes intracellular calcium and activates a nonselective cation conductance in rat spiral ganglion neurons. *Eur. J. Neurosci.* 16, 2095–2102.

Jafri, M. S., and Weinreich, D. (1996). Substance P hyperpolarizes vagal sensory neurones of the ferret. *J. Physiol.* 493(Pt 1), 157–166.

Kaneko, T., Murashima, M., Lee, T., and Mizuno, N. (1998). Characterization of neocortical non-pyramidal neurons expressing preprotachykinins A and B: a double immunofluorescence study in the rat. *Neuroscience* 86, 765–781.

Kaneko, T., Shigemoto, R., Nakanishi, S., and Mizuno, N. (1994). Morphological and chemical characteristics of substance P receptor-immunoreactive neurons in the rat neocortex. *Neuroscience* 60, 199–211.

Kilduff, T. S., Cauli, B., and Gerashchenko, D. (2011). Activation of cortical interneurons during sleep: an anatomical link to homeostatic sleep regulation? *Trends Neurosci.* 34, 10–19.

Kubota, Y., Shigematsu, N., Karube, F., Sekigawa, A., Kato, S., Yamaguchi, N., Hirai, Y., Morishima, M., and Kawaguchi, Y. (2011). Selective coexpression of multiple chemical markers defines discrete populations of neocortical GABAergic neurons. *Cereb. Cortex* 21, 1803–1817.

Labrakakis, C., and MacDermott, A. B. (2003). Neurokinin receptor 1-expressing spinal cord neurons in lamina I and III/IV of postnatal rats receive inputs from capsaicin sensitive fibers. *Neurosci. Lett.* 352, 121–124.

Lacoste, B., Riad, M., and Descarries, L. (2006). Immunocytochemical evidence for the existence of substance P receptor (NK1) in serotonin neurons of rat and mouse dorsal raphe nucleus. *Eur. J. Neurosci.* 23, 2947–2958.

Lee, J. E., and Jeon, C. J. (2005). Immunocytochemical localization of nitric oxide synthase-containing neurons in mouse and rabbit visual cortex and co-localization with calcium-binding proteins. *Mol. Cells* 19, 408–417.

Lieb, K., Ahlvers, K., Dancker, K., Strohbusch, S., Reincke, M., Feige, B., Berger, M., Riemann, D., and Voderholzer, U. (2002). Effects of the neuropeptide substance P on sleep, mood, and neuroendocrine measures in healthy young men. *Neuropsychopharmacology* 27, 1041–1049.

Liu, H., Brown, J. L., Jasmin, L., Maggio, J. E., Vigna, S. R., Mantyh, P. W., and Basbaum, A. I. (1994). Synaptic relationship between substance P and the substance P receptor: light and electron microscopic characterization of the mismatch between neuropeptides and their receptors. *Proc. Natl. Acad. Sci. U.S.A.* 91, 1009–1013.

Liu, R., Ding, Y., and Aghajanian, G. K. (2002). Neurokinins activate local glutamatergic inputs to serotonergic neurons of the dorsal raphe nucleus. *Neuropsychopharmacology* 27, 329–340.

Lüth, H. J., Hedlich, A., Hilbig, H., Winkelmann, E., and Mayer, B. (1994). Morphological analyses of NADPH-diaphorase/nitric oxide synthase positive structures in human visual cortex. *J. Neurocytol.* 23, 770–782.

Mardsen, P., Newton, D., and Tsui, A. (2011). Alternative processing: neuronal nitric oxide synthase. eLS [Online]. Available: http://www.els.net/WileyCDA/ElsArticle/refId-a0005040.html

Martinowich, K., Schloesser, R. J., Jimenez, D. V., Weinberger, D. R., and Lu, B. (2011). Activity-dependent brain-derived neurotrophic factor expression regulates cortistatin-interneurons and sleep behavior. *Mol. Brain* 4, 11.

Maubach, K. A., Cody, C., and Jones, R. S. (1998). Tachykinins may modify spontaneous epileptiform activity in the rat entorhinal cortex *in vitro* by activating GABAergic inhibition. *Neuroscience* 83, 1047–1062.

McConalogue, K., Corvera, C. U., Gamp, P. D., Grady, E. F., and Bunnett, N. W. (1998). Desensitization of the neurokinin-1

receptor (NK1-R) in neurons: effects of substance P on the distribution of NK1-R, Galphaq/11, G-protein receptor kinase-2/3, and beta-arrestin-1/2. *Mol. Biol. Cell* 9, 2305–2324.

Mileusnic, D., Lee, J. M., Magnuson, D. J., Hejna, M. J., Krause, J. E., Lorens, J. B., and Lorens, S. A. (1999). Neurokinin-3 receptor distribution in rat and human brain: an immunohistochemical study. *Neuroscience* 89, 1269–1290.

Morozova, E., Wu, M., Dumalska, I., and Alreja, M. (2008). Neurokinins robustly activate the majority of septohippocampal cholinergic neurons. *Eur. J. Neurosci.* 27, 114–122.

Nakaya, Y., Kaneko, T., Shigemoto, R., Nakanishi, S., and Mizuno, N. (1994). Immunohistochemical localization of substance P receptor in the central nervous system of the adult rat. *J. Comp. Neurol.* 347, 249–274.

Nishino, S., and Fujiki, N. (2007). Neuropeptides as possible targets in sleep disorders. *Expert Opin. Ther. Targets* 11, 37–59.

Page, N. M. (2004). Hemokinins and endokinins. *Cell. Mol. Life Sci.* 61, 1652–1663.

Pagliardini, S., Adachi, T., Ren, J., Funk, G. D., and Greer, J. J. (2005). Fluorescent tagging of rhythmically active respiratory neurons within the pre-Botzinger complex of rat medullary slice preparations. *J. Neurosci.* 25, 2591–2596.

Pasumarthi, R. K., Gerashchenko, D., and Kilduff, T. S. (2010). Further characterization of sleep-active neuronal nitric oxide synthase neurons in the mouse brain. *Neuroscience* 169, 149–157.

Paul, K., and Cox, C. L. (2010). Excitatory actions of substance P in the rat lateral posterior nucleus. *Eur. J. Neurosci.* 31, 1–13.

Paxinos, G., and Franklin, K. (2001). *The Mouse Brain in Stereotaxic Coordinates*. San Diego, CA: Academic Press.

Paxinos, G., and Watson, C. (2007). *The Rat Brain in Stereotaxic Coordinates*. Amsterdam: Elsevier Academic Press.

Pereira, A. Jr., Freire, M. A., Bahia, C. P., Franca, J. G., and Picanco-Diniz, C. W. (2000). The barrel field of the adult mouse SmI cortex as revealed by NADPH-diaphorase histochemistry. *Neuroreport* 11, 1889–1892.

Roche, M., Kerr, D. M., Hunt, S. P., and Kelly, J. P. (2012). Neurokinin-1 receptor deletion modulates behavioural and neurochemical alterations in an animal model of depression. *Behav. Brain Res.* 228, 91–98.

Saffroy, M., Torrens, Y., Glowinski, J., and Beaujouan, J. C. (2003). Autoradiographic distribution of tachykinin NK2 binding sites in the rat brain: comparison with NK1 and NK3 binding sites. *Neuroscience* 116, 761–773.

Shlosberg, D., Buskila, Y., Abu-Ghanem, Y., and Amitai, Y. (2012). Spatiotemporal alterations of cortical network activity by selective loss of NOS-expressing interneurons. *Front. Neural Circuits* 6:3. doi: 10.3389/fncir.2012.00003

Smiley, J. F., Mcginnis, J. P., and Javitt, D. C. (2000). Nitric oxide synthase interneurons in the monkey cerebral cortex are subsets of the somatostatin, neuropeptide Y, and calbindin cells. *Brain Res.* 863, 205–212.

Stacey, A. E., Woodhall, G. L., and Jones, R. S. (2002). Activation of neurokinin-1 receptors promotes GABA release at synapses in the rat entorhinal cortex. *Neuroscience* 115, 575–586.

Stockmeier, C. A., Shi, X., Konick, L., Overholser, J. C., Jurjus, G., Meltzer, H. Y., Friedman, L., Blier, P., and Rajkowska, G. (2002). Neurokinin-1 receptors are decreased in major depressive disorder. *Neuroreport* 13, 1223–1227.

Tomioka, R., Okamoto, K., Furuta, T., Fujiyama, F., Iwasato, T., Yanagawa, Y., Obata, K., Kaneko, T., and Tamamaki, N. (2005). Demonstration of long-range GABAergic connections distributed throughout the mouse neocortex. *Eur. J. Neurosci.* 21, 1587–1600.

Tomioka, R., and Rockland, K. S. (2007). Long-distance corticocortical GABAergic neurons in the adult monkey white and gray matter. *J. Comp. Neurol.* 505, 526–538.

Torsney, C., and MacDermott, A. B. (2006). Disinhibition opens the gate to pathological pain signaling in superficial neurokinin 1 receptor-expressing neurons in rat spinal cord. *J. Neurosci.* 26, 1833–1843.

Valentino, R. J., Bey, V., Pernar, L., and Commons, K. G. (2003). Substance P Acts through local circuits within the rat dorsal raphe nucleus to alter serotonergic neuronal activity. *J. Neurosci.* 23, 7155–7159.

van den Pol, A. N., Yao, Y., Fu, L. Y., Foo, K., Huang, H., Coppari, R., Lowell, B. B., and Broberger, C. (2009). Neuromedin B and gastrin-releasing peptide excite arcuate nucleus neuropeptide Y neurons in a novel transgenic mouse expressing strong Renilla green fluorescent protein in NPY neurons. *J. Neurosci.* 29, 4622–4639.

Vincent, S. R., Satoh, K., Armstrong, D. M., and Fibiger, H. C. (1983). Substance P in the ascending cholinergic reticular system. *Nature* 306, 688–691.

Vruwink, M., Schmidt, H. H., Weinberg, R. J., and Burette, A. (2001). Substance P and nitric oxide signaling in cerebral cortex: anatomical evidence for reciprocal signaling between two classes of interneurons. *J. Comp. Neurol.* 441, 288–301.

Wiencken, A. E., and Casagrande, V. A. (2000). The distribution of NADPH diaphorase and nitric oxide synthetase (NOS) in relation to the functional compartments of areas V1 and V2 of primate visual cortex. *Cereb. Cortex* 10, 499–511.

Wolansky, T., Pagliardini, S., Greer, J. J., and Dickson, C. T. (2007). Immunohistochemical characterization of substance P receptor (NK1R)-expressing interneurons in the entorhinal cortex. *J. Comp. Neurol.* 502, 427–441.

Yan, T. C., McQuillin, A., Thapar, A., Asherson, P., Hunt, S. P., Stanford, S. C., and Gurling, H. (2010). NK1 (TACR1) receptor gene 'knockout' mouse phenotype predicts genetic association with ADHD. *J. Psychopharmacol.* 24, 27–38.

Yousef, T., Neubacher, U., Eysel, U. T., and Volgushev, M. (2004). Nitric oxide synthase in rat visual cortex: an immunohistochemical study. *Brain Res. Brain Res. Protoc.* 13, 57–67.

Zaninetti, M., and Raggenbass, M. (2000). Oxytocin receptor agonists enhance inhibitory synaptic transmission in the rat hippocampus by activating interneurons in stratum pyramidale. *Eur. J. Neurosci.* 12, 3975–3984.

Zhang, G., Wang, L., Liu, H., and Zhang, J. (2004). Substance P promotes sleep in the ventrolateral preoptic area of rats. *Brain Res.* 1028, 225–232.

Conflict of Interest Statement: The authors declare that the research was conducted in the absence of any commercial or financial relationships that could be construed as a potential conflict of interest.

Received: 28 March 2012; paper pending published: 10 April 2012; accepted: 06 May 2012; published online: 05 June 2012.

*Citation: Dittrich L, Heiss JE, Warrier DR, Perez XA, Quik M and Kilduff TS (2012) Cortical nNOS neurons co-express the NK1 receptor and are depolarized by Substance P in multiple mammalian species. Front. Neural Circuits **6**:31. doi: 10.3389/fncir.2012.00031*

frontiers in
NEURAL CIRCUITS

ORIGINAL RESEARCH ARTICLE
published: 07 February 2012
doi: 10.3389/fncir.2012.00003

Spatiotemporal alterations of cortical network activity by selective loss of NOS-expressing interneurons

Dan Shlosberg, Yossi Buskila, Yasmin Abu-Ghanem and Yael Amitai*

Faculty of Health Sciences, Department of Physiology and Neurobiology, Ben-Gurion University of the Negev, Beer-Sheva, Israel

Edited by:
Bruno Cauli, CNRS and UPMC, France

Reviewed by:
Barry W. Connors, Brown University, USA
Kathleen S. Rockland, MIT, USA
Yoshiyuki Kubota, National Institute for Physiological Sciences, Japan

****Correspondence:***
Yael Amitai, Faculty of Health Sciences, Department of Physiology and Neurobiology, Ben-Gurion University of the Negev, POB 653, Beer-Sheva 84015, Israel.
e-mail: yaela@bgu.ac.il

Deciphering the role of GABAergic neurons in large neuronal networks such as the neocortex forms a particularly complex task as they comprise a highly diverse population. The neuronal isoform of the enzyme nitric oxide synthase (nNOS) is expressed in the neocortex by specific subsets of GABAergic neurons. These neurons can be identified in live brain slices by the nitric oxide (NO) fluorescent indicator diaminofluorescein-2 diacetate (DAF-2DA). However, this indicator was found to be highly toxic to the stained neurons. We used this feature to induce acute phototoxic damage to NO-producing neurons in cortical slices, and measured subsequent alterations in parameters of cellular and network activity. Neocortical slices were briefly incubated in DAF-2DA and then illuminated through the 4× objective. Histochemistry for NADPH-diaphorase (NADPH-d), a marker for nNOS activity, revealed elimination of staining in the illuminated areas following treatment. Whole cell recordings from several neuronal types before, during, and after illumination confirmed the selective damage to non-fast-spiking (FS) interneurons. Treated slices displayed mild disinhibition. The reversal potential of compound synaptic events on pyramidal neurons became more positive, and their decay time constant was elongated, substantiating the removal of an inhibitory conductance. The horizontal decay of local field potentials (LFPs) was significantly reduced at distances of 300–400 μm from the stimulation, but not when inhibition was non-selectively weakened with the $GABA_A$ blocker picrotoxin. Finally, whereas the depression of LFPs along short trains of 40 Hz stimuli was linearly reduced with distance or initial amplitude in control slices, this ordered relationship was disrupted in DAF-treated slices. These results reveal that NO-producing interneurons in the neocortex convey lateral inhibition to neighboring columns, and shape the spatiotemporal dynamics of the network's activity.

Keywords: epilepsy, DAF-2DA, nitric oxide, lateral inhibition, barrel cortex, dendritic delay, dendritic inhibition, synaptic integration

INTRODUCTION

It has become widely recognized that discrete inhibitory neuronal populations co-exist in the cerebral cortex and most likely contribute differentially to mold the neuronal network activity. Subtypes of interneurons possess distinct characteristics evident in typical firing patterns, peptide expression, axonal targets, or electrical coupling. These characteristics are well-correlated, implying that specific neuronal-types carry specific circuit functions (e.g., Kawaguchi and Kubota, 1993; Cauli et al., 1997; Gibson et al., 1999). For example, fast-spiking (FS), parvalbumin-expressing (PV+), proximally targeting inhibitory neurons mediate feed-forward inhibition both in the hippocampus and somatosensory cortex (Kiss et al., 1996; Beierlein and Connors, 2002), tightly control spike timing (Pouille and Scanziani, 2002), and promote gamma-band cortical oscillations (Sohal et al., 2009). On the other hand, activation of distally targeting, somatostatin-expressing (SOM+) interneurons elicits IPSPs of smaller amplitude and slower kinetics than proximally evoked IPSPs (e.g., Salin and Prince, 1996; Silberberg and Markram, 2007), and it has been proposed that these IPSPs modulate excitatory synaptic inputs locally. These neurons are recruited by high activity rates to mediate intracortical recurrent inhibition (Kapfer et al., 2007) or feed-forward thalamocortical inhibition at high activity rates (Tan et al., 2008). While intense research has been conducted to describe the cellular attributes of these interneurons subtypes, their specific roles in the network have remained largely ambiguous due to the difficulty to identify and selectively manipulate them. Optogenetics tools have already begun to reveal distinct effects of local inhibitory populations, but these techniques are not free of limitations (for review see Cardin, 2011).

The neuronal isoform of the enzyme nitric oxide synthase (nNOS) is expressed in the neocortex by specific subsets of GABAergic neurons (Karagiannis et al., 2009; Kubota et al., 2011). To simplify available data, one subset comprised mostly SOM+, dendritic targeting interneurons (Lüth et al., 1995; Gonchar and Burkhalter, 1997; Vruwink et al., 2001). Their firing properties have been commonly termed "LTS" after their tendency to fire low threshold spikes (Kawaguchi, 1993), and are identified also by deep and complex AHPs (Beierlein et al., 2003). Another group is composed of some of the neuropeptide Y-expressing (NPY+) or PV+ cells with an adapting firing pattern, which amongst

themselves also display high heterogeneity both in morphology as well as physiology (Karagiannis et al., 2009; Kubota et al., 2011). While it seems that these neuronal groups display overlap in several features, two distinct morphological features appear among the nNOS+ neurons: Neurogliaform neurons which display a dense local axonal arborization (e.g., Uematsu et al., 2008; Karagiannis et al., 2009), and in contrast—long-range projecting GABAergic interneurons, (e.g., Lüth et al., 1995; Gonchar and Burkhalter, 1997; Vruwink et al., 2001). Additional classification scheme divided nNOS-expressing (NOS+) interneurons to type I, characterized by large somata and strong nNOS or NADPH-diaphorase (NADPH-d) reactivity, and type II, characterized by small somata and weaker nNOS/NADPH-d staining (Lee and Jeon, 2005; Kubota et al., 2011).

In a previous study (Buskila et al., 2005) we identified NO-producing neurons in acute cortical slices by using the fluorescent NO indicator diaminofluorescein-2 diacetate (DAF-2DA, Kojima et al., 1998). We found that this indicator indeed stains non-pyramidal neurons in cortical slices with bright puncta which delineate some somata, but are also sparsely scattered in the neuropil. (Buskila et al., 2005, **Figure 1A**). Interestingly, these DAF-positive neurons appeared shrunken under IR/DIC optics and attempts to patch them were not successful, while other non-fluorescent neurons in the visual field were easily patched and displayed normal physiology. Moreover, propidium iodide, an indicator for cell death, was co-localized with the vast majority of DAF-positive neurons (Buskila et al., 2005). We, therefore, used DAF-2DA to induce selective phototoxic damage to NO-producing interneurons in cortical slices, and explored the cellular and network effects of this manipulation. We find that selective damage to this population results in mild disinhibition of the entire cortical network which is especially pronounced at horizontal distances of 300–400 μm from the center of activation, and in severe alterations of the spatio-temporal activity dynamics during repetitive stimulation.

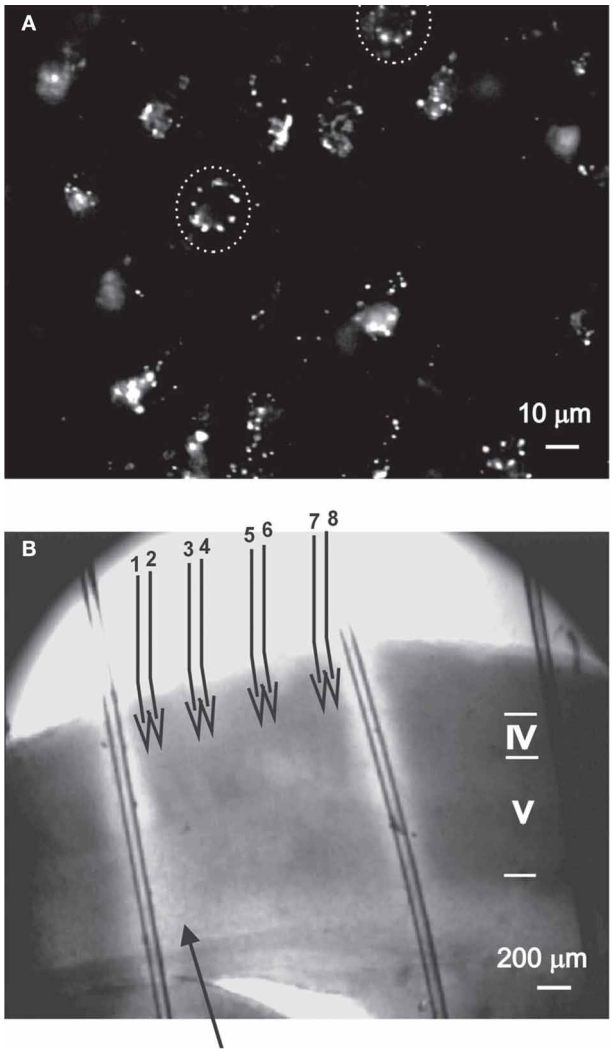

FIGURE 1 | The experimental methods used to evaluate the role of nNOS+ neurons. (A) DAF-2DA staining of neurons in acute slices, as visualized under the 40× objective (details in Buskila et al., 2005). Suspected neuronal somata are surrounded by dashed circle. **(B)** The illustration depicts the experimental paradigm. An acute slice which had been incubated in DAF-2DA is illuminated through the 4× objective (Methods, area displayed in bright light). The stimulating electrode (filled arrow) is placed above the white matter. For LFP recordings, four pairs of micropipettes (numbered open arrows) are placed in layer 2/3, where electrode #1 is in column with the stimulating electrode. Cortical lamina is marked by roman numerals.

MATERIALS AND METHODS

SLICE PREPARATION AND PHOTOTOXICITY INDUCTION

All experiments were carried out in compliance with the ethical guidelines of the NIH Guide for the Care and Use of Laboratory Animals to minimize the number of animals used and their suffering. The Animal Care Committee of Ben-Gurion University approved all procedures. Experiments were carried on mice (CD1, 14–21 days old). The mice were deeply anesthetized with pentobarbital, decapitated, and their brains quickly removed into cold (4°C) physiological solution. Thalamocortical brain slices (350 μm thick) were cut with a vibratome (Campden Instruments, London, UK) and kept in a holding chamber at room temperature for at least 1 h before any manipulation, continuously bubbled by 95% O_2–5% CO_2. The bathing solution in all experiments contained (in mM): 124 NaCl, 3 KCl, 2 $MgSO_4$, 1.25 $NaHPO_4$, 2 $CaCl_2$, 26 $NaHCO_3$, and 10 dextrose, and was saturated with 95% O_2–5% CO_2 (pH 7.4). The temperature was kept at 34°C and slices were continuously perfused. For phototoxicity induction, slices were incubated in diaminofluorescein-2 diacetate (DAF-2DA, 2 μm, Calbiochem, La Jolla, CA) for 10 min before they were transferred to the recording chamber, mounted on an upright microscope equipped with infrared/differential interference contrast (IR/DIC) optics (Nikon Physiostation EC-600, Tokyo, Japan). Illumination was performed using a light source (100 W mercury lamp) via a Nikon filter (excitation wavelength 450–490 nm, emission wavelength 520 nm), using either a 60× fluid immersion objective (for cellular recordings) or 4× objective (for area phototoxicity). Imaging was done using a black and white CCD camera with integrating frame grabber control unit (CCD-300IFG, Dage-MTI, USA), integrating 16 frames for each image. Several DAF-2DA-positive neurons could be identified in almost each visual field by punctate fluorescent

staining (**Figure 1A**, Buskila et al., 2005). Area phototoxicity was induced by exposing the slices to light in the above wave length for a period of 5 min. The light-exposed field had a diameter of about 5 mm (**Figure 1B**), thus we estimate that most of the barrel cortex in the slice was affected.

ELECTROPHYSIOLOGY

Whole-cell recordings were performed in layer 5 of the somatosensory cortex using patch pipettes (3–5 MΩ), containing (in mM): 125 *K*-gluconate, 2 $MgCl_2$, 10 Hepes, 10 EGTA, 5 NaCl, and $2Na_2ATP$. Extracellular stimulations (200 μs, 10–200 μA) were delivered through an AMPI isolation unit (Jerusalem, Israel) using a bipolar concentric microelectrode (Micro Probe Inc.) placed ∼300 μm lateral to the recording electrode to stimulate intracortical axons.

For extracellular recordings, the slices were transferred to a chamber that held the slices at the fluid-gas interface. In some experiments the $GABA_A$ receptor blocker picrotoxin (PTX, 3–8 μM, Sigma-Aldrich) was included in the perfusing solution. Local field potentials (LFPs) were recorded in layer 2/3 of the somatosensory cortex using four pairs of sharpened tungsten electrodes (Micro Probe Inc., 1–2 MΩ). The electrodes in each pair were spaced 100 μm apart and the distance between pairs was 200 μm. Stimulation was delivered vertically under the first electrode of the array and right above the white matter (**Figure 1B**).

NADPH-DIAPHORASE HISTOCHEMISTRY

At the end of recording session, slices were fixed overnight in a solution of paraformaldehyde at 4% in 0.1 M phosphate buffer (pH 7.4), then transferred to a solution of 30% sucrose for cryoprotection, and re-sectioned to 100 μm. NADPH-d histochemistry was conducted according to standard procedures. Briefly, free-floating sections were incubated in a solution containing 1 mM reduced β-NADPH (Sigma-Aldrich, Israel), 0.2 mM nitro blue tetrazolium (Sigma-Aldrich, Israel), 0.1 M phosphate buffer, 0.1% Tween (Sigma-Aldrich, Israel) at 37°C for 3–4 h. The reaction was visually controlled and stopped by washing the sections with phosphate buffered saline at pH 7.4. The sections were then mounted on slides, air-dried, and cover-slipped. Under light microscopy, NADPH-d-positive neurons and blood vessels were identifiable by the presence of dark blue staining.

STATISTICAL ANALYSIS

Statistical analysis was performed using SPSS software. We either used the analysis of variance (ANOVA) test for multiple comparisons, or the Wilcoxon test for paired data, unless noted otherwise. Results are reported as mean ± S.E.M.

RESULTS

NO-PRODUCING INTERNEURONS ARE SELECTIVELY DAMAGED

Our previous findings implied that neurons which exhibited DAF staining, hence NOS positive, were damaged by the light (Buskila et al., 2005). These neurons were expected to be a subset of inhibitory neurons, with non-FS firing properties. We wanted to make use of this finding to selectively eliminate this group, but initially we ascertained the specificity of the phototoxicity.

NADPH-d histochemistry provides a specific histochemical marker for neurons producing nitric oxide (NO) (Hope et al., 1991; Vincent and Kimura, 1992), thus we examined the effect of treatment with DAF-2DA (2 μM, 10 min incubation) and area illumination (5 min through the 4× objective) on the histochemical reaction. Untreated slices displayed a typical image of multiple darkly stained neurons scattered in the neocortex (**Figure 2A**). Higher magnification revealed a dense network of stained axons, passing in all directions (**Figure 2A**, inset). In contrast, no stained neurons were found in the neocortex in slices which had been incubated in DAF-2DA and illuminated, while such neurons appeared in the striatum and midbrain structures of the same slices, distant from the illuminated zone. Interestingly, blood vessels were clearly noted in the neocortex of those same slices following long incubation periods, but not neurons (**Figure 2B**, arrows), suggesting that the weak NADPH-d reactivity of NOS-expressing endothelial cells (e.g., Felaco et al., 2001) was less disturbed by the process. Taken together, the findings confirmed the damage to NOS-expressing neurons in the illuminated zone.

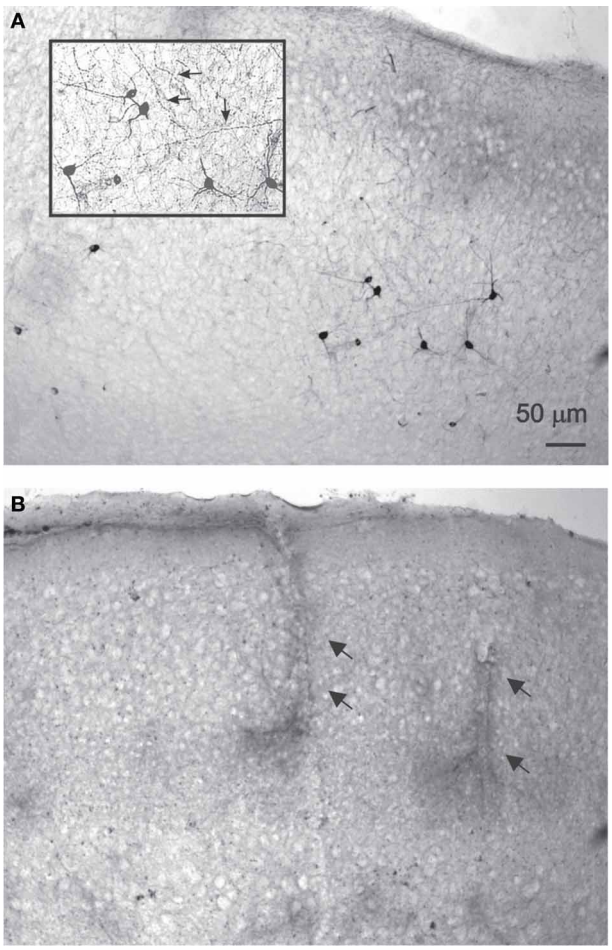

FIGURE 2 | NADPH-d staining is reduced following DAF-2DA incubation and illumination. (A) Control, untreated sections display multiple darkly stained neurons. In the inset, additional magnification highlighting the network of stained axons (arrows). **(B)** Neocortical section which had been treated by DAF-2DA and illumination. The histochemical reaction has been extended for several hours. No neurons are seen, but note darkly stained capillaries.

To further ascertain the selectivity of the damage, we also examined directly the electrophysiological response of DAF-incubated neurons to illumination. Since fluorescent neurons could not be accessed (see above), we patched neurons in layer 5 of the somatosensory cortex in slices which had been incubated in DAF-2DA before opening the fluorescent light shutter. The passive membrane properties were monitored by analyzing voltage deflections to short hyperpolarizing current pulses delivered at 1–3 Hz, before, during, and following illumination. Pyramidal neurons were initially differentiated from interneurons by the shape of their somata and proximal dendrites under IR/DIC optics. Recorded pyramidal neurons ($n = 30$) displayed either regular-spiking (RS) or intrinsically bursting firing patterns (Chagnac-Amitai et al., 1990). Their passive membrane properties remained unchanged throughout the illumination period and afterwards, as long as they were recorded (**Table 1 and Figure 3A**). Similarly, inhibitory FS interneurons, identified by their typical firing pattern (Golomb et al., 2007, $n = 6$) were not affected by the illumination process (**Figure 3B and Table 1**). Notably, none of the pyramidal or FS neurons exhibited a fluorescent response. We also recorded eight neurons which displayed elongated somata and were oriented in the vertical axis as observed under IR/DIC optics. These neurons exhibited a firing pattern which was not FS, but rather compatible with adapting or non-adapting LTS patterns (Gibson et al., 1999; Beierlein et al., 2003; Ma et al., 2006). Out of these, four neurons displayed fluorescence upon illumination (**Figure 3D**). These fluorescent neurons rapidly depolarized, fired few spikes and the recording was abruptly lost, typically within the duration of illumination (**Figure 3C**, right panel). The additional neurons did not fluoresce and a stable recording was held well after the illumination period while their membrane properties remained unchanged (data not shown). Taken together, these results verify our previous data which implied that DAF-2DA fluorescence is toxic to NO-producing neurons.

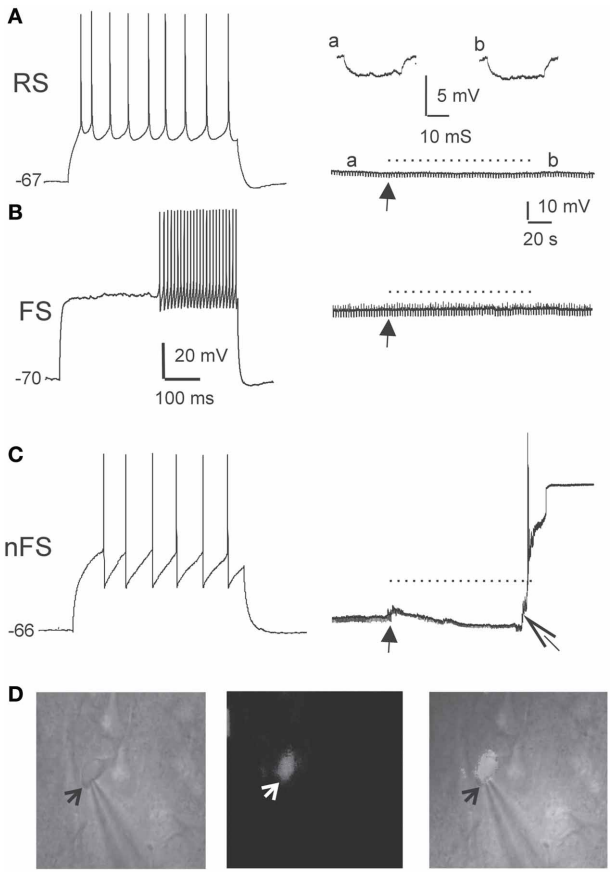

FIGURE 3 | DAF phototoxicity is selective to interneurons with LTS firing pattern. Layer 5 neurons were recorded in slices pre-incubated in DAF-2DA (2 μM, 10 min). **(A)** The left panel displays typical firing pattern of a pyramidal RS neuron in response to depolarizing current pulse. The resting potential is marked to the left. On the right—the recorded trace before opening the fluorescent shutter (arrow), during illumination (dotted line) and afterwards. A hyperpolarizing current pulse monitored the membrane resistance, and examples from time points "a" and "b" are displayed above. **(B)** Example traces of the response of a FS-type interneuron to light. Details as in **(A)**. **(C)** Example traces of the response of a LTS-type interneuron to light. Note on the right panel the appearance of instability of the membrane potential and a reduction of membrane resistance shortly after opening the shutter (closed arrow), and loss of the membrane potential shortly before the end of illumination (open arrow). **(D)** Images of the neuron in **(C)**. On the left is an IR/DIC image of the patched neuron. An arrow points to the tip of the recording pipette. The middle image shows the same field under fluorescent light, showing faint staining in the recorded neuron. On the right is a combined image.

INCREASED NETWORK EXCITABILITY FOLLOWING SELECTIVE LOSS OF NOS+ INTERNEURONS

To damage NO-producing interneurons selectively in a large cortical area, we exposed DAF-incubated slices to light for 5 min through the 4× objective, and investigated the effect of this manipulation on properties of the population activity. Initially, we tested whether the balance between excitation and inhibition in the network has been altered. As expected, the stimulus—response curve of LFPs in DAF-treated slices was steeper compared with untreated slices (**Figure 4A**, slope values – control: 0.17 ± 0.02, $n = 9$; treated: 0.27 ± 0.04, $n = 9$; $p = 0.02$ student

Table 1 | Membrane properties of pyramidal neurons and FS interneurons in DAF-treated slices were not altered by the fluorescent light.

	V_m (mV)	R_{in} (MΩ)	τ (ms)	V_m (mV)	R_{in} (MΩ)	τ (ms)
	Before illumination			After illumination		
Pyramidal ($n = 30$)	-68.4 ± 0.8	218.6 ± 19.6	20.6 ± 1.9	-68.0 ± 0.9	205.1 ± 17.6	19.1 ± 1.6
FS ($n = 6$)	-67.2 ± 1.6	99.2 ± 13.5	13.16 ± 4.6	-64.9 ± 2.6	107.1 ± 17.1	13.14 ± 3.7

Measurements were taken before opening the fluorescent light shutter and 2 min after the termination of a 5 min illumination period. V_m, resting membrane potential; R_{in}, input resistance; τ, the membrane time-constant. Note the stability of parameters throughout the manipulation.

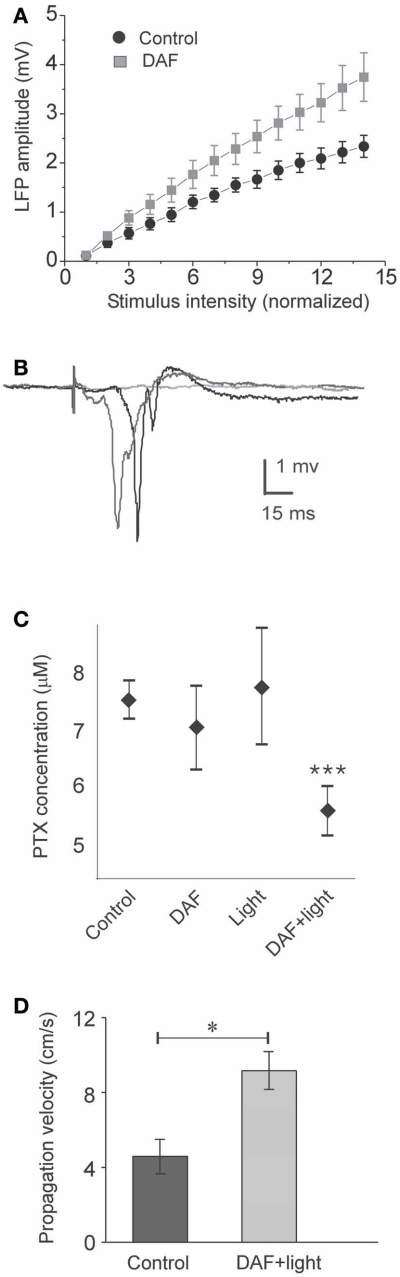

FIGURE 4 | DAF-treated slices are disinhibited. The treatment consisted of 10 min incubation in a solution containing 2 μM DAF-2DA, and 5 min fluorescent illumination through the 4× objective. **(A)** A plot of the average LFP amplitude against the normalized stimulus intensity demonstrates steeper slope for DAF-treated slice ($n = 9$) compared with control slices ($n = 9$). **(B)** An example of three consecutive traces of synchronized epileptic activity recorded at a single point in DAF-treated slice, when inhibition was further reduced by PTX (5 μM), demonstrating a failure and two synchronized events of variable latency (shades of gray). **(C)** Threshold concentrations of PTX required for eliciting epileptic activity as in **(B)**, under different conditions (control – $n = 9$; DAF-2DA – $n = 9$; light – $n = 10$; DAF-2DA + light – $n = 11$). Note significantly reduced dose in slices which have been treated with DAF and illumination. **(D)** The propagation velocity of epileptic discharge at suprathreshold concentrations of PTX is higher in DAF-pretreated slices ($n = 12$) compared with non-treated slices ($n = 13$), reflecting pre-existing disinhibition.

t-test), indicating increased network excitability. When inhibition efficacy in cortical slices is sufficiently reduced, it is possible to evoke synchronized "epileptic" population events, which appear in an all-or-none manner to threshold stimulus intensity, their latency from the stimulation is highly variable, and they can propagate horizontally along the slices without decrement (**Figure 4B**, Chagnac-Amitai and Connors, 1989; Shlosberg et al., 2003). Such synchronized population events did not appear spontaneously and could not be evoked in DAF-treated slices. We thus applied gradually increasing concentrations of the $GABA_A$ receptor blocker picrotoxin (PTX) to the perfusing solution (adding 1 μM every 30 min), noting the minimal concentration required to elicit such synchronized events as an indication of the degree of disruption in the balance between excitation and inhibition. Indeed, DAF-treated slices ($n = 11$) required significantly lower doses of PTX to achieve the pharmacological threshold to epileptic events as compared with untreated slices ($n = 9$), slices that were treated with DAF-2DA alone ($n = 9$), or slices treated with light alone ($n = 10$) ($p < 0.0001$, ANOVA, **Figure 4C**), thus confirming that the manipulation (incubation in DAF-2DA followed by illumination) reduced the inhibition in the network.

Finally, it has been shown both theoretically and experimentally that the propagation velocity of epileptic discharges is dictated by the relative strength of cortical inhibition present (Golomb and Ermentrout, 2001; Shlosberg et al., 2003; Trevelyan et al., 2007). Once epileptic events were elicited in the slices by applying a suprathreshold dose of PTX (7–8 μM), we measured their propagation velocity across a horizontal distance of 1 mm. DAF-treated slices displayed significantly higher propagation velocity than untreated slices (treated -9.2 ± 1 cm/s, $n = 12$; control -4.6 ± 0.9 cm/s, $n = 13$, $p < 0.02$, **Figure 4D**). Taken together, these results ascertain that the procedure of DAF-2DA incubation followed by illumination, shown above to damage NO-producing interneurons, resulted in a significant increase of network excitability, but not sufficiently to instigate synchronized activity.

MODULATION OF SYNAPTIC POTENTIALS FOLLOWING LOSS OF NOS+ NEURONS

A notable subset of the cortical NO-producing interneurons are dendritic–targeting (e.g., Valtschanoff et al., 1993; Lüth et al., 1995; Seress et al., 2005), hence their influence is expected to be electrotonically distant from the somatic integration zone. We explored the effect of the assumed removal of dendritic inhibition on the properties of compound synaptic potentials evoked on pyramidal neurons by activating intracortical pathways and recording PSPs before and after area illumination as above. As already noted, the membrane properties of pyramidal neurons were not altered by the illumination. The reversal potential of the synaptic events (E_{rev}) shifted to more positive values in four neurons, and did not change in two others. Overall, there was a significant adjustment in the average reversal potential of these events ($E_{rev\ control}$ -28.6 ± 7.4 mV; $E_{rev\ treated}$ -14.2 ± 9.2 mV, $p = 0.02$, $n = 6$, **Figure 5A**), indicating that some inhibition has been removed. In accordance, the change in E_{rev} was accompanied by a reduction in the conductance slope of these synaptic

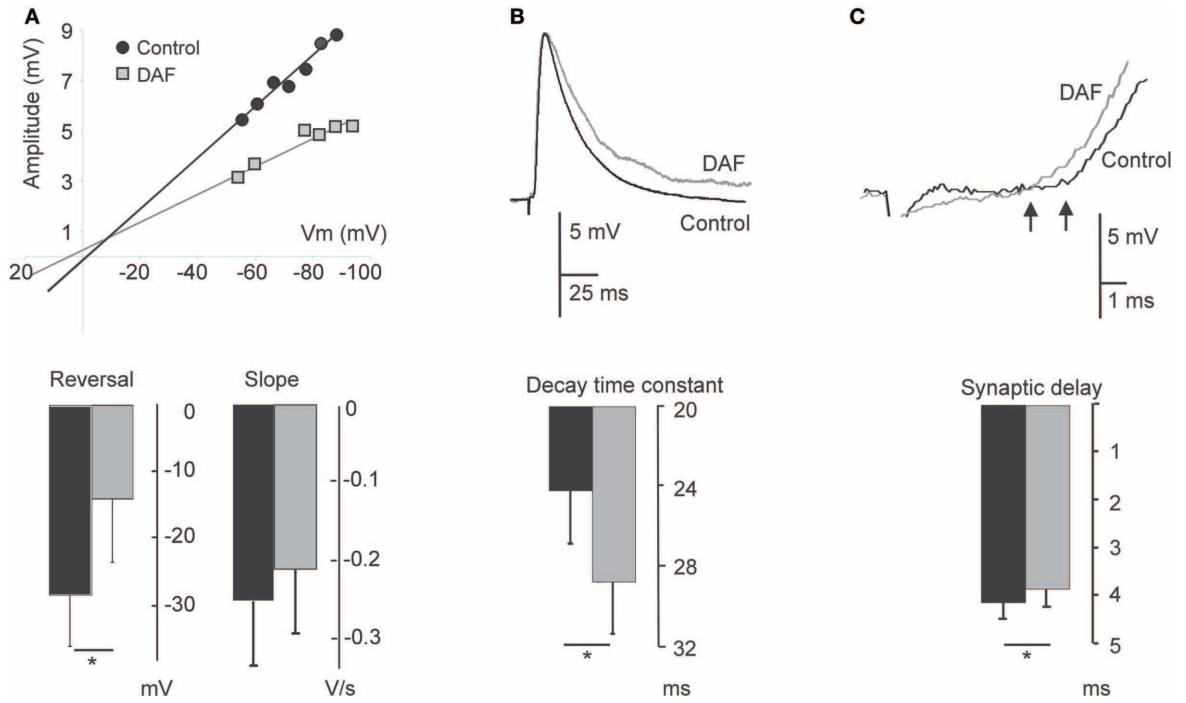

FIGURE 5 | Damage to NOS+ interneurons affects synaptic integration in pyramidal neurons. PSPs evoked on layer 5 pyramidal neurons before 2 min illumination and afterwards are compared. **(A)** Plot of the relationship between PSP amplitude and the membrane potential in a single neuron displays a change both in the reversal potential and slope conductance following illumination (upper panel). The bottom panel displays a summary diagram of these parameters for the population ($n = 6$). **(B)** Example traces of EPSPs before and after illumination, demonstrating an elongation of the decay time (upper panel). The bottom panel displays the summary diagram of the change in the decay time constant ($n = 8$). **(C)** Example traces of EPSPs before and after illumination, demonstrating a decrease in the delay. Arrows point to the deflection points (upper panel). The bottom panel displays a summary diagram of the change in the dendritic delay ($n = 8$). For all panels, recording under control conditions are represented by black bars; recordings following illumination are represented by gray bars.

events (**Figure 5A**). Assessing the shape parameter of synaptic potentials, there was no significant change in the rising slope, but we found elongation of about 17% in the PSPs decay time-constant (τ_s) ($\tau_{s\ control}$ 24.1 ± 2.7 ms; $\tau_{s\ treated}$ 28.7 ± 2.8 ms, $p = 0.018$, $n = 8$, **Figure 5B**). This finding is compatible with an increased resistance at the background of these synaptic events. Since the membrane input resistance was not altered by the illumination, we concluded that other conductances, evoked during the synaptic events, have been subtracted. In addition, a small but significant decrease in the synaptic delay appeared after the illumination (4.1 ± 0.33 ms before and 3.8 ± 0.35 ms after, $p = 0.012$, $n = 8$, **Figure 5C**), likely to reflect a reduction in the time required for the synaptic current to travel along the apical dendrites (Agmon-Snir and Segev, 1993). Altogether, the results reveal multipart modulation of excitatory synaptic integration by the removal of the inhibition mediated by NOS+ neurons.

LOSS OF NOS+ INTERNEURONS PRODUCES SPATIOTEMPORAL ALTERATIONS OF NETWORK ACTIVITY

In the neocortex, the horizontal spread of activity from a center of activation to neighboring regions is powerfully constrained by inhibition (Chagnac-Amitai and Connors, 1989). At least some NOS+ interneurons possess especially long intra-cortical or even projecting axonal arbors (Wang et al., 2004; Higo et al., 2007; Tamamaki and Tomioka, 2010), thus we conjectured that they convey lateral, inter-columnar inhibition. To test this possibility, we placed multiple extracellular microelectrodes in supragranular laminae to monitor the spread of activity by recordings LFPs at horizontal distances up to 1000 μm. When stimulating above the white matter, a typical sharp and negative LFP was recorded by the electrode positioned vertically in line (position 0, **Figure 6A**). The amplitude of LFPs decreased horizontally, reaching around 10% of its maximal amplitude at 1000 μm. The latency difference between LFPs at position 0 and at 1000 μm laterally was around 3 ms (**Figure 6B**). Such a time delay is likely to be contributed mostly by the conductance of the horizontal intracortical excitatory axons (Shlosberg et al., 2008), and not by polysynaptic connections as synchronized population waves of activity propagate (**Figure 4D**, Golomb and Amitai, 1997). In DAF-treated slices, LFPs at 1000 μm reached around 20% of their maximal amplitude. Furthermore, the horizontal decay pattern differed from control slices mainly due to a significant increase in the LFPs' relative amplitude at distances of 300–400 μm (**Figure 6C**), indicating that this region was particularly disinhibited. We then asked whether this finding was specific to the loss of NOS+ interneurons, or was a general feature of cortical disinhibition. We bathed the slices in low concentrations of PTX which

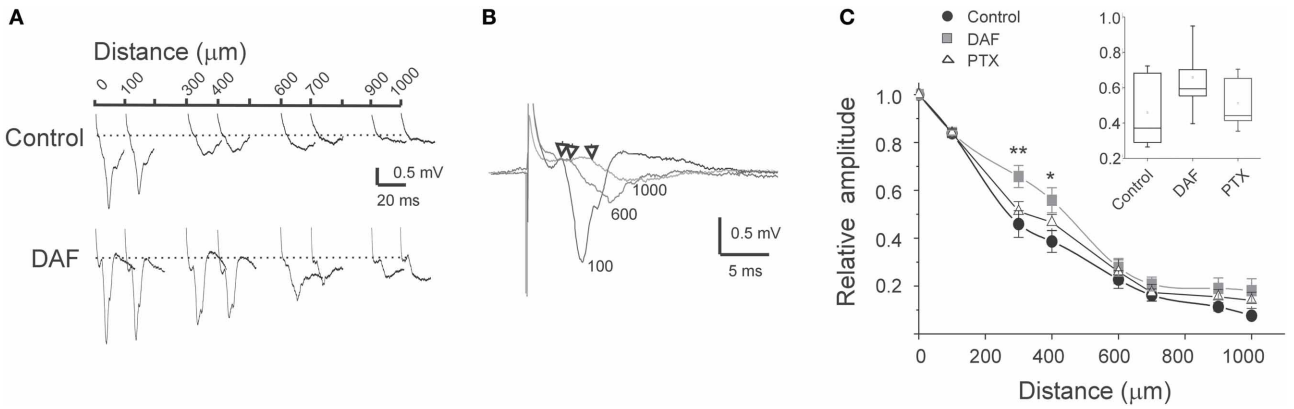

FIGURE 6 | The horizontal pattern of activity spread is affected by damage to NOS+ interneurons. (A) Example traces of simultaneously recorded LFPs at the distances as marked above, in control slice and in DAF-treated slice. **(B)** Example traces from simultaneous recordings of LFPs at three distances from the center of activation (marked by the traces, in μm). Arrows mark the deflection point from baseline. Note the short delay of around 3 ms for a distance of 1000 μm. **(C)** A summary diagram of the LFPs amplitude with distance, normalized to the amplitude above the stimulating electrode (distance 0), for control slices ($n = 16$), DAF-treated slices ($n = 13$), and PTX-treated slices ($n = 10$). Note a significant difference between control and DAF-treated slices at the distances of 300 μm ($p = 0.008$), and 400 μm ($p = 0.02$). The inset displayed the data distribution for the 300 μm point.

resulted in a similar distance of activity spread, and were subthreshold for the induction of synchronized events (3–5 μM). This dose of PTX resulted in a slightly reduced decay of LFPs horizontally compared with control slices, but the relative enhancement of activity at a distance of 300–400 μm was not observed (**Figure 6C**).

Inhibitory interneurons exhibit highly variable short-term dynamics of their synaptic activation. For example, among NOS+ interneurons, the subset of SOM+ cells are activated by pyramidal cells via uniquely facilitating synapses, such that they are strongly recruited at higher frequencies (Beierlein et al., 2003; Markram et al., 2004; Tan et al., 2008). We, therefore, hypothesized that when a single type of interneuron such as NOS+/SOM+ cells is selectively damaged, repetitive stimulation will result in even stronger alteration of the lateral activity spread pattern. Following the same recording scheme as before, we now applied six consecutive stimuli at 40 Hz and compared the spatio-temporal characteristics of activity between control and DAF-treated slices. Under control conditions, LFP frequency-dependent depression was monotonically reduced with distance (**Figure 7A**) while this order was interrupted in DAF-treated slices (**Figure 7B**). We next plotted the voltage attenuation as the ratio between the 6th and the 1st LFP amplitudes in the stimulus train (V6/V1) against the distance along the horizontal axis of the slice. Whereas untreated slices exhibited a highly linear correlation between the voltage attenuation ratio and the horizontal distance, this correlation was completely disrupted in DAF-treated slices (**Figure 7C**). The degree of activity depression at a given location may be correlated with the amplitude of the first LFP in the train, as higher amplitudes reflect higher activity levels of the network, and thus may engage stronger inhibition locally. We thus plotted V6/V1 against the amplitude of the first LFP (V1) at each recording site. Indeed, in control slices, the ratio V6/V1 was linearly correlated with V1 (**Figure 7D**). However, this relationship was not maintained in DAF-treated slices, implying that network recruitment with distance has been altered by the manipulation.

DISCUSSION

In this study we selectively damaged a population of NO-producing interneurons in cortical slices. This manipulation resulted in: (1) elongation of the decay time-constant and reduced dendritic delay of compound PSPs evoked on pyramidal neurons, (2) disinhibition of the network which was especially pronounced at horizontal distances of 300–400 μm from the center of activation, and (3) alterations of the spatio-temporal activity dynamics during repetitive stimulation. Together, our findings demonstrate directly, for the first time, a specific role for NOS+ interneurons in communicating significant lateral inhibition, and shaping the horizontal spread of activity.

THE IDENTITY OF DAF-POSITIVE NEURONS

The morphological identity of DAF-positive neurons was not established directly in this study due to technical difficulties. The few neurons that fluoresced during recording (**Figures 3C,D**) most likely belong to the NOS type I subgroup given their relatively large soma size. Yet, in the lack of direct morphological identification we have to rely on other studies. In the neocortex, nNOS is expressed exclusively by GABAergic neurons, and among them in several specific subpopulations with different expression levels (Kubota et al., 2011). Unsupervised clustering of cortical interneurons based on molecular, morphological, and electrophysiological parameters reveals two major groups (Karagiannis et al., 2009): the first one is relatively homogenous and consists of the FS, PV-expressing interneurons which do not expresses nNOS. Our finding which showed that FS neurons did not exhibit DAF-2DA fluorescence and maintained stable passive membrane properties under illumination is in agreement with these data. The second major cluster according to Karagiannis et al. (2009) exhibits considerable molecular diversity. Among neurons of

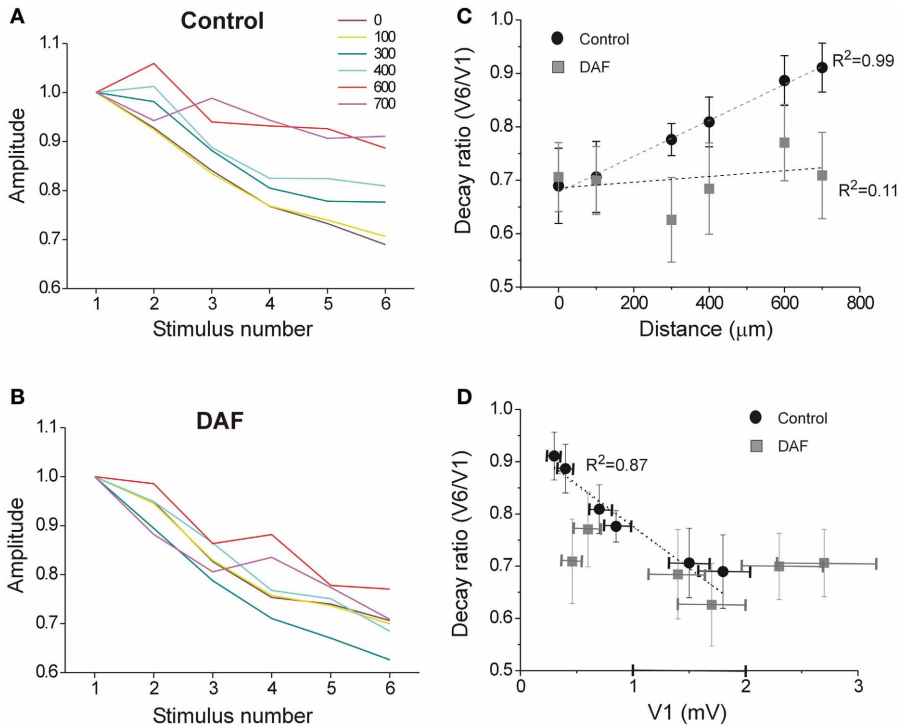

FIGURE 7 | The spatio-temporal dynamics of the network activity are disrupted in DAF-treated slices. A train of six stimuli at 40 Hz was delivered under the first electrode, and LFPs were recorded in layer 2/3 at six horizontal distances (color-coded as marked). **(A)** LFP depression with frequency is displayed for the six distance points in control slices. Each line displays an average of 10 slices (error bars omitted for clarity). **(B)** LFP depression with frequency is displayed for six distance points in DAF-treated slices. Each line displays an average of 11 slices. **(C)** For the same slices as in **A** and **B**, the ratio between the 6th and the 1st LFPs' amplitude is plotted as a function of the distance for control (black circles) and DAF-treated (gray squares) slices. Linear regression lines are plotted for each data set, and the adjusted *R*-square value is marked to the side. **(D)** The same ratio as in **(C)** is plotted as a function of the average amplitude of 1st LFP in the train, Linear regression line is plotted for the control data set. Data points in **(C)** and **(D)** display averages ± SEM.

this second non-fast-spiking cluster, nNOS was co-localized with some of the SOM− and NPY-expressing neurons.

Morphologically, SOM+ neurons have been largely characterized by long axonal projections targeting distal dendrites as well as the pyramidal apical tuft. A study examining synaptic target patterns of unidentified NOS+ neurons confirmed that they target dendritic segments of principal excitatory neurons (Seress et al., 2005). Another morphologically distinct subtype of NOS+ neurons has been associated with "neurogliaform" neurons. The extensive network of axons as revealed by the NADPH-d staining is indeed quite reminiscent of the axonal network of neurogliaform neurons. Interestingly, this type of interneurons is thought to deliver non-synaptic volume inhibition, devoid of any spatial selectivity (Oláh et al., 2009). Hence, we suggest that the more specific spatial alterations in the network behavior following damage to NOS+ interneurons, i.e., reduction of lateral inhibition, is mainly due to damage to the SOM+, dendritic targeting interneurons. NOS+ neurons indeed comprise a prevailing portion of interneurons with long axonal projections. The literature is very consistent and compelling in showing that NOS is expressed by a clear subset of SOM+ interneurons with relatively long axons in all species examined (monkey—Smiley et al., 2000; Tomioka and Rockland, 2007; cat—Higo et al., 2007; rat—Gonchar and Burkhalter, 1997; Vruwink et al., 2001).

Although NADPH-d staining was greatly diminished in treated slices, we cannot rule out that some NOS+ neurons remained. One of the reasons would be incomplete penetrance of the light to the depth of the 350 μm thick slices. DAF fluorescence was visible in the superficial 80–100 μm of the slices. Therefore, the physiological changes we documented are likely to reflect damage inflicted to some fraction of NOS+/SOM+ neurons. Interestingly, in several models of epilepsy, a selective loss of inhibitory SOM+ interneurons has been demonstrated (Sloviter, 1987; Robbins et al., 1991; Cossart et al., 2001). We speculate that the ability to produce NO renders these interneurons more vulnerable under conditions of high metabolic demands (Almeida et al., 2001), thus exacerbating the propensity to develop seizures.

CELLULAR EFFECTS OF NOS+ INTERNEURONS

NOS+/SOM+ interneurons are expected to target the distal dendritic branches. While several powerful mechanisms combine to amplify distal excitatory inputs, there are only a few recognized mechanisms that can support dendritic propagation of IPSPs (e.g., Williams and Stuart, 2003). Therefore, most theories regarding the role of distal dendritic inhibition maintain that it affects dendritic processing locally. By recording compound synaptic events on pyramidal neurons we unraveled several means by

which NOS+ interneurons might be affecting the summed activity. The increase in the EPSPs time constant can evolve directly from the removal of slow IPSPs, or from a secondary decrease in the activation of the hyperpolarization-activated cation channels (Ih), which are abundant in the distal dendrites of pyramidal cells (Gulledge et al., 2005). In both cases, the effect is elongation of the integration time window of neurons, allowing for stronger excitatory summation. Another interesting finding is the shortening of the dendritic delay. Cable theory suggests that the dendritic conduction velocity at a given point is equal to the ratio between the space constant and the time constant (Agmon-Snir and Segev, 1993). Given the increase in the time constant alone one would predict a reduction in the dendritic conduction velocity. On the other hand, the removal of dendritic inhibition is likely to enhance active conductances in the distal segments (Larkum et al., 1999; London and Hausser, 2005), thus enhancing the velocity of distal PSP's in their propagation toward the soma. Taken together these data imply that the damage inflicted to NOS+ neurons alters the overall integration properties of pyramidal neurons.

SPATIOTEMPORAL EFFECT OF NOS+ INTERNEURONS

Studies of cortical network activity have paid little attention to the horizontal, non-epileptic, spread of activity. It has been demonstrated that GABAergic inhibition controls the horizontal (tangential) spread of activity via intracortical connections (Chagnac-Amitai and Connors, 1989), but little is known about specific roles of interneurons subtypes in the spatial shaping of network activity. The short delay between the LFPs recorded at the column of stimulation and 1 mm away (around 3 ms) indicates that activity spread is mediated mostly by intracortical horizontal axons (Shlosberg et al., 2008). Such axons are well-documented, and indeed, monosynaptic horizontal EPSPs can be recorded in cortical slices up to distances of 1–3 mm (e.g., Hirsch and Gilbert, 1991; Telfeian and Connors, 2003). In our experimental setup, some detectable LFP remained 1 mm lateral to the stimulated column in control slices, and at slightly longer distances in disinhibited slices. However, the main difference between DAF-treated slices and controls appeared at horizontal distances of 300–400 μm. The size of a barrel column in the mouse somatosensory cortex is around 200 μm. Previous studies reveal specific interneurons in the barrel cortex with long horizontal axonal projections, expected to provide lateral inhibition (Kisvárday and Eysel, 1993; Helmstaedter et al., 2009). Our data strongly imply that NOS+ neurons provide such inhibition to neighboring columns. This role is in accordance with the anatomy of these neurons, which demonstrate that SOM+/NOS+ neurons have especially long axonal branches crossing columnar boundaries (e.g., Wang et al., 2004; Higo et al., 2007).

Excitatory transmission onto SOM+ interneurons is strongly facilitating, such that these interneurons are recruited by high activity rates (Beierlein et al., 2003; Markram et al., 2004; Silberberg and Markram, 2007; Tan et al., 2008). Given this information, we expected that selective damage to SOM+/NOS+ interneurons will result in reduced horizontal decay with repetitive stimulation, but the results do not support this simplistic hypothesis. We suggest that complex synaptic interactions between SOM+ interneurons and other neuronal types (Gibson et al., 1999) serve to compensate for their selective loss. Another surprising finding is the linear relationship between short-term depression of activity with repeated stimulation and the distance, or the local initial amplitude of the LFP, and the disruption of this relationship in DAF-treated slices. Frequency-dependent activity depression can be caused by the synaptic dynamics (both excitatory and inhibitory), and by the local recruitment of inhibitory neurons. The horizontal excitatory connection themselves demonstrate periodic variability in density (Chervin et al., 1988; Gilbert, 1993). Remarkably, all these parameters even-out in the control situation to yield a smooth reduction of frequency-dependent depression with distance and amplitude. We reason that once a subpopulation of interneurons is damaged, other cells in the network modify their activity rates, but the orderly architecture of network engagement is lost. Other means to selectively damage additional types of interneurons in the cortex will be needed to decipher their specific roles in controlling the spatial attributes of activity.

ACKNOWLEDGMENTS

The study was supported by grants 412/02 and 269/06 from the Israel Science Foundation to Yael Amitai. We thank D. Golomb for his useful comments on the manuscript.

REFERENCES

Agmon-Snir, H., and Segev, I. (1993). Signal delay and input synchronization in passive dendritic structures. *J. Neurophysiol.* 70, 2066–2085.

Almeida, A., Almeida, J., Bolanos, J. P., and Moncada, S. (2001). Different responses of astrocytes and neurons to nitric oxide: the role of glycolytically generated ATP in astrocyte protection. *Proc. Natl. Acad. Sci. U.S.A.* 98, 15294–15299.

Beierlein, M., and Connors, B. W. (2002) Short-term dynamics of thalamocortical and intracortical synapses onto layer 6 neurons in neocortex. *J. Neurophysiol.* 88, 1924–1932.

Beierlein, M., Gibson, J., and Connors, B. W. (2003). Two dynamically distinct inhibitory networks in layer 4 of the neocortex. *J. Neurophysiol.* 90, 2987–3000.

Buskila, Y., Farkash, S., Hershfinkel, M., and Amitai, Y. (2005). Rapid and reactive nitric oxide production by astrocytes in mouse neocortical slices. *Glia* 52, 169–176.

Cardin, J. A. (2011) Dissecting local circuits *in vivo*: integrated optogenetic and electrophysiology approaches for exploring inhibitory regulation of cortical activity. *J. Physiol. Paris* PMID: 21958624.

Cauli, B., Audinat, E., Lambolez, B., Angulo, M. C., Ropert, N., Tsuzuki, K., Hestrin, S., and Rossier, J. (1997). Molecular and physiological diversity of cortical nonpyramidal cells. *J. Neurosci.* 17, 3894–3906.

Chagnac-Amitai, Y., and Connors, B. W. (1989). Horizontal spread of synchronized activity in neocortex and its control by GABA-mediated inhibition. *J. Neurophysiol.* 61, 747–758.

Chagnac-Amitai, Y., Luhmann, H. J., and Prince, D. A. (1990). Burst generating and regular spiking layer 5 pyramidal neurons of rat neocortex have different morphological features. *J. Comp. Neurol.* 296, 598–613.

Chervin, R. D., Pierce, P. A., and Connors, B. W. (1988). Periodicity and directionality in the propagation of epileptiform discharges across neocortex. *J. Neurophysiol.* 60, 1695–1713.

Cossart, R., Dinoncourt, C., Hirsch, J. C., Merchan-Perez, A., De Felipe, J., Ben-Ari, Y., Esclapez, M., and Bernard, C. (2001). Dendritic but not somatic GABAergic inhibition is decreased in experimental epilepsy. *Nat. Neurosci.* 4, 52–62.

Felaco, M., Grilli, A., De Lutiis, M. A., Patruno, A., Libertini, N., Taccardi, A. A., Di Napoli, P., Di Giulio, C., Barbacane, R., and Conti, P. (2001). Endothelial nitric oxide synthase (eNOS) expression and localization in healthy and diabetic rat hearts. *Ann. Lab. Clin. Sci.* 31, 179–186.

Gibson, J. R., Beierlein, M., Connors, B. W. (1999) Two networks of electrically coupled inhibitory neurons in neocortex. *Nature* 402, 75–79.

Gilbert, C. D. (1993). Circuitry, architecture, and functional dynamics of visual cortex. *Cereb. Cortex* 3, 373–386.

Golomb, D., and Amitai, Y. (1997). Propagating neuronal discharges in neocortical slices: computational and experimental study. *J. Neurophysiol.* 78, 1199–1211.

Golomb, D., Donner, K., Shacham, L., Shlosberg, D., Amitai, Y., and Hansel, D. (2007). Mechanisms of firing patterns in fast-spiking cortical interneurons. *PLoS Comput. Biol.* 3, e156. doi: 10.1371/journal.pcbi.0030156

Golomb, D., and Ermentrout, B. G. (2001). Bistability in pulse propagation in networks of excitatory and inhibitory populations. *Phys. Rev. Lett.* 86, 4179–4182.

Gonchar, Y., and Burkhalter, A. (1997). Three distinct families of GABAergic neurons in rat visual cortex. *Cereb. Cortex* 7, 347–358.

Gulledge, A. T., Kampa, B. M., and Stuart, G. J. (2005). Synaptic integration in dendritic trees. *J. Neurobiol.* 64, 75–90.

Helmstaedter, M., Sakmann, B., and Feldmeyer, D. (2009). Neuronal correlates of local, lateral, and translaminar inhibition with reference to cortical columns. *Cereb. Cortex* 19, 926–937.

Higo, S., Udaka, N., and Tamamaki, N. (2007). Long-range GABAergic projection neurons in the cat neocortex. *J. Comp. Neurol.* 503, 421–431.

Hirsch, J. A., and Gilbert, C. D. (1991). Synaptic physiology of horizontal connections in the cat's visual cortex. *J. Neurosci.* 11, 1800–1809.

Hope, B. T., Michael, G. J., Knigge, K. M., and Vincent, S. R. (1991). Neuronal NADPH diaphorase is a nitric oxide synthase. *Proc. Natl. Acad. Sci. U.S.A.* 88, 2811–2814.

Kiss, J., Buzsáki, G., Morrow, J. S., Glantz, S. B., and Leranth, C. (1996). Entorhinal cortical innervation of parvalbumin-containing neurons (Basket and Chandelier cells) in the rat Ammon's horn. *Hippocampus* 6, 239–246.

Kapfer, C., Glickfeld, L. L., Attalah, B. V., and Scanziani, M. (2007). Supralinear increase of recurrent inhibition during sparse activity in the somatosensory cortex. *Nat. Neurosci.* 10, 743–753.

Karagiannis, A., Gallopin, T., Dávid, C., Battaglia, D., Geoffroy, H., Rossier, J., Hillman, E. M., Staiger, J. F., and Cauli, B. (2009). Classification of NPY-expressing neocortical interneurons. *J. Neurosci.* 29, 3642–3659.

Kawaguchi, Y. (1993). Grouping of nonpyramidal and pyramidal cells with specific physiological and morphological characteristics in rat frontal cortex. *J. Neurophysiol.* 69, 416–431.

Kawaguchi, Y., and Kubota, Y. (1993). Correlation of physiological subgroupings of nonpyramidal cells with Parvalbumin and Calbindin D28k-immunoreactive neurons in layer V of rat frontal cortex. *J. Neurophysiol.* 70, 387–396.

Kisvárday, Z. F., and Eysel, U. T. (1993). Functional and structural topography of horizontal inhibitory connections in cat visual cortex. *Eur. J. Neurosci.* 5, 1558–1572.

Kojima, H., Nakatsubo, N., Kikuchi, K., Kawahara, S., Kirino, Y., Nagoshi, H., Hirata, Y., and Nagano, T. (1998). Detection and imaging if nitric oxide with novel fluorescent indicators: diaminofluoresceins. *Anal. Chem.* 70, 2446–2453.

Kubota, Y., Shigematsu, N., Karube, F., Sekigawa, A., Kato, S., Yamaguchi, N., Hirai, Y., Morishima, M., and Kawaguchi, Y. (2011). Selective coexpression of multiple chemical markers defines discrete populations of neocortical GABAergic neurons. *Cereb. Cortex* 8, 1803–1817.

Larkum, M. E., Kaiser, K. M. M., and Sakmann, B. (1999). Calcium electrogenesis in distal apical dendrites of layer 5 pyramidal cells at a critical frequency of back-propagating action potentials. *Proc. Natl. Acad. Sci. U.S.A.* 96, 14600–14604.

Lee, J. E., and Jeon, C. J. (2005). Immunocytochemical localization of nitric oxide synthase-containing neurons in mouse and rabbit visual cortex and co-localization with calcium-binding proteins. *Mol. Cells* 19, 408–417.

London, M., and Hausser, M. (2005). Dendritic computation. *Annu. Rev. Neurosci.* 28, 503–532.

Lüth, H. J., Hedlich, A., Hilbig, H., Winkelmann, E., and Mayer, B. (1995). Postnatal development of NADPH-diaphorase/nitric oxide synthase positive nerve cells in the visual cortex of the rat. *J. Hirnforsch.* 36, 313–328.

Ma, Y., Hu, H., Berrebi, H. S., Mathers, P. H., and Agmon, A. (2006). Distinct subtypes of somatostatin-containing neocortical interneurons revealed in transgenic mice. *J. Neurosci.* 26, 5069–5082.

Markram, H., Toledo-Rodriguez, M., Wang, Y., Gupta, A., Silberberg, G., and Wu, C. (2004). Interneurons of the neocortical inhibitory system. *Nat. Neurosci. Rev.* 5, 793–806.

Oláh, S., Füle, M., Komlósi, G., Varga, C., Báldi, R., Barzó, P., and Tamás, G. (2009). Regulation of cortical microcircuits by unitary GABA-mediated volume transmission. *Nature* 461, 1278–1281.

Pouille, F., and Scanziani, M. (2002). Enforcement of temporal fidelity in pyramidal cells by somatic feed-forward inhibition. *Science* 293, 1159–1163.

Robbins, R. J., Brines, M. L., Kim, J. H., Adrian, T., de Lanerolle, N., Welsh, S., and Spencer, D. D. (1991). A selective loss of somatostatin in the hippocampus of patients with temporal lobe epilepsy. *Ann. Neurol.* 29, 325–332.

Salin, P. A., and Prince, D. A. (1996). Electrophysiological mapping of $GABA_A$ receptor-mediated inhibition in adult rat somatosensory cortex. *J. Neurophysiol.* 75, 1589–1600.

Seress, L., Abraham, H., Hajnal, A., Lin, H., and Totterdell, S. (2005). NOS-positive local circuit neurons are exclusively axo-dendritic cells both in the neo- and archi-cortex of the rat brain. *Brain Res.* 1056, 183–190.

Shlosberg, D., Abu-Ghanem, Y., and Amitai, Y. (2008). Comparative properties of excitatory and inhibitory inter-laminar neocortical axons. *Neuroscience* 155, 366–373.

Shlosberg, D., Patrick, S. L., Buskila, Y., and Amitai, Y. (2003). Inhibitory effect of mouse neocortex layer I on the underlying cellular network. *Eur. J. Neurosci.* 18, 2751–2759.

Silberberg, G., and Markram, H. (2007). Disynaptic inhibition between neocortical pyramidal cells mediated by Martinotti cells. *Neuron* 53, 735–746.

Sloviter, R. S. (1987). Decreased hippocampal inhibition and a selective loss of interneurons in experimental epilepsy. *Science* 235, 73–76.

Smiley, J. F., McGinnis, J. P., and Javitt, D. C. (2000). Nitric oxide synthase interneurons in the monkey cerebral cortex are subsets of the somatostatin, neuropeptide Y, and calbindin cells. *Brain Res.* 863, 205–212.

Sohal, V. S., Zhang, F., Yizhar, O., and Deisseroth, K. (2009). Parvalbumin neurons and gamma rhythms enhance cortical circuit performance. *Nature* 459, 698–702.

Tamamaki, N., and Tomioka, R. (2010). Long-range GABAergic connections distributed throughout the neocortex and their possible function. *Front. Neurosci.* 4, 202. doi: 10.3389/fnins.2010.00202

Tan, Z., Hu, H., Huang, Z. J., and Agmon, A. (2008). Robust but delayed thalamocortical activation of dendritic-targeting inhibitory interneurons. *Proc. Nat. Acad. Sci. U.S.A.* 105, 2187–2192.

Telfeian, A. E., and Connors, B. W. (2003). Widely integrative properties of layer 5 pyramidal cells support a role for processing of extralaminar synaptic inputs in rat neocortex. *Neurosci. Lett.* 343, 121–124.

Tomioka, R., and Rockland, K. S. (2007). Long-distance corticocortical GABAergic neurons in the adult monkey white and gray matter. *J. Comp. Neurol.* 505, 526–538.

Trevelyan, A. J., Sussillo, D., and Yuste, R. (2007). Feedforward inhibition contributes to the control of epileptiform propagation speed. *J. Neurosci.* 27, 3383–3387.

Uematsu, M., Hirai, Y., Karube, F., Ebihara, S., Kato, M., Abe, K., Obata, K., Yoshida, S., Hirabayashi, M., Yanagawa, Y., and Kawaguchi, Y. (2008). Quantitative chemical composition of cortical GABAergic neurons revealed in transgenic Venus-expressing rats. *Cereb. Cortex* 18, 315–330.

Valtschanoff, J. G., Weinberg, R. J., Kharazia, V. N., Schmidt, H. H., Nakane, M., and Rustioni, A. (1993). Neurons in rat cerebral cortex that synthesize nitric oxide: NADPH diaphorase histochemistry, NOS immunocytochemistry, and colocalization with GABA. *Neurosci. Lett.* 157, 157–161.

Vincent, S. R., and Kimura, H. (1992). Histochemical mapping of nitric oxide synthase in the rat brain. *Neuroscience* 46, 755–784.

Vruwink, M., Schmidt, H. H., Weinberg, R. J., and Burette, A. (2001). Substance P and nitric oxide signaling in cerebral cortex: anatomical evidence for reciprocal signaling between two classes of interneurons. *J. Comp. Neurol.* 441, 288–301.

Wang, Y., Toledo-Rodriguez, M., Gupta, A., Wu, C., Silberberg, G., Luo, J., and Markram, H. (2004). Anatomical, physiological and molecular properties of Martinotti cells in the somatosensory cortex of the juvenile rat. *J. Physiol.* 561, 65–90.

Williams, S. R., and Stuart, G. (2003). Voltage- and site-depenedent control of the somatic impact of dendritic IPSPs. *J. Neurosci.* 23, 7358–7367.

Conflict of Interest Statement: The authors declare that the research was conducted in the absence of any commercial or financial relationships that could be construed as a potential conflict of interest.

Received: 15 December 2011; accepted: 23 January 2012; published online: 07 February 2012.

Citation: Shlosberg D, Buskila Y, Abu-Ghanem Y and Amitai Y (2012) Spatiotemporal alterations of cortical network activity by selective loss of NOS-expressing interneurons. Front. Neural Circuits ***6****:3. doi: 10.3389/fncir.2012.00003*

frontiers in
NEURAL CIRCUITS

REVIEW ARTICLE
published: 16 May 2012
doi: 10.3389/fncir.2012.00023

Neurogliaform and Ivy cells: a major family of nNOS expressing GABAergic neurons

Caren Armstrong*, Esther Krook-Magnuson and Ivan Soltesz

Department of Anatomy and Neurobiology, University of California Irvine, Irvine, CA, USA

Edited by:
Ludovic Tricoire, Université Pierre et Marie Curie, France

Reviewed by:
Gianmaria Maccaferri, Northwestern University, USA
Thomas Klausberger, MRC University of Oxford, UK
Linda Overstreet-Wadiche, University of Alabama Birmingham, USA
Marco Capogna, Medical Research Council, UK

****Correspondence:***
Caren Armstrong, Department of Anatomy and Neurobiology, University of California, 192 Irvine Hall, Irvine, CA 92697-1280, USA.
e-mail: cmarmstr@uci.edu

Neurogliaform and Ivy cells are members of an abundant family of neuronal nitric oxide synthase (nNOS) expressing GABAergic interneurons found in diverse brain regions. These cells have a defining dense local axonal plexus, and display unique synaptic properties including a biphasic postsynaptic response with both a slow $GABA_A$ component and a $GABA_B$ component following even a single action potential. The type of transmission displayed by these cells has been termed "volume transmission," distinct from both tonic and classical synaptic transmission. Electrical connections are also notable in that, unlike other GABAergic cell types, neurogliaform family cells will form gap junctions not only with other neurogliaform cells, but also with non-neurogliaform family GABAergic cells. In this review, we focus on neurogliaform and Ivy cells throughout the hippocampal formation, where recent studies highlight their role in feedforward inhibition, uncover their ability to display a phenomenon called persistent firing, and reveal their modulation by opioids. The unique properties of this family of cells, their abundance, rich connectivity, and modulation by clinically relevant drugs make them an attractive target for future studies *in vivo* during different behavioral and pharmacological conditions.

Keywords: feedforward inhibition, persistent firing, opioid, $GABA_B$, $GABA_{A,slow}$

INTRODUCTION

The neurogliaform family of cells is one of the major groups of GABAergic neurons expressing nitric oxide synthase (nNOS). Neurogliaform cells, originally described by Cajal as arachniform cells (Ramón y Cajal, 1922; Ramón y Cajal, 1999), together with the closely related Ivy cells, which were only recently characterized (Fuentealba et al., 2008), are estimated to be the most abundant GABAergic cell type in area CA1 of the hippocampus (Fuentealba et al., 2008). However, the neurogliaform family of cells is found in large numbers not only throughout CA1, but also across a range of brain regions, including the entire hippocampal formation (Vida et al., 1998; Price et al., 2005; Elfant et al., 2008; Price et al., 2008; Karayannis et al., 2010; Szabadics et al., 2010; Armstrong et al., 2011; Krook-Magnuson et al., 2011; Markwardt et al., 2011), the neocortex (Tamas et al., 2003; Simon et al., 2005; Olah et al., 2007; Szabadics et al., 2007; Olah et al., 2009), the piriform cortex (Suzuki and Bekkers, 2012), striatum (Ibanez-Sandoval et al., 2011), and the habenula of the thalamus (Weiss and Veh, 2011). Thus, these cells are not only abundant, but also widespread. Yet their function in the context of local circuit dynamics is only beginning to be unraveled.

Here, in addition to reviewing the known anatomical, synaptic, neuromodulatory, and connective properties of neurogliaform family cells, we discuss their potential network functions, particularly in the hippocampal formation.

UNIQUE AXONS, UNIQUE CONNECTIONS

Despite their wide distribution, cells within the neurogliaform family have very similar characteristics across brain regions, and these unique characteristics clearly set them apart from other GABAergic cell types. Neurogliaform cells have a dense local axonal plexus and generally small, round, somata (**Figure 1**). The axons of neurogliaform cells have frequent, small *en passant* boutons, which despite their small size can form synaptic contacts (Vida et al., 1998; Fuentealba et al., 2008; Olah et al., 2009). The synapses formed by neurogliaform family cell boutons, however, do not necessarily form classical synapses like those of other GABAergic cell classes, in that the synaptic cleft at identified synapses is unusually wide and some boutons, complete with synaptic vesicles, do not have an easily identifiable postsynaptic target in the classical sense (Vida et al., 1998; Olah et al., 2009). Their unique synaptic and axonal morphologies underlie some key features of neurogliaform synaptic transmission (**Figure 2**), namely (1) the ability of neurogliaform cells to mediate GABAergic volume transmission, affecting virtually any processes within their dense axonal plexus, (2) the production of a slow $GABA_A$ current in the postsynaptic cell ($GABA_{A,slow}$), and (3) the postsynaptic $GABA_B$ response to even a single neurogliaform action potential (Tamas et al., 2003; Price et al., 2005; Szabadics et al., 2007; Price et al., 2008; Olah et al., 2009; Karayannis et al., 2010; Capogna and Pearce, 2011).

Neurogliaform cells' ability to induce a biphasic current in the postsynaptic cell, including both a $GABA_A$-mediated and a $GABA_B$-mediated component, is a property which has been consistently observed across brain regions (Tamas et al., 2003; Price et al., 2005; Olah et al., 2007; Szabadics et al., 2007; Armstrong et al., 2011). The $GABA_A$ and $GABA_B$-mediated components can be separated based on reversal potential, since the K^+-mediated $GABA_B$ component and the largely Cl^--mediated $GABA_A$ component reverse at different membrane potentials. Additionally, the $GABA_A$

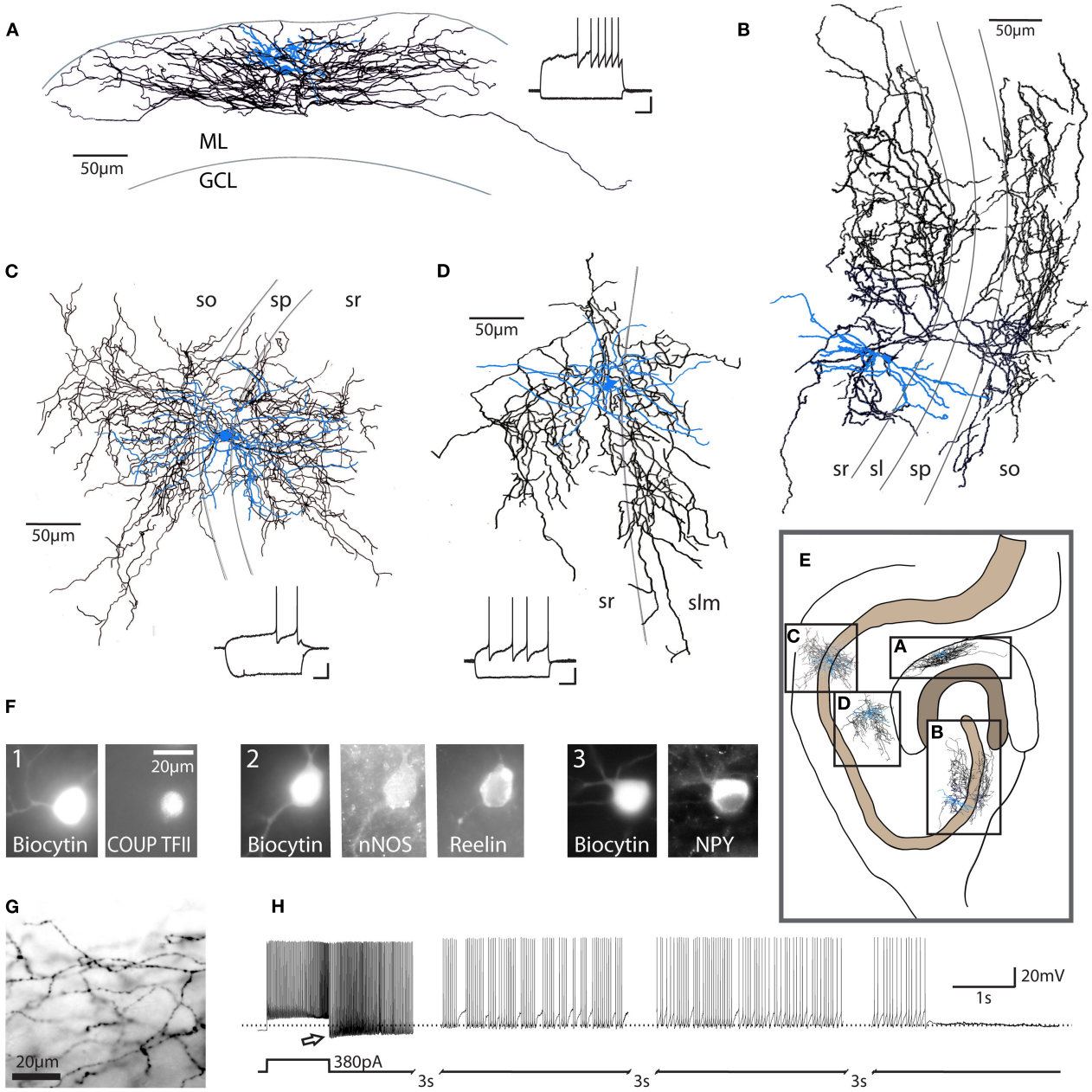

FIGURE 1 | Characteristics of neurogliaform family cells. Neurogliaform and Ivy cells in the hippocampus: **(A)** dentate gyrus neurogliaform cell, **(B)** CA3 Ivy cell, **(C)** CA1 Ivy cell, **(D)** CA1 neurogliaform cell; these cells are characterized by their dense local axonal plexus (black: axon; blue: somata and dendrites). These cells also show a characteristic late-spiking firing pattern in response to depolarizing current steps [insets, **(A,C,D)**; scale bars 20 mV, 200 ms]. ML, molecular layer; GCL, granule cell layer; so, stratum oriens; sp, stratum pyramidale; sl, stratum lucidum; sr, stratum radiatum; slm, stratum lacunosum-moleculare. Cells represented in **(A,B)** are from rat. Examples in **(C,D)** are from mouse. **(E)** Schematic diagram of the hippocampus, illustrating the approximate relative locations of cells in **(A–D)** (scale bar = 100 μm). Note that the Ivy cell reconstructed in **(C)** targets proximal dendrites, while the neurogliaform cell in **(D)** targets distal dendrites of CA1 pyramidal cells. **(F)** Recorded, biocytin-filled cells confirmed as neurogliaform cells in the dentate gyrus (three separate cells, numbered 1–3) express a variety of markers, including COUP TFII, nNOS, reelin, and NPY (scale bar = 20 μm) among others (see text). **(G)** Light microscopic image, showing the characteristic neurogliaform axonal arborization, with multiple axonal branches passing through a single plane of focus and frequent, small en passant boutons [same cell as **(A)**, scale bar 20 μm]. **(H)** In addition to the classical late-spiking pattern characteristic of these cells, a high percentage of neurogliaform and Ivy cells display the recently described phenomenon referred to as persistent firing. After hundreds of action potentials induced by repeated depolarizing current steps (note that only the last depolarizing step is shown here), the cell continues to fire action potentials after the cessation of depolarizing input (bottom trace: schematic of current injection; top trace: current clamp recording, dashed line indicates −60 mV). Note the apparent low action potential threshold (arrow). Due to the long duration of the persistent firing state, the trace has segments omitted (indicated by hash marks) for illustration purposes. Reproduced and modified with permission from Armstrong et al. (2011) **(A,F,G)**, Szabadics et al. (2010) **(B)**, and Krook-Magnuson et al. (2011) **(C,D,H)**.

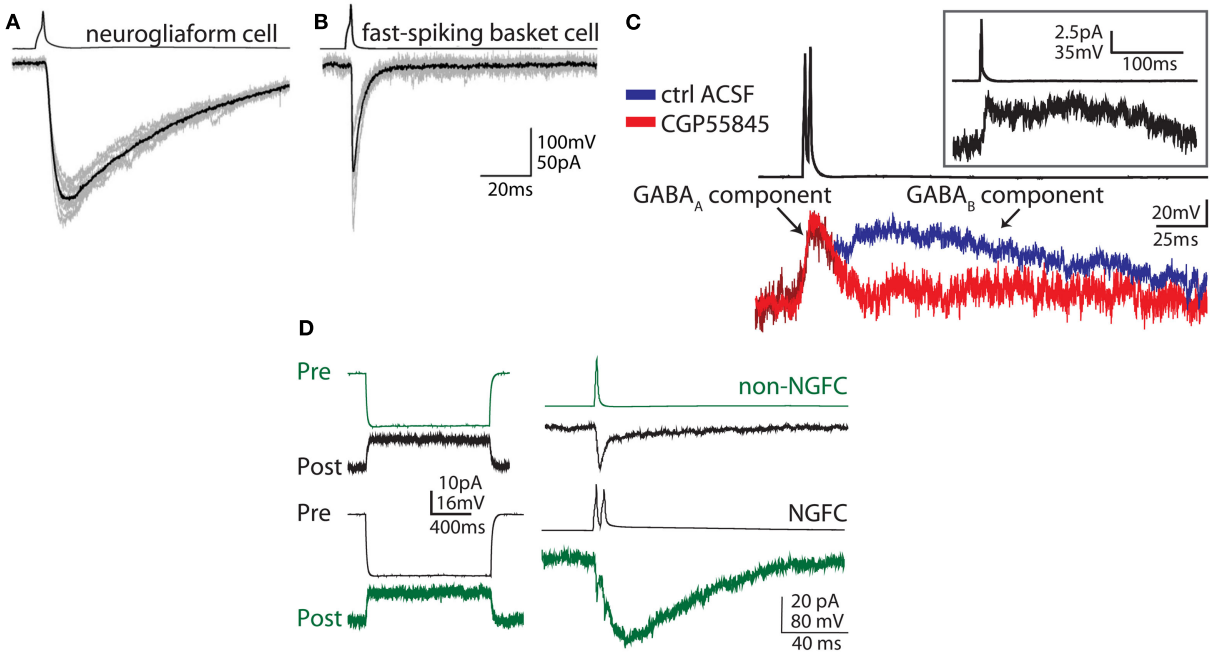

FIGURE 2 | Unique synaptic properties of neurogliaform cells. (A) Action potentials in a neurogliaform cell (top trace, example from neocortex) produce a slow IPSC ($GABA_{A,slow}$ – bottom trace) in the postsynaptic cell. **(B)** In contrast, action potentials in fast-spiking basket cell (top trace) produce an IPSC with fast kinetics in the postsynaptic cell (bottom trace). **(C)** Neurogliaform cells (averaged examples from dentate gyrus) produce a biphasic postsynaptic response, consisting of a slow $GABA_A$ and a $GABA_B$ component, which can be distinguished by application of the $GABA_B$ antagonist CGP55845 (red trace). This biphasic response can be seen following even a single presynaptic action potential (inset). **(D)** Neurogliaform cells (NGFC, black traces) can form both electrical and chemical synaptic connections with other GABAergic cell types. In this example, an electrical and unidirectional synaptic connection between a NGFC (black traces) and a non-NGFC (green traces) can be appreciated (example from dentate gyrus). *Left traces*: a hyperpolarizing current step (Pre, current clamp responses shown in the upper traces of each example), evokes an outward current in the electrically connected cell (Post, voltage clamp responses shown in the lower traces of each example). *Right*: When an action potential is evoked in the presynaptic non-NGFC, only a short inward current, due to electrical coupling, is observed in the connected NGFC, while both electrical and chemical synaptic responses can be appreciated in the postsynaptic non-NGFC in response to NGFC stimulation (upper traces, both pre and postsynaptic traces are averaged). Note the electrical responses in the non-NGFC riding on top of the slow GABA-mediated IPSC. Reproduced and modified with permission from Szabadics et al. (2007) **(A,B)** and Armstrong et al. (2011) **(C,D)**.

and $GABA_B$-mediated components can be pharmacologically separated using specific antagonists for $GABA_A$ and $GABA_B$ receptors (**Figure 2**). Importantly, this biphasic GABA-mediated current results in a large inhibitory charge transfer in the postsynaptic target, and involves even traditionally extrasynaptic receptors, such as δ subunit-containing $GABA_A$ receptors and $GABA_B$ receptors, as well as classically synaptic receptors, e.g., benzodiazepine-sensitive γ subunit-containing $GABA_A$ receptors (Szabadics et al., 2007; Olah et al., 2009; Karayannis et al., 2010).

The kinetics of the neurogliaform cell-evoked $GABA_A$ response are also considerably slower than the kinetics of responses to other GABAergic cell types, and these events, referred to as $GABA_{A,slow}$ (Pearce, 1993; reviewed in Capogna and Pearce, 2011), were shown to arise from neurogliaform cells (Tamas et al., 2003; Price et al., 2005; Szabadics et al., 2007). In theory, $GABA_{A,slow}$ could be due to multiple, asynchronous, vesicular release. However, the kinetics of the $GABA_{A,slow}$ response are not affected by altering release probability through variation of external Ca^{2+} concentration, such that vesicular release properties cannot explain the kinetics (Szabadics et al., 2007). Dendritic filtering of neurogliaform cell input to distal dendrites also cannot explain the slow kinetics, since other dendritically targeting cells (in this case, Martinotti cells) do not induce $GABA_{A,slow}$ (Szabadics et al., 2007). Further, while spillover of GABA does occur, affecting both $GABA_{A,slow}$ and $GABA_B$-mediated events, the extreme kinetics of the responses are not fully explained by GABA spillover. Importantly, the postsynaptic $GABA_{A,slow}$ response is highly sensitive to low-affinity competitive $GABA_A$ receptor antagonists, indicating that low concentrations of GABA at the postsynaptic membrane contribute to the slow unitary kinetics of neurogliaform cell connections (Szabadics et al., 2007). These data suggest that the nature of the GABA transient (the spatiotemporal concentration profile of GABA at the synapse) is largely responsible for the kinetics of neurogliaform connections (Krook-Magnuson and Huntsman, 2007; Szabadics et al., 2007; Karayannis et al., 2010). In turn, this unique GABA transient can be explained by the morphology of the synapse (i.e., the relatively small area combined with the relatively large distances between pre- and post-synaptic processes; Szabadics et al., 2007; Olah et al., 2009). Interestingly, although *in vivo* neurogliaform cells do fire in a phase-locked manner with theta rhythms (Fuentealba et al., 2010), paired neurogliaform cell connections in acute slices demonstrate profound depression with repeated

stimulation (Tamas et al., 2003), an effect which persists in the presence of $GABA_B$ antagonists (Karayannis et al., 2010).

The axonal arbors of neurogliaform cells described above are one of the most distinctive features of these cells. While the axons of neurogliaform cells form a unique dense, local plexus, they can also cross boundaries of brain regions. For example, neurogliaform cells were recently identified in the molecular layer of the dentate gyrus (Armstrong et al., 2011), where importantly, it was found that their axons can cross the hippocampal fissure and extend into the adjacent CA1 or subiculum (Armstrong et al., 2011). Similarly, axons of neurogliaform cells in the CA1 can cross into dentate molecular layer (Ceranik et al., 1997; Price et al., 2005; Fuentealba et al., 2010). This extension of axons across boundaries is a notable feature among GABAergic cells, suggesting that neurogliaform cells may serve to share information between, and coordinate the activities of, distinct brain regions.

Beyond their remarkable chemical synapses, neurogliaform cells are also unusual with regard to their electrical synapses. Interneurons typically form gap junctions preferentially with members of the same cell type. In contrast, neurogliaform cells frequently form gap junctions with a wide variety of other GABAergic cell types (**Figure 2**; Simon et al., 2005; Zsiros and Maccaferri, 2005; Olah et al., 2007; Zsiros and Maccaferri, 2008; Armstrong et al., 2011). This is important when considering the role of neurogliaform cells in hippocampal networks, which will be discussed below.

DIVERSITY AND DIVISIONS

Despite the similarities in axonal and synaptic properties of individual cells of the neurogliaform family, there are some notable differences between them as well. Members of the neurogliaform family may differ in where they reside within a given brain region, the input they receive, and the domain of the postsynaptic cells their axons target, as well as in the neuronal markers that they express.

As mentioned above, the neurogliaform family of cells is composed of neurogliaform cells and Ivy cells. Neurogliaform cells classically target the distal dendrites of principal cells while Ivy cells, which have to date been definitively identified in the CA1 and the CA3 of the hippocampus (Fuentealba et al., 2008; Szabadics and Soltesz, 2009; Szabadics et al., 2010), have a unique position in and around the pyramidal cell layer, where they may have different incoming and outgoing connectivity when compared to neurogliaform cells. In the CA1, where Ivy cells were first described (Fuentealba et al., 2008), neurogliaform cells in and near the stratum lacunosum-moleculare receive excitatory inputs from both the temporo-ammonic pathway and CA3 Schaffer collaterals, and in turn target the distal dendrites of CA1 pyramidal cells (**Figures 1** and **3**; Price et al., 2005; Fuentealba et al., 2010). In contrast, Ivy cells reside in or near the stratum pyramidale, receive excitatory input from local pyramidal cells as well as presumably from CA3 Schaffer collaterals, and target the proximal dendrites of CA1 pyramidal cells (Fuentealba et al., 2008). This differential input means that, while neurogliaform cells near the CA1 lacunosum-moleculare serve a primarily feedforward inhibitory role, Ivy cells near the pyramidale are poised to mediate both feedforward and feedback inhibition to CA1 pyramidal cells. Ivy and neurogliaform cells can also differ in their *in vivo* firing properties and dendritic morphologies (Fuentealba et al., 2008; Fuentealba et al., 2010), and differences in network functions of neurogliaform and Ivy cells *in vivo* will be discussed further below.

Even within the different types of neurogliaform family cells, there are differences in neuronal markers that can be used for identification. Thus, while neuropeptide Y (NPY), nNOS, COUP TFII, α-actinin, $GABA_A\alpha_1$, $GABA_A\delta$, and reelin are notably found in neurogliaform cells (**Figure 1**), there is significant heterogeneity in marker expression from cell to cell such that no one marker or combination of markers captures, uniquely, all neurogliaform cells (Deller and Leranth, 1990; Ratzliff and Soltesz, 2001; Price et al., 2005; Simon et al., 2005; Fuentealba et al., 2008; Karagiannis et al., 2009; Olah et al., 2009; Fuentealba et al., 2010; Tricoire et al., 2010). Ivy cells of the CA1 seem to share many of the same markers as neurogliaform cells, but have not been observed to express reelin (Fuentealba et al., 2010). Interestingly, the presence or absence of nNOS may serve as a marker of developmental origin for both neurogliaform and Ivy cells, that is whether the cells arise from the medial or caudal ganglionic eminences, both of which can generate neurogliaform family cells (Tricoire et al., 2010).

ELECTROPHYSIOLOGICAL PROPERTIES OF NEUROGLIAFORM FAMILY CELLS

As might be expected due to their differential inputs and placement within the CA1, Ivy and neurogliaform cells of the CA1 differ also in their *in vivo* firing patterns. In anesthetized animals, when both theta and gamma oscillations are recorded from the stratum pyramidale, individual Ivy cells fire at a low frequency shortly after the trough of theta – that is, after CA3 input and just after CA1 pyramidal cells fire – and during the trough of gamma oscillations, while staying primarily silent during ripples (Fuentealba et al., 2008; Klausberger and Somogyi, 2008; Mizuseki et al., 2009; Fuentealba et al., 2010). On the other hand, neurogliaform cells fire just after the peak of theta, following input to CA1 from the entorhinal cortex; are phase-coupled with the locally recorded gamma; and are either unmodulated by, or show a decrease in firing during ripples (Buzsaki, 2002; Fuentealba et al., 2010). In awake animals, putative Ivy cells recorded using tetrodes have similar firing properties during theta oscillations and ripples as Ivy cells in anaesthetized animals (Fuentealba et al., 2008).

Despite these differences in firing patterns *in vivo*, when recordings are made from slices in whole-cell patch configuration, both Ivy and neurogliaform cells exhibit a characteristic late-spiking firing pattern, often with a depolarizing ramp and subthreshold oscillations in the gamma frequency range leading up to the first spikes (Szabadics et al., 2007; Armstrong et al., 2011; Krook-Magnuson et al., 2011; Weiss and Veh, 2011; **Figure 1**). While neurogliaform cells of rodents typically do not exhibit a sag upon hyperpolarization, neurogliaform cells of humans and monkeys do (Olah et al., 2007; Povysheva et al., 2007).

Both Ivy and neurogliaform cells exhibit the recently described phenomenon of persistent firing (Krook-Magnuson et al., 2011; **Figure 1**). Persistent firing is a state of continued firing in the absence of continued input (Sheffield et al., 2011). Experimentally, it is induced by repeated somatic current injections, causing the cell to fire hundreds of action potentials over the span of minutes.

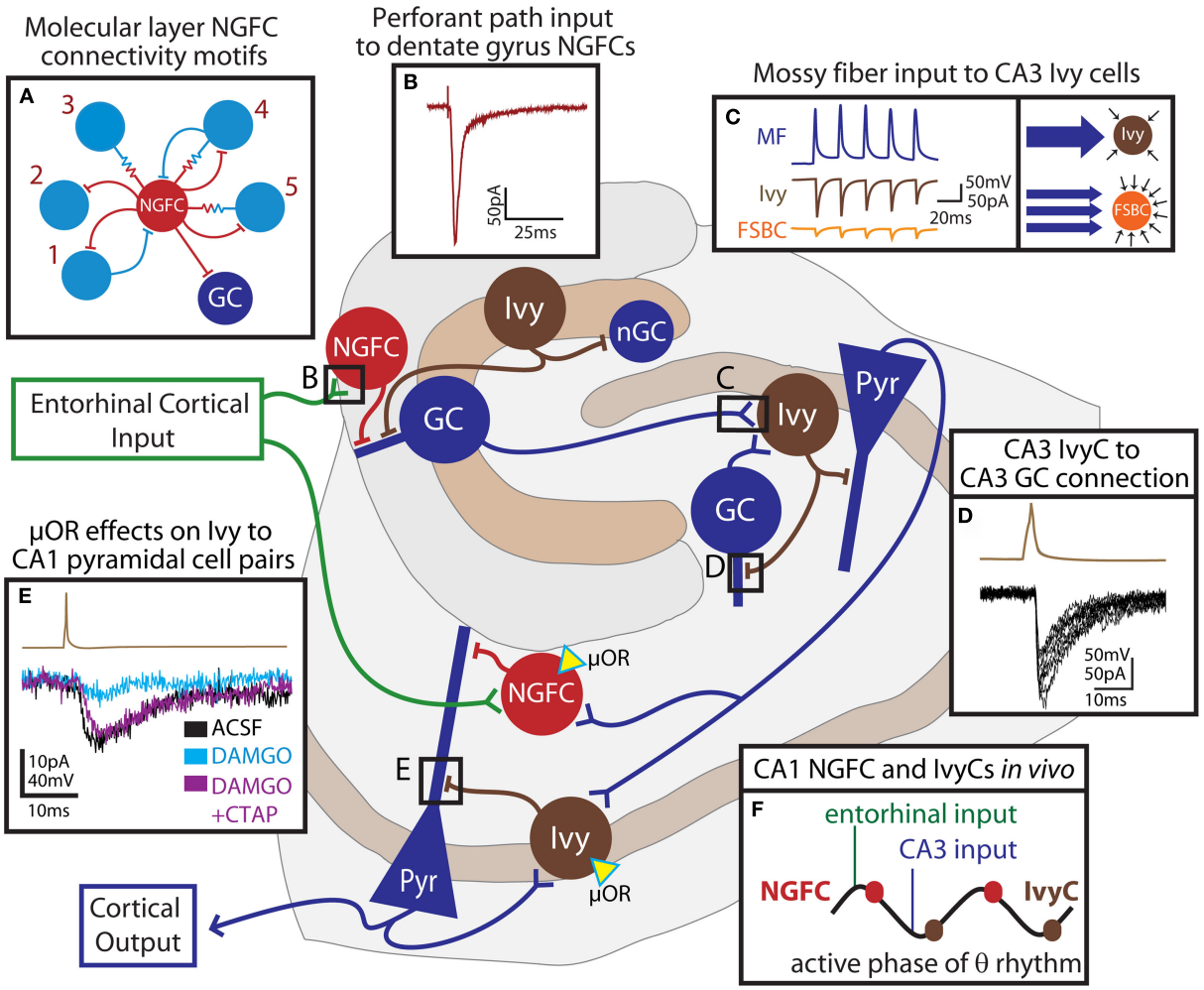

FIGURE 3 | Feedforward network functions of neurogliaform family cells in the hippocampus. The schematic outlines the connectivity of hippocampal neurogliaform and Ivy cells with principal cells. Entorhinal cortical input (green) directly excites NGFCs (red cells) both in the dentate gyrus and in the CA1. These cells provide feedforward inhibition to principal cells (blue) of the dentate gyrus or CA1, respectively. In the dentate, neurogliaform family cells targeting proximal dendrites (Ivy, brown) provide inhibition to both adult granule cells (GC) and newly born granule cells (nGC). Granule cells of the dentate, as well as granule cells of the CA3 provide mossy fiber input to CA3 Ivy cells, which provide both feedforward inhibition to pyramidal cells (Pyr) and feedback inhibition to CA3, but not dentate, granule cells. Schaffer collateral input to the CA1 contacts CA1 NGFCs and presumably, Ivy cells which both provide feedforward inhibition to CA1 pyramidal cells. CA1 pyramidal cells also provide feedback excitation to Ivy cells. Both NGFCs and Ivy cells in the CA1 express the μ-opioid receptor (μOR, yellow triangle). In this simplified schematic, excitatory input to excitatory cells has been omitted. **(A)** indicates the observed connectivity of NGFCs (red) in the dentate gyrus with other interneurons (light blue), consisting of five different connectivity motifs (1: bidirectional chemical synaptic; 2: unidirectional chemical synaptic; 3: electrical only; 4 electrical and bidirectional chemical synaptic; and 5: electrical and unidirectional chemical synaptic). **(B)** shows the response in a dentate gyrus NGFC to perforant path stimulation. **(C)** illustrates that individual mossy fiber boutons (MF, blue trace) form strong unitary connections (left box) with postsynaptic Ivy cells in the CA3 (brown traces) while unitary connections between mossy fiber boutons and fast-spiking basket cells (FSBC, orange traces) are smaller in amplitude. However (right box), while Ivy cells receive relatively fewer individual connections from mossy fibers, FSBCs receive more frequent mossy fiber bouton input. **(D)** demonstrates, in a paired recording, that Ivy cells (action potential, brown trace) provide inhibition to CA3 GCs (IPSCs, black traces). **(E)** shows the effect of the μ-opioid receptor agonist, DAMGO on an Ivy cell (brown trace) to CA1 pyramidal cell (lower traces) pair. The paired connection (control ACSF, black) is nearly abolished by application of DAMGO (light blue), and can be restored by addition of the μ-opioid receptor antagonist, CTAP (DAMGO + CTAP, purple). **(F)** indicates the relative timing of NGFC and Ivy cell firing during theta rhythms recorded from the pyramidal cell layer *in vivo*. NGFCs tend to fire right after the peak of theta, shortly following entorhinal input, while Ivy cells tend to fire right after the trough, shortly following CA3 input and just after the firing of CA1 cells. Reproduced and modified with permission from Armstrong et al. (2011) **(A,B)**; Szabadics and Soltesz (2009) **(C)**; Szabadics et al. (2010) **(D)**, and Krook-Magnuson et al. (2011) **(E)**.

During this time period, there appears to be an integration of spiking information, eventually resulting in the induction of persistent firing. Once this state of persistent firing is achieved, spiking occurs without further input for tens of seconds (though in rare instances it can persist for over 10 min; Sheffield et al., 2011). Persistent firing is not affected by blocking $GABA_A$, $GABA_B$, AMPA, and NMDA

receptors (Sheffield et al., 2011), but induction is inhibited by activation of μ-opioid receptors (Krook-Magnuson et al., 2011). The apparent threshold for firing during persistent firing is very low when recording from the soma, and it has been shown that this is due to the action potentials starting in the axons themselves and back-propagating to the soma (Sheffield et al., 2011). Somatically recorded spikes have an initial component, representing spiking in the axon, and a subsequent component, indicative of a somatodendritic spike (Sheffield et al., 2011). The mechanism permitting the integration of spiking information over the span of minutes, required for the induction of persistent firing, is a matter of open debate and investigation, as are the physiological consequences of persistent firing. Importantly, however, not all interneurons display persistent firing (Krook-Magnuson et al., 2011; Sheffield et al., 2011). Indeed, less than 20% of fast-spiking parvalbumin expressing basket cells display persistent firing, in contrast to over 80% of neurogliaform family cells (Krook-Magnuson et al., 2011).

NETWORK AND FUNCTIONAL ROLES OF NEUROGLIAFORM AND IVY CELLS

Neurogliaform family cells have recently been described in the dentate gyrus (Armstrong et al., 2011; Markwardt et al., 2011). Neurogliaform cells located in the middle and outer molecular layers receive entorhinal input and synapse on distal dendrites of granule cells, meaning that they are capable of providing feedforward inhibition (Armstrong et al., 2011; **Figures 1** and **3**). Compared to granule cells, neurogliaform cells in the dentate molecular layer receive fewer spontaneous inputs (consisting of excitatory and inhibitory events at roughly equal frequencies) to their small dendritic arbors than granule cells. However, like granule cells, they do receive direct perforant path input from the entorhinal cortex. This perforant path input is facilitating at high frequencies, and suggests that neurogliaform cells may act to inhibit granule cells primarily during high frequency incoming activity (Armstrong et al., 2011).

In regions like the dentate gyrus, where granule cells exhibit sparse firing, feedforward GABAergic input has been predicted to play a major role in normal function (Ferrante et al., 2009), including for spatial navigation, as well as in pathological states, such as in epilepsy. Because neurogliaform cells target the distal dendrites of principal cells, they may have stronger effects on the processing of incoming input in dendritic compartments than on spike timing control *per se*. However, inhibitory dendritic input, in addition to its role in dendritic processing, has also recently been shown to have major effects on the firing of postsynaptic cells (Lovett-Barron et al., 2012). Thus, new studies will be necessary to determine what the major effect of neurogliaform cell activation may be during concurrent dendritic input to granule cells from other sources.

The fact that neurogliaform cells form both chemical and electrical synapses with other classes of GABAergic neurons means that they can display a variety of connectivity motifs. In the dentate gyrus molecular layer, for example, every possible two-cell connectivity motif between neurogliaform cells and other types of interneurons was observed (electrical only, unidirectional synaptic, bidirectional synaptic, and combinations of electrical and synaptic connections; Armstrong et al., 2011; **Figure 3**). The microcircuit functions of neurogliaform family cells in this context remain to be determined. This arrangement could serve a number of important roles in the network, possibly synchronizing neuronal subgroups, inhibiting nearby neuronal subgroups, or acting as low-pass filters on incoming input to distinct cell types (Mitchell and Silver, 2003; Zsiros et al., 2007). Computational studies will help to determine the significance of this connectivity for overall network function (Santhakumar et al., 2005; Dyhrfjeld-Johnsen et al., 2007; Morgan and Soltesz, 2008; Ferrante et al., 2009; Cutsuridis and Hasselmo, 2012).

In the dentate, where neurogenesis of granule cells occurs throughout life, cells of the neurogliaform family play another important role, being among the first sources of input to newly born granule cells (Markwardt et al., 2011). Dentate neurogliaform family cells not only inhibit adult granule cells directly, but also inhibit other interneurons (indeed, burst firing in neurogliaform family cells during 4AP application coincided with robust suppression of spontaneous firing of other interneuronal types) and may therefore also disinhibit mature cells (Markwardt et al., 2011). In this way, neurogliaform family cells might coordinate activity of both newly born and adult granule cells, via direct depolarization of newborn granule cells (through depolarizing GABA effects) and coincident disinhibition of mature cells (Markwardt et al., 2011). The advent of novel ways to probe the roles of specific neuronal subgroups *in vivo*, such as optogenetic methods, provide ways of investigating how neurogliaform family cells may enhance or direct the integration of newly born cells into the network, and to better understand under what conditions neurogliaform cells have a predominately inhibitory action on adult granule cells (e.g., feedforward inhibition), and under what conditions neurogliaform cells produce a net disinhibition of granule cells (by inhibiting other interneurons).

Just as neurogliaform cells can mediate feedforward inhibition to dentate granule cells, Ivy cells in the CA3 region are similarly positioned to mediate feedforward inhibition to CA3 pyramidal cells (Szabadics and Soltesz, 2009). In paired recordings between mossy fiber boutons of granule cells and postsynaptic CA3 interneurons, Ivy cells received fewer, but stronger unitary connections from mossy fibers than fast-spiking basket cells (Szabadics and Soltesz, 2009). This arrangement suggests that individual large amplitude inputs from individual mossy fibers to Ivy cells may be capable of inducing feedforward inhibition to CA3 pyramidal cells, while other interneurons, such as fast-spiking basket cells, require greater convergent input from a number of mossy fiber terminals in order to produce feedforward inhibition. Interestingly, granule cells have recently been identified within the CA3, where their excitatory inputs from entorhinal cortex and mossy fiber outputs to both glutamatergic and GABAergic cells of the CA3, as well as their electrophysiological properties, are similar to those of granule cells located in the dentate (Szabadics et al., 2010). Unlike dentate granule cells, however, CA3 granule cells have reciprocal connections with CA3 Ivy cells, as well as with other GABAergic cells of the CA3 (Szabadics et al., 2010; **Figure 3**). Therefore, CA3 granule cells represent a unique, local glutamatergic neuronal subtype which in addition to both exciting CA3 pyramidal cells and GABAergic

cells to drive feedforward inhibition, also receive feedback input from the CA3 GABAergic network. Ivy cells providing simultaneous feedforward inhibition to CA3 pyramidal cells and feedback inhibition of CA3 granule cells, may have important implications for oscillatory activity and spike timing within this brain region.

Finally, neurogliaform cells in CA1 are also positioned to mediate feedforward inhibition, as they receive input from both CA3 and entorhinal cortex, and in turn inhibit CA1 pyramidal cells (in addition to interneurons; Vida et al., 1998; Price et al., 2005; Price et al., 2008). Feedforward inhibition in CA1 can be very strong; following the stimulation of the temporoammonic pathway, a predominately inhibitory response is generated in CA1 pyramidal cells (Soltesz and Jones, 1995). Relevant to our discussion, this inhibitory response consists of both postsynaptic $GABA_A$ and $GABA_B$ components (Empson and Heinemann, 1995), which may implicate involvement of neurogliaform cells.

NEUROMODULATORS AND NEUROGLIAFORM FAMILY CELLS

Neuromodulatory influences onto and arising from neurogliaform family cells are only beginning to be uncovered. One recent interesting finding involves the effects of opioids on these cells in the CA1. In studies of input to CA1 from CA3 and entorhinal cortex, it was noted that stimulating the temporo-ammonic pathway one theta cycle before stimulating Schaffer collateral input leads to inhibition of the second excitatory input to CA1 pyramidal cells in a $GABA_B$-dependent, opioid-sensitive manner (Dvorak-Carbone and Schuman, 1999; McQuiston, 2011). In the context of the known properties of neurogliaform family cells, this observation suggests that neurogliaform cells could be modulated by opioids. In fact, both Ivy and neurogliaform cells were recently found to be highly modulated by μ-opioid receptors (Krook-Magnuson et al., 2011). Activation of μ-opioid receptors produced both somatic hyperpolarization and inhibition of neurotransmitter release from terminals. Indeed, in paired recordings between Ivy and pyramidal cells, activation of μ-opioid receptors nearly abolished the Ivy cell-mediated inhibitory postsynaptic current (IPSC; **Figure 3**). Together these findings and others suggest not only that neurogliaform cells can mediate feedforward inhibition, and that feedforward inhibition interacts with the timing of impinging excitatory inputs to CA1 pyramidal cells, but also that this inhibition is highly modulated by opioids. This has implications both for understanding the mechanisms of action of drugs of abuse that act at the μ-opioid receptor (such as heroin), as well as for the physiological function of CA1 during exploration, learning, and memory. Indeed, μ-opioid receptor knock-out mice show reduced radial-arm maze and Morris water maze performance (Jamot et al., 2003). Further, alterations in the hippocampal opioid system are also seen, for example, in epilepsy and Alzheimer's, indicating a potential role in these disorders (Laorden et al., 1985; Gall, 1988; Gall et al., 1988; D'Intino et al., 2006; Rocha et al., 2007; Cuellar-Herrera et al., 2012). Moreover, in a model of Alzheimer's it was found that the reported increase in enkephalin (an endogenous ligand for μ-opioid receptors) contributed to the cognitive difficulties associated with the disease (Meilandt et al., 2008), indicating that changes in the hippocampal opioid system can have significant functional consequences.

In addition to new insights into the neuromodulation of neurogliaform family output, the expression of such neuroactive markers as NPY and nNOS suggests that neurogliaform family cells may be important sources of both NPY and NO in the brain. NPY is a neuropeptide with a range of reported functions, including stimulating dentate neurogenesis (Howell et al., 2007). Additionally, NPY is implicated in anxiolysis, in the mechanisms of antidepressants (reviewed in Heilig, 2004), and in response to stress–veterans exposed to traumatic experiences but who had higher plasma levels of NPY experienced fewer stress-related sequelae such as post-traumatic stress disorder (PTSD) and depression than those with lower NPY levels (Morgan et al., 2002; Yehuda et al., 2006). Interestingly, NPY may also be important in epilepsy; both the level of NPY protein and its receptor subtypes are robustly changed after seizures, and NPY overexpression is protective against acute and chronic seizures. This suggests that neurogliaform family cells may be important in suppressing seizure activity in epilepsy (Vezzani et al., 1999; Bacci et al., 2002; Noè et al., 2008; Noe et al., 2010; Kovac et al., 2011).

The expression of nNOS by cells of the neurogliaform family is especially interesting since it is not yet known how the interneuronal production of NO may contribute to overall network activity. While the known functions of NO in neuronal and non-neuronal tissues are numerous, the roles of nNOS and NO in specific GABAergic cell types, such as neurogliaform family cells, has yet to be determined. However, NO is a well-known retrograde modulator, and nNOS in neurogliaform cells may therefore involve synapse- and cell type-specific regulation of transmission from both excitatory and inhibitory inputs. This may serve to modulate levels of neurogliaform activity (and thus levels of GABAergic volume transmission) during specific input patterns (Szabadits et al., 2007; Feil and Kleppisch, 2008; Maggesissi et al., 2009; Zanelli et al., 2009; Szabadits et al., 2011), or to affect long term synaptic plasticity (Shin and Linden, 2005; Anwyl, 2006; Lange et al., 2012). In addition, the known vasodilatory role of NO in the peripheral circulatory system and in the CNS (Hall and Behbehani, 1998; Cauli et al., 2004; Corsani et al., 2008; Melikian et al., 2009) suggests the possibility that neurogliaform family cells might play a major role in increasing perfusion to regions that are particularly active (Tamas et al., 2003; Simon et al., 2005). More studies are clearly needed to definitively address the role of nNOS in the function of neurogliaform family cells.

SUMMARY AND OUTLOOK

Neurogliaform family cells have unique intrinsic and synaptic properties and are found in a range of brain regions, including throughout the hippocampal formation. A number of roles for neurogliaform family cells have been proposed. In addition to functions related to their expression of NPY and nNOS, roles in influencing network synchrony and oscillatory activity have been proposed (Tamas et al., 2003; Simon et al., 2005; Zsiros et al., 2007; Fuentealba et al., 2008; Price et al., 2008; Olah et al., 2009; Karayannis et al., 2010). Their modulation by μ-opioid receptors suggests that volume transmission by neurogliaform family cells may play

a major role in the effects of opiates, and may be of importance for future pharmacological insights.

Interestingly, some GABAergic populations have been observed to select postsynaptic partners based on long-range projection patterns. For example, in the entorhinal cortex, CCK-positive basket cells selectively target only those principal cells which project to contralateral extrahippocampal structures, avoiding principal cells which project to the ipsilateral hippocampus and form the perforant path (Varga et al., 2010). In contrast, due to their unique volume neurotransmission, neurogliaform cells are likely to indiscriminately inhibit all cells with processes within their axonal arbors. Thus, neurogliaform cells may represent a GABAergic cell class which coordinates the activity, or level of activity, between neurons processing information destined for distinct brain regions (Krook-Magnuson et al., 2012). This idea is particularly interesting when considering that cells with different long-range projection patterns may intermingle within a single cell layer (Varga et al., 2010). Moreover, as neurogliaform cells have been found to cross boundaries (e.g., the hippocampal fissure), they may also directly regulate concurrent activity in distinct brain regions (Ceranik et al., 1997; Price et al., 2005; Fuentealba et al., 2010; Armstrong et al., 2011).

The role of neurogliaform family cells as important feedforward inhibitors is supported by *in vitro* and existing *in vivo* data, but the wide connectivity and unique properties of these cells with other interneurons complicates our understanding of their true network functions. Ultimately, more studies, including studies *in vivo* in awake, behaving animals are needed to determine how neurogliaform and Ivy cells behave in information processing and network activities during different behavioral states. A comprehensive understanding of the roles of these unique neurons and their peculiar connective properties promises to shed light on new mechanisms by which microcircuits interact within and across brain areas.

ACKNOWLEDGMENTS

This work was supported by the US National Institutes of Health grants NS35915, NS074702, and NS74432, the Epilepsy Foundation (to Caren Armstrong), and the George E. Hewitt Foundation for Medical Research (to Esther Krook-Magnuson).

REFERENCES

Anwyl, R. (2006). Induction and expression mechanisms of postsynaptic NMDA receptor-independent homosynaptic long-term depression. *Prog. Neurobiol.* 78, 17–37.

Armstrong, C., Szabadics, J., Tamas, G., and Soltesz, I. (2011). Neurogliaform cells in the molecular layer of the dentate gyrus as feed-forward gamma-aminobutyric acidergic modulators of entorhinal-hippocampal interplay. *J. Comp. Neurol.* 519, 1476–1491.

Bacci, A., Huguenard, J. R., and Prince, D. A. (2002). Differential modulation of synaptic transmission by neuropeptide Y in rat neocortical neurons. *Proc. Natl. Acad. Sci. U.S.A.* 99, 17125–17130.

Buzsaki, G. (2002). Theta oscillations in the hippocampus. *Neuron* 33, 325–340.

Capogna, M., and Pearce, R. A. (2011). GABAA, slow: causes and consequences. *Trends Neurosci.* 34, 101–112.

Cauli, B., Tong, X.-K., Rancillac, A., Serluca, N., Lambolez, B., Rossier, J., and Hamel, E. (2004). Cortical GABA interneurons in neurovascular coupling: relays for subcortical vasoactive pathways. *J. Neurosci.* 24, 8940–8949.

Ceranik, K., Bender, R., Geiger, J. R., Monyer, H., Jonas, P., Frotscher, M., and Lubke, J. (1997). A novel type of GABAergic interneuron connecting the input and the output regions of the hippocampus. *J. Neurosci.* 17, 5380–5394.

Corsani, L., Bizzoco, E., Pedata, F., Gianfriddo, M., Faussone-Pellegrini, M. S., and Vannucchi, M. G. (2008). Inducible nitric oxide synthase appears and is co-expressed with the neuronal isoform in interneurons of the rat hippocampus after transient ischemia induced by middle cerebral artery occlusion. *Exp. Neurol.* 211, 433–440.

Cuellar-Herrera, M., Velasco, A. L., Velasco, F., Chavez, L., Orozco-Suarez, S., Armagan, G., Turunc, E., Bojnik, E., Yalcin, A., Benyhe, S., Borsodi, A., Alonso-Vanegas, M., and Rocha, L. (2012). Mu opioid receptor mRNA expression, binding, and functional coupling to G-proteins in human epileptic hippocampus. *Hippocampus* 22, 122–127.

Cutsuridis, V., and Hasselmo, M. (2012). GABAergic contributions to gating, timing, and phase precession of hippocampal neuronal activity during theta oscillations. *Hippocampus.*

D'Intino, G., Vaccari, F., Sivilia, S., Scagliarini, A., Gandini, G., Giardino, L., and Calza, L. (2006). A molecular study of hippocampus in dogs with convulsion during canine distemper virus encephalitis. *Brain Res.* 1098, 186–195.

Deller, T., and Leranth, C. (1990). Synaptic connections of neuropeptide Y (NPY) immunoreactive neurons in the hilar area of the rat hippocampus. *J. Comp. Neurol.* 300, 433–447.

Dvorak-Carbone, H., and Schuman, E. M. (1999). Patterned activity in stratum lacunosum moleculare inhibits CA1 pyramidal neuron firing. *J. Neurophysiol.* 82, 3213–3222.

Dyhrfjeld-Johnsen, J., Santhakumar, V., Morgan, R. J., Huerta, R., Tsimring, L., and Soltesz, I. (2007). Topological determinants of epileptogenesis in large-scale structural and functional models of the dentate gyrus derived from experimental data. *J. Neurophysiol.* 97, 1566–1587.

Elfant, D., Pal, B. Z., Emptage, N., and Capogna, M. (2008). Specific inhibitory synapses shift the balance from feedforward to feedback inhibition of hippocampal CA1 pyramidal cells. *Eur. J. Neurosci.* 27, 104–113.

Empson, R. M., and Heinemann, U. (1995). The perforant path projection to hippocampal area CA1 in the rat hippocampal-entorhinal cortex combined slice. *J. Physiol. (Lond.)* 484(Pt 3), 707–720.

Feil, R., and Kleppisch, T. (2008). "NO/cGMP-dependent modulation of synaptic transmission," *Pharmacology of Neurotransmitter Release*, eds T. C. Südhof and K. Starke (Berlin: Springer), 529–560.

Ferrante, M., Migliore, M., and Ascoli, G. A. (2009). Feed-forward inhibition as a buffer of the neuronal input-output relation. *Proc. Natl. Acad. Sci. U.S.A.* 106, 18004–18009.

Fuentealba, P., Begum, R., Capogna, M., Jinno, S., Marton, L. F., Csicsvari, J., Thomson, A., Somogyi, P., and Klausberger, T. (2008). Ivy cells: a population of nitric-oxide-producing, slow-spiking GABAergic neurons and their involvement in hippocampal network activity. *Neuron* 57, 917–929.

Fuentealba, P., Klausberger, T., Karayannis, T., Suen, W. Y., Huck, J., Tomioka, R., Rockland, K., Capogna, M., Studer, M., Morales, M., and Somogyi, P. (2010). Expression of COUP-TFII nuclear receptor in restricted GABAergic neuronal populations in the adult rat hippocampus. *J. Neurosci.* 30, 1595–1609.

Gall, C. (1988). Seizures induce dramatic and distinctly different changes in enkephalin, dynorphin, and CCK immunoreactivities in mouse hippocampal mossy fibers. *J. Neurosci.* 8, 1852–1862.

Gall, C. M., Pico, R. M., and Lauterborn, J. C. (1988). Focal hippocampal lesions induce seizures and long-lasting changes in mossy fiber enkephalin and CCK immunoreactivity. *Peptides* 9(Suppl. 1), 79–84.

Hall, C. W., and Behbehani, M. M. (1998). Synaptic effects of nitric oxide on enkephalinergic, GABAergic, and glutamatergic networks of the rat periaqueductal gray. *Brain Res.* 805, 69–87.

Heilig, M. (2004). The NPY system in stress, anxiety and depression. *Neuropeptides* 38, 213–224.

Howell, O. W., Silva, S., Scharfman, H. E., Sosunov, A. A., Zaben, M., Shatya, A., Mckhann Ii, G., Herzog, H., Laskowski, A., and Gray, W. P. (2007). Neuropeptide Y is important for basal and seizure-induced precursor cell proliferation in the hippocampus. *Neurobiol. Dis.* 26, 174–188.

Ibanez-Sandoval, O., Tecuapetla, F., Unal, B., Shah, F., Koos, T., and Tepper, J. M. (2011). A novel functionally distinct subtype of striatal neuropeptide Y interneuron. *J. Neurosci.* 31, 16757–16769.

Jamot, L., Matthes, H. W., Simonin, F., Kieffer, B. L., and Roder, J. C. (2003). Differential involvement of the mu and kappa opioid receptors in spatial learning. *Genes Brain Behav.* 2, 80–92.

Karagiannis, A., Gallopin, T., David, C., Battaglia, D., Geoffroy, H., Rossier, J., Hillman, E. M., Staiger, J. F., and Cauli, B. (2009). Classification of NPY-expressing neocortical interneurons. *J. Neurosci.* 29, 3642–3659.

Karayannis, T., Elfant, D., Huera-Ocampo, I., Teki, S., Scott, R. S., Rusakov, D. A., Jones, M. V., and Capogna, M. (2010). Slow GABA transient and receptor desensitization shape synaptic responses evoked by hippocampal neurogliaform cells. *J. Neurosci.* 30, 9898–9909.

Klausberger, T., and Somogyi, P. (2008). Neuronal diversity and temporal dynamics: the unity of hippocampal circuit operations. *Science* 321, 53–57.

Kovac, S., Megalogeni, M., and Walker, M. (2011). In vitro effects of neuropeptide Y in rat neocortical and hippocampal tissue. *Neurosci. Lett.* 492, 43–46.

Krook-Magnuson, E., and Huntsman, M. M. (2007). The transience of interneuron circuit diversity just "sped" up. *Proc. Natl. Acad. Sci. U.S.A.* 104, 16723–16724.

Krook-Magnuson, E., Luu, L., Lee, S. H., Varga, C., and Soltesz, I. (2011). Ivy and neurogliaform interneurons are a major target of mu-opioid receptor modulation. *J. Neurosci.* 31, 14861–14870.

Krook-Magnuson, E., Varga, C., Lee, S. H., and Soltesz, I. (2012). New dimensions of interneuronal specialization unmasked by principal cell heterogeneity. *Trends Neurosci.* 35, 175–184.

Lange, M. D., Doengi, M., Lesting, J., Pape, H. C., and Jüngling, K. (2012). Heterosynaptic long-term potentiation at interneuron-principal neuron synapses in the amygdala requires nitric oxide signalling. *J. Physiol. (Lond.)* 590, 131–143.

Laorden, M. L., Olaso, M. J., Miralles, F. S., and Puig, M. M. (1985). Cerebrospinal fluid leucine-enkephalin-like levels in febrile convulsions. *Methods Find Exp. Clin. Pharmacol.* 7, 75–77.

Lovett-Barron, M., Turi, G. F., Kaifosh, P., Lee, P. H., Bolze, F., Sun, X. H., Nicoud, J. F., Zemelman, B. V., Sternson, S. M., and Losonczy, A. (2012). Regulation of neuronal input transformations by tunable dendritic inhibition. *Nat Neurosci.* 15, 423–430.

Maggesissi, R. S., Gardino, P. F., Guimarães-Souza, E. M., Paes-De-Carvalho, R., Silva, R. B., and Calaza, K. C. (2009). Modulation of GABA release by nitric oxide in the chick retina: different effects of nitric oxide depending on the cell population. *Vision Res.* 49, 2494–2502.

Markwardt, S. J., Dieni, C. V., Wadiche, J. I., and Overstreet-Wadiche, L. (2011). Ivy/neurogliaform interneurons coordinate activity in the neurogenic niche. *Nat. Neurosci.* 14, 1407–1409.

McQuiston, A. R. (2011). Mu opioid receptor activation normalizes temporo-ammonic pathway driven inhibition in hippocampal CA1. *Neuropharmacology* 60, 472–479.

Meilandt, W. J., Yu, G. Q., Chin, J., Roberson, E. D., Palop, J. J., Wu, T., Scearce-Levie, K., and Mucke, L. (2008). Enkephalin elevations contribute to neuronal and behavioral impairments in a transgenic mouse model of Alzheimer's disease. *J. Neurosci.* 28, 5007–5017.

Melikian, N., Seddon, M. D., Casadei, B., Chowienczyk, P. J., and Shah, A. M. (2009). Neuronal nitric oxide synthase and human vascular regulation. *Trends Cardiovasc. Med.* 19, 256–262.

Mitchell, S. J., and Silver, R. A. (2003). Shunting inhibition modulates neuronal gain during synaptic excitation. *Neuron* 38, 433–445.

Mizuseki, K., Sirota, A., Pastalkova, E., and Buzsaki, G. (2009). Theta oscillations provide temporal windows for local circuit computation in the entorhinal-hippocampal loop. *Neuron* 64, 267–280.

Morgan Iii, C. A., Rasmusson, A. M., Wang, S., Hoyt, G., Hauger, R. L., and Hazlett, G. (2002). Neuropeptide-Y, cortisol, and subjective distress in humans exposed to acute stress: replication and extension of previous report. *Biol. Psychiatry* 52, 136–142.

Morgan, R. J., and Soltesz, I. (2008). Nonrandom connectivity of the epileptic dentate gyrus predicts a major role for neuronal hubs in seizures. *Proc. Natl. Acad. Sci. U.S.A.* 105, 6179–6184.

Noè, F., Pool, A.-H., Nissinen, J., Gobbi, M., Bland, R., Rizzi, M., Balducci, C., Ferraguti, F., Sperk, G., During, M. J., Pitkänen, A., and Vezzani, A. (2008). Neuropeptide Y gene therapy decreases chronic spontaneous seizures in a rat model of temporal lobe epilepsy. *Brain* 131, 1506–1515.

Noe, F., Vaghi, V., Balducci, C., Fitzsimons, H., Bland, R., Zardoni, D., Sperk, G., Carli, M., During, M. J., and Vezzani, A. (2010). Anticonvulsant effects and behavioural outcomes of rAAV serotype 1 vector-mediated neuropeptide Y overexpression in rat hippocampus. *Gene Ther.* 17, 643–652.

Olah, S., Fule, M., Komlosi, G., Varga, C., Baldi, R., Barzo, P., and Tamas, G. (2009). Regulation of cortical microcircuits by unitary GABA-mediated volume transmission. *Nature* 461, 1278–1281.

Olah, S., Komlosi, G., Szabadics, J., Varga, C., Toth, E., Barzo, P., and Tamas, G. (2007). Output of neurogliaform cells to various neuron types in the human and rat cerebral cortex. *Front. Neural Circuits* 1:4. doi:10.3389/neuro.04.004.2007

Pearce, R. A. (1993). Physiological evidence for two distinct GABAA responses in rat hippocampus. *Neuron* 10, 189–200.

Povysheva, N. V., Zaitsev, A. V., Kroner, S., Krimer, O. A., Rotaru, D. C., Gonzalez-Burgos, G., Lewis, D. A., and Krimer, L. S. (2007). Electrophysiological differences between neurogliaform cells from monkey and rat prefrontal cortex. *J. Neurophysiol.* 97, 1030–1039.

Price, C. J., Cauli, B., Kovacs, E. R., Kulik, A., Lambolez, B., Shigemoto, R., and Capogna, M. (2005). Neurogliaform neurons form a novel inhibitory network in the hippocampal CA1 area. *J. Neurosci.* 25, 6775–6786.

Price, C. J., Scott, R., Rusakov, D. A., and Capogna, M. (2008). GABA(B) receptor modulation of feedforward inhibition through hippocampal neurogliaform cells. *J. Neurosci.* 28, 6974–6982.

Ramón y Cajal, S. (1922). Studien über die Sehrinde der Katze. *J. Psychol. Neurol.* 29, 161–181.

Ramón y Cajal, S. (1999). *Texture of the Nervous System of Man and the Vertebrates.* Barcelona: Spring-Verlag/Wein Springer.

Ratzliff, A. D., and Soltesz, I. (2001). Differential immunoreactivity for alpha-actinin-2, an N-methyl-D-aspartate-receptor/actin binding protein, in hippocampal interneurons. *Neuroscience* 103, 337–349.

Rocha, L., Cuellar-Herrera, M., Velasco, M., Velasco, F., Velasco, A. L., Jimenez, F., Orozco-Suarez, S., and Borsodi, A. (2007). Opioid receptor binding in parahippocampus of patients with temporal lobe epilepsy: its association with the antiepileptic effects of subacute electrical stimulation. *Seizure* 16, 645–652.

Santhakumar, V., Aradi, I., and Soltesz, I. (2005). Role of mossy fiber sprouting and mossy cell loss in hyperexcitability: a network model of the dentate gyrus incorporating cell types and axonal topography. *J. Neurophysiol.* 93, 437–453.

Sheffield, M. E., Best, T. K., Mensh, B. D., Kath, W. L., and Spruston, N. (2011). Slow integration leads to persistent action potential firing in distal axons of coupled interneurons. *Nat. Neurosci.* 14, 200–207.

Shin, J. H., and Linden, D. J. (2005). An NMDA receptor/nitric oxide cascade is involved in cerebellar LTD but is not localized to the parallel fiber terminal. *J. Neurophysiol.* 94, 4281–4289.

Simon, A., Olah, S., Molnar, G., Szabadics, J., and Tamas, G. (2005). Gap-junctional coupling between neurogliaform cells and various interneuron types in the neocortex. *J. Neurosci.* 25, 6278–6285.

Soltesz, I., and Jones, R. S. (1995). The direct perforant path input to CA1: excitatory or inhibitory? *Hippocampus* 5, 101–103.

Suzuki, N., and Bekkers, J. M. (2012). Microcircuits mediating feedforward and feedback synaptic inhibition in the piriform cortex. *J. Neurosci.* 32, 919–931.

Szabadics, J., and Soltesz, I. (2009). Functional specificity of mossy fiber innervation of GABAergic cells in the hippocampus. *J. Neurosci.* 29, 4239–4251.

Szabadics, J., Tamas, G., and Soltesz, I. (2007). Different transmitter transients underlie presynaptic cell type specificity of GABAA,slow and GABAA, fast. *Proc. Natl. Acad. Sci. U.S.A.* 104, 14831–14836.

Szabadics, J., Varga, C., Brunner, J., Chen, K., and Soltesz, I. (2010). Granule cells in the CA3 area. *J. Neurosci.* 30, 8296–8307.

Szabadits, E., Cserép, C., Ludányi, A., Katona, I., Gracia-Llanes, J., Freund, T. F., and Nyíri, G. (2007). Hippocampal GABAergic synapses possess the molecular machinery for retrograde nitric oxide signaling. *J. Neurosci.* 27, 8101–8111.

Szabadits, E., Cserép, C., Szonyi, A., Fukazawa, Y., Shigemoto, R., Watanabe, M., Itohara, S., Freund, T. F., and Nyiri, G. (2011). NMDA receptors in hippocampal GABAergic synapses and their role in nitric oxide signaling. *J. Neurosci.* 31, 5893–5904.

Tamas, G., Lorincz, A., Simon, A., and Szabadics, J. (2003). Identified

sources and targets of slow inhibition in the neocortex. *Science* 299, 1902–1905.

Tricoire, L., Pelkey, K. A., Daw, M. I., Sousa, V. H., Miyoshi, G., Jeffries, B., Cauli, B., Fishell, G., and Mcbain, C. J. (2010). Common origins of hippocampal Ivy and nitric oxide synthase expressing neurogliaform cells. *J. Neurosci.* 30, 2165–2176.

Varga, C., Lee, S. Y., and Soltesz, I. (2010). Target-selective GABAergic control of entorhinal cortex output. *Nat. Neurosci.* 13, 822–824.

Vezzani, A., Sperk, G., and Colmers, W. F. (1999). Neuropeptide Y: emerging evidence for a functional role in seizure modulation. *Trends Neurosci.* 22, 25–30.

Vida, I., Halasy, K., Szinyei, C., Somogyi, P., and Buhl, E. H. (1998). Unitary IPSPs evoked by interneurons at the stratum radiatum-stratum lacunosum-moleculare border in the CA1 area of the rat hippocampus in vitro. *J. Physiol. (Lond.)* 506(Pt 3), 755–773.

Weiss, T., and Veh, R. W. (2011). Morphological and electrophysiological characteristics of neurons within identified subnuclei of the lateral habenula in rat brain slices. *Neuroscience* 172, 74–93.

Yehuda, R., Brand, S., and Yang, R.-K. (2006). Plasma neuropeptide Y concentrations in combat exposed veterans: relationship to trauma exposure, recovery from PTSD, and coping. *Biol. Psychiatry* 59, 660–663.

Zanelli, S., Naylor, M., and Kapur, J. (2009). Nitric oxide alters GABAergic synaptic transmission in cultured hippocampal neurons. *Brain Res.* 1297, 23–31.

Zsiros, V., Aradi, I., and Maccaferri, G. (2007). Propagation of postsynaptic currents and potentials via gap junctions in GABAergic networks of the rat hippocampus. *J. Physiol. (Lond.)* 578, 527–544.

Zsiros, V., and Maccaferri, G. (2005). Electrical coupling between interneurons with different excitable properties in the stratum lacunosum-moleculare of the juvenile CA1 rat hippocampus. *J. Neurosci.* 25, 8686–8695.

Zsiros, V., and Maccaferri, G. (2008). Noradrenergic modulation of electrical coupling in GABAergic networks of the hippocampus. *J. Neurosci.* 28, 1804–1815.

Conflict of Interest Statement: The authors declare that the research was conducted in the absence of any commercial or financial relationships that could be construed as a potential conflict of interest.

Received: 29 February 2012; paper pending published: 22 March 2012; accepted: 13 April 2012; published online: 16 May 2012.

*Citation: Armstrong C, Krook-Magnuson E and Soltesz I (2012) Neurogliaform and Ivy cells: a major family of nNOS expressing GABAergic neurons. Front. Neural Circuits **6**:23. doi: 10.3389/fncir.2012.00023*

frontiers in
NEURAL CIRCUITS

REVIEW ARTICLE
published: 09 August 2012
doi: 10.3389/fncir.2012.00051

The complex contribution of NOS interneurons in the physiology of cerebrovascular regulation

Sonia Duchemin , Michaël Boily† , Nataliya Sadekova and Hélène Girouard*

Department of Pharmacology, Université de Montréal, Montreal, QC, Canada

Edited by:
Bruno Cauli, Centre National de la Recherche Scientifique, France

Reviewed by:
Gilles Bonvento, Centre National de la Recherche Scientifique, France
Elvire Vaucher, Université de Montréal, Canada
Armelle Rancillac, Centre National de la Recherche Scientifique, France

***Correspondence:**
Hélène Girouard, Department of Pharmacology, Cerebrovascular Pharmacology, Université de Montréal, Montreal, QC, Canada.
e-mail: helene_girouard@hotmail.com

† Co-first author.

Following the discovery of the vasorelaxant properties of nitric oxide (NO) by Furchgott and Ignarro, the finding by Bredt and coll. of a constitutively expressed NO synthase in neurons (nNOS) led to the presumption that neuronal NO may control cerebrovascular functions. Consequently, numerous studies have sought to determine whether neuraly-derived NO is involved in the regulation of cerebral blood flow (CBF). Anatomically, axons, dendrites, or somata of NO neurons have been found to contact the basement membrane of blood vessels or perivascular astrocytes in all segments of the cortical microcirculation. Functionally, various experimental approaches support a role of neuronal NO in the maintenance of resting CBF as well as in the vascular response to neuronal activity. Since decades, it has been assumed that neuronal NO simply diffuses to the local blood vessels and produce vasodilation through a cGMP-PKG dependent mechanism. However, NO is not the sole mediator of vasodilation in the cerebral microcirculation and is known to interact with a myriad of signaling pathways also involved in vascular control. In addition, cerebrovascular regulation is the result of a complex orchestration between all components of the neurovascular unit (i.e., neuronal, glial, and vascular cells) also known to produce NO. In this review article, the role of NO interneuron in the regulation of cortical microcirculation will be discussed in the context of the neurovascular unit.

Keywords: astrocyte, autoregulation, cerebral blood flow, GABA, interneuron, magnetic resonance imaging, neurovascular coupling, nitric oxide

INTRODUCTION

Nitric oxide (NO) is a small inorganic, labile gaseous molecule originally identified as endothelium-derived relaxing factor (EDRF) mediating relaxation of blood vessels (Furchgott and Zawadzki, 1980). NO is produced through the enzymatic conversion of L-arginine to L-citrulline by the enzyme NO synthase (NOS). NOS includes three main isoforms: the constitutive endothelial eNOS and neuronal nNOS as well as the inducible iNOS. The discovery by Bredt and colleagues (Bredt and Snyder, 1989) that NO is also produced in the brain led to the finding that NO could act as a neurotransmitter and a modulator of cerebral blood flow (CBF).

CBF is regulated by two main mechanisms: autoregulation and neurovascular coupling (NVC). CBF autoregulation is the primary mechanism ensuring that the flow and supply of oxygen, glucose, and nutrients through the vascular beds remain within the upper and lower limits of the autoregulatory range (50–160 mm Hg) during fluctuations in systemic arterial pressure. NVC is the dynamic link between neuronal energy needs and hemodynamic changes. In the cortex, NVC depends on the complex interplay between neurons, astrocytes, and microvessels (endothelial cells, myocytes, and pericytes) that form the "neurovascular unit" (Iadecola, 2004). NO is known to play a pivotal role in mechanisms underlying both autoregulation and NVC. However, although many studies have attempted to elucidate the role of NO in the CBF regulation, the exact source of NO involved at different levels of CBF regulation as well as its molecular and cellular targets remains unresolved. This review article will focus on the physiological role of a specific subsets NO producing gamma aminobutyric acid (GABA)ergic neurons, the NOS interneurons in control of cortical CBF. The current knowledge on this topic will be critically examined in the context of the neurovascular unit.

ANATOMICAL RELATIONSHIP BETWEEN NO INTERNEURONS AND BLOOD VESSELS

The intracortical NOS interneurons are part of a family of GABA inhibitory interneurons believed to play a pivotal role in CBF regulation. Indeed, NOS interneurons have been demonstrated to be ideally positioned between glutamatergic pyramidal cells and local microvessels (Cauli et al., 2004). Most anatomical studies on NOS interneurons have used immunohistochemistry for the nicotinamide adenine dinucleotide phosphate-diaphorase (NADPHd) which constitutes a histochemical marker for nNOS. This method is prefered for use due to its simplicity compared to NOS immunohistochemistry and *in situ* hybridization since it requires only two reagents, nitro blue tetrazolium and NADPH. Histochemistry for NADPHd is believed to be very specific for nNOS in aldehyde-fixed mammalian brain tissue (Matsumoto et al., 1993). Firstly, in the neocortex of many species the overlap of immunocytochemical staining of nNOS and NADPHd is quasi absolute in neurons. Secondly, *in situ* hybridization for nNOS

mRNA in combination with NADPHd show that each positive cell for NADPHd in rat cerebral cortex also exhibits autoradiographic staining for nNOS mRNA (Bredt et al., 1991). Thirdly, the deletion of the gene coding for nNOS results in the absence of NADPHd staining in mice nervous sytem (Huang et al., 1993).

Cortical NADPHd neurons are divided in type I and type II neurons according to the intensity of staining. Type I cells exhibit large somata and are intensely stained while type II cells are much smaller and weakly stained (Kubota et al., 1994; Yan et al., 1996). Type I neurons are found in the cortex of various species including mouse, cat, monkey, and humans. Their distribution pattern is similar between species and are found in all cortical layers (Sandell, 1986; Mizukawa et al., 1988; Oermann et al., 1999; Garbossa et al., 2005). The numerical density of type I cells is lower in the monkey than in the rat (Yan et al., 1994). Type II cells have a smaller soma and lower NADPHd activity, and are 20-fold more numerous than type I cells in primates. Type II cells are found mainly in the supragranular layers in monkey (Yan et al., 1996) and human (Judas et al., 1999) while, in rodents, they are about twofold more numerous than type I cells and populate all neocortical layers (Perrenoud et al., 2012b). In primates, pyramidal cells also present some NADPHd reactivity or nNOS immunostaining in different cortical areas (Barone and Kennedy, 2000; Garbossa et al., 2005). Although the association of type I interneurons with blood vessels have been recently described in the adult monkey (Rockland and Nayyar, 2012) the association of type II neurons with blood vessels remain to be described.

Around 80% of NADPHd positive cells in the rat cortex contain GABA and they account for 2% of the GABAergic cells (Valtschanoff et al., 1993) which represent about 15% of cortical neurons in rodents (Gabbott et al., 1997). NADPHd-positive interneurons co-express many vasoactive mediators such as GABA, neuropeptide Y (NPY), somatostatin (SOM), and calbindin (Kummer et al., 1992; Kubota et al., 1994; Xiao et al., 1996; Abounader and Hamel, 1997; Gonchar and Burkhalter, 1997; Estrada and DeFelipe, 1998). Indeed, using patch-clamp recordings, biocytin labeling, and single-cell reverse transcriptase-PCR, Karagiannis et al. (2009), showed that nNOS was expressed by 9% of fast spiking parvalbumin (PV)-interneurons, 6% of adapting SOM-interneurons, 2% of adapting vasoactive intestinal peptide (VIP)-interneurons, 0% of bursting VIP-interneurons, and 26% of adapting NPY-interneurons. More recently, double labeling studies showed colocalisation of cytochrome P450 2C11 epoxygenase and soluble epoxygenase with nNOS within perivascular nerves which suggests synthesis of the vasodilator eicosatrienoic acids in nitrergic nerves (Iliff et al., 2007). The authors concluded that both the P450 epoxygenase and NOS pathways seem to be involved in the local CBF response to N-methyl-D-aspartate (NMDA) receptor activation. As in every neuron, NOS interneurons release potassium (K^+), hydrogen ions, and adenosine produced by ATP catabolism in response to neuronal activity (Iliff et al., 2003).

In addition to releasing various vasoactive mediators, nitrergic nerves are strategically positioned in proximity to cerebral arteries. NADPHd positive fibers have been found around pial arteries as well as parenchymal vessels. Pial arteries are innervated by perivascular nitrergic nerves that originate from sphenopalatine, otic, and trigeminal ganglia (Suzuki et al., 1994), while fibers close to parenchymal arteries have been identified as GABAergic interneurons. NOS interneurons have access to parenchymal arterioles but apparently not to arterioles and arteries proximal to the Virchow-Robin space (Abadia-Fenoll, 1969; Busija, 1993). Using electron microscopy, it has been demonstrated that the axons, dendrites, or somata of NADPHd positive neurons contact the basal membrane of blood vessels or the perivascular astroglia (Vaucher et al., 2000). As a matter of fact, a very specific neurovascular connection has been observed in isoled cortical parenchymal arteries where a network of fibers or individual fibers is attached along isolated vessels (Estrada et al., 1988). In a very elegant study, Cauli et al. (2004) identified the subtypes of interneurons associated with rat cortical microvessels in layer I–III. According to this study, at a distance within 50 μm of the blood vessels, the percentage of GABAergic neuron subsets appears to be the following: 39% express VIP or NPY, 28% express NOS, 28% express SOM, some cells co-express more than one marker. This distribution differed considerably with their respective density in the same layers and fields of the somatosensory cortex, which was VIP (46.1%) > SOM (30.4%) > NPY (16.1%) > NOS (7.4%). These results indicate a privileged redistribution of NPY and NOS interneurons in the vicinity of cortical microvessels. Indeed several authors have reported that cortical nitrergic neurons are localized in apposition to cerebral arteries, especially in bifurcation areas surrounding vessels with their projections or sending projections to more distant arterioles and capillaries (Estrada et al., 1993; Iadecola et al., 1993; Regidor et al., 1993; Yan et al., 1996). Using infrared videomicroscopy, Cauli et al. (2004) also demonstrated that the GABAergic neurons not only contacted the neighboring penetrating microvessels, but that their dendrites and/or axonal branches reached for several blood vessels within an area that extended >100 μm away from the cell. In humans, processes of type 1 NADPHd-positive neurons are also intimately entwined with blood vessels in the cortex (DeFelipe, 1993; Garbossa et al., 2005) but their relative vascular and nonvascular distributions have not been investigated.

FUNCTIONAL SIGNIFICANCE OF THE ANATOMICAL RELATIONSHIP BETWEEN NOS INTERNEURONS AND BLOOD VESSELS

NOS interneurons are considered multifunctional as they release various neuromediators with different physiological effects. This multifunctionality requires a well-organized anatomy for a high spatial specificity in NVC. An example of this specificity is the finding of a distribution of an axonal plexus of densely NADPHd positive neurons around a restrictive group of microvessels in human temporal cortex (DeFelipe, 1993). NOS interneurons co-localize with the very powerful vasoconstrictor NPY in the cerebral cortex. Neurovascular associations have been reported for NPY in the human striate cortex (Berman and Fredrickson, 1992). Thus, the local release of NPY through the perivascular axonal plexus may produce a very localized vasoconstriction that will provide a spatial limitation to the vasodilation around the neuronal soma and dendrites (Estrada and DeFelipe, 1998). In contrast, NO possesses a volume of influence of up to 350 μm

from a source point of production and may in effect dilate vessels within this radial length (Santos et al., 2012). Another possible role of NPY in the NOS interneuron-induced vascular response is to timely limit the vasodilation. Indeed, direct activation of a single nitrergic interneuron is sufficient to increase the diameter of a neighboring microvessel, but reversible dilatation is only induced by stimulation of a NOS neuron coexpressing NPY (Cauli et al., 2004).

The role of GABAergic transmission in the control of CBF also remains obscure, but anatomical and physiological evidences suggest that it could directly act on vessels to induce a vasodilation. GABA can induce intraparenchymal dilation through GABAa receptors located on vessels (Fergus and Lee, 1997). Glial cells also possess GABA receptors (Bureau et al., 1995). It is therefore possible that GABA modulates the vascular tone by acting on perivascular astrocytes. Consequently, the net effect of GABA on vascular tone stems from a very complex interaction with vessels, astrocytes as well as cortical interneurons and pyramidal neurons receiving GABAergic innervations.

Cortical NOS interneurons receive projections from the basalocortical Acetylcholine (Ach) and NO-synthesizing fibers as well as from the brainstem 5-hydrotryptamine (5-HT) afferents in both rat and human (Vaucher et al., 1997; Tong and Hamel, 1999). A large proportion (∼30%) of NOS neurons receive both Ach and 5-HT innervations and 60% of these NOS containing neurons contact local blood vessels either with their proximal or distal neurites. Their neuronal processes extend long distances and contact a broad array of microvessels. NOS neurons thus appear exceptionally well positioned to relay Ach and 5-HT afferent information to blood vessels since they also exquisitely contact neighboring and remotely located blood vessels (Estrada and DeFelipe, 1998). Nevertheless, studies with 7-nitroindazole (7-NI), a selective nNOS inhibitor, failed to attenuate the CBF increase in response to basal forebrain activation (Zhang et al., 1995; Iadecola and Zhang, 1996). On the contrary, nonselective NOS inhibitors such as L-N^G-nitroarginine (L-NNA) attenuate the CBF increase induced by stimulation of the basal forebrain (Raszkiewicz et al., 1992). Ach fibers directly contact cortical microvessels or the surrounding astrocytes in rat and man (Mesulam et al., 1992; Vaucher and Hamel, 1995; Tong and Hamel, 1999) and could as a result directly activate eNOS. The lack of an additive CBF effect of the coapplication of muscarinic receptor antagonist, atropine, and nonselective NOS inhibitor, L-NNA, on the cerebral cortex compared to L-NNA alone, suggest that Ach increases CBF possibly through eNOS activation (Zhang et al., 1995). In this context, the direct effect of Ach nerves on the vascular tone may encompass those mediated by nitrergic interneurons. However, in pathological situations where endothelial functions are altered, NO interneurons may significantly control CBF following basal forebrain stimulation.

NEURALLY-DERIVED NITRIC OXIDE AND CEREBROVASCULAR REGULATION

RESTING CEREBRAL BLOOD FLOW

Many evidences suggest that NO plays a role in the cerebrovascular regulation. Various studies demonstrated that systemic or topical administration of non-selective NOS or selective nNOS inhibitors decrease resting CBF in many species. This effect is not observed with the iNOS inhibitor, aminoguanidine (Iadecola et al., 1995). Intraperitoneal injections of 7-NI, an *in vivo* inhibitor of the neuronal isoform of NOS, lower baseline CBF in unanesthetized rats (laser Doppler on the somatosensory cortex) (Montecot et al., 1997) (autoradiography in the barrel cortex) (Gotoh et al., 2001a) and anesthetized mice (laser Doppler on the somatosensory cortex) (Girouard et al., 2007, 2009), cerebral capillary flow in anesthetized rats (intravital microscopy on the right parietal cortex) (Hudetz et al., 1998), global CBF in anesthetized rats (autoradiography) (Cholet et al., 1997), and global CBF in cats (PET scan) (Hayashi et al., 2002a). The decreased cortical CBF ranges from about 10 to 60% depending on the 7-NI concentrations and the cortical areas and it is not accompanied by a decrease in glucose utilization (Kelly et al., 1995; Cholet et al., 1997; Hayashi et al., 2002b).

At resting state, arterioles exhibit slow spontaneous rhythmic diameter and blood flow changes of about 0.1 Hz defined as vasomotion. Vasomotion has been detected in cerebral arteries (Fujii et al., 1990; Filosa et al., 2004) and may be influenced by a variety of physiological factors including NO (Fujii et al., 1990). Mathematical models of myogenic mechanisms have demonstrated that vasomotion oscillations can be propagated locally and self-sustained within a group feeding of vessels (Behzadi and Liu, 2005). These models also suggest that a vessel with an oscillating diameter conducts more flow than a vessel with a static diameter (Meyer et al., 2002). Systemic administration of nonselective NOS inhibitors lead to the enhancement of oscillations within a common feeding vessel that are propagated to downstream branches (Griffith and Kilbourn, 1996; Behzadi and Liu, 2005). However, this phenomenon may be a consequence of the increase in systemic blood pressure and respiratory rate. The administration of a nNOS specific inhibitor or the local application of NOS inhibitors would give more specific information about the role of NO in the regulation of spontaneous vasomotion.

The CBF reduction in the presence of 7-NI is equivalent to the CBF attenuation induced by nonspecific NOS inhibitors which suggests that the neuronal isoform is responsible for the maintenance of resting cerebrovascular tone. Despite this, resting CBF evaluated with the hydrogen clearance method did not significantly differ between wildtype, nNOS- and eNOS-null mice (Atochin et al., 2003). This discrepancy may be explained by compensatory mechanisms in transgenic mice. Another argument for a neuronal specific effect on resting CBF is that the topical application of the specific NMDA receptor antagonist, MK801, reduces resting CBF to the same extent as 7-NI (Girouard et al., 2009). This is consistent with a nNOS role in the maintenance of resting CBF as no functional NMDA receptors in rat and human cerebromicrovascular endothelial cells has been identified (Morley et al., 1998). More importantly, isolated cerebral arteries in a number of species have not been found to dilate in response to application of glutamate or NMDA (Faraci et al., 1993; Simandle et al., 2005) and endothelial damage *in vivo* failed to affect NMDA-induced dilation (Domoki et al., 2002). Interestingly, NOS interneurons are spontaneously active. These spontaneous spikes are likely to be initiated by a baseline NMDA receptor activity detectable during subthreshold synaptic activation

(Katona et al., 2011). It is thus possible that NOS interneuron spontaneous activity participates to maintain a certain level of resting CBF.

Anatomical and physiological evidences suggest the presence of nNOS in arterial smooth muscle. Neuronal NOS has been found in smooth muscle of cerebral vessels (Toda and Okamura, 2011) as well as in the common carotid artery (Brophy et al., 2000). In addition, 7-NI increases contractile response of carotid artery (Brophy et al., 2000). These results brought controversies about the origin of NO that contributes to the maintenance of resting CBF. However, in Brophy's study, 7-NI was applied on isolated arteries whereas 7-NI acts as a preferential nNOS inhibitor when administered systemically only (Babbedge et al., 1993). Using electron microscopy, Wang et al. (2005) did not observe any nNOS in vascular smooth muscle cells, endothelium, or glial processes.

Assuming that NO contributing to the resting CBF comes from neurons, the neuronal subtype responsible for its formation still has to be clearly identified. Although a clear participation of nitrergic nerves from the pterygopalatine ganglion has been demonstrated in the dilation of the middle cerebral artery and the posterior communicating arteries (Toda and Okamura, 2003), no studies have identified the specific neuronal NO origin that control parenchymal arteries tone. The use of Cre-dependent optogenetic transgenic mice for light induced activation and silencing different types of neurons will be necessary to clarify this issue (Madisen et al., 2012).

AUTOREGULATION

Cerebrovascular resistance decreases or increases in response to changes in transmural pressure and blood flow so that flow remains constant. Changes in resistance result from vasodilation and vasoconstriction of the pial and parenchymal vessels (Shapiro et al., 1971). Several studies have investigated the role of NO in the mechanisms involved in autoregulation. Nonspecific NOS inhibitors were administered while arterial pressure was decreased in a stepwise manner in order to test the role of NO in the lower limit of autoregulation. Although data coming from these studies were divergents the lower limit of autoregulation was raised in eNOS knockout mice (Huang et al., 1994) and remained normal in nNOS knockout mice (Huang et al., 1996). In addition, a study showing nonspecific NOS-induced autoregulation dysfunction failed to demonstrate similar effects with the nNOS inhibitor 7-NI (Toyoda et al., 1997) suggesting that eNOS is involved in the vasodilation in response to decreases in arterial pressure. To test the upper limit of autoregulation, arterial presure is gradualy elevated. Contrasting results emerged from studies using nonspecific NOS inhibitors. No effects have been observed with 7-NI (Hardy et al., 1999). Although many questions remain unresolved concerning the effect of NO in the control of autoregulation, there are no indications that (inter)neurons are involved in these mechanisms.

HYPERCAPNIA AND HYPEROXIA

CBF is highly sensitive to alterations in arterial blood gases. For instance, increases in the partial pressure of arterial CO_2 ($PaCO_2$) and O_2 (PaO_2) provoke dilation and constriction, respectively. In several mammalian species including humans, it has been reported that blockade of NO synthesis with NOS inhibitors attenuates CBF responses to hypercapnia (Iadecola, 1992; Wang et al., 1992; Buchanan and Phillis, 1993; Pelligrino et al., 1993; Iadecola and Xu, 1994; Iadecola and Zhang, 1994; Sandor et al., 1994; Heinert et al., 1999) in the entire brain (Bonvento et al., 1994). The participation of NO is more important in mild hypercapnia ($PaCO_2$ = 50–60 mm Hg) (Iadecola and Zhang, 1994). The cellular sources of NO during hypercapnia remain to be established but some evidences suggest a role for nNOS-derived NO in vascular responses to hypercapnia. Hypercapnia increases nNOS-derived NO in rat brain (Harada et al., 1997). Administration of 7-NI reduces the vasodilator and CBF responses to hypercapnia in anesthetized rats, suggesting that NO synthesized by nNOS participates in hypercapnic hyperemia (Wang et al., 1995; Okamoto et al., 1997). Endothelial denudation does not alter basilar and middle cerebral artery dilation in Japanese monkeys and Mongrel dogs in response to moderate hypercapnia (Toda et al., 1996). However, light/dye endothelial injury as well as NOS and soluble guanylate cyclase inhibition reduce hypercapnic cerebrovascular dilatation in anesthetized juvenile pigs, indicating that endothelial NO may play a significant role in the hypercapnic vasodilatation in this model (Willis and Leffler, 2001). Thus, mostly nNOS-derived NO seem to participate in the vascular response to hypercapnia while both eNOS and nNOS derived NO may participate in the autoregulation of the particular piglet cerebrovascular regulation.

The mechanisms by which NO modulates the hypercanic vascular response are not clear. However, hypercapnia provokes H^+ accumulation and acidosis which, by converting Ca^{2+} waves to sparks, leads to the activation of BK(Ca^{2+}) channels to induce dilation of cerebral parenchymal arteries (Dabertrand et al., 2012). This effect may be amplified by the modulating effect of NO on large conductance Ca^{2+}-dependent K^+ (BK) channels. This is consistant with the presence of hypercapnic vasodilation in isolated arteries in concert with NOS participation in the acidosis-induced vasodilation (Niwa et al., 1993) and the permissive role of NO in hypercapnic vasodilation (Iadecola and Zhang, 1994).

Hyperoxia causes a transient decrease in CBF, followed by a later rise. From mice lacking nNOS or eNOS and wild-type mice, Atochin et al. (2003) obtained evidences suggesting that cerebral vasodilatation induced by 60-min exposure to hyperbaric oxygen depends on both nNOS and eNOS. However, the underlying mechanisms remain to be investigated.

NEUROVASCULAR COUPLING

Active neurons send various signals to astrocytes and blood vessels in order to increase CBF and obtain sufficient O_2 and substrates. A number of studies have provided evidences that NOS inhibition attenuates the CBF increase in response to neuronal activity. Indeed, local application of NOS inhibitors suppresses the activity-dependent vasodilation by about 50% (Dirnagl et al., 1994; Irikura et al., 1994; Peng et al., 2004; Girouard et al., 2007; Kitaura et al., 2007). Systemic administration of 7-NI has also been shown to reduce the amplitude of NVC in different experimental paradigm of neuronal activation such as whisker stimulation and electric stimulation of mice forepaw

(Cholet et al., 1996; Bonvento et al., 2000; Girouard et al., 2007; Liu et al., 2008). In both eNOS and nNOS-knockout mice, activity-dependent vascular changes were similar to those in control mice. However, in eNOS null mice, activity-dependent vasodilation was suppressed by NOS inhibitors (Ayata et al., 1996) while in nNOS knockout mice, NVC remained intact in the presence of NOS inhibitors (Ma et al., 1996). These data support the participation of neurogenic NO in NVC.

Reports on awake animals brought controversies about the role of NO on NVC. Studies with nonspecific NOS inhibitors, in which CBF was quantitatively determined in unanesthetized restrained animals, have failed to support such a role for NO (Sokoloff et al., 1992; Wang et al., 1993; Adachi et al., 1994). These results conclude that NVC is modulated by NO in anesthetized conditions only. However, in unanesthetized unrestrained rats, unspecific and specific nNOS inhibition decreases the vascular response to neuronal stimulation (Gotoh et al., 2001b). This discrepancy could be explained by the fact that immobilization of animals is a stressful condition that lowers $paCO_2$, increases circulating catecholamines and therefore alter cerebrovascular regulation (Lacombe and Seylaz, 1984).

Another aspect that may mislead data interpretations is the potential effect of NO on neuronal activity (Lonart et al., 1992; Manzoni and Bockaert, 1993; Schuman and Madison, 1994; Jayakumar et al., 1999) that could explain its effect on NVC. Some studies have shown a decreased amplitude of somatosensory-evoked potentials induced by electrical stimulation of the forepaw or the sciatic nerve in the presence of NOS inhibitors (Ngai et al., 1995; Stefanovic et al., 2007). Other investigations demonstrated that NOS inhibition has no significant effect or a very slight effect on somatosensory evoked potentials (Lindauer et al., 1996; Burke and Buhrle, 2006; Hoffmeyer et al., 2007) or cerebral glucose activation (Cholet et al., 1997). Notwithstanding the observed effects on activated potentials, NOS inhibition was always accompanied by CBF reduction in *in situ* electrical response to neuronal supporting a role in the modulation of the vascular response.

Local NOS interneuron density varies among brain areas. Consequently, in each region, CBF may be differently regulated by NO. Cholet et al. reported that NO plays a role in NVC in the somatosensory area and the thalamus but less so in the trigeminal primary nucleus in rats under peri-oral somatosensory stimulation (Cholet et al., 1997). During vibrissal stimulation in unanesthetized rats, NOS inhibition with L-NAME attenuates the increase in CBF in the ventroposteromedial thalamic nucleus and 7-NI reduces the CBF in both the ventroposteromedial thalamic nucleus and the barrel cortex. NOS inhibitors did not significantly affect CBF in the spinal trigeminal nucleus and the principal sensory trigeminal nucleus (Gotoh et al., 2001a). Electrical somatosensory stimulation in the unilateral cat forepaw elicits an increase in CBF in the contralateral somatosensory cortex and the ipsilateral cerebellum which is attenuated by 7-NI (Hayashi et al., 2002b). These results are consistent with NOS interneuron distribution and strongly support the idea that NO regulating CBF comes from GABAergic neurons (Bertini et al., 1996; Mize et al., 1996).

CBF responses reflect the combined activities of cells and synapses that include both excitatory and inhibitory processes. Hence, depending on the afferent pathway and intensity, distinct population of neurons may be recruited. Electrical stimulation of two different pathways—cortico-cortical (transcallosal) or thalamocortical (infraorbital)—results in increased cortical CBF associated with the recruitment of distinct populations of interneurons and cyclo-oxygenase (COX)2 pyramidal cells (Enager et al., 2009). Analysis of double-immunostained cells with c-Fos and specific neuronal markers indicate that after 4 Hz thalamocortical stimulation, activation of COX2 expressing pyramidal cells and specific subtypes of inhibitory GABA interneurons that contain PV and SOM, a subset of the latter, are also known to contain NOS (Kubota et al., 1994). Transcallosal stimulation at 4 Hz sollicitates more COX2 pyramidal cells and less SOM interneurons (Enager et al., 2009). However, at 30 Hz, a larger fraction of SOM-NOS interneurons were activated together with a subset of VIP interneurons, but there was a silencing of those containing PV. Blood flow responses to these stimulations show a strong correlation between the CBF amplitude and the percentage of the SOM eNOS subset of GABAergic interneurons recruited (Enager et al., 2009).

The NO release from (inter)neurons is stimulated by glutamatergic neurotransmission (Faraci and Breese, 1993). Glutamate binds to its NMDA ionotropic receptors to produce NO by the activation of nNOS, an enzyme tethered to the NMDA receptor NR1 subunit receptor complex by the post-synaptic density protein-95 (Christopherson et al., 1999). This is consistent with the presence of nNOS in post-synaptic dendrites (Wang et al., 2005), NMDA R1 subunit mRNA or immunoreactivity in the majority of nNOS-immunoreactive neurons in rat cerebral cortex (Price et al., 1993). Ionotropic NMDA receptor stimulation results in Ca^{2+} influx, membrane depolarization, activation of nNOS, and the subsequent production of NO, which diffuses out of the neurons and acts on smooth muscle cells in local arterioles and pial arteries to cause vasodilatation (Faraci and Brian, 1995; Meng et al., 1995; Pelligrino et al., 1996; Garthwaite et al., 1989a; Girouard et al., 2009). NO may also directly act on pericytes surrounding terminal arterioles and capillaries (Hamilton et al., 2010).

The hypothesis that the nNOS-induced activation by NMDA receptors contributes to the increase in CBF is supported by the following observations: (1) NMDA increases NO production around arteries as demonstrated by the accumulation of NO degradation products in the cerebrospinal fluid surrounding the arteries (Domoki et al., 2002) or directly in the arteries (methemoglobin detection by spectroscopy) (Gonzalez-Mora et al., 2002) following NMDA application in the cortex and the simultaneous increase in CBF and NO production measured using microdialysis after NMDA perfusion in the striatum (Bhardwaj et al., 2000). (2) Both dilation and NO increases induced by NMDA are reduced by treatment with nonspecific and specific nNOS inhibitors in various animal species (Faraci and Breese, 1993; Faraci and Brian, 1995; Meng et al., 1995; Bhardwaj et al., 2000; Gonzalez-Mora et al., 2002). (3) These effects are abolished by the administration of the sodium channel blocker tetrodotoxin (TTX), an agent which does not usually affect the endothelium (Faraci and Breese, 1993; Pelligrino et al., 1996) whereas endothelial stunning by phorbol 12,13-dibutyrate leaves NMDA-induced

dilation intact (Domoki et al., 2002). Exception has been found in the piglet which seems to be the unique model expressing ionotropic glutamate receptors in the endothelium and where dilator responses of cerebral resistance vessels to glutamate were reported to be intact despite the presence of TTX (Leffler et al., 2006). (4) Tissue plasminogen activator (tPA) is critical to the full expression of the flow increase evoked by activation of the mouse whisker barrel cortex and increases NMDA-induced NO production by increasing nNOS phosphorylation state (Park et al., 2008).

Differential recruitment of ionotropic glutamatergic receptors (GluRs) seems to result from different stimulation frequencies. Indeed, ionotropic nNOS inhibition reduces CBF responses to all stimulation frequencies by 50% (Dirnagl et al., 1993; Hoffmeyer et al., 2007) while NMDA receptor blockade attenuates CBF responses only at high frequencies. This suggests that nNOS activity may be stimulated by NMDA-independent mechanisms. This could involve gating of Ca^{2+} permeables AMPA or kainate receptors as well as opening voltage sensitive Ca^{2+} channels (Goldberg and Yuste, 2005). Application of kainate and AMPA receptor agonists also results in NO production (Garthwaite et al., 1989b; Bhardwaj et al., 1997a) and dilation of cerebral arteries in all species studied when applied to the cerebral cortex. Dilation to kainate is attenuated by inhibition of NOS (Faraci et al., 1994). It also appears that antagonists or blockers of heme oxygenase and COX reduce dilation to kainate (Bari et al., 1997; Ohata et al., 2006) or to the kainate receptor agonist, (*RS*)-2-amino-3-(3-hydroxy-5-*t*-butylisoxazol-4-yl) propionic acid (ATPA) (Robinson et al., 2002). Arterial dilation to AMPA is not restricted by superfusion of NOS inhibitors but is attenuated by adenosine A(2A) and A(2B) receptor antagonists and the HO inhibitor chromium mesoporphyrin (Ohata et al., 2006).

Although glutamate has the potential to induce vasodilation though activation of any of the three ionotropic glutamate receptors, this effect mostly involves NMDA receptors. Thus, MK-801, a selective NMDA receptor antagonist, blocks almost all of the cerebral dilator response to glutamate or NMDA in rabbits, piglets, and rats (Faraci and Breese, 1993; Meng et al., 1995; Pelligrino et al., 1995, 1996; Girouard et al., 2009). This preference for the NMDA receptors in the cortex may be due to their location in the cerebral cortex or due to their greater affinity for glutamate than kainate or AMPA receptors.

In the mouse somatosensory cortex, serotonin $5\text{-}HT_{3A}$ receptors have been identified in neurogliaform like regular spiking neurons corresponding to GABAergic neurons expressing NPY and NOS (Vucurovic et al., 2010; Markwardt et al., 2011). This receptor, which is the only ionotropic serotonergic receptor (Chameau and van Hooft, 2006), mediates fast serotonin-induced excitation (Ferezou et al., 2002). Perrenoud et al. (2012a) found that activation of 5-HT3A-expressing interneurons mostly induces NO-mediated vasodilation and, less frequently, NPY-mediated vasoconstriction. The same study also demonstrated that these effects are absents in Pet-1 knock-out mice which display a drastic depletion of cortical serotoninergic fibers (Kiyasova et al., 2011) supporting NPY/NOS interneuron-dependent vasomotor effects rather than presynaptic 5-HT3 activation of serotonergic axons originating from the raphe nuclei. According to Perrenoud et al. (2012a) activation of the serotonin 5-HT3A receptors triggers NPY and NO release by a mechanism independent of action potential generation, but rather by direct Ca^{2+} influx which may induce Ca^{2+} release from intracellular stores.

NO is one of the vasodilator that diffuses the most rapidly (Wood and Garthwaite, 1994) and its release, in the context of NVC, mostly depends on nNOS activation. The release of NO from neurons depends on intracellular Ca^{2+} elevation similar to other vasoactive mediators derived from neurons (Lauritzen, 2005) and astrocytes (Straub and Nelson, 2007). Thus, a fast activation of nNOS would occur following Ca^{2+} influx after fast neuronal depolarization (10–12 ms) (Petersen et al., 2003) and/or activation of ionotropic receptors while a slower release may be induced through the activation of metabotropic receptors leading to Ca^{2+} release from intracellular stores (Perea and Araque, 2005). Thus, hypothetically, NO may account for the initiation and the maintenance (up to 15 min) of the vasodilatatory response in NVC. This premise is supported by the following observations: (1) NO concentrations increase at the beginning of the stimulation and remain elevated during at least a 2 min duration of neuronal stimulation (de Labra et al., 2009); (2) CBF responses to 1 s stimulation of the mouse hindpaw is reduced by about 50% in nNOS knockout mice or after topical application of L-NA (Kitaura et al., 2007); (3) Topical application of L-NNA dampers the entire NVC; (4) Systemic administration of 7-NI attenuates NVC during long stimulus of more than 60 s (Dirnagl et al., 1993, 1994; Ngai et al., 1995; Lindauer et al., 1999; Peng et al., 2004). NO can either act directly on smooth muscle cells through the guanylate cyclase/cGMP system or indirectly by having a permissive role. In the cerebral cortex, the reduction of the magnitude of the NVC reduced by NOS inhibition could be restored by the normalization of basal NO levels with the infusion of the NO precursor, L-arginine NO (Northington et al., 1992; Lindauer et al., 1999). This effect is not observed after restoration of basal cGMP levels. These observations suggest that, in the cortex, NO is a modulator rather than a mediator of NVC (Iadecola et al., 1994; Lindauer et al., 1999). However, the vasodilation induced by NMDA is completely dependent of nNOS, guanylate cyclase, and protein kinase G (Girouard et al., 2009) which indicates that NO has an obligatory role in the NMDA-induced dilation and thus possibly in the fast ionotropic dependent CBF response to neuronal activation.

In summary, it seems that an initial rise of intracellular NO concentration in interneurons following activation of the glutamatergic or serotoninergic ionotropic receptors is responsible for the initiation of the vascular response whereas during long stimulation, NO would have a permissive role for other mediators to increase CBF.

ROLE OF ASTROCYTES IN THE NO MODULATION OF NEUROVASCULAR COUPLING (FIGURE 1)

Astrocytes are key elements in the neural activity-dependent regulation of vascular tone. Anatomically, astrocytes surround most of the arteriolar and capillary abluminal surface with their endfeet and are uniquely positioned between synapses and vessels. This specific arrangement led to the concept of

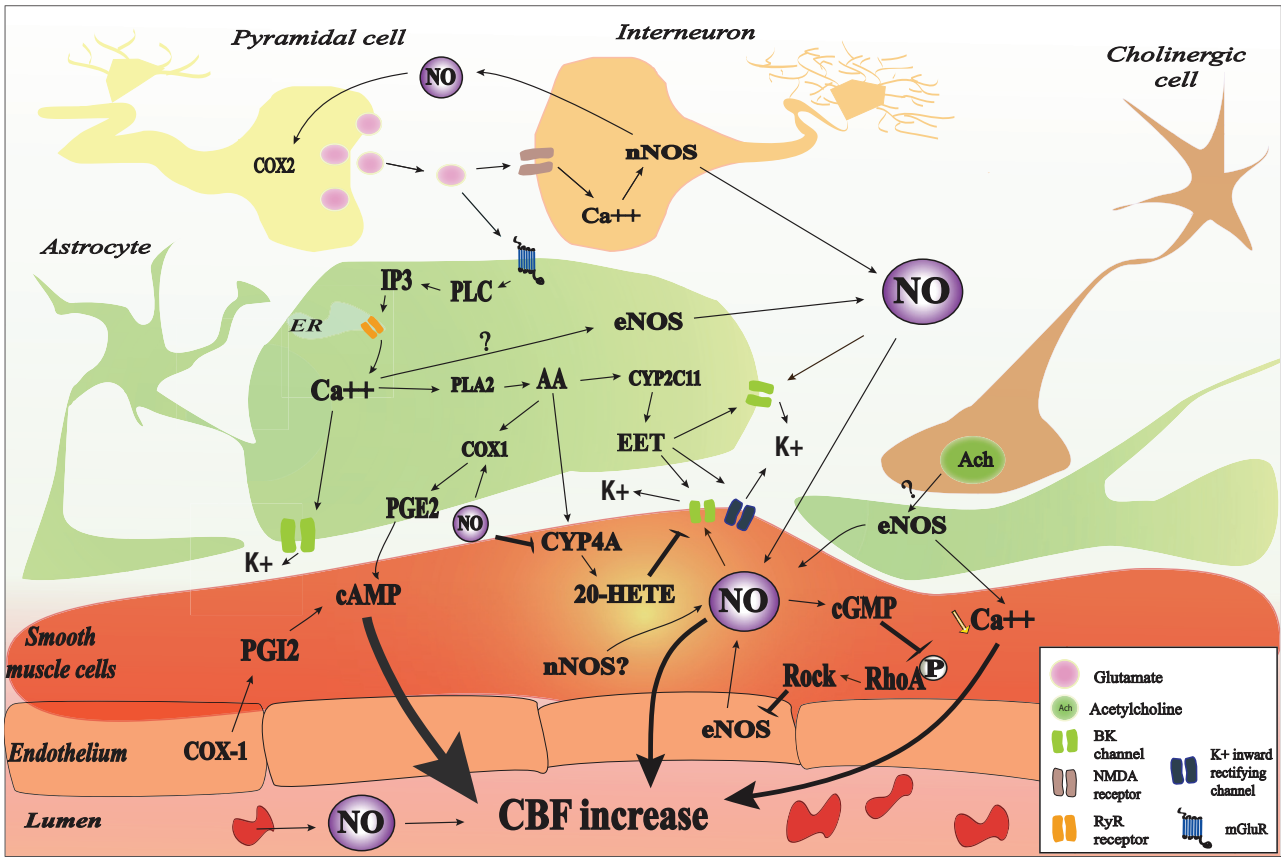

FIGURE 1 | Nitric oxide (NO) interactions in neurovascular coupling (NVC). NO may be released from red blood cells, endothelial cells, smooth muscle cells, astrocyte, interneurons, and some pyramidal cells. NO may be involved in the initiation of NVC through a cyclic guanosine monophosphate (cGMP)-dependent pathway and may modulate NVC probably by interaction with different cGMP-independent pathways. In astrocyte, glutamate released from pyramidal cell binds to the metabotropic glutamate receptor (mGluR) which lead to IP_3 formation and the subsequent release of Ca^{2+}. The increase in intracellular Ca^{2+} activates BK channel and catalyses the phosphorylation of arachidonic acid (AA) by phospholipase A_2 (PLA_2). AA metabolites (PGE2, 20-HETE, and EET) will mediate cerebral blood flow (CBF) through different pathways. NO may interact with different astrocytic pathways such as Ca^{2+} release, Ca^{2+}-activated K^+ channel (BK) opening, and COX1 activity. NO can also decrease 20-HETE formation through the inhibition of CYP4A. Vascular smooth muscle cells are the final integrators of NO-induced signals coming from the endothelium, the blood, neurons, and astrocytes. In the SMC, NO directly mediate vasodilation through the increase in cGMP-PKG activity and the increase of BK channel opening probability and the subsequent hyperpolarization as well as the inhibition of RhoA phosphorylation. The contractile state of VSMC is mainly determined by the phosphorylation level of myosin light chains (MLC). MLC is phosphorylated by the Ca^{2+}/calmodulin-dependent MLCK and dephosphorylated by the Ca^{2+}-independent MLCP. NOS may be inhibited, in turn, by RhoA kinase (ROCK).

a neuron-astrocyte-vasculature tripartite (Vaucher and Hamel, 1995). Functionally, astrocytes can integrate neurotransmitters signals from thousands of synapses (Bushong et al., 2002) and relay this information to the arterioles (Metea and Newman, 2006). Surely, results obtained in cortical brain slices show a temporal link between increases in Ca^{2+} in the astrocyte and the subsequent vasodilation of neighboring arterioles (Zonta et al., 2003a). Then, using two-photon microscopy, Nedergaard's team (Wang et al., 2006) confirmed *in vivo* the physiological involvement of astrocytic Ca^{2+} increase in NVC. In accordance with the functional studies, metabotropic GluRs blockers attenuate the astrocytic Ca^{2+} signal indicating that astrocytes sense and get activated by glutamate. The involvement of astrocytes is likely to occur in the late phase of NVC. Indeed, Calcinaghi et al. (2011) reported that pharmacological blockage of mGluR5 and mGluR1 mostly expressed on astrocytes (Porter and McCarthy, 1996) does not affect NVC in the somatosensory cortex of adult rats on brief whisker stimulation of 4 and 24 s. Whisker stimulation *in vivo* induces CBF increase after 600 ms (Devor et al., 2003) while it activates astrocytes with a latency of 3 s after the stimulus (Wang et al., 2006). *In situ* electrical stimulation within the barrel triggered astrocyte Ca^{2+} transients, which peaked within 1–2 s after stimulation (Schipke et al., 2008). These data strongly suggest that although astrocytic Ca^{2+} rises early after neuronal activation, astrocytic metabotropic activation does not play a significant role in the onset of CBF but is essential for the maintenance of the hemodynamic response during NVC. In addition, the lack of an astrocytic Ca^{2+} rise when neuronal activity is blocked by TTX, indicates that neurons and astrocytes act in series during the delayed phase of NVC.

Some evidences support the hypothesis that NO derived from nNOS participates in the mGluRs induced CBF

increase. The mGluR1 and five agonist, *trans*-1-amino-1,3-cyclopentanedicarboxylic acid (ACPD), is capable of increasing NOS activity *in vivo* through an IP3-dependent mechanism (Bhardwaj et al., 1997b). In addition, nNOS inhibition strongly attenuates the CBF increase to the mGluR1 activation with the agonist (S)-3,5-dihydroxyphenylglycine (DHPG) during the first 10–15 min of superfusion while it does not exert any significant effect after 15 min (Liu et al., 2011). These data suggest that NO interact with different astrocytic pathways instead of acting directly on smooth muscle cells. In the next paragraphs, we will describe the possible interaction of NO with different pathways involved in NVC.

REPORTED EFFECTS OF NO ON ASTROCYTIC Ca^{2+} SIGNALING, BK AND PLA_2 PATHWAYS

For decades, investigators assumed that NO originating from neurons diffuses to smooth muscle cells to induce a vasorelaxation. However, astrocytes are anatomically closer to neurons and nNOS than smooth muscle cells. In addition, an increased cGMP production has been observed in astrocytes in response to exogenous NO as well as to glutamate and NMDA induced NO production (Malcolm et al., 1996). Willmott et al. (2000a) demonstrated that NO-PKG signaling is coupled to Ca^{2+} mobilization in isolated glial cells. In many cellular types, it has been demonstrated that NO induces Ca^{2+} mobilization (Publicover et al., 1993; Willmott et al., 1995a,b; Clementi et al., 1996) through the activation of the cGMP-PKG and ADP-ribosylcyclase and subsequent increase in synthesis of the potent Ca^{2+} ryanodine receptor (RYR) dependent mobilizing agent cyclic ADP-ribose (Galione et al., 1991; Willmott et al., 1995b; Clementi et al., 1996) or the direct nitrosylation of regulatory thiol groups of RYR (Stoyanovsky et al., 1997).

Cytoplasmic and endoplasmic reticulum (ER) Ca^{2+} are important determinant of IP3-mediated Ca^{2+} release, which delivers local Ca^{2+} in astrocytic endfeet for BK channel activation in the endfeet. The release of K^+ into the arteriolar space acts on smooth muscle inward rectifying K^+ channels to hyperpolarize the smooth muscle cell membrane, lower arteriolar smooth muscle $[Ca^{2+}]$ and thereby cause vasodilation (Straub et al., 2006). In several tissues, the cGMP/PKG pathway activates BK channels (Archer et al., 1994; Alioua et al., 1995; Carrier et al., 1997). BK channel activity is regulated by a variety of signaling molecules, including intracellular Ca^{2+} ($[Ca^{2+}]_i$) (Kume et al., 1989), protein kinases (Robertson et al., 1993), tyrosine kinases (Alioua et al., 2002), cytochrome P-450 metabolites of arachidonic acid (Zou et al., 1996), and heme (Tang et al., 2003). BK channels are also directly activated by O_2, CO, and NO as demonstrated in cell-free membrane patches isolated from the intracellular medium (Bolotina et al., 1994). Thus NO may modulate BK channel opening directly or by inducing cytosolic Ca^{2+} increase. BK channels are typically composed of pore-forming α subunits that are encoded by the *Slo1* (or *KCNMA1*) gene, and accessory ß subunits that modulate channel gating (Tanaka et al., 2004). Stimulatory effect of NO on BK channels is likely mediated by the β subunits of BK channel complex. NO elevates BK channel Ca^{2+} sensitivity (Tanaka et al., 2004), enhancing the effective coupling of Ca^{2+} to BK channels (Jaggar et al., 2002).

The level of Ca^{2+} in astrocytic endfeet determines the nature of the vascular response with moderate elevations causing dilation and larger elevations causing constriction. The constrictive responses in preconstricted arteries in brain slices incubated in artificial cerebrospinal fluid with stable levels of oxygen seem to be entirely dependent on BK channels (Girouard et al., 2010). In acute mammalian retina, high doses of the NO donor SNAP (100 μM) blocks light-evoked vasodilations or transforms vasodilations into vasoconstrictions. This effect is prevented with PTIO (a NO scavenger, 2-pyenyl-4,4,5,5-tetramethylimidazoline-3-oxide-1-oxyl). In the presence of L-NAME, light stimulation evokes only vasodilations. All arterioles dilate in response to light when NO is lower than 70 nM. At NO concentrations between 80 nM and 1 μM, light-evoked responses switch from dilation to constriction (Metea and Newman, 2006). Electrical stimulations in brain slices raises NO concentration up to 100 nM as measured by electrodes (Shibuki and Okada, 1991) and levels up to 1–4 μM have been measured in rat brain *in vivo* during ischemia and reperfusion (Malinski et al., 1993). In this context, the NO induced vasoconstriction is probably pathological. The NO capacity to mobilize astrocytic Ca^{2+} and to increase BK channels opening probability may explain why exogenous NO could transform vasodilation into vasoconstriction and support the idea of a modulating role of NO in NVC (**Figure 2**).

Astrocytic cytosolic Ca^{2+} induces arachidonic acid release (Alkayed et al., 1997), which serves as a substrate for the synthesis of epoxyeicosatrienoic acids (EETs) by CYP2C and CYP2J epoxygenases in astrocytes (Alkayed et al., 1996, 1997; Nithipatikom et al., 2001; Peng et al., 2004), prostaglandin E2 (PGE2) by COX1 in astrocytes (Zonta et al., 2003b), and the synthesis of 20-HETE by CYP4A enzymes in cerebral vascular smooth muscle (Dunn et al., 2008). Astrocyte-derived EETs promote increases in astrocyte Ca^{2+} and opening of astrocytic BK channels (Yamaura et al., 2006). They may also diffuse from astrocytes to the adjacent smooth muscle cells to open BK channels and hyperpolarize vascular smooth muscle cells (Alkayed et al., 1997). Specific inhibitors of EET synthesis, MS-PPOH and miconazole, or antagonist of EET receptors, 14,15-EEZE, show that EETs contribute to 40–60% of the CBF response to sensory stimulation (Liu et al., 2011). In contrast, 20-HETE depolarizes smooth muscle cells by inhibiting the opening of K^+ channels (Lange et al., 1997) and enhances Ca^{2+} influx through voltage-dependent Ca^{2+} channels (Gebremedhin et al., 1992). The 20-HETE inhibitor HET0016 blocks the vasoconstriction elicited by electrical activation in rat brain slices (Hama-Tomioka et al., 2009). *In vivo*, HET0016 attenuates the CBF response during the first 5 min of activation of the group I mGluRs with DHPG superfusion, suggesting that 20-HETE might serve as a vasodilator during the first phase of the group I mGluR-induced vasodilation (Liu et al., 2011). This effect may be explained by the conversion of 20-HETE to the vasodilator 20-hydroxy-PGE by COX (McGiff and Quilley, 1999). When mGluR activation is prolonged beyond 30 min, the inhibition of 20-HETE synthesis prevents the decrement of the CBF suggesting that this mediator may limit CBF increase periods (Liu et al., 2011). The other arachidonic acid metabolite, PGE2 released from astrocytes may travel to smooth muscle cells and induce vasodilation by binding to EP_4 prostaglandin receptors

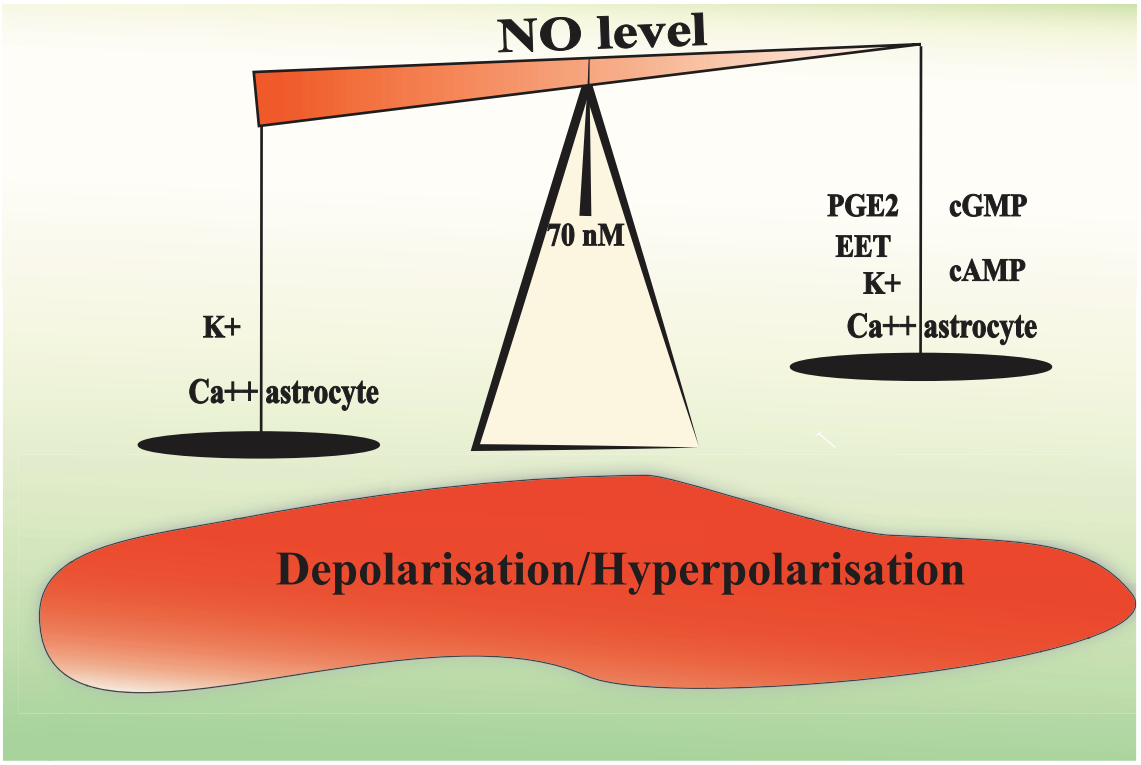

FIGURE 2 | Hypothetical mechanisms underlying the biphasic effect of NO in the modulation of NVC. A moderate or physiological NO increases the release of vasorelaxing factors from the astrocyte and depolarise smooth muscle cells to increase cerebral blood flow. NO levels above 70–80 nM may increase astrocytic Ca^{2+} mobilization and BK channel opening probability to a level that will increase the perivascular K^+ ion concentrations over 20 mM. Such a high K^+ concentration induces smooth muscle membrane depolarization and the consequent vasoconstriction.

(Davis et al., 2004), which increase the activation of protein kinase A by cyclic AMP and as a result decrease the phosphorylation of the myosin light chain (Takata et al., 2009).

NO can affect vasomotor responses by inhibiting ω-hydroxylase, the synthetic enzyme for the vasoconstrictor 20-HETE (Roman, 2002). It also enhances prostaglandin production by COX1 (Fujimoto et al., 2004). The concomitant inhibition of the synthesis of the vasoconstrictor 20-HETE and COX1 expressed in astrocytic endfeet (Gordon et al., 2008) stimulation by NO may underlie a significant fraction of the dilating effect of NO (Sun et al., 2000) and may be another mechanism by which NO modulates NVC in a cyclic GMP-independent manner. Also, by counteracting the decrement of CBF by 20-HETE at the end of the stimulation, NO could increase the length of the CBF response.

NO can also enhance the catalytic activity of COX2 in the brain (Salvemini, 1997). However, although COX1 is present in astrocytes, COX2 is rather present in neurons post and presynapticaly to nNOS neurons (Bidmon et al., 2001). Anatomical evidences suggest a close interaction between COX2 and NO. Firstly, COX2 and nNOS are both prevalent in layer I and III, IV (Degi et al., 1998). Secondly, COX2 are detected in dendrites that are lightly immunolabeled for nNOS. Both COX2 and nNOS are close to walls of penetrating arterioles and capillaries and separated by thin glial processes (Wang et al., 2005), which indicate that their interaction may play a role in the regulation of NVC. However, physiological studies have shown an additive effect with unspecific COX and NOS inhibitions (Kitaura et al., 2007), suggesting independent pathways.

RETROGRADE VASODILATATION (FIGURE 3)

During NVC, local vasodilation must be associated with dilation of upstream pial arteries (Duling et al., 1987). This has been observed in several brain areas. For example, activation of whisker barrel cortex increases vascular diameter in pial arterioles that are several hundred micrometers away from the site of activation (Ngai et al., 1988; Cox et al., 1993; Erinjeri and Woolsey, 2002). Several possible mechanisms have been proposed for this complex and coordinated chain of events, including widespread neurovascular innervation, propagation of astrocytic Ca^{2+} waves and "intramural" signaling within the vascular wall. Vascular smooth muscle cells probably receive and integrate signals coming from neurons, glia, endothelial cells as well as mechanical forces. Indeed, neurons release NO, glutamate, and ATP that have been shown to play a role in the astrocytic Ca^{2+} wave propagation. NO is a good candidate for the propagation of neuronal signals since it can diffuse very rapidly and propagate to a distance of up to 100 μM. NO can also potentiate the propagation by amplifying the astrocytic signals such as Ca^{2+} waves and ATP and glutamate release from astrocytes. Indeed, the addition of puffs of aqueous

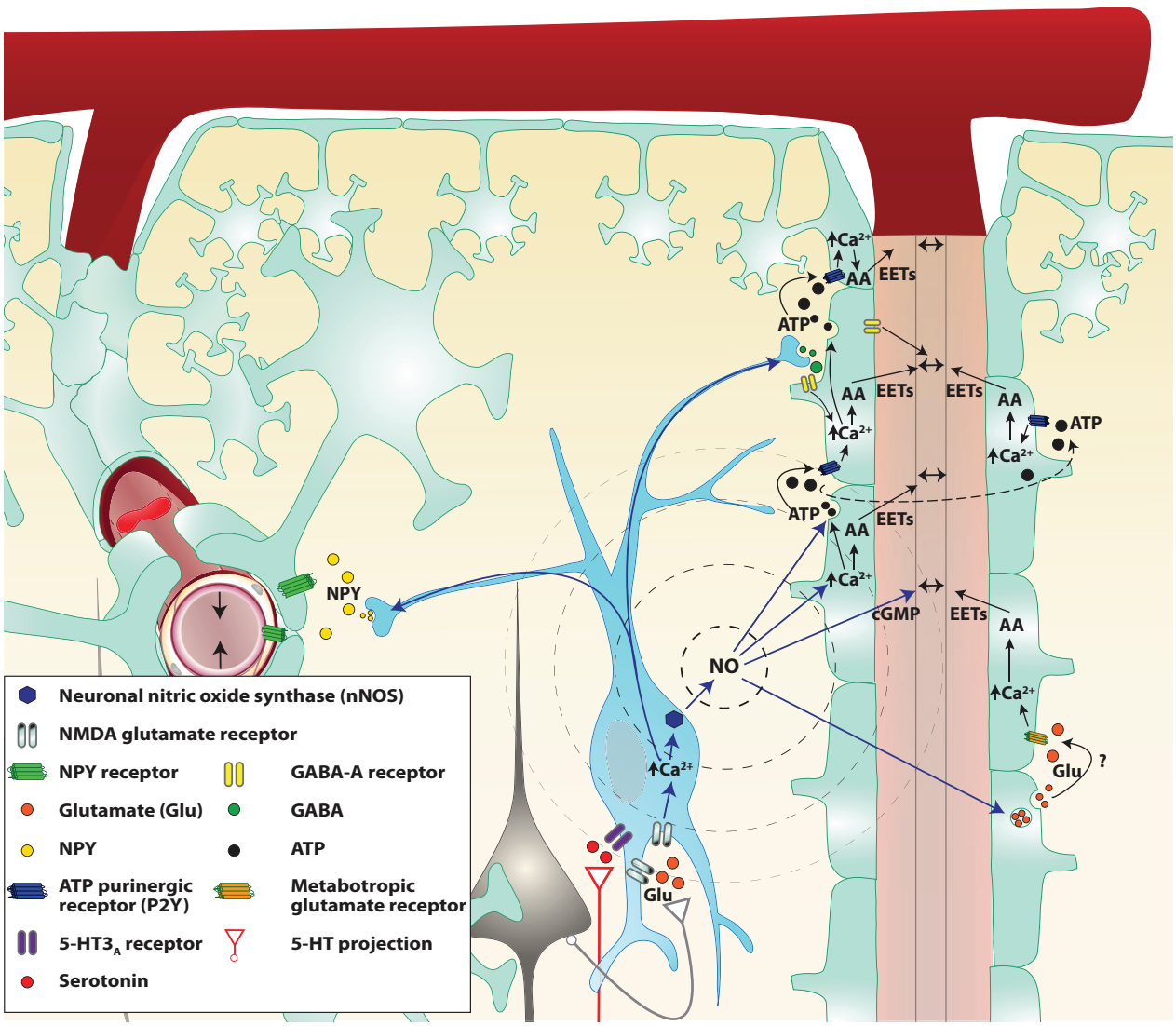

FIGURE 3 | Proposed mechanisms by which NO interneurons may propagate the signal in the cortex. Two parenchymal descending arteries (left and right of the figure) are branching from a pial artery. Astrocytes (light green cells) cover descending arteries with their specialized projections: the astrocytic endfeet, with the exception of the pial artery and parenchymal arteries portion separated by the Virchow–Robin space. Following local neuronal activity, pyramidal cells (black cells) stimulate nitrergic interneurons (blue cell), through their glutamate NMDA receptors. The influx of calcium (Ca^{2+}) in the cell allows activation of the neuronal NO synthase (nNOS) and the production of NO. NO diffuses freely through cell membranes and reaches the astrocytic endfeet where it could modulate the release of various vasoactive metabolites. NO may be involved in retrograde vasodilation either through astrocyte signaling modulation or by acting directly on smooth muscle cells. Indeed NO can increase the release of ATP and glutamate from astrocytes. ATP released from vesicles goes from one astrocyte to the next stimulating P2Y purinergic receptors, creating a Ca^{2+} wave. These Ca^{2+} waves enhance the production of arachidonic acid (AA) derived vasodilation mediators like epoxyeicosatrienoic acids (EETs) or activate large conductance Ca^{2+}-dependent K^+ channels thus causing arterial vasodilation. NO also directly increases astrocytic Ca^{2+} and might therefore facilitate the production of vasodilators. Finally, NO binds to smooth muscle guanylate cyclase and increases the cGMP levels. Stimulated nitrergic interneurons also release GABA which could act either on astrocytes or smooth muscles GABA-A receptors to cause vasodilation. However, GABA seems to restrain the astrocytic signal propagation. Simultaneously, Neuropeptide Y (NPY) is released most probably to a remote vascular bed (on the left of the illustration) to cause a vasoconstriction and concentrate the blood flow close to the neuronal activation.

NO induces large astrocytic Ca^{2+} transients that propagate to a group of up to 20 cells (Willmott et al., 2000b). This effect seems to be mediated through PKG and RyR-linked Ca^{2+} release as well as gap junction (Bolanos and Medina, 1996; O'Donnell and Grace, 1997). Astrocytes are known to have a vesicular pool of glutamate (and possibly ATP) that is rapidly exocytosed in response to agonists such as NO that raise intracellular Ca^{2+} (Maienschein et al., 1999; Pasti et al., 2001). Nanomolars levels of ATP can act via extracellular mediators and may carry information between astrocytes (Scemes, 2000). NO is also known to

cause rapid glutamate release from neurons (Meffert et al., 1994). Thus NO may propagate the neuro-astrocytic signals directly by increasing intracellular concentrations of Ca^{2+} or through the release of ATP and glutamate. ATP may also be metabolized and produce adenosine, a potent vasodilator. Adenosine has long been implicated as a mediator of NVC (Ko et al., 1990; Dirnagl et al., 1994). Indeed, adenosine A_{2A} receptors have a role in dilation of upstream pial arterioles during neuronal activation or direct activation of GluRs (Iliff et al., 2003; Ohata et al., 2006). In addition to acting on vascular adenosine receptors, adenosine could act on astrocytes, which also express various types of adenosine receptors (Fields and Burnstock, 2006). Activation of A_{2B} receptors can increase intracellular Ca^{2+} in astrocytes and might participate in the propagation of increased Ca^{2+} throughout the astrocyte processes (Pilitsis and Kimelberg, 1998). Ordinarily, an increase in Ca^{2+} is associated with release of ATP through connexin hemichannels, and A_{2B} receptors potentiate the ATP-evoked Ca^{2+} response (Jimenez et al., 1999; Alloisio et al., 2004). Finally, the release of GABA from interneurons restricts the astrocytic response to the barrel column (Benedetti et al., 2011).

Endothelial and smooth muscle cells in the brain are connected by homocellular gap junctions and can propagate vasodilation in a retrograde fashion (Dietrich et al., 1996; Sokoya et al., 2006). Local vasodilation increases flow velocity in upstream branches which, due to increased shear stress, leads to the local release of endothelium-dependent vasodilators (Busse and Fleming, 2003). These vasodilators relax the larger arteries and amplify the increase of flow, but there is limited evidence supporting this possibility in the neocortical microcirculation. The hyperpolarization of vascular smooth muscle travels rapidly through gap junctions for millimeters (de Wit, 2010) or within the endothelial tissue through the small (KCa 2.3; KCNN3)-and intermediate (KCa 3.1; KCNN4)-conductance Ca^{2+}-activated K+ channels (SKCa/IKCa) (Behringer and Segal, 2012).

WHAT IS THE SPECIFIC ROLE OF INTERNEURON-DERIVED NO IN THE CONTROL OF CBF AMONG OTHER SOURCES?

There are multiple sources of NO and all cell types of the brain can produce NO. NO derives from three NOS isoforms as well as from nitrite. In the central nervous system, the nNOS isoform is present in interneurons, some pyramidal cells as well as nitrergic nerves originating from pterygopalatine ganglia although their extraneuronal presence is still a matter of controversies. There are at least three nNOS alternative-splice variants: nNOSα, nNOSβ, and nNOSγ (Putzke et al., 2000; Saur et al., 2000). The mitNOS corresponds to the nNOSα variant and could be inhibited by 7-NI. In addition, only the nNOSα variant is knocked out in the nNOS null mice (Putzke et al., 2000), which means that these mice lack both neuronal and mitochondrial NOS. Neuronal NOSα null mice are resistant to NMDA-induced neurotoxicity (Dawson et al., 1996; Ayata et al., 1997). In a culture of rat hippocampal neurons, it has been demonstrated that nNOS is totally localized into mitochondria and activated by NMDA (Marks et al., 2005). Therefore, it is very difficult to conclude the source of NO using nNOS transgenic mice or 7-NI. Since NOS interneurons are very specifically localized and serve as a relay to pyramidal neurons, we could hypothesize that their primary function is the control of NVC and local resting CBF rather than global CBF changes such as in autoregulation or responses to (Ulker et al., 2009) systemic changes in $paCO_2$ or paO_2. However, the subcellular localization of NOS in interneurons remains controversial (Mizukawa et al., 1988; Wolf et al., 1992; Aoki et al., 1993; Wiencken and Casagrande, 2000).

Although, we already mentioned studies about the role of NOS isoforms in resting CBF, autoregulation as well as responses to $paCO_2$ or paO_2 variations, it is interesting to stress out the possible involvement of NO from blood cells in these mechanisms. Although blood cells can produce a considerable amount of NO, this aspect is rarely considered in neurovascular studies. Shear stress, defined as the tangential forces acting on the luminal surface of the vessel as a result of flow, could activate eNOS in the endothelium as well as red blood cells NOS which is very similar to eNOS (Ulker et al., 2009). In this regard, both endothelial and red blood cells would play a role in CBF autoregulation. Interestingly, red blood cells also contain functional NMDA receptors, which upon activation increase NOS-dependent NO production (Makhro et al., 2010). This may explain why resting CBF is decreased in the presence of the NMDA inhibitor MK-801 although the effect of 7-NI on red blood cell NOS remain to be assessed.

Another important source of NO in the brain is nitrite. However, nitrite was recently found to have a direct effect on resting CBF in a rat model (Rifkind et al., 2007) and on the CBF in response to hypercapnia and hypoxia in human (Peebles et al., 2008). Nitrite concentrations in different mammalian tissues are in general in micromolar range of 0.5–20 μM (Samouilov et al., 2007; Feelisch et al., 2008). Nitrite can be converted into NO through the nitrite reductase activity of deoxyhemoglobin (Cosby et al., 2003), xanthine oxidase (Li et al., 2008), aldehyde oxidase (Li et al., 2009), carbonic anhydrase (Aamand et al., 2009), and all isoforms of NOS (Mikula et al., 2009).

Overall, anatomical and physiological studies support a role of NOS interneurons in NVC while other NOS containing cells or nitrite seem to be rather responsible for the control of autoregulation or the responses to hypercapnia and hypoxia. Nevertheless, the development of specific NOS inhibitors is necessary to bring appropriate answers to questions related to the origin of NO in CBF regulation.

NO AND FUNCTIONAL BRAING IMAGING

Functional magnetic resonance imaging (fMRI) is often used as a marker of changes in neuronal spiking activity. In reality, fMRI detects CBF through the arterial spin label method or blood oxygenation levels (BOLD) which reflects the shift of the ratio between the local concentration of oxygenated and deoxygenated hemoglobin due to increased oxygen extraction and increased oxygen supply. Unfortunately, the relationship between hemodynamic changes and the actual underlying response is still poorly understood. Anatomical and physiological data about NOS interneurons strongly suggest a non-linear relationship between neuronal activity and fMRI signals. In fact, NOS interneurons account for 0.3% of all cortical neurons but for about 50% of the vascular response to neuronal stimulation.

In addition, the inhibition of nNOS with 7-NI clearly reduces the BOLD response upon electrical forepaw stimulation while the somatosensory-evoked potentials are still clearly detectable and only slightly reduced in amplitude (Burke and Buhrle, 2006). Overall, these studies strongly support the concept of a non-linear relationship between the BOLD-fMRI signal and neuronal stimulation (Membre et al., 1997; Yang et al., 2000).

However, interneurons may act as "local integrators" of cortical activity and therefore have important implications for the resulting neuronal activity and functional brain imaging (Buzsaki et al., 2007). The resulting neuronal activity correlates with increases in local field potentials rather than spikes. For example, if the balance between excitation and inhibition does not lead to the firing of action potentials, as demonstrated in the visual cortex, the CBF response correlates with local field potentials but not with spikes. Thus, local field potentials reflect synchronized or correlated neuronal activity and are associated with incoming input and local processing (Logothetis et al., 2001). So, the CBF increase best reflects signal processing by interneurons and electrophysiological events that do not result in spikes. Nonetheless, the majority of studies suggest that the relationship between CBF or BOLD signal and local field potentials is non-linear. Consequently, fMRI signals should be carefully interpreted as a non-linear result of local field potential and the significance of NOS interneurons in this signal remain to be elucidated.

CONCLUSION

NOS interneurons are strategically positioned close to blood vessels and seem to be involved in the control of CBF. In NVC, the mechanisms by which NO intervenes are particularly complex. Actual data suggest that NO from interneurons play a cGMP-dependent mediator role in the initiation of the vascular response to neuronal activation followed by a cGMP-independent modulatory role of astrocytic signals, which could lead to a vasodilation at moderate concentrations or a vasoconstriction at higher concentrations. NO from different sources also seems to coordinate the signal propagation of vasodilation upstream as well as the length of the response. The involvement of inhibitory NOS interneurons in NVC implies that the relationship between neuronal activity and CBF is non-linear. Therefore, a better understanding of the role of NOS interneurons in the control of CBF will allow a better modelization and interpretation of BOLD signal used in fMRI studies.

FUTURE DIRECTIONS

Since the discovery that NO is a powerful vasodilator, we have made many observations to support its pivotal role in the cerebrovascular regulation. However, a complete understanding of the origin of NO and the pathways by which it controls the vascular tone is still missing. Additional studies will have to be conducted to further determine how NO intervene in NVC, how it is released upon activation and how it interact with astrocytes. As pharmacological blockers show evident limitations when it comes to cell-type specificity, new techniques to unveil the direct involvement of NOS expressing interneurons in NVC have yet to be developed. A few transgenic mice models like the Arx (Colombo et al., 2007; Price et al., 2009) and the Tsc1 (Fu et al., 2011) mutant mice, present a diminished expression of NPY interneurons in the cortex. It would be interesting to verify whether CBF regulation is impaired in these models and what proportion of the remaining interneurons expresses nNOS. As these transgenic mice model might present compensatory mechanism and reorganization of the neural circuitry, more targeted approaches might be needed. Recently, a new method for specific elimination of nNOS expressing interneurons in acute slices using induced photo-toxicity has been elaborated (Shlosberg et al., 2012). However, the most promising tool will be conditional transgenic optogenetic silencing using Cre driver lines allowing the investigations of neural circuit function with unprecedented reliability and accuracy.

ACKNOWLEDGMENTS

Hélène Girouard was supported by funds from the Canadian Institutes in Health Research (CIHR), the Natural Sciences and Engineering Research Council of Canada (NSERC), the "Fonds de Recherche en Santé du Québec" (FRSQ) and the Canada Found for Innovation (CFI). She was also the holder of new investigator awards from the FRSQ and the Heart and Stroke Foundation of Canada (HSFC). Nataliya Sadekova is the holder of a student award from the "Société Québécoise d'Hypertension Artérielle."

REFERENCES

Aamand, R., Dalsgaard, T., Jensen, F. B., Simonsen, U., Roepstorff, A., and Fago, A. (2009). Generation of nitric oxide from nitrite by carbonic anhydrase: a possible link between metabolic activity and vasodilation. *Am. J. Physiol. Heart Circ. Physiol.* 297, H2068–H2074.

Abadia-Fenoll, F. (1969). Structure of the leptomeninx and cerebral vessels of the cat. II. Constituent elements of the intracerebral vessel wall (analogy with the meninges). *Angiology* 20, 535–562.

Abounader, R., and Hamel, E. (1997). Associations between neuropeptide Y nerve terminals and intraparenchymal microvessels in rat and human cerebral cortex. *J. Comp. Neurol.* 388, 444–453.

Adachi, K., Takahashi, S., Melzer, P., Campos, K. L., Nelson, T., Kennedy, C., and Sokoloff, L. (1994). Increases in local cerebral blood flow associated with somatosensory activation are not mediated by NO. *Am. J. Physiol.* 267, H2155–H2162.

Alioua, A., Huggins, J. P., and Rousseau, E. (1995). PKG-I alpha phosphorylates the alpha-subunit and upregulates reconstituted GKCa channels from tracheal smooth muscle. *Am. J. Physiol.* 268, L1057–L1063.

Alioua, A., Mahajan, A., Nishimaru, K., Zarei, M. M., Stefani, E., and Toro, L. (2002). Coupling of c-Src to large conductance voltage- and Ca2+-activated K+ channels as a new mechanism of agonist-induced vasoconstriction. *Proc. Natl. Acad. Sci. U.S.A.* 99, 14560–14565.

Alkayed, N. J., Birks, E. K., Narayanan, J., Petrie, K. A., Kohler-cabot, A. E., and Harder, D. R. (1997). Role of P-450 arachidonic acid epoxygenase in the response of cerebral blood flow to glutamate in rats. *Stroke* 28, 1066–1072.

Alkayed, N. J., Narayanan, J., Gebremedhin, D., Medhora, M., Roman, R. J., and Harder, D. R. (1996). Molecular characterization of an arachidonic acid epoxygenase in rat brain astrocytes. *Stroke* 27, 971–979.

Alloisio, S., Cugnoli, C., Ferroni, S., and Nobile, M. (2004). Differential modulation of ATP-induced calcium signalling by A1 and A2 adenosine receptors in cultured cortical astrocytes. *Br. J. Pharmacol.* 141, 935–942.

Aoki, C., Fenstemaker, S., Lubin, M., and Go, C. G. (1993). Nitric oxide synthase in the visual cortex of monocular monkeys as revealed by light and electron microscopic

immunocytochemistry. *Brain Res.* 620, 97–113.

Archer, S. L., Huang, J. M., Hampl, V., Nelson, D. P., Shultz, P. J., and Weir, E. K. (1994). Nitric oxide and cGMP cause vasorelaxation by activation of a charybdotoxin-sensitive K channel by cGMP-dependent protein kinase. *Proc. Natl. Acad. Sci. U.S.A.* 91, 7583–7587.

Atochin, D. N., Demchenko, I. T., Astern, J., Boso, A. E., Piantadosi, C. A., and Huang, P. L. (2003). Contributions of endothelial and neuronal nitric oxide synthases to cerebrovascular responses to hyperoxia. *J. Cereb. Blood Flow Metab.* 23, 1219–1226.

Ayata, C., Ayata, G., Hara, H., Matthews, R. T., Beal, M. F., Ferrante, R. J., Endres, M., Kim, A., Christie, R. H., Waeber, C., Huang, P. L., Hyman, B. T., and Moskowitz, M. A. (1997). Mechanisms of reduced striatal NMDA excitotoxicity in type I nitric oxide synthase knock-out mice. *J. Neurosci.* 17, 6908–6917.

Ayata, C., Ma, J., Meng, W., Huang, P., and Moskowitz, M. A. (1996). L-NA-sensitive rCBF augmentation during vibrissal stimulation in type III nitric oxide synthase mutant mice. *J. Cereb. Blood Flow Metab.* 16, 539–541.

Babbedge, R. C., Bland-ward, P. A., Hart, S. L., and Moore, P. K. (1993). Inhibition of rat cerebellar nitric oxide synthase by 7-nitro indazole and related substituted indazoles. *Br. J. Pharmacol.* 110, 225–228.

Bari, F., Louis, T. M., and Busija, D. W. (1997). Kainate-induced cerebrovascular dilation is resistant to ischemia in piglets. *Stroke* 28, 1272–1276. discussion: 1277.

Barone, P., and Kennedy, H. (2000). Non-uniformity of neocortex: areal heterogeneity of NADPH-diaphorase reactive neurons in adult macaque monkeys. *Cereb. Cortex* 10, 160–174.

Behringer, E. J., and Segal, S. S. (2012). Tuning electrical conduction along endothelial tubes of resistance arteries through Ca2+-activated K+ channels. *Circ. Res.* 110, 1311–1321.

Behzadi, Y., and Liu, T. T. (2005). An arteriolar compliance model of the cerebral blood flow response to neural stimulus. *Neuroimage* 25, 1100–1111.

Benedetti, B., Matyash, V., and Kettenmann, H. (2011). Astrocytes control GABAergic inhibition of neurons in the mouse barrel cortex. *J. Physiol.* 589, 1159–1172.

Berman, N. E., and Fredrickson, E. (1992). Morphology and laminar distribution of neuropeptide Y immunoreactive neurons in the human striate cortex. *Synapse* 11, 20–27.

Bertini, G., Peng, Z. C., and Bentivoglio, M. (1996). The chemical heterogeneity of cortical interneurons: nitric oxide synthase vs. calbindin and parvalbumin immunoreactivity in the rat. *Brain Res. Bull.* 39, 261–266.

Bhardwaj, A., Northington, F. J., Carhuapoma, J. R., Falck, J. R., Harder, D. R., Traystman, R. J., and Koehler, R. C. (2000). P-450 epoxygenase and NO synthase inhibitors reduce cerebral blood flow response to N-methyl-D-aspartate. *Am. J. Physiol. Heart Circ. Physiol.* 279, H1616–H1624.

Bhardwaj, A., Northington, F. J., Ichord, R. N., Hanley, D. F., Traystman, R. J., and Koehler, R. C. (1997a). Characterization of ionotropic glutamate receptor-mediated nitric oxide production *in vivo* in rats. *Stroke* 28, 850–856. discussion: 856–857.

Bhardwaj, A., Northington, F. J., Martin, L. J., Hanley, D. F., Traystman, R. J., and Koehler, R. C. (1997b). Characterization of metabotropic glutamate receptor-mediated nitric oxide production *in vivo*. *J. Cereb. Blood Flow Metab.* 17, 153–160.

Bidmon, H. J., Emde, B., Kowalski, T., Schmitt, M., Mayer, B., Kato, K., Asayama, K., Witte, O. W., and Zilles, K. (2001). Nitric oxide synthase-I containing cortical interneurons co-express antioxidative enzymes and anti-apoptotic Bcl-2 following focal ischemia: evidence for direct and indirect mechanisms towards their resistance to neuropathology. *J. Chem. Neuroanat.* 22, 167–184.

Bolanos, J. P., and Medina, J. M. (1996). Induction of nitric oxide synthase inhibits gap junction permeability in cultured rat astrocytes. *J. Neurochem.* 66, 2091–2099.

Bolotina, V. M., Najibi, S., Palacino, J. J., Pagano, P. J., and Cohen, R. A. (1994). Nitric oxide directly activates calcium-dependent potassium channels in vascular smooth muscle. *Nature* 368, 850–853.

Bonvento, G., Cholet, N., and Seylaz, J. (2000). Sustained attenuation of the cerebrovascular response to a 10 min whisker stimulation following neuronal nitric oxide synthase inhibition. *Neurosci. Res.* 37, 163–166.

Bonvento, G., Seylaz, J., and Lacombe, P. (1994). Widespread attenuation of the cerebrovascular reactivity to hypercapnia following inhibition of nitric oxide synthase in the conscious rat. *J. Cereb. Blood Flow Metab.* 14, 699–703.

Bredt, D. S., Hwang, P. M., Glatt, C. E., Lowenstein, C., Reed, R. R., and Snyder, S. H. (1991). Cloned and expressed nitric oxide synthase structurally resembles cytochrome P-450 reductase. *Nature* 351, 714–718.

Bredt, D. S., and Snyder, S. H. (1989). Nitric oxide mediates glutamate-linked enhancement of cGMP levels in the cerebellum. *Proc. Natl. Acad. Sci. U.S.A.* 86, 9030–9033.

Brophy, C. M., Knoepp, L., Xin, J., and Pollock, J. S. (2000). Functional expression of NOS 1 in vascular smooth muscle. *Am. J. Physiol. Heart Circ. Physiol.* 278, H991–H997.

Buchanan, J. E., and Phillis, J. W. (1993). The role of nitric oxide in the regulation of cerebral blood flow. *Brain Res.* 610, 248–255.

Bureau, M., Laschet, J., Bureau-heeren, M., Hennuy, B., Minet, A., Wins, P., and Grisar, T. (1995). Astroglial cells express large amounts of GABAA receptor proteins in mature brain. *J. Neurochem.* 65, 2006–2015.

Burke, M., and Buhrle, C. (2006). BOLD response during uncoupling of neuronal activity and CBF. *Neuroimage* 32, 1–8.

Bushong, E. A., Martone, M. E., Jones, Y. Z., and Ellisman, M. H. (2002). Protoplasmic astrocytes in CA1 stratum radiatum occupy separate anatomical domains. *J. Neurosci.* 22, 183–192.

Busija, D. W. (1993). "The role of central neural pathways in the regulation of cerebral blood flow," in *The Regulation Cerebral Blood Flow*, ed J. W. Phillis (New York, NY: CRC Press), 65–77.

Busse, R., and Fleming, I. (2003). Regulation of endothelium-derived vasoactive autacoid production by hemodynamic forces. *Trends Pharmacol. Sci.* 24, 24–29.

Buzsaki, G., Kaila, K., and Raichle, M. (2007). Inhibition and brain work. *Neuron* 56, 771–783.

Calcinaghi, N., Jolivet, R., Wyss, M. T., Ametamey, S. M., Gasparini, F., Buck, A., and Weber, B. (2011). Metabotropic glutamate receptor mGluR5 is not involved in the early hemodynamic response. *J. Cereb. Blood Flow Metab.* 31, e1–e10.

Carrier, G. O., Fuchs, L. C., Winecoff, A. P., Giulumian, A. D., and White, R. E. (1997). Nitrovasodilators relax mesenteric microvessels by cGMP-induced stimulation of Ca-activated K channels. *Am. J. Physiol.* 273, H76–H84.

Cauli, B., Tong, X. K., Rancillac, A., Serluca, N., Lambolez, B., Rossier, J., and Hamel, E. (2004). Cortical GABA interneurons in neurovascular coupling: relays for subcortical vasoactive pathways. *J. Neurosci.* 24, 8940–8949.

Chameau, P., and van Hooft, J. A. (2006). Serotonin 5-HT(3) receptors in the central nervous system. *Cell Tissue Res.* 326, 573–581.

Cholet, N., Bonvento, G., and Seylaz, J. (1996). Effect of neuronal NO synthase inhibition on the cerebral vasodilatory response to somatosensory stimulation. *Brain Res.* 708, 197–200.

Cholet, N., Seylaz, J., Lacombe, P., and Bonvento, G. (1997). Local uncoupling of the cerebrovascular and metabolic responses to somatosensory stimulation after neuronal nitric oxide synthase inhibition. *J. Cereb. Blood Flow Metab.* 17, 1191–1201.

Christopherson, K. S., Hillier, B. J., Lim, W. A., and Bredt, D. S. (1999). PSD-95 assembles a ternary complex with the n-methyl-d-aspartic acid receptor and a bivalent neuronal NO synthase PDZ domain. *J. Biol. Chem.* 274, 27467–27473.

Clementi, E., Riccio, M., Sciorati, C., Nistico, G., and Meldolesi, J. (1996). The type 2 ryanodine receptor of neurosecretory pc12 cells is activated by cyclic adp-ribose. role of the nitric oxide/cgmp pathway. *J. Biol. Chem.* 271, 17739–17745.

Colombo, E., Collombat, P., Colasante, G., Bianchi, M., Long, J., Mansouri, A., Rubenstein, J. L., and Broccoli, V. (2007). Inactivation of arx, the murine ortholog of the X-linked lissencephaly with ambiguous genitalia gene, leads to severe disorganization of the ventral telencephalon with impaired neuronal migration and differentiation. *J. Neurosci.* 27, 4786–4798.

Cosby, K., Partovi, K. S., Crawford, J. H., Patel, R. P., Reiter, C. D., Martyr, S., Yang, B. K., Waclawiw, M. A., Zalos, G., Xu, X., Huang, K. T., Shields, H., KIM-shapiro, D. B., Schechter, A. N., Cannon, R. O. 3rd., and Gladwin, M. T. (2003). Nitrite reduction to nitric oxide by deoxyhemoglobin vasodilates the human circulation. *Nat. Med.* 9, 1498–1505.

Cox, S. B., Woolsey, T. A., and Rovainen, C. M. (1993). Localized

dynamic changes in cortical blood flow with whisker stimulation corresponds to matched vascular and neuronal architecture of rat barrels. *J. Cereb. Blood Flow Metab.* 13, 899–913.

Dabertrand, F., Nelson, M. T., and Brayden, J. E. (2012). Acidosis dilates brain parenchymal arterioles by conversion of calcium waves to sparks to activate BK channels. *Circ. Res.* 110, 285–294.

Davis, R. J., Murdoch, C. E., Ali, M., Purbrick, S., Ravid, R., Baxter, G. S., Tilford, N., Sheldrick, R. L., Clark, K. L., and Coleman, R. A. (2004). EP4 prostanoid receptor-mediated vasodilatation of human middle cerebral arteries. *Br. J. Pharmacol.* 141, 580–585.

Dawson, V. L., Kizushi, V. M., Huang, P. L., Snyder, S. H., and Dawson, T. M. (1996). Resistance to neurotoxicity in cortical cultures from neuronal nitric oxide synthase-deficient mice. *J. Neurosci.* 16, 2479–2487.

DeFelipe, J. (1993). A study of NADPH diaphorase-positive axonal plexuses in the human temporal cortex. *Brain Res.* 615, 342–346.

Degi, R., Bari, F., Beasley, T. C., Thrikawala, N., Thore, C., Louis, T. M., and Busija, D. W. (1998). Regional distribution of prostaglandin H synthase-2 and neuronal nitric oxide synthase in piglet brain. *Pediatr. Res.* 43, 683–689.

de Labra, C., Rivadulla, C., Espinosa, N., Dasilva, M., Cao, R., and Cudeiro, J. (2009). Different sources of nitric oxide mediate neurovascular coupling in the lateral geniculate nucleus of the cat. *Front. Syst. Neurosci.* 3:9. doi: 10.3389/neuro.06.009.2009

de Wit, C. (2010). Different pathways with distinct properties conduct dilations in the microcirculation *in vivo*. *Cardiovasc. Res.* 85, 604–613.

Devor, A., Dunn, A. K., Andermann, M. L., Ulbert, I., Boas, D. A., and Dale, A. M. (2003). Coupling of total hemoglobin concentration, oxygenation, and neural activity in rat somatosensory cortex. *Neuron* 39, 353–359.

Dietrich, H. H., Kajita, Y., and Dacey, R. G. Jr. (1996). Local and conducted vasomotor responses in isolated rat cerebral arterioles. *Am. J. Physiol.* 271, H1109–H1116.

Dirnagl, U., Lindauer, U., and Villringer, A. (1993). Role of nitric oxide in the coupling of cerebral blood flow to neuronal activation in rats. *Neurosci. Lett.* 149, 43–46.

Dirnagl, U., Niwa, K., Lindauer, U., and Villringer, A. (1994). Coupling of cerebral blood flow to neuronal activation: role of adenosine and nitric oxide. *Am. J. Physiol.* 267, H296–H301.

Domoki, F., Perciaccante, J. V., Shimizu, K., Puskar, M., Busija, D. W., and Bari, F. (2002). N-methyl-D-aspartate-induced vasodilation is mediated by endothelium-independent nitric oxide release in piglets. *Am. J. Physiol. Heart Circ. Physiol.* 282, H1404–H1409.

Duling, B. R., Hogan, R. D., Langille, B. L., Lelkes, P., Segal, S. S., Vatner, S. F., Weigelt, H., and Young, M. A. (1987). Vasomotor control: functional hyperemia and beyond. *Fed. Proc.* 46, 251–263.

Dunn, K. M., Renic, M., Flasch, A. K., Harder, D. R., Falck, J., and Roman, R. J. (2008). Elevated production of 20-HETE in the cerebral vasculature contributes to severity of ischemic stroke and oxidative stress in spontaneously hypertensive rats. *Am. J. Physiol. Heart Circ. Physiol.* 295, H2455–H2465.

Enager, P., Piilgaard, H., Offenhauser, N., Kocharyan, A., Fernandes, P., Hamel, E., and Lauritzen, M. (2009). Pathway-specific variations in neurovascular and neurometabolic coupling in rat primary somatosensory cortex. *J. Cereb. Blood Flow Metab.* 29, 976–986.

Erinjeri, J. P., and Woolsey, T. A. (2002). Spatial integration of vascular changes with neural activity in mouse cortex. *J. Cereb. Blood Flow Metab.* 22, 353–360.

Estrada, C., and DeFelipe, J. (1998). Nitric oxide-producing neurons in the neocortex: morphological and functional relationship with intraparenchymal microvasculature. *Cereb. Cortex* 8, 193–203.

Estrada, C., Mengual, E., and Gonzalez, C. (1993). Local NADPH-diaphorase neurons innervate pial arteries and lie close or project to intracerebral blood vessels: a possible role for nitric oxide in the regulation of cerebral blood flow. *J. Cereb. Blood Flow Metab.* 13, 978–984.

Estrada, C., Triguero, D., Munoz, J., and Sureda, A. (1988). Acetylcholinesterase-containing fibers and choline acetyltransferase activity in isolated cerebral microvessels from goats. *Brain Res.* 453, 275–280.

Faraci, F. M., and Breese, K. R. (1993). Nitric oxide mediates vasodilatation in response to activation of N-methyl-D-aspartate receptors in brain. *Circ. Res.* 72, 476–480.

Faraci, F. M., Breese, K. R., and Heistad, D. D. (1993). Nitric oxide contributes to dilatation of cerebral arterioles during seizures. *Am. J. Physiol.* 265, H2209–H2212.

Faraci, F. M., Breese, K. R., and Heistad, D. D. (1994). Responses of cerebral arterioles to kainate. *Stroke* 25, 2080–2083. discussion: 2084.

Faraci, F. M., and Brian, J. E. Jr. (1995). 7-Nitroindazole inhibits brain nitric oxide synthase and cerebral vasodilatation in response to N-methyl-D-aspartate. *Stroke* 26, 2172–2175. discussion: 2176.

Feelisch, M., Fernandez, B. O., Bryan, N. S., Garcia-saura, M. F., Bauer, S., Whitlock, D. R., Ford, P. C., Janero, D. R., Rodriguez, J., and Ashrafian, H. (2008). Tissue processing of nitrite in hypoxia: an intricate interplay of nitric oxide-generating and -scavenging systems. *J. Biol. Chem.* 283, 33927–33934.

Ferezou, I., Cauli, B., Hill, E. L., Rossier, J., Hamel, E., and Lambolez, B. (2002). 5-HT3 receptors mediate serotonergic fast synaptic excitation of neocortical vasoactive intestinal peptide/cholecystokinin interneurons. *J. Neurosci.* 22, 7389–7397.

Fergus, A., and Lee, K. S. (1997). GABAergic regulation of cerebral microvascular tone in the rat. *J. Cereb. Blood Flow Metab.* 17, 992–1003.

Fields, R. D., and Burnstock, G. (2006). Purinergic signalling in neuron-glia interactions. *Nat. Rev. Neurosci.* 7, 423–436.

Filosa, J. A., Bonev, A. D., and Nelson, M. T. (2004). Calcium dynamics in cortical astrocytes and arterioles during neurovascular coupling. *Circ. Res.* 95, E73–E81.

Fu, C., Cawthon, B., Clinkscales, W., Bruce, A., Winzenburger, P., and Ess, K. C. (2011). GABAergic Interneuron Development and Function Is Modulated by the Tsc1 Gene. *Cereb. Cortex*. doi: 10.1093/cercor/bhr300. [Epub ahead of print].

Fujii, K., Heistad, D. D., and Faraci, F. M. (1990). Vasomotion of basilar arteries *in vivo*. *Am. J. Physiol.* 258, H1829–H1834.

Fujimoto, Y., Uno, E., and Sakuma, S. (2004). Effects of reactive oxygen and nitrogen species on cyclooxygenase-1 and -2 activities. *Prostaglandins Leukot. Essent. Fatty Acids* 71, 335–340.

Furchgott, R. F., and Zawadzki, J. V. (1980). The obligatory role of endothelial cells in the relaxation of arterial smooth muscle by acetylcholine. *Nature* 288, 373–376.

Gabbott, P. L., Dickie, B. G., Vaid, R. R., Headlam, A. J., and Bacon, S. J. (1997). Local-circuit neurones in the medial prefrontal cortex (areas 25, 32 and 24b) in the rat: morphology and quantitative distribution. *J. Comp. Neurol.* 377, 465–499.

Galione, A., Lee, H. C., and Busa, W. B. (1991). Ca(2+)-induced Ca2+ release in sea urchin egg homogenates: modulation by cyclic ADP-ribose. *Science* 253, 1143–1146.

Garbossa, D., Fontanella, M., Tomasi, S., Ducati, A., and Vercelli, A. (2005). Differential distribution of NADPH-diaphorase histochemistry in human cerebral cortex. *Brain Res.* 1034, 1–10.

Garthwaite, J., Garthwaite, G., Palmer, R. M., and Moncada, S. (1989a). NMDA receptor activation induces nitric oxide synthesis from arginine in rat brain slices. *Eur. J. Pharmacol.* 172, 413–416.

Garthwaite, J., Southam, E., and Anderton, M. (1989b). A kainate receptor linked to nitric oxide synthesis from arginine. *J. Neurochem.* 53, 1952–1954.

Gebremedhin, D., Ma, Y. H., Falck, J. R., Roman, R. J., Vanrollins, M., and Harder, D. R. (1992). Mechanism of action of cerebral epoxyeicosatrienoic acids on cerebral arterial smooth muscle. *Am. J. Physiol.* 263, H519–H525.

Girouard, H., Bonev, A. D., Hannah, R. M., Meredith, A., Aldrich, R. W., and Nelson, M. T. (2010). Astrocytic endfoot Ca2+ and BK channels determine both arteriolar dilation and constriction. *Proc. Natl. Acad. Sci. U.S.A.* 107, 3811–3816.

Girouard, H., Park, L., Anrather, J., Zhou, P., and Iadecola, C. (2007). Cerebrovascular nitrosative stress mediates neurovascular and endothelial dysfunction induced by angiotensin II. *Arterioscler. Thromb. Vasc. Biol.* 27, 303–309.

Girouard, H., Wang, G., Gallo, E. F., Anrather, J., Zhou, P., Pickel, V. M., and Iadecola, C. (2009). NMDA receptor activation increases free radical production through nitric oxide and NOX2. *J. Neurosci.* 29, 2545–2552.

Goldberg, J. H., and Yuste, R. (2005). Space matters: local and global dendritic Ca2+ compartmentalization in cortical interneurons. *Trends Neurosci.* 28, 158–167.

Gonchar, Y., and Burkhalter, A. (1997). Three distinct families of

GABAergic neurons in rat visual cortex. *Cereb. Cortex* 7, 347–358.

Gonzalez-Mora, J. L., Martin, F. A., Rojas-diaz, D., Hernandez, S., Ramos-Perez, I., Rodriguez, V. D., and Castellano, M. A. (2002). *In vivo* spectroscopy: a novel approach for simultaneously estimating nitric oxide and hemodynamic parameters in the rat brain. *J. Neurosci. Methods* 119, 151–161.

Gordon, G. R., Choi, H. B., Rungta, R. L., Ellis-davies, G. C., and Macvicar, B. A. (2008). Brain metabolism dictates the polarity of astrocyte control over arterioles. *Nature* 456, 745–749.

Gotoh, J., Kuang, T. Y., Nakao, Y., Cohen, D. M., Melzer, P., Itoh, Y., Pak, H., Pettigrew, K., and Sokoloff, L. (2001a). Regional differences in mechanisms of cerebral circulatory response to neuronal activation. *Am. J. Physiol. Heart Circ. Physiol.* 280, H821–H829.

Gotoh, T., Terada, K., and Mori, M. (2001b). hsp70-DnaJ chaperone pairs prevent nitric oxide-mediated apoptosis in RAW 264.7 macrophages. *Cell Death Differ.* 8, 357–366.

Griffith, O. W., and Kilbourn, R. G. (1996). Nitric oxide synthase inhibitors: amino acids. *Methods Enzymol.* 268, 375–392.

Hama-Tomioka, K., Kinoshita, H., Azma, T., Nakahata, K., Matsuda, N., Hatakeyama, N., Kikuchi, H., and Hatano, Y. (2009). The role of 20-hydroxyeicosatetraenoic acid in cerebral arteriolar constriction and the inhibitory effect of propofol. *Anesth. Analg.* 109, 1935–1942.

Hamilton, N. B., Attwell, D., and Hall, C. N. (2010). Pericyte-mediated regulation of capillary diameter: a component of neurovascular coupling in health and disease. *Front. Neuroenergetics* 2:5. doi: 10.3389/fnene.2010.00005

Harada, M., Fuse, A., and Tanaka, Y. (1997). Measurement of nitric oxide in the rat cerebral cortex during hypercapnoea. *Neuroreport* 8, 999–1002.

Hardy, P., Nuyt, A. M., Dumont, I., Peri, K. G., Hou, X., Varma, D. R., and Chemtob, S. (1999). Developmentally increased cerebrovascular NO in newborn pigs curtails cerebral blood flow autoregulation. *Pediatr. Res.* 46, 375–382.

Hayashi, S., Osawa, T., and Tohyama, K. (2002a). Comparative observations on corneas, With special reference to Bowman's layer and Descemet's membrane in mammals and amphibians. *J. Morphol.* 254, 247–258.

Hayashi, T., Katsumi, Y., Mukai, T., Inoue, M., Nagahama, Y., Oyanagi, C., Yamauchi, H., Shibasaki, H., and Fukuyama, H. (2002b). Neuronal nitric oxide has a role as a perfusion regulator and a synaptic modulator in cerebellum but not in neocortex during somatosensory stimulation–an animal PET study. *Neurosci. Res.* 44, 155–165.

Heinert, G., Nye, P. C., and Paterson, D. J. (1999). Nitric oxide and prostaglandin pathways interact in the regulation of hypercapnic cerebral vasodilatation. *Acta Physiol. Scand.* 166, 183–193.

Hoffmeyer, H. W., Enager, P., Thomsen, K. J., and Lauritzen, M. J. (2007). Nonlinear neurovascular coupling in rat sensory cortex by activation of transcallosal fibers. *J. Cereb. Blood Flow Metab.* 27, 575–587.

Huang, P. L., Dawson, T. M., Bredt, D. S., Snyder, S. H., and Fishman, M. C. (1993). Targeted disruption of the neuronal nitric oxide synthase gene. *Cell* 75, 1273–1286.

Huang, Z., Huang, P. L., Ma, J., Meng, W., Ayata, C., Fishman, M. C., and Moskowitz, M. A. (1996). Enlarged infarcts in endothelial nitric oxide synthase knockout mice are attenuated by nitro-L-arginine. *J. Cereb. Blood Flow Metab.* 16, 981–987.

Huang, Z., Huang, P. L., Panahian, N., Dalkara, T., Fishman, M. C., and Moskowitz, M. A. (1994). Effects of cerebral ischemia in mice deficient in neuronal nitric oxide synthase. *Science* 265, 1883–1885.

Hudetz, A. G., Shen, H., and Kampine, J. P. (1998). Nitric oxide from neuronal NOS plays critical role in cerebral capillary flow response to hypoxia. *Am. J. Physiol.* 274, H982–H989.

Iadecola, C. (1992). Does nitric oxide mediate the increases in cerebral blood flow elicited by hypercapnia? *Proc. Natl. Acad. Sci. U.S.A.* 89, 3913–3916.

Iadecola, C. (2004). Neurovascular regulation in the normal brain and in Alzheimer's disease. *Nat. Rev. Neurosci.* 5, 347–360.

Iadecola, C., Beitz, A. J., Renno, W., Xu, X., Mayer, B., and Zhang, F. (1993). Nitric oxide synthase-containing neural processes on large cerebral arteries and cerebral microvessels. *Brain Res.* 606, 148–155.

Iadecola, C., Pelligrino, D. A., Moskowitz, M. A., and Lassen, N. A. (1994). Nitric oxide synthase inhibition and cerebrovascular regulation. *J. Cereb. Blood Flow Metab.* 14, 175–192.

Iadecola, C., and Xu, X. (1994). Nitro-L-arginine attenuates hypercapnic cerebrovasodilation without affecting cerebral metabolism. *Am. J. Physiol.* 266, R518–R525.

Iadecola, C., and Zhang, F. (1994). Nitric oxide-dependent and -independent components of cerebrovasodilation elicited by hypercapnia. *Am. J. Physiol.* 266, R546–R552.

Iadecola, C., and Zhang, F. (1996). Permissive and obligatory roles of NO in cerebrovascular responses to hypercapnia and acetylcholine. *Am. J. Physiol.* 271, R990–R1001.

Iadecola, C., Zhang, F., and Xu, X. (1995). Inhibition of inducible nitric oxide synthase ameliorates cerebral ischemic damage. *Am. J. Physiol.* 268, R286–R292.

Iliff, J. J., Close, L. N., Selden, N. R., and Alkayed, N. J. (2007). A novel role for P450 eicosanoids in the neurogenic control of cerebral blood flow in the rat. *Exp. Physiol.* 92, 653–658.

Iliff, J. J., D'Ambrosio, R., Ngai, A. C., and Winn, H. R. (2003). Adenosine receptors mediate glutamate-evoked arteriolar dilation in the rat cerebral cortex. *Am. J. Physiol. Heart Circ. Physiol.* 284, H1631–H1637.

Irikura, K., Maynard, K. I., and Moskowitz, M. A. (1994). Importance of nitric oxide synthase inhibition to the attenuated vascular responses induced by topical L-nitroarginine during vibrissal stimulation. *J. Cereb. Blood Flow Metab.* 14, 45–48.

Jaggar, J. H., Leffler, C. W., Cheranov, S. Y., Tcheranova, D. E. S., and Cheng, X. (2002). Carbon monoxide dilates cerebral arterioles by enhancing the coupling of Ca2+ sparks to Ca2+-activated K+ channels. *Circ. Res.* 91, 610–617.

Jayakumar, A. R., Sujatha, R., Paul, V., Asokan, C., Govindasamy, S., and Jayakumar, R. (1999). Role of nitric oxide on GABA, Glutamic acid, Activities of GABA-T and GAD in rat brain cerebral cortex. *Brain Res.* 837, 229–235.

Jimenez, A. I., Castro, E., Mirabet, M., Franco, R., Delicado, E. G., and Miras-Portugal, M. T. (1999). Potentiation of ATP calcium responses by A2B receptor stimulation and other signals coupled to Gs proteins in type-1 cerebellar astrocytes. *Glia* 26, 119–128.

Judas, M., Sestan, N., and Kostovic, I. (1999). Nitrinergic neurons in the developing and adult human telencephalon: transient and permanent patterns of expression in comparison to other mammals. *Microsc. Res. Tech.* 45, 401–419.

Karagiannis, A., Gallopin, T., David, C., Battaglia, D., Geoffroy, H., Rossier, J., Hillman, E. M., Staiger, J. F., and Cauli, B. (2009). Classification of NPY-expressing neocortical interneurons. *J. Neurosci.* 29, 3642–3659.

Katona, G., Kaszas, A., Turi, G. F., Hajos, N., Tamas, G., Vizi, E. S., and Rozsa, B. (2011). Roller Coaster Scanning reveals spontaneous triggering of dendritic spikes in CA1 interneurons. *Proc. Natl. Acad. Sci. U.S.A.* 108, 2148–2153.

Kelly, P. A., Ritchie, I. M., and Arbuthnott, G. W. (1995). Inhibition of neuronal nitric oxide synthase by 7-nitroindazole: effects upon local cerebral blood flow and glucose use in the rat. *J. Cereb. Blood Flow Metab.* 15, 766–773.

Kitaura, H., Uozumi, N., Tohmi, M., Yamazaki, M., Sakimura, K., Kudoh, M., Shimizu, T., and Shibuki, K. (2007). Roles of nitric oxide as a vasodilator in neurovascular coupling of mouse somatosensory cortex. *Neurosci. Res.* 59, 160–171.

Kiyasova, V., Fernandez, S. P., Laine, J., Stankovski, L., Muzerelle, A., Doly, S., and Gaspar, P. (2011). A genetically defined morphologically and functionally unique subset of 5-HT neurons in the mouse raphe nuclei. *J. Neurosci.* 31, 2756–2768.

Ko, K. R., Ngai, A. C., and Winn, H. R. (1990). Role of adenosine in regulation of regional cerebral blood flow in sensory cortex. *Am. J. Physiol.* 259, H1703–H1708.

Kubota, Y., Hattori, R., and Yui, Y. (1994). Three distinct subpopulations of GABAergic neurons in rat frontal agranular cortex. *Brain Res.* 649, 159–173.

Kume, H., Takai, A., Tokuno, H., and Tomita, T. (1989). Regulation of Ca2+-dependent K+-channel activity in tracheal myocytes by phosphorylation. *Nature* 341, 152–154.

Kummer, W., Fischer, A., Mundel, P., Mayer, B., Hoba, B., Philippin, B., and Preissler, U. (1992). Nitric oxide synthase in VIP-containing vasodilator nerve fibres in the guinea-pig. *Neuroreport* 3, 653–655.

Lacombe, P., and Seylaz, J. (1984). Significance of the cerebrovascular effects of immobilization stress in the rabbit. *J. Cereb. Blood Flow Metab.* 4, 397–406.

Lange, A., Gebremedhin, D., Narayanan, J., and Harder, D.

(1997). 20-Hydroxyeicosatetraenoic acid-induced vasoconstriction and inhibition of potassium current in cerebral vascular smooth muscle is dependent on activation of protein kinase C. *J. Biol. Chem.* 272, 27345–27352.

Lauritzen, M. (2005). Reading vascular changes in brain imaging: is dendritic calcium the key? *Nat. Rev. Neurosci.* 6, 77–85.

Leffler, C. W., Parfenova, H., Fedinec, A. L., Basuroy, S., and Tcheranova, D. (2006). Contributions of astrocytes and CO to pial arteriolar dilation to glutamate in newborn pigs. *Am. J. Physiol. Heart Circ. Physiol.* 291, H2897–H2904.

Li, H., Cui, H., Kundu, T. K., Alzawahra, W., and Zweier, J. L. (2008). Nitric oxide production from nitrite occurs primarily in tissues not in the blood: critical role of xanthine oxidase and aldehyde oxidase. *J. Biol. Chem.* 283, 17855–17863.

Li, H., Kundu, T. K., and Zweier, J. L. (2009). Characterization of the magnitude and mechanism of aldehyde oxidase-mediated nitric oxide production from nitrite. *J. Biol. Chem.* 284, 33850–33858.

Lindauer, U., Megow, D., Matsuda, H., and Dirnagl, U. (1999). Nitric oxide: a modulator, But not a mediator, Of neurovascular coupling in rat somatosensory cortex. *Am. J. Physiol.* 277, H799–H811.

Lindauer, U., Megow, D., Schultze, J., Weber, J. R., and Dirnagl, U. (1996). Nitric oxide synthase inhibition does not affect somatosensory evoked potentials in the rat. *Neurosci. Lett.* 216, 207–210.

Liu, X., Li, C., Falck, J. R., Roman, R. J., Harder, D. R., and Koehler, R. C. (2008). Interaction of nitric oxide, 20-HETE, And EETs during functional hyperemia in whisker barrel cortex. *Am. J. Physiol. Heart Circ. Physiol.* 295, H619–H631.

Liu, X., Li, C., Gebremedhin, D., Hwang, S. H., Hammock, B. D., Falck, J. R., Roman, R. J., Harder, D. R., and Koehler, R. C. (2011). Epoxyeicosatrienoic acid-dependent cerebral vasodilation evoked by metabotropic glutamate receptor activation *in vivo*. *Am. J. Physiol. Heart Circ. Physiol.* 301, H373–H381.

Logothetis, N. K., Pauls, J., Augath, M., Trinath, T., and Oeltermann, A. (2001). Neurophysiological investigation of the basis of the fMRI signal. *Nature* 412, 150–157.

Lonart, G., Wang, J., and Johnson, K. M. (1992). Nitric oxide induces neurotransmitter release from hippocampal slices. *Eur. J. Pharmacol.* 220, 271–272.

Ma, J., Ayata, C., Huang, P. L., Fishman, M. C., and Moskowitz, M. A. (1996). Regional cerebral blood flow response to vibrissal stimulation in mice lacking type I NOS gene expression. *Am. J. Physiol.* 270, H1085–H1090.

Madisen, L., Mao, T., Koch, H., Zhuo, J. M., Berenyi, A., Fujisawa, S., Hsu, Y. W., Garcia, A. J. 3rd., Gu, X., Zanella, S., Kidney, J., Gu, H., Mao, Y., Hooks, B. M., Boyden, E. S., Buzsaki, G., Ramirez, J. M., Jones, A. R., Svoboda, K., Han, X., Turner, E. E., and Zeng, H. (2012). A toolbox of Cre-dependent optogenetic transgenic mice for light-induced activation and silencing. *Nat. Neurosci.* 15, 793–802.

Maienschein, V., Marxen, M., Volknandt, W., and Zimmermann, H. (1999). A plethora of presynaptic proteins associated with ATP-storing organelles in cultured astrocytes. *Glia* 26, 233–244.

Makhro, A., Wang, J., Vogel, J., Boldyrev, A. A., Gassmann, M., Kaestner, L., and Bogdanova, A. (2010). Functional NMDA receptors in rat erythrocytes. *Am. J. Physiol. Cell Physiol.* 298, C1315–C1325.

Malcolm, C., Grieve, A., Ritchie, L., Schousboe, A., and Griffiths, R. (1996). NMDA receptor-mediated cGMP synthesis in primary cultures of mouse cerebellar granule cells appears to involve neuron-astrocyte communication with NO operating as the intercellular messenger. *J. Neurosci. Res.* 45, 129–142.

Malinski, T., Bailey, F., Zhang, Z. G., and Chopp, M. (1993). Nitric oxide measured by a porphyrinic microsensor in rat brain after transient middle cerebral artery occlusion. *J. Cereb. Blood Flow Metab.* 13, 355–358.

Manzoni, O., and Bockaert, J. (1993). Nitric oxide synthase activity endogenously modulates NMDA receptors. *J. Neurochem.* 61, 368–370.

Marks, J. D., Boriboun, C., and Wang, J. (2005). Mitochondrial nitric oxide mediates decreased vulnerability of hippocampal neurons from immature animals to NMDA. *J. Neurosci.* 25, 6561–6575.

Markwardt, S. J., Dieni, C. V., Wadiche, J. I., and Overstreet-Wadiche, L. (2011). Ivy/neurogliaform interneurons coordinate activity in the neurogenic niche. *Nat. Neurosci.* 14, 1407–1409.

Matsumoto, T., Nakane, M., Pollock, J. S., Kuk, J. E., and Forstermann, U. (1993). A correlation between soluble brain nitric oxide synthase and NADPH-diaphorase activity is only seen after exposure of the tissue to fixative. *Neurosci. Lett.* 155, 61–64.

McGiff, J. C., and Quilley, J. (1999). 20-HETE and the kidney: resolution of old problems and new beginnings. *Am. J. Physiol.* 277, R607–R623.

Meffert, M. K., Premack, B. A., and Schulman, H. (1994). Nitric oxide stimulates Ca(2+)-independent synaptic vesicle release. *Neuron* 12, 1235–1244.

Membre, N., Berna, A., Neutelings, G., David, A., David, H., Staiger, D., Saez vasquez, J., Raynal, M., Delseny, M., and Bernier, F. (1997). cDNA sequence, genomic organization and differential expression of three Arabidopsis genes for germin/oxalate oxidase-like proteins. *Plant Mol. Biol.* 35, 459–469.

Meng, W., Tobin, J. R., and Busija, D. W. (1995). Glutamate-induced cerebral vasodilation is mediated by nitric oxide through N-methyl-D-aspartate receptors. *Stroke* 26, 857–862. discussion: 863.

Mesulam, M. M., Hersh, L. B., Mash, D. C., and Geula, C. (1992). Differential cholinergic innervation within functional subdivisions of the human cerebral cortex: a choline acetyltransferase study. *J. Comp. Neurol.* 318, 316–328.

Metea, M. R., and Newman, E. A. (2006). Glial cells dilate and constrict blood vessels: a mechanism of neurovascular coupling. *J. Neurosci.* 26, 2862–2870.

Meyer, C., De Vries, G., Davidge, S. T., and Mayes, D. C. (2002). Reassessing the mathematical modeling of the contribution of vasomotion to vascular resistance. *J. Appl. Physiol.* 92, 888–889.

Mikula, I., Durocher, S., Martasek, P., Mutus, B., and Slama-Schwok, A. (2009). Isoform-specific differences in the nitrite reductase activity of nitric oxide synthases under hypoxia. *Biochem. J.* 418, 673–682.

Mize, R. R., Banfro, F. T., and Scheiner, C. A. (1996). Pre- and postnatal expression of amino acid neurotransmitters, calcium binding proteins, and nitric oxide synthase in the developing superior colliculus. *Prog. Brain Res.* 108, 313–332.

Mizukawa, K., McGeer, P. L., Vincent, S. R., and McGeer, E. G. (1988). Ultrastructure of reduced nicotinamide adenine dinucleotide phosphate (NADPH) diaphorase-positive neurons in the cat cerebral cortex, Amygdala and caudate nucleus. *Brain Res.* 452, 286–292.

Montecot, C., Borredon, J., Seylaz, J., and Pinard, E. (1997). Nitric oxide of neuronal origin is involved in cerebral blood flow increase during seizures induced by kainate. *J. Cereb. Blood Flow Metab.* 17, 94–99.

Morley, P., Small, D. L., Murray, C. L., Mealing, G. A., Poulter, M. O., Durkin, J. P., and Stanimirovic, D. B. (1998). Evidence that functional glutamate receptors are not expressed on rat or human cerebromicrovascular endothelial cells. *J. Cereb. Blood Flow Metab.* 18, 396–406.

Ngai, A. C., Ko, K. R., Morii, S., and Winn, H. R. (1988). Effect of sciatic nerve stimulation on pial arterioles in rats. *Am. J. Physiol.* 254, H133–H139.

Ngai, A. C., Meno, J. R., and Winn, H. R. (1995). L-NNA suppresses cerebrovascular response and evoked potentials during somatosensory stimulation in rats. *Am. J. Physiol.* 269, H1803–H1810.

Nithipatikom, K., Grall, A. J., Holmes, B. B., Harder, D. R., Falck, J. R., and Campbell, W. B. (2001). Liquid chromatographic-electrospray ionization-mass spectrometric analysis of cytochrome P450 metabolites of arachidonic acid. *Anal. Biochem.* 298, 327–336.

Niwa, K., Lindauer, U., Villringer, A., and Dirnagl, U. (1993). Blockade of nitric oxide synthesis in rats strongly attenuates the CBF response to extracellular acidosis. *J. Cereb. Blood Flow Metab.* 13, 535–539.

Northington, F. J., Matherne, G. P., and Berne, R. M. (1992). Competitive inhibition of nitric oxide synthase prevents the cortical hyperemia associated with peripheral nerve stimulation. *Proc. Natl. Acad. Sci. U.S.A.* 89, 6649–6652.

O'Donnell, P., and Grace, A. A. (1997). Cortical afferents modulate striatal gap junction permeability via nitric oxide. *Neuroscience* 76, 1–5.

Oermann, E., Bidmon, H. J., Mayer, B., and Zilles, K. (1999). Differential maturational patterns of nitric oxide synthase-I and NADPH diaphorase in functionally distinct cortical areas of the mouse cerebral cortex. *Anat. Embryol.* 200, 27–41.

Ohata, H., Cao, S., and Koehler, R. C. (2006). Contribution of adenosine A2A and A2B receptors and heme oxygenase to AMPA-induced dilation of pial arterioles in rats. *Am. J. Physiol. Regul. Integr. Comp. Physiol.* 291, R728–R735.

Okamoto, H., Hudetz, A. G., Roman, R. J., Bosnjak, Z. J., and Kampine, J. P. (1997). Neuronal NOS-derived NO plays permissive role in cerebral blood flow response to hypercapnia. *Am. J. Physiol.* 272, H559–H566.

Park, L., Gallo, E. F., Anrather, J., Wang, G., Norris, E. H., Paul, J., Strickland, S., and Iadecola, C. (2008). Key role of tissue plasminogen activator in neurovascular coupling. *Proc. Natl. Acad. Sci. U.S.A.* 105, 1073–1078.

Pasti, L., Zonta, M., Pozzan, T., Vicini, S., and Carmignoto, G. (2001). Cytosolic calcium oscillations in astrocytes may regulate exocytotic release of glutamate. *J. Neurosci.* 21, 477–484.

Peebles, K. C., Richards, A. M., Celi, L., McGrattan, K., Murrell, C. J., and Ainslie, P. N. (2008). Human cerebral arteriovenous vasoactive exchange during alterations in arterial blood gases. *J. Appl. Physiol.* 105, 1060–1068.

Pelligrino, D. A., Gay, R. L. 3rd., Baughman, V. L., and Wang, Q. (1996). NO synthase inhibition modulates NMDA-induced changes in cerebral blood flow and EEG activity. *Am. J. Physiol.* 271, H990–H995.

Pelligrino, D. A., Koenig, H. M., and Albrecht, R. F. (1993). Nitric oxide synthesis and regional cerebral blood flow responses to hypercapnia and hypoxia in the rat. *J. Cereb. Blood Flow Metab.* 13, 80–87.

Pelligrino, D. A., Wang, Q., Koenig, H. M., and Albrecht, R. F. (1995). Role of nitric oxide, Adenosine, N-methyl-D-aspartate receptors, And neuronal activation in hypoxia-induced pial arteriolar dilation in rats. *Brain Res.* 704, 61–70.

Peng, X., Zhang, C., Alkayed, N. J., Harder, D. R., and Koehler, R. C. (2004). Dependency of cortical functional hyperemia to forepaw stimulation on epoxygenase and nitric oxide synthase activities in rats. *J. Cereb. Blood Flow Metab.* 24, 509–517.

Perea, G., and Araque, A. (2005). Properties of synaptically evoked astrocyte calcium signal reveal synaptic information processing by astrocytes. *J. Neurosci.* 25, 2192–2203.

Perrenoud, Q., Rossier, J., Férézou, I., Geoffroy, H., Gallopin, T., Vitalis, T., and Rancillac, A. (2012a). Activation of cortical 5-HT3 receptor-expressing interneurons induces NO mediated vasodilatations and NPY mediated vasoconstrictions. *Front. Neural Circ.* 6:50. doi: 10.3389/fncir.2012.00050

Perrenoud, Q., Rossier, J., Geoffroy, H., Vitalis, T., and Gallopin, T. (2012b). Diversity of GABAergic interneurons in Layer VIa and VIb of Mouse Barrel Cortex. *Cereb. Cortex*. doi: 10.1093/cercor/bhs032. [Epub ahead of print].

Petersen, C. C., Grinvald, A., and Sakmann, B. (2003). Spatiotemporal dynamics of sensory responses in layer 2/3 of rat barrel cortex measured *in vivo* by voltage-sensitive dye imaging combined with whole-cell voltage recordings and neuron reconstructions. *J. Neurosci.* 23, 1298–1309.

Pilitsis, J. G., and Kimelberg, H. K. (1998). Adenosine receptor mediated stimulation of intracellular calcium in acutely isolated astrocytes. *Brain Res.* 798, 294–303.

Porter, J. T., and McCarthy, K. D. (1996). Hippocampal astrocytes in situ respond to glutamate released from synaptic terminals. *J. Neurosci.* 16, 5073–5081.

Price, M. G., Yoo, J. W., Burgess, D. L., Deng, F., Hrachovy, R. A., Frost, J. D. Jr., and Noebels, J. L. (2009). A triplet repeat expansion genetic mouse model of infantile spasms syndrome, Arx(GCG)10+7, With interneuronopathy, Spasms in infancy, Persistent seizures, and adult cognitive and behavioral impairment. *J. Neurosci.* 29, 8752–8763.

Price, R. H. Jr., Mayer, B., and Beitz, A. J. (1993). Nitric oxide synthase neurons in rat brain express more NMDA receptor mRNA than non-NOS neurons. *Neuroreport* 4, 807–810.

Publicover, N. G., Hammond, E. M., and Sanders, K. M. (1993). Amplification of nitric oxide signaling by interstitial cells isolated from canine colon. *Proc. Natl. Acad. Sci. U.S.A.* 90, 2087–2091.

Putzke, J., Seidel, B., Huang, P. L., and Wolf, G. (2000). Differential expression of alternatively spliced isoforms of neuronal nitric oxide synthase (nNOS) and N-methyl-D-aspartate receptors (NMDAR) in knockout mice deficient in nNOS alpha (nNOS alpha(Delta/Delta) mice). *Brain Res. Mol. Brain Res.* 85, 13–23.

Raszkiewicz, J. L., Linville, D. G., Kerwin, J. F. Jr., Wagenaar, F., and Arneric, S. P. (1992). Nitric oxide synthase is critical in mediating basal forebrain regulation of cortical cerebral circulation. *J. Neurosci. Res.* 33, 129–135.

Regidor, J., Edvinsson, L., and Divac, I. (1993). NOS neurones lie near branchings of cortical arteriolae. *Neuroreport* 4, 112–114.

Rifkind, J. M., Nagababu, E., Barbiro-Michaely, E., Ramasamy, S., Pluta, R. M., and Mayevsky, A. (2007). Nitrite infusion increases cerebral blood flow and decreases mean arterial blood pressure in rats: a role for red cell NO. *Nitric Oxide* 16, 448–456.

Robertson, B. E., Schubert, R., Hescheler, J., and Nelson, M. T. (1993). cGMP-dependent protein kinase activates Ca-activated K channels in cerebral artery smooth muscle cells. *Am. J. Physiol.* 265, C299–C303.

Robinson, J. S., Fedinec, A. L., and Leffler, C. W. (2002). Role of carbon monoxide in glutamate receptor-induced dilation of newborn pig pial arterioles. *Am. J. Physiol. Heart Circ. Physiol.* 282, H2371–H2376.

Rockland, K. S., and Nayyar, N. (2012). Association of type I neurons positive for NADPH-diaphorase with blood vessels in the adult monkey corpus callosum. *Front. Neural Circuits* 6:4. doi: 10.3389/fncir.2012.00004

Roman, R. J. (2002). P-450 metabolites of arachidonic acid in the control of cardiovascular function. *Physiol. Rev.* 82, 131–185.

Salvemini, D. (1997). Regulation of cyclooxygenase enzymes by nitric oxide. *Cell. Mol. Life Sci.* 53, 576–582.

Samouilov, A., Woldman, Y. Y., Zweier, J. L., and Khramtsov, V. V. (2007). Magnetic resonance study of the transmembrane nitrite diffusion. *Nitric Oxide* 16, 362–370.

Sandell, J. H. (1986). NADPH diaphorase histochemistry in the macaque striate cortex. *J. Comp. Neurol.* 251, 388–397.

Sandor, P., Komjati, K., Reivich, M., and Nyary, I. (1994). Major role of nitric oxide in the mediation of regional CO2 responsiveness of the cerebral and spinal cord vessels of the cat. *J. Cereb. Blood Flow Metab.* 14, 49–58.

Santos, R. M., Lourenco, C. F., Ledo, A., Barbosa, R. M., and Laranjinha, J. (2012). Nitric oxide inactivation mechanisms in the brain: role in bioenergetics and neurodegeneration. *Int. J. Cell Biol.* 2012, 391914.

Saur, D., Paehge, H., Schusdziarra, V., and Allescher, H. D. (2000). Distinct expression of splice variants of neuronal nitric oxide synthase in the human gastrointestinal tract. *Gastroenterology* 118, 849–858.

Scemes, E. (2000). Components of astrocytic intercellular calcium signaling. *Mol. Neurobiol.* 22, 167–179.

Schipke, C. G., Heidemann, A., Skupin, A., Peters, O., Falcke, M., and Kettenmann, H. (2008). Temperature and nitric oxide control spontaneous calcium transients in astrocytes. *Cell Calcium* 43, 285–295.

Schuman, E. M., and Madison, D. V. (1994). Nitric oxide and synaptic function. *Annu. Rev. Neurosci.* 17, 153–183.

Shapiro, H. M., Stromberg, D. D., Lee, D. R., and Wiederhielm, C. A. (1971). Dynamic pressures in the pial arterial microcirculation. *Am. J. Physiol.* 221, 279–283.

Shibuki, K., and Okada, D. (1991). Endogenous nitric oxide release required for long-term synaptic depression in the cerebellum. *Nature* 349, 326–328.

Shlosberg, D., Buskila, Y., Abu-ghanem, Y., and Amitai, Y. (2012). Spatiotemporal alterations of cortical network activity by selective loss of NOS-expressing interneurons. *Front. Neural Circuits* 6:3. doi: 10.3389/fncir.2012.00003

Simandle, S. A., Kerr, B. A., Lacza, Z., Eckman, D. M., Busija, D. W., and Bari, F. (2005). Piglet pial arteries respond to N-methyl-D-aspartate *in vivo* but not *in vitro*. *Microvasc. Res.* 70, 76–83.

Sokoloff, L., Kennedy, C., Adachi, K., Wang, F., Takahashi, S., and Melzer, P. (1992). "Effects of inhibition of nitric oxide synthase on resting local cerebral blood flow and on changes in- duced by hypercapnia or local functional activity," in *Pharmacology of Cerebral Ischemia,* ed J. Krieglstein, (Stuttgart: Wissenschaftliche Verlagsgesellschaft), 371–381.

Sokoya, E. M., Burns, A. R., Setiawan, C. T., Coleman, H. A., Parkington, H. C., and Tare, M. (2006). Evidence for the involvement of myoendothelial gap junctions in EDHF-mediated relaxation in the rat middle cerebral artery. *Am. J. Physiol. Heart Circ. Physiol.* 291, H385–H393.

Stefanovic, B., Schwindt, W., Hoehn, M., and Silva, A. C. (2007). Functional uncoupling of hemodynamic from neuronal response by inhibition of neuronal nitric oxide synthase. *J. Cereb. Blood Flow Metab.* 27, 741–754.

Stoyanovsky, D., Murphy, T., Anno, P. R., Kim, Y. M., and Salama, G. (1997). Nitric oxide activates skeletal and cardiac ryanodine receptors. *Cell Calcium* 21, 19–29.

Straub, S. V., Bonev, A. D., Wilkerson, M. K., and Nelson, M. T. (2006). Dynamic inositol trisphosphate-mediated calcium signals within astrocytic endfeet underlie vasodilation of cerebral arterioles. *J. Gen. Physiol.* 128, 659–669.

Straub, S. V., and Nelson, M. T. (2007). Astrocytic calcium signaling: the information currency coupling neuronal activity to the cerebral microcirculation. *Trends Cardiovasc. Med.* 17, 183–190.

Sun, C. W., Falck, J. R., Okamoto, H., Harder, D. R., and Roman, R. J. (2000). Role of cGMP versus 20-HETE in the vasodilator response to nitric oxide in rat cerebral arteries. *Am. J. Physiol. Heart Circ. Physiol.* 279, H339–H350.

Suzuki, N., Fukuuchi, Y., Koto, A., Naganuma, Y., Isozumi, K., Konno, S., Gotoh, J., and Shimizu, T. (1994). Distribution and origins of cerebrovascular NADPH-diaphorase-containing nerve fibers in the rat. *J. Auton. Nerv. Syst.* 49(Suppl.), S51–S54.

Takata, F., Dohgu, S., Nishioku, T., Takahashi, H., Harada, E., Makino, I., Nakashima, M., Yamauchi, A., and Kataoka, Y. (2009). Adrenomedullin-induced relaxation of rat brain pericytes is related to the reduced phosphorylation of myosin light chain through the cAMP/PKA signaling pathway. *Neurosci. Lett.* 449, 71–75.

Tanaka, Y., Koike, K., Alioua, A., Shigenobu, K., Stefani, E., and Toro, L. (2004). Beta1-subunit of MaxiK channel in smooth muscle: a key molecule which tunes muscle mechanical activity. *J. Pharmacol. Sci.* 94, 339–347.

Tang, X. D., Xu, R., Reynolds, M. F., Garcia, M. L., Heinemann, S. H., and Hoshi, T. (2003). Haem can bind to and inhibit mammalian calcium-dependent Slo1 BK channels. *Nature* 425, 531–535.

Toda, N., Ayajiki, K., and Okamura, T. (1996). Hypercapnia relaxes cerebral arteries and potentiates neurally-induced relaxation. *J. Cereb. Blood Flow Metab.* 16, 1068–1074.

Toda, N., and Okamura, T. (2003). The pharmacology of nitric oxide in the peripheral nervous system of blood vessels. *Pharmacol. Rev.* 55, 271–324.

Toda, N., and Okamura, T. (2011). Modulation of renal blood flow and vascular tone by neuronal nitric oxide synthase-derived nitric oxide. *J. Vasc. Res.* 48, 1–10.

Tong, X. K., and Hamel, E. (1999). Regional cholinergic denervation of cortical microvessels and nitric oxide synthase-containing neurons in Alzheimer's disease. *Neuroscience* 92, 163–175.

Toyoda, K., Fujii, K., Ibayashi, S., Nagao, T., Kitazono, T., and Fujishima, M. (1997). Role of nitric oxide in regulation of brain stem circulation during hypotension. *J. Cereb. Blood Flow Metab.* 17, 1089–1096.

Ulker, P., Sati, L., Celik-ozenci, C., Meiselman, H. J., and Baskurt, O. K. (2009). Mechanical stimulation of nitric oxide synthesizing mechanisms in erythrocytes. *Biorheology* 46, 121–132.

Valtschanoff, J. G., Weinberg, R. J., Kharazia, V. N., Schmidt, H. H., Nakane, M., and Rustioni, A. (1993). Neurons in rat cerebral cortex that synthesize nitric oxide: NADPH diaphorase histochemistry, NOS immunocytochemistry, And colocalization with GABA. *Neurosci. Lett.* 157, 157–161.

Vaucher, E., and Hamel, E. (1995). Cholinergic basal forebrain neurons project to cortical microvessels in the rat: electron microscopic study with anterogradely transported *Phaseolus vulgaris* leucoagglutinin and choline acetyltransferase immunocytochemistry. *J. Neurosci.* 15, 7427–7441.

Vaucher, E., Linville, D., and Hamel, E. (1997). Cholinergic basal forebrain projections to nitric oxide synthase-containing neurons in the rat cerebral cortex. *Neuroscience* 79, 827–836.

Vaucher, E., Tong, X. K., Cholet, N., Lantin, S., and Hamel, E. (2000). GABA neurons provide a rich input to microvessels but not nitric oxide neurons in the rat cerebral cortex: a means for direct regulation of local cerebral blood flow. *J. Comp. Neurol.* 421, 161–171.

Vucurovic, K., Gallopin, T., Ferezou, I., Rancillac, A., Chameau, P., Van Hooft, J. A., Geoffroy, H., Monyer, H., Rossier, J., and Vitalis, T. (2010). Serotonin 3A receptor subtype as an early and protracted marker of cortical interneuron subpopulations. *Cereb. Cortex* 20, 2333–2347.

Wang, H., Hitron, I. M., Iadecola, C., and Pickel, V. M. (2005). Synaptic and vascular associations of neurons containing cyclooxygenase-2 and nitric oxide synthase in rat somatosensory cortex. *Cereb. Cortex* 15, 1250–1260.

Wang, Q., Kjaer, T., Jorgensen, M. B., Paulson, O. B., Lassen, N. A., Diemer, N. H., and Lou, H. C. (1993). Nitric oxide does not act as a mediator coupling cerebral blood flow to neural activity following somatosensory stimuli in rats. *Neurol. Res.* 15, 33–36.

Wang, Q., Paulson, O. B., and Lassen, N. A. (1992). Effect of nitric oxide blockade by NG-nitro-L-arginine on cerebral blood flow response to changes in carbon dioxide tension. *J. Cereb. Blood Flow Metab.* 12, 947–953.

Wang, Q., Pelligrino, D. A., Baughman, V. L., Koenig, H. M., and Albrecht, R. F. (1995). The role of neuronal nitric oxide synthase in regulation of cerebral blood flow in normocapnia and hypercapnia in rats. *J. Cereb. Blood Flow Metab.* 15, 774–778.

Wang, X., Lou, N., Xu, Q., Tian, G. F., Peng, W. G., Han, X., Kang, J., Takano, T., and Nedergaard, M. (2006). Astrocytic Ca2+ signaling evoked by sensory stimulation *in vivo*. *Nat. Neurosci.* 9, 816–823.

Wiencken, A. E., and Casagrande, V. A. (2000). The distribution of NADPH diaphorase and nitric oxide synthetase (NOS) in relation to the functional compartments of areas V1 and V2 of primate visual cortex. *Cereb. Cortex* 10, 499–511.

Willis, A. P., and Leffler, C. W. (2001). Endothelial NO and prostanoid involvement in newborn and juvenile pig pial arteriolar vasomotor responses. *Am. J. Physiol. Heart Circ. Physiol.* 281, H2366–H2377.

Willmott, N. J., Galione, A., and Smith, P. A. (1995a). A cADP-ribose antagonist does not inhibit secretagogue-, Caffeine- and nitric oxide-induced Ca2+ responses in rat pancreatic beta-cells. *Cell Calcium* 18, 411–419.

Willmott, N. J., Galione, A., and Smith, P. A. (1995b). Nitric oxide induces intracellular Ca2+ mobilization and increases secretion of incorporated 5-hydroxytryptamine in rat pancreatic beta-cells. *FEBS Lett.* 371, 99–104.

Willmott, N. J., Wong, K., and Strong, A. J. (2000a). A fundamental role for the nitric oxide-G-kinase signaling pathway in mediating intercellular Ca(2+) waves in glia. *J. Neurosci.* 20, 1767–1779.

Willmott, N. J., Wong, K., and Strong, A. J. (2000b). Intercellular Ca(2+) waves in rat hippocampal slice and dissociated glial-neuron cultures mediated by nitric oxide. *FEBS Lett.* 487, 239–247.

Wolf, G., Wurdig, S., and Schunzel, G. (1992). Nitric oxide synthase in rat brain is predominantly located at neuronal endoplasmic reticulum: an electron microscopic demonstration of NADPH-diaphorase activity. *Neurosci. Lett.* 147, 63–66.

Wood, J., and Garthwaite, J. (1994). Models of the diffusional spread of nitric oxide: implications for neural nitric oxide signalling and its pharmacological properties. *Neuropharmacology* 33, 1235–1244.

Xiao, Y. M., Diao, Y. C., and So, K. F. (1996). A morphological study of neurons expressing NADPH diaphorase activity in the visual cortex of the golden hamster. *Brain Behav. Evol.* 48, 221–230.

Yamaura, K., Gebremedhin, D., Zhang, C., Narayanan, J., Hoefert, K., Jacobs, E. R., Koehler, R. C., and Harder, D. R. (2006). Contribution of epoxyeicosatrienoic acids to the hypoxia-induced activation of Ca2+ -activated K+ channel current in cultured rat hippocampal astrocytes. *Neuroscience* 143, 703–716.

Yan, X. X., Garey, L. J., and Jen, L. S. (1994). Development of NADPH-diaphorase activity in the rat neocortex. *Brain Res. Dev. Brain Res.* 79, 29–38.

Yan, X. X., Garey, L. J., and Jen, L. S. (1996). Prenatal development of NADPH-diaphorase-reactive neurons in human frontal cortex. *Cereb. Cortex* 6, 737–745.

Yang, Y., Engelien, W., Pan, H., Xu, S., Silbersweig, D. A., and Stern, E. (2000). A CBF-based event-related brain activation paradigm: characterization of impulse-response function and comparison to BOLD. *Neuroimage* 12, 287–297.

Zhang, F., Xu, S., and Iadecola, C. (1995). Role of nitric oxide and acetylcholine in neocortical hyperemia elicited by basal forebrain stimulation: evidence for an involvement of endothelial nitric oxide. *Neuroscience* 69, 1195–1204.

Zonta, M., Angulo, M. C., Gobbo, S., Rosengarten, B., Hossmann, K. A.,

Pozzan, T., and Carmignoto, G. (2003a). Neuron-to-astrocyte signaling is central to the dynamic control of brain microcirculation. *Nat. Neurosci.* 6, 43–50.

Zonta, M., Sebelin, A., Gobbo, S., Fellin, T., Pozzan, T., and Carmignoto, G. (2003b). Glutamate-mediated cytosolic calcium oscillations regulate a pulsatile prostaglandin release from cultured rat astrocytes. *J. Physiol.* 553, 407–414.

Zou, A. P., Fleming, J. T., Falck, J. R., Jacobs, E. R., Gebremedhin, D., Harder, D. R., and Roman, R. J. (1996). 20-HETE is an endogenous inhibitor of the large-conductance Ca(2+)-activated K+ channel in renal arterioles. *Am. J. Physiol.* 270, R228–R237.

Conflict of Interest Statement: The authors declare that the research was conducted in the absence of any commercial or financial relationships that could be construed as a potential conflict of interest.

Received: 01 May 2012; accepted: 19 July 2012; published online: 09 August 2012.
Citation: Duchemin S, Boily M, Sadekova N and Girouard H (2012) The complex contribution of NOS interneurons in the physiology of cerebrovascular regulation. Front. Neural Circuits ***6****:51. doi: 10.3389/fncir.2012.00051*

frontiers in
NEURAL CIRCUITS

ORIGINAL RESEARCH ARTICLE
published: 20 February 2012
doi: 10.3389/fncir.2012.00004

Association of type I neurons positive for NADPH-diaphorase with blood vessels in the adult monkey corpus callosum

Kathleen S. Rockland [1,2] **** and Naema Nayyar*** [2]

[1] *Laboratory for Cortical Organization and Systematics, RIKEN Brain Science Institute, Wako-shi, Saitama, Japan*
[2] *Picower Institute of Learning and Memory, Massachusetts Institute of Technology, Cambridge, MA, USA*

Edited by:
Yoshiyuki Kubota, National Institute for Physiological Sciences, Japan

Reviewed by:
Noritaka Ichinohe, National Center of Neurology and Psychiatry, Japan
Bruno Cauli, CNRS and UPMC, France

****Correspondence:***
Kathleen S. Rockland, RIKEN-MIT Center for Neural Circuit Genetics, Picower Institute for Learning and Memory, Massachusetts Institute of Technology, 77 Massachusetts Avenue, Building 46, Cambridge, MA 02139, USA.
e-mail: kathrock@mit.edu

Sagittal sections through the corpus callosum of adult macaque monkeys ($n = 7$) reveal a subpopulation of neurons positive for NADPH-diaphorase (NADPHd). These are sparsely distributed, with 2–12 neurons scored over the anterior two-thirds of the callosum (about 14 mm). Neurons are densely labeled, type 1; but on the basis of soma and dendritic morphology, these neurons exhibit distinct heterogeneity. In one subpopulation, the cell body is narrowly attenuated (7–10 μm in width). These have bipolar dendrites, extending 300–800 μm from the cell body. One or both of the dendrites is often closely associated with blood vessels and tends to be aligned dorso-ventral, perpendicular to the body of the callosum. Another subpopulation of neurons has a larger soma (typically, 15 μm × 20 μm) and more multipolar dendrites, which are not as obviously associated with blood vessels. White matter neurons positive for NADPHd have previously been observed as a transient population, most numerous during development, in the human corpus callosum, as well as in that of other species. Their persistence in the corpus callosum of adult macaques and their close association with blood vessels has not previously been reported and is suggestive of roles other than axon guidance.

Keywords: neurovascular, white matter neurons, acetylcholine, callosal septa

INTRODUCTION

GABAergic neurons in the cortical white matter (WM) have been repeatedly demonstrated in multiple species (Kostovic and Rakic, 1980; Sandell, 1986; Chun and Shatz, 1989; Yan et al., 1996; Clancy et al., 2001; Jovanov-Milosevic et al., 2009; Suarez-Sola et al., 2009). Recent experiments have shown that at least some of these send long-distance connections into the cortical gray matter (Tomioka et al., 2005; Tomioka and Rockland, 2007; Higo et al., 2009), and thus presumably have a significant role in the cortical circuitry.

White matter neurons occur either subjacent to layer 6 or deeper in the WM core (Clancy et al., 2001; García-Marín et al., 2010). A subset has been identified within the parenchyma of the corpus callosum, where a role in circuitry might seem less likely. Since these neurons are more abundant in development, they have been considered as likely to figure in processes of axon guidance (Riederer et al., 2004; Niquille et al., 2009).

In this paper, we demonstrate that neurons positive for NADPH-diaphorase (NADPHd+) occur in the corpus callosum of adult macaque monkeys. NADPH-diaphorase is an enzyme that oxidizes the reduced form of nicotinamide adenine dinucleotide phosphate (NADPH), and is found in a small population of GABAergic neurons (reviewed in Yan et al., 1996). The population of NADPHd+ neurons has been further subdivided into at least two broad categories: type 1, with a larger soma (diameter > 20 μm; Yan et al., 1996) and dense, Golgi-like staining and type 2, with smaller soma and lighter more diffuse staining. The neurons reported here uniformly belong to the densely stained type 1 subpopulation, but exhibit distinct variability of soma size and dendritic arbors. Some of these neurons are conspicuously associated with blood vessels. This localization in the corpus callosum and the persistence into adulthood are strongly suggestive of roles other than in axon guidance.

MATERIALS AND METHODS

Tissue from seven adult macaque monkeys (4–6 kg) was used in this study. Monkeys were sedated with ketamine (11 mg/kg i.m.), deeply anesthetized with an overdose of Nembutal (75 mg/kg), and perfused transcardially in sequence with 0.9% saline, 4% paraformaldehyde, and three runs (250, 250, and 500 ml) of chilled 0.1 M phosphate buffer (PB) with 10, 20, or 30% sucrose, respectively. Brains were removed from the skull, bisected in the midline, placed in cold 30% sucrose until sinking (1–2 days), and cut serially in the sagittal plane (at 50 μm) by frozen microtomy. Three of the hemispheres had unilateral injections of biotinylated dextran amine in a sterile surgery procedure, 18–21 days before the perfusion (Zhong and Rockland, 2003). All animal procedures were carried out in conformity with institutionally approved protocols (RIKEN, Brain Science Institute), and in accordance with the US National Institutes of Health Guide for the Care and Use of Laboratory Animals.

For six of the seven hemispheres, alternate sections were reacted for NADPHd (Scherer-Singler et al., 1983). Substrate solution contained, per 50 ml of Tris buffer (TB; pH 7.4), 400 μl Triton-X, 40 mg NADPH (Sigma-Aldrich), 35 mg Nitroblue tetrazolium

(Sigma-Aldrich), and 60 mg sodium malate (Fisher Scientific). Tissue sections were rinsed in TB and incubated free-floating, in 8-compartment, netted "pie-plate" holders, at 37° until the desired intensity of staining was reached (usually about 45–90 min). Degree of staining was evaluated by viewing wet tissue under a dissecting microscope. At completion of the reaction, tissue was rinsed 3× in TB, mounted onto coated slides, dehydrated, and coverslipped. A second series of alternating sections was reacted by immunocytochemistry for parvalbumin (PV) or acetylcholinesterase (AChE). One hemisphere (R116) was processed in repeating series of three for NADPHd, acetylcholinesterase, and calbindin (the latter is not reported). The additional procedures were initially carried out as part of other studies. We include here results from the PV and AChE processing, since (1) there is an established link between AChE positive fibers and NADPHd+ neurons (Vaucher et al., 1997; Kalinchuk et al., 2010; Kilduff et al., 2011) and (2) continued work on the distribution of NADPHd+ neurons may show a relationship to what appear to be PV+ compartments.

PV immunohistochemistry was carried out on free-floating sections. These were placed for 1 h at room temperature, in 0.1 M phosphate buffered saline (PBS; pH 7.3), containing 0.5% Triton-X 100 and 5% normal goat serum (PBS–TG), and then incubated for 40–48 h at 4°C with PBS–TG containing mouse monoclonal anti-PV antibody (Swant, Bellinzona, Switzerland; 1:50,000). After rinsing, sections were continued to biotinylated goat anti-mouse IgG (Vector Laboratories, Burlingame, CA, USA; 1:200) for 1.5 h at room temperature. Immunoreactivity was visualized by the ABC protocol (one drop of reagent per 7 ml of 0.1 M PB; ABC Elite kits; Vector), followed by diaminobenzidine histochemistry with 0.03% nickel ammonium sulfate. Sections were mounted, dehydrated, and coverslipped. AChE histochemistry was carried out on free-floating sections, according to a standard protocol (Geneser-Jensen and Blackstad, 1971). Incubation time in substrate was prolonged to 2–3 days at room temperature, for the sake of enhancing reaction product in the comparatively AChE-poor cortical regions.

DATA ANALYSIS

Analysis was restricted to the medial most portion (1–2 mm) of the corpus callosum, in order to avoid confounds with the adjoining, non-callosal WM. Midline was determined by reference to the midline of the gross brain, as bisected after removal from the skull, and by reference to adjoining structures. That is, sections of interest were medial to the caudate nucleus. The posterior most portion of the corpus callosum (splenium) was not available. For the seven brains, the available portion of the corpus callosum comprised the anterior most 6, 7, 10, 15, 15, 22, and 25 mm.

Sections were scanned by using an Olympus VS120 light microscope equipped with a VC50 camera, captured by using a 10× or 40× objective (equivalent to 100× or 400× base magnification), and digitized as virtual slides. Most of the higher magnification scans were acquired in Z-mode to utilize the extended depth of focus feature. Sections were scored for number of cells positive for NADPHd; and these cells were subsequently analyzed for soma size and dendritic features. Long and short axes of the soma were obtained using VS120 measurement tools applied to the metadata of the captured image. Size, brightness, and contrast were adjusted to reflect the real image, by Photoshop software (Adobe Systems, San Jose, CA, USA).

RESULTS

In all seven brains, neurons positive for NADPHd occurred in the parenchyma of the corpus callosum. These were sparsely distributed, with 2–12 neurons per section (**Figure 1**). Neurons were typically isolated, but groups of three to four neurons, spaced 500–700 μm apart, were also found, especially in the region of the genu (**Figure 2**).

In addition to the sparsely scattered NADPHd neurons within the corpus callosum, positive neurons were evident along both the dorsal and ventral margins. These were less sparsely distributed (**Figures 1** and **3**); but since we consider these as a separate subpopulation, on the grounds of location and orientation, they were not included in further analysis. NADPHd neurons with soma within 100 μm of either margin were also excluded.

Positive neurons were densely filled, in Golgi-like detail, and therefore unambiguously classified as type 1 (Yan et al., 1996; Estrada and DeFelipe, 1998). No examples of type 2 neurons, defined as small, lightly stained neurons, were evident. Within the broad category of type 1, however, further subpopulations were indicated on the basis of several morphological criteria. First, soma size and shape were distinctly varied (**Figures 1–4**). Soma size ranged from 12.5 to 44.3 μm in the long axis and 4.5–13.6 μm in the short axis (**Table 1**). A few neurons had somas that were almost round; but the majority had an elongated soma, where the long axis was two or three times the length of the short axis (four times, for cell 11, R30). For four brains, the average length and width was calculated: R30, 20.4 μm × 8.3 μm; R31, 22.7 μm × 10.8 μm; P3, 26.1 μm × 11.4 μm; R19L, 19.9 μm × 10.7 μm (see **Table 1**).

Second, the configuration of proximal dendrites was distinctive. Two broad groupings on the basis of primary branch configuration at the soma are: bipolar or multipolar (**Figures 1–4**). Within the multipolar group, a small further subset could be identified by having one notably thick side dendrite (**Figure 3D**).

Third, the dendritic arborization could be described as bipolar, bitufted, multipolar, or asymmetric, with one vertical and one multipolar dendrite (**Figures 2–4**). Dendrites could commonly be followed 350–550 μm from the soma in single sections. These were typically beaded, but could also have a sparse distribution of spines (**Figures 1** and **4**). A striking feature was the close association of the bipolar neurons in particular with blood vessels (**Figures 3E** and **4C–E**). Dendrites of multipolar neurons often approached blood vessels (**Figures 2** and **4**), but it was hard to judge if these actually formed direct contacts.

Morphological heterogeneity has been previously reported for NADPHd+ neurons in the cortical gray matter (Estrada and DeFelipe, 1998). In our sample, strictly bipolar neurons (**Figures 3E** and **4E**), with two oppositely oriented primary dendrites extending distally, were a small minority. Either the ascending or descending dendrite was often tightly intertwined with one or more branches. Bitufted cells were more frequently observed (**Figure 4C**); and multipolar neurons were the most numerous (**Figures 3C** and **4A**). As our material consisted of alternating, not sequential, sections,

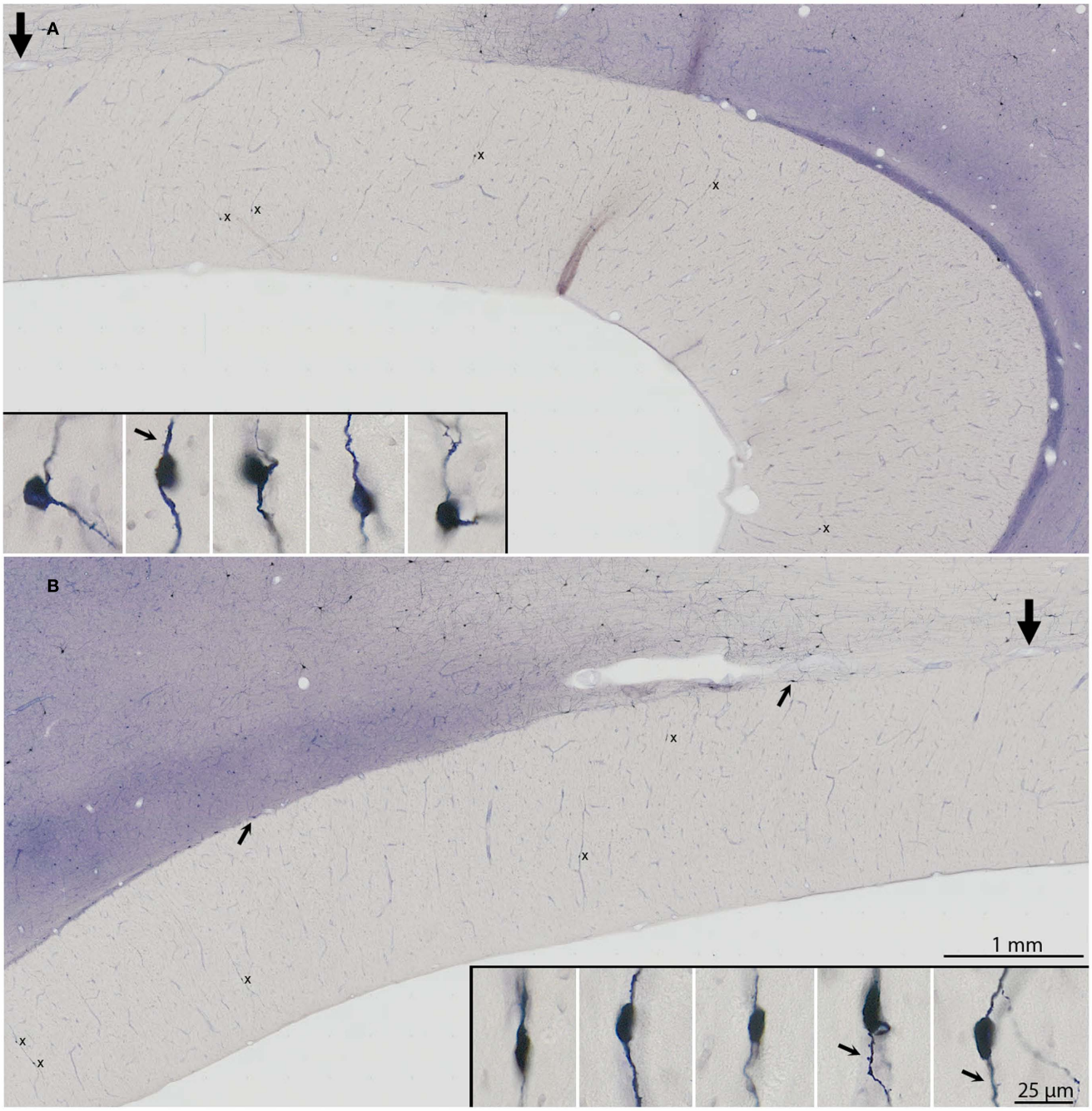

FIGURE 1 | (A,B) Low magnification photomicrograph of a mid-sagittal section through the corpus callosum in case R30. **(B)** is a posterior continuation of the portion in **(A)**, such that the thick arrows in **(A,B)** demarcate corresponding blood vessels. Ten neurons that are NADPHd+ are identified, and indicated by x in **(A,B)**. Somas and proximal dendrites of these neurons are shown in higher magnification insets. The five neurons in **(A)** are arranged from anterior (at right) to posterior (at left), and the lower five, similarly, for the segment shown in **(B)**. Arrows in three of the insets point to sparsely distributed dendritic spines. Neurons have been rotated so that the major axis is perpendicular to the dorsal surface of the brain. NADPHd+ neurons are also obvious at the dorsal margin of the callosum [two small arrows in **(B)**] and in the overlying cortical white matter.

we are limiting ourselves to these observations, which will need to be followed up by more detailed analysis and/or additional criteria for classifications.

Finer processes, possibly corresponding to axons, could often be identified (**Figure 3D**, inset), but no close association with blood vessels could be confidently discerned.

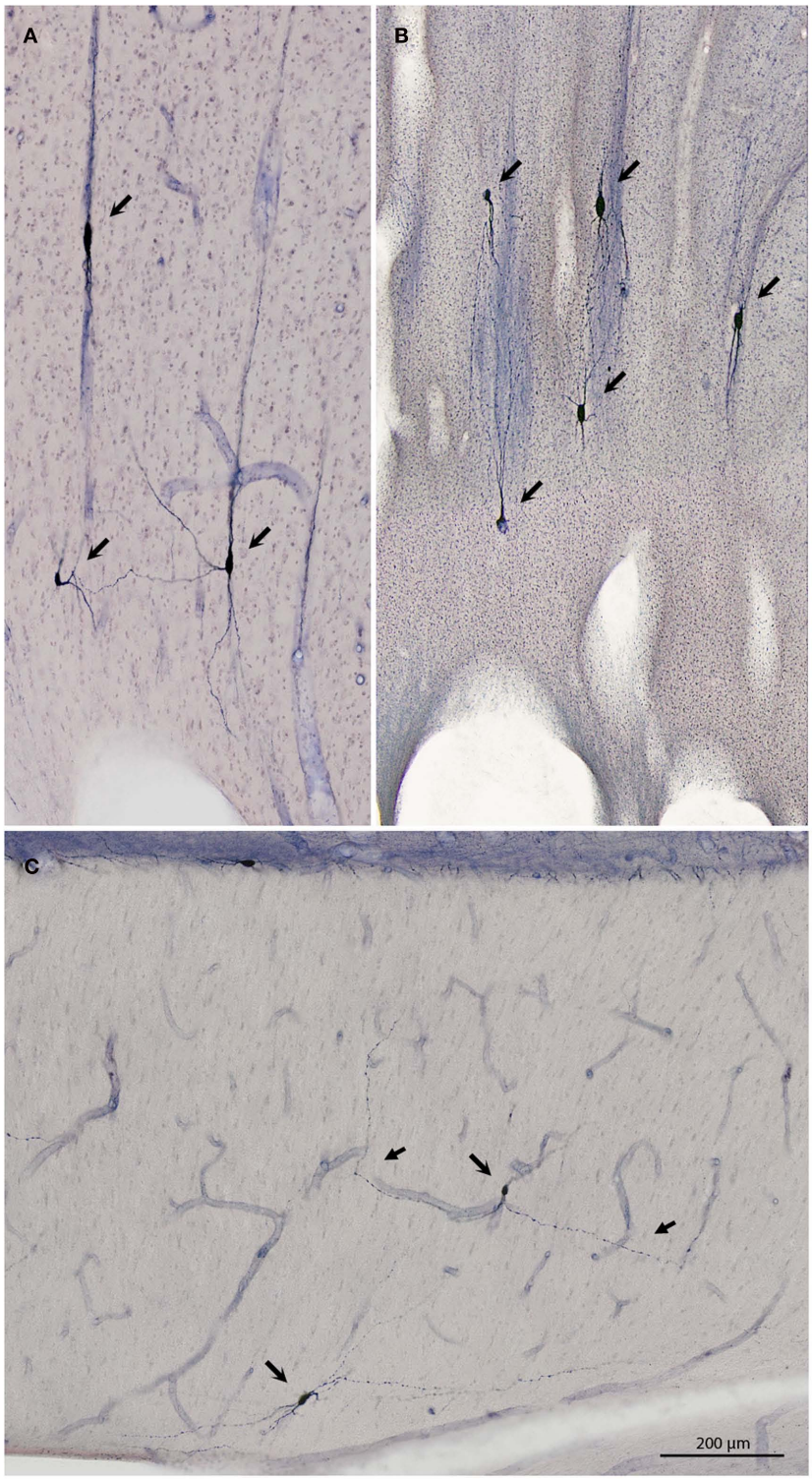

FIGURE 2 | Three examples of small groups of NADPHd+ neurons. (A) Three neurons (arrows), at the genu (case R30). The dendritic portion of a fourth neuron is visible at the right. **(B)** Five neurons (arrows), also at the genu (case P3). In **(A,B)**, the field has been rotated 90° counter-clockwise, for the sake of formatting. **(C)** Two neurons (right pointing arrows) in the body of the callosum (case R31). Distal portions of the dendrite of the more dorsal neuron are indicated by left-pointing arrows. The left dendrite parallels one of the blood vessels for >200 µm.

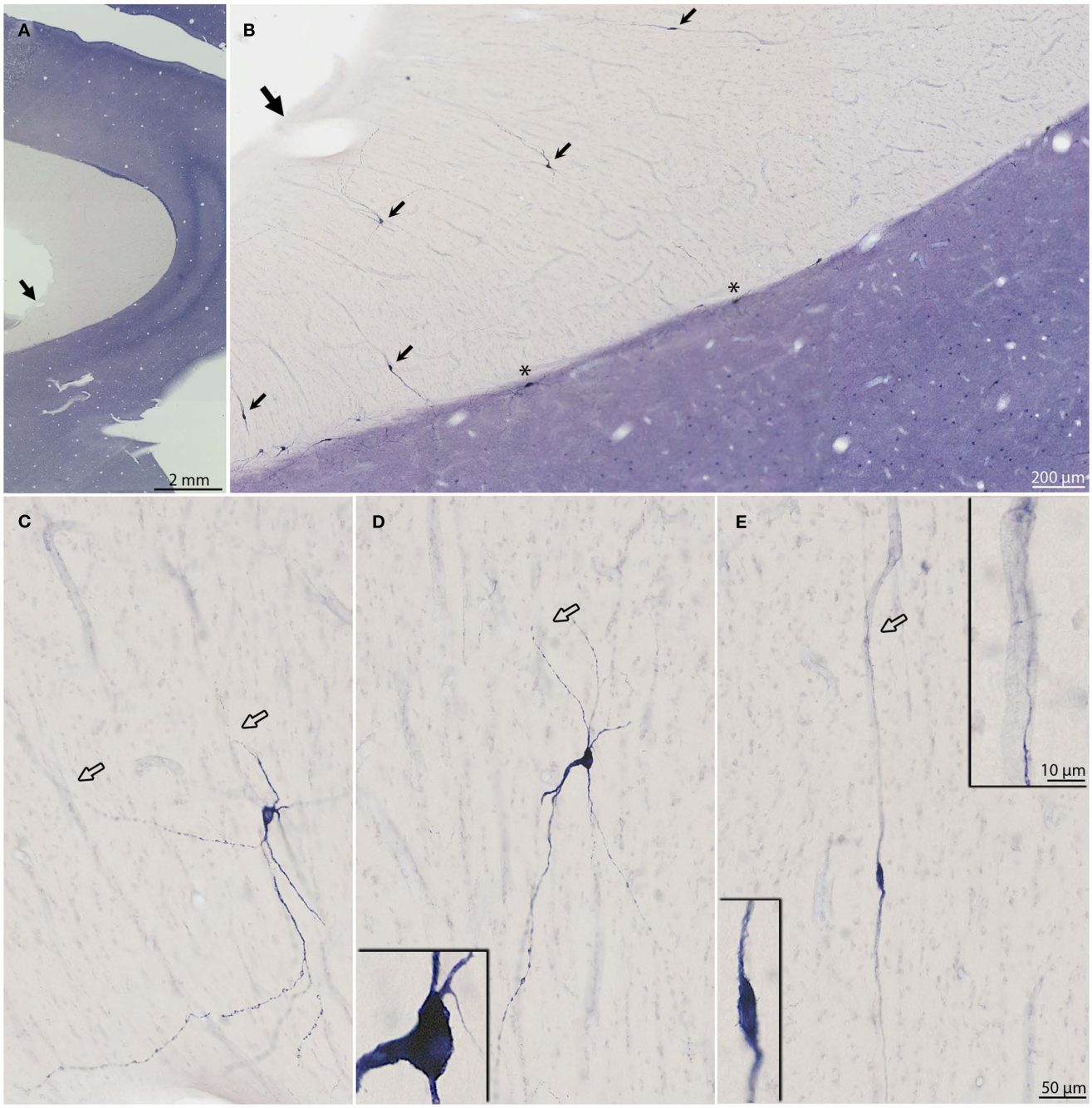

FIGURE 3 | (A,B) Progressively higher magnifications of a mid-sagittal section through the corpus callosum in R31. Thick arrows demarcate corresponding blood vessels in **(A,B)**. Scattered neurons that are NADPHd+ are evident at the ventral margin of the callosum [asterisk in **(B)**]. Five neurons positive for NADPHd are indicated by short arrows in **(B)**. **(C–E)** Higher magnification views of three of the NADPHd+ neurons to show dendritic detail. Inset in **(D)** is an example of a neuron with one very thick dendrite. Inset in [**(E)** at lower left] is an example of a neuron with thin soma and bipolar dendritic arborization. Inset in [**(E)** at upper right] shows close association of dendrite and blood vessel. Individual neurons have been rotated so that they are approximately perpendicular to the dorsal surface of the brain. Hollow arrows indicate points where NADPHd+ dendrites are in close proximity to blood vessels.

OTHER MARKERS

In one brain, stained for acetylcholinesterase (AChE), occasional neurons were evident in the callosum (**Figure 5**). AChE+ fibers were also detected. These were usually oriented dorso-ventrally, perpendicular to the long axis of the corpus callosum (**Figure 5**). Positive neurons were not found in tissue stained for parvalbumin (PV; **Figure 6**).

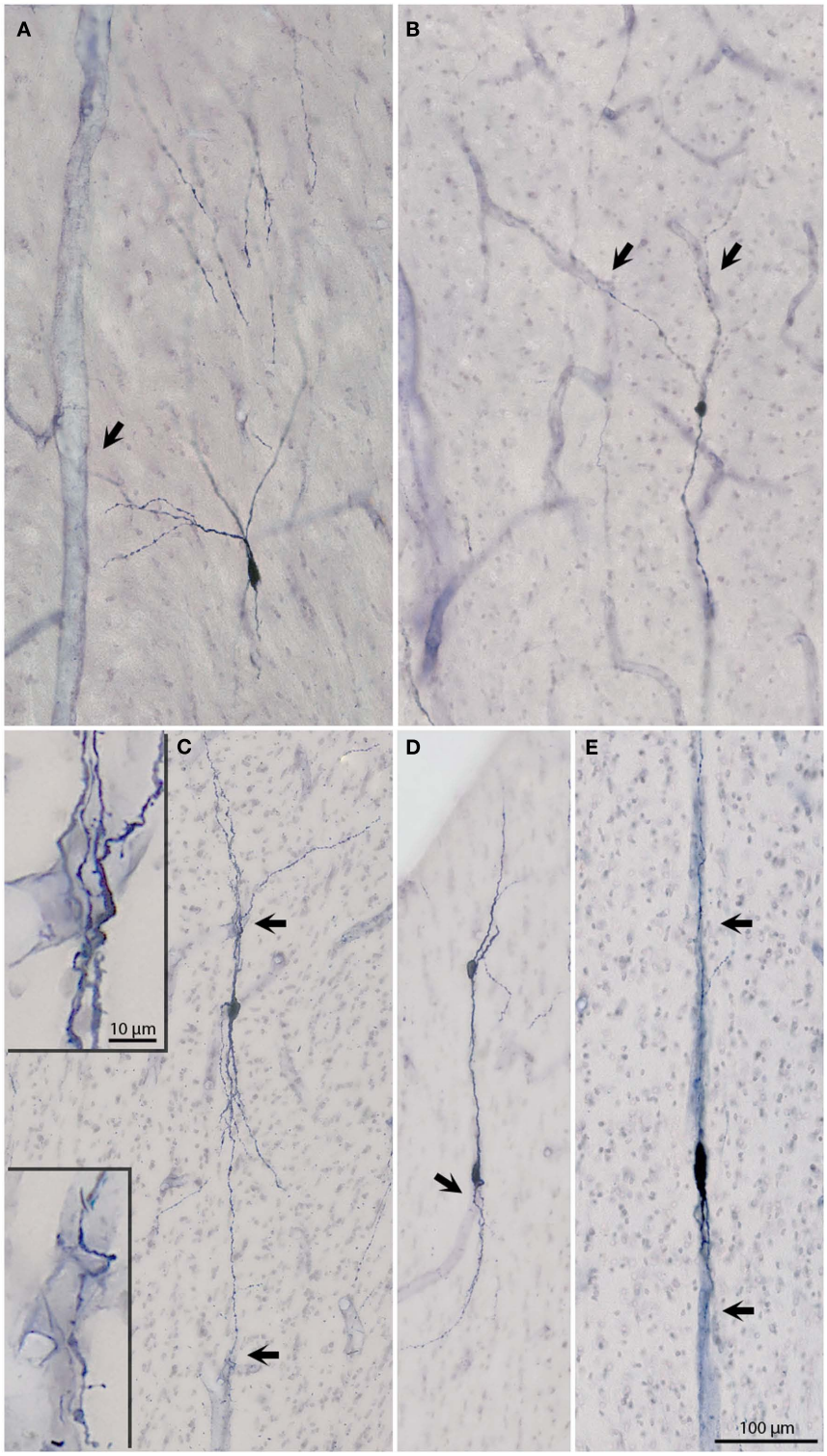

FIGURE 4 | (A–E) Micrographs of six additional NADPHd+ neurons to show soma and dendritic arbors. Arrows point to blood vessels, which are in apparent close association with dendrites. The association is particularly evident for the neurons in **(C–E)**. The two higher magnification insets in **(C)** depict dendrites intertwining around blood vessels. Sparse dendritic spines are evident on both segments. The two vertically aligned neurons in **(D)**, have partially overlapping dendrites, giving an illusory appearance of being conjoined. The neurons in **(D)** are from the posterior most x in **Figure 1**; the other four neurons are from R19L **(A)**, R31 **(B)**, and R30 **(C,E)**.

Table 1 | Soma size of NADPHd+ intracallosal cells from four brains.

Case	Cell	Length × width (μm)
R30	1 (s. 8A)	15.1 × 9.9
	2 (s. 8A)	15.1 × 8.4
	3 (s. 8A)	13.6 × 9.2
	4 (s. 8A)	12.5 × 7.7
	5 (s. 8A)	18.6 × 4.5
	6 (s. 8A)	15.5 × 6.1
	7 (s. 8A)	18.8 × 8.4
	8 (s. 8A)	21.8 × 6.1
	9 (s. 8B)	16.8 × 8.3
	10 (s. 8B)	16.9 × 10.2
	11 (s. 4B)	29.3 × 6.8
	12 (s. 2C)	29.5 × 11.4
	13 (s. 2C)	19.5 × 7.1
	14 (s. 2C)	44.3 × 11.7
	15 (s. 2C)	19.1 × 8.3
		Average 20.4 × 8.3
R31	1 (s. 4)	22.6 × 12.9
	2 (s. 7)	20.0 × 9.7
	3 (s. 7)	28.4 × 11.5
	4 (s. 7)	32.2 × 10.3
	5 (s. 7)	16.6 × 11.0
	6 (s. 7)	16.1 × 9.1
		Average 22.7 × 10.8
P3	1 (s. 7)	30.5 × 12.5
	2 (s. 7)	20.8 × 8.9
	3 (s. 7)	27.6 × 12.8
	4 (s. 7)	26.2 × 9.1
	5 (s. 7)	23.0 × 10.9
	6 (s. 7)	33.2 × 11.4
	7 (s. 7)	23.2 × 12.7
	8 (s. 7)	25.1 × 12.5
	9 (s. 7)	15.9 × 11.2
	10 (s. 5)	24.0 × 11.5
	11 (s. 5)	31.1 × 12.4
	12 (s. 3)	21.2 × 12.5
	13 (s. 3)	37.3 × 9.8
		Average 26.1 × 11.4
R19L	1 (s. 9)	20.9 × 7.6
	2 (s. 9)	20.9 × 13.4
	3 (s. 9)	19.3 × 12.3
	4 (s. 9)	18.8 × 11.6
	5 (s. 12)	19.9 × 7.7
	6 (s. 12)	19.1 × 11.6
	7 (s. 12)	17.7 × 11.5
	8 (s. 12)	23.8 × 13.6
	9 (s. 12)	16.4 × 9.7
	10 (s. 12)	18.5 × 7.1
	11 (s. 11)	15.8 × 12.0
	12 (s. 11)	27.5 × 10.7
		Average 19.9 × 10.7

Average length × width is given for the four groups of cells. s., Section containing the particular neurons.

CALLOSAL SEPTA

In tissue reacted for PV, alternating zones could be discerned, about 150–200 μm across, where callosal fibers were differentially oriented. That is, PV+ segments were either mainly in cross section (asterisks, **Figure 6**) or occurred in short, obliquely cut segments (arrows, **Figure 6**). The PV+ fibers presumably originate from subpopulations of large, PV+ pyramids in layer 5 of some cortical areas (Ichinohe et al., 2004).

DISCUSSION

One main point of the present report is the persistence of NADPHd+ neurons in the corpus callosum of adult macaque monkeys. Previous reports have demonstrated neurons in the corpus callosum, but have found that these neurons decrease significantly in the postnatal period. In cats, the number drops from about 570 at birth to 200 in the adult, and the distribution becomes restricted to the rostrum (Riederer et al., 2004). In humans, what were called "intracallosal" neurons are most numerous in the second half of gestation and the early postnatal years, but are found only sporadically in the adult brain (Jovanov-Miloševic et al., 2010). In our adult monkey material, NADPHd+ neurons were sparsely distributed, but readily identified. Consistent with Riederer et al. although the neurons were found throughout the body of the callosum, the rostrum, and genu was a preferential location (splenium was not examined). Since the present report was restricted to adult material, we cannot comment on a developmentally related decrease in density, although this would seem likely.

A second point is the striking morphological heterogeneity of the NADPHd+ neurons. This feature has consistently been noted in reports dealing with both gray matter and WM populations. Dendritic morphology is described as bipolar, bitufted, or multipolar; and neurons visualized by immuno-staining for nitric oxide synthetase (NOS) are further distinguishable based on whether NOS is co-localized with neuropeptide-Y or somatostatin (Yan et al., 1996; Estrada and DeFelipe, 1998; Cauli et al., 2004).

A third point is the conspicuous association of at least some of these neurons with blood vessels. An association of NADPHd+ neurons with blood vessels has been remarked previously, but primarily as pertains to neurons in the gray matter (Vaucher et al., 1997; Hamel, 2006; Suarez-Sola et al., 2009; Cauli and Hamel, 2010, among others). In the gray matter, NOS+ neurons are considered to act in conjunction with acetylcholine, serotonin, and an assortment of signaling molecules to transmute neural signals to vascular responses, in an activity-related cycle of vasodilatations and constrictions (Cauli et al., 2004; Iadecola, 2004; Kocharyan et al., 2008; Lecrux and Hamel, 2011). Owing to the diffusion properties of NO, a given NOS+ neuron has been estimated to have an effective sphere of influence of about 100 μm radius (Wood and Garthwaite, 1994; Estrada and DeFelipe, 1998), and is thought to influence several microvessels (Cauli et al., 2004). Some of the intracallosal neurons reported here appeared to contact several microvessels. Others, however, seemed closely associated with a single blood vessel (**Figures 3** and **4**). Moreover, in view of the sparse distribution of the NADPHd+ neurons, it is evident that these are associated with only a subset of microvessels.

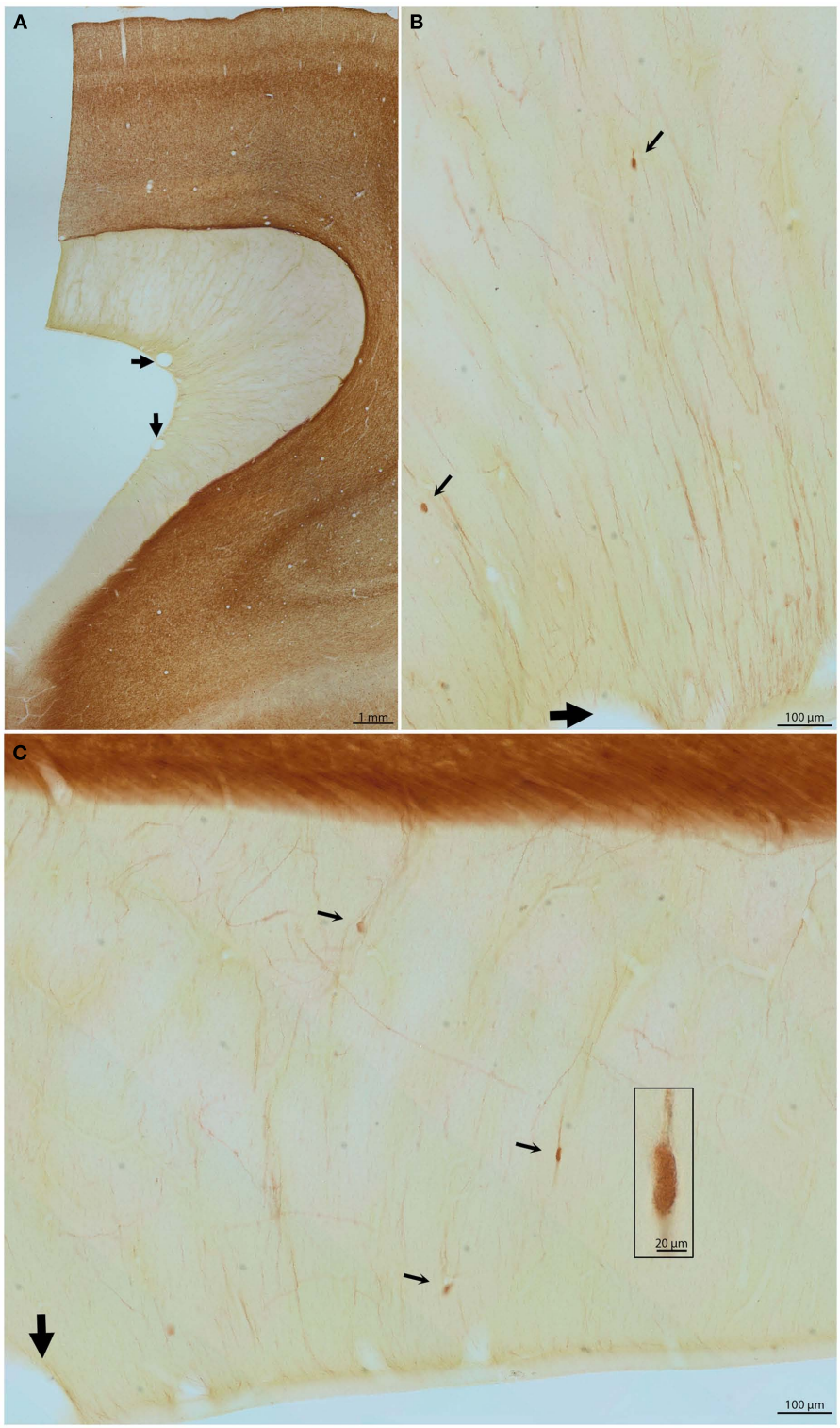

FIGURE 5 | (A) Low magnification view of a mid-sagittal section through the genu and rostrum of the corpus callosum, reacted for acetylcholinesterase (AChE). **(B,C)** Higher magnifications from upper arrow **(B)** and lower arrow **(C)**, showing AChE fibers and scattered AChE+ neurons (small arrows). The field in **(B)** has been rotated so as to be perpendicular to the dorsal surface of the brain. One neuron [in **(C)**] with thin soma and bipolar proximal dendrites is shown at higher magnification in the box at the right.

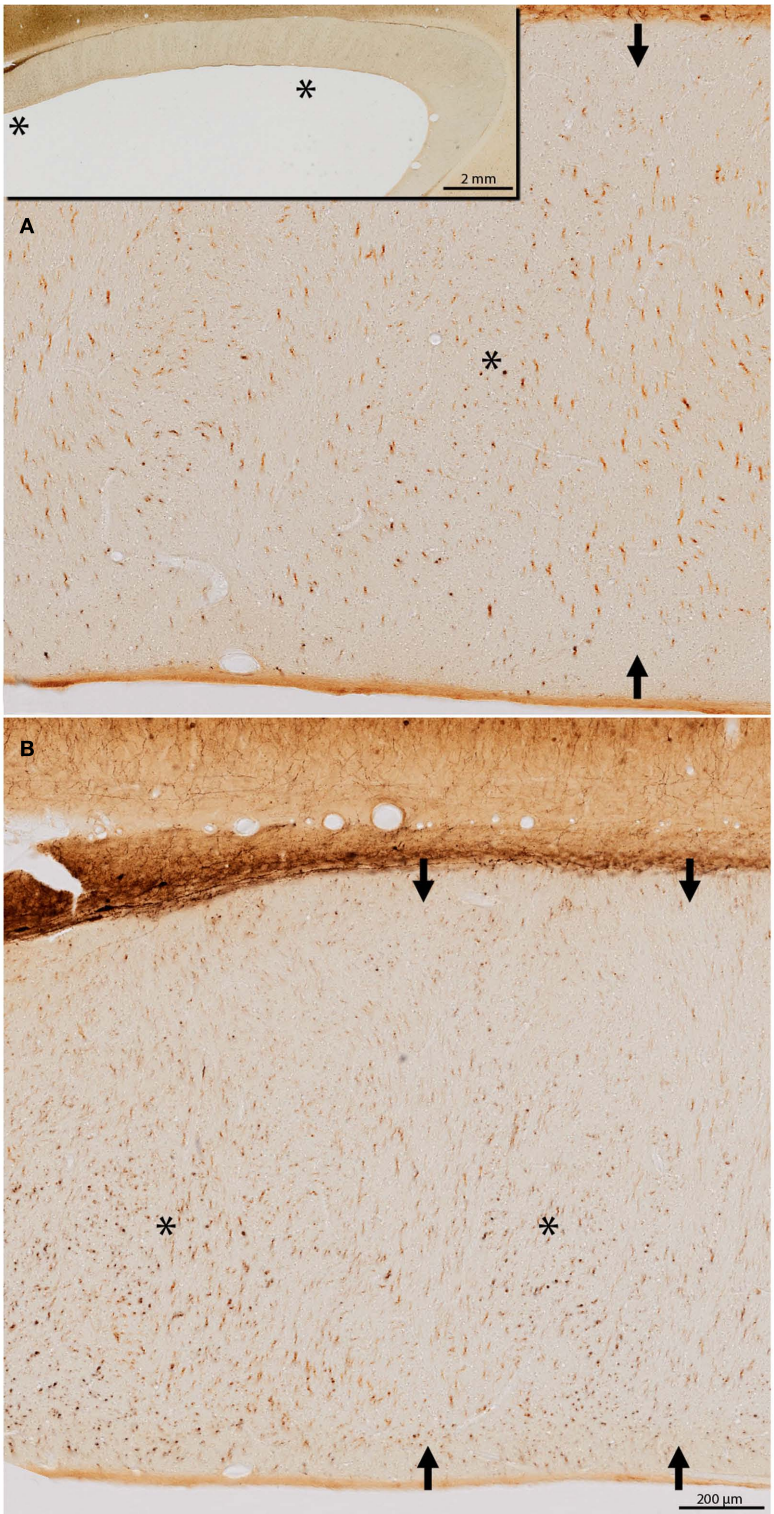

FIGURE 6 | (A,B) Two fields through the body of the callosum, reacted for parvalbumin (PV). The location of the two fields is indicated by asterisks in the low magnification inset in **(A)** [**(A)** is more anterior; **(B)** is more posterior]. Subpopulations of PV+ fibers are cut predominantly in cross section (asterisks) or oblique section (arrows), with some indication of a regular alternation.

An obvious question is whether the NADPHd+ neurons in the deep WM of the callosum have the same role (i.e., part of an activity-related neurovascular unit) as has been defined for those in the overwhelmingly more cell-dense gray matter. Possibly relevant in this regard is evidence from *in vitro* experiments on rat optic nerve, showing that there are persistent signals from eNOS+ microvascular cells to axons, and that these generate both tonic and phasic nitric oxide (NO) signals (Garthwaite et al., 2006). These results pertain specifically to eNOS, but can be taken to indicate some effect of NO directly on axons. Alternatively, nNOS may figure in activity-dependent modulation of the myelin sheath by an axon (Stys, 2011) or, more particularly, in a neurovascular unit where axons and myelination, not spiking neurons, are the interacting components.

Other recent studies have reported release of vesicular glutamate at discrete sites along axons in the WM (Kukley et al., 2007). This has been interpreted in the context of inotropic glutamatergic receptors on oligodendrocyte precursor cells (Kukley et al., 2007). Given that NO can amplify glutamate release and interact with NMDA receptors (Kara and Friedlander, 1998), this might be another influence of the NADPHd+ neurons.

With the discovery that some NADPHd+ neurons have long-distance projections (Tomioka et al., 2005; Tomioka and Rockland, 2007; Higo et al., 2009), these have also been discussed in a network context; and *in vitro* experiments have verified that WM neurons participate in functional circuitry in the gray matter (Clancy et al., 2001; von Engelhardt et al., 2011). Thus, another possibility is that NADPHd+ neurons in the callosum may participate in a widespread network, either involving neurons in the overlying gray matter or, perhaps more likely given their distance from the gray matter, similar neurons, or neuron–glia–vascular units in the deep WM.

Expression studies of cFOS-labeled neurons have implicated cortical nNOS+ interneurons in slow wave sleep (Kilduff et al., 2011), although these were described in the cortical gray matter. Another aspect of the sleep cycle, however, is cholinergic input from the basal forebrain (Vaucher et al., 1997; Kalinchuk et al., 2010; Kilduff et al., 2011). Interestingly, we observed cholinergic fibers and cells in the callosum in the present report; but further work will be necessary to determine if there is significant cholinergic input to the intracallosal NADPHd+ cells.

Finally, it is worth noting that NADPHd+ intracallosal neurons tend to have a vertical orientation, extended in the dorso-ventral plane. This may be related to the dorso-ventrally oriented septa described in the developing human callosum (Jovanov-Miloševic et al., 2010). These have been reported as transient modules; but some indication of what might be comparable septa in the adult macaque can be detected in our PV material (**Figure 6**).

CONCLUSION

In summary, we have demonstrated the persistence of NADPHd+ neurons in the corpus callosum of adult macaque monkeys. Their persistence in the adult and their apparent association with blood vessels argues for a role other than in axon guidance. Other possibilities as to their function include a role in widespread network organization, possibly related to sleep cycles, or in interactions of axons, myelination, and vasculature. Multiple roles of NOS are summarized in Calabrese et al., 2007. Presumably, since a role in axon guidance has been repeatedly demonstrated for transient intracallosal neurons (Riederer et al., 2004; Niquille et al., 2009), these neurons undergo changing roles over the course of the lifetime (Friedlander and Torres-Reveron, 2009).

ACKNOWLEDGMENTS

We would like to thank Professors E. Vaucher and E. Hamel for kind discussion. Funding is gratefully acknowledged from RIKEN Brain Science Institute, and the RIKEN-MIT Center for Neural Circuit Genetics.

REFERENCES

Calabrese, V., Mancuso, C., Calvani, M., Rizzarelli, E., Butterfield, D. A., and Stella, A. M. (2007). Nitric oxide in the central nervous system: neuroprotection versus neurotoxicity. *Nat. Rev. Neurosci.* 8, 766–775.

Cauli, B., and Hamel, E. (2010). Revisiting the role of neurons in neurovascular coupling. *Front. Neuroenergetics* 2:9. doi:10.3389/fnene.2010.00009

Cauli, B., Tong, X. K., Rancillac, A., Serluca, N., Lambolez, B., Rossier, J., and Hamel, E. (2004). Cortical GABA interneurons in neurovascular coupling: relays for subcortical vasoactive pathways. *J. Neurosci.* 24, 8940–8949.

Chun, J. J., and Shatz, C. J. (1989). Interstitial cells of the adult neocortical white matter are the remnant of the early generated subplate neuron population. *J. Comp. Neurol.* 282, 555–569.

Clancy, B., Silva-Filho, M., and Friedlander, M. J. (2001). Structure and projections of white matter neurons in the postnatal rat visual cortex. *J. Comp. Neurol.* 434, 233–252.

Estrada, C., and DeFelipe, J. (1998). Nitric oxide-producing neurons in the neocortex: morphological and functional relationship with intraparenchymal microvasculature. *Cereb. Cortex* 8, 193–203.

Friedlander, M. J., and Torres-Reveron, J. (2009). The changing roles of neurons in the cortical subplate. *Front. Neuroanat.* 3:15. doi:10.3389/neuro.05.015.2009

García-Marín, V., Blazquez-Llorca, L., Rodriguez, J. R., Gonzalez-Soriano, J., and DeFelipe, J. (2010). Differential distribution of neurons in the gyral white matter of the human cerebral cortex. *J. Comp. Neurol.* 518, 4740–4759.

Garthwaite, G., Bartus, K., Malcolm, D., Goodwin, D., Kollb-Sielecka, M., Dooldeniya, C., and Garthwaite, J. (2006). Signaling from blood vessels to CNS axons through nitric oxide. *J. Neurosci.* 26, 7730–7740.

Geneser-Jensen, F. A., and Blackstad, T. W. (1971). Distribution of acetyl cholinesterase in the hippocampal region of the guinea pig. I. Entorhinal area, parasubiculum, and presubiculum. *Z. Zellforsch. Mikrosk. Anat.* 114, 460–481.

Hamel, E. (2006). Perivascular nerves and the regulation of cerebrovascular tone. *J. Appl. Physiol.* 100, 1059–1064.

Higo, S., Akashi, K., Sakimura, K., and Tamamaki, N. (2009). Subtypes of GABAergic neurons project axons in the neocortex. *Front. Neuroanat.* 3:25. doi:10.3389/neuro.05.025.2009

Iadecola, C. (2004). Neurovascular regulation in the normal brain and in Alzheimer's disease. *Nat. Rev. Neurosci.* 5, 347–360.

Ichinohe, N., Watakabe, A., Miyashita, T., Yamamori, T., Hashikawa, T., and Rockland, K. S. (2004). A voltage-gated potassium channel, Kv3.1b, is expressed by a subpopulation of large pyramidal neurons in layer 5 of the macaque monkey cortex. *Neuroscience* 129, 179–185.

Jovanov-Milosevic, N., Culjat, M., and Kostovic, I. (2009). Growth of the human corpus callosum: modular and laminar morphogenetic zones. *Front. Neuroanat.* 3:6. doi:10.3389/neuro.05.006.2009

Jovanov-Miloševic, N., Petanjek, Z., Petrovic, D., Judaš, M., and Kostovic, I. (2010). Morphology, molecular phenotypes and distribution of neurons in developing human corpus callosum. *Eur. J. Neurosci.* 32, 1423–1432.

Kalinchuk, A. V., McCarley, R. W., Porkka-Heiskanen, T., and Basheer, R. (2010). Sleep deprivation triggers inducible nitric oxide-dependent nitric oxide production in wake-active basal forebrain neurons. *J. Neurosci.* 30, 13254–13264.

Kara, P., and Friedlander, M. J. (1998). Dynamic modulation of cerebral cortex synaptic function by nitric oxide. *Prog. Brain Res.* 118, 183–198.

Kilduff, T. S., Cauli, B., and Gerashchenko, D. (2011). Activation of cortical interneurons during sleep: an anatomical link to homeostatic sleep regulation? *Trends Neurosci.* 34, 10–19.

Kocharyan, A., Fernandes, P., Tong, X. K., Vaucher, E., and Hamel, E. (2008). Specific subtypes of cortical GABA interneurons contribute to the neurovascular coupling response to basal forebrain stimulation. *J. Cereb. Blood Flow Metab.* 28, 221–231.

Kostovic, I., and Rakic, P. (1980). Cytology and time of origin of interstitial neurons in the white matter in infant and adult human and monkey telencephalon. *J. Neurocytol.* 9, 219–242.

Kukley, M., Capetillo-Zarate, E., and Dietrich, D. (2007). Vesicular glutamate release from axons in white matter. *Nat. Neurosci.* 10, 311–320.

Lecrux, C., and Hamel, E. (2011). The neurovascular unit in brain function and disease. *Acta Physiol.* 203, 47–59.

Niquille, M., Garel, S., Mann, F., Hornung, J. P., Otsmane, B., Chevalley, S., Parras, C., Guillemot, F., Gaspar, P., Yanagawa, Y., and Lebrand, C. (2009). Transient neuron populations are required to guide callosal axons: a role for semaphorin 3C. *PLoS Biol.* 7, e1000230. doi:10.1371/journal.pbio.1000230

Riederer, B. M., Berbel, P., and Innocenti, G. M. (2004). Neurons in the corpus callosum of the cat during postnatal development. *Eur. J. Neurosci.* 19, 2039–2046.

Sandell, J. H. (1986). NADPH diaphorase histochemistry in the macaque striate cortex. *J. Comp. Neurol.* 251, 388–397.

Scherer-Singler, U., Vincent, S. R., Kimura, H., and McGeer, E. G. (1983). Demonstration of a unique population of neurons with NADPH-diaphorase histochemistry. *J. Neurosci. Methods* 9, 229–234.

Stys, P. K. (2011). The axo-myelinic synapse. *Trends Neurosci.* 34, 393–400.

Suarez-Sola, M. L., Gonzalez-Delgado, F. J., Pueyo-Morlans, M., Medina-Bolivar, O. C., Hernandez-Acosta, N. C., Gonzalez-Gomez, M., and Meyer, G. (2009). Neurons in the white matter of the adult human neocortex. *Front. Neuroanat.* 3:7. doi:10.3389/neuro.05.007.2009

Tomioka, R., Okamoto, K., Furuta, T., Fujiyama, F., Iwasato, T., Yanagawa, Y., Obata, K., Kaneko, T., and Tamamaki, N. (2005). Demonstration of long-range GABAergic connections distributed throughout the mouse neocortex. *Eur. J. Neurosci.* 21, 1587–1600.

Tomioka, R., and Rockland, K. S. (2007). Long-distance corticocortical GABAergic neurons in the adult monkey white and gray matter. *J. Comp. Neurol.* 505, 526–538.

Vaucher, E., Linville, D., and Hamel, E. (1997). Cholinergic basal forebrain projections to nitric oxide synthase-containing neurons in the rat cerebral cortex. *Neuroscience* 79, 827–836.

von Engelhardt, J., Khrulev, S., Eliava, M., Wahlster, S., and Monyer, H. (2011). 5-HT3A receptor-bearing white matter interstitial GABAergic interneurons are functionally integrated into cortical and subcortical networks. *J. Neurosci.* 31, 16844–16854.

Wood, J., and Garthwaite, J. (1994). Models of the diffusional spread of nitric oxide: implications for neural nitric oxide signalling and its pharmacological properties. *Neuropharmacology* 33, 1235–1244.

Yan, X. X., Jen, L. S., and Garey, L. J. (1996). NADPH-diaphorase-positive neurons in primate cerebral cortex colocalize with GABA and calcium-binding proteins. *Cereb. Cortex* 6, 524–529.

Zhong, Y. M., and Rockland, K. S. (2003). Inferior parietal lobule projections to anterior inferotemporal cortex (area TE) in macaque monkey. *Cereb. Cortex* 13, 527–540.

Conflict of Interest Statement: The authors declare that the research was conducted in the absence of any commercial or financial relationships that could be construed as a potential conflict of interest.

Received: 05 January 2012; paper pending published: 18 January 2012; accepted: 01 February 2012; published online: 20 February 2012.

*Citation: Rockland KS and Nayyar N (2012) Association of type I neurons positive for NADPH-diaphorase with blood vessels in the adult monkey corpus callosum. Front. Neural Circuits **6**:4. doi: 10.3389/fncir.2012.00004*

frontiers in
NEURAL CIRCUITS

ORIGINAL RESEARCH ARTICLE
published: 10 August 2012
doi: 10.3389/fncir.2012.00050

Activation of cortical 5-HT$_3$ receptor-expressing interneurons induces NO mediated vasodilatations and NPY mediated vasoconstrictions

Quentin Perrenoud, Jean Rossier, Isabelle Férézou†, Hélène Geoffroy, Thierry Gallopin, Tania Vitalis and Armelle Rancillac*

Laboratoire de Neurobiologie, CNRS UMR 7637, ESPCI ParisTech, Paris, France

Edited by:
Bruno Cauli, UPMC, France

Reviewed by:
Kathleen S. Rockland, Massachusetts Institute of Technology, USA
Salah El Mestikawy, Université Pierre et Marie Curie, France
Helene Girouard, Universite de Montreal, Canada

***Correspondence:**
Armelle Rancillac, Laboratoire de Neurobiologie, CNRS UMR 7637, ESPCI ParisTech, 10 rue Vauquelin, 75005 Paris, France.
e-mail: armelle.rancillac@espci.fr

†Present address:
Isabelle Férézou, Unité de Neurosciences Information et Complexité, Centre National de la Recherche Scientifique, Gif sur Yvette, France.

GABAergic interneurons are local integrators of cortical activity that have been reported to be involved in the control of cerebral blood flow (CBF) through their ability to produce vasoactive molecules and their rich innervation of neighboring blood vessels. They form a highly diverse population among which the serotonin 5-hydroxytryptamine 3A receptor (5-HT$_{3A}$)-expressing interneurons share a common developmental origin, in addition to the responsiveness to serotonergic ascending pathway. We have recently shown that these neurons regroup two distinct subpopulations within the somatosensory cortex: Neuropeptide Y (NPY)-expressing interneurons, displaying morphological properties similar to those of neurogliaform cells and Vasoactive Intestinal Peptide (VIP)-expressing bipolar/bitufted interneurons. The aim of the present study was to determine the role of these neuronal populations in the control of vascular tone by monitoring blood vessels diameter changes, using infrared videomicroscopy in mouse neocortical slices. Bath applications of 1-(3-Chlorophenyl)biguanide hydrochloride (mCPBG), a 5-HT$_3$R agonist, induced both constrictions (30%) and dilations (70%) of penetrating arterioles within supragranular layers. All vasoconstrictions were abolished in the presence of the NPY receptor antagonist (BIBP 3226), suggesting that they were elicited by NPY release. Vasodilations persisted in the presence of the VIP receptor antagonist VPAC1 (PG-97-269), whereas they were blocked in the presence of the neuronal Nitric Oxide (NO) Synthase (nNOS) inhibitor, L-NNA. Altogether, these results strongly suggest that activation of neocortical 5-HT$_{3A}$-expressing interneurons by serotoninergic input could induces NO mediated vasodilatations and NPY mediated vasoconstrictions.

Keywords: neurovascular coupling, mCPBG, serotonin, U46619, Pet1 knock-out mouse, vasoactive intestinal peptide, brain slices, neurogliaform cells

INTRODUCTION

Within the cerebral cortex, different types of GABAergic inhibitory interneurons have been described according to their distinctive morphological, molecular, and electrophysiological characteristics (Cauli et al., 1997; Markram et al., 2004; Vitalis and Rossier, 2011). Although the final classification scheme of cortical interneurons is still a matter of debate (Ascoli et al., 2008), data from *in vitro* and *in vivo* experiments tend to demonstrate that distinct subpopulations of inhibitory interneurons exert specific functional roles in the integrative processes of the cortical network (Whittington and Traub, 2003; Markram et al., 2004; Fanselow and Connors, 2010; Gentet et al., 2010; Mendez and Bacci, 2011). Furthermore, some GABAergic interneurons have been reported recently to be involved in the control of cerebral blood flow (CBF) through their ability to express and release vasoactive molecules (Cauli et al., 2004; Cauli and Hamel, 2010). However, further characterization of these vasoactive interneurons subpopulations remains to be established.

Interestingly, the robust cortical serotoninergic innervation from raphe nuclei (Reinhard et al., 1979; Steinbusch, 1981; Tork, 1990), which modulate cortical activity (Takeuchi and Sano, 1984; Papadopoulos et al., 1987; DeFelipe et al., 1991) and CBF (Rapport et al., 1948; Cohen et al., 1996; Riad et al., 1998), preferentially targets inhibitory interneurons (DeFelipe et al., 1991; Smiley and Goldman-Rakic, 1996; Paspalas and Papadopoulos, 2001). However, the processes by which 5-hydroxytryptamine (serotonin, 5-HT) acts on the cortical network and CBF are complex and deserve to be further understood. Indeed, responses to 5-HT seem to depend upon the nature of the receptors involved, and the recruited neuronal populations (Underwood et al., 1992; Cohen et al., 1996; Foehring et al., 2002).

Serotonin can notably induce a fast excitation of specific interneuron subpopulations through the activation of the 5-hydroxytryptamine 3A receptor (5-HT$_{3A}$) (Ferezou et al., 2002; Lee et al., 2010) which is the only ionotropic serotonergic receptor (Barnes and Sharp, 1999; Chameau and van Hooft, 2006). In the mouse primary somatosensory cortex, the 5-HT$_{3A}$ receptor is expressed by two distinct types of interneurons (Vucurovic et al., 2010). The first one was characterized by a bipolar/bitufted morphology, an adaptative or bursting firing behavior and the

frequent expression of the vasoactive intestinal peptide (VIP), reported to be a vasodilator in the cerebral cortex (McCulloch and Edvinsson, 1980; Yaksh et al., 1987; Dacey et al., 1988), whereas the second population of interneurons includes neurogliaform like regular spiking neurons and therefore frequently expressed the neuropeptide Y (NPY), a potent vasoconstrictor (Dacey et al., 1988; Abounader et al., 1995; Cauli et al., 2004). In rat neocortical slices, it has been shown that electrical stimulation of a single VIP- or NOS/NPY-expressing interneuron was able to induce a dilation of nearby microvessels, probably by releasing vasoactive molecules. Additionally, direct perfusion of VIP or NO donor onto cortical slices dilated blood vessels, whereas perfusion of NPY induced vasoconstrictions (Cauli et al., 2004).

In the present study, we investigated how the pharmacological activation of 5-HT$_{3A}$-expressing interneurons can induce blood vessel diameter changes by means of infrared videomicroscopy on mice cortical slices. We find that activation of 5-HT$_{3A}$-expressing interneurons mostly induced vasodilations mediated by NO release and also, but less frequently, vasoconstrictions through NPY release. Our results show that these interneurons are strategically positioned to transmute incoming neuronal afferent signals into vascular responses.

MATERIALS AND METHODS

ANIMALS AND SURGERY

Animal procedures were conducted in strict compliance with approved institutional protocols and in accordance with the provisions for animal care and use described in the *European Communities Council directive of 24 November 1986 (86-16-09/EEC)*.

C57Bl6J mice (14–21 days old; Charles River) were used for vascular reactivity. All animals were housed in a temperature-controlled (21–25°C) room under daylight conditions. They arrived in the laboratory at least 1 week before initiating experiments to acclimate to their new environment.

Immunohistochemistry was performed on a transgenic mouse line expressing the enhanced green fluorescent protein (GFP) under the control of the 5-HT$_{3A}$ promoter (5-HT3A:GFP). This line, obtained by using modified bacterial artificial chromosomes (BACs) was provided by the GENSAT Consortium (Rockefeller University-GENSAT Consortium; (Heintz, 2004) and maintained under the Swiss genetic background by breeding heterozygous mice. The selective expression of GFP in 5-HT$_3$ expressing neurons has been previously controlled in the cortex of these mice (Lee et al., 2010; Vucurovic et al., 2010).

The Pet1 knock-out mouse line (gift from Evan Deneris, Case Western Reserve University, Cleveland, OH) was maintained on a C57BL6 genetic background. Heterozygous Pet1$^{+/-}$ females were mated with Pet1$^{+/-}$ or Pet1$^{-/-}$ males to produce mixed litters. Genotyping of the progeny was done by PCR analysis of tail DNA as described previously (Hendricks et al., 2003).

IMMUNOHISTOCHEMISTRY

Neuronal populations expressing 5-HT$_{3A}$:GFP were analyzed at postnatal day P18–P25 ($n = 6$). Animals were deeply anesthetized with an intraperitoneal (IP) injection of pentobarbital (150 mg/kg body weight) and perfused transcardially with 4% paraformaldehyde (PFA). Brains were cryoprotected in 30% sucrose and cut on a freezing microtome (35 µm). For immunofluorescence, sections were incubated overnight at 4°C with the following antibodies diluted in phosphate buffer (PS) saline (PBS): chicken anti-GFP (1:1000, Molecular Probes) and rabbit anti-NPY (1:500, Amersham), rabbit anti-VIP (1:800, Incstar) or rabbit anti-nNOS (1:400, Santa-Cruz). After washing in PBS, sections were incubated in alexa 568 conjugated goat anti-rabbit and alexa 488 conjugated goat anti-chicken antibodies (1:300; Molecular Probes).

Sections were rinsed in PB, mounted in Vectashield (Vector) containing 4′,6′-diamidino-2-phenylindole (DAPI) and were observed with a fluorescent microscope (Leica, DMR). Images were acquired with a Coolsnap camera (Photometrics). Quantifications of GFP:5-HT$^+_{3A}$ and NOS$^+$, NPY$^+$, or VIP$^+$ cells were performed at the level of the primary somatosensory cortex, in 500 µm-wide cortical strips (data are expressed as percentages). Three adjacent sections of at least five animals were used.

The estimation of the neuronal density at specific distances from the closest penetrating blood vessel was performed on coronal brain slices (60 µm thick) that were fixed by immersion overnight in PFA. Slices were then rinsed in PBS prior immunolabeling. For immunofluorescence, sections were incubated sequentially overnight at 4°C with the following antibodies diluted in PBS: rabbit anti-GFP (1:1000, Molecular Probes) and goat anti-collagen IV (1:400, Millipore). After washing in PBS, sections were incubated in CY3 conjugated rabbit anti-goat and alexa 488 conjugated chicken anti-rabbit antibodies (1:300; Molecular Probes). Sections were rinsed in PB, mounted in Vectashield (Vector) containing 4′,6′-diamidino-2-phenylindole (DAPI) and were observed with a fluorescent microscope (Zeiss). Images were acquired at the level of the somatosensory cortex with a Zeiss microscope equiped with an AxioCam MRm CDC camera (Zeiss) and three adjacent sections of four animals were used. When two penetrating blood vessels were identified the distance of GFP:5-HT$^+_{3A}$ cells within the region defined by these two blood vessels was determined. The distance from the closest penetrating blood vessel was calculated using Image J software. The distance from the closest blood vessel and the center of two adjacent penetrating blood vessels was subsequentially subdivided in four equal parts. The percentages of 5-HT$_{3A}$:GFP$^+$ cells located within these four radial bins were then calculated.

Some captions were also taken with a Nikon confocal system and maximal projections were used for illustration.

PREPARATION OF ACUTE CORTICAL SLICES

Mice were rapidly decapitated and brains were quickly removed and placed into cold (∼4°C) slicing solution containing (in mM): 110 choline chloride, 11.6 Na-ascorbate, 7 $MgCl_2$, 2.5 KCl, 1.25 NaH_2PO_4, and 0.5 $CaCl_2$, continuously bubbled with 95% O_2–5% CO_2. Coronal brain slices (300 µm thick) containing the primary somatosensory cortex were cut with a vibratome (VT1200S; Leica), and transferred to a holding chamber enclosing artificial cerebrospinal fluid (ACSF) containing (in mM): 126 NaCl, 2.5 KCl, 1.25 NaH_2PO_4, 2 $CaCl_2$, 1 $MgCl_2$,

26 $NaHCO_3$, 20 glucose and 1 kynurenic acid (a nonspecific glutamate receptor antagonist, Sigma), constantly oxygenated (95% O_2–5% CO_2), kept 30 min at 35°C and then held at room temperature. Individual slices were next placed in a submerged recording chamber kept at 32°C and perfused (1.5 ml/min) with oxygenated ACSF (in the absence of kynurenic acid). Blood vessels were visualized using infrared videomicroscopy with Dodt gradient contrast optics (Luigs and Neumann) mounted on an upright microscope (Zeiss) equipped with a CDD camera (Hamamatsu).

DRUGS

The 5-HT$_3$ receptor selective agonist (1-(3-Chlorophenyl) biguanide hydrochloride, mCPBG, 100 μM, Sigma) was used to stimulate specifically 5-HT$_3$-expressing interneurons. To block neuronal synaptic transmission, mCPBG was applied in the presence and after 10 min application of tetrodotoxin (TTX; 1 μM; Latoxan). To block the nNOS, slices were treated for at least 1 h with an irreversible inhibitor of constitutive nitric oxide synthase (nNOS) and a reversible inhibitor of inducible nitric oxide synthase (iNOS), Nω-Nitro-L-arginine (L-NNA; 100 μM; Sigma). NPY Y1 receptors were blocked with the selective antagonist N2-(Diphenylacetyl)-N-[(4-hydroxyphenyl) methyl]-D-arginine amide (BIBP 3226; 100 μM; Sigma). VIP type 1 (VPAC1) receptors of VIP were blocked with the high-affinity, selective antagonist PG-97-269 (100 nM; Biochem, Shanghai). The thromboxane A_2 receptors agonist (9,11-dideoxy-11a,9a-epoxymethanoprostaglandin F2α, U46619, 5 nM, Sigma) was used to pre-constrict the blood vessels.

VASCULAR REACTIVITY

Arterioles remaining in focal plane, exhibiting a well-defined luminal diameter (10–20 μm) and located in the supragranular layers of the somatosensory cortex were selected for vascular reactivity. Images of arterioles were acquired every 15 s (Media Cybernetics). The eventual drift of the images along the time of the recording was corrected on-line for the z-drift and off-line for *x* and *y* directions using Image Pro Plus 7.0. Manual replacement of the images to minimize the differences between two consecutive frames was realized by using a subtraction tool from Image Pro Plus and luminal diameters were quantified at different locations along the blood vessel using custom written routines running within IgorPro (WaveMetrics) to determine the location that moved the most.

Control baselines were determined for 5 min at the start of the recording. Unresponsive blood vessels or vessels with unstable baseline were discarded from the analysis. Vessels were considered unstable when their diameter moved more than 5% during the control baseline. Only one vessel per slice was recorded.

As blood vessels in the slice preparation lack intraluminal flow and pressure (Sagher et al., 1993; Cauli et al., 2004), vasomotor movements were detected in vessels pre-constricted for 10 min with the thromboxane agonist U46619 (5 nM), which was applied throughout the experiment. Only blood vessels that presented a diameter reduction of at least 10% were kept for analyses. The vasoconstriction of blood vessels induced by U46619 followed an exponential progression along the time. This exponential drifting contraction was fitted and subtracted from the recordings using IgorPro.

Maximal vasomotor responses were then expressed as percentages of the mean baseline diameter, which is the averaged diameter measured during the control period of one minute, after correction for the pre-constriction and just before the mCPBG application.

The maximal response diameter was averaged between the fifth and sixth minute after the onset of the mCPBG application for vasodilations and between the fourth and the fifth minute for vasoconstrictions.

STATISTICAL ANALYSES

Data were expressed as mean ± standard error of the mean (SEM). A paired *t*-test was used to determine the statistical significance of vasomotor responses to mCPBG application under the same conditions and a *t*-test was used to determine the statistical significance of response amplitudes between different set of experiments.

RESULTS

DISTRIBUTION OF 5-HT$_{3A}$-EXPRESSING NEURONS AND CO-EXPRESSION OF VASOACTIVE MOLECULES IN TRANSGENIC 5-HT$_{3A}$:GFP MICE

In order to determine the laminar distribution of 5-HT$_3$-expressing interneurons and the vasoactive molecules that they express, we used a reporter mouse strain in which the enhanced GFP expression is under the control of the 5-HT$_{3A}$ promoter (Heintz, 2001). This 5-HT$_{3A}$:GFP mouse line provided by GENSAT shows similar distribution of cortical 5-HT$_{3A}$:GFP$^+$ neurons, compared to the expression pattern of 5-HT$_{3A}$ transcripts observed in wild type animals (Vucurovic et al., 2010). The 5-HT$_3$-expressing interneurons are distributed in all cortical layers (**Figure 1**), with a higher density in supragranular layers.

We next performed immunohistochemical analyses to assess the expression of vasoactive molecules in 5-HT$_{3A}$-expressing interneurons. Within the primary somatosensory cortex, 5-HT$_{3A}$:GFP$^+$ cells frequently co-expressed NPY (31 ± 4.3%), VIP (30.2 ± 5.2% or nNOS (9.8 ± 0.9%; **Figure 2**). These nNOS$^+$/GFP$^+$ cells correspond to 34.4 ± 0.9% of type II nNOS cells (see Perrenoud et al., 2012), whereas no type I nNOS cell were found to express 5-HT$_3$.

The proportion of cells in which GFP was co-detected with one of the three markers is layer dependent (**Figure 2D**). Indeed, VIP$^+$/GFP$^+$ interneurons were preferentially located in layers II-III, while nNOS$^+$/GFP$^+$ and NPY$^+$/GFP$^+$ interneurons were distributed in all cortical layers. These distributions correspond to those recently reported by Lee and collaborators for the NPY and VIP (Lee et al., 2010).

We then determined the relative distribution of 5-HT$_{3A}$:GFP$^+$ neurons in relation with the closest large penetrating blood vessel identified on a coronal section at the level of the somatosensory cortex (17–32 μm, **Figure 3**). This was done in layer I and in layer II were subsequent analyses were performed. In layer I the distribution of 5-HT$_{3A}$:GFP$^+$ cells was homogenous between two penetrating blood vessels (**Figure 3A**). By contrast, in layer II, both multipolar 5-HT$_{3A}$:GFP$^+$ neurons (**Figure 3B**) and bipolar

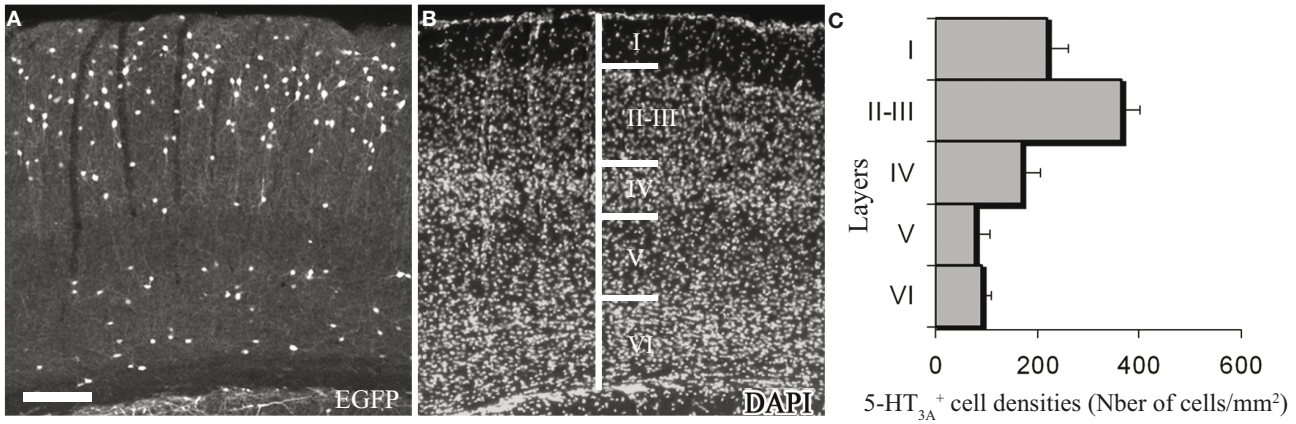

FIGURE 1 | Expression of 5-HT$_{3A}$ within the somatosensory cortex. **(A,B)** Coronal section of a 5-HT$_{3A}$:GFP mouse counterstained with DAPI showing the preferential location of 5-HT$_{3A}$-expressing cells in supragranular layers. **(C)** Density of 5-HT$_{3A}$-expressing cells from transgenic 5-HT$_{3A}$:GFP mice in the different layers of the primary somatosensory cortex. Scale bar: 250 μm.

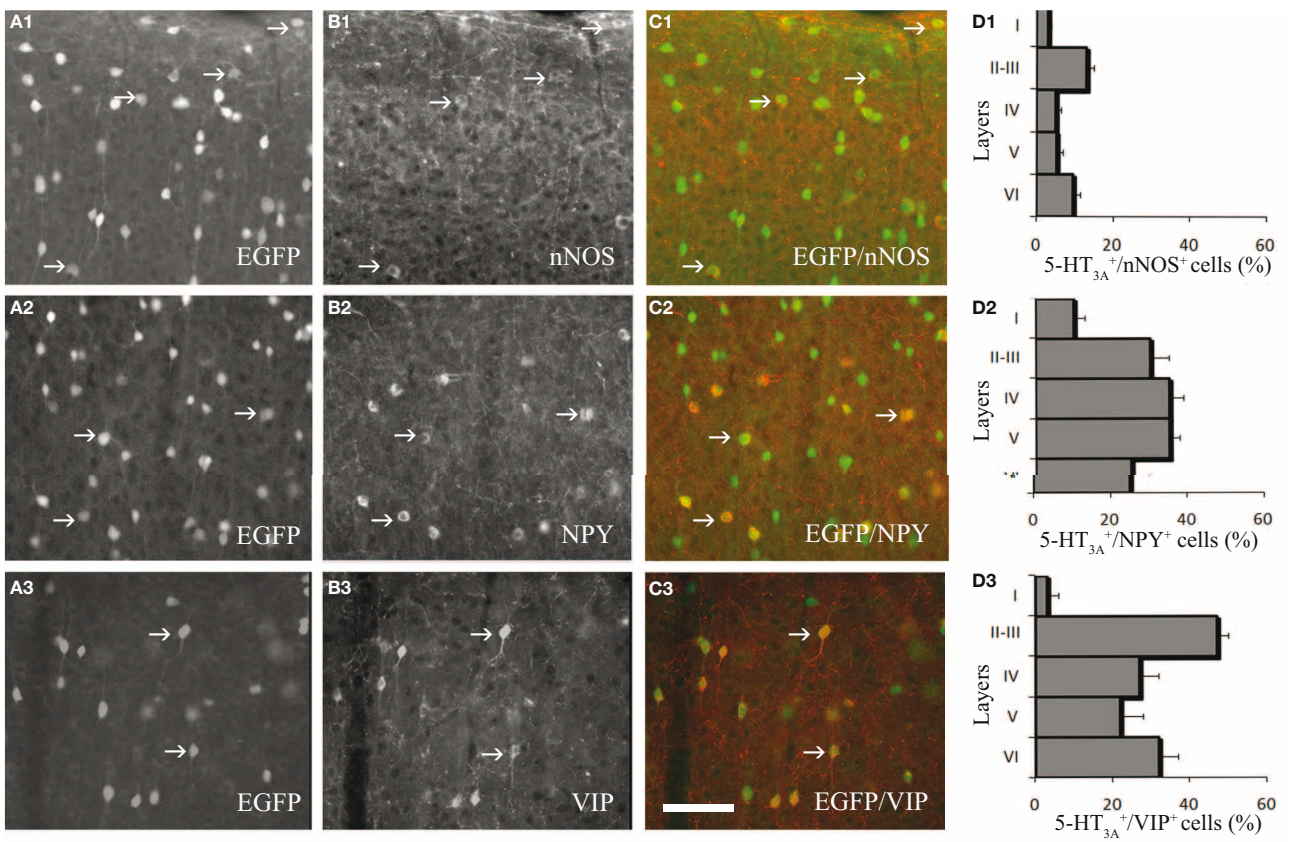

FIGURE 2 | Expression of vasoactive molecules in 5-HT$_{3A}$-expressing interneurons. (A1–3) Immunodetection of GFP-expressing neurons within the primary somatosensory cortex of 5-HT$_{3A}$:GFP$^+$ mice. **(B1–3)** Immunodetection of nNOS (B1), NPY (B2) and VIP (B3) within the same areas as in (A). **(C1–3)** Overlays showing the colocalization of GFP with nNOS (C1), NPY (C2), or VIP (C3). **(D1–3)**, Density of 5-HT$_{3A}$-expressing cells colocalized with nNOS (D1), NPY (D2), or VIP (D3) in the different layers of the somatosensory cortex. Examples of co-labeled neurons are pointed by arrows. Scale bar: 65 μm.

5-HT$_{3A}$:GFP$^+$ neurons (**Figure 3C**) showed an non-uniform distributions as the densities of 5-HT$_{3A}$:GFP$^+$ neurons were higher closest two the penetrating blood vessel (0–25% away from the closest blood vessel) then away from it (75–100% for multipolar 5-HT$_{3A}$:GFP$^+$ neurons, $P < 0.05$ and 50–100% for bipolar 5-HT$_{3A}$:GFP$^+$ neurons, $P < 0.01$).

PHARMACOLOGICAL STIMULATION OF 5-HT$_{3A}$-EXPRESSING INTERNEURONS IN CORTICAL SLICES INDUCES VASOMOTOR MOVEMENTS RECORDED BY INFRARED VIDEOMICROSCOPY

The stimulation of GABAergic interneurons can induce vasomotricity via the production of vasoactive substances such as VIP, NPY, or nitric oxide (NO), a highly diffusible gas which is known to be a potent vasodilator (Estrada and DeFelipe, 1998; Cauli et al., 2004; Rancillac et al., 2006). Here we investigated the functional role of 5-HT$_3$-expressing interneurons in the control of vascular tone within the supragranular layers of the cortex. In this aim, we applied a 5-HT$_3$R selective agonist mCPBG (100 μM) for 6 min, directly onto acute slices while recording associated blood vessel movements using infrared videomicroscopy. We focused our study on penetrating arterioles that are known to be of prime importance in feeding deeply located microvessels and neurons (Nishimura et al., 2007). Well defined arterioles of supragranular layers were therefore selected for quantitative analyses. As blood vessels in the slice preparation lack intraluminal flow and pressure (Sagher et al., 1993; Cauli et al., 2004), vasomotor changes were detected in pre-constricted arterioles using the thromboxane agonist U46619 (5 nM) throughout the experiment. When bath applied, mCPBG (100 μM) induced

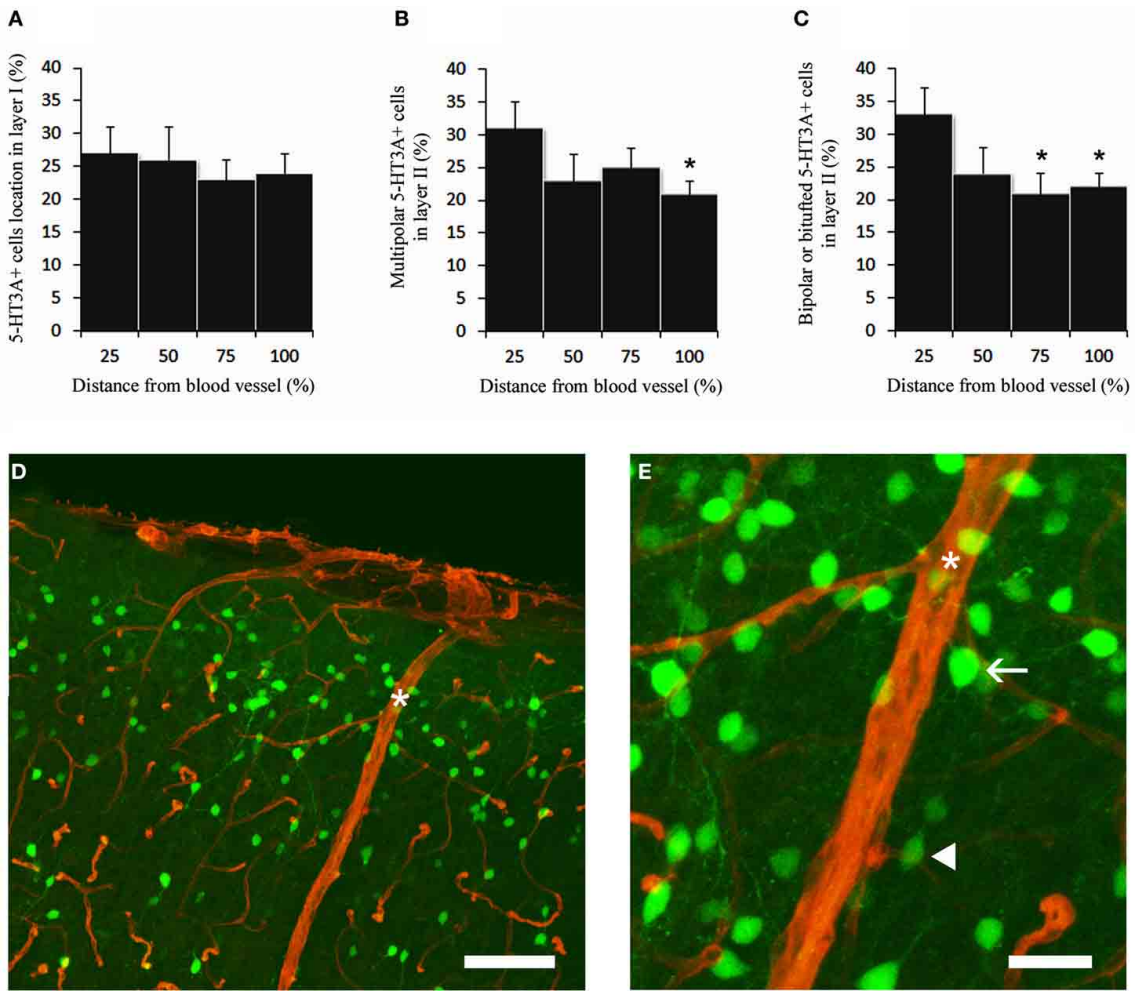

FIGURE 3 | 5-HT$_{3A}$:GFP$^+$ neurons in relation with the closest large penetrating blood vessel. (A) In layer I, 5-HT$_{3A}$:GFP$^+$ neurons do not show specific preferences to be located close to large penetrating blood vessels. **(B,C)** By contrast in layer II multipolar and bipolar/bitufted 5-HT$_{3A}$:GFP$^+$ neurons are preferentially positioned in the vicinity of penetrating blood vessels. **(D)** Confocal picture of a coronal section taken at the level of the supragranular layers of the somatosensory cortex showing the distribution of 5-HT$_{3A}$:GFP$^+$ neurons (green) in relation with blood vessels stained by collagen IV (red). Large penetrating blood vessel is indicated by a star. **(E)** Higher power view of the caption shown in **(D)**. The arrow points to a multipolar 5-HT$_{3A}$:GFP$^+$ neurons displaying a large soma. The filled arrowhead points to a bipolar 5-HT$_{3A}$:GFP$^+$ neurons displaying a fusiform shape. Scale bars: (D) 130 μm; (E) 35 μm.

either reversible vasodilations ($111.11 \pm 3.03\%$ over baseline, $n = 9/17$; $P < 0.01$; **Figures 4A** and **B**) or reversible vasoconstrictions ($90.04 \pm 3.15\%$ over baseline, $n = 4/17$; $P < 0.05$; **Figures 4C** and **D**).

VASODILATIONS ARE MAINLY MEDIATED BY NO WHEREAS VASOCONSTRICTIONS ARE DUE TO NPY RELEASE

We hypothesized that mCPBG induced vasodilation could be due to NO and/or VIP release by 5-HT$_{3A}$R-interneurons, whereas vasoconstriction could be caused by NPY release. To determine the molecular events underlying vasomotor changes, we successively blocked different possible mechanisms. Lowering basal NO levels by treatment with the constitutive nNOS inhibitor L-NNA (100 μM) strongly reduced the proportion of vasodilations observed in response to mCPBG applications from 69% in control conditions to 11% ($n = 1/9$) and favored vasoconstrictions from 31% in control condition to 80% (93.83 ± 1.60 of baseline diameter; $n = 4/9$, $P < 0.01$) (**Figures 5A** and **6**).

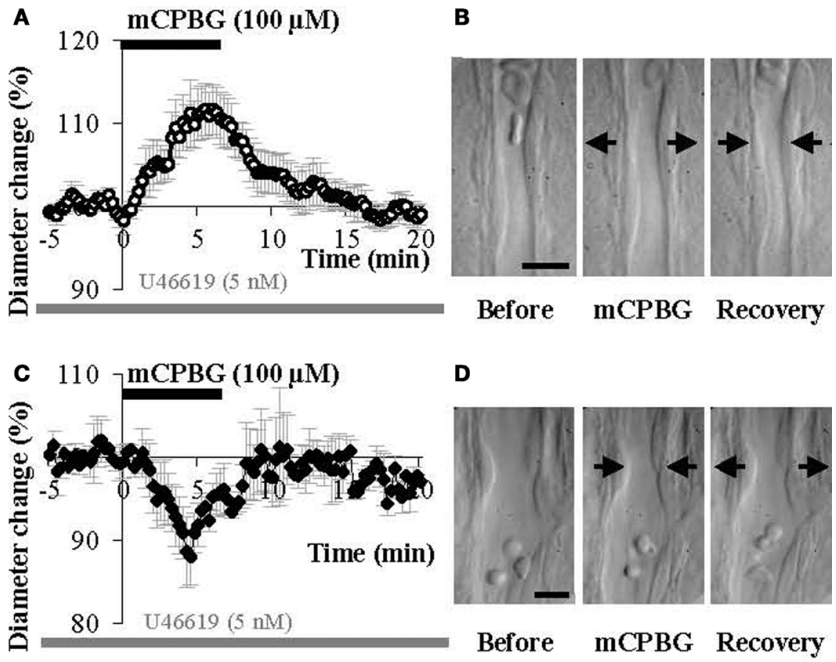

FIGURE 4 | mCPBG induces both vasodilations and vasoconstrictions in somatosensory cortical slices. (A) Mean vascular dilation ($n = 9$) induced by mCPBG (100 μM). **(B)** Infrared images of a penetrating blood vessel that reversibly dilated in response to bath application of mCPBG (100 μM). Arrows indicate region of high vascular reactivity. **(C)** Mean vascular constriction ($n = 4$) induced by mCPBG (100 μM). **(D)** Infrared images of a penetrating blood vessel that reversibly constricted in response to bath application of mCPBG (100 μM). Scale bar: 10 μm.

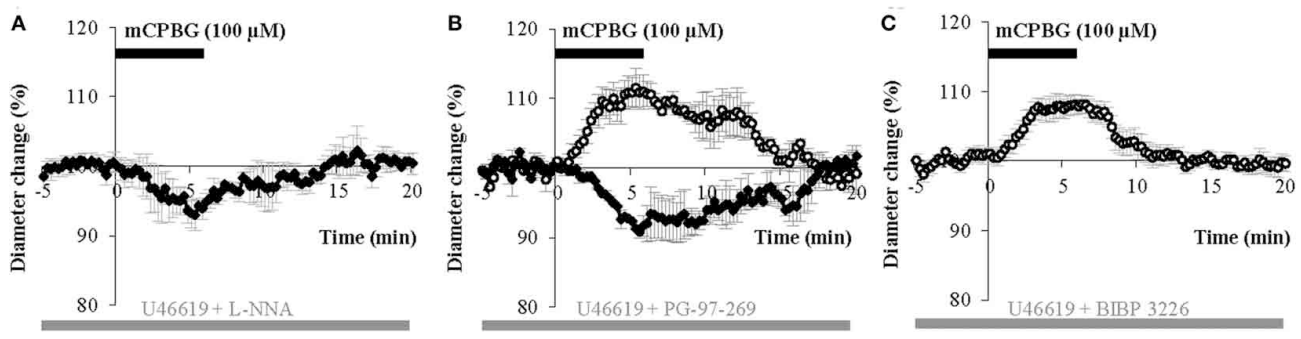

FIGURE 5 | mCPBG induced vasodilations are mediated by NO while constrictions are mediated by NPY. (A) Mean vasoconstriction ($n = 4$) induced by mCPBG (100 μM) in the presence of nNOS inhibitor L-NNA (100 μM) and the preconstricting agent U46619 (5 nM). **(B)** Mean vascular dilation ($n = 4$; white circle) and mean vascular constriction ($n = 2$; black diamond) induced by mCPBG (100 μM) in the presence of the VIP receptor VPAC1 antagonist PG-97-269 (100 nM) and U46619 (5 nM). **(C)** Vasodilation ($n = 9$) induced by mCPBG (100 μM) in the presence of the NPY Y1 receptor antagonist BIBP 3226 (1 μM) and U46619 (5 nM).

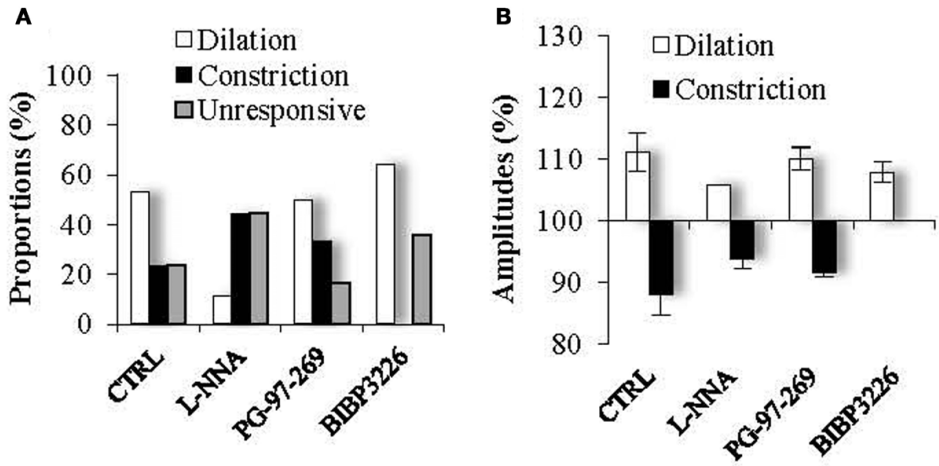

FIGURE 6 | Proportions (A) and amplitudes (B) of dilating or constricting blood vessels in control condition (CTRL) and in the presence of the pharmacological blockers used in Figure 5. Note that in presence of the nNOS inhibitor, L-NNA, as in the presence the Y1 NPY receptor antagonist, BIBP 3226, the occurrence of dilations *versus* contractions was reduced or favored respectively, without impacting their amplitudes. On the opposite, in the presence of the VPAC1 receptor antagonist of VIP, PG-97-269, no changes were observed compared to control conditions.

These results suggest that mCPBG-induced vasodilations are mostly mediated by NO release. The remaining vasodilation observed in the presence of L-NNA could be mediated by VIP release. However, in the presence of the VIP receptor VPAC1 antagonist, PG-97-269 (100 nM), mCPBG application induced 60% of vasodilations ($110.01 \pm 1.87\%$; $n = 3/6$; $P < 0.05$) and 40% of vasoconstrictions (92.04 ± 0.61; $n = 2/6$; $P < 0.05$) of similar proportions and amplitudes compared to control conditions (**Figures 5B** and **6**). Then, to determine the molecular pathway underlying vasoconstrictions, treatment of mCPBG was reproduced in the presence of NPY Y1 receptor antagonist (BIBP 3226, 1 μM). Indeed, vasoconstrictions mediated by NPY are known to be mediated by smooth muscle NPY Y1 vascular receptor (Abounader et al., 1999). Under BIBP 3226, constrictions where blocked and only dilations ($108.28 \pm 1.62\%$; $n = 9/14$; $P < 0.01$) could be recorded (**Figures 5C** and **6**). Amplitudes of vasomotor responses under these different conditions were not statistically different from control condition (**Figure 6B**). Altogether, these data strongly suggest that pharmacological stimulations of 5-HT$_{3A}$-expressing interneurons mainly induce vasodilations through NO release, whereas they induce to a less extensive vasoconstrictions through NPY release and activation of its Y1 receptor.

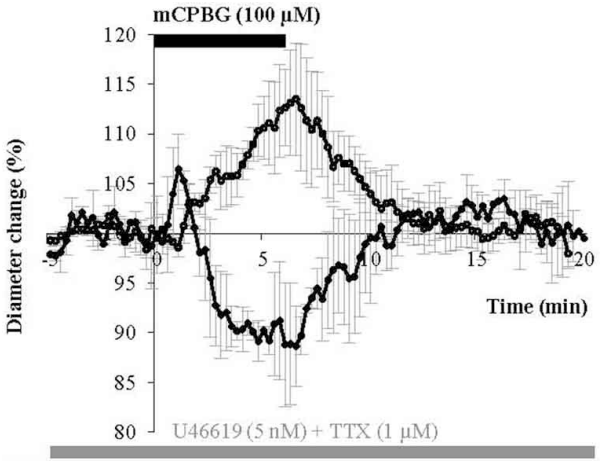

FIGURE 7 | mCPBG induces TTX-insensitive vasodilations and vasoconstrictions. Mean vascular dilation ($n = 5$) and constriction ($n = 2$) induced by mCPBG (100 μM) in the presence of TTX (1 μM) and U46619 (5 nM).

TTX-INSENSITIVE PEPTIDERGIC AND NO RELEASE

It is assumed that peptidergic release requires repetitive action potentials at high frequencies (Zupanc, 1996; Ludwig and Pittman, 2003; Baraban and Tallent, 2004) and that nNOS activation depends on Ca^{2+} entry (Garthwaite, 2008). Therefore, we tested mCPBG stimulation in the presence of tetrodotoxin (TTX, 1 μM) to block action potential generation and propagation. However, this treatment failed to prevent mCPBG-induced vasodilations ($111.45 \pm 4.81\%$; $n = 5/10$, $P < 0.05$) or vasoconstrictions ($90.04 \pm 2.1\%$; $n = 2/10$, $P < 0.05$), (**Figure 7**). This suggests that the vasomotor changes observed in response to 5-HT$_3$R activation may depend on the Ca^{2+} influx through 5-HT$_3$R rather than on action potential generation.

ORIGIN OF 5-HT$_3$R INDUCED NO RELEASE

In the neocortex the 5-HT$_{3A}$R is exclusively located on GABAergic interneurons (Morales and Bloom, 1997; Ferezou et al., 2002; Chameau and van Hooft, 2006; Vucurovic et al., 2010). However, 5-HT inputs from the raphe also express presynaptic 5-HT$_{3A}$Rs regulating neurotransmitter release (Jackson and Yakel, 1995; Roerig et al., 1997; Nayak et al., 1999). As the presence of NOS in 5-HT-containing axons from dorsal raphe has been already reported in the somatosensory cortex (Simpson et al., 2003) the pharmacological stimulation of 5-HT$_3$Rs realized

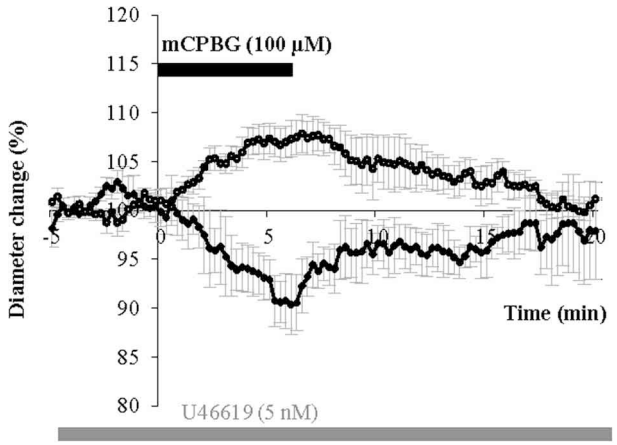

FIGURE 8 | mCPBG induces vasodilations and vasoconstrictions in Pet1$^{-/-}$ mice. Mean vasodilation ($n = 6$) and vasoconstriction ($n = 3$) induced by mCPBG (100 µM) in Pet1$^{-/-}$ mice.

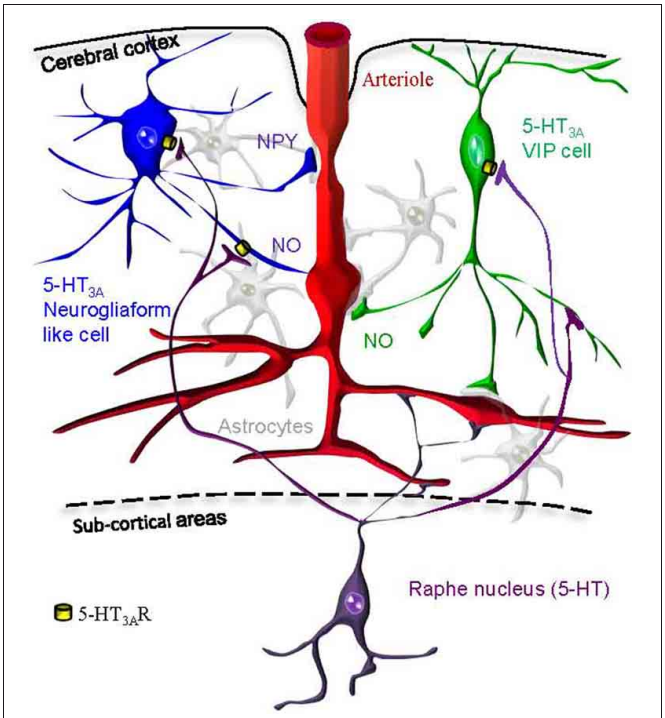

FIGURE 9 | Hypothetical schematic representation of the 5-HT$_{3A}$R induction of neurovascular coupling within the somatosensory cortex. We find that pharmacological stimulation of 5-HT$_{3A}$-expressing neurogliaform like cells (in blue) or VIP cells (in green) could either lead to vasodilation via NO release or vasoconstriction via NPY release. Cortical penetrating arterioles (in red) are also directly innervated by serotoninergic fibers originating from raphe nuclei (in purple). Astrocytes are shown in gray.

in this study could also have induced NO release from the NOS-containing fibers originating from raphe nuclei. In order to evaluate the contribution of such a NO release in our experiments, we used Pet1$^{-/-}$ (Pheochromocytoma 12 ETS factor-1) knock-out mice, in which raphe projections to the somatosensory cortex were found to be strongly reduced (Hendricks et al., 1999; Liu et al., 2010). In this mutant mice, we found that pharmacological stimulation of 5-HT$_3$R could still induce vasodilations ($107.07 \pm 1.67\%$; $n = 6/11$, $P < 0.01$) or vasoconstrictions ($93.45 \pm 2.60\%$; $n = 3/11$, $P < 0.05$), (**Figure 8**). These vasomotor changes were not significantly different than those induced in control condition neither in amplitude nor in proportion (from 69 to 67% for vasodilations and from 31 to 33% for vasoconstrictions), suggesting a postsynaptic origin of NO release.

DISCUSSION

5-HT$_{3A}$-expressing interneurons are composed of two different populations: neurogliaform like interneurons expressing NPY and bipolar/bitufted interneurons expressing VIP that are likely candidates to control cortical blood vessels tonus via neuronally derived vasoactive messengers. In this article we show that in supragranular layers of the mouse somatosensory cortex, pharmacological activation of 5-HT$_3$-expressing interneurons can release of NO to dilate, or NPY to constrict arterioles (**Figure 9**).

5-HT$_{3A}$R ACTIVATION INDUCES VASCULAR RESPONSES THROUGH THE ACTIVATION OF SPECIFIC GABAergic INTERNEURONS SUBPOPULATIONS

The mechanisms underlying the vasoactive action of serotonin in the cerebral cortex are not completely understood at present time. Our results demonstrate that the selective activation of the ionotropic 5-HT receptor, 5-HT$_3$R, induces a complex vascular response including both local vasoconstrictions and vasodilations.

These vasomotor changes are not mediated by the presynaptic 5-HT$_3$R activation of serotonergic axons originating from raphe nuclei that could potentially release vasoactive substances. Indeed, they were also observed in Pet-1$^{-/-}$ knock-out mice, which display a drastic depletion of cortical serotoninergic fibers (Hendricks et al., 1999; Liu et al., 2010; Kiyasova et al., 2011). Conversely, our hypothesis is that a specific activation of local 5-HT$_{3A}$-expressing GABAergic interneurons is responsible for the observed vasomotor responses.

Indeed, it has been reported that 5-HT$_{3A}$ expression is confined to GABAergic interneurons in both rat and primate cerebral cortex (Morales and Bloom, 1997; Jakab and Goldman-Rakic, 2000; Ferezou et al., 2002). This has been recently confirmed in the mouse somatosensory cortex since neither the pyramidal cell marker Satb2 nor the oligodendrocyte marker Olig2 could be detected in 5-HT$_{3A}$-expressing cells (Lee et al., 2010).

5-HT$_{3A}$-expressing interneurons constitutes nearly 30% of the total interneuronal population (Rudy et al., 2011), which accounts for ∼15% of the overall cortical neurons in rodents (Beaulieu, 1993; Gabbott et al., 1997). Using an unsupervised cluster analysis based on 28 electrophysiological parameters, we have shown in a previous study (Vucurovic et al., 2010) that 5-HT$_{3A}$-expressing interneurons are segregated into two distinct subpopulations within the somatosensory cortex. The first one was characterized by the frequent expression of the NPY (87%)

and a multipolar morphology, while the second one expressed frequently the VIP (73%), and presented a bipolar somatodendritic shape. Subsequently, in an article published in 2010, Lee et al. have suggested, based on immunohistochemical analyses and electrophysiological recordings, a much broader diversity of the 5-HT$_{3A}$-expressing neuronal population. Indeed, analyzing the intrinsic membrane properties and the morphology of these neurons, they distinguished seven types of 5-HT$_{3A}$-expressing interneurons. Although our separation of these neurons in two subpopulations could therefore appear restrictive; we consider it is meaningful since it relies on a solid statistical classification analysis (unsupervised clustering). However, we do not exclude the existence of some diversity within these two groups.

In the present study, we analyzed the laminar distribution of these neuronal populations. We observed that the cell bodies of more than two-thirds of these interneurons were positioned within superficial layers (L1, $13 \pm 0.9\%$; L2/3, $51 \pm 1.2\%$) in agreement with what was recently described (Lee et al., 2010; Vucurovic et al., 2010). We further revealed that the nNOS is also expressed by a subset of 5-HT$_{3A}$-expressing interneurons. These neurons corresponded to type II NOS$^+$ cells, since they were smaller than type I and weakly immunohistochemically-stained for nNOS (Yan et al., 1996; Cho et al., 2010; Perrenoud et al., 2012). Thus, the distribution and the expression of vasoactive substances within 5-HT$_{3A}$-expressing interneurons put them in a unique position to induce a fast and effective modulation of vascular tone in response to 5-HT.

DUAL ROLE OF 5-HT$_{3A}$-EXPRESSING INTERNEURONS ON VASOMOTOR CONTROL

In line with our finding that 5-HT$_{3A}$-expressing interneurons produce several vasoactive substances, our results indicate that their activation induces a complex vascular response. Indeed the selective 5-HT$_3$R agonist mCPBG induced either constrictions (30%) or dilations (70%) of penetrating arterioles within supragranular layers. All vasoconstrictions were abolished in the presence of the NPY receptor antagonist (BIBP 3226), suggesting that they were elicited by NPY release. Conversely, mCPBG-induced dilations were blocked in the presence of a nNOS inhibitor suggesting that NO is the predominant messenger inducing the vasodilation, in line previous studies performed in the cerebellum (Yang et al., 1999, 2000; Rancillac et al., 2006) and in the cortex (Estrada and DeFelipe, 1998; Lovick et al., 1999; Brown et al., 2000; Tong and Hamel, 2000; Cauli et al., 2004; Liu et al., 2008; Rancillac et al., 2012). Interestingly, a recent study on epileptic seizures has revealed that 5-HT$_3$ activation can stimulate NO synthesis (Gholipour et al., 2010).

The NPY-mediated constrictions confirm and extend prior studies implicating NPY in vasoconstrictions (Dacey et al., 1988; Abounader et al., 1995; Cauli et al., 2004) and are likely to be caused by the activation of NPY/5-HT$_{3A}$-expressing neurogliaform-like cells (Lee et al., 2010; Vucurovic et al., 2010).

On the other hand, it has been shown that neurogliaform cells substantially express nNOS (Karagiannis et al., 2009; Kubota et al., 2011; Perrenoud et al., 2012) and are thus well positioned to mediate NO-induced vasodilations. In addition, we have recently found that a significant proportion of nNOS type II cells express VIP (Perrenoud et al., 2012). Therefore, a subset of VIP/5-HT$_3$-expressing cells could also release NO following 5-HT$_{3A}$R stimulation (**Figure 9**).

5-HT$_{3A}$-nNOS-expressing interneurons could also form a small third class of 5-HT$_{3A}$-expressing interneurons that express neither NPY nor VIP. Although this population has not been isolated with the cluster analysis of these interneurons (Vucurovic et al., 2010), further triple immunolabeling would be necessary to assess this possibility.

Unexpectedly, although VIP is present in 5-HT$_{3A}$-expressing interneurons, the mCPBG-induced dilations persisted in the presence of the VIP receptor VPAC1 antagonist, suggesting that VIP release acting on VPAC1 receptors is not involved in this response. This was surprising since the VPAC1 receptor is a postsynaptic receptor predominantly and uniformly expressed by smooth muscle cells in cerebral arteries and arterioles (Fahrenkrug et al., 2000) and that direct perfusion of VIP as well as electrical stimulation of a single VIP-expressing interneuron have been reported to dilate microvessels onto rat slices (Cauli et al., 2004). Moreover, both light and electron microscopy have revealed that some VIP$^+$ neurons are closely associated with blood vessels, providing a neuroanatomic substrate for the role of VIP in the regulation of cerebral blood circulation in the rat cerebral cortex (Eckenstein and Baughman, 1984; Chédotal et al., 1994a,b; Fahrenkrug et al., 2000).

In the presence of a nNOS inhibitor, one dilation out of nine tested blood vessels was still observed (**Figure 6A**). This dilation could have been mediated by an activation of perivascular astrocytes resulting from the evoked action potential discharge of 5-HT$_3$ interneurons. Indeed, astrocytes are known as cellular intermediaries that couple neuronal activity to local blood flow changes through the phospholipase A_2 (PLA_2)-mediated synthesis of arachidonic acid, which leads to production of prostaglandins and epoxyeicosatrienoic acids (Petzold and Murthy, 2011). However, Kitaura et al. (2007) have shown that hindpaw stimulation-induced cortical vasodilations were suppressed in mice lacking nNOS, while they were unchanged in mice lacking cytosolic phospholipase A2 alpha (cPLA2α).

Together, our observations that in the somatosensory cortex a selective 5-HT$_3$R agonist induce NO mediated vasodilations confirms and extends prior studies reinforcing the central role of NO in the neurovascular coupling.

TTX-INSENSITIVE VASOMOTOR CHANGES

The cellular mechanisms underlying the release of vasoactive compounds within the cortex are still poorly considered. Here we observed that the vascular responses induced by 5-HT$_{3A}$R activation were unaffected by the bath application of TTX. This result indicates that the release of NO, NPY, and VIP by 5-HT$_3$-expressing interneurons is independent of subthreshold activity, raising the question of the mode of secretion of these molecules in the neutrophil.

Studies of hypothalamic neuroendocrine cells indicate that neuropeptides are confined to large dense-core vesicles and

released from dendrites and axons (Ludwig and Pittman, 2003) following high intracellular Ca^{2+} concentrations (Kits and Mansvelder, 2000). Action potentials originating at the neuronal soma trigger neuropeptide release from terminals, whereas Ca^{2+} release from intracellular stores signals dendritic peptide release (Ludwig et al., 2002). Similarly, the nNOS enzyme, which immunoreactivity spreads throughout the cytoplasm of neuronal cell bodies and their processes (Batista et al., 2001), is well known to be activated by Ca^{2+} associated with calmodulin (Bredt et al., 1991).

Therefore, if these mechanisms are conserved within the cortex, NPY and NO release should also be dependent on high intracellular Ca^{2+} concentrations influx. Since 5-HT$_{3A}$Rs are predominantly expressed at the somatodendritic level in the cortex (Morales et al., 1996; Jakab and Goldman-Rakic, 2000), our study indicates that the application of mCPBG is likely to evoke enough intracellular Ca^{2+} influx through 5-HT$_{3A}$R to induce Ca^{2+} release from intracellular stores and trigger NPY and NO release.

Several lines of evidence support this hypothesis. In heterologous expression systems, the Ca^{2+} permeability of the 5-HT$_3$R has been reported to be enhanced by co-assembly of the 5-HT$_{3A}$ subunit with the α-4 subunit of the nicotinic acetylcholine receptor (van Hooft et al., 1998; Sudweeks et al., 2002). The existence of functional heteromeric 5-HT$_{3A/}$nACh$_{α4}$ receptors has been described in CA1 hippocampal interneurons (Sudweeks et al., 2002). Lee et al. (2010), recently reported that in the mouse somatosensory cortex, like in the rat somatosensory cortex (Ferezou et al., 2002), 5-HT$_{3A}$-expressing neurons respond to both 5-HT$_3$R and nAChR agonists. Hence, heteromeric 5-HT$_{3/}$nACh$_{α4}$ receptors are probably present on the membrane of cortical 5-HT$_{3A}$-expressing interneurons and potentiate the Ca^{2+} influx evoked by the mCPBG. Altogether, these results suggests that NPY and NO release were not triggered by action potential generation, but rather by direct Ca^{2+} entry through homomeric or heteromeric 5-HT$_{3A}$R channels in response to mCPBG application, supporting the fact that TTX blocked neither NO nor neuropeptides induced vasomotor responses.

IMPACT OF 5-HT$_{3A}$-EXPRESSING INTERNEURONS ACTIVATION ON THE CORTICAL NETWORK

In vitro electrophysiological studies have shown that ionotropic serotonergic receptor agonists induce a fast excitation of 5-HT$_{3A}$-expressing interneurons through the activation of postsynaptic somatodendritic receptors (Porter et al., 1999; Zhou and Hablitz, 1999; Ferezou et al., 2002; Lee et al., 2010). This activation is likely to have inhibitory impact on the cortical network. Indeed, because supragranular interneurons innervate pyramidal cells, their activation will induce inhibitory post-synaptic currents in pyramidal neurons and thus inhibits their firing activity (Zhou and Hablitz, 1999; Moreau et al., 2010).

Nonetheless, the physiological release of 5-HT by the fibers originating from the raphe nuclei activate not only 5-HT$_{3A}$Rs, but also metabotropic serotonin receptors subtypes that are divided into six classes (5-HT$_1$R, 5-HT$_2$R, and 5-HT$_4$R–5-HT$_7$R) (Hoyer et al., 1994; Walstab et al., 2010; Pytliak et al., 2011). The consequences of intracerebrally released 5-HT, both on the cortical network activity and on the CBF will be based on its various actions through different 5-HTRs (Cohen et al., 1996; Andrade, 2011). Indeed, 5-HT has been reported to have both inhibitory and excitatory effects on the cortical network (Krnjevic and Phillis, 1963; Reader, 1978; Waterhouse et al., 1990; Zhou and Hablitz, 1999; Puig et al., 2005), while it has a negative impact on the CBF in the neocortex through a major vasoconstrictor role of 5-HT through 5-HT$_{1B}$ receptors (Cohen et al., 1996; Riad et al., 1998).

CONCLUSION

Altogether, this study indicates that 5-HT$_{3A}$-expressing interneurons occupy a strategic position in superficial layers to convey fast effects of serotonergic modulation, thus modulating cortical network activity and blood supply. The brainstem 5-HT pathway, in addition to its direct projections and vasomotor effects on cortical blood vessels, can use 5-HT$_{3A}$-expressing interneurons to control and adapt CBF. These results suggest that blood flow could be enhanced prior to the onset of any metabolic deficit, reinforcing the "neurogenic" hypothesis of the neurovascular coupling versus the "metabolic" one (Rossier, 2009).

ACKNOWLEDGMENTS

We thank Alain Couvineau (U773) for the generous gift of PG-97-269, Evan Deneris for the gift of the Pet-1$^{-/-}$ mice, Patricia Gaspar for maintaining the Pet-1$^{-/-}$ line and providing the animals. We are grateful to Marcel Leopoldie for excellent animal husbandry and Raphael Tomasi and Céline Boisserie for technical support. This work was supported by the French National Research Agency (ANR-06-NEURO-033-01grant), ESPCI ParisTech., CNRS and Inserm.

REFERENCES

Abounader, R., Elhusseiny, A., Cohen, Z., Olivier, A., Stanimirovic, D., Quirion, R., and Hamel, E. (1999). Expression of neuropeptide Y receptors mRNA and protein in human brain vessels and cerebromicrovascular cells in culture. *J. Cereb. Blood Flow Metab.* 19, 155–163.

Abounader, R., Villemure, J. G., and Hamel, E. (1995). Characterization of neuropeptide Y (NPY) receptors in human cerebral arteries with selective agonists and the new Y1 antagonist BIBP 3226. *Br. J. Pharmacol.* 116, 2245–2250.

Andrade, R. (2011). Serotonergic regulation of neuronal excitability in the prefrontal cortex. *Neuropharmacology* 61, 382–386.

Ascoli, G. A., Alonso-Nanclares, L., Anderson, S. A., Barrionuevo, G., Benavides-Piccione, R., Burkhalter, A., Buzàki, G., Cauli, B., Defelipe, J., Faién, A., Feldmeyer, D., Fishell, G., Fregnac, Y., Freund, T. F., Gardner, E. P., Goldberg, J. H., Helmstaedter, M., Hestrin, S., Karube, F., Kisvàrday, Z. F., Lambolez, B., Lewis, D. A., Marin, O., Markram, H., Munoz, A., Packer, A., Petersen, C. C., Rockland, K. S., Rossier, J., Rudy, B., Somogy, P., Staiger, J. F., Tamas, G., Thomson, A. M., Toledo-Rodriguez, M., Wang, Y., West, D. C., and Yuste, R. (2008). Petilla terminology: nomenclature of features of GABAergic interneurons of the cerebral cortex. *Nat. Rev. Neurosci.* 9, 557–568.

Baraban, S. C., and Tallent, M. K. (2004). Interneuron diversity series: interneuronal neuropeptides–

endogenous regulators of neuronal excitability. *Trends Neurosci*. 27, 135–142.

Barnes, N. M., and Sharp, T. (1999). A review of central 5-HT receptors and their function. *Neuropharmacology* 38, 1083–1152.

Batista, C. M., De Paula, K. C., Cavalcante, L. A., and Mendez-Otero, R. (2001). Subcellular localization of neuronal nitric oxide synthase in the superficial gray layer of the rat superior colliculus. *Neurosci. Res*. 41, 67–70.

Beaulieu, C. (1993). Numerical data on neocortical neurons in adult rat, with special reference to the GABA population. *Brain Res*. 609, 284–292.

Bredt, D. S., Glatt, C. E., Hwang, P. M., Fotuhi, M., Dawson, T. M., and Snyder, S. H. (1991). Nitric oxide synthase protein and mRNA are discretely localized in neuronal populations of the mammalian CNS together with NADPH diaphorase. *Neuron* 7, 615–624.

Brown, L. A., Key, B. J., and Lovick, T. A. (2000). Fluorescent imaging of nitric oxide production in neuronal varicosities associated with intraparenchymal arterioles in rat hippocampal slices. *Neurosci. Lett*. 294, 9–12.

Cauli, B., Audinat, E., Lambolez, B., Angulo, M. C., Ropert, N., Tsuzuki, K., Hestrin, S., and Rossier, J. (1997). Molecular and physiological diversity of cortical nonpyramidal cells. *J. Neurosci*. 17, 3894–3906.

Cauli, B., and Hamel, E. (2010). Revisiting the role of neurons in neurovascular coupling. *Front. Neuroenergetics* 2:9. doi: 10.3389/fnene.2010.00009

Cauli, B., Tong, X. K., Rancillac, A., Serluca, N., Lambolez, B., Rossier, J., and Hamel, E. (2004). Cortical GABA interneurons in neurovascular coupling: relays for subcortical vasoactive pathways. *J. Neurosci*. 24, 8940–8949.

Chameau, P., and van Hooft, J. A. (2006). Serotonin 5-HT(3) receptors in the central nervous system. *Cell Tissue Res*. 326, 573–581.

Chédotal, A., Cozzari, C., Faure, M. P., Hartman, B. K., and Hamel, E. (1994a). Distinct choline acetyltransferase (ChAT) and vasoactive intestinal polypeptide (VIP) bipolar neurons project to local blood vessels in the rat cerebral cortex. *Brain Res.* 646, 181–193.

Chédotal, A., Umbriaco, D., Descarries, L., Hartman, B. K., and Hamel, E. (1994b). Light and electron microscopic immunocytochemical analysis of the neurovascular relationships of choline acetyltransferase and vasoactive intestinal polypeptide nerve terminals in the rat cerebral cortex. *J. Comp. Neurol*. 343, 57–71.

Cho, K. H., Jang, J. H., Jang, H. J., Kim, M. J., Yoon, S. H., Fukuda, T., Tennigkeit, F., Singer, W., and Rhie, D. J. (2010). Subtype-specific dendritic Ca(2+) dynamics of inhibitory interneurons in the rat visual cortex. *J. Neurophysiol*. 104, 840–853.

Cohen, Z., Bonvento, G., Lacombe, P., and Hamel, E. (1996). Serotonin in the regulation of brain microcirculation. *Prog. Neurobiol*. 50, 335–362.

Dacey, R. G. Jr., Bassett, J. E., and Takayasu, M. (1988). Vasomotor responses of rat intracerebral arterioles to vasoactive intestinal peptide, substance P, neuropeptide Y, and bradykinin. *J. Cereb. Blood Flow Metab*. 8, 254–261.

DeFelipe, J., Hendry, S. H., Hashikawa, T., and Jones, E. G. (1991). Synaptic relationships of serotonin-immunoreactive terminal baskets on GABA neurons in the cat auditory cortex. *Cereb. Cortex* 1, 117–133.

Eckenstein, F., and Baughman, R. W. (1984). Two types of cholinergic innervation in cortex, one co-localized with vasoactive intestinal polypeptide. *Nature* 309, 153–155.

Estrada, C., and DeFelipe, J. (1998). Nitric oxide-producing neurons in the neocortex: morphological and functional relationship with intraparenchymal microvasculature. *Cereb. Cortex* 8, 193–203.

Fahrenkrug, J., Hannibal, J., Tams, J., and Georg, B. (2000). Immunohistochemical localization of the VIP1 receptor (VPAC1R) in rat cerebral blood vessels: relation to PACAP and VIP containing nerves. *J. Cereb. Blood Flow Metab*. 20, 1205–1214.

Fanselow, E. E., and Connors, B. W. (2010). The roles of somatostatin-expressing (GIN) and fast-spiking inhibitory interneurons in UP-DOWN states of mouse neocortex. *J. Neurophysiol*. 104, 596–606.

Ferezou, I., Cauli, B., Hill, E. L., Rossier, J., Hamel, E., and Lambolez, B. (2002). 5-HT3 receptors mediate serotonergic fast synaptic excitation of neocortical vasoactive intestinal peptide/cholecystokinin interneurons. *J. Neurosci*. 22, 7389–7397.

Foehring, R. C., Van Brederode, J. F., Kinney, G. A., and Spain, W. J. (2002). Serotonergic modulation of supragranular neurons in rat sensorimotor cortex. *J. Neurosci*. 22, 8238–8250.

Gabbott, P. L., Dickie, B. G., Vaid, R. R., Headlam, A. J., and Bacon, S. J. (1997). Local-circuit neurones in the medial prefrontal cortex (areas 25, 32 and 24b) in the rat: morphology and quantitative distribution. *J. Comp. Neurol*. 377, 465–499.

Garthwaite, J. (2008). Concepts of neural nitric oxide-mediated transmission. *Eur. J. Neurosci*. 27, 2783–2802.

Gentet, L. J., Avermann, M., Matyas, F., Staiger, J. F., and Petersen, C. C. (2010). Membrane potential dynamics of GABAergic neurons in the barrel cortex of behaving mice. *Neuron* 65, 422–435.

Gholipour, T., Ghasemi, M., Riazi, K., Ghaffarpour, M., and Dehpour, A. R. (2010). Seizure susceptibility alteration through 5-HT(3) receptor: modulation by nitric oxide. *Seizure* 19, 17–22.

Heintz, N. (2001). BAC to the future: the use of bac transgenic mice for neuroscience research. *Nat. Rev. Neurosci*. 2, 861–870.

Heintz, N. (2004). Gene expression nervous system atlas (GENSAT). *Nat. Neurosci*. 7, 483.

Hendricks, T., Francis, N., Fyodorov, D., and Deneris, E. S. (1999). The ETS domain factor Pet-1 is an early and precise marker of central serotonin neurons and interacts with a conserved element in serotonergic genes. *J. Neurosci*. 19, 10348–10356.

Hendricks, T. J., Fyodorov, D. V., Wegman, L. J., Lelutiu, N. B., Pehek, E. A., Yamamoto, B., Silver, J., Weeber, E. J., Sweatt, J. D., and Deneris, E. S. (2003). Pet-1 ETS gene plays a critical role in 5-HT neuron development and is required for normal anxiety-like and aggressive behavior. *Neuron* 37, 233–247.

Hoyer, D., Clarke, D. E., Fozard, J. R., Hartig, P. R., Martin, G. R., Mylecharane, E. J., Saxena, P. R., and Humphrey, P. P. (1994). International union of pharmacology classification of receptors for 5-hydroxytryptamine (Serotonin). *Pharmacol. Rev*. 46, 157–203.

Jackson, M. B., and Yakel, J. L. (1995). The 5-HT3 receptor channel. *Annu. Rev. Physiol*. 57, 447–468.

Jakab, R. L., and Goldman-Rakic, P. S. (2000). Segregation of serotonin 5-HT2A and 5-HT3 receptors in inhibitory circuits of the primate cerebral cortex. *J. Comp. Neurol*. 417, 337–348.

Karagiannis, A., Gallopin, T., David, C., Battaglia, D., Geoffroy, H., Rossier, J., Hillman, E. M., Staiger, J. F., and Cauli, B. (2009). Classification of NPY-expressing neocortical interneurons. *J. Neurosci*. 29, 3642–3659.

Kitaura, H., Uozumi, N., Tohmi, M., Yamazaki, M., Sakimura, K., Kudoh, M., Shimizu, T., and Shibuki, K. (2007). Roles of nitric oxide as a vasodilator in neurovascular coupling of mouse somatosensory cortex. *Neurosci. Res*. 59, 160–171.

Kits, K. S., and Mansvelder, H. D. (2000). Regulation of exocytosis in neuroendocrine cells: spatial organization of channels and vesicles, stimulus-secretion coupling, calcium buffers and modulation. *Brain Res. Brain Res. Rev.* 33, 78–94.

Kiyasova, V., Fernandez, S. P., Laine, J., Stankovski, L., Muzerelle, A., Doly, S., and Gaspar, P. (2011). A genetically defined morphologically and functionally unique subset of 5-HT neurons in the mouse raphe nuclei. *J. Neurosci*. 31, 2756–2768.

Krnjevic, K., and Phillis, J. W. (1963). Iontophoretic studies of neurones in the mammalian cerebral cortex. *J. Physiol*. 165, 274–304.

Kubota, Y., Shigematsu, N., Karube, F., Sekigawa, A., Kato, S., Yamaguchi, N., Hirai, Y., Morishima, M., and Kawaguchi, Y. (2011). Selective coexpression of multiple chemical markers defines discrete populations of neocortical GABAergic neurons. *Cereb. Cortex* 21, 1803–1817.

Lee, S., Hjerling-Leffler, J., Zagha, E., Fishell, G., and Rudy, B. (2010). The largest group of superficial neocortical GABAergic interneurons expresses ionotropic serotonin receptors. *J. Neurosci*. 30, 16796–16808.

Liu, C., Maejima, T., Wyler, S. C., Casadesus, G., Herlitze, S., and Deneris, E. S. (2010). Pet-1 is required across different stages of life to regulate serotonergic function. *Nat. Neurosci*. 13, 1190–1198.

Liu, X., Li, C., Falck, J. R., Roman, R. J., Harder, D. R., and Koehler, R. C. (2008). Interaction of nitric oxide, 20-HETE, and EETs during functional hyperemia in whisker barrel cortex. *Am. J. Physiol. Heart Circ. Physiol*. 295, H619–H631.

Lovick, T. A., Brown, L. A., and Key, B. J. (1999). Neurovascular

relationships in hippocampal slices: physiological and anatomical studies of mechanisms underlying flow-metabolism coupling in intraparenchymal microvessels. *Neuroscience* 92, 47–60.

Ludwig, M., and Pittman, Q. J. (2003). Talking back: dendritic neurotransmitter release. *Trends Neurosci*. 26, 255–261.

Ludwig, M., Sabatier, N., Bull, P. M., Landgraf, R., Dayanithi, G., and Leng, G. (2002). Intracellular calcium stores regulate activity-dependent neuropeptide release from dendrites. *Nature* 418, 85–89.

Markram, H., Toledo-Rodriguez, M., Wang, Y., Gupta, A., Silberberg, G., and Wu, C. (2004). Interneurons of the neocortical inhibitory system. *Nat. Rev. Neurosci*. 5, 793–807.

McCulloch, J., and Edvinsson, L. (1980). Cerebral circulatory and metabolic effects of vasoactive intestinal polypeptide. *Am. J. Physiol*. 238, H449–H456.

Mendez, P., and Bacci, A. (2011). Assortment of GABAergic plasticity in the cortical interneuron melting pot. *Neural Plast*. 2011, 976856.

Morales, M., Battenberg, E., De, L. L., Sanna, P. P., and Bloom, F. E. (1996). Cellular and subcellular immunolocalization of the type 3 serotonin receptor in the rat central nervous system. *Brain Res. Mol. Brain Res*. 36, 251–260.

Morales, M., and Bloom, F. E. (1997). The 5-HT3 receptor is present in different subpopulations of GABAergic neurons in the rat telencephalon. *J. Neurosci*. 17, 3157–3167.

Moreau, A. W., Amar, M., Le, R. N., Morel, N., and Fossier, P. (2010). Serotoninergic fine-tuning of the excitation-inhibition balance in rat visual cortical networks. *Cereb. Cortex* 20, 456–467.

Nayak, S. V., Ronde, P., Spier, A. D., Lummis, S. C., and Nichols, R. A. (1999). Calcium changes induced by presynaptic 5-hydroxytryptamine-3 serotonin receptors on isolated terminals from various regions of the rat brain. *Neuroscience* 91, 107–117.

Nishimura, N., Schaffer, C. B., Friedman, B., Lyden, P. D., and Kleinfeld, D. (2007). Penetrating arterioles are a bottleneck in the perfusion of neocortex. *Proc. Natl. Acad. Sci. U.S.A*. 104, 365–370.

Papadopoulos, G. C., Parnavelas, J. G., and Buijs, R. M. (1987). Light and electron microscopic immunocytochemical analysis of the serotonin innervation of the rat visual cortex. *J. Neurocytol*. 16, 883–892.

Paspalas, C. D., and Papadopoulos, G. C. (2001). Serotoninergic afferents preferentially innervate distinct subclasses of peptidergic interneurons in the rat visual cortex. *Brain Res*. 891, 158–167.

Perrenoud, Q., Geoffroy, H., Gauthier, B., Rancillac, A., Kessaris, N., Rossier, J., Vitalis, T., and Gallopin, T. (2012). Characterization of Type I and Type II nNOS expressing neurons in the barrel cortex of mouse. *Front. Neuronal Circuits* 6:36. doi: 10.3389/fncir.2012.00036

Petzold, G. C., and Murthy, V. N. (2011). Role of astrocytes in neurovascular coupling. *Neuron* 71, 782–797.

Porter, J. T., Cauli, B., Tsuzuki, K., Lambolez, B., Rossier, J., and Audinat, E. (1999). Selective excitation of subtypes of neocortical interneurons by nicotinic receptors. *J. Neurosci*. 19, 5228–5235.

Puig, M. V., Artigas, F., and Celada, P. (2005). Modulation of the activity of pyramidal neurons in rat prefrontal cortex by raphe stimulation *in vivo*: involvement of serotonin and GABA. *Cereb. Cortex* 15, 1–14.

Pytliak, M., Vargova, V., Mechirova, V., and Felsoci, M. (2011). Serotonin receptors—from molecular biology to clinical applications. *Physiol. Res*. 60, 15–25.

Rancillac, A., Goeffroy, H., and Rossier, J. (2012). Impaired neurovascular coupling in the APPxPS1 mouse model of Alzheimer's disease. *Curr. Alzheimer Res.* [Epub ahead of print].

Rancillac, A., Lainé, J., Perrenoud, Q., Geoffroy, H., Ferezou, I., Vitalis, T., and Rossier, J. (2010). Degenerative abnormalities in transgenic neocortical neuropeptide Y interneurons expressing tau-green fluorescent protein. *J. Neurosci. Res*. 88, 487–99.

Rancillac, A., Rossier, J., Guille, M., Tong, X. K., Geoffroy, H., Amatore, C., Arbault, S., Hamel, E., and Cauli, B. (2006). Glutamatergic control of microvascular tone by distinct GABA neurons in the cerebellum. *J. Neurosci*. 26, 6997–7006.

Rapport, M. M., Green, A. A., and Page, I. H. (1948). Serum vasoconstrictor, serotonin; isolation and characterization. *J. Biol. Chem*. 176, 1243–1251.

Reader, T. A. (1978). The effects of dopamine, noradrenaline and serotonin in the visual cortex of the cat. *Experientia* 34, 1586–1588.

Reinhard, J. F. Jr., Liebmann, J. E., Schlosberg, A. J., and Moskowitz, M. A. (1979). Serotonin neurons project to small blood vessels in the brain. *Science* 206, 85–87.

Riad, M., Tong, X. K., El, M. S., Hamon, M., Hamel, E., and Descarries, L. (1998). Endothelial expression of the 5-hydroxytryptamine1B antimigraine drug receptor in rat and human brain microvessels. *Neuroscience* 86, 1031–1035.

Roerig, B., Nelson, D. A., and Katz, L. C. (1997). Fast synaptic signaling by nicotinic acetylcholine and serotonin 5-HT3 receptors in developing visual cortex. *J. Neurosci*. 17, 8353–8362.

Rossier, J. (2009). Wiring and plumbing in the brain. *Front. Hum. Neurosci*. 3:2. doi: 10.3389/neuro.09.002.2009

Rudy, B., Fishell, G., Lee, S., and Hjerling-Leffler, J. (2011). Three groups of interneurons account for nearly 100% of neocortical GABAergic neurons. *Dev. Neurobiol*. 71, 45–61.

Sagher, O., Zhang, X. Q., Szeto, W., Thai, Q. A., Jin, Y., Kassell, N. F., and Lee, K. S. (1993). Live computerized videomicroscopy of cerebral microvessels in brain slices. *J. Cereb. Blood Flow Metab*. 13, 676–682.

Simpson, K. L., Waterhouse, B. D., and Lin, R. C. (2003). Differential expression of nitric oxide in serotonergic projection neurons: neurochemical identification of dorsal raphe inputs to rodent trigeminal somatosensory targets. *J. Comp. Neurol*. 466, 495–512.

Smiley, J. F., and Goldman-Rakic, P. S. (1996). Serotonergic axons in monkey prefrontal cerebral cortex synapse predominantly on interneurons as demonstrated by serial section electron microscopy. *J. Comp. Neurol*. 367, 431–443.

Steinbusch, H. W. (1981). Distribution of serotonin-immunoreactivity in the central nervous system of the rat-cell bodies and terminals. *Neuroscience* 6, 557–618.

Sudweeks, S. N., Hooft, J. A., and Yakel, J. L. (2002). Serotonin 5-HT(3) receptors in rat CA1 hippocampal interneurons: functional and molecular characterization. *J. Physiol*. 544, 715–726.

Takeuchi, Y., and Sano, Y. (1984). Serotonin nerve fibers in the primary visual cortex of the monkey. Quantitative and immunoelectronmicroscopical analysis. *Anat. Embryol. (Berl.)* 169, 1–8.

Tong, X. K., and Hamel, E. (2000). Basal forebrain nitric oxide synthase (NOS)-containing neurons project to microvessels and NOS neurons in the rat neocortex: cellular basis for cortical blood flow regulation. *Eur. J. Neurosci*. 12, 2769–2780.

Tork, I. (1990). Anatomy of the serotonergic system. *Ann. N.Y. Acad. Sci*. 600, 9–34.

Underwood, M. D., Bakalian, M. J., Arango, V., Smith, R. W., and Mann, J. J. (1992). Regulation of cortical blood flow by the dorsal raphe nucleus: topographic organization of cerebrovascular regulatory regions. *J. Cereb. Blood Flow Metab*. 12, 664–673.

van Hooft, J. A., Spier, A. D., Yakel, J. L., Lummis, S. C., and Vijverberg, H. P. (1998). Promiscuous coassembly of serotonin 5-HT3 and nicotinic alpha4 receptor subunits into Ca(2+)-permeable ion channels. *Proc. Natl. Acad. Sci. U.S.A*. 95, 11456–11461.

Vitalis, T., and Rossier, J. (2011). New insights into cortical interneurons development and classification: contribution of developmental studies. *Dev. Neurobiol*. 71, 34–44.

Vucurovic, K., Gallopin, T., Ferezou, I., Rancillac, A., Chameau, P., van Hooft, J. A., Geoffroy, H., Monyer, H., Rossier, J., and Vitalis, T. (2010). Serotonin 3A receptor subtype as an early and protracted marker of cortical interneuron subpopulations. *Cereb. Cortex* 20, 2333–2347.

Walstab, J., Rappold, G., and Niesler, B. (2010). 5-HT(3) receptors: role in disease and target of drugs. *Pharmacol. Ther*. 128, 146–169.

Waterhouse, B. D., Azizi, S. A., Burne, R. A., and Woodward, D. J. (1990). Modulation of rat cortical area 17 neuronal responses to moving visual stimuli during norepinephrine and serotonin microiontophoresis. *Brain Res*. 514, 276–292.

Whittington, M. A., and Traub, R. D. (2003). Interneuron diversity series: inhibitory interneurons and network oscillations *in vitro*. *Trends Neurosci*. 26, 676–682.

Yaksh, T. L., Wang, J. Y., and Go, V. L. (1987). Cortical vasodilatation produced by vasoactive intestinal polypeptide (VIP) and by physiological stimuli in the cat. *J. Cereb. Blood Flow Metab*. 7, 315–326.

Yan, X. X., Jen, L. S., and Garey, L. J. (1996). NADPH-diaphorase-positive neurons in primate cerebral cortex colocalize with GABA and

calcium-binding proteins. *Cereb. Cortex* 6, 524–529.

Yang, G., Chen, G., Ebner, T. J., and Iadecola, C. (1999). Nitric oxide is the predominant mediator of cerebellar hyperemia during somatosensory activation in rats. *Am. J. Physiol*. 277, R1760–R1770.

Yang, G., Huard, J. M., Beitz, A. J., Ross, M. E., and Iadecola, C. (2000). Stellate neurons mediate functional hyperemia in the cerebellar molecular layer. *J. Neurosci*. 20, 6968–6973.

Zhou, F. M., and Hablitz, J. J. (1999). Activation of serotonin receptors modulates synaptic transmission in rat cerebral cortex. *J. Neurophysiol*. 82, 2989–2999.

Zupanc, G. K. (1996). Peptidergic transmission: from morphological correlates to functional implications. *Micron* 27, 35–91.

Conflict of Interest Statement: The authors declare that the research was conducted in the absence of any commercial or financial relationships that could be construed as a potential conflict of interest.

Received: 28 March 2012; paper pending published: 03 May 2012; accepted: 10 July 2012; published online: 10 August 2012.

Citation: Perrenoud Q, Rossier J, Férézou I, Geoffroy H, Gallopin T, Vitalis T and Rancillac A (2012) Activation of cortical 5-HT$_3$ receptor-expressing interneurons induces NO mediated vasodilatations and NPY mediated vasoconstrictions. Front. Neural Circuits ***6****:50. doi: 10.3389/fncir.2012.00050*